TRANSFORMATION AND HARDENABILITY IN STEELS

Symposium: February 27-28, 1967

TRANSFORMATION AND HARDENABILITY IN STEELS

Symposium sponsored by
CLIMAX MOLYBDENUM COMPANY OF MICHIGAN (INCORPORATED)
an AMAX subsidiary
and the **UNIVERSITY OF MICHIGAN**
Department of Chemical and Metallurgical Engineering
in cooperation with
The University of Michigan Extension Service

5780023905 .

Climax Molybdenum Company of Michigan (Incorporated)

An AMAX Subsidiary • 1600 Huron Parkway, Ann Arbor, Michigan 48105

Table of Contents

Introduction

A. J. HERZIG
President, Climax Molybdenum Company of Michigan
a subsidiary of American Metal Climax, Inc.

In extending greetings to you on this occasion, and in expressing thanks to you for your participation in the deliberations we will undertake, I have chosen, by way of introduction, to comment briefly on man's experience with iron.

Some time ago I read that around 1250 B.C., King Hattushish, of the Hittites, sent a letter to King Ramses II of Egypt covering the delivery of a defective dagger. An excerpt from that letter might well serve as a keynote for this symposium. I quote from the letter:

> *"As to the good iron in my sealed house in Kissuwadna, it is a bad time to make iron, but I have written ordering them to make good iron. So far they have not finished it. When they finish it, I will send it to you."*

It occurs to me that in the long lines of communications which followed, each of us has accepted the task assigned in that letter, but, alas, we have not yet finished it! Those who might not like such a fantastic interpretation of the King's words could at least surmise that he had composed a very early apology for low hardenability or poor hardening practice.

Whether or not he appreciated the vast implications of his discovery, the first man who recognized the combination of hardness, strength, and malleability — which characterizes the metallic state — started a long chain of investigation. Whether or not some later man appreciated the implications of his discovery, that second man who hardened a piece of iron–carbon alloy, by heating and cooling it, performed the first experiment in the specific field of metals/materials science which brings us together at this symposium. It matters not to us whether these men were motivated as scientists or by the forces that carry the artisan through the long process of trial and error. A tremendous potential had been disclosed for the use of metallic materials.

Without belaboring the point at which art becomes science, or without conjecture as to how the rate of effort over the long years may have been affected by budgets and/or marketing programs, the potential of iron was largely pursued on an empirical basis until 1863 when the first examinations of the microstructure of iron were undertaken. In a relatively short span of years, these and subsequent examinations, as well as the deductions therefrom, led us to the knowledge that the basis for the extraordinary response of iron–carbon alloys to heat treatment resided in the solid-state transformations to which they were inherently susceptible.

By the early years of this century, the exploitation of iron and steel had been of such scope and intensity, it can be said that although man's organic substantive existence is based on carbon, hydrogen, and oxygen–his power, his security, and the standard of living he enjoys are predominantly based on his use of iron and carbon. In view of the predominance of this technology, it was inevitable that we would delve deeply into an understanding of the environmental parameters that maximize the response of iron to the treatments we had learned to apply to it.

Since the recognition, beginning in 1930, of a quantitative relationship between composition, temperature, time, transformation products, stress, and rate of transformation of austenite, every discipline to which our profession has access has been employed in the procurement of more data and the appraisal of detailed studies of all of the phenomena that attend the formation and decomposition of austenite. All this effort was and still is indeed focused on the objective that we might eventually secure for society-at-large the ultimate capability of iron–carbon alloys.

It is appropriate at such a time to acknowledge all who have preceded us in this effort. It is also appropriate to be mindful of those contemporaries who for any reason whatsoever are not with us today. Since it is the purpose of such a symposium to share our experiences on the basis of our opportunities to enjoy them, it is not necessary to identify and pass judgment on individual contributions either ancient or modern.

On behalf of our company and in acknowledgment of the cooperation of the University of Michigan, I thank you for your participation in this meeting where, although we may not improve upon the King's English, we may have done something toward perfecting his iron.

The Formation of Austenite

H. W. PAXTON
Carnegie Institute of Technology
Pittsburgh, Pennsylvania

INTRODUCTION

The value of a moderately fine-grain size in austenite has been recognized for many years in ferrite–pearlite (FP) structural steels, and in those steels customarily quenched and tempered. Whereas in high speed steels, fine austenite grain size has implied grain diameters of the order 5μ (ASTM 12), in quenched and tempered (QT) steels, it was generally believed that 40/50μ (ASTM 6 or 7) was adequate; in structural steels the austenite grains were often much larger.

The yield strength and ductility parameters of QT steels were shown in 1939 (by Janitzky and Baeyertz)[1]* to be virtually independent of the then conventional *austenite* grain size range. The dependence of these properties in the FP steels on the *ferrite* grain size has been known for well over ten years, and comprehensive publications from the United Steel Companies Ltd.[2] have documented the effect convincingly. The resistance of QT steels to impulsive loading has long been known to be improved by refinement of austenite grain size, and that of FP steels by the smaller ferrite grain size which generally results from a small austenite grain size.

The austenite grain size in low alloy hypoeutectoid QT steels is typically in the range of ASTM 6/8 after the heating necessary to assure a matrix with virtually no undissolved carbides and only modest compositional gradients, and which would thus give the maximum hardenability on quenching.

Methods of producing significantly smaller austenite grain diameters in these materials were first reduced to practice by Grange.[3] They include the classical method of "cold" deformation of austenite followed by recrystallization, and the somewhat less obvious method of repeated rapid heating of ferrite–carbide aggregates into the lower end of the single-phase austenite range. Grain sizes of ASTM 12 (6μ diameter) and in appropriate cases, sizes even smaller than this, are not too difficult to produce by these methods, but practical and economic considerations have made commercial exploitation somewhat limited at present.

In the FP steels, especially those containing less than 0.1% C, austenite grain sizes are frequently not known, but ferrite grain sizes of ASTM 12/13 are produced with no unusual difficulty commercially.

The purposes of this paper are to survey the parameters which can influence austenite grain size, to enquire if grain sizes much smaller than ASTM 12 are realistically possible in all steels, and to explore possibilities of producing a grain size of ASTM 12 by means other than those which have already been proposed.

SOME EXPERIMENTAL OBSERVATIONS ON AUSTENITE FORMATION

There appear to be only two available and currently practical methods of producing essentially strain-free grains of austenite. One is by recrystallization, and the other involves formation by a phase change, most commonly up-quenching of a ferrite–carbide aggregate. We shall ignore here formation of austenite by vapor deposition or from the liquid, including the possibility of grains nucleating from a "splat cooled" amorphous film of austenite. The two more usual processes will be considered in turn.

Recrystallization of Austenite

Modern theories of recrystallization take into account the structures produced by deformation which can serve to provide a viable nucleus without invoking thermal activation over an unreasonable volume.[4]

*See references.

This paper is a summary of work performed under the sponsorship of the Office of Naval Research (Contract Nonr 1-51005-TO 14), the Army Research Office, Durham (1-50014-A 33), and the National Science Foundation (1-55092-NSF 134).

In both bcc and fcc materials of high stacking fault energy, the dislocations form "cells" of about 1μ in diameter within the grains after modest deformations (10/30%) at T/T_m 0.2/0.3. The center of each cell is virtually free of dislocations, and the dislocations in the wall possess such a density that estimates of their number are questionable. At rather higher temperatures, e.g., T/T_m 0.3/0.4, the dislocations in the cell walls are more likely to form networks, and the cell size increases, although not by more than a factor of two.

Since all the theories of recrystallization involve the idea that one of these cells is the existing nucleus, and grows by one means or another, one would expect the minimum grain size after recrystallization to be some small multiple of the cell size. (The dislocation arrangements forming cell walls are not considered to be high angle grain boundaries, and the coalescence of two, three, or more cells is necessary to produce these.) On this basis, then, the expected minimum grain size in these materials after complete recrystallization and before any substantail grain growth would perhaps be about 5μ.

On the other hand, materials with low stacking fault energy, which includes some austenites, do not show clearly defined cells.[5] Rather, the dislocations remain co-planar to a great extent, and occasionally one may form deformation twins. A good example of this is given by Leslie and Miller[6] in a 0.27% C — 11% Mn steel where the twins are 25 to 250 Å thick, and spaced about 50 to 5,000 Å apart. The recrystallization behavior of such materials has not been studied extensively. It remains to be seen whether the nucleation rate can be made sufficiently high and the growth rate sufficiently low that a grain diameter of, for example, 1μ or about ASTM 17 can result. It might be possible to arrange for a finely dispersed precipitate to form during the heating for recrystallization, which would reduce boundary velocities; this point will be discussed more extensively in a later section.

In the cold working of a phase containing hard dispersed particles, cells also form and it appears that they may be somewhat smaller than those in homogeneous materials, e.g., perhaps one-quarter or one-half of a micron instead of a micron. The possibility of utilizing this idea during the hot-rolling of austenite prior to expected recrystallization may be interesting. However, the experimental difficulties of checking the underlying premises are formidable and an appropriate dispersion of particles may cause other complications. The effect on recrystallization behavior seems to be a function of size and spacing of particles. The most obvious area for testing in the ferrous field is in hypereutectoid alloy steels, where results on carefully controlled deformation have not been reported extensively, and some degree of control over carbide precipitation can be achieved.

The whole subject of recrystallization of two-phase alloys is complex; for a review of current opinions and experiments, the reader is referred to a recent survey by Cahn.[7]

The possibility also exists that by careful control of rolling and recrystallization, it may be possible to produce an austenite with a strong preferred orientation, which may result in a product having interesting anisotropic properties. The value of this approach in producing deep drawing sheet by rolling and recrystallizing ferrite has been especially evident over the last few years.

Formation of Austenite by a Phase Transformation

It is also possible to nucleate austenite, presumably generally relatively undeformed, from other phases which exist, either stably or metastably at or near room temperature. These phases may be ferrite–carbide aggregates or may contain substantial amounts of martensite (which may or may not temper significantly on heating).

There is now clear evidence that, depending on circumstances, austenite may form either by classical heterogeneous nucleation at a carbide–ferrite interface, or by a shear reaction on a specific habit-plane. The possibility also exists, but the evidence is less convincing at the moment, that a massive reaction may occur in some cases.

A graphic illustration of the formation of austenite by diffusionless shear is given by the work of Zerwekh and Wayman,[8] who, under certain conditions, could transform single crystal whiskers of pure iron by a single interface shear transformation in a temperature gradient. The habit plane was close to, but not exactly, $\{110\}\alpha$ and could be satisfactorily understood by the phenomenological theory of "martensite" transformations.

Superficially similar results were found by Grozier[9] in an investigation of the formation of austenite

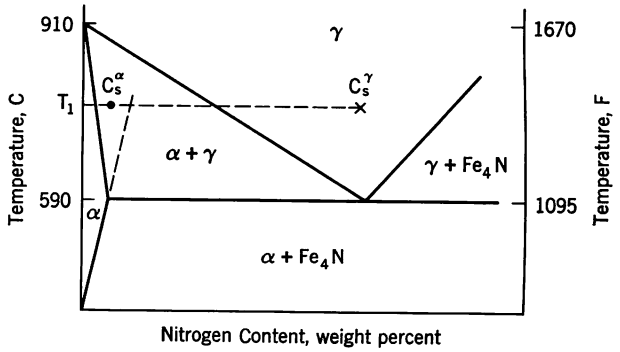

FIGURE 1. Schematic of the iron–nitrogen system showing typical conditions in Grozier's experiment to grow isothermal acicular austenite. The composition given by the intersection of the dotted lines would be in equilibrium with Fe_4N. C_s^α is in metastable equilibrium with C_s^γ, and is supersaturated with respect to the $\alpha/(\alpha+\gamma)$ phase boundary

during the nitriding of single crystals of zone refined iron. A schematic of his experimental concept is shown in Figure 1. α-crystals several millimeters in diameter and about 1 mm thick were exposed at temperature T_1 to an NH_3/H_2 mixture with a nitrogen activity such that at equilibrium an austenite of composition C_s^γ would result; the same atmosphere produces a surface concentration in ferrite of C_s^α until austenite nucleates.

If the surface was rendered quite imperfect, by mechanical abrasion for example, austenite nucleated quite easily and profusely. The austenite grains impinged rapidly, and eventually grew inwards in a classical columnar fashion with an average α–γ interface parallel to the external surface. The rate of growth inwards was capable of being calculated on the basis that nitrogen diffusion through austenite was dominant and that local equilibrium existed at the external and internal surfaces of the austenite. The experimental results were in excellent agreement with these calculations.

On the other hand, if the surfaces prior to nitriding were carefully prepared, e.g., by prolonged electropolishing, the pattern of austenite formation was very different. Nucleation of austenite became much more difficult and was restricted to local heterogeneities such as grain boundaries, inclusions, or deliberately introduced scratches. The growth of austenite was acicular and displayed a marked shear on the polished surface of an α-crystal. Mid-ribs were often visible during hot-stage examination.

It was possible to make measurements of growth rate; the length of a given grain was directly proportional to the elapsed time after nucleation and very sensitive to temperature and supersaturation of nitrogen in the ferrite. The crystallography of the plates was not simple. α-crystals with surface poles in the region of the unit triangle bounded by [100] – [110] – [112] had habit planes of $\{110\}\alpha$, those in the remainder of the unit triangle had habit planes of $\{112\}\alpha$. This growth habit is not understood at present, and may have some similarities to the formation of certain of the bainitic structures described later in this conference.

Since the growth, although the interface advances by a cooperative shear, appears to be controlled by nitrogen diffusion from supersaturated ferrite to the advancing austenite, it is perhaps more appropriate to think of this transformation as Widmanstätten rather than "martensitic."

In similar experiments using CO/CO_2 or CH_4/H_2 mixtures, Judd[10] was able to display the same phenomenon for carbon austenite. However, due to difficulties in reproducibility, perhaps related to catalytic difficulties in maintaining a constant carbon potential over iron at the relatively low temperature involved, it was not possible to obtain the same kind of quantitative data on growth rates for carbon austenite as for nitrogen austenite. There appears to be no reason, however, to question the hypothesis that the two elements behave in a very similar fashion.

As a qualitative experiment to confirm the idea that austenite might grow into ferrite with an associated shear if the supersaturation is sufficiently high, two different types of experiments were performed. In the first,[9] an iron crystal was uniformly nitrided in the solid solution range at 650 C (1200 F) to 0.055% N, which is close to the solubility limit at this temperature. The specimen was then up-quenched to 825 C (1515 F) for one hour and water quenched. A large fraction of the austenite formed was in the interiors of the grains and acicular with a habit plane close to $\{110\}\alpha$. In similar experiments, with a lower temperature utilized for up-quenching, thus producing lower supersaturations, the austenite tended to nucleate more and more at ferrite grain boundaries and at the external surface, and the fraction of idiomorphic austenite increased.

In the second series of experiments performed by Judd,[10] Fe_3C was used as a solid source of carbon. Carbon dissolves rapidly in ferrite and diffuses substantially in times which, under the proper conditions, are short relative to the times necessary for austenite nucleation. In large-grained crystals of iron (from a zone refined base) containing well-dispersed carbides, up-quenching to sufficiently high temperatures also produced acicular austenite on $\{110\}\alpha$. At lower supersaturations, or when austenite nucleation was facilitated by α grain boundaries, idiomorphs of austenite resulted (frequently with noticeable deviations from sphericity in the form of flat facets).

To summarize the above information, it appears to be quite evident that the acicular mode of austenite formation can occur in a variety of situations when the supersaturation, and hence the driving free energy of transformation, are sufficiently high and the rate of conventional nucleation is low for any reason. In some cases, shear is clearly observed; in others it appears by analogy to be probable. It should be pointed out that the transformations are not necessarily all diffusionless even though shear may be involved.

THE FORMATION OF AUSTENITE IN STEELS

In applying the thoughts above to practical considerations in the formation of austenite in commercial steels, there are several questions which are of concern:

(1) What are the rate and mechanism of austenite nucleation at carbide particles in grain boundaries and in grains?

(2) How does this rate vary with variation in composition or coherency of the carbide?

(3) What factors contribute to the rate of growth of austenite prior to impingement?

(4) How rapid is grain growth following impingement?

It will be convenient to discuss each of these in turn.

Nucleation of Austenite at Carbide Particles

The difficulties of predicting nucleation rates in solid-solid transformation have been discussed by many authors. Even experimental measurements are not particularly simple, and furthermore are tryingly tedious.

In the classic early work of Roberts and Mehl,[11] the formation of austenite was investigated from various microstructures, largely eutectoid pearlites of various spacing. The view was taken that a constant nucleation rate per unit volume of pearlite, N_v, was appropriate, and this could then be calculated from the Johnson-Mehl formalism and the curves of fraction transformed versus time. The calculated values of N_v varied by many orders of magnitude, but the resulting values of grain size, calculated from these N_v and observed growth rates (from measurements of maximum austenite nodule radius versus time) were not very different. All values were essentially ASTM 7 ± 1. Fracture grain size measurements were generally in good agreement with calculations.

Whether or not one should use N_v or should express a nucleation rate in terms of the carbide–ferrite interfacial area is a debatable point. In principle, the area measurement is probably the more realistic, but in practice, the variation in area possible with most achievable carbide distributions is not large compared with potential variations in nucleation rate caused by other factors such as temperature, supersaturation and coherency.

Experimental measurements of nucleation rate in well defined experimental situations are sparse. In aggregates of spheroidal carbides in ferrite, with carbide diameters of the order of a few microns, a spectrum of nucleation times exists for austenite forming at carbide particles when the superheating is small. In some experiments performed by Judd[10] (to be discussed later) on 0.1% C steels, where the carbide spacing is 12/15μ, it was possible to make approximate measurements of nucleation rate between 750 and 787 C (1400 and 1450 F) since, in general, the austenite patches do not impinge. The results are shown in Table I, expressed as percent of carbide particles per second which nucleate austenite.

On the other hand, experiments by Molinder[12] on a 1.27% C steel in which the carbide size is comparable to Judd's, but the carbide spacing is only 2 to 3μ, show that when the nucleation rate is low, a different pattern of austenite formation can hold. It is possible to have austenite grow sufficiently rapidly that it engulfs many carbides; the necessity for further nucleation is thereby avoided and the carbide merely dissolves in the austenite without any further obvious effect on austenite grain size.

We are then concerned with effective nucleation rate in determining the number of austenite grains produced before impingement. It may be in many cases that the clear increase in austenite nucleation rate observed when carbides are in ferrite grain boundaries leads to this effect dominating nucleation and hence austenite grain size (i.e., carbides in α-grain interiors may have little effect as nuclei).

In the formation of austenite from as-quenched acicular alloy martensite, it is not unusual for the austenite also to be acicular.[13,14] With many carbide particles and α-α boundaries available as potential nuclei, the effect is complex and the microstructure can depend on the alloying elements present and on available free energies. Aaronson, in his investigation[15] of this effect, is led to the conclusion that the austenite growth is diffusion limited.

Provided that more than one carbide particle per ferrite grain nucleates austenite and that each austenite grain during a subsequent cooling transformation produces one or more ferrite grains, a progressive refinement is obviously possible. The experiments of Grange [3,16] are in accord with this line of reasoning. A saturation exists after 2 to 4 cycles in the range ASTM 12 to ASTM 17 in that the austenite grain size cannot be further refined. This latter figure is consistent with a very efficiently nucleating carbide particle of a few thousand Ångstroms diameter or a number of rather less efficient carbides of the same total volume. Carbides greater than 1μ diameter can presumably not lead to ultrafine austenite grain sizes, at least in a single heat treatment.

Evidence for the formation of austenite from ferrite by diffusionless shear in fine grained steels containing carbides is still rather indirect. The locus of T_o is known quite well above A_1 for carbon and low alloy steels, but the locus of A_s remains questionable. By analogy with the reverse problem, the relative location of T_o and M_s, one might expect at least for carbon contents greater than about 0.1% that A_s would be some 200 C (360 F) above T. This is approximately true (at lower temperatures) in the reversion of Fe–Ni martensites. However, the value of (T_o–M_s) in very low carbon steels has been the subject of recent debate, and it seems incontestable that the value of ΔG involved in the diffusionless transformation of ferrite to austenite in nearly pure iron can hardly exceed about 18 cal/mol, a full order of magnitude less than that for the austenite–martensite transformation in carbon steels and Fe–Ni alloys. In recent work, Albutt and Garber[17] have suggested that ferrite (in a 0.08% C steel) can transform to austenite by a diffusionless transformation at about 920 C (1690 F) at rates of heating

above about 1000 C/sec (1800 F/sec). If this is true, the driving force is indeed quite small. Albutt and Garber state clearly that they did not attempt to decide whether the transformation is massive or martensitic.

In any case, in the normal circumstances associated with austenite formation from ferrite–carbide aggregates at temperatures low enough so grain growth is reasonably low, i.e., 850 C (1560 F) or less, the ferrite composition is virtually independent of the number and size of the carbides, it cannot transform by a diffusionless shear, and will thus transform by nucleation and normally incoherent growth of austenite. Rapid heating rates per se are not relevant in producing "martensitic austenite."

An illustration of this point is given in work by Speich, Szirmae and Fisher[18] who used laser heating to permit very short isothermal holding times to study the response of a 0.77% C alloy. The heating rate was of order 10^6 C/sec (1.8×10^6 F/sec) and cooling rate 10^5 C/sec (1.8×10^5 F/sec). A specimen held for 0.02 sec at 845 C (1555 F) showed a uniform austenite rim around each carbide and the same was true for a specimen held 0.008 seconds at 885 C (1625 F). It is noteworthy that the nucleation time is very short, and all carbides had formed austenite around them. However, virtually all the carbides were in grain boundaries, and the increased catalytic potency of these is clearly an important factor.

Thus the experiments of Grozier and Judd, which established the possibility of acicular austenite, do not seem to have any proven application to practical austenite grain size control. It would be necessary to have a dense uniform array of fine carbides in a very coarse-grained ferrite, and no way of doing this is apparent to the author.

Effect of Coherency and Composition of Carbides

The theory of the nucleation of a third phase from a mixture of two others is not developed to any significant extent. However, the qualitative ideas from a solid–solid transformation when only two phases are

TABLE I Observed Experimental Material Parameters

Temperature C	Temperature F	Material	$\bar{r}_o$	r_{max}	N	t_o sec
750	1380	Small grain*	1.57	3.25	12	9
		Large grain†	2.75	3.67	1.43	32
		Mn alloy	1.28	3.29	2.86	20
		Blackplate	1.04	3.52	—	14
762.5	1405	Small grain	1.63	3.44	28.2	6.75
		Large grain	2.18	3.89	4.5	18.8
		Mn alloy	1.87	3.75	25	10.5
		Blackplate	0.94	3.07	22.5	10.2
775	1425	Small grain	1.53	2.90	≧100	7
		Large grain	1.90	2.99	10.7	14
		Mn alloy	1.20	3.20	30	9.7
		Blackplate	1.49	2.81	73	9
787.5	1450	Small grain	2.06	2.56	≧100	4
		Large grain	1.83	2.40	33⅓	10.1
		Mn alloy	1.50	3.22	≧100	6
		Blackplate	1.60	2.31	≧100	6

*Small grain indicates small grain zone refined Fe–C alloy (~0.1% C).

†Large grain indicates large grain zone refined Fe–C alloy (~0.1% C).

Composition**

	% Mn	% C	% Si	% S	% P	% Cr	% Cu	% Mo	% Ni
Fe–Mn–C	0.49	0.1	0.04	0.012	—	—	—	—	—
Blackplate	0.45	0.09	0.008	0.019	0.007	0.02	0.02	0.01	0.02

$\bar{r}_o$ = mean radius of Fe_3C

r_{max} = maximum radius of Fe_3C

N = nucleation rate in percent of carbide particles per sec

t_o = incubation time

** = weight percent

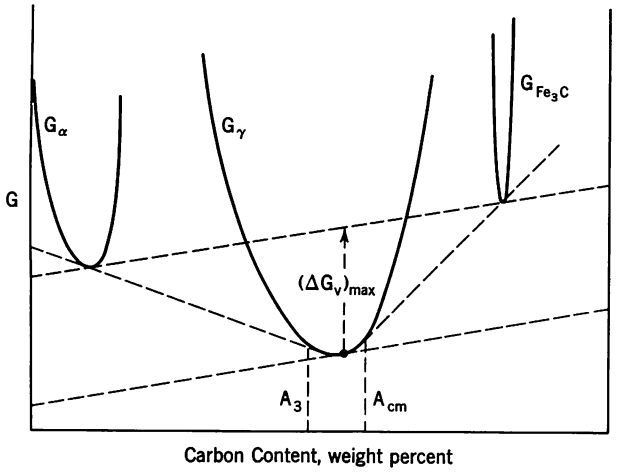

FIGURE 2. Schematic of probable nucleation conditions for austenite from a ferrite–carbide aggregate

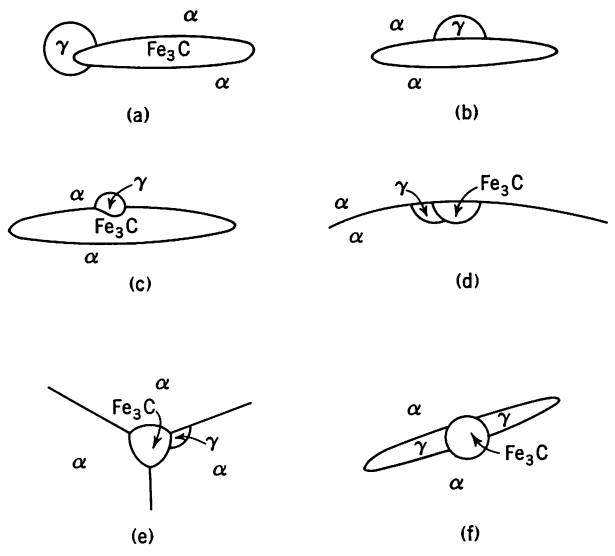

FIGURE 3. Some possible nucleation geometries for austenite at an α–Fe_3C interface. Only in (f) is any special low energy interface for α–γ considered

involved can probably be applied with some confidence. We can outline here only the formalism. In particular, we are interested as usual in:

(a) the free energy change per unit volume;

(b) the net increase in surface energy for a given volume of austenite, which obviously depends on the geometry;

(c) strain energy contributions.

The free energy change depends on the "composition" of the austenite nucleus. This is maximized for the situation shown in Figure 2, and unless the surface free energy is a strong function of composition, this probably is the effective situation in pure iron–carbon alloys. In steels containing other elements, which in general would diffuse slowly, the situation

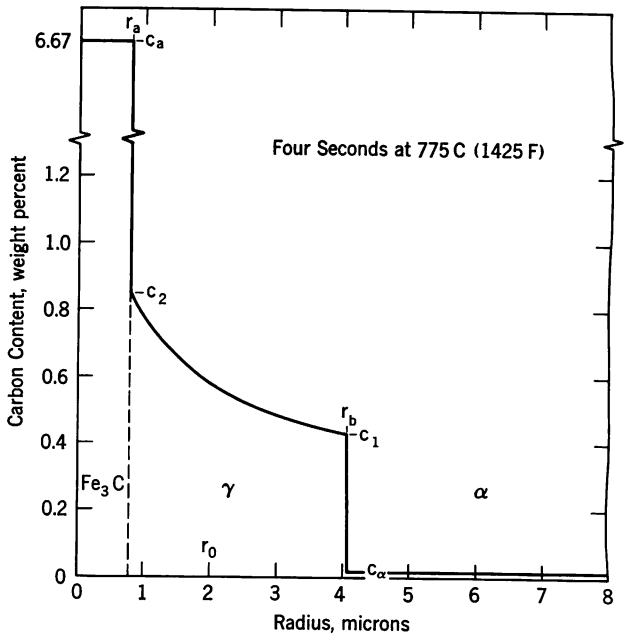

FIGURE 4. Concentration of carbon vs distance along a radius from the center of a spherical carbide particle four seconds after nucleation of austenite at 775 C (1425 F). r_0 is the original carbide–ferrite interface. c_a, c_2, and c_1 are given by the phase diagram

is rather more complex, and the free energy change will not be the maximum possible (a constraint of constant N_{Fe}/N_x is probably usually operative, for example). Since the free energy enters as the exponent $\{-\text{ const}/(\Delta G_v)^2\}$, the possible effect may be large, but is impossible to calculate with present knowledge. Judd's experiments (Table I) suggest a somewhat slower nucleation rate in his 0.5% Mn alloy and in blackplate.

Some possible geometries of austenite nucleation are shown in Figure 3. The most favorable situations are c, d and e, especially if $\frac{\gamma_{a\gamma}}{\gamma_{a_c}} < 1$ or $\frac{\gamma_{a\gamma}}{\gamma_{aa}} < 1$.

Whether (c) is generally likely is not known; (d) and (e) are certainly common, and examples have already been cited. Alloy additions which promote coherent carbides and therefore reduce γ_{a_c} would be expected to suppress still more cases (a) and (b).

Factors Contributing to the Rate of Growth of Austenite prior to Impingement

Since the finest grain sizes will be produced by a very large number of austenite nuclei per unit volume (i.e., many fine carbides all of which have a chance to produce a nucleus before they are engulfed by austenite nucleated elsewhere), the chances of sufficient time being available for this to occur are obviously improved by a low growth rate of austenite. The factors which can affect this rate will therefore be considered.

The simplest model which can be chosen for theoretical study would assume a spherical carbide particle of radius r_0 on which a uniform shell of austenite nucleates after an incubation period t_0. This shell dissolves carbon from the carbide and as this diffuses outward, ferrite is consumed. A schematic of concentration along a radius is shown in Figure 4, where the concentrations c_α and c_a represent the solubility of carbon in ferrite, and the weight percent of carbon in cementite respectively.

If the concentrations at r_a and r_b represent the limits of the austenite stability range at the temperature of interest, it is possible to calculate r_a and r_b as a function of time after t_0 assuming that the rate controlling step is the diffusion of carbide through austenite. The details of the calculations are published elsewhere, but some typical examples of the results are shown in Figures 5 and 6.

By incorporating measured nucleation rates, and the above calculations for growth rate, it is possible to check the validity of the assumption that D is the rate controlling parameter. In a series of experiments performed by Judd over the temperature range 750 to 787 C (1400 to 1450 F), this assumption does indeed appear to be true for a 0.1% C material prepared by gaseous carburization of zone refined iron, whether this had a "small" ferrite grain size (~ASTM 6) with essentially all carbides in grain boundaries or a considerably larger ferrite grain size (~1 mm) where most of the carbides were intragranular. However, in a similar alloy prepared with 0.5% Mn in addition, or in commercial blackplate, the rate of growth at small supersaturations was very noticeably less than that characterized by carbon diffusion control. The reasons for this are not clearly established, but the most reasonable explanation is that the diffusion gradient in the austenite is reduced by a change in the carbon activity at the carbide–austenite interface due to previous partitioning of manganese preferentially to the carbide, and to the sluggish diffusion of this manganese away from the interface after some carbide dissolution. At higher temperatures, where diffusion gradients are steeper, this effect would be expected to be less dominant as is indeed observed.

Various other experiments have been performed in the author's laboratory to investigate the conditions under which austenite grows by diffusion-limited transport of an interstitial. The experiments of Grozier[9] cited earlier showed that an appropriate NH_3/H_2 environment would cause nitrogen–austenite to grow in a planar fashion into zone refined iron at a rate which could be predicted accurately from the phase diagram, the diffusion coefficient D_N^γ, and Wagner's analysis of the moving boundary problem.

However, if various alloying elements are added to the iron, in amounts of about one atom percent, the pattern of growth changes in a more or less systematic fashion.[19] Additions of nickel, cobalt or manganese produced little change in the pattern of inward growth of austenite. Additions of vanadium, titanium, chromium, silicon or aluminum showed a much smaller growth rate of this austenite rim, a very ragged interface and a considerable penetration of austenite down the ferrite grain boundaries ahead of the rim. This extra penetration is absent in zone-refined iron or in the nickel, cobalt or manganese alloys.

Molybdenum was added to the extent of one weight percent and behaved like nickel, cobalt and manganese. However, one weight percent is only about 0.5 atom percent and so comparisons are not necessarily fruitful or meaningful. Some illustrations of

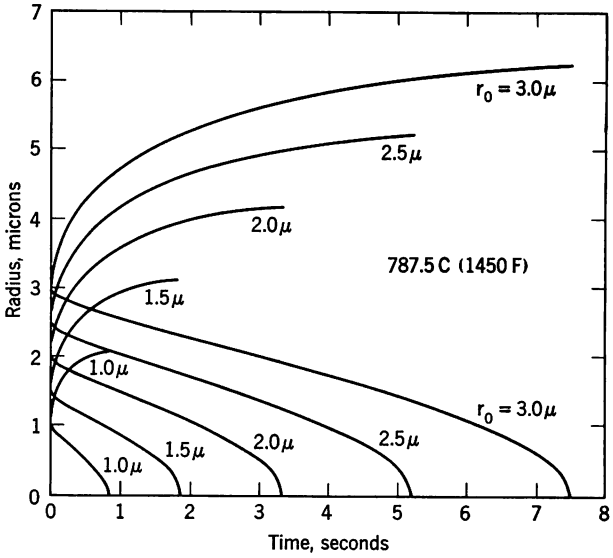

FIGURE 5. Variation of r_a (lower curves) and r_b (upper curves) for typical values of r_0 during austenite formation at 787.5 C (1450 F). The curves are terminated when the carbide is dissolved; further and slower increase in r_b occurs by homogenization

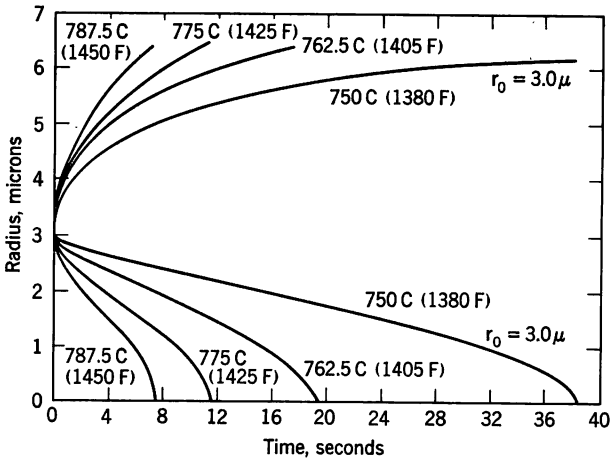

FIGURE 6. Variation of r_a and r_b with time at various temperatures for a starting r_0 of 3μ

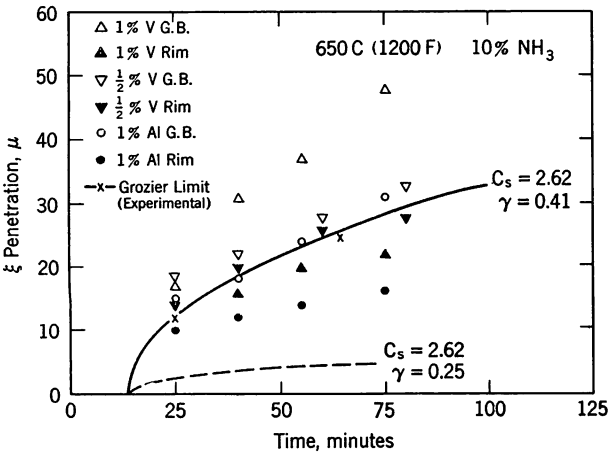

FIGURE 7. Penetration at α grain boundaries and within α grains for various alloys vs time of exposure, compared to the experimental rim penetration in zone-refined iron under equivalent conditions of temperature and atmosphere. 650 C (1200 F), 10% NH_3 in H_2. The dashed line shows the predicted rim penetration using diffusion data of Grieveson and Turkdogan

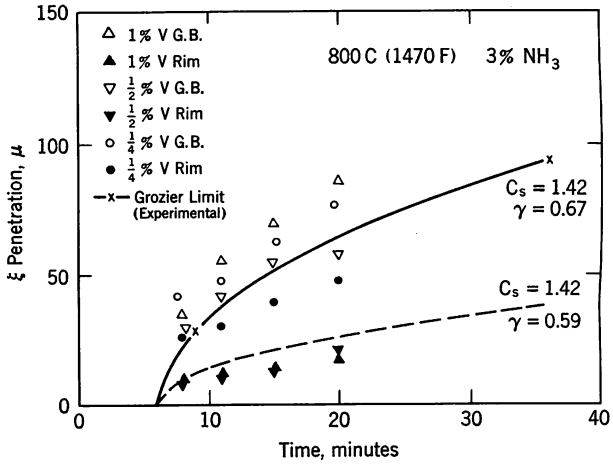

FIGURE 8. Penetration at α grain boundaries and within α grains for various alloys vs time of exposure, compared to the experimental rim penetration in zone-refined iron under equivalent conditions of temperature and atmosphere. 800 C (1470 F), 3% NH_3 in H_2. The dashed line shows the predicted rim penetration using diffusion data of Grieveson and Turkdogan

this effect are shown in Figures 7 and 8, for the nitrogen–austenite growth rates in zone-refined iron and in iron containing various amounts of vanadium. The parabolae cited as the "Grozier limit" are those for a given surface concentration (in weight percent nitrogen) and the value of γ in Wagner's equation $\xi = 2\gamma\sqrt{D_N^\gamma t}$, where γ is a function of the interface concentrations and of D_N^γ/D_N^α.[9] The effect of vanadium is seen to be more significant at the lower temperature

Some possible explanations of this effect have been discussed elsewhere in a paper by Pavlick, Mullins and Paxton.[19] It was not possible to reach firm conclusions on the mechanism, but one attractive theory held that particles of, for example, vanadium nitride formed during the growth of austenite and acted as a barrier to growth in a similar manner to that envisioned many years ago by Zener[20] for recrystallizing grains. For these particles to be effective in explaining the results, it is necessary in this case that they be in the size range of a few hundred Ångstroms, in order to maintain the necessary radii of curvature in the α–γ interface.

Mravic[26] has examined iron–vanadium specimens after exposure to NH_3/H_2 and has clearly shown the presence of vanadium nitride which formed in the ferrite ahead of the advancing interface. An example of a replica (taken on what is now martensite) is shown in Figure 9.

Another interesting observation noted by Mravic is that by systematic temperature variation, precipitation of VN in ferrite can be in bands, etching "dark" and "light" in nital, parallel to the external surface of the specimen. These bands represent areas of coarse and fine vanadium nitride particles respectively, and are analogous to many observations on internal oxidation. It is interesting (Figure 10) that austenite spreading laterally from an α–α grain boundary shows a good deal more growth along the paths where larger nitrides are present than in those where smaller nitrides occur (as predicted by the theory).

Growth of Austenite Grains after Impingement

As soon as austenite grains impinge, although the driving force for boundary migration is reduced by one to two orders of magnitude, the normal process of grain coarsening will proceed unless the boundaries are effectively locked by dispersed particles. Experimental measurements are possible directly if the temperature is sufficiently high for thermionic emission microscopy,[21] i.e., usually at least 950 C (1740 F), or if the grain size is sufficiently coarse so that conventional techniques using controlled transformation can be effective in delineating the structure characteristic of the elevated temperature. However, it seems probable that severe difficulties will be experienced with the various possible "grain outlining" techniques below about ASTM 8/10 in low carbon steels,[22] although with medium carbon steels, Grange[16] has been able to measure well below ASTM 12. Nutting and Rouze[21] have experimentally measured mean approximate migration rates of 0.02μ/sec in a low carbon alloy steel at 975/1075 C (1785/1965 F) by thermionic emission microscopy. A suitable method to extrapolate their results to isothermal coarsening at lower temperatures is not obvious. Furthermore, they point out that boundaries

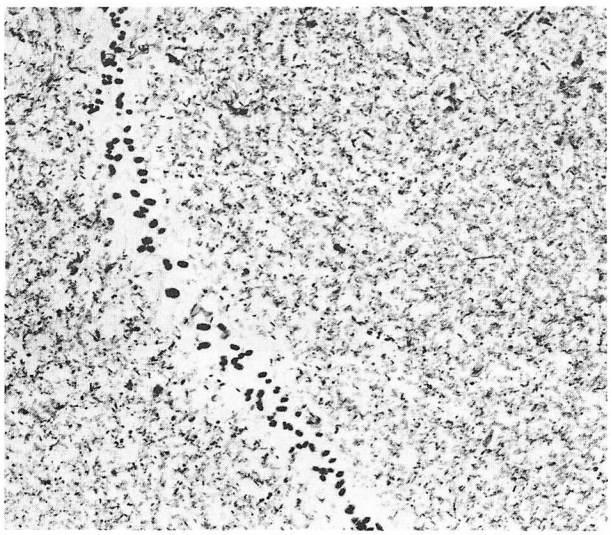

FIGURE 9. Precipitates of VN in 0.5% V austenite (now martensite) after exposure to 4% NH_3 in H_2 for 60 min at 750 C (1380 F). The region of larger particles is at grain boundary in the austenite. Extraction replica 12,000 X

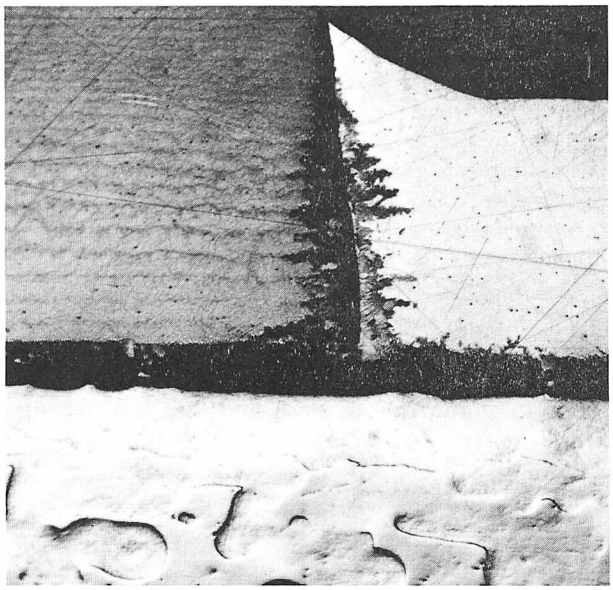

FIGURE 10. Penetration of austenite into ferrite in which bands of coarse and fine precipitates of VN have been manufactured by systematic temperature variation. The austenite penetrates preferentially along the paths where the nitrides are coarser. 2% V in ferrite exposed to 4% NH_3 in H_2 for nine hours at 750 C (1380 F). 95 X

often move quite rapidly to a local metastable position, and then remain virtually immobile for extended periods until readjustments some distance away cause another wave of equilibration at grain corners to pass through the specimen. This behavior is reproduced quite exactly in more conventional foams such as bubbles on a soap solution or on beer.

The theories of boundary migration are complex[23] and have been compared quantitatively only for quite dilute solutions of alloying elements. With these theories, based on no direct pinning by second phase particles, but perhaps a drag on the boundary caused by the necessity of adsorbed impurity atoms to be carried along, various degrees of agreement with experiment in aluminum and lead alloys have been observed. At the present time, it appears that speculation on application to austenite at T/T_m of about 0.6 or higher is fruitless; experimental measurements would, on the other hand, be very helpful.

SUMMARY AND OBSERVATIONS

Straightforward considerations suggest that what one would like to have in controlling austenite grain size is a situation where austenite is nucleated profusely with a very narrow spread in nucleation times, so as to produce a uniform and small grain size. The slower the growth rate after nucleation but before impingement, the bigger the spread in nucleation times can be while still retaining close to maximum effectiveness.

In conventional heating for austenitizing, the carbides presumably act as nuclei over a range of temperature above Ac_1. Since at low superheatings the nucleation rate is also low, it might be interesting to insert a hold time just above Ac_1, to ensure that all carbide particles have a chance to nucleate an austenite crystal before they are engulfed by other growing austenite. The growth rate is a minimum just above Ac_1. Depending on the composition of the steel, and thus particularly at carbon contents in the range of 0.1/0.2% C, it should be possible to produce isolated islands of austenite. Using Judd's observations,[10] a period of a few seconds is all that is necessary even as low as 750 C (1380 F).

Continued heating to some temperature low in the single-phase austenite range seems unlikely to produce a grain size larger than continuous heating directly to this same temperature. On the other hand, a very rapid heating can in principle cause instabilities in the austenite–ferrite interface and perhaps cause acicular austenite to grow. Whether or not this makes a difference to the austenite grain size or to its subsequent decomposition may be intriguing.

The effect of potential precipitates during the transformation is of obvious interest[24] from two points of view. Large particles (a few thousand Ångstrom) can act to pin austenite grain boundaries, and growth would be influenced by solution or agglomeration of these particles.[25] However, much finer particles could act in a fashion similar to that suggested by the work of Pavlick[19] and Mravic[26] during the formation stage of the austenite. The relevance of this possibility has not yet been quantitatively established in a convincing fashion to the author's knowledge.

It would be of potential interest perhaps to compute curves for the amount of austenite formed during continuous heating in a number of ferrite–carbide aggregates at various rates in an analogous fashion to curves for austenite decomposition. The possibility of programmed heating and of the growth-limiting effects of precipitates could be built into the model using the data of Judd,[10] Mravic[26] or other suitably isothermal observations.

Nothing has been said in all of the above discussions about the effects of very fine austenite grain size on subsequent hardenability. The effects are complex[16] and need more work to enable the improved strength and toughness to be consistently reached in heavy sections. Work on weldability is also necessary.

Finally, the engineering problems in controlling a reproducible and sophisticated time–temperature cycle are obviously not easy. However, if it can be shown that an economic advantage really exists with ultrafine grained austenite, as seems likely, the challenge will doubtless lead to the customary ingenious solutions.

ACKNOWLEDGMENTS

The author is grateful to many of his friends and colleagues for discussions of this subject, in particular J. D. Grozier, R. R. Judd, W. C. Leslie, B. Mravic, W. W. Mullins, T. Osuka, and J. E. Pavlick. The support of the National Science Foundation, Army Research Office (Durham) and the Office of Naval Research has made possible much of the time and effort on this problem over a period of years.

REFERENCES

1. E. J. Janitzky and M. Baeyertz, *Metals Handbook*, American Society for Metals, Cleveland, 1939, 515
2. K. J. Irvine and F. B. Pickering, *Metallurgical Developments in Carbon Steels*, Special Report 81, The Iron and Steel Institute (London), 1963, Discussion, 21-24, 83
3. R. A. Grange, U. S. Patents 3,201,288 and 3,178,324 (1965)
4. R. W. Cahn, *Recrystallization, Grain Growth and Textures*, American Society for Metals, Metals Park, 1966, 99
5. P. R. Swann, Corrosion *19*. 102t (1963)
6. W. C. Leslie and R. L. Miller, Trans. ASM *57*. 972 (1964)
7. R. W. Cahn, *Recrystallization, Grain Growth and Textures*, American Society for Metals, Metals Park, 1966, 109-116
8. R. P. Zerwekh and C. M. Wayman, Acta Met. *13*. 99 (1965)
9. J. D. Grozier, H. W. Paxton and W. W. Mullins, Trans. AIME *233*. 130 (1965)
10. R. R. Judd, Ph.D. Thesis, Carnegie Institute of Technology, 1966
11. G. A. Roberts and R. F. Mehl, Trans. ASM *31*. 613 (1943)
12. G. Molinder, Acta Met. *4*. 565 (1956)
13. A. E. Nehrenberg, Trans. AIME *188*. 162, 1376 (1950)
14. V. G. Gorbach and V. D. Sadovskii, Fiz. Metall. Metalloved. *6*. 106, 665 (1958)
15. H. I. Aaronson, Private Communication, Ford Scientific Laboratory, Ford Motor Company
16. R. A. Grange, Trans. ASM *59*. 26 (1966)
17. K. J. Albutt and S. Garber, J. Iron and Steel Inst. (London), *204*. 1217 (1966)
18. G. R. Speich, A. Szirmae and R. M. Fisher, "A Laser Heating Device for Metallographic Studies," *Advances in Electron Metallography*, Vol. 6, ASTM-STP 396, Philadelphia, 1966, 97
19. J. E. Pavlick, W. W. Mullins and H. W. Paxton, Trans. AIME *236*. 875 (1966)
20. C. S. Smith, Trans. AIME *175*. 15 (1948), referring to C. Zener's work
21. J. Nutting and S. R. Rouze, *Fifth International Congress for Electron Microscopy*, Academic Press, New York, 1962, CC7
22. R. Phillips and J. A. Chapman, "Methods of Determining Austenite Grain Size, and Grain Coarsening of Mild Steels Containing Niobium and Titanium," *Metallurgical Developments in Carbon Steels*, Special Report 81, The Iron and Steel Institute (London), 1963, 60
23. P. Gordon and R. A. Vandermeer, *Recrystallization, Grain Growth and Textures*, American Society for Metals, Metals Park, 1966, 205
24. W. C. Leslie, J. T. Michalak and F. W. Aul, *Iron and Its Dilute Solid Solutions*, Interscience, New York, 1963, 119
25. T. Gladman, "The Effect of Aluminium Nitride on the Grain Coarsening Behaviour of Austenite," *Metallurgical Developments in Carbon Steels*, Special Report 81, The Iron and Steel Institute (London), 1963, 68
26. B. Mravic, Private Communication, Carnegie Institute of Technology

ORAL DISCUSSION OF

The Formation of Austenite

Presented by H. W. PAXTON

J. W. SPRETNAK (Ohio State University). Rather than a question, I would just like to make a comment or two on Professor Paxton's presentation. Underlying all formation of austenite, of course, is the lattice transformation. It is very important to realize that we can induce this lattice transformation by at least two physical manifestations of the driving force. One is a simple superheating of alpha iron above the temperature at which the gamma form is stable; for example, if you rapidly heat the steel, you will superheat alpha matrix at temperatures above 910 C (1670 F). This we can call the thermal type of driving force. The second possibility is this effect of supersaturation with respect to the solute; for example, experiments have been performed in which nitrogen or carbon drives the transformation. We do not have the thermal driving for the lattice transformation in these isothermal studies, but rather supersaturation with respect to the solute. This, I believe, is what complicates the kinetics of formation of austenite. Professor Gordon Powell and myself have been doing work along this line; we find that, in general, for an isothermal transformation such as this (equilibration of iron–(iron–carbon) couples at 850 C, 1560 F) you do find physical manifestations of supersaturation with respect to the solute (carbon) which is the driving force for the lattice transformation. We also find that the kinetics of motion of the α–γ interface depend on whether the rate controlling process is the interface reaction or the supply of solute to the interface; the interface reaction is usually unspecified in detail. It is suggested that in these experiments, the interface reaction is the lattice transformation. In high purity iron–carbon alloys, the transformation is not rate controlling; the kinetics depends on the rate at which you get this critical supersaturation of carbon, so that the classical $t^{1/2}$ dependence works nicely. When alloying elements such as manganese and molybdenum are added to the system, the lattice transformation becomes rate-controlling, rather than the rate of supply of carbon. Professor Paxton mentioned that molybdenum simply immobilizes this interface. We do not observe the planar motion of the interface at all, but rather penetration of carbon down the grain boundaries of the alpha phase, eventually forming pockets of gamma phase, particularly at grain junctions. Some of the complexity of austenite formation, therefore, arises in the fact that two physical manifestations of the driving force for the lattice transformation can be operative. I think that Professor Paxton's comments were very timely and appropriate in bringing these situations to our attention.

AUTHOR'S REPLY. Yes, we have discussed this before, and all you are saying is indeed possible and correct. I am not yet convinced that the lattice transformation in the molybdenum case is rate-controlling. In any case, one can explain quite nicely why austenite can form ahead of the interface in isolated patches. (See reference to Pavlick *et al.*)

W. MCFARLAND (Inland Steel Company). Have you done any work on the effect of heating rates on the temperature of transformation at A_1 and A_3?

AUTHOR'S REPLY. We have not done any serious work on this, other people have; perhaps some of you have seen the very interesting paper by Albutt and Garber in last month's JISI. I don't think there is anything very magical about heating rates; I think there have been some questionable ideas written on the possibility of martensite being formed below T_0. I have not seen anything yet on rapid heating rates which I can't understand fairly well on relatively naive pictures. I wouldn't think we have to start a new cult.

M. COHEN (Massachusetts Institute of Technology). Professor Spretnak has just pointed out that there is considerable Russian literature on the problem of rapid austenitizing by pulse heating by either resistivity or induction heating by Professor Sadovskiy of Moscow State University.

AUTHOR'S REPLY. There are some very interesting effects, but they often do them on unusual steels. It is hard to obtain qualitative ideas on mechanisms.

M. COHEN. You refer to massive transformation as being diffusionless. The correct statement would be yes, there is no long-range diffusion, and there is no change in composition between parent and the product phases; but there certainly is diffusion across the interface.

AUTHOR'S REPLY. I don't think we have any differences in viewpoint; it is just a matter of choice of words. I certainly agree that there is no long-range diffusion involved.

M. COHEN. The word "massive" appears two or three times in the abstract.

D. L. ALBRIGHT (International Harvester Research). Measurement of true austenitic grain size constitutes a distinct problem. With this in mind we have been experimenting with the technique of thermal etching of grain boundaries, a method that has been carefully evaluated by Day and Austin.* The advantages of the thermal

*M. J. Day and J. B. Austin, Trans. ASM, *28*. 354 (1940)

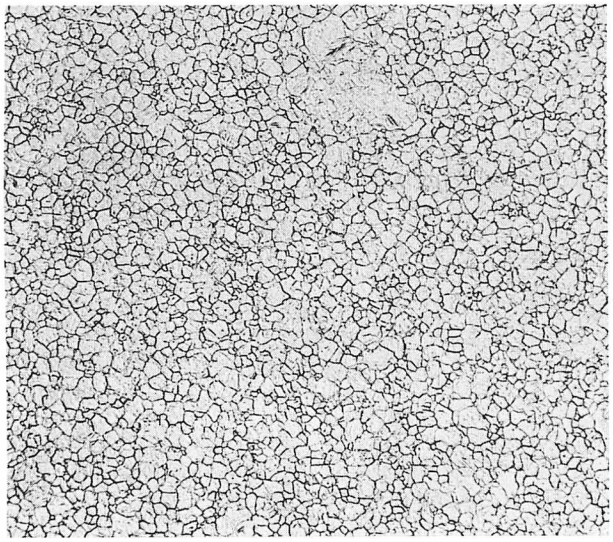

FIGURE A. "Fine-grained" 8620 steel thermally etched two hours at 925 C (1700 F). 100 X

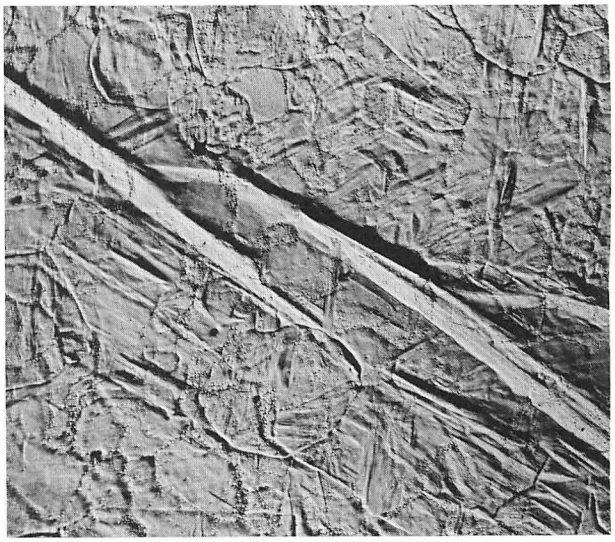

FIGURE B. "Fine-grained" 8620 steel thermally etched 11 hours at 925 C (1700 F). 8 X

FIGURE C. "Fine-grained" 8620 steel thermally etched 11 hours at 925 C (1700 F). 500 X

etching technique render it a prime candidate for use in steel plant quality control, especially in view of the decreased time between melt and final product in modern integrated mills.

One interesting point that has arisen in our experiments involves interpretation of the grain size as established by various techniques. Specifically, an 8620 steel which was typed as fine-grain by the McQuaid-Ehn test (using both 6 and 11 hour treatments) was also examined after thermal etching. The micrograph of Figure A generally confirms this fine-grained structure as revealed after thermal etching for two hours at 925 C (1700 F) in a purified argon atmosphere. However, after eleven hours of thermal etching at 925 C (1700 F), the same time and temperature as in one of the McQuaid-Ehn treatments, a duplex grain structure had developed. This partial coarsening is indicated in the 8 X macrograph of Figure B, with one particular area shown at 500 X in Figure C. (It is important to note that the presence of martensite in this structure greatly aids the measurement of prior austenitic grain size.) Thus it is apparent that the carbon pickup in the McQuaid-Ehn test has inhibited the formation of the inherent duplex grain structure of the steel. Do you feel that this is a valid point for practical consideration, or is the influence of grain size on properties so minor as to minimize the importance of the discrepancy?

AUTHOR'S REPLY. The only reply I would make is that when anyone shows me thermally-etched structures, my immediate reaction is to find what's wrong with them. I think you ought to be very, very careful when using thermal grooving as a method of measuring grain sizes. It does not automatically give wrong answers, but it can be misleading on enough occasions that I urge this caution.

Structure and Growth of Widmanstätten Ferrite and Bainite

J. M. OBLAK
Research Associate
Advanced Materials Research & Development Laboratory
Pratt & Whitney Corporation
formerly Graduate Student, Department of Metallurgy
Case Institute of Technology

R. F. HEHEMANN
Professor of Physical Metallurgy
Case Institute of Technology
Cleveland, Ohio

INTRODUCTION

The important role that the transformation of austenite to bainite plays in the hardenability of alloy steels as well as the attractive properties frequently associated with bainitic structures have generated much interest in the study of austenite decomposition at intermediate temperatures. At least two variants of bainite have been recognized since the early metallographic studies[1]* which, following Mehl,[2] have generally been termed upper and lower bainite.

Replica and transmission electron microscopy has clarified considerably the structural and crystallographic features of these two forms of bainite. Specifically,[3-8] the classical upper bainite structure forms as an aggregate of lath or needle-like ferrite particles with cementite precipitated parallel to the needle axis. The structure resembles closely that of tempered low carbon martensite. The morphology of lower bainite is quite similar to that of tempered high carbon martensite and consists of ferrite plates with carbides precipitated at an angle of about 60° to the major axis of the plate. Unfortunately, it is not always possible to distinguish between the two forms of bainite on this simple basis and intermediate structures such as the granular bainites discussed by Habraken[9] are known to exist. The crystallographic relationship between the ferrite and carbide components of bainite has served to characterize further the two forms of bainite[8,10] and has strengthened the concept that the carbide in upper bainite precipitates from carbon enriched austenite trapped between ferrite needles whereas that in lower bainite precipitates from supersaturated ferrite.

A close connection between bainitic and martensitic transformations received added emphasis with the observation that surface tilts accompany the formation of bainite.[11] However, bainite plates grow slowly[11-15] and this constitutes a major obstacle to the concept that either form of bainite arises initially as supersaturated ferrite with a carbon content above that permitted by metastable equilibrium between ferrite and austenite. Christian[25] has concluded that surface tilts need not constitute evidence for a diffusionless transformation when the diffusivity of the solute greatly exceeds that of the solvent as in these interstitial solid solutions. This apparent dichotomy between the structural and kinetic observations has not yet been satisfactorily resolved.

Surface relief also has been observed in the transformation of austenite to Widmanstätten ferrite[16] and, in plain carbon steels at least, there is no discontinuity in growth rate between Widmanstätten ferrite and upper bainite.[17] This has led to the concept that Widmanstätten ferrite and the two forms of bainite constitute a continuous series of decomposition products in which the growth rate is coupled to the flux of carbon through austenite away from a coherent or semi-coherent interface.[18,19,20] The gross morphological features as well as the growth kinetics, therefore, are most logically rationalized in terms of the Zener-Hillert model which has been elegantly applied to the present problem by Kaufman, Radcliffe and Cohen.[19] However, the structures of bainites are much more complicated than had been recognized and it appears that the structural details must be given explicit consideration in the treatment of growth kinetics. More specifically, diffusion (or interface

* See references.

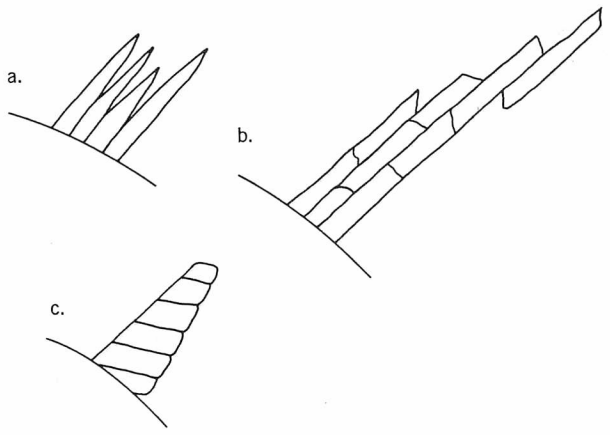

FIGURE 1. Schematic illustration of structures produced by (a) diffusion controlled growth, (b) and (c) repeated nucleation of subunits, which rapidly attain a limiting size

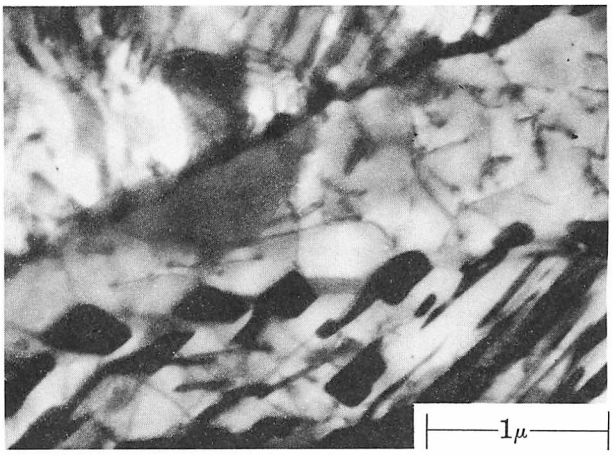

FIGURE 2. Widmanstätten ferrite and pearlite in 1040 steel transformed at 575 C (1070 F) for three minutes. 21,200 X

controlled) models for growth are based on the concept that the transformation product develops by the continued advance of a unique interface as illustrated schematically in Figure 1a. Bainites, on the other hand, may "grow"[26,29] by repeated nucleation of a more basic substructural unit as suggested in Figures 1b and 1c. This distinction is fundamental to the comparison of experimental growth rates with those predicted by diffusion controlled or other models. If, for example, the basic units develop rapidly to a limiting size, then experimental growth rates refer primarily to the rate at which these units nucleate and the slow observed growth rates do not demand that the extensive partition of carbon necessary for metastable equilibrium between ferrite and austenite arises during evolution of the individual substructural units. This argument has been advanced frequently in various ways during the past 35 years but has not received general acceptance.

The present work attempts to determine if Widmanstätten ferrite and the two forms of bainite can be differentiated from a structural standpoint and to explore the extent to which the known substructure of bainites has entered into growth measurements.

EXPERIMENTAL

The compositions of the steels employed in this investigation are given in Table I. The 1040, 5140, and 2340 steels were employed to compare the structures of upper bainite and proeutectoid ferrite whereas the nature of upper and lower bainite was examined in greater detail in the remaining alloys.

The steels were received as hot rolled rounds which were rolled to flats and machined to sheets approximately 0.007 in. thick.

Heat treatment was conducted with the samples encapsulated in Vycor capsules evacuated to 10^{-5} mm Hg. Austenitizing was conducted at 1095 C ± 6 C (2000 F ± 10 F) and isothermal transformation was accomplished in salt baths controlled to ± 3 C (5 F).

Thin foils for electron microscopy were prepared using two methods. The thinning of sheet specimens was accomplished by electropolishing in a solution of 135 grams acetic acid, 25 grams CrO_3, and 7 ml H_2O at 25 volts using a modified Bollman technique. Disc specimens were dimpled to 0.001 in. thickness with a jet of 10% perchloric-acetic solution at 25 ma current and then electropolished to perforation in a solution of one part anhydrous sodium chromate and five parts acetic acid at 35 volts.

A Jem 6A microscope operated at 100 KV was employed for the transmission microscopy and growth measurements were made with conventional hot stage microscopy techniques.

RESULTS AND DISCUSSION

Internal Structure of Proeutectoid Ferrite and Upper Bainite

Studies of isothermal transformations in alloy steels in which the proeutectoid and pearlite reactions are clearly separated from the bainite reaction have revealed a temperature, designated B_s, above which austenite will not transform to bainite.[21] In lower

TABLE I Analyses of Steels*

Steel	%C	%Mn	%Si	%Cr	%Mo	%Ni
1040	0.43	0.69	0.22	—	—	—
5140	0.41	0.90	0.27	1.04	—	0.04
2340	0.40	0.89	0.31	0.11	—	3.34
9N3	0.29	0.69	0.31	—	—	8.80
9N5	0.50	0.68	0.36	—	—	8.70
M	0.69	0.85	0.70	0.85	0.81	1.80
S	0.60	0.86	2.00	0.31	—	—

* Weight percent.

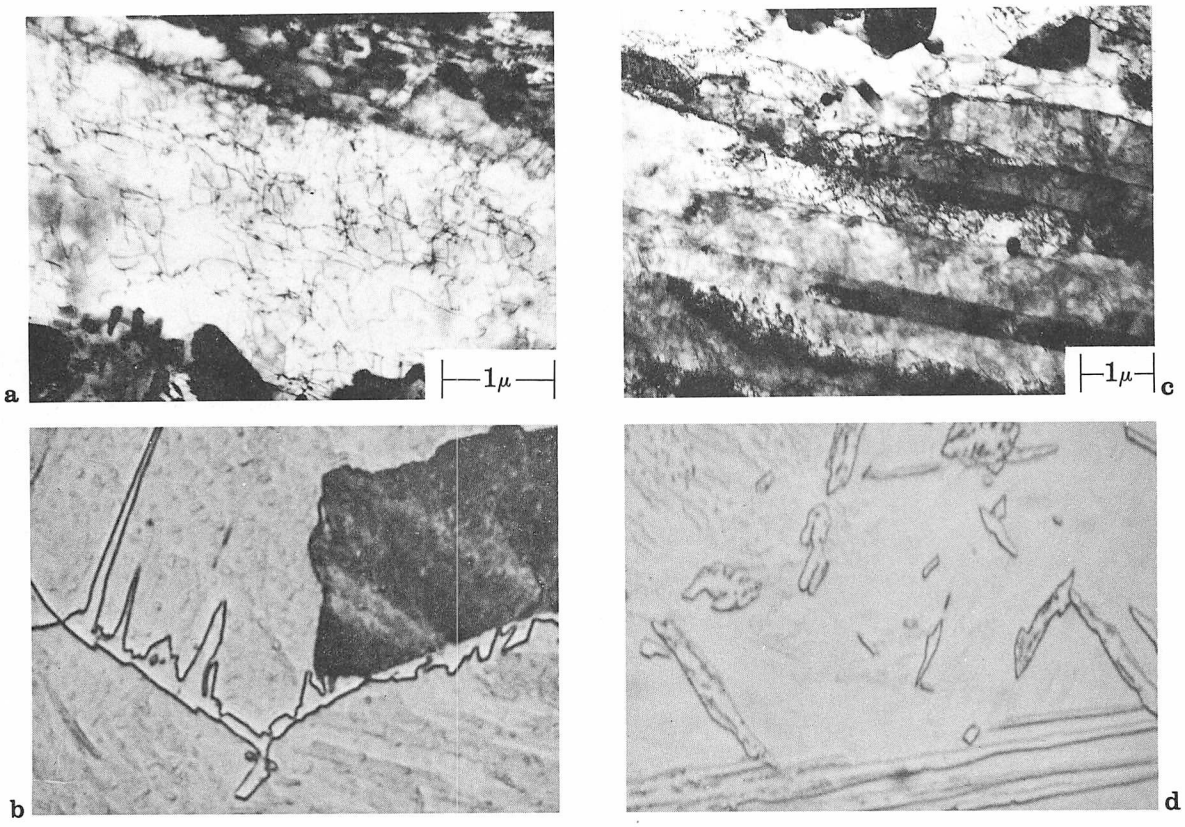

FIGURE 3. Widmanstätten ferrite and upper bainite structures in 5140 steel

a. Widmanstätten ferrite after 4-hr transformation at 565 C (1050 F). 13,000 X

b. Widmanstätten ferrite after 30-sec transformation at 595 C (1100 F). 1000 X

c. upper bainite after 4-hr transformation at 550 C (1020 F). 10,000 X

d. upper bainite after 20-sec transformation at 540 C (1000 F). 1500 X

alloy steels and particularly in unalloyed steels, extensive overlapping of the bainite and higher temperature reactions makes it difficult to determine B_s. In fact, the view that acicular ferrite and bainite constitute a continuous series of decomposition products demands that B_s be identified with the maximum temperature at which acicular ferrite forms. This temperature approaches and may exceed the A_1 temperature whereas B_s temperatures determined kinetically rarely, if ever, exceed approximately 565 C (1050 F). The kinetic studies indicate that alloying elements influence the overall rates and presumably also the growth rates of the ferrite and bainite transformations differently and it therefore becomes of interest to determine if a structural distinction exists between acicular ferrite and upper bainite. This comparison was made on a plain carbon and two low alloy steels using, respectively, treatments resulting in complete isothermal transformation to proeutectoid ferrite and pearlite or to bainite and pearlite. These treatments were used in order to avoid the almost impossible task of differentiating in transmission micrographs between upper bainite and the low carbon martensite that would form in these steels if partially transformed samples were quenched to room temperature. Conventional metallography was conducted on partially transformed samples.

Proeutectoid ferrite exhibited both grain boundary and Widmanstätten morphologies in 5140 and 1040; however, as reported by Aaronson,[22] grain boundary allotriomorphs were the only form of proeutectoid ferrite observed in 2340. A typical example of Widmanstätten ferrite is illustrated in Figure 2. Each plate could be traced continuously from its tip to the grain boundary allotriomorph from which it originated. There were no indications of an aggregate lath or cell substructure and the widths of the plates measured on transmission micrographs agreed well with those observed by optical microscopy. A plate of acicular ferrite consists of a single crystal of ferrite containing a rather low dislocation density, and, consequently this structure is consistent with that expected to result from either diffusion or interface controlled growth (Figure 1a).

An abrupt change in structure was observed in the 5140 and 2340 steels when the transformation temperature was reduced below the B_s temperature as determined from dilatometric studies. These tem-

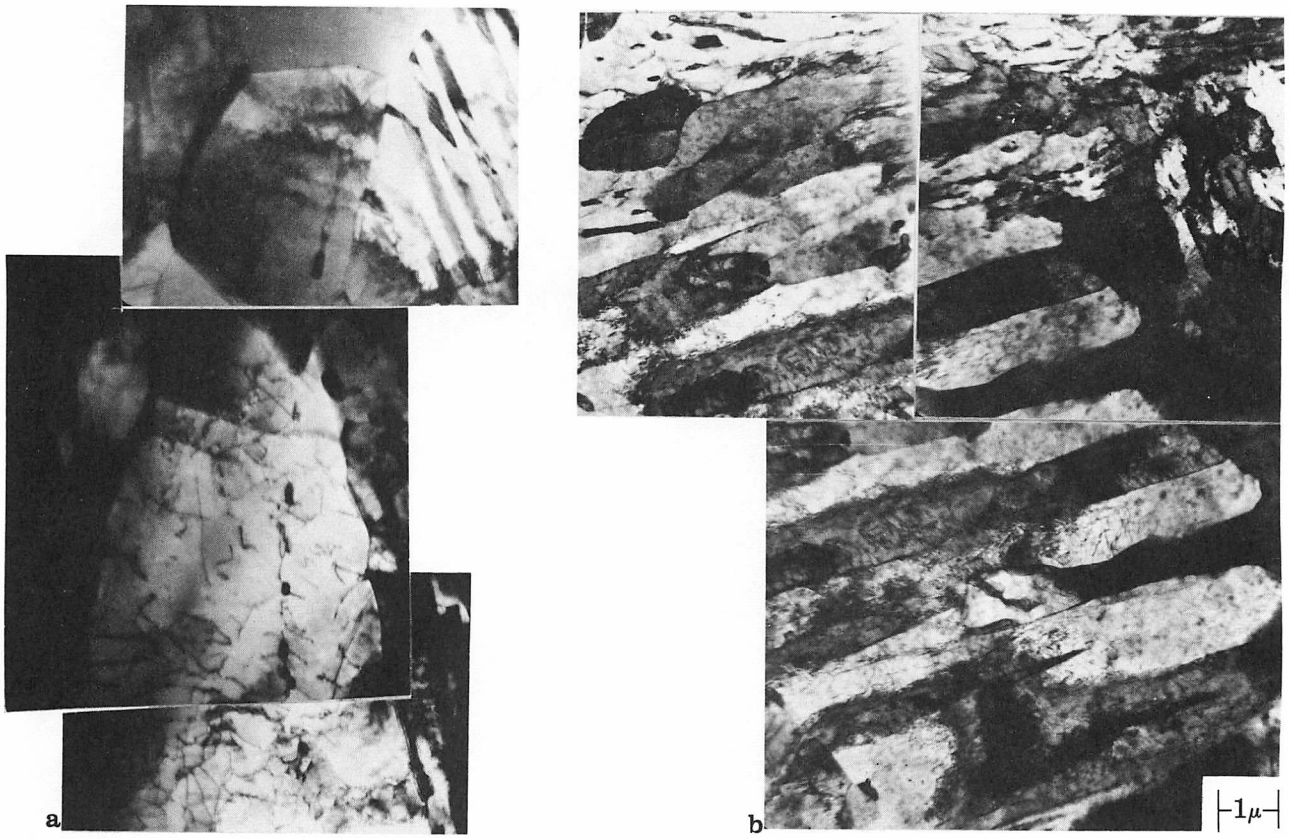

FIGURE 4. Comparison of proeutectoid ferrite and upper bainite in 2340

a. proeutectoid ferrite after 12-hr transformation at 595 C (1100 F). 6500 X

b. upper bainite after 15-hr transformation at 540 C (1000 F). 8000 X

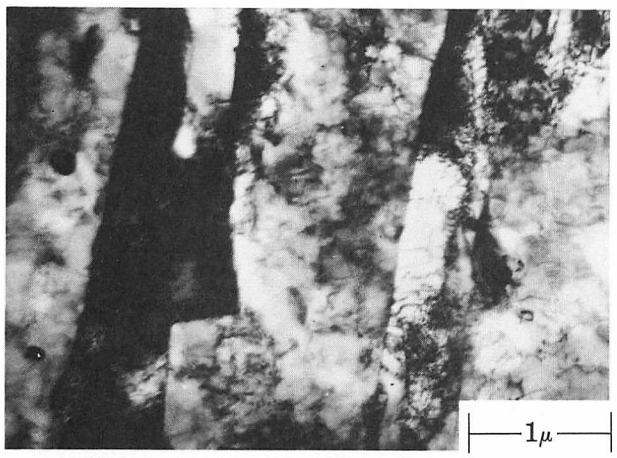

FIGURE 5. Upper bainite in 5140 steel transformed at 530 C (990 F) for 17 hr and aged 4-hr at 565 C (1050 F). 17,900 X

peratures are 565 C (1050 F) for 5140 and 540/550 C (1000/1025 F) for 2340.[23] Figures 3 and 4 compare the structures observed immediately above and below B_s. The structure of Widmanstätten ferrite in 5140 (Figure 3a) was identical with that in 1040. The correspondence of the structures observed by optical and transmission microscopy is apparent and the fine structure of upper bainite differs significantly from that of acicular ferrite. As reported in the literature,[6,7,10] upper bainite is characterized by a parallel arrangement of ferrite laths exhibiting an extremely high dislocation density. The laths are in immediate contact with each other and are of the order of 0.5 to 0.7 μ wide. The bainitic regions illustrated in the optical micrograph have attained widths of 2 to 4 μ and consequently are composed of a number of these substructural units. Occasional carbides are apparent in Figure 3d and presumably have precipitated from carbon enriched austenite trapped between the laths. These same lath-like structures characterize upper bainite in 2340 in spite of the fact that Widmanstätten ferrite was not observed in this steel when transformed above B_s. As suggested by Aaronson[20,24] these lath-like structures evolve as a result of sympathetic nucleation; however, the reason why this process suddenly becomes operative at the B_s temperature is in need of clarification.

In spite of the striking difference in structure between Widmanstätten ferrite and upper bainite, the possibility exists that both structures may have formed initially in much the same way. For example, normal recovery processes may have annihilated a lath structure created during the initial formation of

Widmanstätten ferrite. To check this, bainite was produced in 5140 at 530 C (990 F) and then upquenched to 565 C (1050 F) for the time allotted formation of Widmanstätten ferrite at this temperature. The resulting structure (Figure 5) indicates that the lath interfaces are relatively immobile at 565 C (1050 F) and that the high dislocation density of the bainite laths has not been reduced significantly by the subsequent annealing treatment. It is concluded that Widmanstätten ferrite did not originally form as an aggregate from which the substructure was lost by an annealing process. Clearly, significant structural differences distinguish Widmanstätten ferrite from upper bainite. Thus, a B_s temperature can be defined in structural terms which agrees well with that determined kinetically.* The surface relief associated with acicular ferrite apparently reflects simply a partially coherent interface and does not signify that acicular ferrite and bainite form by the same mechanism.

Role of Structure in the Growth of Upper Bainite

The fine structure and morphology of Widmanstätten ferrite are consistent with that expected for interface or diffusion controlled growth. This also would apply to the growth of upper bainite if the substructure units simply develop at or behind a unique interface. However, detailed comparison of optical and transmission micrographs suggests that bainites develop by the repeated nucleation of the substructural units.

An optical micrograph of 5140 reacted for 10 seconds at 540 C (1000 F) is compared with a transmission micrograph of a sample fully transformed at 550 C (1020 F) in Figure 6. Each of the bainitic needles in the optical micrograph consists of several subunits which are less than one micron wide and of the order of 10 microns long. A one to one correspondence between the substructure in the transmission micrograph and the elementary growth units indicated by arrows in the optical micrograph appears to exist. The separation between the units in the optical micrograph indicates that they develop separately rather than arising behind a continuous interface. Growth of upper bainite in this steel is best described by the condition visualized in Figure 1b.

The critical question concerns the rate at which these units increase in length. Unfortunately, hot stage microscopy has not answered this question unequivocally. Upper bainite exhibits multiple relief (Figure 7) and the several units in a given group do not advance at precisely the same rate.[15] This apparently discontinuous growth is consistent with the optical and transmission micrographs which indicate that the individual units do not grow continuously but achieve limited lengths in the range of 10 to 15 μ. One way in which this happens is indicated rather clearly in the optical micrograph of Figure 6. As indicated by the arrows, individual laths have nucleated at the side of the others and have propagated well in advance of the main group before their growth has been terminated.

The diffusion models for growth of bainite presumably refer to propagation of the individual subunits in the bainitic aggregate; however, the apparently discontinuous rather than continuous

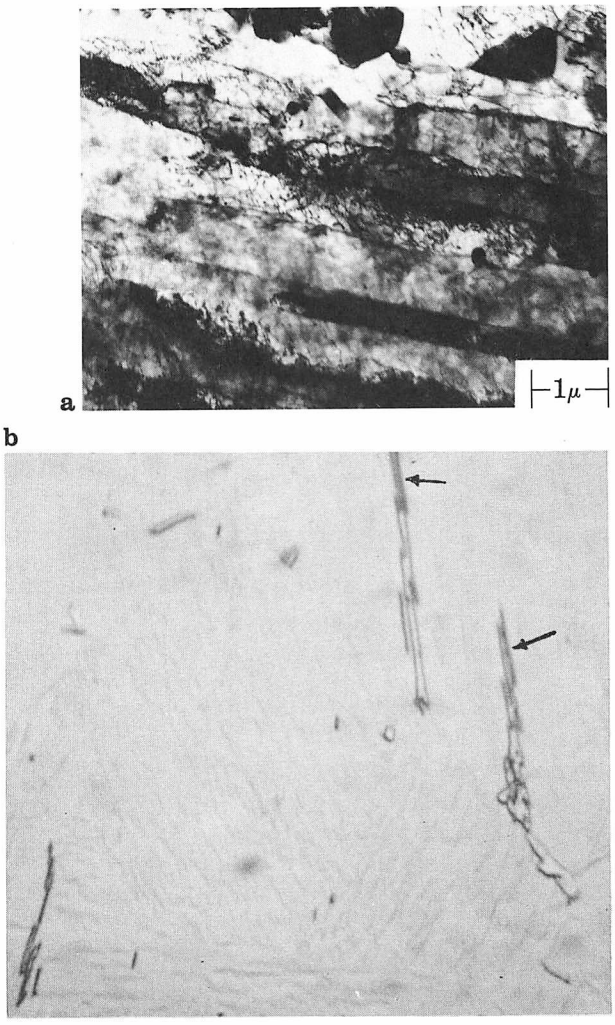

FIGURE 6. Comparative micrographs of 5140 steel

a. transmission micrograph of structure after 4-hr transformation at 550 C (1020 F). 10,000 X

b. optical micrograph of structure after 10-sec transformation at 540 C (1000 F). 1500 X

* The 1040 steel reacted too rapidly to permit the heat treating techniques employed in this study to be used at temperatures near the nose. The structure of upper bainite produced at 480 C (900 F) and below was identical with that observed in 5140 and 2340. Since Widmanstätten ferrite forms in this steel at 575 C (1070 F) (Figure 2) a B_s temperature, as defined by the structural transition, exists and is below 575 C (1070 F).

growth is highly significant. We conclude that upper bainite needles develop by the repeated nucleation of a more basic unit which propagates to a limited size at a high but presently unknown rate. On this basis, hot stage microscopy measures primarily the rate at which these units nucleate. Since the growth rates predicted by the diffusion model are approximately one order of magnitude higher than observed growth rates even in high purity iron–carbon alloys,[19] it is conceivable that propagation of the individual laths is diffusion limited as visualized in the models; however, discontinuous propagation and other observations to be considered shortly appear to favor the view that the individual laths develop at rates substantially higher than those permitted by the flux of carbon in austenite.

Other Variants of Upper Bainite

Upper bainite in the M and S steels was characterized by the same lath arrangements described above, however, transformation in the upper bainite range does not always result in these lath-like arrangements. For example, granular bainites have been considered by Habraken[9] and Shackleton and Kelly[10]

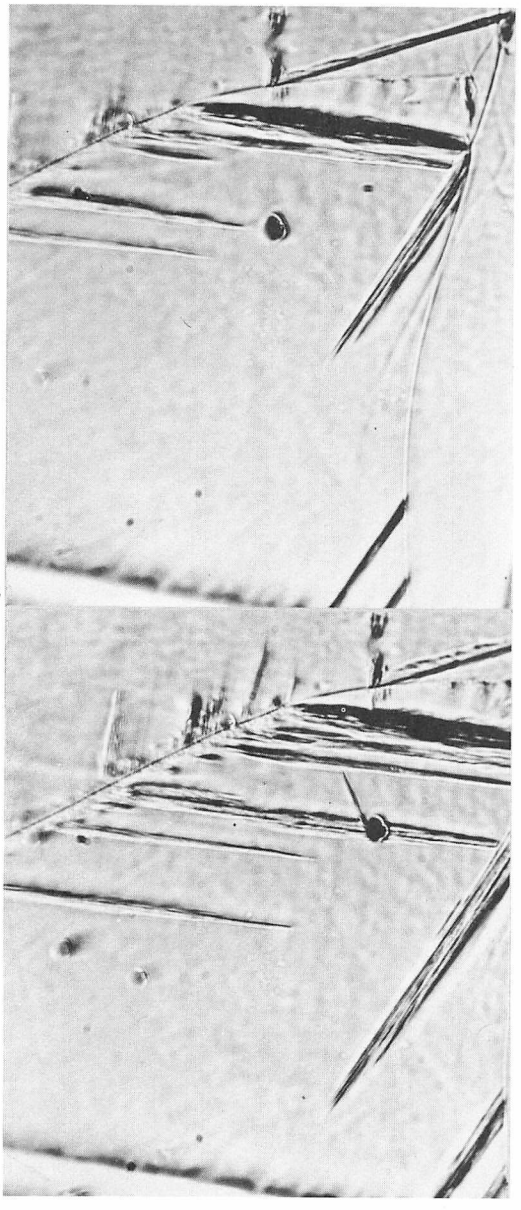

FIGURE 7. Surface relief produced by transformation to upper bainite at 400 C (750 F) of a 0.1% C–9% Ni steel. 460 X

a. transformation time 49 min
b. transformation time 56 min

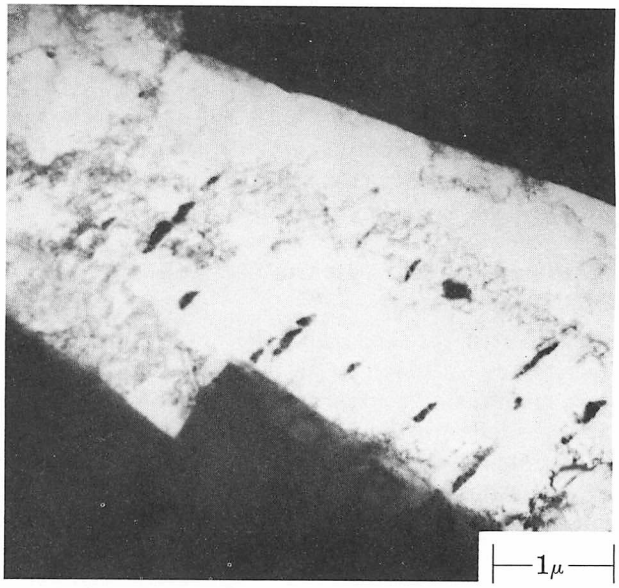

FIGURE 8. Upper bainite in 9N3 steel transformed at 405 C (760 F) for eight hours. 16,300 X

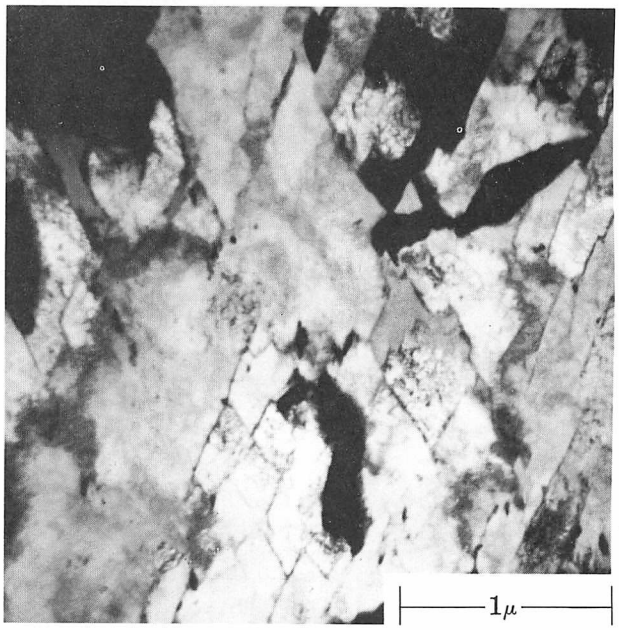

FIGURE 9. Textured bainite structure in S steel transformed at 480 C (900 F) for six minutes. 27,700 X

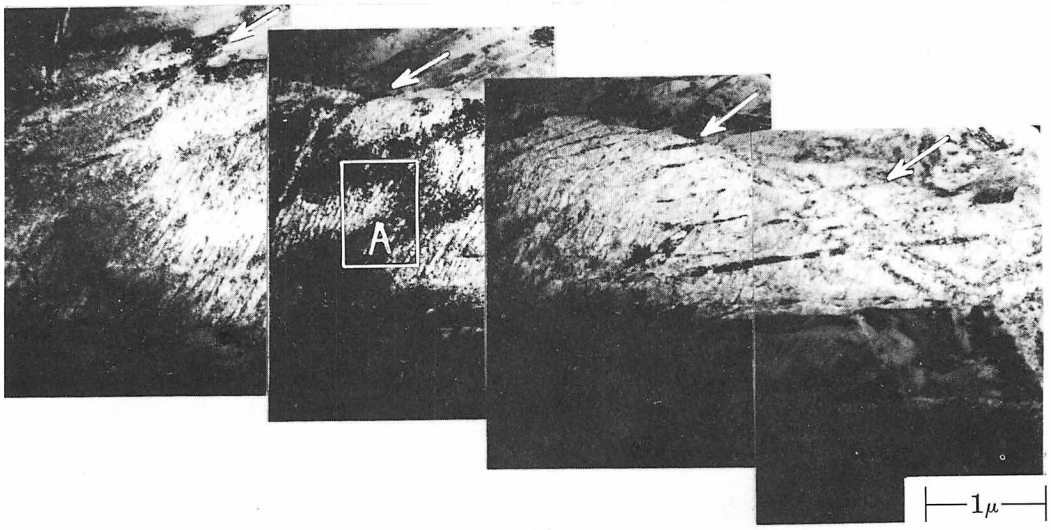

FIGURE 10. Lower bainite plate and martensite matrix in M steel transformed at 270 C (520 F) for 30 min. The plate has one straight edge and is subdivided into a number of smaller particles, indicated by arrows, which contain a fine dislocation structure. 16,900 X

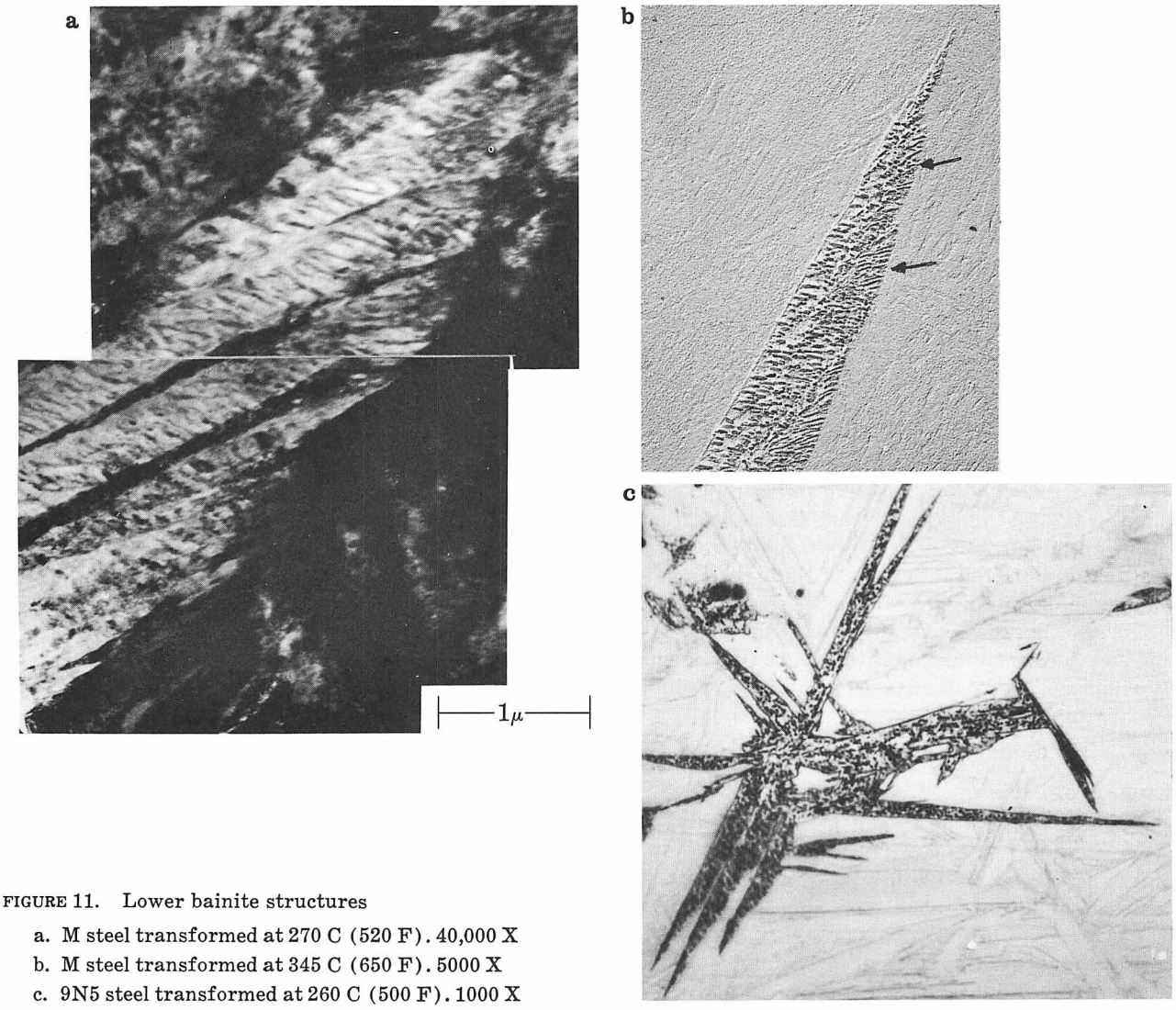

FIGURE 11. Lower bainite structures

a. M steel transformed at 270 C (520 F). 40,000 X
b. M steel transformed at 345 C (650 F). 5000 X
c. 9N5 steel transformed at 260 C (500 F). 1000 X

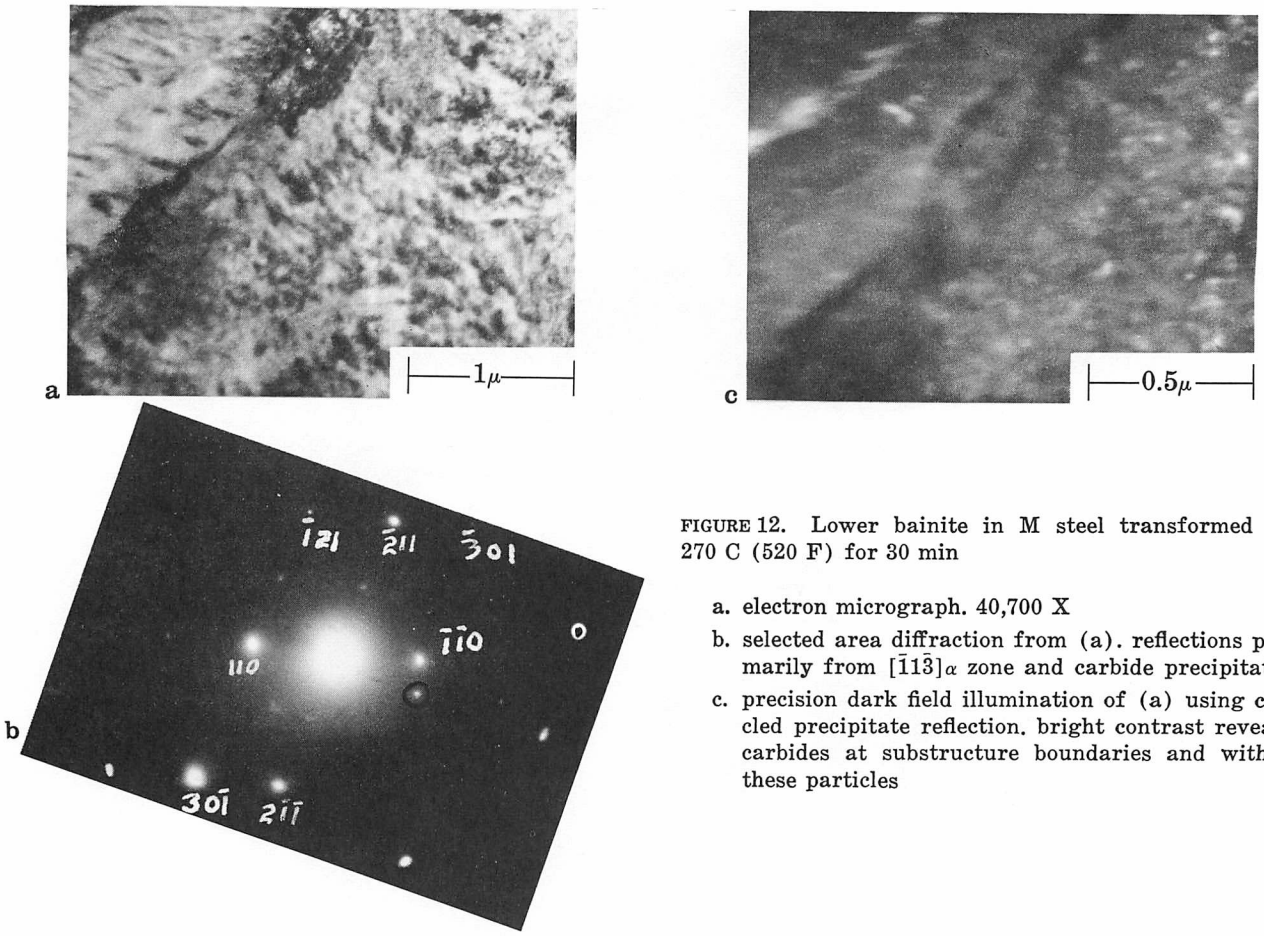

FIGURE 12. Lower bainite in M steel transformed at 270 C (520 F) for 30 min

a. electron micrograph. 40,700 X
b. selected area diffraction from (a). reflections primarily from $[\bar{1}1\bar{3}]\alpha$ zone and carbide precipitates
c. precision dark field illumination of (a) using circled precipitate reflection. bright contrast reveals carbides at substructure boundaries and within these particles

have observed structures consisting of massive regions of ferrite with embedded carbides. A similar massive form of upper bainite occurred in the 9% Ni steels (Figure 8) at the complete exclusion of the lath-like structures and massive structures also were observed at higher temperatures in the S steel (Figure 9) where their formation competed with that of the classical upper bainites (Figure 15).

The formation of both massive and lath-like structures in the S steel suggests that these constituents result from competitive modes of austenite decomposition. Presumably, the rates of these reactions are influenced differently by various solutes so that control over composition and heat treatment parameters may provide considerable latitude in the development of controlled microstructures exhibiting optimum mechanical properties.

Lower Bainite

The higher carbon M, S, and 9N5 steels were employed to study the structure of lower bainite. In these higher carbon materials, martensite and bainite can be distinguished in transmission micrographs so that it was possible to examine the structures at quite early stages of transformation. A typical lower bainite plate is illustrated in Figure 10 and the tip of another plate is shown in Figure 11a. As is evident in Figure 11, the entire bainitic region in the transmission micrographs corresponds to one plate as observed with the optical microscope as has been confirmed by numerous measurements of the widths of lower bainite plates in similar optical, replica and transmission micrographs. The now well known structure of lower bainite consisting of numerous carbides oriented at a characteristic angle to the growth direction is quite apparent—particularly in Figure 11. Precision dark field techniques using a carbide reflection were employed to confirm that the markings were indeed carbides with the positive result presented in Figure 12.

Although the substructure units in lower bainite appear to be very similar to the laths that characterize upper bainite, stereographic analysis of many lower bainite plates has demonstrated that they are not identical. Specifically, the trace of the laths in upper bainite consistently falls upon the trace of $(110)\alpha$ planes whereas the units in lower bainite do not consistently parallel the trace of any one crystallographic plane in the ferritic phase. It has not yet been possible to determine the crystallographic features of these lower bainite plates.

The similarity between lower bainite and high carbon martensite has been noted by many investi-

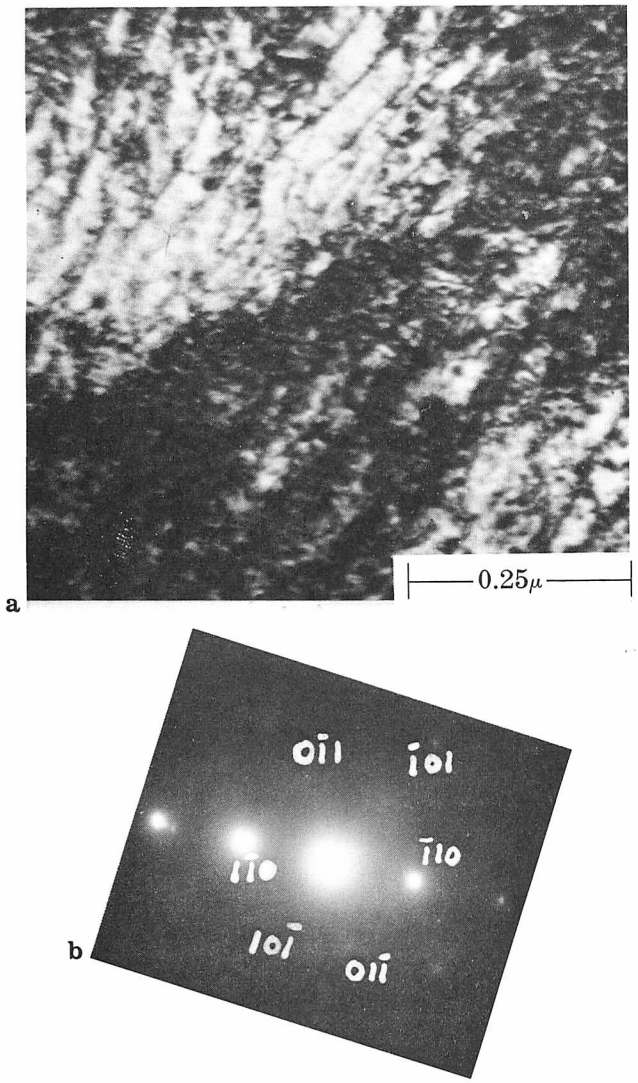

FIGURE 13. Lower bainite structure in M steel transformed at 270 C (520 F) for 30 min

a. fine dislocation structure taken from Area A, Figure 10. 117,000 X

b. selected area diffraction from (a). reflections from [111]α zone

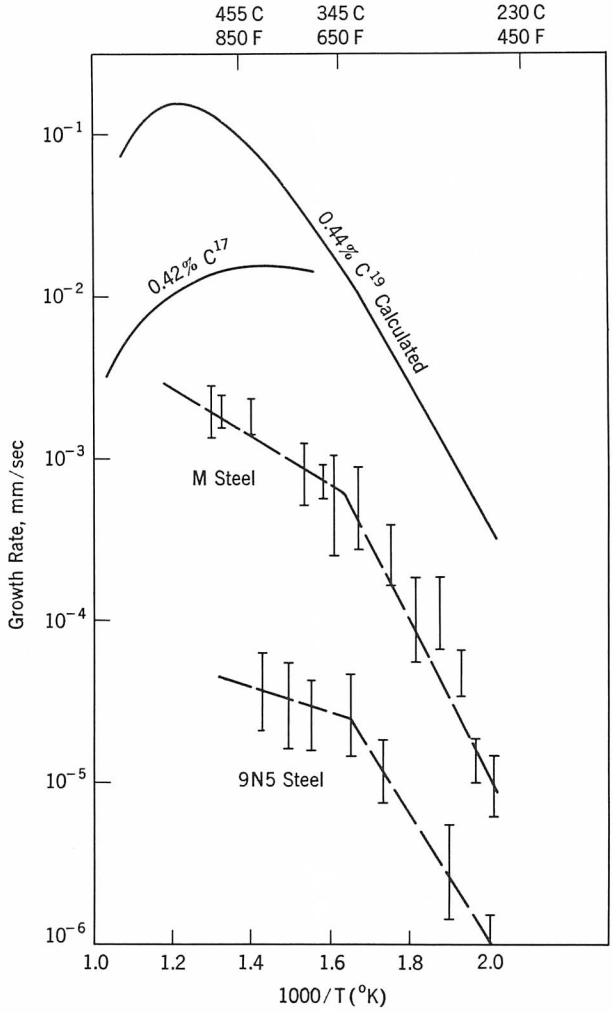

FIGURE 14. Comparison of calculated and observed growth rates of Widmanstätten ferrite and bainite

gators. Generally, it has been inferred from this that lower bainite initially forms with an internally twinned structure and that carbides precipitate at the twin boundaries. However, none of the previous investigators have reported that twins are observed in lower bainite.[6,7,10] A careful search for internal twins in lower bainite formed in the M, S and 9N5 steels also was unsuccessful. Although the twins in martensite gradually anneal out during tempering, the time and temperature conditions for this[27] are considerably more severe than those required for the early stages of bainite formation examined in this study. Therefore, it appears that growth of lower bainite does not involve a stage in which an internally twinned product develops. This, nevertheless, does not exclude a close structural connection with martensites. Figure 13, which is an enlargement of region A in Figure 10, reveals a dislocation network similar to that which replaces the internal twins in many martensitic structures.[28]

The general features that characterized lower bainite in the M steel also were observed in the 9% Ni and S steels. More complicated structures also were observed but will not be considered further here in spite of their obvious implications with regard to the mechanical behavior of heat treated steels.

Structure and Growth of Lower Bainite

Growth rates of bainite in the M and 9% Ni steels are compared with those calculated from the carbon diffusion model in Figure 14. The range of isothermal growth rates observed experimentally, represented in Figure 14 by bars around each datum point, is quite large and amounts to a factor between two and five. This large variation in isothermal growth rates

also has been observed in other studies[12-14] and is less difficult to understand if growth occurs by repeated nucleation.

The diffusion model predicts the temperature dependence of the growth rate in a generally satisfactory way; however, in these alloy steels observed growth rates are lower than expected by several orders of magnitude. The structural transition between upper and lower bainite occurs at about 345 C (650 F) in all of these steels and Figure 14 suggests that the temperature dependence of the growth rate changes more rapidly in this temperature range than expected from diffusion controlled growth.

It is extremely difficult to establish whether the structural difference between upper and lower bainite is responsible for the relatively minor kinetic differences between these constituents. Attention will be directed first to the question of whether lower bainite also forms by repeated nucleation of a more basic unit. Figure 11 compares optical, replica and transmission micrographs of lower bainite. Substructural units are indicated in Figure 11b by arrows and comparison of the three micrographs provides a striking illustration of the concept[26] that lower bainite plates increase in width from only one side. These units are oriented at an angle to the major growth direction (as in Figure 1c), and all of the subunits exhibit nearly the same width. While growth of lower bainite by repeated nucleation of subunits cannot be proven conclusively at this time, the orientation of the subunits and the uniformity of their widths strongly favor this view over one based on propagation of a continuous interface.

Even in the absence of direct measurements of the rates at which the substructure units either nucleate or propagate, the high and uniform density of carbides over the entire plate suggests that carbides precipitate from supersaturated ferrite. This can be most easily understood if the individual growth steps occur rapidly without partition of carbon to austenite. Lower bainite plates thicken at a rate low compared to that at which they increase in length[12,13] so that the uniform distribution of carbides implies further that thickening also occurs in short discrete steps resulting in a supersaturated ferrite from which carbides subsequently precipitate.*

* The alternative to this is that lower bainite plates lengthen at a rate controlled by diffusion of carbon in austenite and thicken by a different mechanism involving either the cooperative and simultaneous growth of ferrite and cementite into austenite or alternatively the diffusion of carbon from austenite through ferrite to internally precipitated carbides.[13] The fine structure and the uniform distribution of carbides lead us to prefer the discontinuous growth concept.

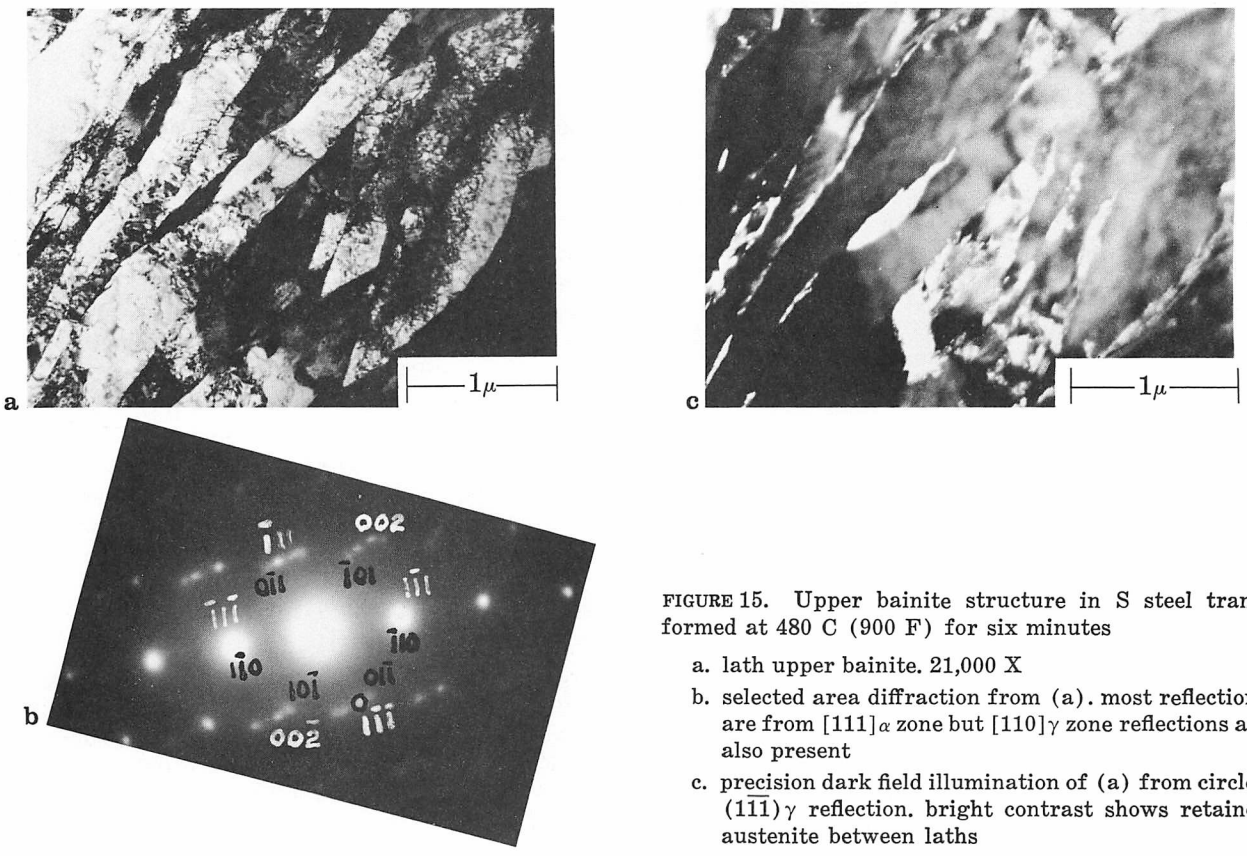

FIGURE 15. Upper bainite structure in S steel transformed at 480 C (900 F) for six minutes

a. lath upper bainite. 21,000 X
b. selected area diffraction from (a). most reflections are from [111]α zone but [110]γ zone reflections are also present
c. precision dark field illumination of (a) from circled $(1\bar{1}\bar{1})\gamma$ reflection. bright contrast shows retained austenite between laths

Origin of Carbides in Upper and Lower Bainite

Whether the carbides in upper and lower bainite precipitate from supersaturated ferrite or from carbon enriched austenite is fundamental to the bainite problem and deserves further consideration. There can be no doubt that much of the carbides in upper bainite form from enriched austenite trapped between ferrite laths. It is less clear, however, that all of the carbide in upper bainite arises in this fashion and the uniform density of carbide in lower bainite points strongly to precipitation exclusively from supersaturated ferrite. The crystallographic relationship between the ferrite and carbide also indicates extensive precipitation from enriched austenite for upper bainite and from supersaturated ferrite for lower bainite[8,10] and Pickering will report further on these studies at this symposium.

The rate at which carbon precipitates from supersaturated ferrite is of decisive importance in examining this issue.[30] Even if bainite develops in short, incremental steps which occur at high velocity,* subsequent partition of carbon between ferrite and austenite should occur to establish metastable equilibrium between these phases at the immobile interfaces where they are in contact. The magnitude of this partition will be determined largely by the rate at which carbide precipitates within the ferritic phase. If this rate is low, substantial partition will occur and if it is high, virtually none.

It is well established in the tempering of martensite[31] that ϵ carbide precipitates extremely rapidly from supersaturated ferrite and that ϵ is subsequently replaced by cementite. As in other precipitation systems, this indicates that precipitation of ϵ and precipitation of cementite are competing processes which occur at significantly different rates. It is expected that both reactions would exhibit the customary maximum rate as a function of temperature and the metastable nature of ϵ suggests that an upper temperature for its formation should exist. Silicon retards significantly the rate of precipitation of cementite from ferrite but exerts virtually no effect on that of ϵ.[32] Thus, the transformation behavior of silicon steels provides unique insight regarding the formation of supersaturated ferrite during transformation to bainite.[30]

Lower Bainite

Transmission micrographs of upper and lower bainite in the silicon steel are presented in Figures 15 to 17. Although minor differences exist, the structures of both constituents are similar to their counterparts in the low-silicon steels. The most important difference between the silicon and non-silicon steels concerns the large amount of retained austenite associated with upper bainite in the silicon steel. This retained austenite is revealed clearly by the precision dark field micrograph in Figure 15c, and also in the electron diffraction patterns obtained from the austenitic region in Figure 16. Confirming an earlier X-ray diffraction study[30] there were no carbides associated with upper bainite in this steel. All of the carbon was dissolved in ferrite and carbon enriched austenite.

Transformation to lower bainite was not accompanied by retention of detectable amounts of enriched austenite. Rather, as in the other steels, carbides (in this case ϵ) were precipitated uniformly throughout the ferritic matrix as indicated by the precision dark field micrograph in Figure 18. So far as is known, ϵ has never been observed to precipitate from austenite. Thus, the uniform density of ϵ particles in this steel provides unequivocal evidence that lower bainite formed initially as a highly supersaturated ferrite.

When samples of the silicon steel, fully transformed to lower bainite, are tempered at higher temperatures, cementite replaces ϵ and this process is accompanied by a large contraction in volume.[30] By comparing these volume changes with those that occur in the tempering of martensite, Deliry[33] has demonstrated that the amount of ϵ carbide in lower bainite corresponds to the total carbon content of the steel and concludes that lower bainite initially forms as a supersaturated ferrite which inherits the bulk carbon content of the original austenite. Combination of the structural observations (Figures 17 and 18) with the X-ray,[30] crystallographic[8,10] and dilatometric[30,33] data leaves little room to doubt that lower bainite initially inherits virtually, if not the entire, carbon content of the austenite. Thus, the slow apparent growth of lower bainite can be most readily understood if lower bainite actually forms by the rapid and discontinuous growth envisioned here.

These same conclusions apply to lower bainite in the low-silicon steels in spite of the difficulty in observing ϵ carbide in these materials. The carbide distribution in these steels (Figure 12) results from precipitation out of supersaturated ferrite and the fact that these carbides generally have been reported to be cementite[10] reflects simply the high rate at which tempering occurs in the absence of silicon.[30]

Upper Bainite

The large amount of enriched austenite associated with upper bainite in the silicon steel is entirely consistent with the concept that growth of upper bainite

* The rates need only be high relative to that permitted by diffusion of carbon in austenite and need not be at near sonic velocities. If the propagation rate is not exceptionally high then some partition of carbon to austenite may be expected to occur as the unit develops.

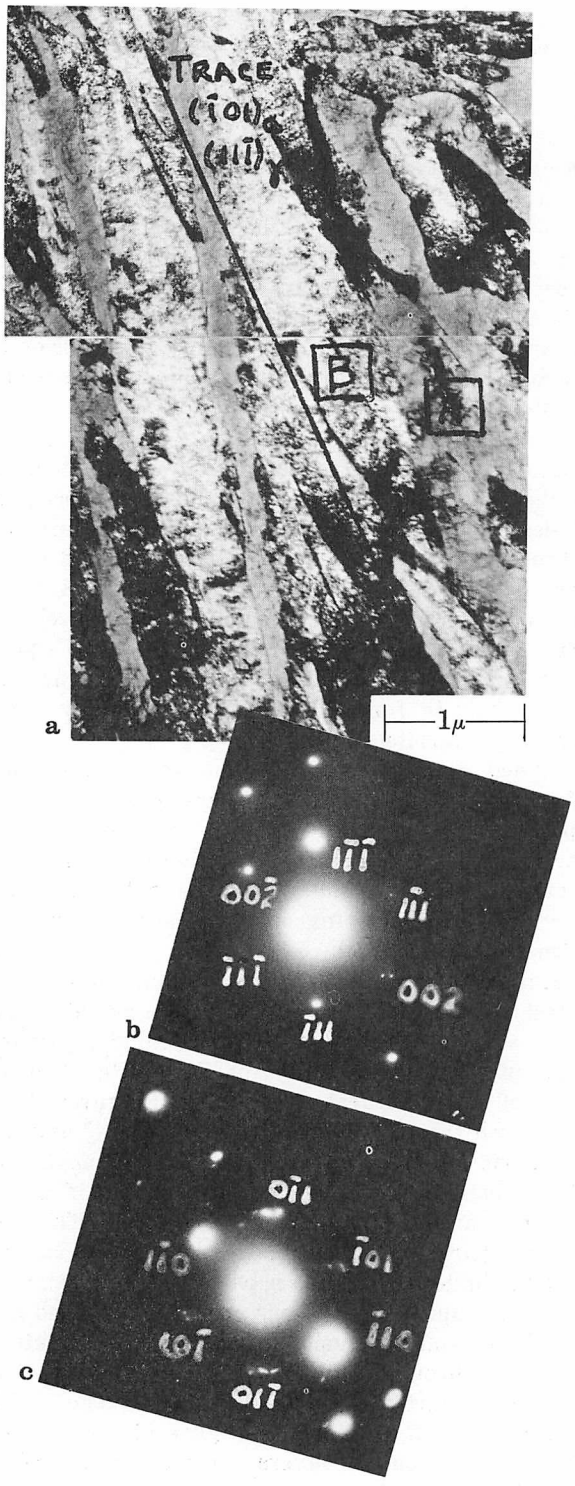

FIGURE 16. Bainite structure with retained austenite in S steel transformed at 400 C (750 F) for 20 min

a. aggregates of bainite laths separated by retained austenite. 17,000 X

b. selected area diffraction from Area A in (a). reflections from retained austenite [110]γ zone

c. selected area diffraction from bainite of Area B in (a). reflections from [111]α zone. present laths lie along traces of coincident $(\bar{1}01)\alpha$ and $(\bar{1}1\bar{1})\gamma$ planes

FIGURE 17. Aggregate lower bainite in S steel transformed at 275 C (525 F) for 17 hr. 21,200 X

is paced by the diffusion of carbon in austenite away from the tip of a ferrite needle. However, the existence of this enriched austenite may be highly misleading so far as the reaction mechanism is concerned. Specifically, it is proposed that, as with metastable phases in other systems, ϵ will not precipitate from supersaturated ferrite above some critical temperature which appears to be near 350 C (660 F). The ability of silicon to retard the precipitation of cementite from supersaturated ferrite then permits carbon to partition to the austenite.

The extent to which carbon partitions to austenite at an immobile austenite/supersaturated ferrite boundary should be determined in part by the rate at which cementite precipitates within the ferritic phase. In silicon steels this rate is very low* which allows the virtually complete partition observed here. In the absence of silicon (or other elements such as aluminum that have the same ability) part of the cementite should precipitate within the individual ferrite laths if these initially form at a high velocity resulting in supersaturated ferrite. A transmission micrograph of upper bainite formed in 1040 is presented in Figure 19. A relatively high density of

* However, it is the ability of silicon to retard precipitation of cementite from austenite that makes it possible to observe the large amount of carbon enriched austenite associated with upper bainite in the steel.

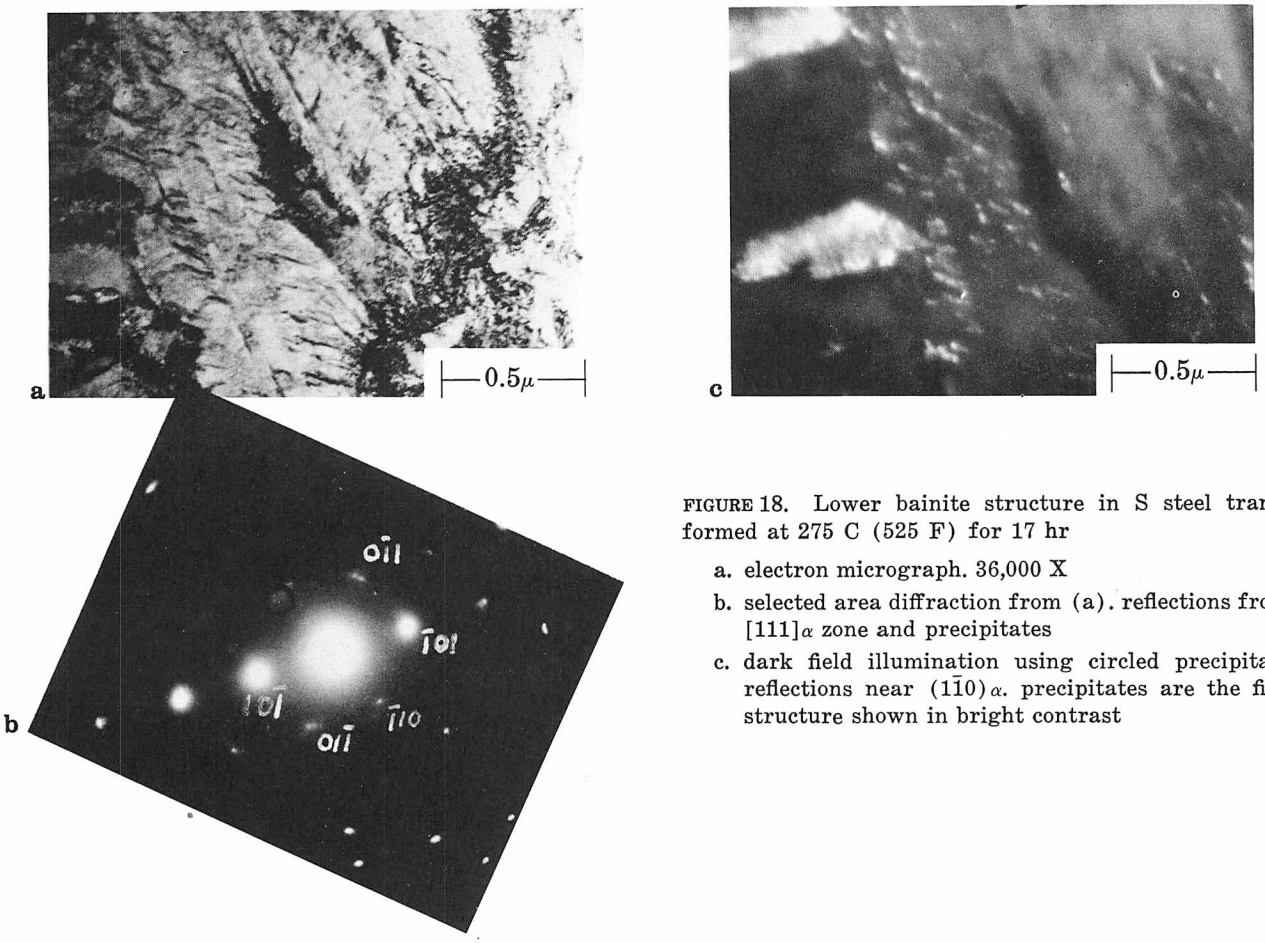

FIGURE 18. Lower bainite structure in S steel transformed at 275 C (525 F) for 17 hr

a. electron micrograph. 36,000 X

b. selected area diffraction from (a). reflections from $[111]\alpha$ zone and precipitates

c. dark field illumination using circled precipitate reflections near $(1\bar{1}0)\alpha$. precipitates are the fine structure shown in bright contrast

carbide particles precipitated within the laths is clearly evident. Although there is no question that a major portion of the carbide in upper bainite precipitates from enriched austenite, it is felt that this enriched austenite arises largely after the laths have formed and as a result of carbon equilibrating between ferrite and austenite at a now immobile interface. In spite of the lack of direct, positive evidence for limited, rapid growth, it seems most likely that the substructural units in both upper and lower bainite form initially with supersaturation well above that permitted by metastable equilibrium with austenite during diffusion controlled growth. It is hoped that emission microscopy or other techniques with higher resolving power than the hot stage microscope will eventually provide conclusive evidence regarding the mechanism by which bainites grow.

Growth Mechanisms

The complexity of bainitic structures and the lack of more detailed information on substructure development preclude a complete analysis of bainite formation at the present time. Nevertheless, some qualitative considerations deserve discussion.

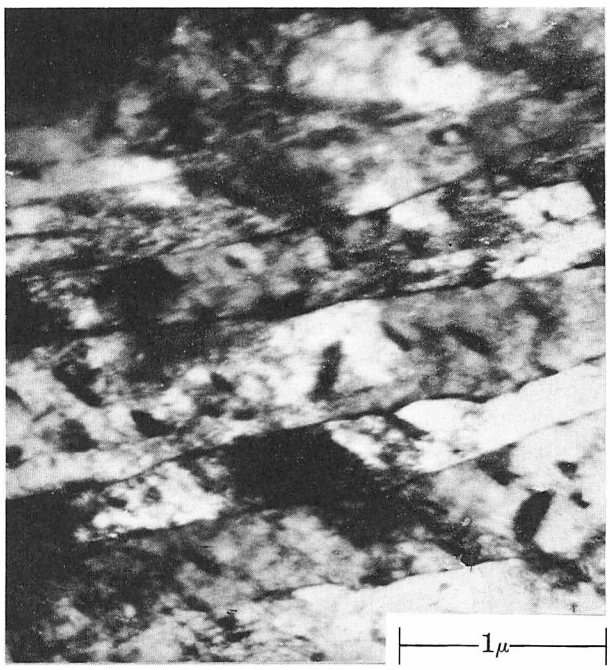

FIGURE 19. Upper bainite containing internal carbides in 1040 steel transformed at 435 C (815 F) for ten minutes. 27,700 X

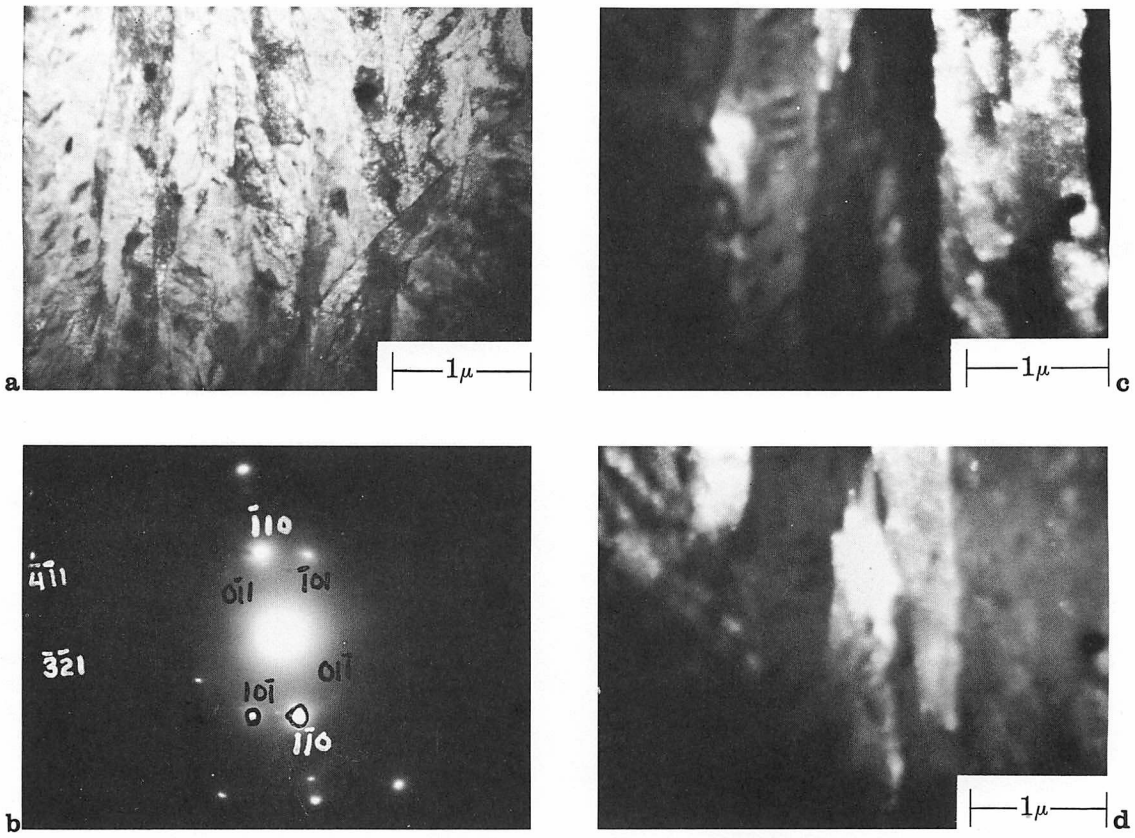

FIGURE 20. Lower bainite structure in 9N5 steel transformed at 270 C (520 F) for nine hours

a. electron micrograph. 19,000 X

b. selected area diffraction from (a). reflections from [111]α and [115]α zones. diffraction pattern should be rotated clockwise 14.5° to coincide with (a)

c. dark field illumination from $(1\bar{1}0)\alpha$ reflection, [115]α zone

d. dark field illumination from $(10\bar{1})\alpha$ reflection, [111]α zone. reversal of contrast in (c) and (d) shows plates alternate in orientation

The concept that bainite "grows" by repeated nucleation of some substructural unit that propagates rapidly to a limited size focuses attention on these substructural units. If this picture is correct, it will be necessary to understand what limits the size attained by a particular unit, how rapidly it attains this size and what determines the rate at which the units continue to nucleate. Neither these nor other equally important questions can presently be answered; however, as has been suggested frequently in the past[11,34] the development of bainitic structures appears to be intimately connected with relaxation of stresses associated with the volume and/or shape change of the transformation.

The structural transition between Widmanstätten ferrite and upper bainite may provide an important clue in the eventual resolution of these issues. Specifically, the lack of significant substructure in Widmanstätten ferrite may signify that these stresses are accommodated by short range mass transport; whereas, the high dislocation density and substructure of bainite suggest accommodation of transformation strain by slip in the parent and/or product phases. As with martensites, the shape strain can be minimized if adjacent subunits undergo self accommodating shears permitted by different variants of the martensite crystallography. Evidence that this occurs in the formation of upper bainite is provided by the alternating contrast between adjacent laths in Figure 4b. However, such alternating contrast is not observed with the regularity that one would desire. Figure 20 indicates that a similar situation sometimes prevails in the formation of lower bainite and these effects should be of importance in the application of the crystallographic theories to bainite and martensite formation. It is proposed that modifications in the processes whereby these strains are accommodated and relaxed are responsible for the transition from upper to lower bainite and this concept will be discussed more fully elsewhere.

According to these concepts, the limited size attained by the subunits in bainite is dictated by strain

accumulation in the austenite and the rate at which these units continue to nucleate is controlled by relaxation of these strains. The ideas expressed here are not new. For example, Ko and Cottrell[11] suggested that carbide precipitation from supersaturated ferrite controlled the growth rate of lower bainite. While this may be one of the factors, other relaxation processes also should contribute. Perhaps, the pronounced influence of alloying elements on the growth rate of bainite (Figure 14) results from the ability of these elements to strengthen austenite and ferrite and to lower the rate of various relaxation processes in each of these phases.

SUMMARY AND CONCLUSIONS

Transmission electron microscopy has been used to demonstrate that, structurally, Widmanstätten ferrite, upper bainite and lower bainite do not form a continuous series of decomposition products. Widmanstätten ferrite forms as single crystals with a low and random dislocation density; whereas, upper bainite exhibits a lath-like substructure with a high dislocation density. This structural transition occurs discontinuously at the B_s temperature as determined from kinetic measurements. A further change in fine structure of bainite occurs at a temperature near 350 C (660 F) and characterizes the transition from upper to lower bainite.

Diffusion controlled growth models are based on the concept that the elementary growth unit (whether this be the gross bainite plate observed by optical microscopy or one of the substructural units observed in transmission microscopy) advances continuously at a rate coupled to the removal of carbon into the surrounding austenite. Comparison of optical and electron micrographs provides indirect evidence that bainite does not form in this fashion. Rather, it is proposed that both upper and lower bainite increase in size by the repeated nucleation of substructural units which propagate rapidly to a limited size. Growth rates measured by hot stage microscopy thus are determined by the rate at which these substructural units nucleate.

It is concluded that both upper and lower bainite form initially with substantial supersaturation. The rate at which carbon precipitates from this supersaturated ferrite is responsible for the difference between upper and lower bainite. Rapid precipitation of ϵ carbide in lower bainite prevents significant carbon enrichment of austenite; whereas, delayed precipitation of cementite from upper bainite permits substantial partition of carbon to austenite trapped between ferritic laths. Cementite may subsequently precipitate from this enriched austenite, however, its presence is not required as a criterion defining bainite as in silicon steels.

Growth by repeated nucleation of particles which rapidly attain a limited size focuses attention on these substructural units. The quite old concept that bainitic growth is intimately connected with relaxation of transformation strain is reaffirmed but an analytical treatment has not been accomplished.

ACKNOWLEDGMENTS

The authors wish to express their appreciation to the Office of Naval Research, U.S. Navy for their support of this work. One of us (J. M. O.) also expresses his appreciation to the National Science Foundation for the award of a Cooperative Fellowship.

REFERENCES

1. E. S. Davenport and E. C. Bain, Trans. AIME, *90*. 117 (1930)
2. R. F. Mehl, "Hardenability of Alloy Steels," ASM (1939), 1
3. Series of Reports by Subcommittee XI of ASTM Committee E4, Proc. ASTM, *50*. 444 (1950), *52*. 543 (1952), *54*. 568 (1954)
4. S. Modin, Jernkontorets Ann., *142*. 37 (1958)
5. A. Schrader and F. Wever, Arch. Eisenhüttenw., *23*. 489 (1952)
6. K. Shimizu and Z. Nishiyama, Mem. Inst. Sci. Ind. Res. Osaka, Univ., *20*. 43 (1963)
7. P. M. Kelly and J. Nutting, J. Iron and Steel Inst. (London), *197*. 199 (1961)
8. K. J. Irvine and F. B. Pickering, "High-Carbon Bainitic Steels," *Physical Properties of Martensite and Bainite*, Special Report 93, The Iron and Steel Institute (London), 1965, 110
9. L. Habraken, Compt. Rend. Rech. Trav. du Centre National de Recherches Metallurgiques, Nov. 1957, No. 19
10. D. N. Shackleton and P. M. Kelly, "Morphology of Bainite," *Physical Properties of Martensite and Bainite*, Special Report 93, The Iron and Steel Institute (London), 1965, 126
11. T. Ko and S. A. Cottrell, J. Iron and Steel Inst. (London), *172*. 307 (1952)
12. G. R. Speich and M. Cohen, Trans. AIME, *218*. 1050 (1960)
13. G. R. Speich, "Growth Kinetics of Bainite in a Three Per Cent Chromium Steel," *Decomposition of Austenite by Diffusional Processes*, edited by V. F. Zackay and H. I. Aaronson, Interscience, New York, 1962, 353
14. K. Tsuya, J. Mech. Lab. Japan, *2*. 20 (1956)
15. R. H. Goodenow, S. J. Matas and R. F. Hehemann, Trans. AIME, *227*. 651 (1963)

16. A. P. Miodownik, J. Inst. Metals (London), *83*. 561 (1954-1955) Discussion

17. M. Hillert, Unpublished data referred to in Ref. 19

18. M. Hillert, "The Formation of Pearlite," *Decomposition of Austenite by Diffusional Processes*, edited by V. F. Zackay and H. I. Aaronson, Interscience, New York, 1962, 197

19. L. Kaufman, S. V. Radcliffe and M. Cohen, "Thermodynamics of the Bainite Reaction," *Decomposition of Austenite by Diffusional Processes*, edited by V. F. Zackay and H. I. Aaronson, Interscience, New York, 1962, 313

20. H. I. Aaronson, "The Proeutectoid Ferrite and the Proeutectoid Cementite Reactions," *Decomposition of Austenite by Diffusional Processes*, edited by V. F. Zackay and H. I. Aaronson, Interscience, New York, 1962, 387

21. T. Lyman and A. R. Troiano, Trans. AIME, *162*. 196 (1945)

22. H. I. Aaronson and H. A. Domian, Trans. AIME, *236*. 781 (1966)

23. A. R. Troiano, Trans. ASM, *41*. 1093 (1949)

24. H. I. Aaronson and C. Wells, Trans. AIME, *206*. 1216 (1956)

25. J. W. Christian, "The Origin of Surface Relief Effects in Phase Transformations," *Decomposition of Austenite by Diffusional Processes*, edited by V. F. Zackay and H. I. Aaronson, Interscience, New York, 1962, 371

26. R. H. Goodenow, R. H. Barkalow and R. F. Hehemann, "Bainite Transformations in Hypoeutectoid Steels," *Physical Properties of Martensite and Bainite*, Special Report 93, The Iron and Steel Institute (London), 1965, 135

27. E. Tekin and P. M. Kelly, "Precipitation from Iron Base Alloys," AIME Met. Soc. Conf. Vol. 28, 1965, Gordon and Breach, New York, p. 173

28. C. M. Wayman, "Ferrous Martensites," *Physical Properties of Martensite and Bainite*, Special Report 93, The Iron and Steel Institute (London), 1965, 153

29. R. H. Goodenow and R. F. Hehemann, Trans. AIME, *233*. 1777 (1965)

30. S. J. Matas and R. F. Hehemann, Trans. AIME, *221*. 179 (1961)

31. F. E. Werner, B. L. Averbach and M. Cohen, Trans. ASM, *49*. 823 (1957)

32. W. S. Owen, Trans. ASM, *46*. 824 (1954)

33. J. Deliry, Mem. Sci. Rev. Met. (Paris), *62*. 527 (1965)

34. C. Zener, Trans. AIME, *167*. 550 (1946)

ORAL DISCUSSION OF

Structure and Growth of Widmanstätten Ferrite and Bainite

Presented by R. F. HEHEMANN

G. R. SRINIVASAN (Cornell University). The findings of Oblak and Hehemann on the structure of lower bainite are in general agreement with those of our thin foil studies carried out at the University of Illinois. Some of the results of these studies were reported by Professor C. M. Wayman and myself at the Chicago AIME meeting last fall.

These studies made on a ferrous alloy containing 1.11% C + 7.9% Cr indicate that lower bainite exhibits the basic characteristics of a shear transformation. Measurement of the crystallographic parameters of the transformation shows that these are consistent with the phenomenological theories of martensite transformation. There are, however, some significant differences in the shear modes between the martensite and lower bainite transformations in the same alloy. The two differ in their habit planes, shape deformation and in their lattice invariant deformation. As Professor Hehemann pointed out, lower bainite formation, unlike the formation of martensite, does not seem to be associated with internal twinning. This is consistent with the observation of Shimizu, Ko and Nishiyama* and of Shackleton and Kelly.** Furthermore, our studies show that lower bainite in this alloy is consistent with a double shear on the bcc slip planes along the common slip direction. We believe that on the basis of these studies lower bainite cannot be equated to autotempered martensite.

Structurally, the lower bainite in our alloy seems to form in a similar fashion to that reported by Professor Hehemann. The bainite forms as a plate as shown in the composite micrograph of Figure A. Figure B shows that the plate has a straight planar side from which the growth seems to take place. This immobile side of the plate corresponds to the habit plane of the theories.

The internal structure of this bainite consists of car- of the plate. There are also some cementite platelets at bide particles precipitated on striations along the length a characteristic angle of 55 to 60° to the growth direc-

*K. Shimizu, T. Ko and Z. Nishiyama, Trans. Japan Inst. Met., *5*. 225 (1964)

**D. N. Shackleton and P. M. Kelly, "Morphology of Bainite," *Physical Properties of Martensite and Bainite*, Special Report 93, The Iron and Steel Institute (London), 1965, 126

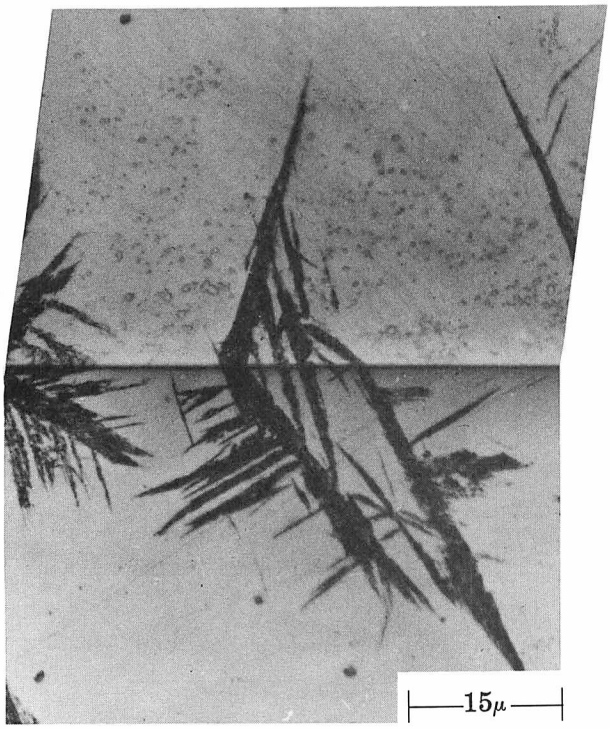

FIGURE A. Two-surface composite micrograph of lower bainite in an Fe–7.9 Cr–1.1C alloy

FIGURE B. Lower bainite plates in surface relief; oblique illumination

FIGURE C. Transmission electron micrograph of lower bainite showing the types and distribution of carbides

tion. These platelets exhibit the standard orientation relationship with the bainitic ferrite. This carbide structure is shown in Figure C. Unlike the lower bainite in Oblak and Hehemann's alloys, the bainite plate in our alloy does not show any subunits of ferrite or multiple relief.

It is interesting to note that no upper bainite forms in this alloy. Instead, in the temperature range usually associated with upper bainite, austenite decomposes into plates of ferrite and carbide. The lower bainite does not form until the temperature is lowered to below 300 C (570 F). These observations can be explained on the basis of the carbon enrichment models of upper bainite formation. It is also our belief that upper bainite and lower bainite are different products of austenite decomposition differing in morphology, kinetics, crystallography, and perhaps transformation mechanism.

AUTHOR'S REPLY. The multiple relief exhibited in our Figure 7 represented upper bainite. We also see single relief for lower bainite just as you have seen.

G. R. SRINIVASAN. The point I was making was that we did not see any subgrowth units in our bainite. The electron diffraction patterns taken over the entire bainite plate showed single bcc orientation. This seems to be the difference between our observations on the two alloys.

AUTHOR'S REPLY. The absence of subgrowth units in lower bainite in the high chromium steel studied by Dr. Srinivasan emphasizes further the effects of composition on structure and morphology of bainite. In spite of the subgrowth units in the bainites we have examined,

electron diffraction patterns exhibit a single bcc orientation for the entire plate. This agrees with the results of Dr. Srinivasan. Evidently, as in upper bainite, there are only slight misorientations between the subgrowth units.

S. V. RADCLIFFE (Case Institute of Technology). Several years ago, Kaufman, Cohen, and myself attempted to develop a general model to account for the transformations from austenite to bainite and Widmanstätten ferrite. Although the model seemed satisfactory, it is clear from Professor Hehemann's observations that our assumption of carbon-diffusion dominated processes may have to be altered. I have not yet talked about this with Professor Cohen and he may have some reservations.

M. COHEN (Massachusetts Institute of Technology). I'm neutral.

S. V. RADCLIFFE. It seems clear that in the lower bainite phase, the additional feature of ferrite nucleation now must be taken into account. On the other hand, I do not believe Professor Hehemann is completely justified in feeling that this may become the rate controlling factor instead of carbon diffusion. What is now needed is a general model which incorporates the new facts which have been reported and takes into account both ferrite nucleation and carbon diffusion, which, in a sense, may be intercontrolling.

Some support of Professor Hehemann's remarks on the constancy of the temperature "boundary" between the upper and lower bainite ranges is provided by results reported recently.† Figure D shows the effects on the martensite transformation in Fe–C alloys of altering the temperature at which martensite is allowed to form by imposing high pressure. The upper two lines show the shift in the M_s temperature with increase in pressure from atmospheric pressures to 40 kilobars. The corresponding microstructures (defined from transmission electron microscopy studies) are indicated by the lower band which shows that the composition of the transition from the lath martensite to internally twinned martensite is lowered at the high pressure. At one atmosphere, the transition takes place in the region of 0.4 w/o C, whereas at the high pressure internally twinned martensite occurs as low as 0.1 w/o C. However, the more interesting fact for the present discussion is that the corresponding M_s for this structural transition is about 300/350 C (570/660 F) at 40 kilobars and 350 C (660 F) at one atmosphere. Thus, the constant temperature "boundary" that Professor Hehemann referred to in connection with upper and lower bainite also appears to correspond to a temperature which relates to a change in the martensitic structure.

AUTHOR'S REPLY. We appreciate very much the comments of Professor Radcliffe. The influence of pressure on the structure of martensite appears to emphasize further the structural connection between lath martensite and upper bainite and that between twinned martensite and lower bainite. It is, however, somewhat disturbing that internal twins have thus far escaped

†R. F. Vyhnal and S. V. Radcliffe, Acta Met., in press

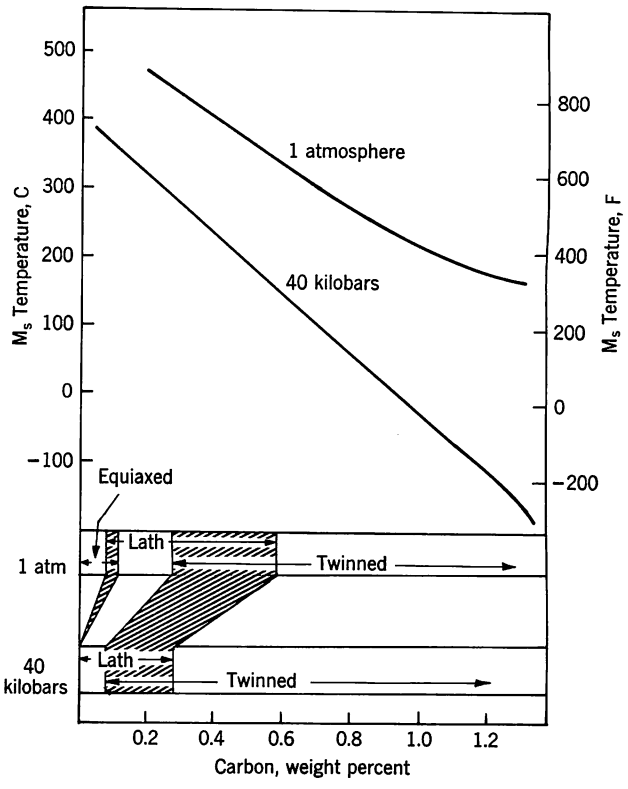

FIGURE D. Schematic representation of electron microstructures observed at atmospheric pressure and 40 kilobars. Also included is the effect of pressure and composition on M_s of iron–carbon alloys

detection in lower bainite. This point requires further experimental study and clarification.

The question of the rate controlling factor in the growth of bainite is particularly complex. We wish to emphasize again our concern regarding the role of substructure in the growth of both upper and lower bainite. Many of the hot-stage growth measurements appear to refer to a rate at which these units nucleate, and further work employing more sensitive techniques will be required to resolve the factors controlling the growth process.

T. G. NILAN (United States Steel Corporation). I would like to comment upon Dr. Aaronson's discussion.* Would you expect the T_0 curve to be altered if we were to consider, rather than bulk thermodynamic properties of the materials, something more pertinent to the interface, i.e., on the scale of atomic dimensions?

H. I. AARONSON. The assumption that macroscopic thermodynamics is applicable to processes taking place on an atomic scale is usually regarded as acceptable when the number of atoms involved is large. This condition is normally fulfilled during growth. The use of conventional thermodynamics in the context of nucleation

*See following written discussion from K. R. Kinsman and H. I. Aaronson

theory, on the other hand, represents a much more complex problem. Even if the considerable progress which has been made in resolving this problem should prove unacceptable to the discusser, the macroscopic T_0 temperature will surely prevent *growth* without a change in composition from taking place, and will thus make such a mode of transformation experimentally undetectable.

A. J. McEvily (Ford Motor Company). I would like to ask Professor Hehemann a question. In a very low carbon steel, what would be the distinction, if any, between Widmanstätten ferrite and upper bainite? Is it possible that both form by the same mechanism, with the lower dislocation content of the Widmanstätten ferrite simply reflecting the fact that the transformation occurs in austenite of relatively weaker strength because of the higher transformation temperatures involved?

Author's Reply. As suggested by Dr. McEvily, the distinction between upper bainite and Widmanstätten ferrite may arise simply from an increased dislocation density in upper bainite produced by the increased resistance to deformation as the reaction temperature is lowered. However, this leaves unanswered the question of why the sheaf structure of upper bainite arises discontinuously at the B_s temperature. This occurs even when ferrite does not adopt a Widmanstätten morphology at temperatures above B_s as in the 2340 steel. The development of these sheaf structures appears to be intimately connected with accommodation of transformation strain.

WRITTEN DISCUSSION

K. R. Kinsman and H. I. Aaronson (Ford Motor Company). The authors consider that both upper and lower bainite are composed of sheaves of individual ferrite plates or "subunits". Although there are a number of differences in detail between the two forms of bainite, the authors urge a central theme common to both. This theme is that the subunits grow at rates substantially higher than those which would be permitted if growth were controlled by the diffusion of carbon in austenite under the condition that the ferrite and austenite in contact with the advancing austenite: ferrite boundaries had the compositions corresponding to the extrapolated $\alpha/\alpha + \gamma$ and $\gamma/\alpha + \gamma$ (Ae_3) curves, respectively, at the reaction temperature. It follows directly from this mechanism that the ferritic component of bainite is substantially supersaturated in carbon with respect to the $\alpha/\alpha + \gamma$ curve. Also on this basis, the rates of lengthening and of thickening of bainite sheaves measured with the presently available technique of low-resolution hot stage (optical) microscopy reflect primarily the rate of sympathetic nucleation,[1] rather than the rate of growth of the component subunits.

The purpose of this discussion is to present a thermodynamic analysis of the authors' mechanism, with particular attention being paid to the application of this mechanism to upper bainite. The quantitative experimental data presently available are insufficient to allow a decision to be made as to the thermodynamic plausibility of their mechanism on the basis of this analysis. It is hoped, however, that the analysis will be of assistance in the design of future experimental studies of the growth mechanisms of bainite. The formation of the first subunit of a sheaf by the Oblak-Hehemann mechanism will be shown to be thermodynamically feasible in the alloys which they employed. Kinetic considerations will then be invoked to demonstrate that the formation of subsequent subunits results in the development of a thermodynamic barrier which can eventually seriously inhibit growth of the subunits by this mechanism. We shall conclude by giving a brief summary of our views on the mechanism of formation of bainite sheaves and a description of a critical growth kinetics experiment which should allow unequivocal distinction between the two mechanisms. Since this experiment will be quite difficult to perform, however, it seems desirable at this juncture to examine the possibilities for differentiation offered by the thermodynamic type of analysis.

Determining whether or not the first subunit of a bainite sheaf can form with essentially the same carbon content as the parent austenite in a given alloy requires that the position of the T_0 temperature (at which stress-free austenite and ferrite of the same composition are in metastable equilibrium)[2] relative to the bainite range be established. This has already been done for iron–carbon alloys as a function of carbon content, using high-purity materials to determine the upper temperature limit of the bainite range (the B_s temperature) and several different methods to calculate the T_0 temperature.[3] It was found that sheaves of bainite form in an increasingly wide range of temperatures above T_0 as the carbon content exceeds that of the eutectoid. These bainite structures have a similar appearance to those formed in hypoeutectoid alloys,[4] wherein the bainite range does lie below the T_0-composition curve. This suggests that in neither range of composition did the ferrite inherit the full carbon content of the parent austenite. Inasmuch as the hypereutectoid bainites were not examined with electron microscopy, however, this evidence may not be considered decisive with respect to the present situation. We accordingly consider the problem of calculating the T_0 temperature for some of the lower carbon, multi-component alloys used by Oblak and Hehemann. This calculation has been considered in some detail for Fe–C–X alloys.[5] The insufficiency of the data on the temperature-dependence of the activity of carbon in austenite in such alloys was considered to restrict this calculation to a slight elaboration of the simple method of Zener.[2] Comparison of the results of the Zener method, as applied to iron–carbon alloys, with those obtained from more accurate relationships indicates, however, that the Zener T_0's are somewhat high at the carbon contents of interest here, and much too high in hypereutectoid steels. We shall therefore convert one of the more accurate iron–carbon relationships to Fe–C–X usage, though perforce retaining the iron–carbon standard state constants, in the hope that this procedure will yield a net improvement in accuracy.

The best available treatment of the statistical thermodynamics of interstitial solid solutions is that due to Lacher[6] and Fowler and Guggenheim[7] (termed LFG). To take

account of the effects of a substitutional alloying element, this analysis has been combined with Zener's[8] treatment of the separate effects of alloying elements upon the magnetic and the non-magnetic components of the free energy change accompanying the austenite→ferrite transformation in pure iron, $\Delta F_{Fe}^{\gamma\rightarrow\alpha}$ [5]. Since the steels used by Oblak and Hehemann contained appreciable percentages of several alloying elements, this approach will be extended to multi-component alloys by simply assuming that the effects of these elements upon $\Delta F_{Fe}^{\gamma\rightarrow\alpha}$ are additive. The free energy change associated with the formation of ferrite of the same carbon and alloy contents as the parent austenite ($\Delta F^{\gamma\rightarrow\alpha}$) is thus written as:

$$(1)\quad \Delta F^{\gamma\rightarrow\alpha} = RT\Big\{6x\ln\frac{(\delta+1-3x)}{(\delta-1+3x)} - 6(1-x)\ln\frac{[1-2J_\gamma+(4J_\gamma-1)x-\delta]}{2J_\gamma(2x-1)} + 6x\ln x - 4(1-x)\ln(1-x) + 5(1-2x)\ln(1-2x)\Big\} + x[\overline{\Delta H}_C^{\alpha} - 10525 - (E+2.34)T - RT\ln 3] + (1-x)\Big[141\sum_i y_i(\Delta T_{Mag_i} - \Delta T_{NM_i}) + \Delta F^{\gamma\rightarrow\alpha}\Big\{T - 100\sum_i y_i\Delta T_{Mag_i}\Big\}\Big]$$

$$(1a)\quad \delta = [1-2(1+2J_\gamma)\,x + (1+8J_\gamma)x^2]^{1/2}$$

$$(1b)\quad J_\gamma = 1 - e^{-\bar{w}_\gamma/RT}$$

(We note here that the first term in equation (1) was incorrectly written as $6x\ln\frac{x(\delta+1-3x)}{(\delta-1+3x)}$ in equation (35) of reference (5).) In these relationships, R = gas constant, T = absolute temperature, x = mole fraction of carbon in austenite and in ferrite, $\bar{w}_\gamma$ = weighted average of the pairwise interaction energy of carbon atoms in the alloyed austenite, $\overline{\Delta H}_C^{\alpha}$ = partial molar heat of solution of carbon in ferrite, E = standard state constant for ferrite and y = mole fraction of substitutional alloying element in austenite or in ferrite (disregarding the presence of carbon). $\Delta F_{Fe}^{\gamma\rightarrow\alpha}\Big\{T - 100y_i.\Delta T_{Mag_i}\Big\}$ = free energy change accompanying the $\gamma\rightarrow\alpha$ transformation in pure iron at temperature $T - 100y_i.\Delta T_{Mag_i}$, ΔT_{Mag_i} and ΔT_{NM_i} = displacement in T, per atomic percent of the i'th substitutional alloying element, at which $\Delta F_{Fe}^{\gamma\rightarrow\alpha}$ is computed as a result of changes produced in the magnetic and the non-magnetic components of this free energy change, respectively. The summations extend over the alloying elements present. An expanded Table of ΔT_{NM} values, and plots of w_γ vs y for various alloying elements from which $\bar{w}_\gamma = \sum_i y_i w_{\gamma i}$ may be computed, are included in reference (5). Since this analysis proved unsatisfactory for chromium, no calculations were made for the two steels containing appreciable amounts of this element; the small chromium contents of the other alloys were disregarded. The value of $\overline{\Delta H}_C^{\alpha}$ for iron–carbon alloys is presently much in dispute.[9-12] Two values of $\overline{\Delta H}_C^{\alpha}$, and their corresponding values of E [3], representing the extrema of the range over which these disagreements extend, are accordingly employed in these calculations.

At the T_0 temperature, $\Delta F^{\gamma\rightarrow\alpha} = 0$. The value of x at which this condition is fulfilled was determined as a function of temperature. Most of the results obtained are plotted in Figures E to H.

In the present context, it is also of interest to determine the Ae_3 curves under the condition that no partition of alloying element takes place between austenite and ferrite. On the basis of electron probe studies conducted on simpler alloys,[13] it may be considered very likely that partition was absent under the conditions of interest here. Calculation was made on the basis of the LFG-type equation[16] of reference,[5] with summations introduced as in equation (1). These results are also included in Figures E to H.

Oblak and Hehemann provided information on the B_s temperature (which they here defined as the highest temperature at which sheaves appear) for only two alloys. In the 1040 (plain carbon) steel, it could only be said that the B_s temperature lies somewhere within the temperature range indicated in Figure E. The T_0 temperature, as calculated on both values of $\overline{\Delta H}_C^{\alpha}$, lies 50 to 75C (90 to 135F) above the upper limit of this range. Figure F shows that the B_s temperature is almost identical to the T_0 temperature for $\overline{\Delta H}_C^{\alpha}$ = 26160 cal/mole in the 2340 steel. If we assume that the kinetic B_s temperature, which is defined on a TTT-curve criterion,[14] corresponds to the special microstructural B_s defined by the authors, then some additional

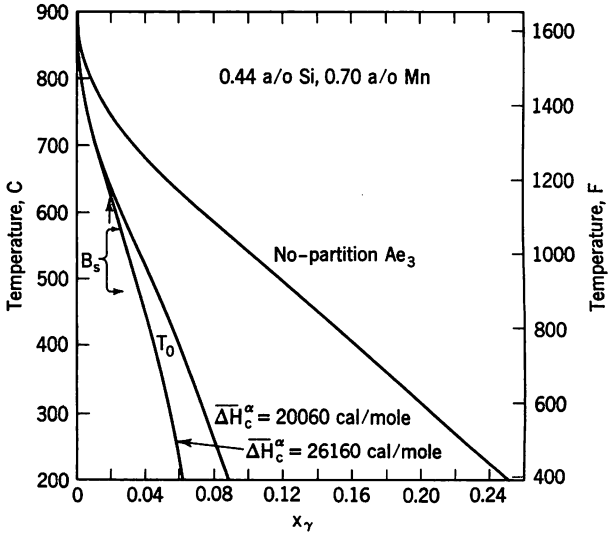

FIGURE E. Calculated no-partition Ae_3 curve and two versions of calculated T_0 curve for steels with alloy content of the Oblak–Hehemann 1040 steel (0.22 w/o Si, 0.69 w/o Mn). Vertical arrow indicates the carbon content of this steel (0.43 w/o or x_γ = 0.0196). Horizontal arrows indicate range within which Oblak and Hehemann established the B_s temperature

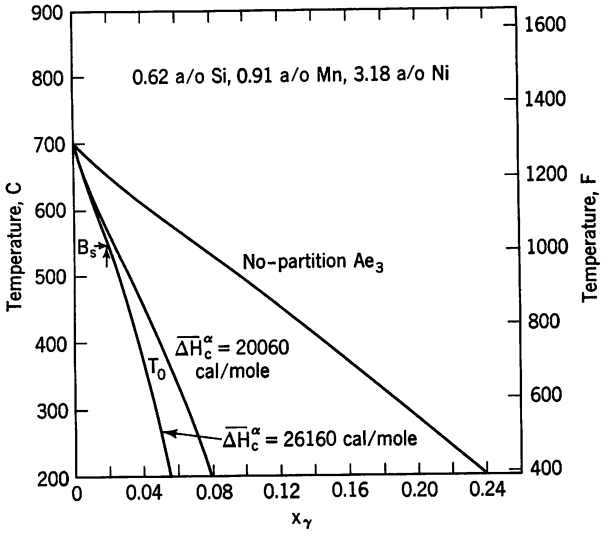

FIGURE F. Calculated no-partition Ae_3 curve and two versions of calculated T_0 curve for steels with the alloy content of the Oblak–Hehemann 2340 steel (0.31 w/o Si, 0.89 w/o Mn, 3.34 w/o Ni). Vertical arrow indicates the carbon content of this steel (0.40 w/o or $x_\gamma = 0.0183$). Horizontal arrow indicates B_s temperature determined by Oblak and Hehemann

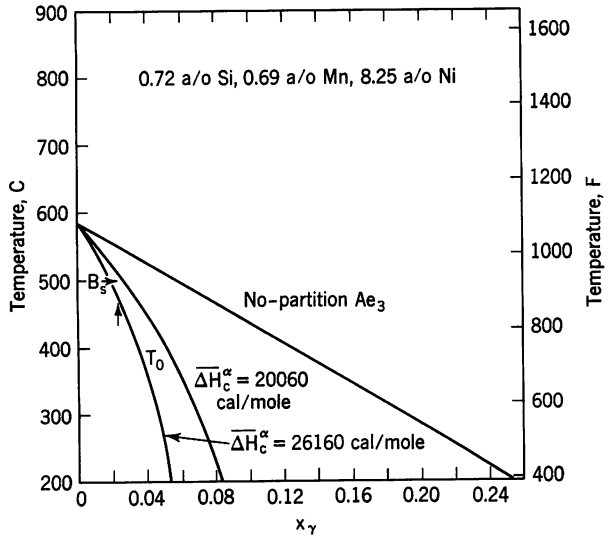

FIGURE G. Calculated no-partition Ae_3 curve and two versions of calculated T_0 curve for steels with the alloy content of the Oblak–Hehemann 9N5 steel (0.36 w/o Si, 0.68 w/o Mn, 8.70 w/o Ni). Vertical arrow indicates the carbon content of this steel (0.50 w/o or $x_\gamma = 0.0228$). Horizontal arrow indicates kinetic B_s temperature interpolated from TTT-diagrams of Sheehan et al[15]

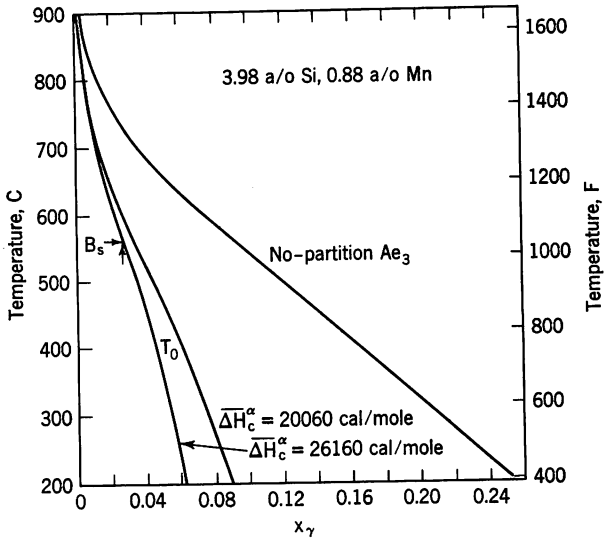

FIGURE H. Calculated no-partition Ae_3 curve and two versions of calculated T_0 curve for steels with the alloy content of the Oblak–Hehemann S steel (2.00 w/o Si, 0.86 w/o Mn). Vertical arrow indicates the carbon content of this steel (0.60 w/o or $x_\gamma = 0.0268$). Horizontal arrow indicates kinetic B_s temperature from TTT-diagram by Hultgren[16] for a similar steel

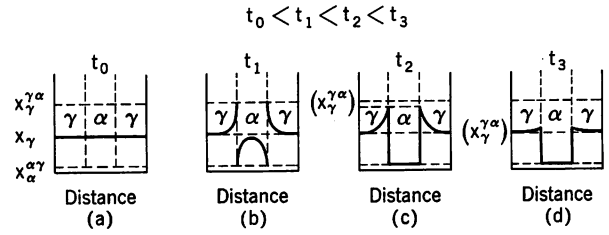

FIGURE I. Schematics of carbon distribution in ferrite and in austenite at successively increasing times (t_i) after growth of a ferrite subunit has ceased

experimental data can be extracted from the literature. From TTT-curves published by Sheehan, Julien and Troiano[15] for iron–carbon–nickel alloys and by Hultgren[16] for an iron–carbon–silicon alloy of compositions bracketing or similar to the 9N5 and S steels, respectively, the experimental B_s temperatures for these alloys were entered on Figures G and H. The agreement between the T_0 and the experimental B_s temperatures in Figures F to H is so good that it might appear significant. We prefer to reserve judgment, however, pointing to the divergence evident in Figure E, and to the outright disagreement in hypereutectoid iron–carbon alloys[3] previously noted. In the sense of the present discussion, however, it must be said that the microstructures with which the authors dealt lie below the T_0 temperature, and thus that the formation of the first subunit of the sheaves in these alloys without change in composition is thermodynamically possible.

Let us now consider the variation with time of the carbon concentration gradients in ferrite and in austenite with the

assistance of the schematic concentration-penetration curves of Figure I. On the basis of the authors' mechanism, the ferrite initially inherits all (or essentially all) of the carbon content of the parent austenite, and the austenite: ferrite boundary is assumed to be immobile for an appreciable time interval before another subunit is sympathetically nucleated at the immobilized austenite:ferrite boundary. At t_0 (Figure Ia), growth of the first subunit has just stopped, and the carbon contents of the bainitic ferrite and the abutting austenite are identical. The metastable equilibrium compositions $x_\gamma^{\gamma\alpha}$ and $x_\alpha^{\alpha\gamma}$ will be reached immediately afterwards at the austenite:ferrite boundary. ($x_\gamma^{\gamma\alpha}$ = mole fraction of carbon in austenite at the austenite:ferrite boundary corresponding to the no-partition Ae_3, $x_\alpha^{\alpha\gamma}$ = mole fraction of carbon in ferrite at the austenite:ferrite boundary given by the no-partition $\alpha/\alpha + \gamma$ curve and x_γ = mole fraction of carbon in austenite prior to transformation.) As indicated in Figure Ib, the carbon then diffuses out of the ferrite into the austenite. Since the diffusivity of carbon in ferrite is much more rapid than in austenite, the rate of decarburization of the ferrite should be controlled by the diffusion of carbon in austenite until the concentration gradients remaining in ferrite become very small. This means that the composition $x_\gamma^{\gamma\alpha}$ can be maintained as the upper bound to carbon diffusion in austenite effectively throughout the decarburization process. Since $x_\gamma^{\gamma\alpha}$ is, of course, higher than the carbon content corresponding to the T_0 curve (Figures E to H), formation of ferrite without a composition change by nucleation at the immobilized austenite:ferrite boundary is thermodynamically impossible during this time interval.

Once decarburization is effectively complete, however, the carbon content in austenite in contact with the boundary will begin to fall, as in Figure Ic. Eventually, only an imperceptible gradient of carbon will remain (Figure Id) if sympathetic nucleation of the next subunit is sufficiently long delayed. Growth of a new subunit without a change in composition cannot take place until the carbon content in austenite at the austenite:ferrite boundary has dropped below that corresponding to T_0 at the temperature of transformation.

Quantitative evaluation of the possibility of accounting for the kinetics of thickening on the Oblak–Hehemann mechanism in the face of these restrictions divides naturally into two steps. The first is to determine the time required to decarburize the initially supersaturated ferrite, and thus the time interval during which the carbon content in austenite at the boundary will be maintained at $x_\gamma^{\gamma\alpha}$. This is given by:

$$(2)\quad \left(\frac{W}{2}\right)(x_\gamma - x_\alpha^{\alpha\gamma}) = \int_0^{s'} x_\gamma\{s, t\}\, ds$$

where w = width of a subunit, $x_\gamma\{s, t\}$ = mole fraction of carbon in austenite as a function of distance, s, normal to the austenite:ferrite boundary and of diffusion time, t . The cut-off limit to be imposed upon s, termed s′, beyond which enrichment of the austenite can be considered negligible, is here defined as the value of s at which

$$x = x_\gamma + 0.001\,(x_\gamma^{\gamma\alpha} - x_\gamma).$$

The austenite:ferrite boundary is assumed to be planar, since the broad faces of a subunit provide most of the interfacial area through which carbon can diffuse out into the austenite; the length/thickness ratio is taken to be sufficiently high so that loss of carbon through the edges of the subunit can be disregarded. On a standard solution to Fick's Second Law for diffusion initiated from a stationary planar boundary, at which the composition is maintained constant, and proceeding into a semi-infinite volume of material:

$$(3)\quad x_\gamma\{s, t\} = x_\gamma + (x_\gamma^{\gamma\alpha} - x_\gamma)\,[1 - \mathrm{erf}\,(s/2\sqrt{Dt})]$$

where D = diffusivity of carbon in austenite at $x_\gamma^{\gamma\alpha}$. Substituting into equation (2) and integrating,

$$(4)\quad \frac{W}{2}(x_\gamma - x_\alpha^{\alpha\gamma}) = x_\gamma^{\gamma\alpha}\, s' - (x_\gamma^{\gamma\alpha} - x_\gamma)\,[s'\,\mathrm{erf}\,(s'/2\sqrt{Dt}) + 2\sqrt{Dt/\pi}\,(e^{-s'^2/4Dt} - 1)]$$

Inserting $s' = 4.654(Dt)^{1/2}$ into this relationship and rearranging, the time interval during which $x_\gamma^{\gamma\alpha}$ can be maintained at the boundary is:

$$(5)\quad t = \frac{\pi w^2 (x_\gamma - x_\alpha^{\alpha\gamma})^2}{4D(1.991\, x_\gamma^{\gamma\alpha} + 3.524\, x_\gamma)^2}$$

Only one thickening rate could be estimated from the authors' micrographs, and this, unfortunately, was in the 5140 steel, for which the T_0 and Ae_3 curves could not be calculated. Both of these curves, however, should be reasonably well approximated by those for the 1040 steel (Figure E). From the authors' Figure 3d, this rate $\approx 7 \times 10^{-6}$ cm/sec at 540C (1000F). Making the appropriate substitutions in equation (5), t = 0.003 sec. Since the average width of a subunit is 6×10^{-5} cm, on the Oblak–Hehemann mechanism the average interval of time elapsing between the nucleation of successive subunits is about 10 sec. Decarburization of a ferrite subunit whose growth has ceased is thus virtually instantaneous compared to the time between successive nucleation events.

Once decarburization has been completed, $x_\gamma^{\gamma\alpha}$ will begin to fall below its equilibrium value as the build-up of carbon in front of the austenite:ferrite boundary begins to dissipate into the surrounding austenite. We shall estimate the kinetics of decrease in $x_\gamma^{\gamma\alpha}$ on the basis of the assumption that the concentration-penetration curve of carbon in austenite at the instant decarburization of the ferrite is complete has a rectangular form rather than the approximately right triangular shape actually applicable. In the terminology of Crank[17], this is "an extended source of limited extent". At the austenite:ferrite boundary, Crank's relationship, as rewritten for $x_\gamma = 0$, reduces to:

$$(6)\quad (x_\gamma^{\gamma\alpha}) = (x_\gamma^{\gamma\alpha} - x_\gamma)\,\mathrm{erf}\,(h/2\sqrt{Dt}) + x_\gamma$$

where $(x_\gamma^{\gamma\alpha})$ = carbon concentration in austenite at the boundary in the situation of Figure Ic, i.e., when $x_\gamma < (x_\gamma^{\gamma\alpha}) < x_\gamma^{\gamma\alpha}$, and h = width of the "extended source". Since $s' = 1.8 \times 10^{-5}$ cm, we shall set $h = 10^{-5}$ cm in order to make the areas under the assumed and the actual concentration-penetration curves approximately equal. With t = 10 sec, $(x_\gamma^{\gamma\alpha}) = 0.022$. During the initial stage of its growth, the next subunit formed must thus transform to ferrite of the same composition as austenite whose carbon content has been increased by 10% relative to x_γ. When nine consecutive subunits have formed at this temperature, the carbon content (immediately in contact with the ferrite) which must be taken into solution in the growing ferrite, will exceed that of the higher of the two T_0 curves in Figure E. Assuming that subunits form on both sides of the initial one, a sheaf width of 1.1×10^{-3} cm can be attained before a decrease in the initial overall rate of thickening is required to make further transformation by this mechanism thermodynamically permissible. Carbide precipitation in austenite would serve the same purpose. The use of a silicon steel, however,

should avoid this complication. There is no evidence of a limiting size for bainite sheaves, though the point does not appear to have been specifically investigated. In order to apply properly this test of the Oblak–Hehemann mechanism, much more extensive data on the overall thickening kinetics of sheaves and the width of subunits are needed, particularly in a simple iron–carbon–silicon alloy in which the carbon content is close to or even above T_0 at some temperatures in the upper bainite range. For the present, we can only state that a thermodynamic barrier to the operation of this mechanism has been shown to develop increasingly with the successive nucleation of subunits, but that insufficient experimental data are available to ascertain whether or not the proposed mechanism is thermodynamically allowable. Even should the Oblak–Hehemann mechanism prove acceptable on this basis, however, the more critical test shortly to be described must be passed before it can be said with confidence that this is, in fact, *the* mechanism (among any number of other, equally permissible ones) which is actually operative.

The following is a summary of our views on the mechanism of formation of sheaves of upper bainite. On the basis of a general theory of morphology,[18] anisotropic precipitate shapes, such as plates, form because a substantial barrier to growth is present at one orientation of the interphase boundary. This theory has now received direct experimental support in several alloy systems. In particular, the rate of thickening of proeutectoid ferrite plates (formed, unfortunately for present purposes, at quite high reaction temperatures) has been shown to be significantly less than that allowed by the diffusion of carbon in austenite.[19] This theory should be equally applicable to the subunits comprising bainite sheaves, each of which is perhaps more usefully described as an individual ferrite plate. On this basis, individual plates should lengthen at rates approximately equal to those allowed by the diffusion of carbon in austenite. Thickening, on the other hand, should take place more slowly, and should cause $x_\gamma^{\gamma\alpha}$, and thus $x_\alpha^{\alpha\gamma}$ to fall below their metastable equilibrium values. Sheaves are considered to be assembled from individual plates by sympathetic nucleation—defined as the nucleation of a precipitate crystal at the interphase boundary of another crystal of the same phase when the composition of the precipitate differs from that of the matrix.[1] The low supersaturations under which sympathetic nucleation must normally take place require that the net interfacial free energy needed during nucleation be strictly minimized if a detectable rate of sympathetic nucleation is to be attained.[1] Since the energy of the interphase boundary enclosing a precipitate plate should be sharply orientation-dependent,[1,18] this accounts for the rather high degree of internal organization within sheaves, as may be seen from the authors' electron micrographs. Thickening and lengthening of an individual ferrite plate within a sheaf are taken to be interrupted by the sympathetic nucleation of new ferrite plates at the exposed broad faces and edges of the growing plate. On this basis, there is no need to hypothesize that a self-stopping mechanism halts the growth process. In order to have some supersaturation of the ferrite relative to the α/α + carbide phase boundary, and thus allow isothermal precipitation of carbides within ferrite, it is also unnecessary to postulate that growth takes place more rapidly than diffusion control allows. Calculations made on the basis of published X-ray data on the average carbon content of the retained austenite associated with bainite demonstrate that the average carbon content of bainitic ferrite lies in between the $\alpha/\alpha + \gamma$ and the α/α + carbide equilibrium curves,[4] in agreement with the deduction previously noted. Some carbide precipitation can thus take place within the ferrite.

As Oblak and Hehemann have indicated, at-temperature measurements of the growth kinetics of individual subunits by a high resolution technique such as thermionic emission microscopy would provide the vehicle for performing the necessary critical experiment. On their model, the individual subunits should both lengthen and thicken more rapidly than diffusion control would permit, while on our model thickening should proceed more slowly and lengthening at about the rate allowed by the diffusion of carbon in austenite. Unfortunately, the temperatures at which sheaves form lie appreciably below those at which a thermionic emission microscope is normally operable.[20] Efforts are being made to extend the temperature range available, however, and it is hoped that performance of the critical experiment will eventually become feasible. In the meantime, thermodynamic analyses should be of value in ascertaining whether or not the various mechanisms proposed for the formation of bainite are at least possible.

REFERENCES

1. H. I. Aaronson and C. Wells, Trans. AIME *206*. 1216 (1956)
2. C. Zener, Trans. AIME *167*. 550 (1946)
3. H. I. Aaronson, H. A. Domian and G. M. Pound, Trans. AIME *236*. 753 (1966)
4. H. I. Aaronson, to be published
5. H. I. Aaronson, H. A. Domian and G. M. Pound, Trans. AIME *236*. 768 (1966)
6. J. R. Lacher, Proc. Cambridge Phil. Soc. *33*. 518 (1937)
7. R. H. Fowler and E. A. Guggenheim, *Statistical Thermodynamics*, Macmillan, New York, 1939, p. 442 and preceding
8. C. Zener, Trans. AIME *203*. 619 (1955)
9. R. P. Smith, J. Am. Chem. Soc. *68*. 1163 (1946)
10. L. Kaufman, S. V. Radcliffe and M. Cohen, "Thermodynamics of the Bainite Reaction," *Decomposition of Austenite by Diffusional Processes*, edited by V. F. Zackay and H. I. Aaronson, Interscience, New York, 1962, 313
11. R. B. McLellan, Trans. AIME *233*. 1664 (1965)
12. T. Bell and W. S. Owen, Trans. AIME, in press
13. H. I. Aaronson and H. A. Domian, Trans. AIME *236*. 781 (1966)
14. R. F. Hehemann and A. R. Troiano, Metal Progr. *70*. (2). 97 (1956)
15. J. P. Sheehan, C. A. Julien and A. R. Troiano, Trans. ASM *41*. 1165 (1949)
16. A. Hultgren, Kgl. Svenska Vetenskapsakad. Handl. *4*. (3). 3 (1953)

17. J. Crank, *The Mathematics of Diffusion*, Oxford at the Clarendon Press, Oxford, 1957, pp 13-14
18. H. I. Aaronson, "The Proeutectoid Ferrite and the Proeutectoid Cementite Reactions," *Decomposition of Austenite by Diffusional Processes*, edited by V. F. Zackay and H. I. Aaronson, Interscience, New York, 1962, 387
19. K. R. Kinsman, E. Eichen and H. I. Aaronson, unpublished research
20. K. R. Kinsman and H. I. Aaronson, this symposium

AUTHOR'S REPLY. The thermodynamic and kinetic calculations of Drs. Kinsman and Aaronson should be of considerable aid in the evaluation of various models proposed for the bainite reaction. It is gratifying that the thermodynamic calculations indicate that the B_s temperatures for our steels do not exceed T_0. It is becoming increasingly clear, however, that austenite decomposes by more than one mechanism in the bainite range. Thus, as indicated by the discussers, the fact that B_s in hypereutectoid steels is above T_0 need not signify that the bainite in these high carbon steels forms by the same mechanism as that in the lower carbon steels. The problem in the high carbon steels often is complicated further by the precipitation of proeutectoid cementite so that the bainite may then form in an austenite of substantially reduced carbon content. Careful structural studies will be required to resolve these questions.

In their kinetic considerations, the discussers have focussed attention primarily on the thickening of bainite sheaves. It is perhaps worth noting that the incomplete nature of the bainite reaction provides indirect experimental evidence for the fact that bainite sheaves do attain limited thicknesses at temperatures near B_s. This limitation may arise from the thermodynamic barrier proposed in the discussion. However, continued holding should permit the accumulated carbon to be alleviated by diffusion into austenite and by carbide precipitation. Thus, it is not clear why thickening does not continue at least at a greatly reduced rate. The problem, we feel, is one involving nucleation and is intimately connected with relaxation of transformation strain.

Finally, with regard to lengthening, Drs. Kinsman and Aaronson propose that individual subunits grow at a rate controlled by diffusion of carbon in austenite and that their length is limited by sympathetic nucleation. Accordingly, the growth rate should not be less than that permitted by carbon diffusion. However, at least in alloy steels, bainite lengthens more slowly than that predicted for growth controlled by carbon diffusion. The experiments outlined by the discussers should decide whether the individual subunits grow at a rate dictated by carbon diffusion or whether they grow rapidly to some limiting size.

Influence of Molybdenum and Manganese on the Kinetics of the Proeutectoid Ferrite Reaction

K. R. KINSMAN and H. I. AARONSON
Metallurgy Department
Scientific Laboratory
Ford Motor Company
Dearborn, Michigan

INTRODUCTION

Understanding the mechanisms through which alloying elements influence the kinetics of the decomposition of austenite is both an old problem and an important one. Of the several diffusional reactions by which austenite can decompose — proeutectoid ferrite, proeutectoid cementite, pearlite and bainite — the proeutectoid ferrite reaction is industrially the most important. This is the first transformation to occur over wide ranges of temperature and composition in most steels produced in large quantities. The kinetics of this reaction thus determine the hardenability of these steels, and at lower cooling rates play a major role in establishing their mechanical properties. The proeutectoid ferrite reaction is also the simplest from the viewpoint of ascertaining the effects of alloying elements upon the fundamental quantities determining the kinetics of a diffusional transformation, namely, the rates of nucleation and the rates of growth.[1]* The present study deals primarily with the influence of alloying elements upon the isothermal growth kinetics of proeutectoid ferrite, though nucleation rates were calculated by an indirect method. It is anticipated that future investigations in this laboratory will extend these studies to direct measurements of the rates of nucleation.

Although the morphologies of proeutectoid ferrite are complex, they have been documented in detail.[2] These complexities are evidently caused primarily by the presence of a sessile dislocation structure at certain orientations of the austenite:ferrite boundaries.[2] Such structures change the mechanism, significantly reduce the kinetics and substantially alter the morphology of growth.[2,3] The interpretative complications thus introduced can be largely avoided by confining kinetic studies to measurements of the thickening rates of grain boundary allotriomorphs — crystals which nucleate at the grain boundaries in the matrix phase and grow preferentially and more or less smoothly along them.[2,4] These crystals are usually enclosed by austenite:ferrite boundaries whose structure is largely of the disordered or incoherent type, and thus offers no barrier to the growth process.[2] An allotriomorph is sketched in idealized form in Figure 1a; arrowheads indicate the directions in which thickening takes place. Examples of typical allotriomorphs are shown in Figures 1b and 1c. In the case of Figure 1c, a growth barrier has clearly inhibited thickening in one direction. In this situation, measurement of thickening kinetics was restricted to the other face of the allotriomorph, whose growth kinetics did not appear to be so affected. In the absence of a barrier to growth, the thickening of a ferrite allotriomorph can be modeled mathematically as a planar austenite:ferrite boundary whose migration kinetics are controlled by the diffusion of carbon in austenite. This theoretical problem is straightforward in principle and has been solved for a concentration-independent diffusivity by Dubé[5,6] and by Zener.[7] The well-known variation of the diffusivity of carbon in austenite with carbon content[8] can be reasonably taken into account by means of an approximation due to Wagner.[9] The inclusion of an iron–carbon alloy in the present study will enable us to demonstrate that the correspondence between the growth process measured experimentally and the theoretical model is quite satisfac-

*See references.

tory, in confirmation of a conclusion which had been previously drawn on the basis of less complete[2] and of less directly applicable[10] experimental evidence.

The role played by alloying elements in determining the rate of movement of a planar austenite:ferrite boundary with a disordered structure has been considered theoretically by Kirkaldy and co-workers[11,13] and by Aaronson, Domian and Pound.[14] Both groups of investigators concluded that the composition of the austenite in contact with the boundary is the paramount factor affecting growth kinetics. Electron probe analysis has shown that below a characteristic critical temperature the proportion of alloying element in proeutectoid ferrite is the same as that in the parent austenite;[1,13] no partition of the alloying element takes place between the two phases under this condition. In the Fe–C–X alloys (where X is any substitutional alloying element) investigated by Aaronson and Domian,[1] this temperature was experimentally indistinguishable from the equilibrium Ae_3, or $\gamma/\alpha + \gamma$ temperature, and thus partition was not observed, when X = silicon, cobalt, molybdenum, aluminum, chromium or copper.[1] However, the characteristic critical temperature lies an increasingly wide temperature interval below the equilibrium Ae_3 when X = platinum,[1] nickel[1] and manganese.[1,13] In this investigation, attention was

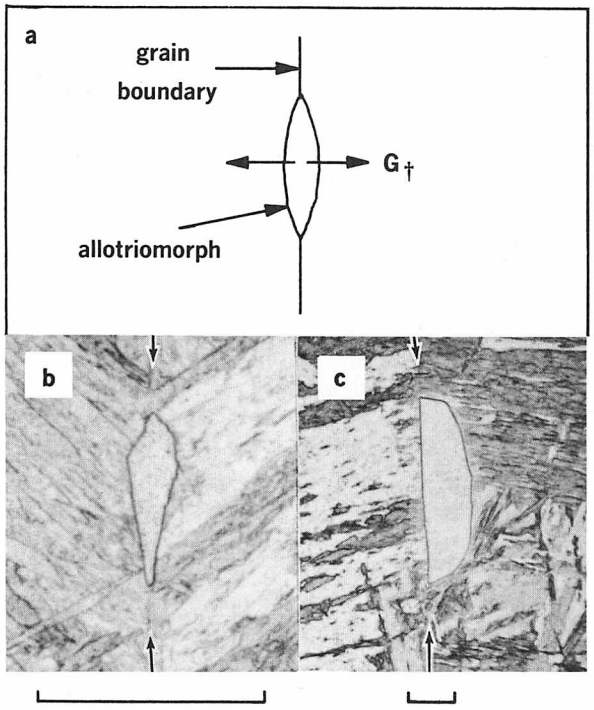

FIGURE 1. (a) Grain boundary allotriomorph in idealized form; (b) and (c) are micrographs of typical allotriomorphs experimentally encountered (Fe–0.12% C–2.98% Cu reacted at 750 C (1380 F) for 1000 sec). In (b) thickening has occurred equally into both austenite grains, in (c) a growth barrier has inhibited growth into one austenite grain. Magnification bars indicate 0.03 mm

confined to the temperature–composition region in which partition was absent. In order to define the carbon content of the austenite in contact with the austenite:ferrite boundary under this circumstance, Aaronson, Domian and Pound proposed the concept of the "no-partition Ae_3" and the "no-partition $\alpha/\alpha + \gamma$" metastable equilibrium curves. The carbon contents of the austenite and the ferrite at the boundary are considered to adjust to values (both less than those of the equilibrium Ae_3 and $\alpha/\alpha + \gamma$ curves) at which the partial molar free energies of carbon in the two phases, and also of the Fe–X substitutional base, are equal at the boundary. The resultant metastable equilibrium is maintained until the alloying element eventually begins to partition toward its equilibrium distribution between austenite and ferrite. The no-partition Ae_3 was identified with the experimentally determined characteristic critical temperature. In contrast, Kirkaldy et al suggested that the equilibrium Ae_3 and $\alpha/\alpha + \gamma$ compositions of all three elements are maintained at disordered austenite:ferrite boundaries even in the absence of "macroscopic" partition (as demonstrated by electron probe analysis). This suggestion, however, is open to serious theoretical objections;[1] only the no-partition curve concept was therefore utilized in this present study.

On the basis of this concept, a qualitative theory of the effects of alloying elements upon the rates of nucleation and of growth of proeutectoid ferrite has been proposed.[1,14] Those elements which raise the no-partition Ae_3 of an Fe–C–X alloy to temperatures higher than that of the equilibrium Ae_3 of an Fe–C alloy of the same carbon content should increase both rates by increasing the volume free energy change driving the nucleation process and the concentration gradient which provides the driving force for growth. Cobalt, aluminum and silicon are in this category, and are found[1] to displace the TTT-curves for the initiation of the proeutectoid ferrite reaction to shorter times, in agreement with the theory. Nickel, and especially manganese, lower the equilibrium Ae_3 and reduce still further the temperature level of the no-partition Ae_3; these elements should therefore decrease the nucleation and growth rates of ferrite, again in qualitative accord with TTT-diagram data.[1] On this basis, however, the behavior of molybdenum is anomalous. Although molybdenum effects only small changes in the location of the no-partition Ae_3 relative to the equilibrium Ae_3 of iron–carbon alloys, it is evidently even more effective than manganese in decreasing the rates of formation of proeutectoid ferrite. Since molybdenum should thus have little influence upon rates of growth, it was concluded that this element exerts its great effects upon hardenability almost entirely by reducing the rate of nucleation; this reduction was suggested to be produced by an increase in the net interfacial free energy required to form a ferrite

nucleus.[1,14]

This investigation was undertaken to test the principal growth aspects of this theory. An Fe–0.5 a/o C alloy was chosen to provide the reference standard. Fe–0.5 a/o C–1.0 a/o Mn was selected to test the prediction that manganese appreciably reduces rates of growth at a given reaction temperature relative to those of the iron–carbon alloy; manganese was chosen instead of nickel in order to maximize the effect obtained. An Fe–0.5 a/o C–1.0 a/o Mo alloy was included to ascertain whether or not molybdenum actually is ineffective in changing rates of growth. If the growth kinetics data on iron–carbon–manganese can be quantitatively accounted for in terms of the no-partition Ae_3 curve, the predictions made with respect to the effects of the other alloying elements (molybdenum excepted) on growth kinetics may then be viewed more favorably, and analogous effects should be expected in future studies of nucleation kinetics. If an equivalent accounting can be made of growth kinetics in iron–carbon–molybdenum, good support would be provided for the deduction that the influence of this element upon hardenability can be explained entirely upon the basis of its effects upon nucleation kinetics.

EXPERIMENTAL METHODS AND PROCEDURES

The three alloys used in this investigation were vacuum melted, and then vacuum cast into ingots about 3 in. in diameter. Their compositions are given in Table I. The two Fe–C–X alloys were redundantly worked by forge pressing, then rolled into bars 1¼ by 1¼ in. in cross-section; the Fe–C ingot was simply rolled directly into this form. Blocks 1 by 1 in. in cross-section were machined from the centers of these bars. The blocks of Fe–C–X alloy were homogenized for three days at 1300 C (2370 F), using a technique previously described.[1] Although the changes in carbon content during the homogenization anneals were less than ± 0.1 a/o, the carbon contents of the Fe–C–X alloys recorded in Table I are those determined after these anneals.

The TTT-diagrams for the alloys were determined and supplementary studies were performed by means of the conventional isothermal transformation technique. Specimens ¼ by 1/32 in. were austenitized for 15 min at 1300 C (2370 F) in an argon-protected salt bath[15] and isothermally reacted in lead baths covered with powdered graphite. Both salt and lead baths were continuously deoxidized by immersed graphite rods. The austenite grain size produced by 15 min at 1300 C (2370 F) was ASTM no. 1 to 2 in the Fe–C alloy and no. 1 to –3 in the Fe–C–X alloys.

Measurement of the thickening kinetics of the grain boundary allotriomorphs, on the other hand, presented a special problem which could not be effectively dealt with by means of the conventional technique. Suppose a series of specimens were to be isothermally reacted for successively increasing times at a given temperature. If the allotriomorph with the largest apparent thickness in each were sought as a basis for determining the growth kinetics, the random angles made by the planes of polish with respect to the average interfacial planes of the allotriomorphs would make the results virtually meaningless. Since allotriomorphs usually do not thicken much, and most of the thickening which does take place occurs quickly, additional and quite stringent requirements are imposed with respect to the accuracy of any alternative experimental method used to make these measurements. Some form of high temperature metallography which permits thickening to be observed continuously while the transformation is taking place should be able to provide a solution to both the sectioning angle and the accuracy problems. Since allotriomorphs do not appear to exhibit sharply angled surface relief effects[16] — a point which was confirmed in this study — hot stage optical microscopy cannot provide the accuracy of measurement required. Thermionic emission microscopy, on the other hand, a technique which yields a higher resolution than optical microscopy[17,18] and does not depend upon surface relief for satisfactory operation, has been found to be eminently suitable for this purpose.

The thermionic emission microscope used in this investigation was designed and constructed by Dr. Erwin Eichen and his associates.[19,20] Although detailed descriptions are available of this instrument in particular[19,20] and of the technique of thermionic emission microscopy in general,[17,18] a brief summary of the principles of this still quite unfamiliar form of microscopy appears to be in order in the present context. Thermionic emission microscopy is based upon the variation of the work function with the crystallographic orientation exposed at the surface of a flat specimen. Electron emission is stimulated by

Table I Chemical Analysis of Alloys*

	%C	%Mn	%Mo	%Si	%P	%S	%Ni	N**	O**
Fe–C	0.11	0.01	0.02	0.01	0.004	0.005	0.02	0.2	12
Fe–C–Mn	0.11	1.01	0.02	0.01	0.004	0.009	0.02	0.4	18
Fe–C–Mo	0.11	0.01	1.95	0.01	0.003	0.005	0.02	0.7	15

*Weight percent except for nitrogen and oxygen.
**Ppm.

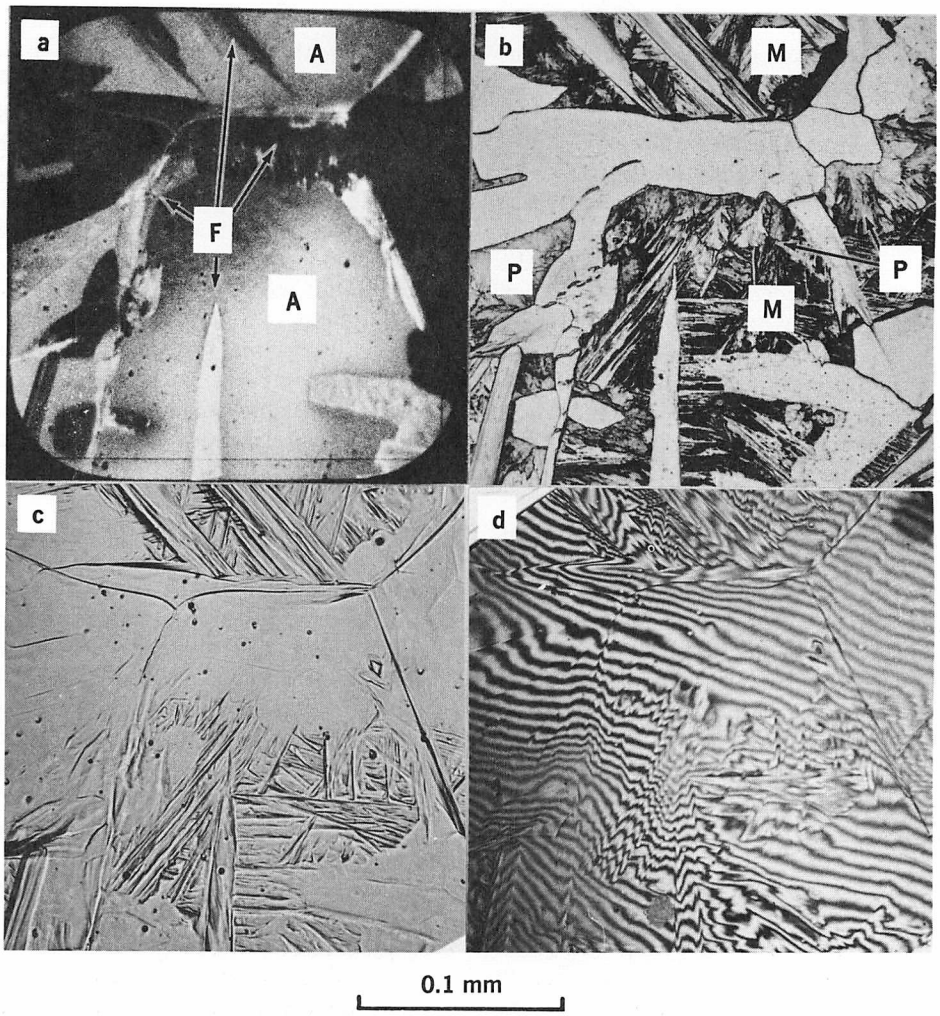

FIGURE 2. Comparative micrographs of a single area of an Fe–0.2% C alloy partially transformed to ferrite at 720 C (1330 F): (a) is a thermionic emission micrograph taken an instant before the specimen was quenched, (c) is the appearance of the free surface after quenching and (d) is an interferogram of that surface. Light polishing and etching (b) reveal good correspondence between the quenched microstructure and that at the reaction temperature. The constituent phases are ferrite (F) and austenite (A) at the reaction temperature (a), and ferrite (F), pearlite (P) and martensite (M) in the quenched specimen — (b), (c) and (d)

heating the specimen, by lightly covering its surface with an "activator" — a substance insoluble in the substrate which reduces the work function (barium was employed in this investigation) — and by applying a high voltage (15/45 kV) to the specimen. The electrons thus emitted are focussed onto a fluorescent screen, providing a readily interpretable metallographic-type image as illustrated by Figure 2a. Figure 2b is an optical micrograph of the same area taken after polishing and etching in 2% nital. As a result of polishing, the location of the surfaces from which these two photographs were taken is slightly different. When allowance is made for this difference, good correspondence is found between the thermionic emission and the optical microscope images. By its nature, this technique provides a method for observing transformations continuously while they are actually occurring at elevated temperatures. The use of barium as an activator placed, in fact, a lower temperature limit of about 725 C (1335 F) on the observations made on the iron–carbon and iron–carbon–molybdenum alloys; in the iron–carbon–manganese alloy, it was fortunately practicable to extend the observations down to 620 C (1150 F). One of the unique advantages of the instrument of Eichen et al is that the thermocouple, in contact with the specimen, and associated temperature measuring circuitry are isolated at the potential of the specimen, thereby permitting small fractions of a millivolt to be measured despite the presence of a specimen potential of many kilovolts.[20] Using the transformation temperature in pure iron and the Ae_1 and Ae_3 temperatures in high-purity iron–carbon alloys for calibration, this temperature measurement system has been found to be accurate to within ± 2 C (3.6 F), rather than ± 5 C (9 F) as originally reported.[17]

To prepare specimens for the thermionic emission microscope, slices 0.025 in. thick were cut from the 1 by 1 in. blocks. Since this was the smallest thickness conveniently and reproducibly obtainable in this manner, further reduction, to 0.013 in., was accomplished by cold rolling; subsequent metallographic polishing gave a final thickness of about 0.010 in. Normally a recrystallization anneal is given thermionic emission specimens so that they may be bent at the edges in order to fit securely onto the heating element of the microscope. In this investigation, a recrystallization anneal was avoided in order to prevent changes in carbon content. The specimens were therefore spot welded onto annealed backing plates made from the same alloy, and, as illustrated in Figure 3, the backing plates were bent to fit onto the heating stage.

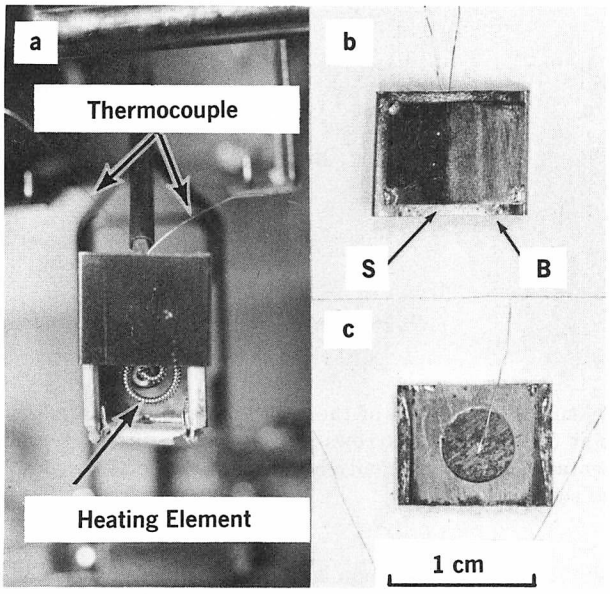

FIGURE 3. Usual thermionic emission specimen on the microscope heating stage, shown in a raised position to reveal the heating element. The spot welded configuration of specimen (S) and backing plate (B) used in this investigation is shown in (b) front view and (c) rear view

With the exception noted below, all heat treatments for the growth rate studies were conducted within the thermionic emission microscope. The normal operating vacua were 2×10^{-7} torr at room temperature and at the reaction temperature, and about 10^{-6} torr at 1300 C (2370 F). Since a vac-ion rather than an oil diffusion pump is used in this instrument, the latter pressure proved sufficient to avoid entirely either carburization or decarburization during these treatments. This was demonstrated experimentally: the carbon content of a specimen heat treated in the microscope was identical to that of a specimen of the same alloy which had not been so treated, and the Ae_3 temperatures of the alloys determined in the microscope were the same as those determined by means of the salt and lead baths. Austenitizing treatments were conducted at 1300 C (2370 F), the iron–carbon and iron–carbon–manganese alloys being held for 15 min at this temperature and the iron–carbon–molybdenum alloy for five minutes. The onset of thermal faceting was responsible for the shorter austenitizing time used for the latter alloy. The temperature of the specimens was then

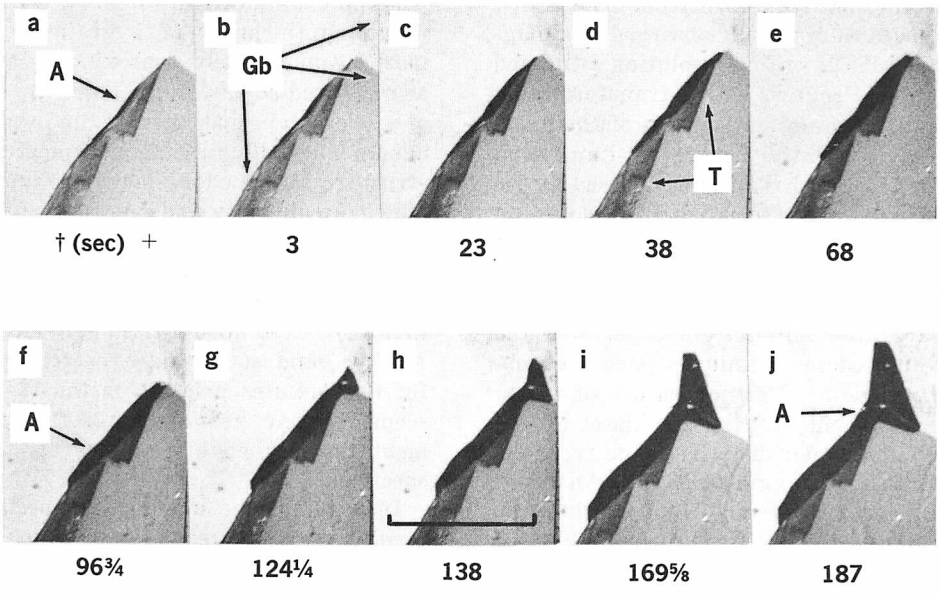

FIGURE 4. Selected ciné pictures of a ferrite allotriomorph, taken as it grew in the iron–carbon–molybdenum alloy at 830 C (1525 F). The allotriomorph (A) is black. The grain boundary along which it initially formed is labelled Gb. Cumulative time in seconds is indicated below each frame. A stepped austenite twin boundary is indicated in (d). The bar in (h) represents 0.1 mm

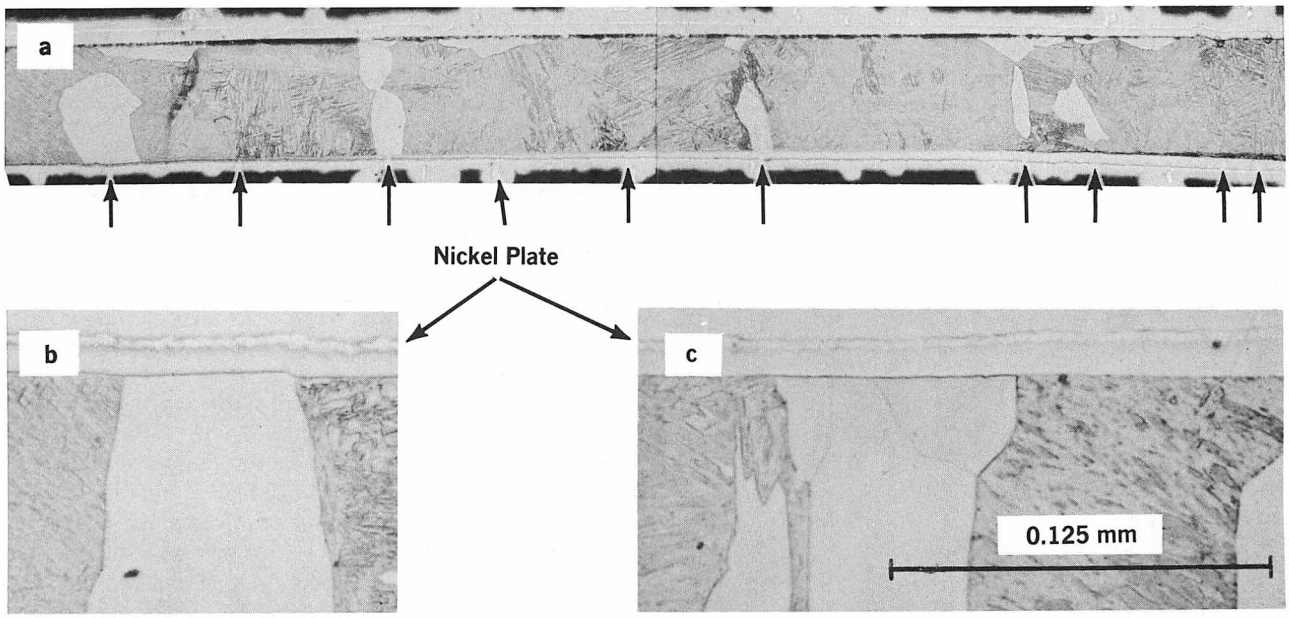

FIGURE 5. A partially transformed and quenched thermionic emission specimen of the Fe–C–Mo alloy, nickel plated to preserve the edge. The bamboo grain structure is apparent at 50 X in (a) — arrows indicate the position of prior austenite grain boundaries. (b) and (c), at 400 X, are representative of the normally high angle of incidence of the allotriomorph–austenite (martensite) interface with the free surface

lowered to about 15/30 C (27/54 F) above the Ae_3 (i.e., to 900 C (1650 F) for the iron–carbon alloy, 840 C (1545 F) for the iron–carbon–manganese and 930 C (1705 F) for the iron–carbon–molybdenum) and barium was evaporated onto their surfaces. The time spent at this temperature varied from eight to ten minutes. Upon completion of the activation process, the specimen was quickly lowered to that intended for isothermal transformation. The transformation processes were usually observed at a magnification of about 350 X, with a resolution estimated to be about 1000 Å. Progress of the transformation was recorded by taking motion pictures of the fluorescent screen, using a Pathé camera with an f 0.95 lens and 16 mm Linograph Pan film, exposed at the rate of eight frames per second and developed to an ASA speed of 900. Figure 4, portraying the growth of a ferrite allotriomorph in the iron–carbon–molybdenum alloy at 830 C (1525 F) over a period of about three minutes, demonstrates the clarity with which these techniques permitted observations to be made at the temperature of transformation. Measurements of the thickness of the grain boundary allotriomorphs were made from the motion picture films. A Vanguard Motion Analyzer, with an accuracy of measurement of 0.001 in., was used for this purpose at a film magnification of 11.8 X. Measurements were made normal to the advancing austenite:ferrite boundaries, using the position originally occupied by the austenite grain boundary as the origin. Isothermal reaction temperatures employed ranged from 810/730 C (1490/1345 F) in the iron–carbon alloy, 875/725 C (1605/1335 F) in the iron–carbon–molybdenum alloy and 800/620 C (1470/1150 F) in the iron–carbon–manganese alloy.

The high temperature used for the austenitizing treatments was dictated in part by the need to grow the austenite grains entirely through the specimens, so that the grain boundaries would be approximately perpendicular to their surfaces. In this manner, the measured thickness of a grain boundary allotriomorph would closely approximate its true thickness as measured normal to the boundary. A cross-section of a microscope specimen of the iron–carbon–molybdenum alloy, illustrating a typical austenite grain structure developed, is shown in Figure 5a. Considerably more difficulty was experienced in obtaining this type of structure in the iron–carbon alloy. Therefore this material had to be given a preliminary heat treatment in the salt and lead baths. Specimens of this alloy were austenitized for one hour at 1300 C (2370 F) and isothermally reacted at 700 C (1290 F) for five minutes prior to installation in the microscope. The Ae_3 test indicated that this heat treatment did not change the carbon content of the specimens.

In a number of instances a specimen was transformed several times, with re-austenitizing being accomplished by re-heating only to the activation temperature for another application of barium. Repeated cycling produced no detectable effect upon either the morphology or the rate of growth of ferrite.

A fair degree of selectivity had to be exerted in order to confine the measurements to allotriomorphs which seemed likely to match in reasonable fashion the model used in the analysis of the data, i.e., planar boundaries moving at diffusion-controlled rates. A number of morphological configurations were thus avoided. Such structures included those in which an interface barrier to growth was clearly operative: the growth of the allotriomorph followed an irregular path, extensive growth appeared to be taking place from the interior toward the surface of the specimen, and the evolution of either sawteeth or sideplates took place from the allotriomorphs during an early stage of growth.

When events occurring in three dimensions are followed by observing their traces on a free surface, two types of special precaution must be taken. First it is necessary to be certain that the surface per se is not affecting these events. For example, surface diffusion might accelerate the growth of ferrite; or by analogy to grain growth, thermal grooving and/or other surface effects might retard growth. To test these hypotheses, perpendicular sections were taken through several specimens which had been partially transformed and then quenched to room temperature in the microscope with a stream of purified helium. Two such sections are shown as Figures 5b and c. Note that while the ferrite is not always exactly perpendicular to the free surface, there is no evidence for particularly rapid or retarded growth at this surface. These micrographs are representative, and lead to the conclusion that the surface does not affect the transformation. The second general matter for concern is whether or not the surface is giving a representative cross-section through the three-dimensional microstructures. The deliberate formation of a "bamboo grain structure" in the austenite (Figure 5a) adequately resolved this problem, though the inevitable moderate deviations of the grain boundaries from perpendicularity with respect to the surface are doubtless responsible for at least some of the scatter obtained in the experimental data. In the particular case of thermionic emission microscopy, one must also be certain that the activator on the surface of the specimen remains completely passive with respect to the reaction studied. Past and current experience[3, 17, 18] confirms that this is so for barium, the activator used in this investigation.

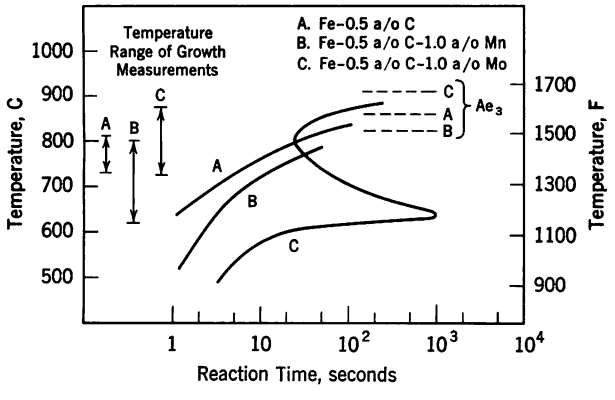

FIGURE 6. Superposition of the isothermal transformation diagrams determined for the three alloys investigated. Temperature ranges of the growth measurements are indicated

A brief supplementary study of the three alloys was made by means of transmission electron microscopy. Samples of each were rolled to a thickness of 0.006 in. and heat treated in the manner employed for the TTT-curve determinations. The specimens were quenched after they had been partially transformed to proeutectoid ferrite, and thinned in a solution consisting of nine parts glacial acetic acid and one part perchloric acid. They were observed in a Phillips EM 200 electron microscope fitted with a tilt-rotation stage and operated at 100 kV.

RESULTS

Figure 6 shows, in superimposed fashion, the TTT-curves for the initiation of transformation in the three alloys studied. The experimentally determined Ae_3 temperatures and the temperature ranges in which the kinetic measurements were made are also included.

During the diffusion-controlled migration of a planar interphase boundary, the position of the boundary, s, should vary with growth time, t, as [5-7]:

$$s = \alpha t^{1/2} \qquad (1)$$

where α is termed the parabolic rate constant. Figures 7a-c contain representative plots of the position of the broad faces of allotriomorphs as a function of $t^{1/2}$ for each of the three alloys studied. All of these plots are seen to be quite satisfactorily linear. Particular attention is called to Figure 7c, in which this result also obtains when the iron–carbon–molybdenum alloy was reacted at temperatures below and at the 800 C (1470 F) nose of the TTT-diagram (Figure 6) as well as above this temperature. Since the thermionic emission microscope permitted the growth time of the allotriomorphs to be determined rather than merely the total isothermal reaction time, these plots should pass through the origin. Within the quite low limits of experimental error, all of the plots behave in just this manner.

From the slopes of the s vs $t^{1/2}$ plots, α was evaluated. Figures 8a-c are plots of α vs reaction temperature for the three alloys. The considerable scatter in these plots is certainly real in the sense that, as typified by Figure 7, the uncertainty in each individual value of α is much less than the differences among the various values obtained at each

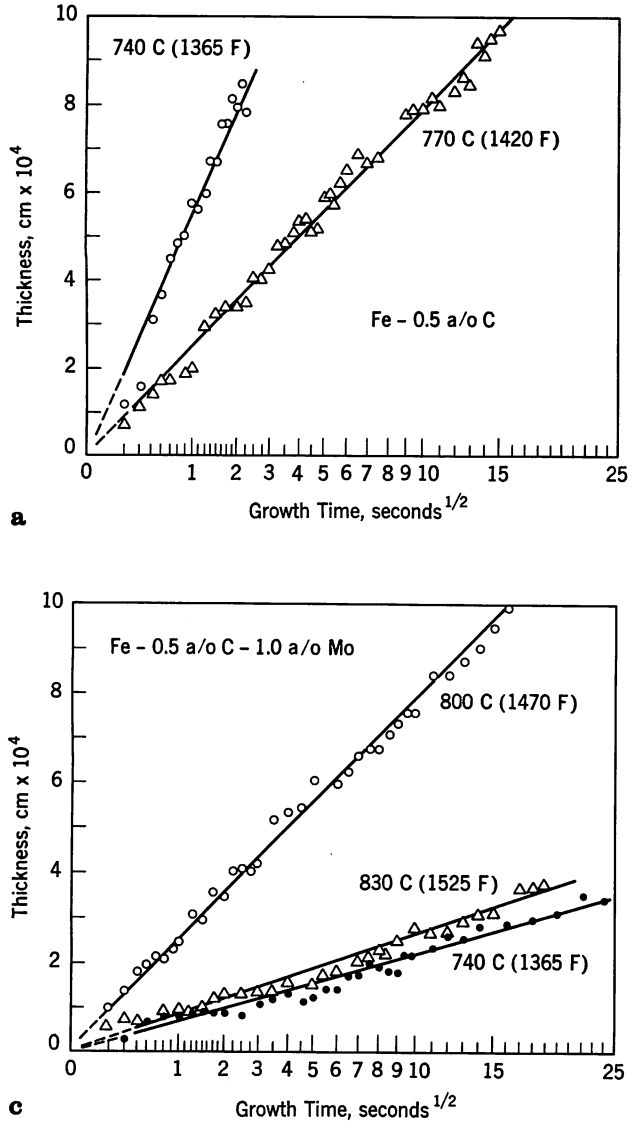

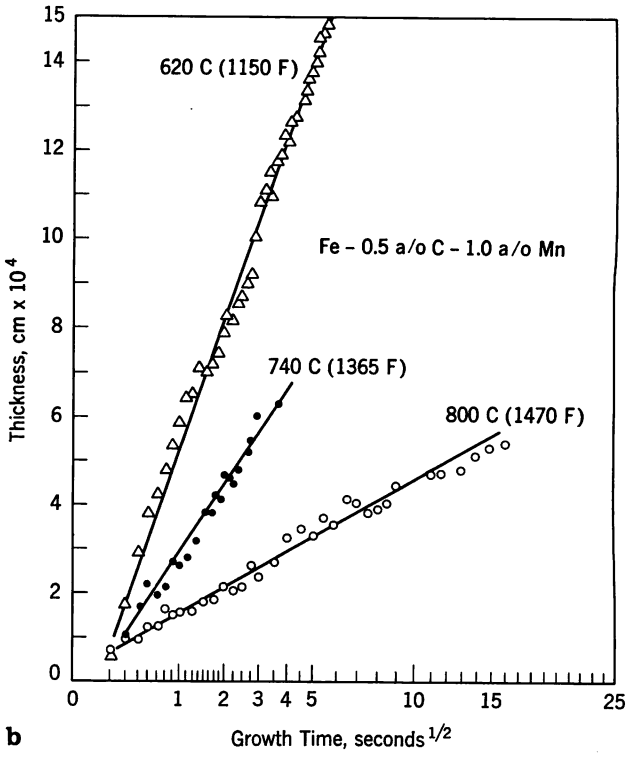

FIGURE 7. Plots of allotriomorph thickness, measured from the austenite grain boundary to the ferrite:austenite interface along a fiducial line, as a function of growth time at representative temperatures in each of the alloys investigated: (a) iron–carbon, (b) iron–carbon–manganese, (c) iron–carbon–molybdenum

temperature. The previously mentioned sectioning problem is probably responsible for a portion of this scatter. Irregularities in the thickening process occasioned by the development of small areas of dislocation facet which serve as a local barrier to growth, however, are considered to be an important source of the differences obtained. The proportional area occupied by such facets and their orientation should depend upon the orientation of the grain boundary with respect to the habit plane of the nuclei of the allotriomorphs, and will thus be different from one grain boundary to the next. This is thus a residual, and unavoidable effect of crystallography upon the thickening of allotriomorphs.

In order to be certain that most of the interphase boundaries enclosing the ferrite allotriomorphs have largely disordered structures, a specimen partially transformed in the microscope was rapidly quenched to room temperature with a stream of purified helium. Figure 2c and 2d (showing the same area as Figures 2a and 2b) indicate by means of optical and interference microscopy, respectively, that both Widmanstätten ferrite and martensite plates exhibit geometric relief effects,[21] but that ferrite allotriomorphs do not.

A comparison of representative electron microstructures of the alloys investigated is provided by Figure 9. As shown in Figures 9a-c, there is no distinguishing feature of the ferrite:austenite (martensite) interface which sets apart any one of the alloys from the other two. In particular, there are similar concentrations of particles in all three ferrite matrices. A common feature is that much of the plastic strain associated with transformation of the remaining austenite to martensite (M) by quenching is accommodated by the generation of dislocations in the ferrite (F) adjacent to the interphase boundary. This is particularly clear in Figure 9b for the ferrite in the neighborhood of the ends of the martensite laths. Ferrite well behind the ferrite: martensite interfaces contains a relatively low dislocation density, as would be expected at the isothermal reaction temperatures used. Plastic strains accompanying the formation of ferrite are normally relieved at the reaction temperature by strain-induced migration of ferrite grain boundaries —.this

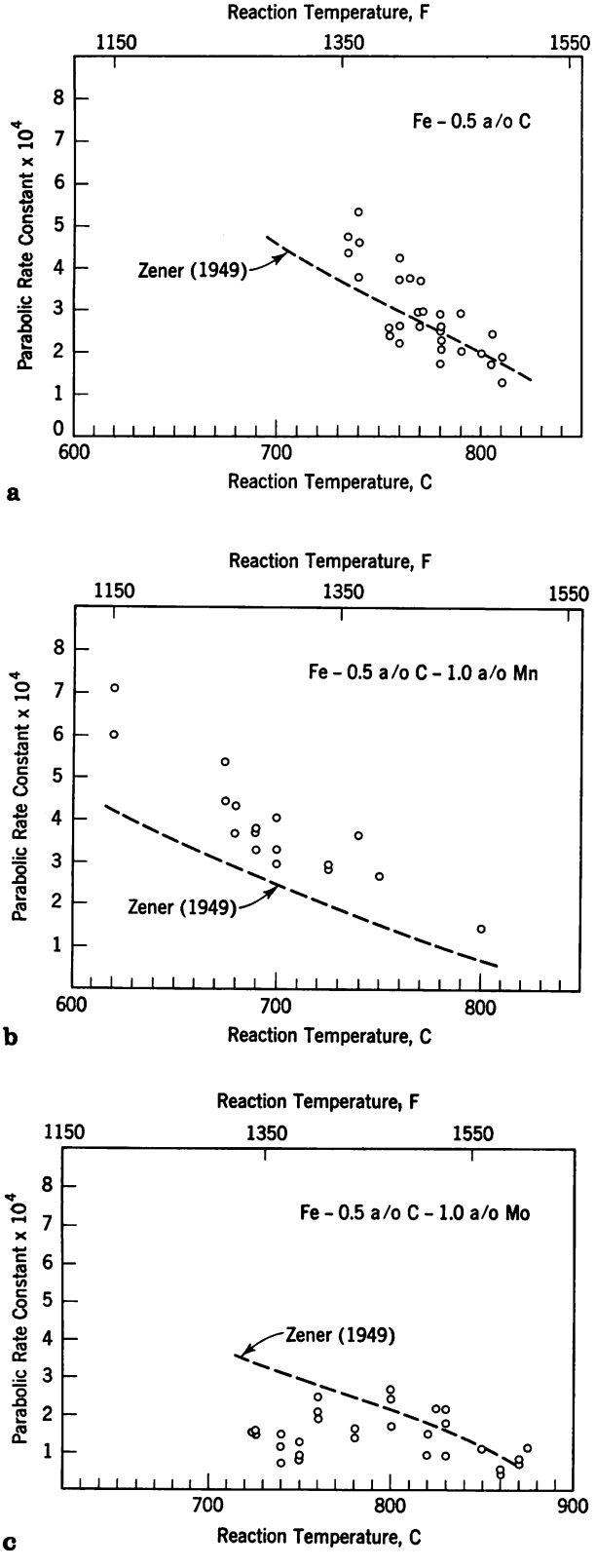

FIGURE 8. Plots of the experimentally determined parabolic rate constant, α, as a function of reaction temperature for the alloys investigated: (a) iron–carbon, (b) iron–carbon–manganese, (c) iron–carbon–molybdenum. Dashed lines indicate α calculated from equation (2)

was observed directly by thermionic emission microscopy — and by the formation of subgrains, as depicted in Figures 9d, e and h. Subgrain boundaries, a common site for precipitation, were found to be relatively clean in all of the alloys, though occasionally carbides were found at them, as at the boundary designated by the arrow in Figure 9g. Tiny carbides, perhaps formed during the quench, are evident in all of the micrographs, and are usually associated with dislocations. (The mottled etching effect in Figure 9g gives a false impression of a high carbide density.)

DISCUSSION

TTT-Diagrams

Figure 6 shows that the TTT-curve for the initiation of transformation in the iron–carbon–manganese alloy lies at significantly longer times than that for the iron–carbon alloy. On the other hand, at temperatures above 800 C (1470 F), the TTT-curve for the iron–carbon–molybdenum alloy is displaced to shorter times relative to the iron–carbon curve. The equilibrium Ae_3 curve for iron–carbon is plotted in Figure 10 together with the no-partition Ae_3 curves for iron–carbon–manganese and iron–carbon–molybdenum of the alloy contents used in this investigation. These curves were calculated as described by Aaronson, Domian and Pound.[14] At the 0.5 a/o C level, the displacement of the no-partition Ae_3 for iron–carbon–molybdenum to a higher temperature and that of iron–carbon–manganese to a lower temperature correctly predict, on the theory of Aaronson, Domian and Pound, the displacements in time noted in the TTT-curves for these alloys.

At temperatures below 800 C (1470 F), on the other hand, the iron–carbon–molybdenum alloy exhibits an entirely different kind of behavior. TTT-curves determined for several Fe–C–X alloys which raise the no-partition Ae_3 temperature[1] suggest that the curve for the iron–carbon–molybdenum alloy also ought to have but one "nose," and that this nose should lie in the range 600/700 C (1110/1290 F). Instead, a rather deep bay centered at about 650 C (1200 F) appears within this range, producing a "premature" nose at 800 C (1470 F), and presumably another one at some temperature below 500 C (930 F). Figure 6 clearly indicates that the formation of the bay plays a major role in the remarkably potent effect which molybdenum exerts upon transformation kinetics. The data of this figure suggest that were it not for the truncation by the bay of the normally expected TTT-curve, molybdenum would act in the manner of cobalt, aluminum and silicon, displacing the TTT-curve to shorter times than in an iron–carbon alloy of the same carbon content, and thus decreasing, rather than markedly increasing the hardenability of steel.

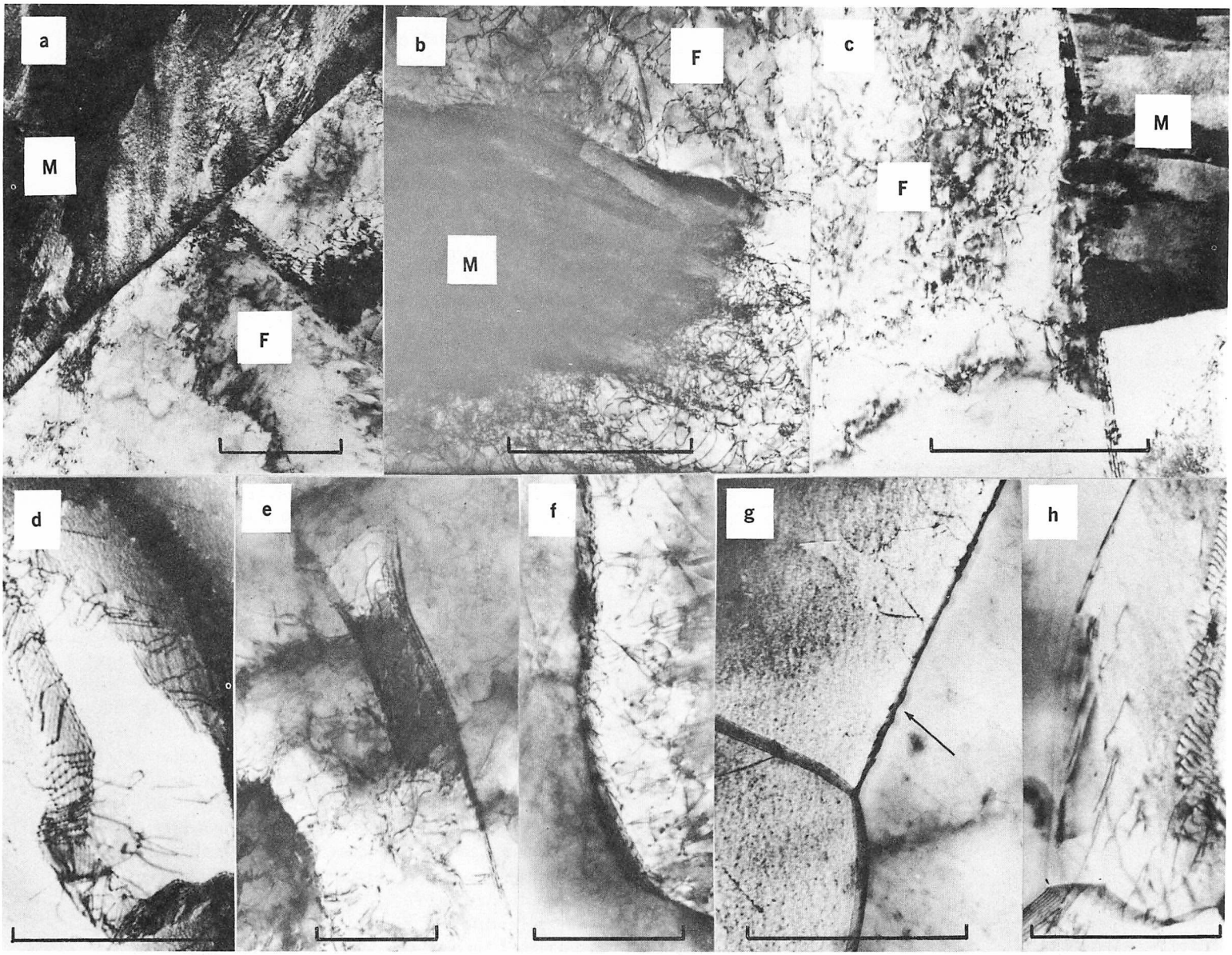

FIGURE 9. Transmission electron micrographs of specimens austenitized for 15 min at 1300 C (2370 F) and isothermally reacted as follows: (a) and (d) — iron–carbon alloy, reacted 15 sec at 700 C (1290 F); (b), (e) and (f) — iron–carbon–manganese alloy, reacted 20 sec at 650 C (1200 F); (c), (g) and (h) — iron–carbon–molybdenum alloy, reacted 150 sec at 750 C (1380 F). Ferrite (F) and martensite (M) are labelled in (a), (b) and (c). Only ferrite is present in (d) through (h). The bar in each figure represents 1μ

Allotriomorph Thickening Kinetics

On the Dubé[5,6]-Zener[7] analysis, the constant α in equation (1) is determined by trial and error from the following transcendental equation:

$$\frac{2(x_\gamma^{\gamma\alpha} - x_\gamma)}{x_\gamma^{\gamma\alpha} - x_\alpha^{\alpha\gamma}} \sqrt{\frac{D}{\pi}} = \alpha \, e^{\alpha^2/4\,D} \left[1 - \operatorname{erf}\left(\frac{\alpha}{2\sqrt{D}} \right) \right] \quad (2)$$

where $x_\gamma^{\gamma\alpha}$ = mole fraction of carbon in austenite corresponding to the no-partition Ae_3 curve (Figure 10), $x_\alpha^{\alpha\gamma}$ = mole fraction of carbon in ferrite at the no-partition $\alpha/\alpha + \gamma$ curve (calculated as in reference (14)), x_γ = mole fraction of carbon in the untransformed austenite and D = diffusivity of carbon in austenite. Following the Wagner approximation,[9] the value of D corresponding to $x_\gamma^{\gamma\alpha}$ is employed. The data of Wells, Batz and Mehl[8] indicate that the amount of manganese present in the iron–carbon–manganese alloy has an insignificant effect on D. The results of Ham[22] suggest that molybdenum may

increase D, but the effect is incompletely defined and is also likely to be small. The data on D in iron–carbon alloys reported by Wells, Batz and Mehl[8] and correlated empirically by Kaufman, Radcliffe and Cohen[23] are therefore used for all three alloys.

The plots of α vs temperature computed from equation (2) are superimposed on Figures 8a-c. Referring first to Figure 8a, for the iron–carbon alloy, the calculated curve is seen to fall largely within the scatter band of the experimental data, though tending to be a trifle low at the lower temperatures. This rather small discrepancy probably results from the failure of equation (2) to take proper account of the increase in D with carbon content even when the Wagner approximation is utilized, since under this circumstance α becomes larger as the difference between $x_\gamma^{\gamma\alpha}$ and x_γ increases.[24, 25] The overall agreement between the calculated and measured values of α can be considered to be very good, however, and to permit the conclusion to be drawn that the thickening of ferrite allotriomorphs is controlled by the diffusion of carbon in austenite. The evidence provided by Figure 8a for this conclusion is substantially better than that previously available.[2]

Figure 8b shows that essentially the same situation obtains in the iron–carbon–manganese alloy. Here the calculated values lie somewhat below those measured experimentally. Consideration of possible error in D and in $x_\gamma^{\gamma\alpha}$ proved unprofitable. Much of this difference is probably due to the D vs carbon content effect upon α discussed in connection with the results on the iron–carbon alloy. Lower temperatures were employed for many of the iron–carbon–manganese measurements. D increases more rapidly with carbon content over a given range of composition at these temperatures.[8] The level of agreement is sufficiently good, however, to allow the conclusion that allotriomorphs in iron–carbon–manganese also thicken at rates determined by carbon diffusion in austenite.

Figure 8c shows that when the iron–carbon–molybdenum alloy is reacted at temperatures above about 800 C (1470 F) very good agreement is obtained between the calculated and measured values of α. At lower temperatures, however, the experimental values decrease, while those calculated continue to rise, thus paralleling (from the experimental viewpoint only) the behavior of the TTT-diagram. In this situation, the divergence between the calculated and experimental curves cannot be explained in terms of the deficiencies in equation (2). No plausible change in the shape of the no-partition Ae_3 curve or in the temperature and composition dependencies of D can be invoked to rationalize the unexpected experimental results. These results thus indicate that a different type of growth behavior becomes operative below 800 C (1470 F). While these data must certainly be extended to lower temperatures in order to explore more fully the magnitude and the variation with temperature of this effect (despite the experimental problems which this poses in connection with operation of the thermionic emission microscope at such temperatures), the existence of the effect can be considered to be well established by the experimental data and the calculations reported in Figure 8c.

Rao and Winchell[26] have recently found that bainite plates formed at 400 C (750 F) in low carbon steels containing 10 a/o Ni lengthen at rates two orders of magnitude less than those calculated from a carbon diffusion control model. Particularly since adequate agreement between calculated and experimental lengthening rates is obtained for iron–carbon alloys,[2, 23, 27] the presence of a really effective dislocation-type barrier at the edges of bainite plates in Fe–C–10 a/o Ni is as unlikely as at the broad faces of ferrite allotriomorphs in the present Fe–C–1.0 a/o Mo alloy. Paxton[28] has considered the effects of a very fine dispersion of very small particles upon the movement of an interphase boundary, and has obtained indications that such a dispersion can serve as a growth barrier. Figure 9 indicates, however, that this kind of situation is not present in the iron–carbon–molybdenum alloy. Evidently still another type of growth barrier exists in solid–solid transformations. We propose that this may be an "impurity drag" effect, such as is long familiar from studies of grain growth and recrystallization[29] in

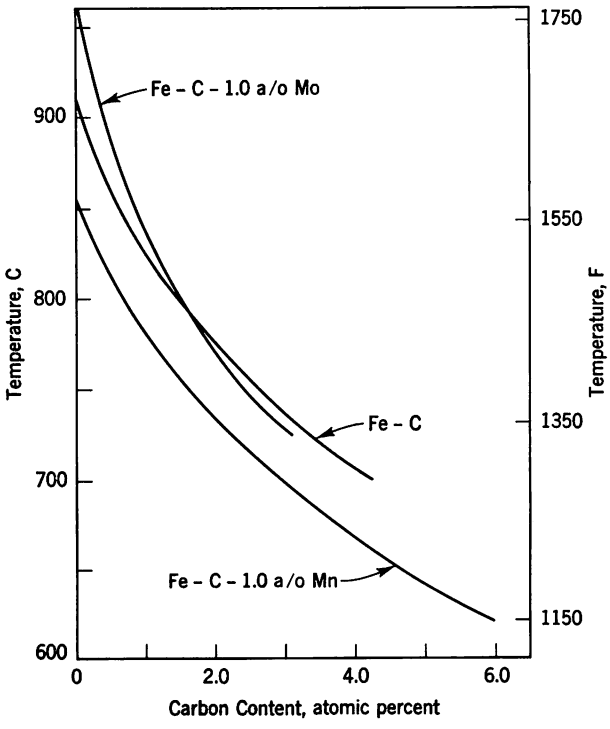

FIGURE 10. Calculated equilibrium Ae_3 for iron–carbon and calculated no-partition Ae_3 for Fe–C–1.0 a/o Mn and Fe–C–1.0 a/o Mo

single phase materials. This may arise here because molybdenum, a strong carbide-former, should tend to be bound to disordered austenite:ferrite boundaries, at which high carbon concentrations are present. Unlike the usual grain growth situation, molybdenum cannot be dragged along with the boundaries by volume diffusion[30] or by a volume diffusion-like process[29] in the temperature range so far investigated. The values of α in Figure 8c are much too high for such an effect to be operative. Instead, molybdenum atoms may be required to diffuse for short distances along the austenite:ferrite boundaries before completing their transfer to the ferrite phase, or alternatively, may simply serve as immobile "pinning points" around which the boundary must bend before it can break away.

While a quantitative treatment of the mechanism of the impurity drag effect will have to await the availability of data on α throughout the temperature range of the bay, several qualitative implications of the existence of such an effect should now be noted. The disappearance of the molybdenum effect at high temperatures (Figure 8c) is explained on this basis as the usual effect of entropy in reducing the gain in free energy accompanying the lodging of an atom in a site which reduces its enthalpy.[31] Both the disordered structure and the high carbon concentration ($x_\gamma^{\gamma\alpha}$) at the boundaries of allotriomorphs contribute to the enthalpic effect; with increasing temperature, however, the decrease in $x_\gamma^{\gamma\alpha}$ will aid the entropic effect in reducing the mean time of stay of molybdenum atoms at austenite:ferrite boundaries. Similarly, the combination of the increase in the effectiveness of the molybdenum drag effect with decreasing temperature and of the simultaneous increase in the driving force for growth provides a basis for explaining the bay in the TTT-diagram. The deepest portion of the bay thus develops when the increased driving force finally begins to overpower the drag effect. The complete cessation of transformation during its early stages at these temperatures[32] thus corresponds to the situation in which the drag effect is at or near its maximum net effectiveness. The increased amounts of transformation permitted at lower temperatures[32] result from the increasing effect of the higher driving force. Note, however, that the TTT-curve for iron–carbon–molybdenum does not rejoin that for the iron–carbon alloy even at the lowest temperatures studied (Figure 6), suggesting that the drag effect is still operative despite the obviously much more rapid growth now permitted. Finally, the absence of a bay when the alloying element is a non-carbide former, e.g., nickel, silicon, aluminum and cobalt, suggests that the impurity drag effect of these elements, when compared with that of molybdenum at a constant atomic percent, is substantially smaller as a result of their lesser binding energy to the austenite:ferrite boundaries. The absence of a drag effect in Fe–C–1 a/o Mn is consistent with the weak carbide forming tendency of manganese. Conversely, the alloying elements which are very strong carbide formers, e.g., titanium, columbium and vanadium, should be even more effective than molybdenum in this regard.

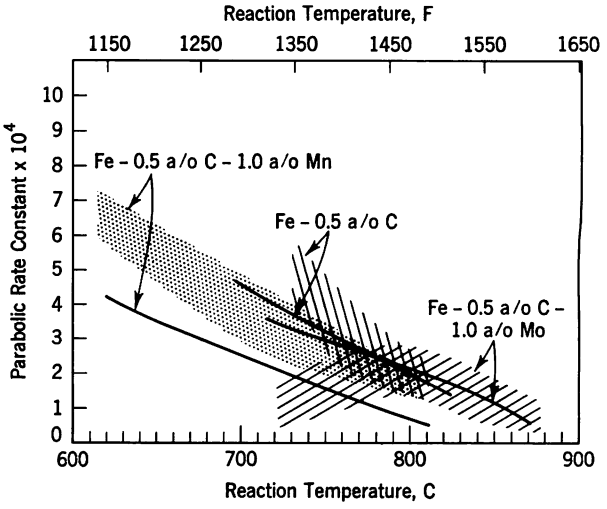

FIGURE 11. Comparison of the data scatter bands of the parabolic rate constant, α, vs reaction temperature for the alloys investigated. Superimposed, as solid lines, are the respective calculated curves of α as a function of reaction temperature according to Zener (1949)

Having discussed in detail the α data obtained from the individual alloys, we now briefly compare the data from the three alloys with the assistance of Figure 11, in which the data scatter bands of Figure 8 are superimposed as shaded bands without data points. In the vicinity of 800 C (1470 F), and at somewhat higher temperatures, reached by extrapolating the iron–carbon and iron–carbon–manganese data, α is highest in the iron–carbon–molybdenum alloy, intermediate in the iron–carbon and lowest in iron–carbon–manganese, all in parallel with the relative disposition of the TTT-curves and in agreement with the theory of Aaronson, Domian and Pound.[14] This positioning of the iron–carbon–manganese data relative to that for iron–carbon remains the same at lower temperatures, whereas α and the TTT-curve for iron–carbon–molybdenum pass through a maximum and thence decline as previously noted. Before deciding whether or not the parallel behavior of the data for the iron–carbon–molybdenum alloy makes growth kinetics wholly responsible for the bay in the TTT-diagram, however, we must attempt to estimate the effects of molybdenum upon the rate of nucleation of ferrite allotriomorphs.

Allotriomorph Nucleation Kinetics

Although no measurements were made of the rates of nucleation of ferrite allotriomorphs, estimates of these rates can be made by calculation from the ex-

perimental data on the TTT-curves and α. This may be done on the basis of a modification of the Johnson-Mehl equation[33] developed by Dubé:[5]

$$f(t) = 1 - \exp\left(- \frac{8}{15} \pi N_v \alpha^3 t^{5/2} \right) \qquad (3)$$

where $f(t)$ = the fraction of the austenite transformed to ferrite and N_v = the rate of nucleation of allotriomorphs per unit volume of austenite. This equation was derived under the assumptions that the allotriomorphs are spheres growing in accordance with equation (1) (with the radius of a sphere substituted for s) and that they are randomly distributed. Neither assumption is fulfilled experimentally, but neither is grossly incorrect when usage of the equation is confined to the earliest stages of reaction and to the higher reaction temperatures.[5] Fortunately, the conditions under which the TTT-curves were determined largely fulfill these conditions. Estimating $f(t) = 0.001$, reading t from the TTT-curves and taking α from curves averaged through the experimental scatter bands, N_v was calculated as a function of temperature for all three alloys. Because

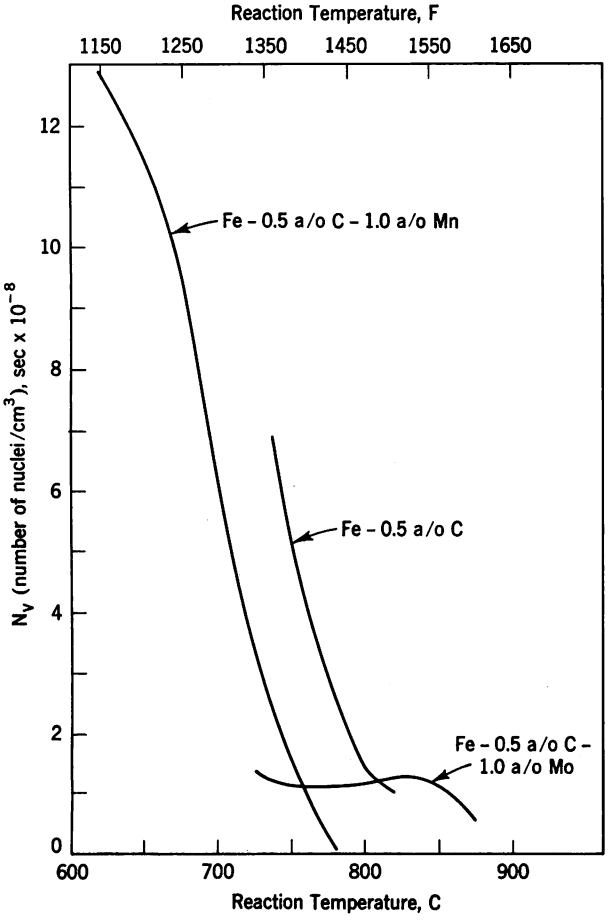

FIGURE 12. Rate of nucleation of ferrite allotriomorphs per unit volume of austenite (N_v) as a function of reaction temperature

of the particular method used to determine the time for the initiation of transformation — that required to form ferrite crystals visible at 100 X at one-half of the austenite grain boundaries — the usual practice of converting N_v to N_s (the rate of nucleation per unit of grain boundary area) was not followed. Because the iron–carbon alloy had a smaller grain size range than the Fe–C–X alloys, the estimate of $f(t)$ as 0.001 was likely somewhat low, on a relative basis, for this alloy. Since N_v varies as $\ln f(t)$, however, the resultant error in N_v for the iron–carbon alloy is unlikely to be much more than 10%.

N_v is plotted as a function of temperature for the three alloys in Figure 12. At a given temperature, N_v in iron–carbon–manganese is seen to fall well below that in the iron–carbon alloy. A similar result was obtained for α (Figure 11). These results bear out the prediction of Aaronson, Domian and Pound[14] that manganese should decrease both the rates of nucleation and the rates of growth of ferrite allotriomorphs. A quite different pattern of behavior is apparent in the case of the iron–carbon–molybdenum alloy. Instead of the customary swift rise with decreasing temperature anticipated from nucleation theory[34] and actually exhibited in the iron–carbon and iron–carbon–manganese alloys, N_v in iron–carbon–molybdenum is nearly independent of temperature. Once the iron–carbon and iron–carbon–manganese alloys have been sufficiently undercooled relative to their Ae_3 temperatures, N_v in these alloys becomes much larger than in iron–carbon–molybdenum. The prediction that molybdenum will decrease rates of nucleation relative to those in iron–carbon alloys[14] is thus also confirmed. However, the fact that the variation of α with temperature follows a path generally parallel to that of the TTT-curve whereas that of N_v does not in this alloy indicates that low values of α, rather than of N_v,[14] are responsible for the powerful effects of molybdenum upon the overall kinetics of the proeutectoid ferrite reaction. The failure of N_v to decrease significantly at temperatures below the 800 C (1470 F) nose suggests that the influence of molybdenum upon α is wholly responsible for the bay. Certainly, extension of the α data to lower temperatures, and direct measurements, rather than indirect calculations of N_v are required before N_v can be wholly ruled out as a significant factor in these effects.

Two comments upon the calculated N_v data per se are now necessary. The values of N_v in Figure 12 are about two orders of magnitude higher than those previously reported for the proeutectoid ferrite reaction in these temperature ranges.[2] The earlier data were obtained from counts of numbers of ferrite crystals, apparently not made at the very earliest stages of transformation. The difficulty of seeing ferrite:ferrite boundaries when ferrite:martensite boundaries are prominent in the microstructure, and the occurrence of substantial grain growth within

impinged aggregates of ferrite crystals[2,35] suggest that these data may be serious underestimates of the rates of nucleation actually operative.

Cahn and Hagel[36] are critical of determinations of N_v performed in the general manner employed in this study. The special form of this method which we used, however, should materially reduce the applicability of such criticisms. At the times chosen to mark the beginning of transformation, "site saturation" had not occurred at any save possibly the lowest reaction temperatures. The variation of N_v with time was partially discounted by selecting a very early stage in the transformation. Finally, the nonparallel behavior of N_v and α in iron–carbon–molybdenum is not "the standard result," i.e., parallel variations with temperature, which Cahn and Hagel conclude is due to misuse of this method.

SUMMARY

The kinetics of the proeutectoid ferrite reaction were investigated in high-purity Fe–0.5 a/o C, Fe–0.5 a/o C–1.0 a/o Mn and Fe–0.5 a/o C–1.0 a/o Mo alloys. TTT-curves for the initiation of isothermal transformation were determined by the conventional experimental technique. The parabolic rate constant, α, for the thickening of grain boundary allotriomorphs* was evaluated at temperatures above about 725 C (1335 F) in the iron–carbon and iron–carbon–molybdenum alloys and at and above 620 C (1150 F) in the iron–carbon–manganese alloy by means of thermionic emission microscopy and cinematography. Rates of nucleation of allotriomorphs per unit volume of austenite, N_v, were estimated from these data by application of an indirect method.

The thickening kinetics of ferrite allotriomorphs are accurately described by a parabolic time law at all temperatures and all compositions studied. In the iron–carbon and iron–carbon–manganese alloys, and in the iron–carbon–molybdenum alloy at temperatures above 800 C (1470 F), the values of α determined experimentally are in reasonable (or better) agreement with those calculated on the assumption that thickening is controlled by volume diffusion of carbon in austenite.

The TTT-curves, α and N_v values for the iron–carbon–manganese alloy lie at longer times or at lower values than those of the iron–carbon alloy throughout the temperature range in which these data were obtained on both alloys. Aaronson, Domian and Pound[14] have proposed that the no-partition Ae_3 temperature of an Fe–C–X alloy relative to that of the equilibrium Ae_3 temperature of an iron–carbon alloy with the same carbon content normally determines the effects of the alloying element upon both N_v and α of proeutectoid ferrite. Since the no-partition Ae_3 of the iron–carbon–manganese alloy is lower, the results obtained are in good accord with this theory.

The TTT-curve of the iron–carbon–molybdenum alloy exhibits a nose at 800 C (1470 F) and a rather deep bay between 600 and 700 C (1110 and 1290 F). In this alloy, α lies above that for the iron–carbon and iron–carbon–manganese alloys at temperatures above about 800 C (1470 F). Since molybdenum raises the no-partition Ae_3 temperature relative to the equilibrium Ae_3 for iron–carbon, this result is also in accord with the theory. At 800 C (1470 F), however, the α vs temperature curve displays a maximum, and then decreases continuously at lower temperatures; such behavior is not predicted by this theory. The α and the TTT-curves for iron–carbon–molybdenum thus exhibit parallel behavior in the temperature range in which both were determined. The calculated N_v data for this alloy are also unusual: they are both low and nearly independent of temperature. The prediction of Aaronson et al that molybdenum should decrease rates of nucleation is thus confirmed, but their suggestion that molybdenum would leave α substantially unchanged (or, in effect, increase α in the iron–carbon–molybdenum alloy used in this study) is not sustained. Instead, the anomalous effect of molybdenum upon α, rather than its influence upon N_v, is responsible for the "premature" occurrence of a nose in the TTT-curve at a relatively long reaction time at 800 C (1470 F), rather than at a quite short time within the 600/700 C (1110/1290 F) range anticipated from the no-partition Ae_3 temperature of the alloy. This effect evidently also produces the bay in the TTT-curve at lower temperatures. It is this striking influence of molybdenum upon growth kinetics which is probably responsible for the anomalous and remarkably potent effect exerted by molybdenum upon the kinetics of the proeutectoid ferrite reaction and the hardenability of steel. This anomaly is tentatively ascribed to an "impurity drag effect," such as would accompany a high binding energy of molybdenum, a strong carbide-former, to the carbon-rich interphase boundaries of ferrite allotriomorphs.

ACKNOWLEDGMENTS

We are particularly grateful to Dr. Erwin Eichen for technical advice on the use and operation of the thermionic emission microscope. Without this instrument, of Dr. Eichen's design, this investigation could not have been performed. W. Stewart, C. Amberger and E. T. Kennedy provided valuable assistance in the laboratory. Appreciation is also expressed to Dr. N. A. Gjostein for his critique of the manuscript.

* The rate of thickening $= \alpha/2t^{1/2}$, where t = isothermal reaction time.

REFERENCES

1. H. I. Aaronson and H. A. Domian, Trans. AIME *236*. 781 (1966)
2. H. I. Aaronson, "The Proeutectoid Ferrite and the Proeutectoid Cementite Reactions," *Decomposition of Austenite by Diffusional Processes*, edited by V. F. Zackay and H. I. Aaronson, Interscience, New York, 1962, 387
3. K. R. Kinsman, E. Eichen and H. I. Aaronson, unpublished research
4. C. A. Dubé, H. I. Aaronson and R. F. Mehl, Rev. Met. (Paris), *55*. 201 (1958)
5. C. A. Dubé, Ph.D. Thesis, Carnegie Institute of Technology, 1948
6. R. F. Mehl and C. A. Dubé, "The Eutectoid Reaction," *Phase Transformations in Solids*, edited by R. Smoluchowski, J. E. Mayer and W. A. Weyl, Wiley, New York, 1951, 545
7. C. Zener, J. Appl. Phys. *20*. 950 (1949)
8. C. Wells, W. Batz and R. F. Mehl, Trans. AIME *188*. 553 (1950)
9. C. Wagner, Trans. AIME *194*. 91 (1952)
10. G. R. Purdy and J. S. Kirkaldy, Trans. AIME *227*. 1255 (1963)
11. J. S. Kirkaldy, Can. J. Phys. *36*. 907 (1958)
12. J. S. Kirkaldy, "Theory of Diffusional Growth in Solid-Solid Transformations," *Decomposition of Austenite by Diffusional Processes*, edited by V. F. Zackay and H. I. Aaronson, Interscience, New York, 1962, 39
13. G. R. Purdy, D. H. Weichert and J. S. Kirkaldy, Trans. AIME *230*. 1025 (1964)
14. H. I. Aaronson, H. A. Domian and G. M. Pound, Trans. AIME *236*. 768 (1966)
15. H. I. Aaronson, N. A. Gjostein, H. W. Paxton and R. W. Heckel, Rev. Sci. Instr. *28*. 579 (1957)
16. T. Ko, J. Iron and Steel Inst. (London), *175*. 16 (1953)
17. E. Eichen, *High-Temperature High-Resolution Metallography*, edited by H. I. Aaronson and G. S. Ansell, Gordon and Breach, New York, 1967
18. E. Eichen, *Techniques in Metals Research, 2*, Wiley, New York, 1967
19. E. Eichen, R. L. Forgacs and B. A. Parafin, Rev. Sci. Instr. *37*. 438 (1966)
20. R. L. Forgacs, B. A. Parafin and E. Eichen, Rev. Sci. Instr. *36*. 1198 (1966)
21. C. Laird and H. I. Aaronson, Acta Met. *15*. 73 (1967)
22. J. L. Ham, R. M. Parke and A. J. Herzig, Trans. ASM *31*. 877 (1943)
23. L. Kaufman, S. V. Radcliffe and M. Cohen, "Thermodynamics of the Bainite Reaction," *Decomposition of Austenite by Diffusional Processes*, edited by V. F. Zackay and H. I. Aaronson, Interscience, New York, 1962, 313
24. R. Trivedi, Ph.D. Thesis, Carnegie Institute of Technology, 1966
25. C. Atkinson, University of Sheffield, private communication
26. M. Rao and P. G. Winchell, Trans. AIME, in press
27. H. W. Paxton and G. M. Pound, Trans. AIME *227*. 957 (1963)
28. H. W. Paxton, this symposium
29. P. Gordon and R. A. Vandermeer, *Recrystallization, Grain Growth and Textures*, American Society for Metals, Metals Park, Ohio, 1966, 205
30. K. Lücke and K. Detert, Acta Met. *5*. 628 (1957)
31. D. McLean, *Grain Boundaries in Metals*, Oxford at the Clarendon Press, Oxford, 1957, 118
32. R. F. Hehemann and A. R. Troiano, Metal Progr. *70*. (2). 97 (1956)
33. W. A. Johnson and R. F. Mehl, Trans. AIME *135*. 416 (1939)
34. J. H. Hollomon and D. Turnbull, "Nucleation," *Progress in Metal Physics*, edited by B. Chalmers, Interscience, New York, 1953, Vol. 4, 370
35. H. C. H. Carpenter and J. M. Robertson, J. Iron and Steel Inst. (London), *123*. 345 (1931)
36. J. W. Cahn and W. C. Hagel, "Theory of the Pearlite Reaction," *Decomposition of Austenite by Diffusional Processes*," edited by V. F. Zackay and H. I. Aaronson, Interscience, New York, 1962, 131

ORAL DISCUSSION OF

Influence of Molybdenum and Manganese on the Kinetics of the Proeutectoid Ferrite Reaction

Presented by K. R. KINSMAN

J. W. SPRETNAK (Ohio State University). Looking at these same observations of the increase of the rate constant alpha, with increasing undercooling, and if this is indeed a diffusion process and D is exponentially related to the temperature, why does one get an increase in the rate constant?

AUTHOR'S REPLY. The increase in rate constant with decreasing temperature is the result of the increased driving force overbalancing the decrease in diffusivity. Below the "nose" of the α versus temperature curve, of course, the direction of the balance reverses. This concept was pointed out by Mehl years ago.

J. W. SPRETNAK. Do you have a steadily rising curve in the alpha temperature range?

AUTHOR'S REPLY. Yes, this corresponds to an increasing growth rate as we decrease the temperature. The temperature range is still above the "growth nose."

J. W. SPRETNAK. Would you expect it to go through a maximum with decreasing temperature?

AUTHOR'S REPLY. Yes, we would expect growth to go through a maximum. The calculations certainly show that it does.

J. W. SPRETNAK. You are talking about impurity drag effects. I assume that you are talking about a noncoherent interface?

AUTHOR'S REPLY. Yes, we are.

J. W. SPRETNAK. Do you have any evidence of the interface being noncoherent?

AUTHOR'S REPLY. The grain boundary allotriomorphs chosen for measurement did not develop sharp facets during the experimental observations; they seemed to grow smoothly, with no distinct crystallographic features. We assume, therefore, no interface inhibition to growth and infer essentially diffusion-controlled growth.

J. W. SPRETNAK. You don't get that classical hemispheric growth seen in textbooks characterizing N and G reactions?

AUTHOR'S REPLY. Grain boundary allotriomorphs begin to grow in a comparatively lens-shape fashion, grow very rapidly along the boundary and then thicken. In the first film sequence we saw just this type of rapid movement along the boundary and thickening. Almost before the measurements were made, the allotriomorph had swept along the boundary. In the second film sequence the more "classic" lenticular shape was maintained for a much longer time. (See Figure 4 in the paper.)

J. W. SPRETNAK. Does not the observed morphology concern you, inasmuch as it is interpreted to reflect a nucleation and growth phenomenon?

AUTHOR'S REPLY. The morphology observed was clearly that which you would expect during diffusional growth of a grain boundary precipitate; there is no reason to believe that there is significant interface inhibition. Now, what may disturb you is the fact that I mentioned that there is a certain irregularity in the growth of the allotriomorphs; at later stages of the reaction, some of the allotriomorphs can generate facets that are apparently strong interface barriers, but the measurements as you see here are made at short reaction times. Measurements were not carried beyond 30 seconds growth time. Although, depending on temperature and relative growth rates, different degrees of "maturity" were attained, the measurements were confined essentially to the early stages of growth.

J. W. SPRETNAK. This is an extremely critical point, i.e., the nature of the interface?

AUTHOR'S REPLY. Yes, it is.

J. W. SPRETNAK. And if it is indeed noncoherent you can evoke the impurity drag effect. If it is coherent and martensitic in nature, then we must look to the effects of these elements, particularly molybdenum, in impeding the actual lattice transformation, which is what our current research seems to indicate.

H. I. AARONSON (Coauthor). Grain boundary allotriomorphs were deliberately chosen in order to avoid, insofar as practicable, interface barriers to growth. Ferrite allotriomorphs bear the Kurdyumov and Sachs lattice orientation relationships with respect to their parent austenite grain. Since the angle which the lath- or plate-shaped ferrite nucleus of an allotriomorph makes with respect to the grain boundary at which it formed will normally be large, at most orientations of the austenite-

ferrite boundary growing into the parent austenite grain, the structure of the boundary will be of the disordered type. However, small facets of dislocation-interfacial structure will inevitably be present at the boundary orientation corresponding to that of the habit plane of the nucleus. These facets are known to offer a serious barrier to growth at their orientation of the boundary. As long as the proportion of the boundary area which these facets comprise is small, however, the disordered areas of the boundary will be able to grow around the dislocation segments (see Figure 13a, p. 406, *Decomposition of Austenite by Diffusional Processes*, John Wiley and Sons, New York, [1962]) and thus minimize their effect upon the growth process. That this effect is not entirely avoided, however, is indicated by the scatter in the plots of parabolic rate constant (α) versus temperature (Figures 8a-c). The satisfactory overall agreement between the experimentally measured values of α and those calculated on the assumption that growth is controlled by the diffusion of carbon in austenite (Figures 8a and b, and Figure 8c at temperatures above 800 C, 1470 F), however, strongly supports these considerations. Since the anomalously low values of α in the iron–carbon–molybdenum alloy at temperatures below 800 C (1470 F) are not accompanied by changes in the morphology of the ferrite allotriomorphs, it would also appear that crystallographic effects upon growth cannot be held responsible for this result. Relief effects formed at a free surface provide an overall sampling of the structure of interphase boundaries. The absence of martensite-like relief effects in association with grain boundary allotriomorphs (Figure 2b-d) also leads to the conclusion that the interphase boundaries of these crystals are predominantly of the disordered type.

H. W. PAXTON (Carnegie Institute of Technology). I have one comment on the molybdenum effects — you are doing a reverse of the transformation which Pavlick was studying. In his observations, molybdenum seemed to have no effect on the rate of austenite growing into ferrite, whereas you say at about the same temperatures ferrite growing into austenite is quite markedly affected. I don't know if there should be an image, but there isn't.

AUTHOR'S REPLY. That is an interesting observation. Pavlick used nominally 1 wt % Mo in his steel, compared to the 1.95 wt % (1 a/o) we employed. That difference in molybdenum content coupled with the difference in systems studied, iron–carbon–molybdenum versus iron–nitrogen–molybdenum, may be significant enough to result in the apparent asymmetry of the observed effect. Of course, at this juncture, grounds for comparison can only be obtained in comparable experiments.

R. F. HEHEMANN (Case Institute of Technology). Do the allotriomorphs grow into both grains or only into one?

AUTHOR'S REPLY. In most cases allotriomorphs were found to grow into both grains; however, growth into only one grain was also commonly observed.

R. F. HEHEMANN. Did the allotriomorphs show any relief on at least one side of the grain boundary, i.e., are the interfaces incoherent on both sides?

AUTHOR'S REPLY. The normal surface rumpling associated with a volume change across an incoherent interface was observed in all cases. No unique surface relief feature could be associated with "one-sided" growth. Only where flat facets evolved did the surface distortion assume the degree of angularity ("geometric surface relief") consistent with a partially coherent interface.

F. B. PICKERING (United Steel Companies Ltd.). I believe you stated that the grain-boundary nucleated ferrite could, at a later stage in its growth, develop faceted interfaces with the austenite, or even a plate-like growth. Is the interface of the faceted ferrite completely incoherent, or does it possess some degree of semicoherency? Have in fact any experimental observations been made on the nature of the ferrite-austenite interface? If the interface of the faceted ferrite growth is partially coherent, by what mechanism do you envisage that an initially incoherent interface is converted during the growth of the ferrite into a partially coherent interface?

AUTHOR and H. I. AARONSON. We have observed that in the later stages of growth of grain boundary ferrite allotriomorphs facets occasionally evolve. In such cases the ferrite-austenite interface would appear to be completely incoherent in the initial stages of growth where measurements were made, partially coherent facets emerging to minimize interfacial energy in the later growth stages. The details of evolution from an initially incoherent to a partially coherent interface are envisioned as follows. When an area of a disordered interphase boundary migrates into an orientation where it can acquire a dislocation interfacial structure, its rate of growth will be sharply curtailed immediately. When the driving force for growth is large and the angle which the dislocation orientation makes with respect to the plane of the grain boundary is also large, disordered segments of the boundary will soon "wrap around" and eliminate the dislocation facets. When the driving force for growth has diminished, near the end of transformation, another factor can come into play to a significant extent. This factor is the minimization of the total interfacial free energy. It will cause the opposite pattern of boundary migration: the dislocation facets will tend to increase in area at the expense of the disordered segments of the boundary. In the case where two facets at an angle to one another are joined by a curved boundary the growth barrier at the planar facets would be expected to force the curved area to grow out allowing the planar facets to join; this exact behavior has been observed on a number of occasions in the course of the experiments. The nature of the interface has been inferred only through observations of growth kinetics and morphology; direct experimental observations of the ferrite-austenite interfacial structure is a most difficult problem, one yet to be solved.

Austenite Decomposition at High Pressure

T. G. NILAN
United States Steel Corporation
Applied Research Laboratory
Monroeville, Pennsylvania

INTRODUCTION

High pressure has been characterized as a new dimension in metallurgy. This is true when one considers that the wealth of experimental data upon which our understanding of present technology is based has been garnered at atmospheric pressure in terms of two primary thermodynamic variables of state, temperature and composition. The remaining variable, pressure, has, until recently, been inaccessible to the metallurgist. This placed him in a position similar to the hypothetical two-dimensional creatures in Abbott's "Flatland," who were faced with describing a three-dimensional world in terms of two dimensions.[1]*

The importance of the pressure variable to an understanding of metallurgical phenomena was recognized early in the development of the science. The first experimental observation that a solid could transform under pressure to a phase not found at atmospheric pressure was made by LeChatelier in 1883.[2] Roberts-Austen reported pressure-induced changes in the temperature of recalescence of steel in 1893.[3] Benedicks speculated on the role of the pressures developed during austenite decomposition upon microstructure in 1908.[4] Ordinarily, interest in an area by men of this stature would spark an extensive study, but in the instance of the pressure variable, this did not happen simply because the experimental demands of simultaneous high pressure and high temperature could not be satisfied. Percy Bridgman, shortly after the turn of the century, began a study of high pressure effects that was to continue throughout his scientific career.[5] Even his highly ingenious techniques, however, did not extend the pressure–temperature limits to those of metallurgical interest. As late as 1951 calculations showed that pressures attained in the laboratory up to that time were too low to alter significantly the kinetics and morphology of high-temperature austenite decomposition.[6] In 1952, however, Kulin, Cohen, and Averbach,[7] using a Bridgman apparatus at subzero temperatures, demonstrated that high pressure lowered the martensite start (M_s) temperature.

The present generation of high pressure studies had its beginning in 1955 with the work at the General Electric Laboratory, which culminated in the syntheses of diamonds.[8] Here at last were the pressures and temperatures needed by the metallurgist. Hilliard applied these ultra-high pressure techniques to a study of the phase equilibria, summarized in Figure 1, and showed that composition and temperature of the eutectoid point were lowered to 0.4% C and 660 C (1220 F) at 30 kbar† and to 0.18% C and

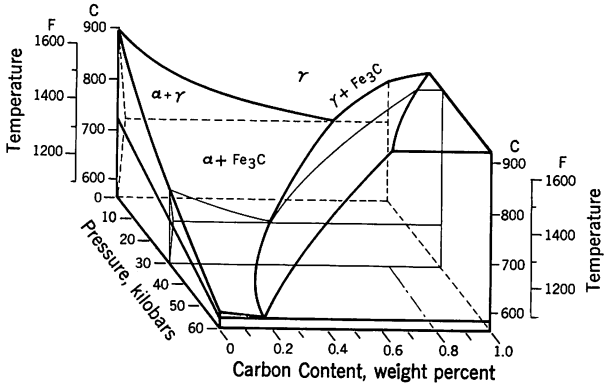

FIGURE 1. Iron – carbon phase equilibria as a function of temperature, composition, and pressure

*See references.

†1 kilobar = 14.5 ksi = 14,500 psi = 987 atmosphere.

580 C (1076 F) at 60 kbar. Subsequent work by the General Electric and ManLabs groups showed that pressure markedly retarded the rates of austenite decomposition.[10,11] Thus, these studies indicated that pressure, of the order of tens of thousands of atmospheres, has a very significant metallurgical effect. In the particular case of austenite decomposition, the phenomenological base for the existing theories of the reaction, namely the phase equilibria, and the morphology and kinetics of formation of the reaction products are all pressure-dependent. The value of the pressure variable as an investigative tool in clarifying the mechanisms of austenite decomposition is predicated on a progressive effect, or con-

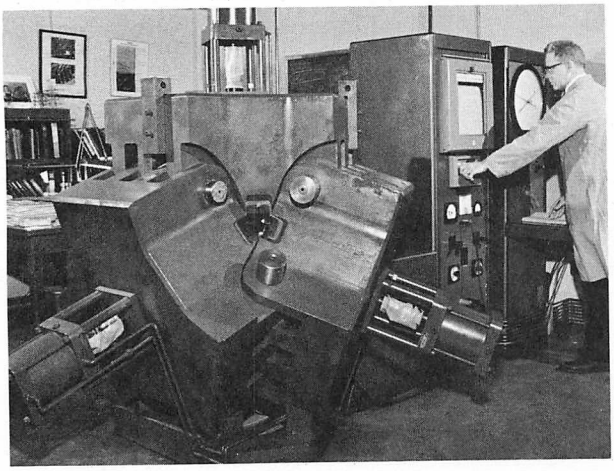

FIGURE 2. Tetrahedral anvil press

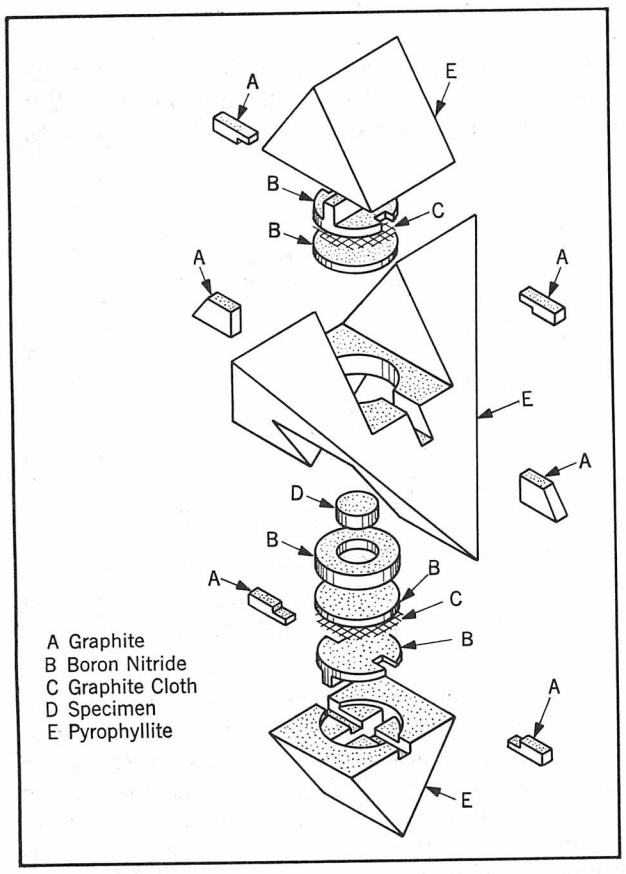

FIGURE 3. Arrangement of the working chamber within the tetrahedral anvil press

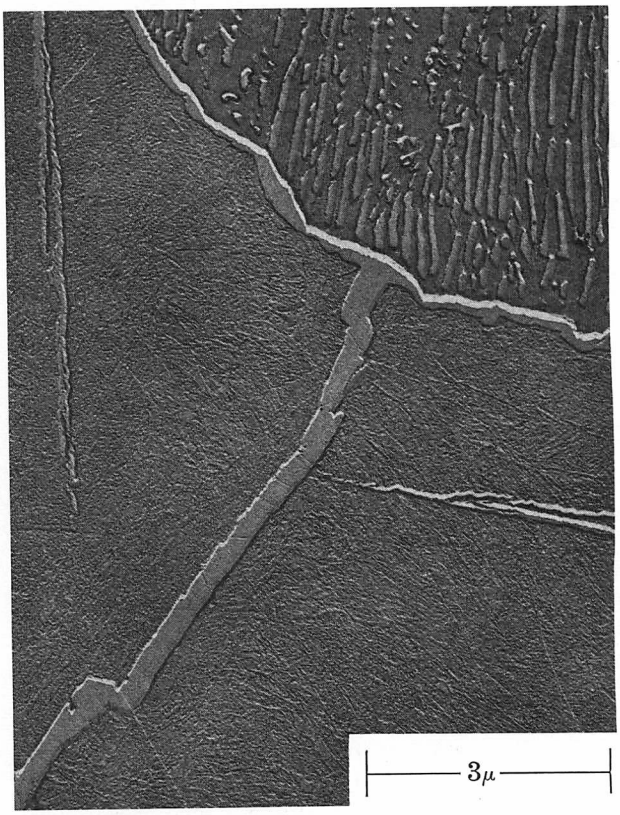

FIGURE 4. Electron micrograph of hypereutectoid morphology developed in 0.82% C steel at 480 C (900 F) and 30 kbar

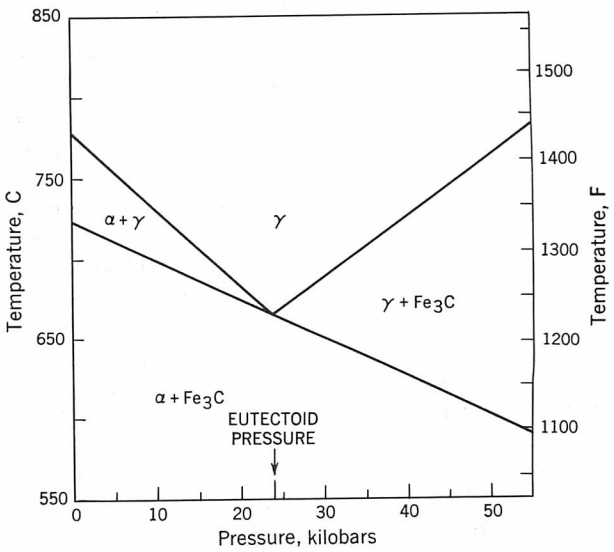

FIGURE 5. Temperature – pressure iron – carbon phase diagram at 0.44% C

tinuity of these mechanisms up to ultrahigh pressures. A discontinuous change in morphology or kinetics at pressures above atmospheric would compound, rather than alleviate, the difficulty of interpretation. The Applied Research Laboratory of U. S. Steel is currently engaged in a study, in some detail, of austenite decomposition under pressure to determine whether such continuity of mechanism exists, and if it does, to use the results to cast more light on the basic nature of the processes involved in the response of steel to heat treatment.

The pressure-generating device used (Figure 2) is an 8,000-ton-capacity tetrahedral anvil press composed of four "platens" (three are shown here), each containing a 16-in.-diameter piston. At the maximum fluid pressure of 20 ksi,* each anvil exerts a 2,000-ton force on the solid experimental volume, developing a pressure of 70 kbar, or over 1,000,000 psi on the specimen. The experimental volume, shown in exploded view (Figure 3), is a pyrophyllite tetrahedron, 3 in. on edge, machined to accommodate both a ⅛-in.-high by ⅜-in.-diameter specimen and heating devices. The heaters are graphite cloth discs, connected by graphite tabs to two of the anvils and in turn to the electrical current supply. The remaining two anvils connect to the chromel-alumel thermocouple, which contacts the specimen. The specimen is encapsulated in boron nitride to minimize nonhydrostatic shear stresses at the specimen. This arrangement has permitted anneals of several hours duration at 1095 C (2000 F) for austenitization and isothermal anneals as long as a week at 595 C (1100 F), and lower, for transformation studies.

The experimental work has been primarily concerned with 0.44 and 0.82% C steels. The 0.82% C steel, eutectoid at one atmosphere, becomes increasingly hypereutectoid with increasing pressure. This is reflected in the microstructure observed (Figure 4). At 30 kbar, transformation of the 0.82% C steel at 480 C (900 F) produces a hypereutectoid morphology with grain boundary and Widmanstätten carbides.

The temperature–pressure section (Figure 5) of the pressure-phase diagram of the iron–carbon system at 0.44% C shows that as pressure increases, this material, which is hypoeutectoid at one atmosphere, becomes eutectoid at 24 kbar and hypereutectoid above 24 kbar. The microstructure as a function of pressure ranges from hypoeutectoid at one atmosphere (Figure 6) where the proeutectoid component is ferrite, through eutectoid at 24 kbar to hypereutectoid at 34 kbar, where now the grain boundary phase is cementite, (Figure 7).

Perhaps the most significant effect of pressure (Figure 8) is the greater hardenability of steel transformed under pressure. Here are plotted the TTT diagrams of the 0.44% C steel at one atmos-

*1 ksi = 1000 psi = 6.9 MN/m²

FIGURE 6. Light micrograph of 0.44% C steel as normalized at one atmosphere

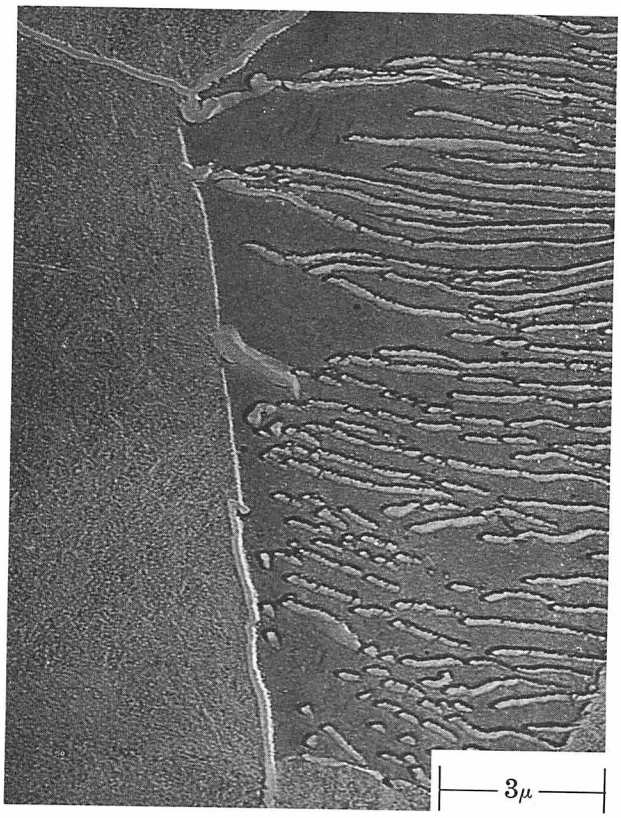

FIGURE 7. Electron micrograph of hypereutectoid microstructure of 0.44% C steel transformed at 480 C (900 F) and 34 kbar

phere and at the eutectoid pressure of 24 kbar. The nose of the C curve has been displaced by pressure from approximately 0.6 sec at one atmosphere to 600 sec at 24 kbar—a 1000-fold increase in transformation start time. The A_1 and M_s temperatures have been lowered respectively by about 55 C (100 F) and 110 C (200 F).

The microstructures developed at 24 kbar, through the pearlite and bainite reactions down to 315 C (600 F), are morphologically similar to those observed in eutectoid decomposition at one atmosphere.

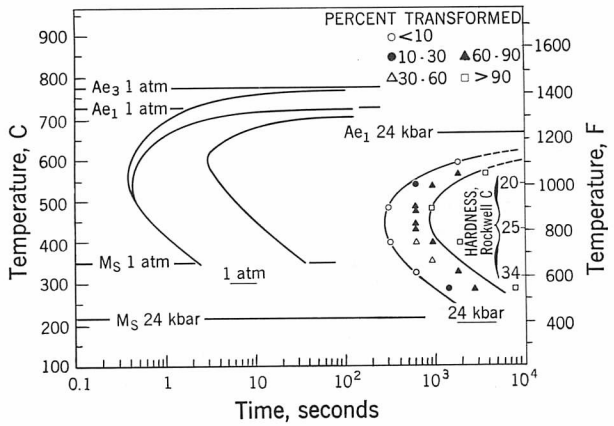

FIGURE 8. Isothermal transformation diagrams of 0.44% C steel at one atmosphere and at 24 kbar

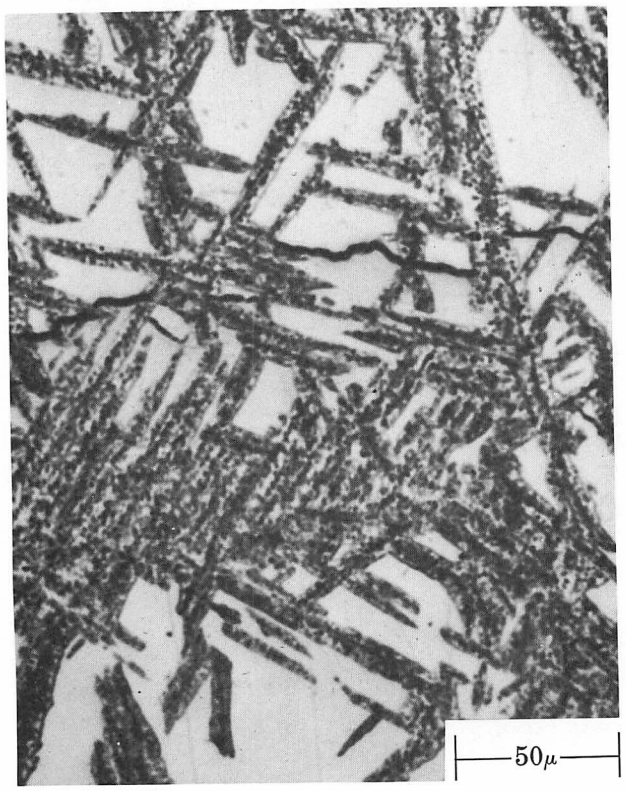

FIGURE 9. Light micrograph of bainite formed at 315 C (600 F) and 24 kbar

In particular, the bainite formed at 315 C (600 F) and 24 kbar (Figure 9) retains the acicularity of one-atmosphere bainite. To investigate this morphology in greater detail, a two-surface study was carried out at electron-microscope magnifications. In Figure 10 are shown mutually perpendicular sections of bainite laths. Note that on both planes bainite appears similar in character with small carbides oriented mostly transverse to the length of the lath. With the technique employed, as can be seen, there is no edge rounding of the specimen. Figure 11, another area of the same specimen, shows dissimilar structures on the two surfaces, that is, the predominantly transverse carbide arrangement on one surface, while on the other the carbides are parallel to the longitudinal axis of the lath. These microstructures are interpreted as different sections of one morphology. The habit plane of the bainite lath structure was found to be the same as that found in bainite formed in eutectoid decomposition at one atmosphere.[12, 13]

The correspondence of the microstructures found after transformation of the 0.4% C steel at eutectoid pressure with those observed in eutectoid decomposition at one atmosphere was not observed in the 290 C (550 F) transformations. At this temperature, a "blocky," columnar morphology is evident (Figure 12). This 290 C (550 F) transformation product nucleates preferentially at grain boundaries, as does fine pearlite, and definitely lacks the acicular character of higher temperature bainite. At much higher magnification (Figure 13), the microstructure formed at 290 C (550 F) and 24 kbar, is composed of fan-shaped regions of fine carbides originating from a point just below and slightly to the left of center and is sheathed on the sides by a coarser ferrite–carbide aggregate. The advancing front is almost planar and unsheathed. The characteristics of this columnar bainite are more clearly evident (Figure 14) in a 290 C (550 F), 30 kbar transformation of the 0.82% C steel. The sheath carbides are, in general, perpendicular to the axis of the fan-shaped region. The primary structure is considered to be the fan-shaped carbide area and the sheath, a secondary growth structure. This microstructure is not new, but it has not been reported in carbon steels below 1.4% C at one atmosphere. Greninger and Troiano[13] and Vilella[14] presented light micrographs of this structure in 1.4 and 1.8% C steels, as did Jellinghaus[15] and Speich and Cohen,[16] in high-carbon steels alloyed with manganese and chromium. This structure occurred at temperatures between 290 and 345 C (550 and 650 F) in all cases.

Figure 15 presents a possible rationale for the appearance of this microstructure. Here is depicted the carbon dependence of the M_s temperature at one atmosphere and at 30 kbar. The shaded region above the one atmosphere M_s represents the region in which Matas and Hehemann[17] observed the bainite

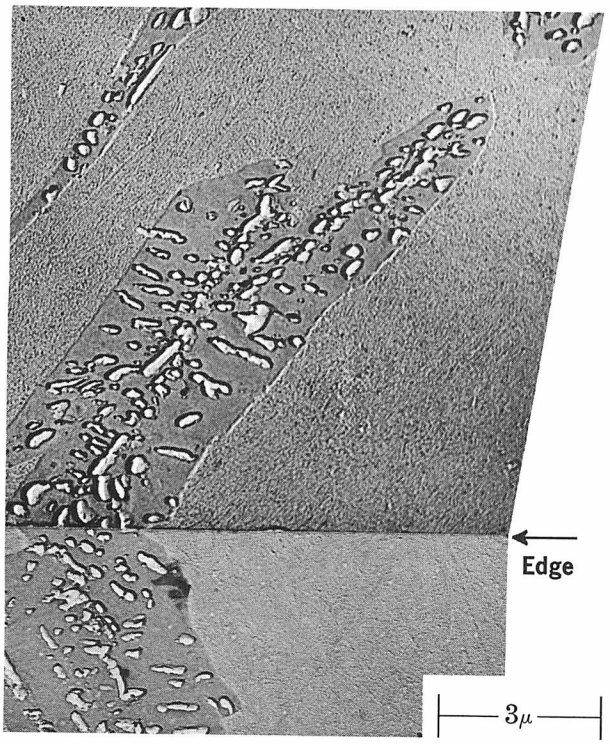

FIGURE 10. Electron micrograph of orthogonal section of 315 C (600 F) – 24 kbar bainite exhibiting the same structure on both surfaces

FIGURE 12. Light micrograph of columnar bainite formed at 290 C (550 F) and 24 kbar

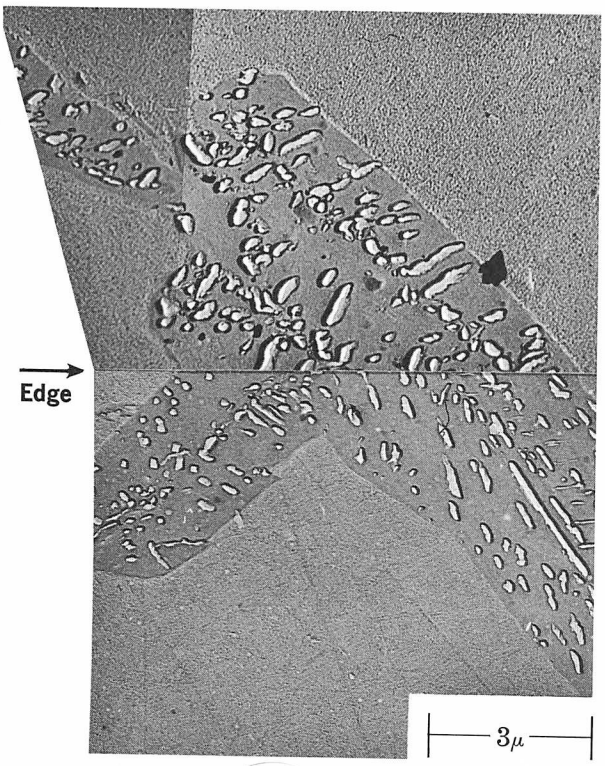

FIGURE 11. Electron micrograph of orthogonal section of 315 C (600 F) – 24 kbar bainite exhibiting dissimilar structure on each surface

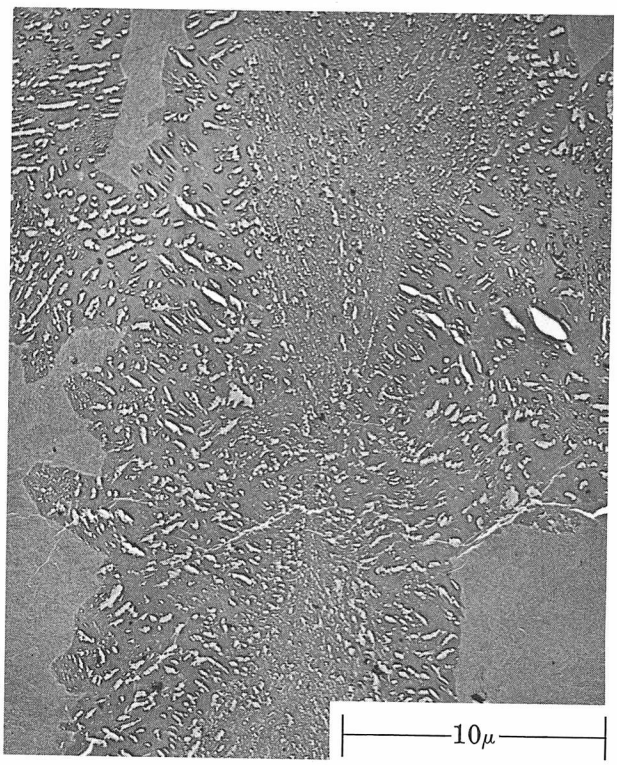

FIGURE 13. Electron micrograph of columnar bainite formed in 0.44% C steel at 290 C (550 F) and 24 kbar

decomposition sequence, $\gamma \rightarrow \epsilon$-Carbide $+ \alpha \rightarrow Fe_3C + \alpha$, that is, the same sequence as observed in the tempering of martensite. The points designate the composition and temperature at which the columnar microstructure has been observed at one atmosphere or at high pressure. Note that the high-pressure points are located at a lower temperature than the one-atmosphere points by approximately the same amount as the pressure lowers the eutectoid temperature. It is hypothesized that the columnar bainite process is a nucleation-and-growth reaction that will occur only in the absence of a lower bainite reaction related to the martensitic process. In this scheme, Figure 16, the bainitic reaction occurring above the M_s is considered to be the isothermal growth of martensite embryos, which can occur over a temperature range above the M_s. Where the embryo reaction overlaps the nucleation-and-growth processes, the nucleation reaction is overriden. At one-atmosphere and low-carbon levels the upper temperature limit of the embryo process is sufficiently high that the columnar reaction, presumed to be a nucleation reaction, does not occur. However, high-carbon and alloy levels depress the M_s temperature and the upper temperature limit of the embryo process so that the columnar morphology can form at one atmosphere. High pressure, with its concomitant depression of the martensitic reaction temperatures, similarly permits this structure to form at the lower 0.4 and 0.8% C levels.

With regard to the morphology of austenite decomposition at high pressure, these results indicate that the pressures thus far investigated do not lead to microstructures substantially different from those found in steel heat-treated at one atmosphere. However, in each particular steel the microstructures, and hence the decomposition mechanisms, are intimately related to the phase equilibria existing at the time of transformation and change as the phase relations are shifted at high pressure.

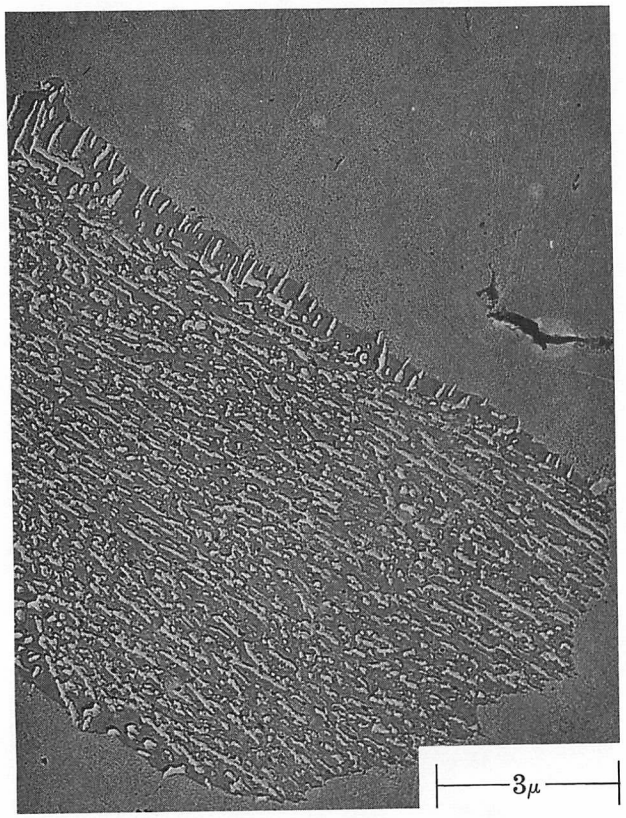

FIGURE 14. Electron micrograph of columnar bainite formed in 0.82% C steel at 290 C (550 F) and 30 kbar

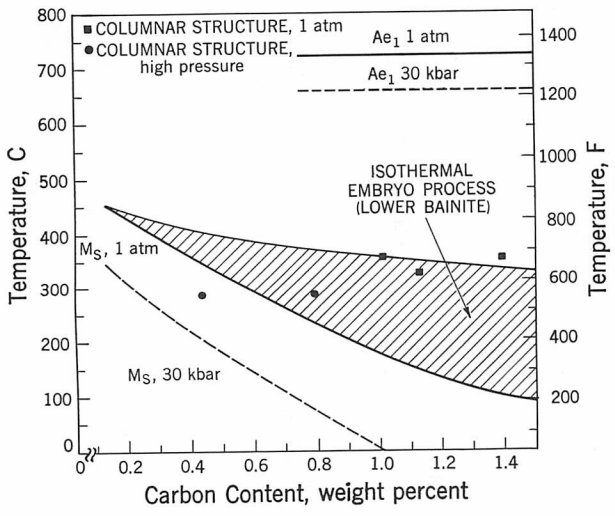

FIGURE 15. Relationship of columnar microstructures to martensitic reactions

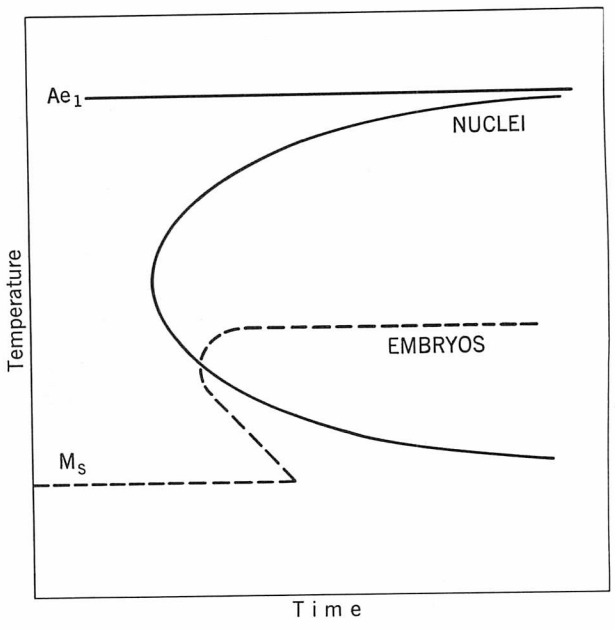

FIGURE 16. Schematic TTT diagram of nuclei and embryo reactions

Preliminary work has been started on the effect of pressure on alloyed steels. A 0.24% Mo addition was made to the 0.4% C steel discussed earlier, and isothermal transformation studies were carried out at the eutectoid pressure of 24 kbar. The TTT results (Figure 17) once again indicate the marked retardation of the decomposition by pressure and also reveal the effect of the molybdenum addition in the steel by the separation of the pearlitic and bainitic reactions.

When a comparison is made between the data for the molybdenum-bearing steel and those for the steel without molybdenum (the dashed curves), it is evident that there are disparate pressure effects on the pearlite and bainite reactions. The austenite grain size at 24 kbar was the same for both steels. The bainite reactions in both steels are essentially the same at 24 kbar; however, the pearlite reaction in the molybdenum-alloyed steel is retarded to a greater degree, there being a maximum increase of 50-fold in transformation start time for the molybdenum steel at 480 C (900 F). Blanchard, Parke, and Herzig of the Climax Molybdenum Laboratory,[18] in their study of the effect of molybdenum on eutectoid decomposition at one atmosphere, found the same time–temperature separation of the reactions and disparate effects on the rates of the bainite and pearlite reactions. According to their data, 0.24% Mo increases the maximum transformation start time by 30-fold at one atmosphere. Once again, austenite decomposition reactions operative at eutectoid composition at one atmosphere are found to be essentially the same as at eutectoid pressure, though the rates are retarded.

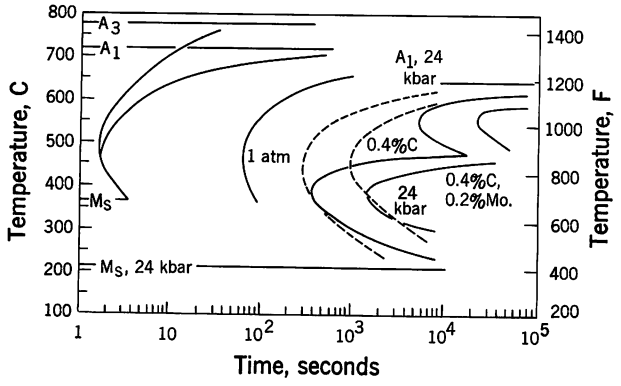

FIGURE 17. TTT diagrams of 0.4% C — 0.24% Mo steel at one atmosphere and at 24 kbar and comparison with TTT curve of 0.4% C steel at 24 kbar

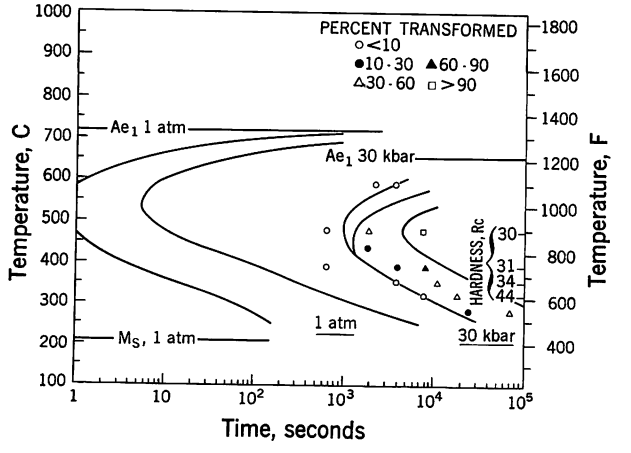

FIGURE 18. Isothermal transformation diagrams of 0.82% C steel at one atmosphere and at 30 kbar

Figure 17 illustrates two determinants of the transformation rate of austenite–alloy concentration and pressure. Ever since Davenport and Bain[19] displayed the kinetics of austenite decomposition in the form of TTT diagrams, efforts have been made to determine the nature of the rate-limiting processes. What are the rate-limiting processes? Carbon diffusion, diffusion of solute atoms, and the mobility of the interface between the transformed and parent phases have been proposed, but it has not been possible to decide between them on the basis of one-atmosphere transformation data alone.

Sufficient data are now available to attempt an analysis of decomposition kinetics in terms of the pressure variable. Referring to the TTT diagram for the 0.82% C steel in Figure 18, the pressure phenomena that must be accounted for are (1) the increase in transformation start time and (2) the increase in time from start to completion of transformation. The first factor is principally dependent on the rate of nucleation of the decomposition products, and the second primarily on the rate of growth of the new phases. Johnson and Mehl[20] described the progress of transformation analytically in terms of these rates, and such an analysis can be used here if it is restricted to the transformation start curve.[21,22] The mathematical expression for fraction transformed at a given temperature,

$$f = 1 - e^{-(\pi/3)Iu^3t^4} \qquad (1)$$

gives the fraction f in terms of I, the nucleation rate; u, the growth rate; and t, the time at temperature.

The transformation start curves at one atmosphere and at pressure both denote the same fraction transformed, $f_o = f_p$, and hence, the fractions being equal, the exponents of equation (1) are also equal.

$$I_o u_o^3 t_o^4 = I_p u_p^3 t_p^4 \qquad (2)$$

In the present work, the transformation times have been determined. Hilliard[23] has measured the changes in growth rate of pearlite at 30 kbar. The change in nucleation rate due to pressure can then be obtained in terms of ratios of rates and times at high pressure to those at one atmosphere.

$$\frac{I_o}{I_p} = \left(\frac{u_p}{u_o}\right)^3 \left(\frac{t_p}{t_o}\right)^4 \qquad (3)$$

Now, for the 1000-fold increase in transformation start time observed and the 40-fold reduction in growth rate found by Hilliard, this relation indicates that 30 kbar pressure reduces the nucleation rate by a factor of 16,000,000.

The energetics of a nucleation process are described in Figure 19. Below T_c, where phase II is stable, the formation of nuclei will initially entail an increase in energy, because of surface energy increments; but beyond the critical size i* volumetric energy changes dominate and result in a net energy decrease and nucleation of the new phase II. The energy barrier Δ^*g must be exceeded before the phase II is nucleated.

The energy increase upon nucleation, $\Delta_i g$, is given in terms of the nucleus size (i), the interfacial surface energy (σ), and the free-energy difference between phases I and II (Δg).

$$\Delta_i g = a\sigma i^{2/3} - \Delta g i \tag{4}$$

Δg is pressure dependent as

$$\Delta_p g = \Delta_o g - P\delta v \tag{5}$$

If the volume change (δv) upon transformation is positive, that is, a volume increase, Δg will be reduced as in the case of austenite decomposition. The pressure-induced changes in the nucleation barrier and the critical nucleus size can then be derived to be

$$\Delta_p{}^*g = \frac{\Delta_o{}^*g}{\left(1 - \frac{P\delta v}{\Delta_o g}\right)^2} \tag{6}$$

$$i_p{}^* = \frac{i_o{}^*}{\left(1 - \frac{P\delta v}{\Delta_o g}\right)^3} \tag{7}$$

The nucleation barrier and critical nucleus size will be greater at high pressure than at one atmosphere; thus, nucleation will be inhibited by pressure.

The kinetics of nuclei growth will be dependent on (Figure 20) (1) the energy difference between phase I and II (Δg), (2) the amount of work that must be done in the process of transformation (Δ^*f), and (3) the rate at which attempts to transform occur (ν_o). The net frequency of transformation (ν') will be the difference between the frequency of transformation from I to II and the reverse transformation, II to I.

$$\nu' = \nu_{I \longrightarrow II} - \nu_{II \longrightarrow I} = \nu_o e^{-\frac{\Delta^*f}{kT}}\left(1 - e^{-\frac{\Delta g}{kT}}\right) \tag{8}$$

The nucleation rate, I, is then given by $N^* n^* \nu'$, where $N^* = Ne^{-\frac{\Delta^*g}{kT}}$ is the number of nuclei of critical size; $n^* = bi^{*2/3}$, the number of atoms surrounding a nucleus capable of rendering it viable, and finally, ν', the frequency at which these atoms transform. If one assumes that the transformation process involved in nucleation is the same as that occurring in the subsequent growth of the nucleus, then the growth rate u can be expressed as $\lambda\nu'$, where λ is an increment of linear growth of phase II. One can then write

$$I = \nu_o b i^{*2/3} N\left(1 - e^{-\frac{\Delta g}{kT}}\right)e^{-\frac{\Delta^*f + \Delta^*g}{kT}} \tag{9}$$

$$u = \lambda\nu_o e^{-\frac{\Delta^*f}{kT}}\left(1 - e^{-\frac{\Delta g}{kT}}\right) \tag{10}$$

The factors Δg and Δ^*f in these expressions are pressure dependent. As before, $\Delta_o g$, the one-atmosphere energy difference, will be decreased by pressure if δv is positive. The transformation barrier potential $\Delta^*{}_o f$ will be modified by the amount Pv^*, where v^* is termed the activation volume of the transformation process.

$$\Delta_p{}^*f = \Delta_o{}^*f + Pv^* \tag{11}$$

When the expressions for nucleation and growth rates are written in terms of these energies at one atmosphere and at pressure, ratios of the transformation rates at one atmosphere to those at high pressure can be obtained.

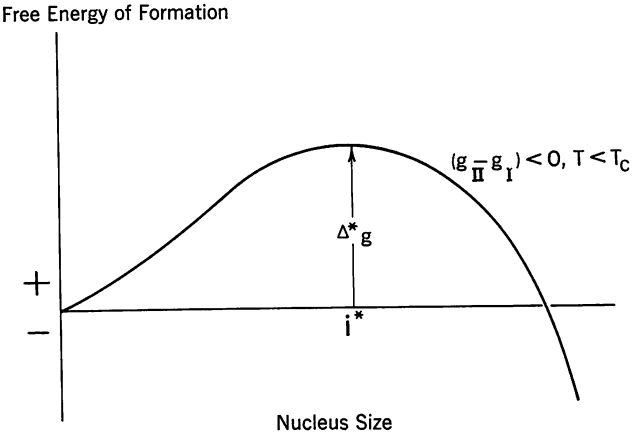

FIGURE 19. Energetics of nucleation

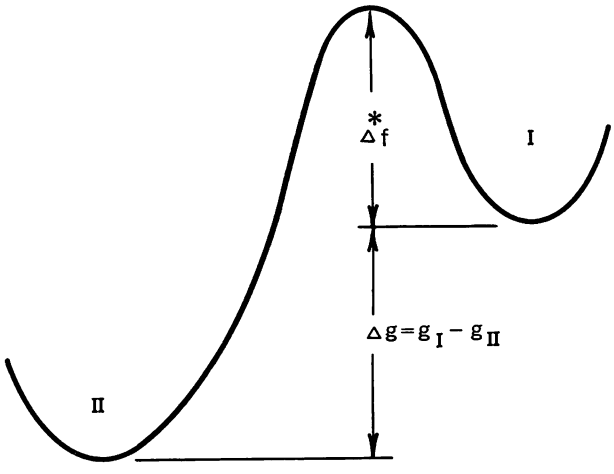

FIGURE 20. Energetics of the transformation from phase I to phase II

$$\frac{I_o}{I_p} = \left(1 - \frac{P\delta v}{\Delta_o g}\right) e^{\frac{P\,(v^* + \delta v i_o^*)}{kT}} \quad (12)$$

$$\frac{u_o}{u_p} = \frac{e^{\frac{Pv^*}{kT}}}{\left(1 - \frac{P\delta v}{\Delta_o g}\right)} \quad (13)$$

It was shown in equation (2) that through the Johnson-Mehl equation, transformation times are related to nucleation and growth-rate ratios. Thus, it is possible to obtain the ratio for transformation start time at pressure P to that at one atmosphere at a given temperature in terms of the parameters of transformation δv, V* and nucleus size i_o^*.

$$\frac{t_p}{t_o} = \left[\frac{I_o}{I_p}\left(\frac{u_o}{u_p}\right)^3\right]^{1/4} = \left(1 - \frac{P\delta v}{\Delta_o g}\right)^{-1/2} e^{\frac{P(v^* + 1/4\,\delta v i_o^*)}{kT}} \quad (14)$$

Note that the ratio of transformation start times is exponentially dependent on the pressure P. Therefore, while 30,000 atmospheres results in a 1000-fold increase in transformation start time, 1000-atmosphere pressure would increase the start time by only 25%. Only when pressure is of the order of 10,000 atmospheres and higher are the pressure effects on austenite transformation rates of consequence. Now, δv, the volume change on transformation at pressure is approximately the same as for transformation at one atmosphere, 0.1 cc/mole at 480 C (900 F). The energy difference, $\Delta_o g$, at one atmosphere and 480 C (900 F) is known, 350 cal/mole. u_o/u_p and t_p/t_o were determined from the pressure studies. Hence, v* and i_o^* can be calculated from the derived expressions. For the time ratio equal to 1000 and the growth rate ratio equal to 40, as determined at 30 kbar, the activation volume for austenite decomposition (V*) is found to be 7 cc/mole at 480 C (900 F). Hilliard and Tully[24] determined the activation volume for carbon diffusion in austenite to be approximately 1 cc/mole. Therefore, carbon diffusion does not appear to be the rate controlling process. On the other hand, 7 cc/mole is somewhat larger than the activation volume observed in self-diffusion or substitutional atom diffusion, which for iron is 6 cc/mole.[25,26]

It is not likely that the rate-controlling step is determined by bulk diffusion of either carbon or lattice atoms. Frye and coworkers have shown that the activation energies for the austenite decomposition process are composition-dependent and are considerably lower than those observed for lattice atom diffusion.[27] Their proposal that the rate-controlling process is localized at the phase interface seems to be supported by the present investigation and analysis.

The size of the critical nucleus at one atmosphere and 480 C (900 F), i_o^*, is computed to be 280 atoms. This size is consistent with Turnbull's estimate of nucleus size.[28]

This analysis has been premised upon the pressure-dependence of Δg and the barrier potential $\Delta^* f$. Hagel, Pound, and Mehl[29] determined the composition-dependence of Δg, and the work by Frye[27] provides evidence of the dependence of $\Delta^* f$ on the alloy content of the steel. The analysis derived above in terms of the pressure variable, can be carried through in terms of alloying-element concentrations. The changes in Δg and $\Delta^* f$ are expressed as a coefficient multiplied by the percentage of alloying element in the steel as:

$$\Delta g' = \Delta_o g + a\% \quad (15)$$

$$\Delta^* f' = \Delta_o^* f + b\% \quad (16)$$

In the expressions the primed quantity in each instance refers to the alloyed material. The expressions for growth rate and transformation time ratios will then be:

$$\frac{u_o}{u'} = \frac{e^{\frac{b\%}{kT}}}{\left(1 + \frac{a\%}{\Delta_o g}\right)} \quad (17)$$

$$\frac{t'}{t_o} = \left(1 + \frac{a\%}{\Delta_o g}\right)^{-1/2} e^{\frac{\%\,(b - 1/4\,a i_o^*)}{kT}} \quad (18)$$

In the case of manganese, which decreases the driving force Δg, the coefficient a is negative; manganese also increases the activation barrier ($\Delta^* f$), hence, the coefficient b is positive. Thus, for manganese steels, these expressions would indicate a slower growth rate and longer transformation time, that is, increased hardenability. On the other hand, the coefficient a is positive for cobalt, and the coefficient b is negative, indicating that cobalt additions increase the growth rate and shorten the transformation time; this is, in fact, the observed effect of cobalt on the transformation kinetics of steels.

For the case of several alloying additions, the changes in Δg and $\Delta^* f$ will be additive for small alloy levels,

$$\Delta g' = \Delta_o g + a_1\%_1 + a_2\%_2 \quad (19)$$

$$\Delta^* f' = \Delta_o^* f + b_1\%_1 + b_2\%_2 \quad (20)$$

The resulting expression for the ratio of transformation start times involves a multiplication of exponential factors of the individual alloy concentration.

$$t'/t_o = \left(1 + \frac{a_1\%_1 + a_2\%_2}{\Delta_o g}\right)^{-1/2} e^{\frac{\%_1(b_1 - 1/4 a_1 i_o^*)}{kT}} \times e^{\frac{\%_2(b_2 - 1/4 a_2 i_o^*)}{kT}} \quad (21)$$

When the exponential terms are expanded to first order,

$$\frac{t'}{t_o} = (1 + B_1\%_1)\,(1 + B_2\%_2) \quad (22)$$

the result is consistent with the empirical expression for the calculation of hardenability (the pre-exponential factor is of the order of one) where multiply-

ing factors are used to express the individual hardenability contribution of alloy elements. At the present time, alloy steels are being investigated and this analytical approach is being assessed.

In summary, there is no question but that high pressure is an important metallurgical variable. The effects of pressure on austenite decomposition are not discontinuous and, within the limits of pressure investigated, have not produced microstructures that would indicate a fundamental change by pressure in the mechanisms of decomposition. The decomposition processes are intimately related to the phase relationships, producing similar morphologies for the same relationship whether that relationship is determined by composition or pressure. With such continuity of mechanisms up to high pressures, the pressure variable should be a powerful investigative tool, yielding not only information on pressure effects per se, but, by improving our understanding of basic metallurgical phenomena, it may help materially in the systematic optimization of steel compositions and heat treatment at one atmosphere.

REFERENCES

1. E. Abbott, *Flatland*, Dover, New York, 1963
2. E. Mallard and H. LeChatelier, Compt. Rend. (Paris), *97*. 102 (1883)
3. W. C. Roberts-Austen, Proc. Inst. Mech. Engrs. 102 (1893)
4. C. Benedicks, J. Iron and Steel Inst. (London), *77*. 153 (1908)
5. P. W. Bridgman, *The Physics of High Pressure*, G. Bell and Sons, London, 1958
6. M. B. Bever and R. Rocca, Rev. Met. (Paris), *48*. 363 (1951)
7. S. A. Kulin, M. Cohen and B. L. Averbach, J. Metals *4*. 661 (1952)
8. F. P. Bundy, H. T. Hall, H. M. Strong and R. H. Wentorf, Jr., Nature *176*. 51 (1955)
9. J. E. Hilliard, Trans. AIME *227*. 429 (1963)
10. J. E. Hilliard and J. W. Cahn, "The Effect of Pressure on Transformation Rates," *Progress in Very High Pressure Research*, edited by F. P. Bundy, W. R. Hibbard, Jr., and H. M. Strong, Wiley, New York, 1961, 109
11. S. V. Radcliffe, M. Schatz and S. A. Kulin, J. Iron and Steel Inst. (London), *201*. 143 (1963)
12. G. V. Smith and R. F. Mehl, Trans. AIME *150*. 211 (1942)
13. A. B. Greninger and A. R. Troiano, Trans. AIME *140*. 311 (1940)
14. J. R. Vilella, Trans. AIME *140*. 332 (1940)
15. W. Jellinghaus, Arch. Eisenhüttenw. *28*. 469 (1957)
16. G. R. Speich and M. Cohen, Trans. AIME *218*. 1050 (1960)
17. S. J. Matas and R. F. Hehemann, Trans. AIME *221*. 179 (1961)
18. J. R. Blanchard, R. M. Parke and A. J. Herzig, Trans. ASM *31*. 849 (1943)
19. E. S. Davenport and E. C. Bain, Trans. AIME *90*. 117 (1930)
20. W. A. Johnson and R. F. Mehl, Trans. AIME *135*. 416 (1939)
21. J. W. Cahn, Acta Met. *4*. 449 (1956)
22. M. Avrami, J. Chem. Phys. *9*. 177 (1941)
23. J. E. Hilliard, ASD Tech. Rept. TDR-62-479, Part I, May 1963
24. J. E. Hilliard and W. R. Tully, ASD Tech. Rept. TDR-61-21, Part I, May 1961
25. D. Lazarus and N. H. Nachtrieb, "Effect of High Pressure on Diffusion," *Solids Under Pressure*, edited by W. Paul and D. M. Warschauer, McGraw-Hill, New York, 1963, 43
26. J. I. Goldstein, R. E. Hanneman and R. E. Ogilvie, Trans. AIME *233*. 812 (1965)
27. J. H. Frye, Jr., E. E. Stansbury and D. L. McElroy, Trans. AIME *197*. 219 (1953)
28. D. Turnbull, "Phase Changes," *Solid State Physics*, edited by F. Seitz and D. Turnbull, Academic Press, New York, 1956, Vol. 3, 225
29. W. C. Hagel, G. M. Pound and R. F. Mehl, Acta Met. *4*. 37 (1956)

ORAL DISCUSSION OF

Austenite Decomposition at High Pressure

Presented by T. G. NILAN

S. V. RADCLIFFE (Case Institute of Technology). There is some recent work by Homan at Waterliet Arsenal* which clearly indicates, in the temperature range of interest, a significant effect of pressure on carbon diffusion in alpha-iron.

One of the points which kept coming out during the talk was that pressure only modifies slightly the structures formed on austenite decomposition. However, everything we have talked about this morning deals with what are really metastable structures which form in the Fe–C system, i.e., not the equilibrium iron–graphite system. I would not like this audience to go away with the idea that decomposition behavior at pressure is a simple continuation of that at atmospheric pressure. In fact, there is direct experimental evidence** that one can create completely different structures at pressure from those discussed here. This is not to question the "continuity" of the effect; obviously if the pressure is raised progressively, there is a corresponding shift of the phase boundaries, a retarding effect on the kinetics, and a modest change in structures. However, at some point, another intermediate transformation may take over, as being capable of a higher rate under the imposed conditions. Thus for example, there can be direct precipitation of carbide from austenite, and consequently, the bainitic structures do not appear.

AUTHOR'S REPLY. I have made a comparison between the activation volume for the transformation (7 cc/mole) and the activation volume for carbon diffusion in austenite (1 cc/mole) to put in question those theoretical models of the transformation in which the diffusivity of carbon in austenite is considered to be the rate-limiting step. The work by Homan, which to my knowledge has not yet been published, would also necessitate a reexamination of those theories of pearlite growth based upon carbon diffusivity.

The fact that we do not observe decomposition phenomena in our pressure studies which would indicate a fundamental change in decomposition mechanisms should not be extrapolated beyond our studied range of pressure. It is entirely reasonable to expect modifications of these mechanisms by sufficiently high pressure. It is important, however, to recognize that, within a range of pressure in which there are significant changes in kinetics and morphology of the decomposition of austenite, the fundamental mechanisms appear to be the same as at one atmosphere. The aim of our studies is to exploit the pressure variable as a means to clarify one atmosphere phenomena, and such continuity of mechanisms is essential for our purpose. There are differences in detail with increasing pressure even within this range, just as variations in composition will change the details of morphology at one atmosphere. Gross morphological changes, however, were not found. The columnar bainite microstructure is an example.

M. COHEN (Massachusetts Institute of Technology). What is the carbide in that constituent?

AUTHOR'S REPLY. The carbides extracted from the columnar bainites were found to be Fe_3C. There was no evidence of ϵ carbide.

D. L. ALBRIGHT (International Harvester Research). When you used the two surface technique to examine the bainite and subsequently disputed the 55° growth form, did you observe any other preferred angle of growth?

AUTHOR'S REPLY. From the two surface micrography study we have proposed a spatial arrangement for the carbides that would give rise to the various observed microstructures when sectioned. The bainite structure is considered a lath with the lenticular carbides arrayed parallel to the direction of most rapid growth of the lath and to the smaller transverse lath dimension. A transverse section would then show the carbides perpendicular to the longer transverse dimension, as can be inferred from Figure 10.

*C. G. Homan and J. F. Cox, *Physics of Solids at High Pressures*, Academic Press, New York, 1965

**S. V. Radcliffe, M. Schatz and S. A. Kulin, J. Iron and Steel Inst. (London), *201*. 143 (1963)

Bainitic Microstructures in Low-Carbon Alloy Steels and Their Mechanical Properties

L. J. HABRAKEN
Centre National de Recherches Métallurgiques
and Associate Professor at the University of Liège

M. ECONOMOPOULOS
Centre National de Recherches Métallurgiques
Liège, Belgium

INTRODUCTION

Since Davenport and Bain succeeded in 1930 in producing by isothermal treatments a structure intermediate between the equilibrium constituents of steel and martensite, a considerable number of investigations have been carried out in this field.[1-5]* They have been aimed at determining the kinetics of formation of this intermediate structure on the one hand and its mechanical properties in view of possible practical applications on the other. The more recent studies devoted to bainitic structures clearly reveal these two lines of thought. Some have a fundamental character and concern mainly the thermodynamics and more particularly the kinetics of the bainite reaction; while others have more practical aims, mostly concerned with the mechanical properties of bainitic structures.

In our opinion, it is useful to emphasize here the difference between these two points of view. Indeed the interpretation of the observed phenomena, at least from the fundamental viewpoint, must be sought in the most intimate mechanisms of solid-state transformations. In this respect, transmission electron microscopy is a particularly good means of investigation. On the other hand, the user is interested in the mechanical properties of bainitic structures and it appears possible to relate the tensile strength, impact toughness and ductility to more "macroscopic" factors such as the bainitic grain size, and the size and distribution of carbides.

Furthermore, whatever point of view is adopted, due consideration must be given to whether the bainitic structures are the result of an isothermal transformation or whether they are produced on continuous cooling. Actually, the paths followed by the austenite in the metastable field — that is, between the A_3 point and the temperature at which transformation starts — are vastly different in the two cases. As a result, although the fundamental mechanisms involved do not necessarily differ, their effects, that is, the microstructures produced, can.

The present trend in the field of structural steels is to increase their alloy content with a view to obtaining high strengths without having to resort to heat treatment. As a result, increasing amounts of bainitic structures can be expected in parts made from such steels, even from the so-called low-alloy grades. In fact, some steels are already being used in the fully bainitic condition. Accordingly, it becomes increasingly necessary to improve our understanding of the intermediate structures and in particular to determine the factors underlying the strengthening of the bainitic structures and to evaluate the possibilities of influencing the intrinsic properties of these structures through modifications in composition or thermomechanical treatment. This kind of knowledge would make it possible to define composition

*See references.

ranges that would be conducive to improved strength combined with a given set of other mechanical properties.

The present paper is intended as a contribution to the above topics. We shall first describe the intermediate structures occurring in steels, especially those with a fairly low carbon content (under 0.3%). This will enable us to ascertain the hardening mechanisms operative in bainite and to propose a tentative transformation mechanism. In the second part of the paper, a study of the mechanical properties of the various structures occurring in the bainitic field will let us determine whether a given structure is more beneficial than another.

PART ONE. MICROSTRUCTURES IN THE INTERMEDIATE TRANSFORMATION FIELD: THEIR CHARACTERISTICS AND KINETICS OF FORMATION

GENERAL DEFINITION OF BAINITIC STRUCTURES

The definition of bainite currently found in technical literature[7,8] is along the following lines: Bainite is a constituent of steels which is formed by the decomposition of austenite within a temperature range located between the field of martensite formation and that of ferrite and pearlite formation. This constituent consists of an aggregate of acicular ferrite and carbides. Its morphology changes progressively with the transformation temperature in that the size of the particles and the acicularity of the structure increase as the temperature decreases. The bainitic transformation field is often divided into two parts according to the structural aspect of the product. In many steels the transition between the two types of structure lies around 350 C (660 F). As a first approximation, this temperature does not seem to be greatly dependent on composition.

Numerous electron-microscopic investigations have shown that in lower bainite, i.e., that obtained below 350 C (660 F), the carbides lie at an angle of approximately 60° to the axis of the ferrite plates.[2,3,9] In general, the tips of the ferrite plates are tapered and appear to be free of carbides. The lateral boundaries of the plates are often practically plane and the carbides are in contact with them.[10] According to the ASTM Subcommittee No. XI,[2] Hehemann[4] and Pomey,[11] the first type of carbide to form is ϵ iron carbide. Cementite, however, is generally substituted for this carbide at a later stage. Nevertheless, the ferrite seems to remain saturated with carbon.

Upper bainite, which forms above 350 C (660 F), comprises larger ferrite plates bounded by Fe_3C precipitates formed directly from the austenite. The carbides lie parallel to the direction of preferred growth of the ferrite plates. During the formation of upper bainite, the carbon content of the austenite increases so the ferrite formed is practically free of carbon. According to some authors, enrichment of the austenite in carbon also precedes the transformation.[3,12-16] Finally, the ferrite plates produced in the upper part of the temperature range for bainite transformation are very large and often are surrounded with groups of cementite particles formed in the supersaturated austenite.

IDENTIFICATION AND MORPHOLOGY OF INTERMEDIATE STRUCTURES IN LOW-CARBON STEELS

In the course of several investigations concerned with the morphology and mechanical properties of various steels, we have had the opportunity to observe numerous aspects of the so-called bainitic structures.[3,17-21] In many cases we have been able to show the occurrence of structures that did not correspond to the accepted definition given above in medium or low-alloy steels with up to 0.3% C treated in the intermediate range. These structures consisted of ferrite and carbon-rich zones, partly transformed into martensite, that did not necessarily contain carbides. It should be noted that these structures were more easily produced by continuous cooling than by isothermal holding.

Steels Investigated

The chemical compositions of the steels that will be discussed in the present paper are listed in Table I. The steels chosen were not only low-carbon steels but also some high-carbon steels and one ferrous alloy to permit a comparison of the structures obtained. They include:

- a eutectoid steel with 0.87% C investigated by ASTM Subcommittee XI
- a chromium–vanadium steel with 0.63% C and a nickel–chromium–molybdenum die-block steel
- a chromium–cobalt ferrous alloy with under 0.005% C
- a chromium–molybdenum tubing steel
- a group of low-alloy structural steels
- an ultrahigh-strength nickel–cobalt steel

Typical continuous-cooling transformation diagrams as well as micrographs of representative

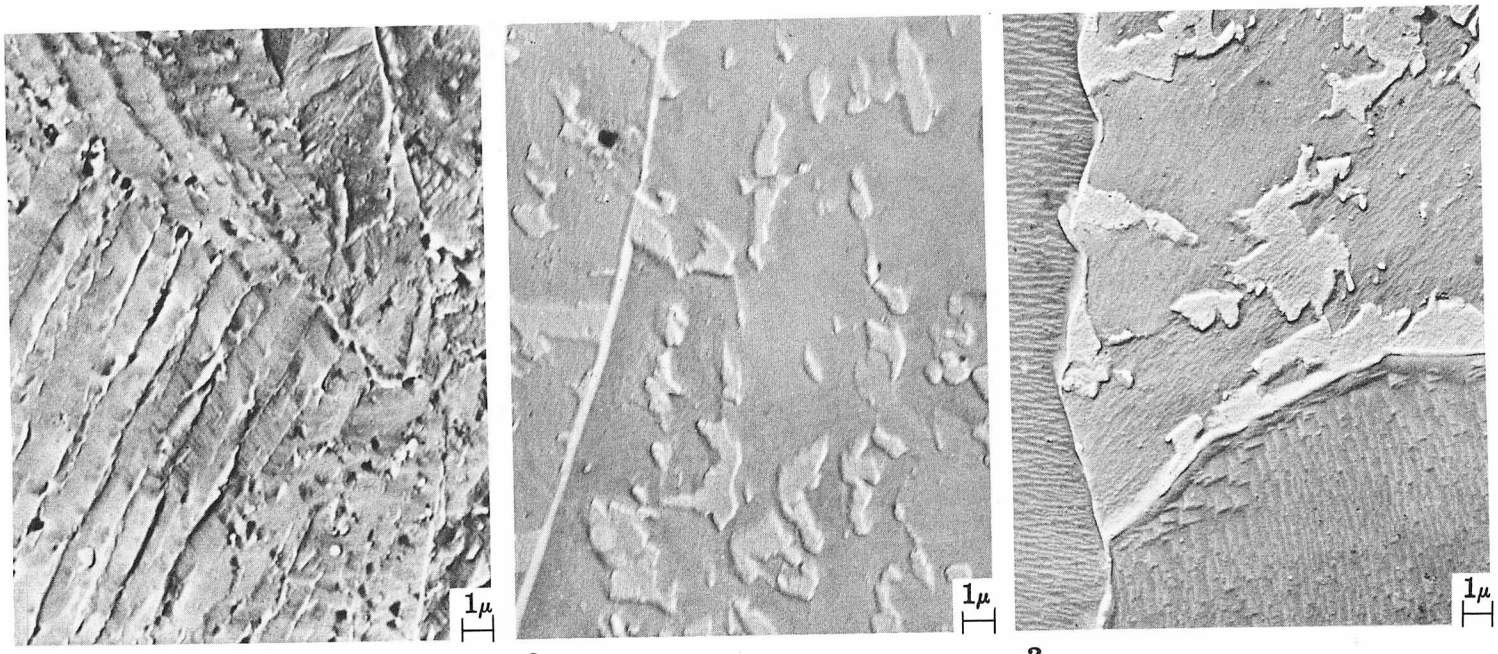

	1	2	3
Cooling rate	2400 C/min (4320 F/min)	220 C/min (395 F/min)	1.1 C/min (2 F/min)

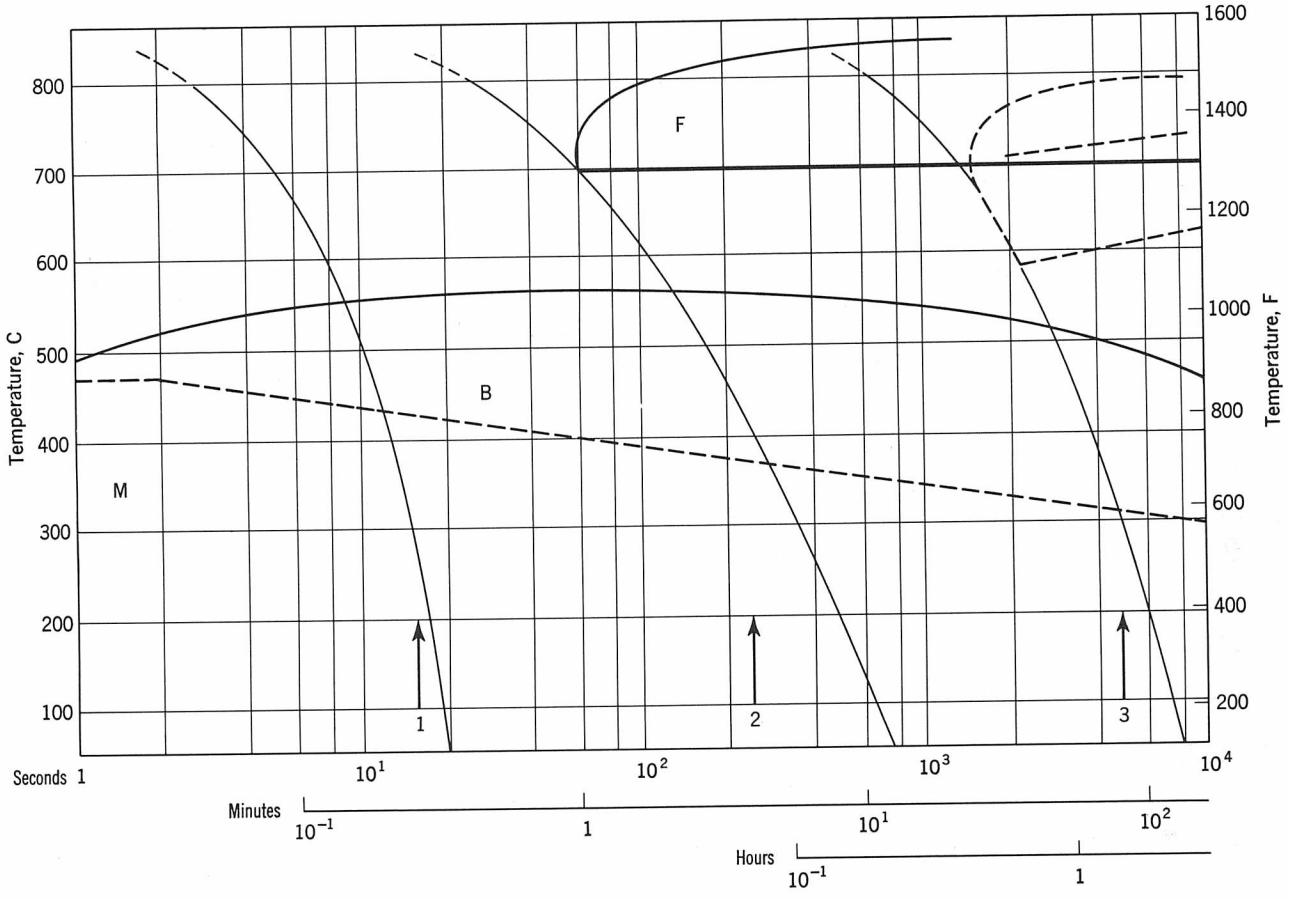

FIGURE 1. CCT diagram of 2¼% Cr–1% Mo steel V. Electron micrographs, plastic negative replicas, of structures produced in bainitic range on continuous cooling at indicated rates

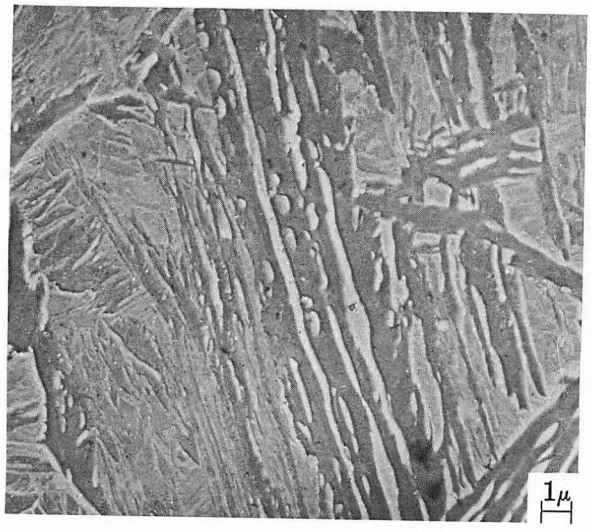

1 Cooling rate 790 C/min (1422 F/min)

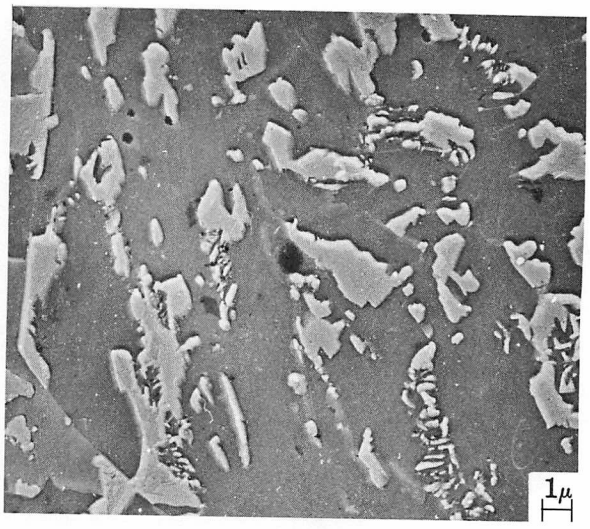

2 60 C/min (110 F/min)

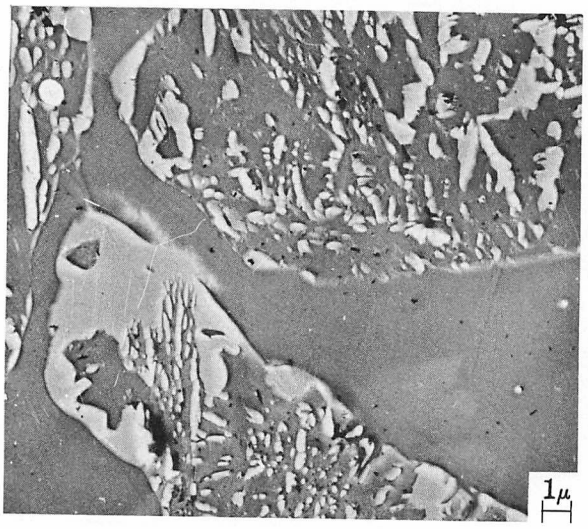

3 1.25 C/min (2.25 F/min)

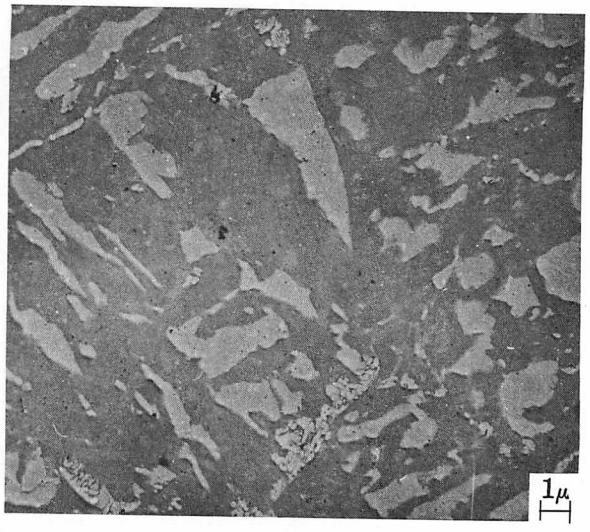

4 One hour at 550 C (1020 F)

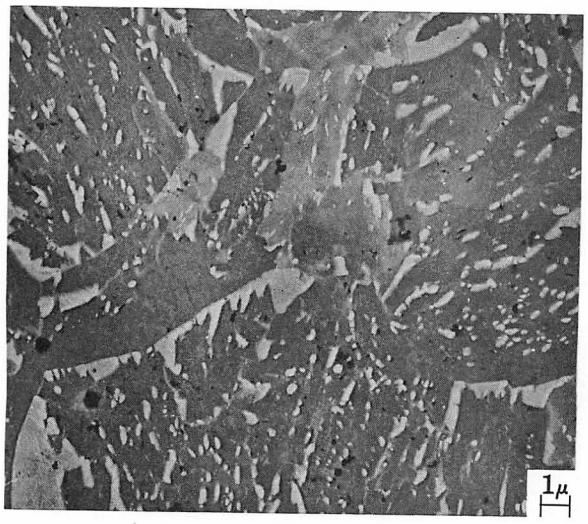

5 One hour at 500 C (930 F)

FIGURE 2. CCT diagram of 1.5% Mn–0.5% Mo–B steel VII. Electron micrographs, plastic negative replicas, of structures produced in bainitic range on continuous cooling at indicated rates (no. 1, 2 and 3) and on isothermal holding (no. 4 and 5). (See diagram on opposite page)

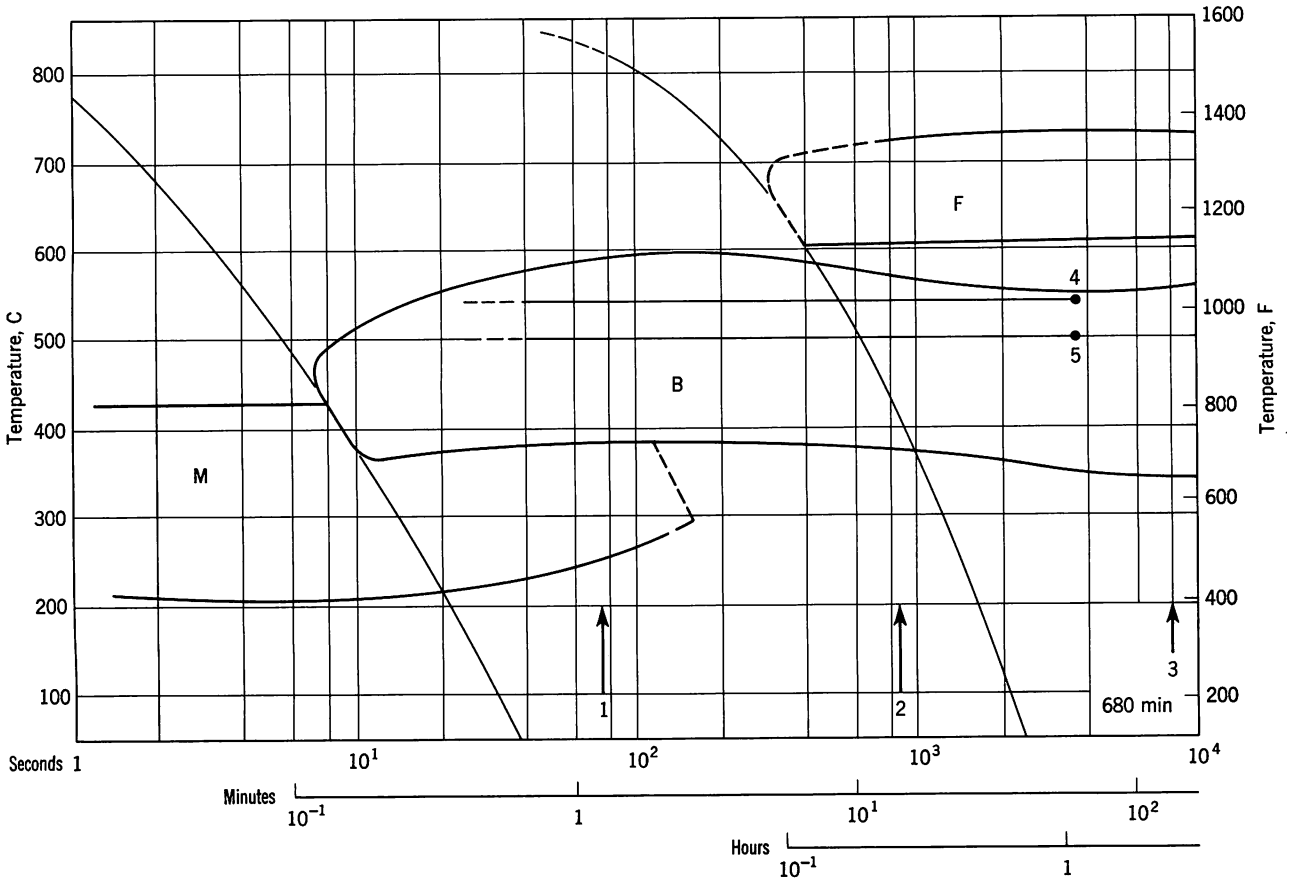

TABLE I Chemical Composition of Steels Investigated*

		%C	%Mn	%Si	%S	%P	%Cr	%Mo	%Ni	%V	%B	% Other
II	Eutectoid Steel	0.87	0.44	0.17	0.021	0.013	0.21	—	0.39	—	—	—
XI	1% Cr–V Steel	0.63	0.49	0.25	—	—	0.92	0.05	—	0.2	—	—
XII	Die-Block Steel	0.54	0.55	0.26	—	—	1.16	0.48	4.12	—	—	0.80 W
III	Fe–12% Cr–10% Co Alloy	0.005	—	—	—	—	12.	—	—	—	—	10 Co
V	2¼% Cr–1% Mo Steel	0.11	0.41	0.43	0.012	0.012	2.10	1.02	0.25	—	—	—
VII	1.5% Mn–0.5% Mo–B Structural Steel	0.21	1.46	0.38	0.019	0.016	—	0.45	—	—	0.0017	—
VIII	1% Cr–0.5% Mo Structural Steel	0.19	0.60	0.30	0.021	0.023	1.07	0.48	—	—	—	0.047 Al
IX	1% Cr–0.5% Mo–B Structural Steel	0.19	0.62	0.36	0.025	0.022	1.03	0.49	—	—	0.006	0.041 Al
X	2.7% Ni–0.9% Cr–0.25% Mo–B Structural Steel	0.19	0.57	0.35	0.009	0.018	0.87	0.25	2.72	0.10	0.0017	—
XIII	9% Ni–4% Co Ultrahigh-Strength Steel	0.32	0.13	0.15	0.005	0.090	—	—	9.05	—	—	4.07 Co

* Weight percent.

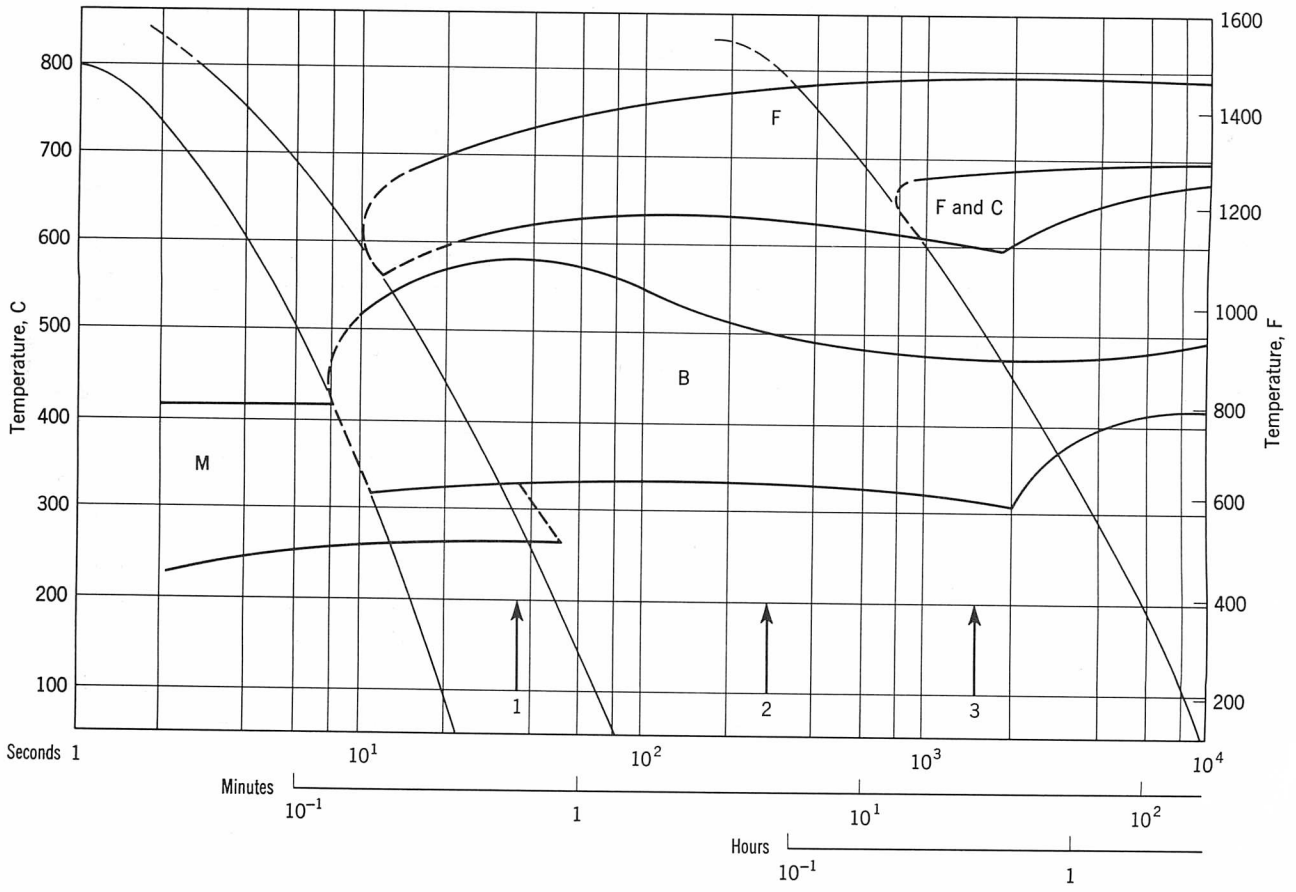

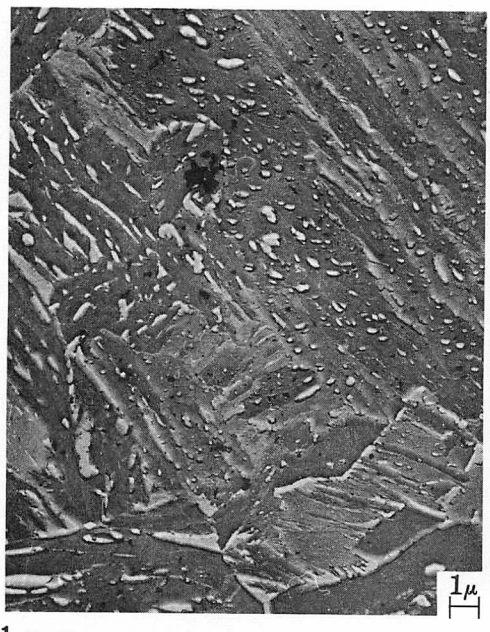

1 Cooling rate 1440 C/min (2590 F/min)

2 168 C/min (300 F/min)

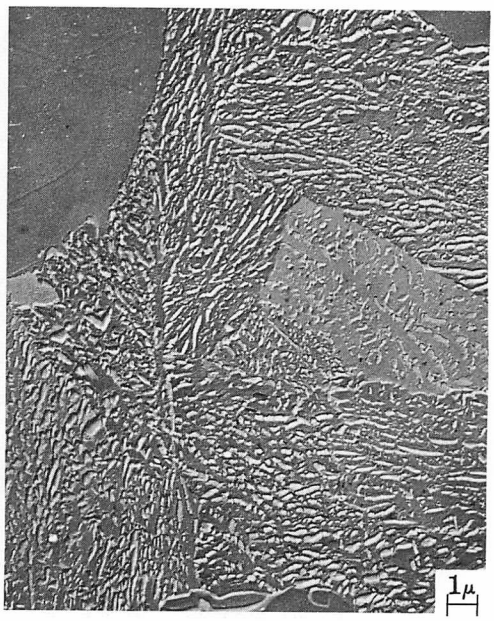

3 44 C/min (79 F/min)

FIGURE 3. CCT diagram of 1% Cr–0.5% Mo steel VIII. Electron micrographs, plastic negative replicas, of structures produced in bainitic range on continuous cooling at indicated rates

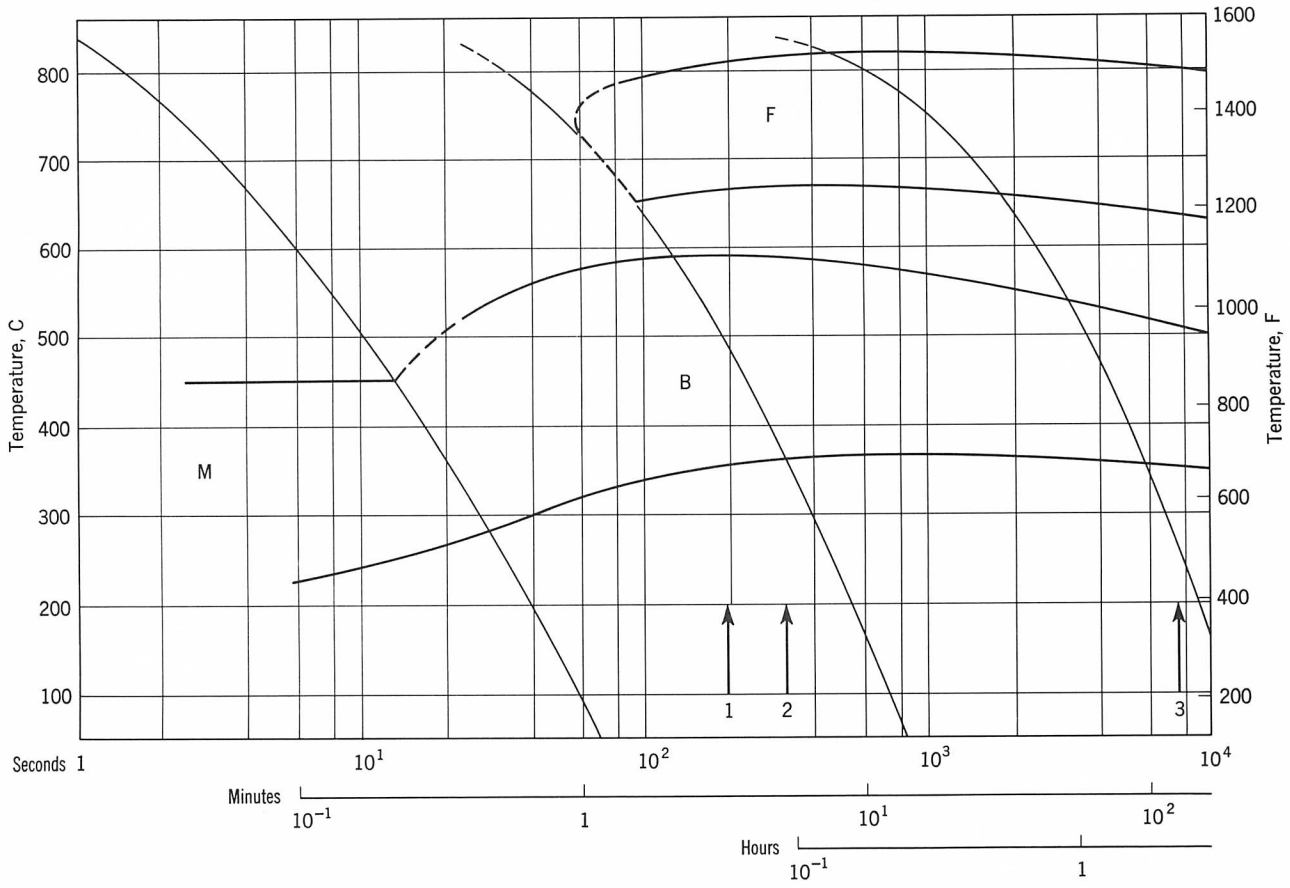

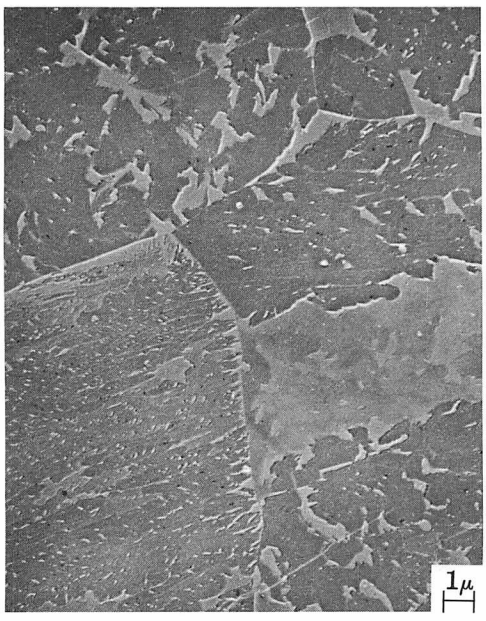

1
Cooling rate 270 C/min (485 F/min)

2
168 C/min (300 F/min)

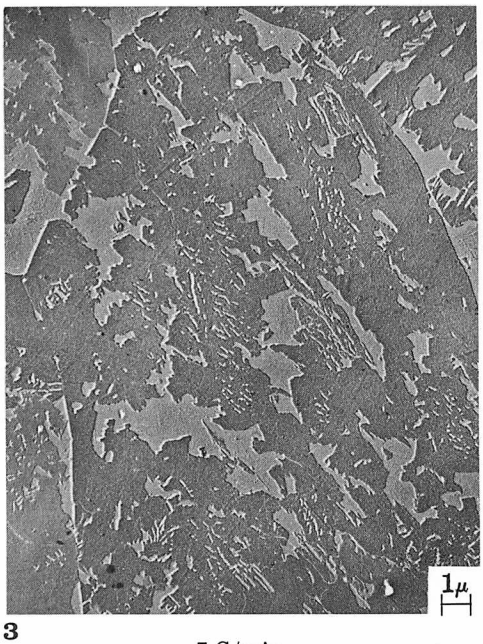

3
7 C/min (13 F/min)

FIGURE 4. CCT diagram of 1% Cr–0.5% Mo–B steel IX. Electron micrographs, plastic negative replicas, of structures produced in bainitic range on continuous cooling at indicated rates

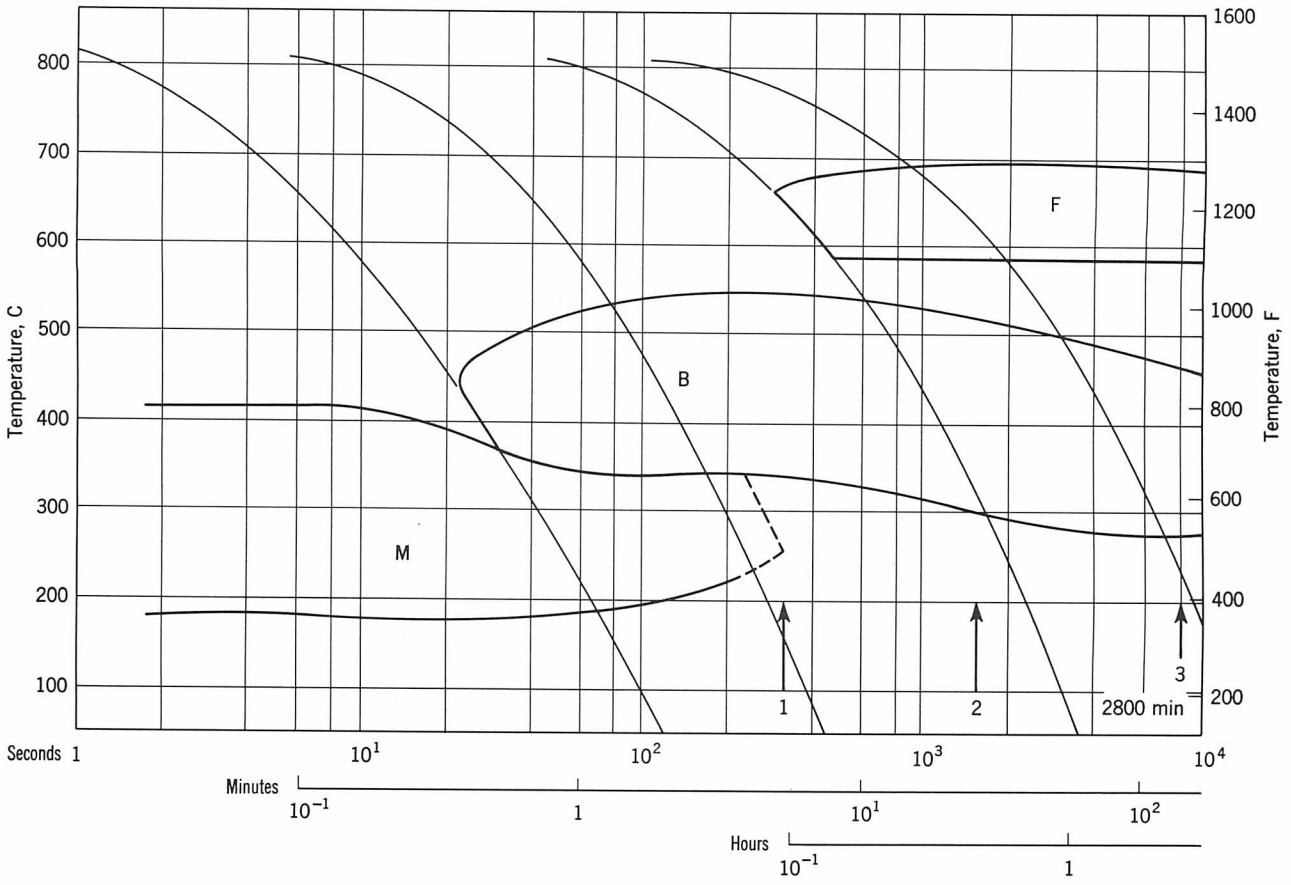

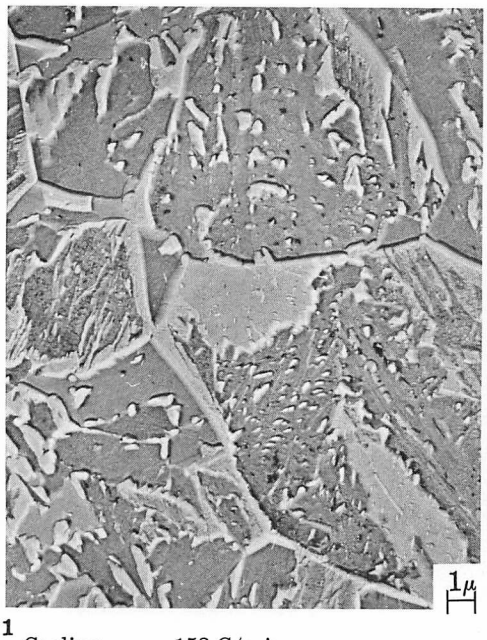

1
Cooling rate 158 C/min (285 F/min)

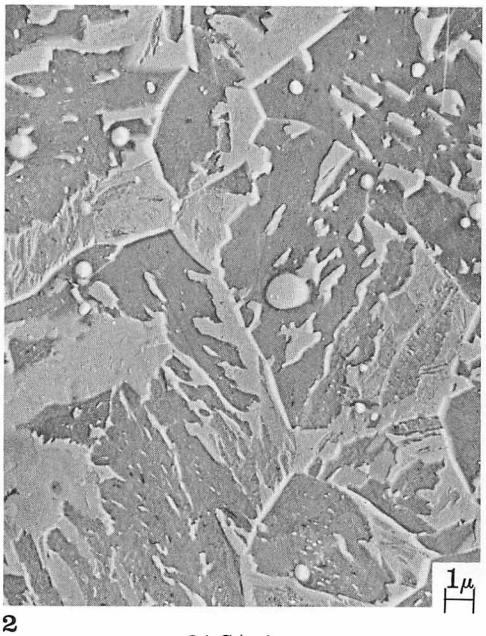

2
34 C/min (60 F/min)

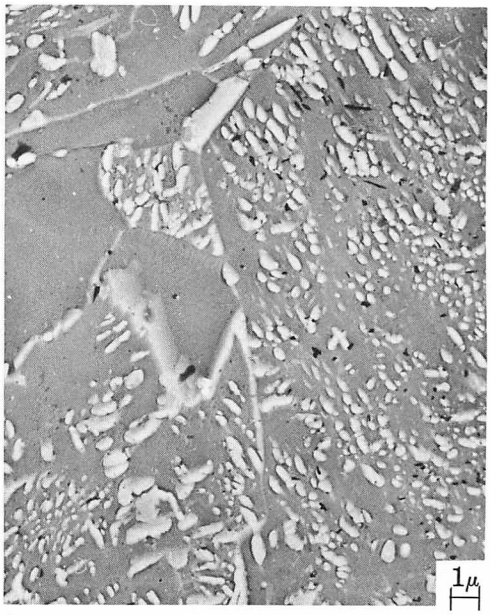

3
0.31 C/min (0.56 F/min)

FIGURE 5. CCT diagram of 2.7% Ni–0.9% Cr–0.25% Mo–B steel X. Electron micrographs, plastic negative replicas, of structures produced in bainitic range on continuous cooling at indicated rates

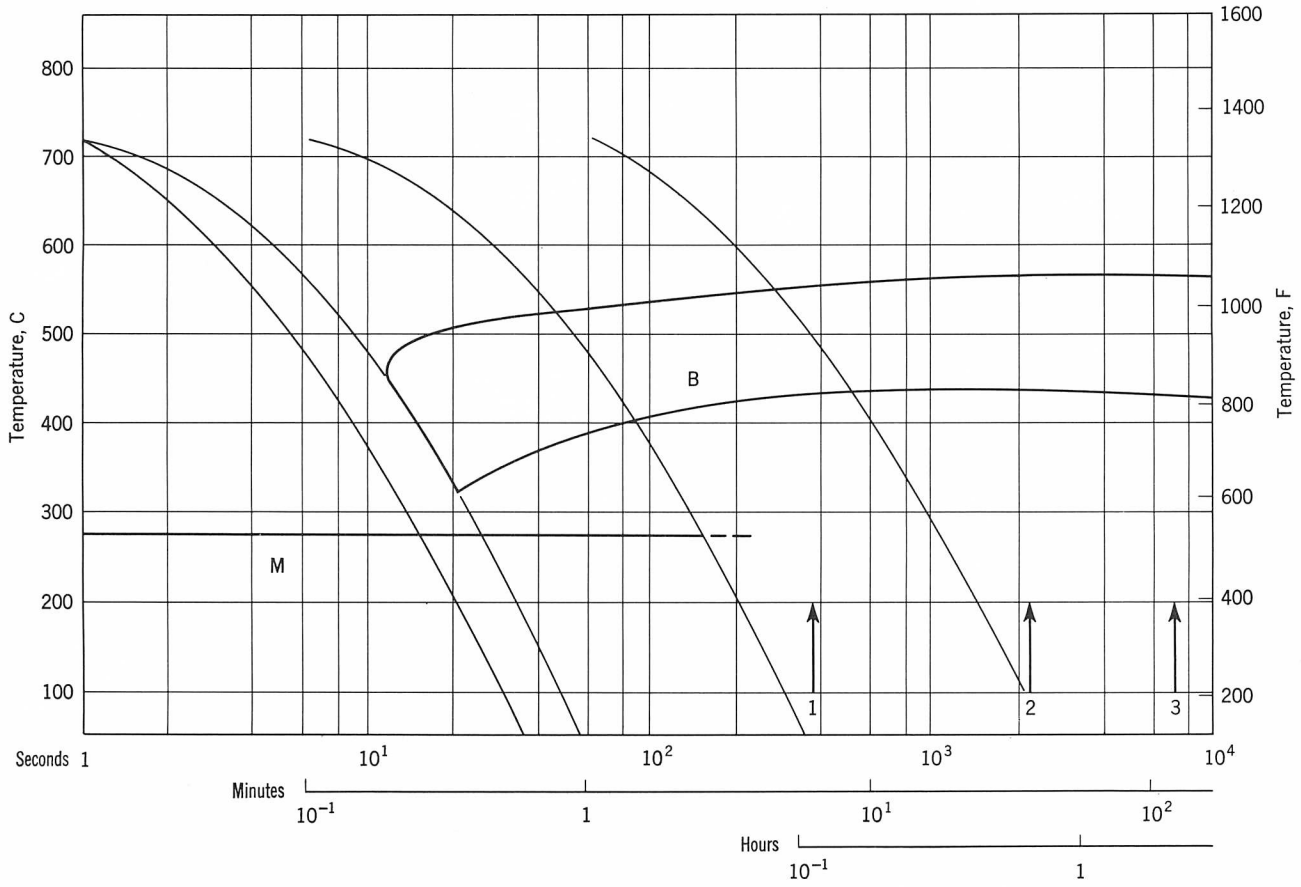

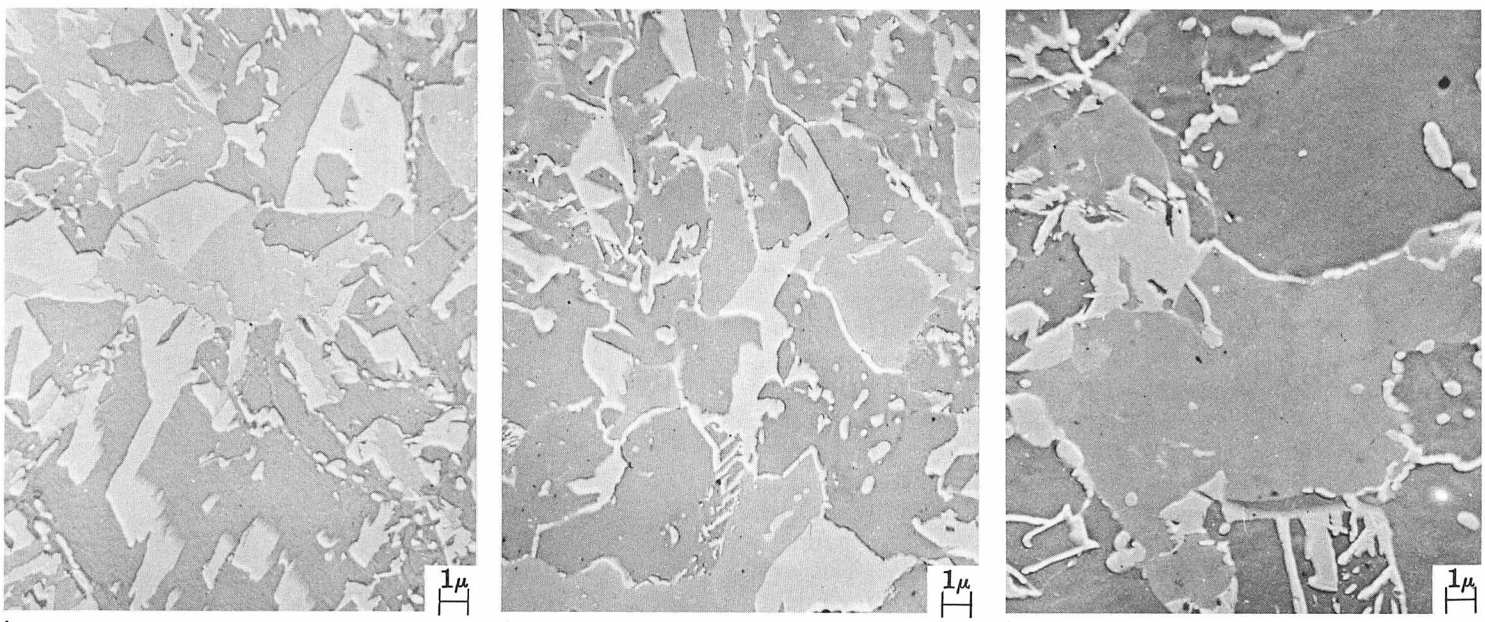

	1	2	3
Cooling rate	110 C/min (200 F/min)	21 C/min (38 F/min)	5 C/min (9 F/min)

FIGURE 6. CCT diagram of 9% Ni–4% Co ultrahigh-strength steel XIII. Electron micrographs, plastic negative replicas, of structures produced in bainitic range on continuous cooling at indicated rates

structures are shown in Figures 1 through 6. The cooling rates of the continuously cooled specimens illustrated in the micrographs are indicated in the diagrams by arrows while the horizontal lines refer to the isothermally transformed specimens.

We do not intend to consider systematically each of the steels listed above. Rather, we shall endeavor to define for each the different aspects of the intermediate structures that can be obtained. We shall then attempt to classify these structures and to compare them with conventional bainites.

Methods of Investigation

The continuous-cooling transformation diagrams were established by thermal and dilatometric analysis combined with metallographic observations.

Dilatometric Analysis A special dilatometer was used to achieve the widest possible range of cooling rates with good reproducibility of tests. The principle of this dilatometer is described at length in the papers listed under reference 22 and may be briefly outlined as follows: Changes in the length of the specimen are transmitted to a displacement sensor (differential transformer) and alter the balance of an AC Wheatstone bridge. After amplification and filtering, the out-of-balance voltage is fed to a recording potentiometer. Consequently, the displacement of the recording pen is proportional to the variation in length of the specimen. A second potentiometer connected to a thermocouple welded to the specimen records the latter's temperature as a function of time.

The specimens were cylinders, 4 mm in diameter by 30 mm long. For the tests involving the fastest cooling rates, the specimen diameter was reduced to 2.6 mm to decrease the thermal inertia. The cooling rates that were achieved ranged from 750 to 3600 C/hr (1350 to 6480 F/hr.) It should be added that the accuracy of the measurements decreased as the cooling rate approached either limiting value.

Absolute Thermal Analysis The curves indicating the noses of the stable or metastable transformation in some grades lie very close to the vertical axis with transformation setting in after times of the order of 0.01/0.1 sec. In these cases it was necessary to resort to absolute thermal analysis. The principle of the apparatus used is given in references 23 and 24. The specimens were small discs, 4 mm in diameter by 0.5/2 mm thick, with very low thermal inertia. The temperature was measured by means of a thermocouple welded to the specimen. Cooling rates from 2 to 900 C/sec (3.6 to 1620 F/sec) were achieved by blowing compressed nitrogen over the specimen.

Metallography and X-Ray Diffraction Extensive use of the replica technique in electron metallography often made it possible to differentiate clearly

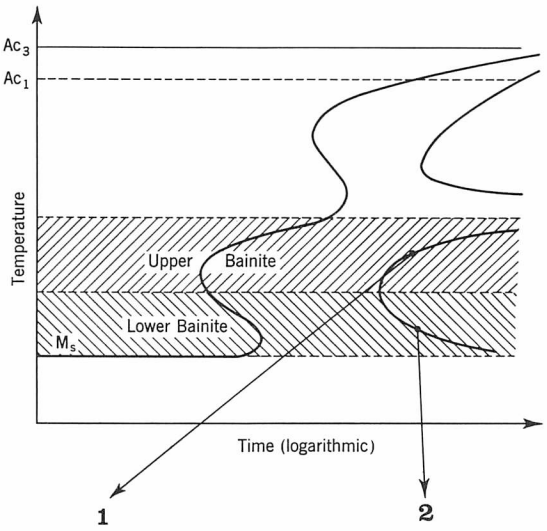

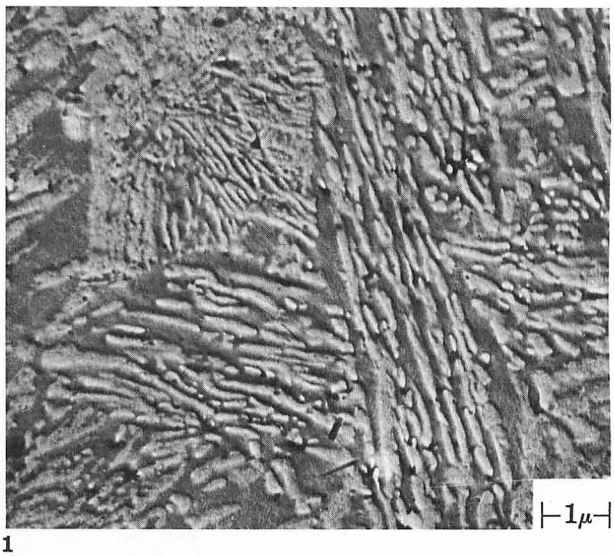

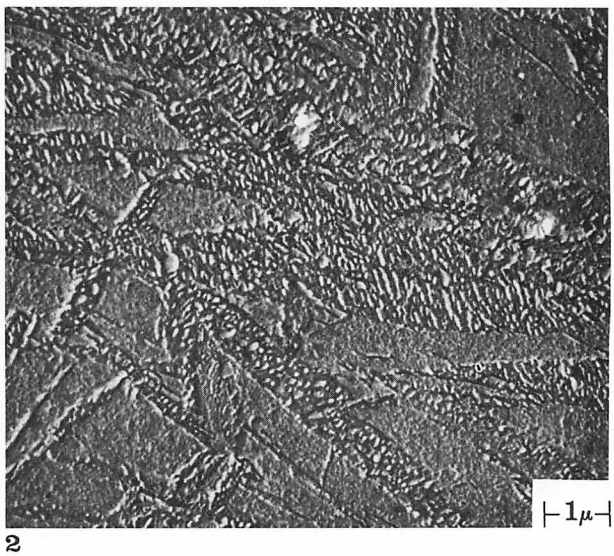

FIGURE 7. Typical structures of conventional upper and lower bainites in high-carbon steels. Electron micrographs, plastic negative replicas. 5000 X

among the structures present, especially in the bainitic field, even at relatively low magnifications of the order of 5000 X.

We made a special effort to obtain the maximum amount of information on the austenitic-martensitic structures encountered. The metallographic techniques let us estimate the volume percentage of these structures while the percent austenite could be determined by an X-ray analysis method. The latter newly developed method is based on statistical treatment of the data by computer so the detrimental effects of extinction and microabsorption can be eliminated.[25]

Finally, more exhaustive structural analyses were carried out on selected specimens by electron microscopy using the thin-foil technique. The joint use of diffraction and microscopy made it possible to define the orientation relations among the structures.

Characteristic Microstructures

Our systematic investigation resulted in the identification of several types of microstructures as having been produced in the intermediate transformation zone on isothermal holding as well as continuous cooling.

In the isothermal transformation (IT) diagram, the bainitic field is usually divided into two horizontal bands corresponding to upper and lower bainite (Figure 7). By analogy, the bainitic field in a continuous-cooling transformation (CCT) diagram can be divided into two or more vertical bands corresponding to different types of bainites. The analogy will be complete if the variable plotted along the horizontal axis is not elapsed time but the cooling time between two given temperatures, for instance 800 and 500 C (1470 and 930 F), as shown in Figure 8.

Actually, we were able to identify three types of structures: ferrite–carbide structures; carbide-free acicular structures; and almost granular structures or structures consisting of coarse plates. For some grades these structures were more clearly distinguishable as isothermally transformed than as continuously cooled; but for most grades they were better defined in continuous-cooled specimens than after isothermal transformation.

Ferrite–Carbide Structures The conventional upper and lower bainitic structures, such as mentioned above, occur over the entire bainitic field in the case of high-carbon steels such as the eutectoid steel II and the chromium–vanadium steel XI of this paper. Isothermal treatments produce well-defined structures of this type, such as the typical examples illustrated in Figure 7, micrograph 1 (upper bainite in eutectoid steel II) and micrograph 2 (lower bainite in the chromium–vanadium steel XI). On the other hand, continuous cooling gives rise to a mixture of these two structures unless the transformation is substantially suppressed by the prior occurrence of the equilibrium transformation. As far as the two high-carbon steels considered here are concerned, it is known that the bainitic transformation in the eutectoid steel is suppressed on continuous cooling. On the contrary, it occurs very distinctly in the chromium–vanadium steel since the pearlitic transformation in this steel is shifted to the right so the bainitic transformation has an opportunity to take place. In this case, the bainitic transformation is restricted to the left vertical band in the diagram of Figure 8 and leads to the formation only of ferrite and carbides. The position and size of the equilibrium transformation regions make it impossible to obtain other structures.

There is some occurrence of structures of this type in lower carbon alloy steels although they are generally less clearly defined here with a more irregular carbide distribution. In addition, since the martensitic transformation here occurs at higher temperatures, it often happens that only upper bainite can form (Figure 4, micrograph 1; Figure 5, micrograph 1; and Figure 8, micrograph 1). Furthermore it is very difficult to distinguish between lower bainite and self-tempered martensite. Finally, certain steels sometimes exhibit significant differences between the microstructures produced by isothermal holding and those obtained by continuous cooling as will be seen later.

It should further be noted that in many low-carbon low-alloy steels where transformation in the intermediate zone occurs on continuous cooling at relatively low rates, the bainitic transformation follows the formation of a large amount of proeutectoid ferrite. It then produces microstructures of the type represented in Figure 8, micrograph 3. Here again mixtures of structures similar to those observed above are found with two constituents, ferrite and Fe_3C carbides. While distributions of these precipitates in bainitic ferrite resembling lower or upper bainite are sometimes found, more-or-less evenly distributed agglomerates of carbides also occur occasionally. These agglomerates will be understood better once we have analyzed the other types of intermediate structures. They actually form in an austenite whose carbon content has been raised as a result of the previous transformation. Thus, up to a certain point, they may be compared with the structures found in higher carbon steels. It is also evident that they are the only structures that perfectly fit the definition of bainite given above. Actually, they are also the only intermediate structures that have been investigated systematically. Recent electron-microscopic examinations and electron-diffraction analyses on thin foils have established accurately the orientation relations existing between ferrite, cementite and austenite.[16] In particular they have confirmed that in lower bain-

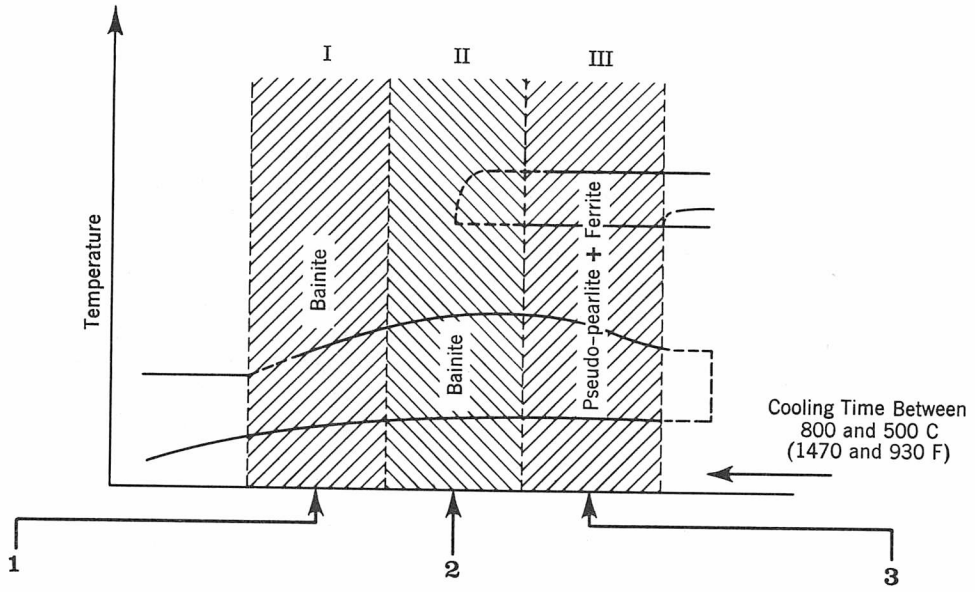

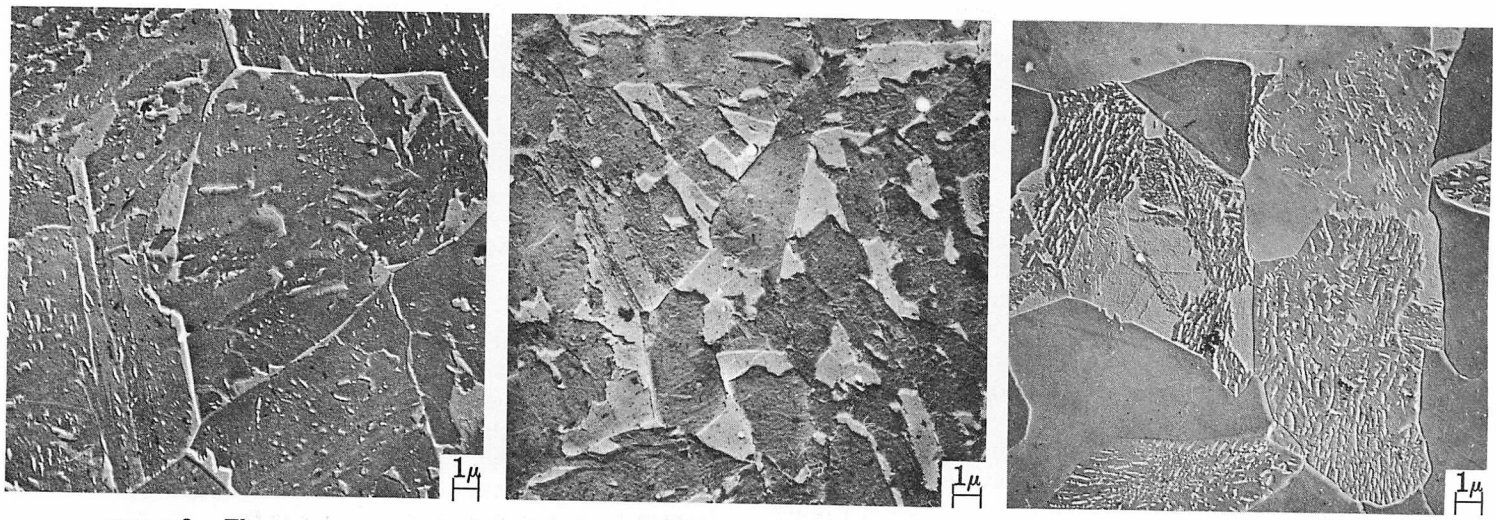

FIGURE 8. Three zones in intermediate transformation range defined in terms of temperature and cooling time between 800 and 500 C (1470 and 930 F) and illustrated by typical microstructures

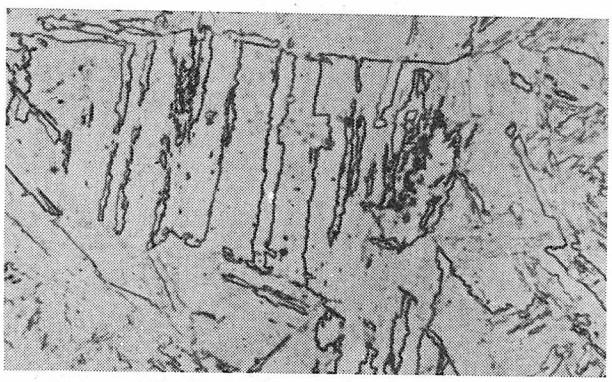

FIGURE 9. Coarse structure in iron–chromium–cobalt alloy III produced by intermediate cooling rate after austenitizing is similar to massive martensite defined by Owen and Wilson.[5] Specimen austenitized one hour at 1100 C (2010 F) and cooled at 3000 C/min (5400 F/min). 110 X

ite the cementite forms in ferrite plates supersaturated with carbon while in upper bainite the carbides form in the austenite. This work permits definition of the kinetics of formation of bainite formation.

Carbide-Free Acicular Structures Structures differing from those discussed above can be identified within the intermediate transformation field of low-carbon steels, especially in the case of the 2¼% Cr–1% Mo steel V, which contains only 0.1% C, as well as in some of the low-alloy structural steels with 0.2% C. In specimens continuously cooled at the highest rates giving bainitic structures, etching for a sufficient time reveals a microstructure consisting of plates lying side by side and often growing from an austenite grain boundary. In the case of the 2¼% Cr–1% Mo steel V, no carbides are observed, either inside the plates or along their boundaries. On the

other hand, some almost unetched particles can occasionally be detected (Figure 1, micrograph 1). In the same condition, another steel examined (1.5% Mn–0.5% Mo–B steel VII) exhibits a lamellar structure. As indicated in Figure 2, micrograph 1, the ferrite plates are separated by bands or aligned nodules of the same almost unetched particles.

After isothermal holding, the structures exhibited by the same steels are somewhat unexpected. In the chromium–molybdenum steel V, the same structures as described above are again found after isothermal transformation in the part of the bainitic field between 440 and 380 C (825 and 715 F). On the contrary in steel VIII, ferrite–carbide structures often resembling conventional bainites are observed after holding one hour at 450 or 400 C (840 or 750 F). Thus, in this particular case, there is a fundamental difference between the structures formed on isothermal holding and those produced on continuous cooling.

The structures just described are characteristic of those found in low-alloy low-carbon steels after transformation in the first bainitic zone (I of Figure 8) on continuous cooling or by isothermal transformation at temperatures between the M_s point and approximately 450 C (840 F).

Massive or Granular Structures The terms massive or granular will be used hereafter to designate respectively the structures consisting of coarse plates and those with an almost entirely granular aspect.

Ferrous Alloy III In addition to acicular and lamellar structures, very coarse massive structures are also observed in alloy III in the intermediate transformation field. The boundaries are very much indented and often consist of a series of straight segments. Figure 9 is a typical example. Similar structures are produced in this alloy by continuous cooling over a wide range of rates.

0.1% C and 0.2% C Steels (V, VI to X) All these steels exhibit structures very similar to that shown in Figure 8, micrograph 2, for a range of cooling rates varying from one steel to the next. The most typical structures occur for the following cooling rates:

Steel V	220 C/min (395 F/min)
Steel VII	60 C/min (110 F/min)
Steel VIII	168 C/min (298 F/min)
Steel IX	100 C/min (180 F/min)
Steel X	35 C/min (65 F/min)

They are clearly revealed by electron-microscopic examination of replicas as shown by the second micrographs in Figures 1 to 6. The austenitic grain boundaries are almost always visible as they are delineated by irregularly shaped, lightly etched particles.

Some bainite grains occur inside the prior austenite grains although their boundaries are not clearly defined in certain of the steels. Very often particles similar to the lightly etched particles referred to above seem to occur inside the bainite grains. In a given prior austenite grain, they sometimes give the impression of being oriented along the principal (111) planes of the austenite.

Some acicularity is observed in the 1.5% Mn–0.5% Mo–B steel VII. Since the structure is more or less isotropic in the other steels, we have generally included it in the granular bainite class.

In some cases, the light-etching particles appear to be partly decomposed to ferrite and carbides (Figure 10). This would account for occasional occurrence of ferritic-bainitic regions containing carbide clusters in the third bainitic band (Figure 8, micrograph 3).

0.3% C Steel with a High Substitutional-Element Content Structures similar to those described above but much coarser are produced in steel XIII by continuous cooling over a very broad range of rates. An acicular martensitic structure can often be detected in the lightly etched areas, clearly in the center but less distinctly at the edges (Figure 11).

Analysis of Massive or Granular Structures

In order to establish the nature of these lightly etched particles and thus to secure some information on their composition, we carried out systematic analyses of a large number of specimens.

X-ray analysis of these specimens generally re-

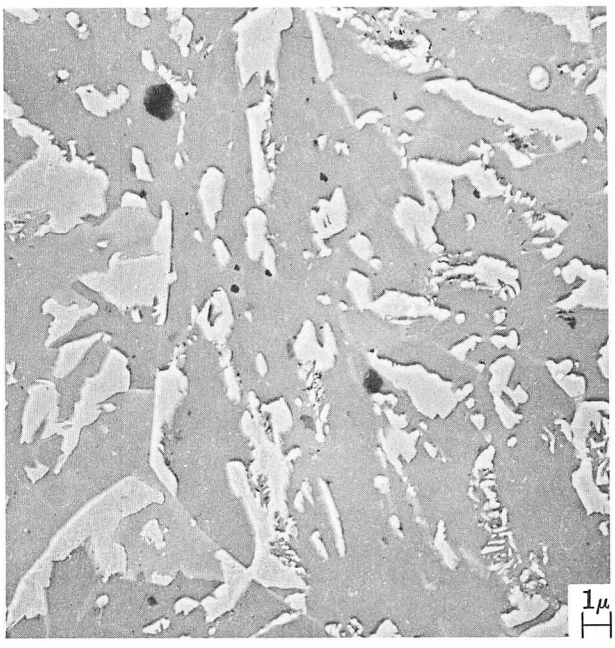

FIGURE 10. Slightly etched particles appear to represent austenitic-martensitic zones partially decomposed into ferrite and carbides. 1.5% Mn–0.5% Mo–B steel VII cooled from austenitizing temperature at 60 C/min (110 F/min)

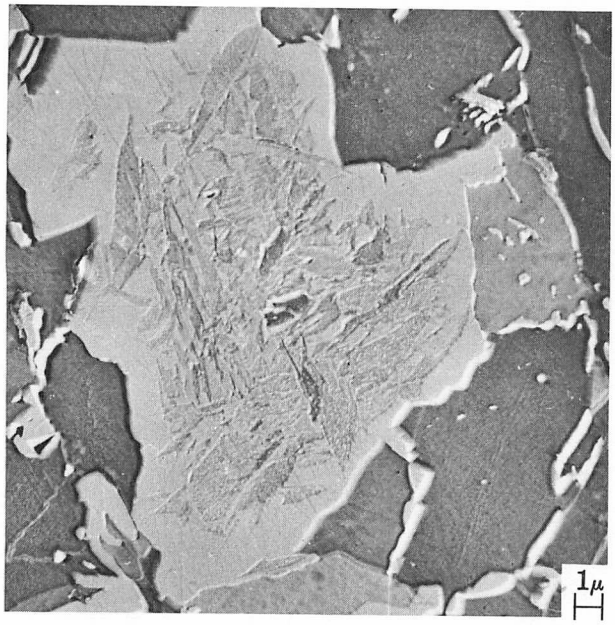

FIGURE 11. Occurrence of acicular martensite in center of lightly etched areas in bainitic structure of 9% Ni–4% Co ultrahigh-strength steel XIII

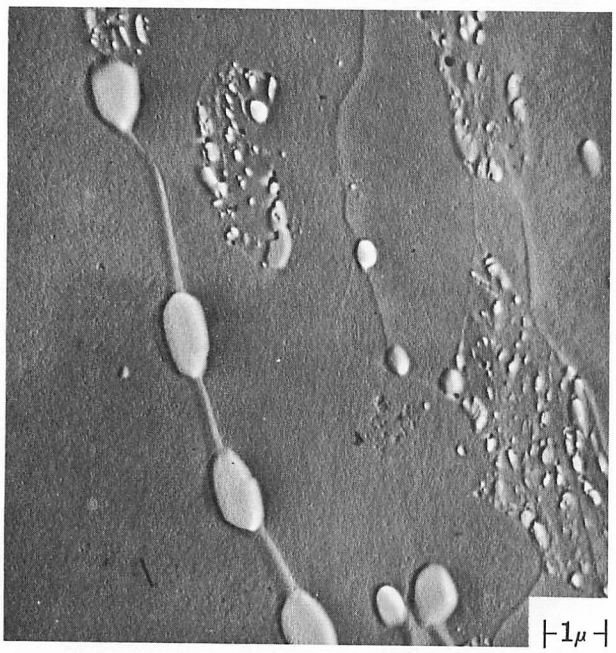

FIGURE 12. Decomposition of austenitic-martensitic nodules into ferrite and carbides in 2¼% Cr–1% Mo steel V cooled in air and tempered at 450 C (840 F)

vealed the presence of residual austenite. There was, however, no direct correlation between the amount of residual austenite detected by X-ray analysis and the volume of particles as determined by point counting under the electron microscope. These tests clearly confirmed the fact that some of these particles are two-phase austenite-martensite in spite of their appearance. The austenite content in a steel such as

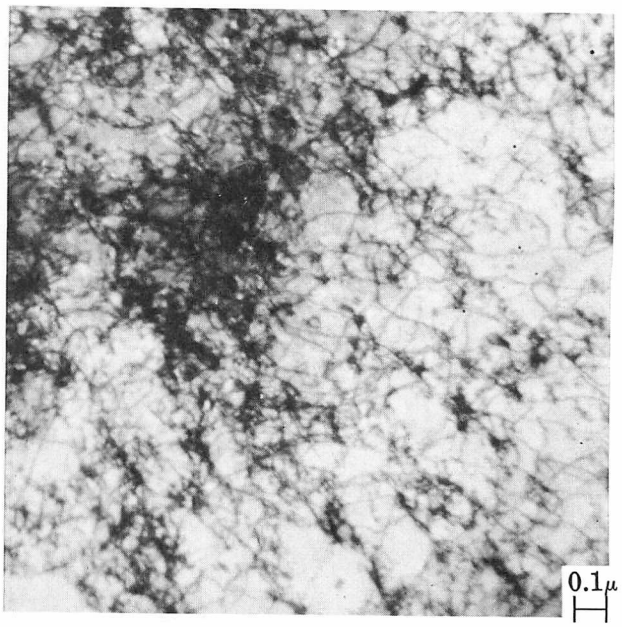

FIGURE 13. High dislocation density in bainitic ferrite of 1.5% Mn–0.5% Mo–B steel VII cooled at 60 C/min (110 F/min)

VII is 8% by X-ray analysis. The highest residual-austenite content of bainite is found with granular or massive structures and up to 30% austenite was detected in certain steels such as steel XII. With steel VII, X-ray analysis gave an austenite content of 8% whereas electron-microscopic point counting indicated 15% of light-etching structures.

We have been unable to ascertain whether the substitutional-element content of this austenite is different from that of the bulk material but its interstitial-element content is raised considerably. After tempering a typical structure of this type in the chromium–molybdenum steel V at 450 C (840 F), these zones have clearly become aggregates of carbides in ferrite (Figure 12). Furthermore, the carbon content of this ferrite is generally significant since this chromium–molybdenum steel exhibits a secondary-hardening effect involving formation of Mo_2C carbides after tempering for very long times.[17]

The thin-foil technique was used to examine some typical granular or massive structures, particularly in steels VII, X and XIII. Accumulations of dislocations could be easily detected at magnifications of 30,000 X (Figure 13). Regardless of the grade, the density of dislocations in the bainitic ferrite was very high.

The austenitic-martensitic regions are easily identified in the thin foils as again they are lightly etched. Because of their lack of transparency, however, they are often difficult to examine but in the most favorable cases diffraction spots corresponding to a face-centered cubic lattice were observed. Thin martensite needles were often detected, particularly in steel VII. Occasionally, Fe_3C precipitates or twins seem to

occur in the needles. Some needles also appeared to have been self tempered and others in the higher carbon steels were combined with the bainitic needles.

Even more specific is the possibility of detecting at the highest magnifications (50,000 to 80,000 X) areas that, depending on the steel, are globular or consist of plates and are "darker" than the rest of the microstructure. Such areas occur on the boundaries as well as inside of the austenitic-martensitic regions. Some of the darker bainitic ferrite particles lie at the boundaries of austenite or bainite grains while others are inside ferritic grains. In the latter case, the electron diffraction from the surrounding ferrite areas indicates exactly the same orientation. In addition, the bainitic ferrite near the austenitic-martensitic particles often contains a high density of dislocations.

Finally, examination of the tool steel (XII), which contained undissolved $M_{23}C_6$ carbides after austenitizing, reveals the aspects illustrated in Figure 14. Since X-ray diffraction analysis indicates 30% austenite overall, the particles shown in the figure may be assumed to be entirely austenitic. Carbides and dislocations as well as the dark areas referred to above can be detected inside them.

Additional Observations

Effect of Composition Generally speaking, the various types of structure described have been observed in various proportions in all the low-carbon steels examined. Their location and extent depend on the transformation rate and austenitization parameters. Alloying elements also play an appreciable role in determining the morphology of these structures. Thus, the high-manganese steel and the high-chromium high-cobalt ferrous alloy usually exhibit structures comprising long coarse plates with these transformed regions extending across prior austenite grains. On the other hand, the structure is less acicular in the chromium–molybdenum steel V and grows along the grain boundaries. Often it deserves the general designation "granular," which we have given it.[3]

Difference Between Isothermal and Continuous-Cooled Microstructures This difference is far from negligible and some of its features have already been discussed. First of all, in some steels there is hardly any bainitic transformation on continuous cooling although isothermal holding produces typical bainitic structures. As is well known, this is the case for the eutectoid steel (II).

In the various low-carbon steels considered, the morphology often differs according to the path followed by the metastable austenite. Thus, in steel VII (Figure 2, micrograph 5), a ferrite–carbide structure is produced by isothermal holding at a low temperature around 400 C (750 F) but continuous cooling

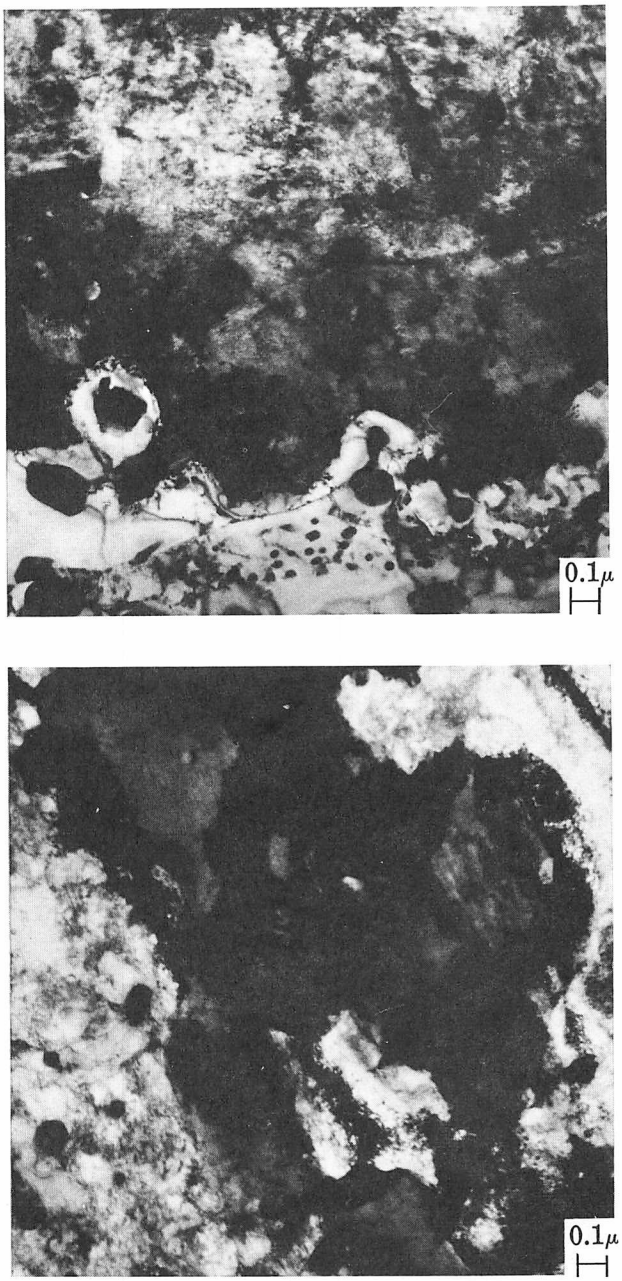

FIGURE 14. Structure of austenitic-martensitic areas in die block steel XII with dark regions in form of elongated cells resulting from enrichment of austenite in metastable range. Thin-foil electron micrographs

gives an acicular structure consisting of ferrite plus some austenitic-martensitic areas. This difference also exists for other steels although it is less sharp.

In most of the steels investigated, the massive or granular structure we have described occurs only after continuous cooling in the second bainitic band of Figure 8. In general, just as with martensitic transformations, the extent of the transformation depends on the final temperature. What happens is a partial transformation to massive structures, the extent of which depends on the difference between B_s

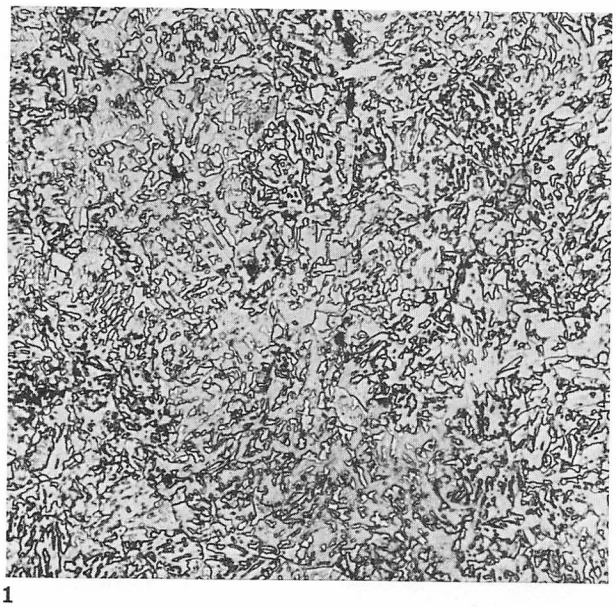

1

15% + 15% deformation between
950 C (1740 F) and 830 C (1525 F)

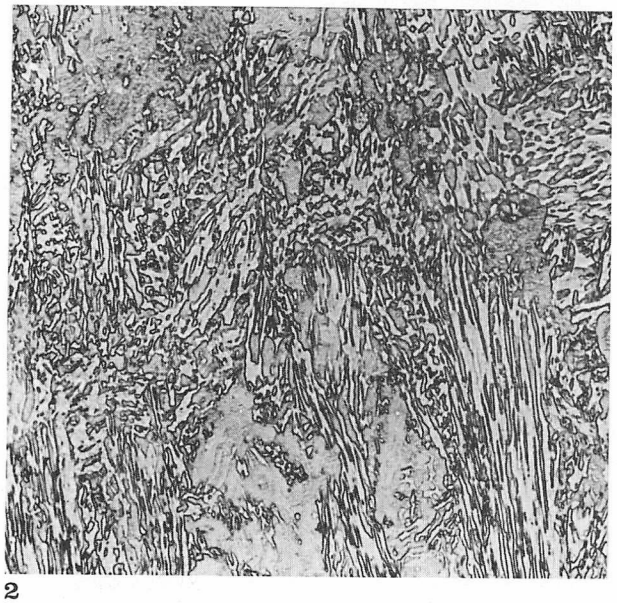

2

15% + 15% + 30% deformation between
800 C (1470 F) and 700 C (1290 F)

FIGURE 15. Only ferrite and austenite-martensite are present after thermomechanical treatment of 1.5% Mn–0.5% Mo–B steel VII at 950/830 C (1740/1525 F) and 800/700 C (1470/1290 F) followed by air cooling at 80 C/min (145 F/min). Optical micrographs. 500 X

and the transformation temperature. At least for the various steels studied, the massive or granular structure cannot be produced by isothermal treatment even at the highest transformation temperatures. In fact, the transformation does not progress with time or only at a very low rate. In steel V, for instance, examination of specimens water quenched after holding from 32 min to 64 hr at 525 C (975 F) shows that the percentage of transformation (percentage of acicular martensite) remains practically the same. When the specimen is air cooled after holding one hour at 500 C (930 F), however, the massive structure appears throughout the specimen as transformation has been completed during the five minutes required to cool from 500 C (930 F) to room temperature. What is certain is that transformation at the higher temperatures within the bainitic field is not yet complete after holding ten hours or more whereas with continuous cooling it is complete after a few minutes.

Finally the third transformation band (Figure 8) is essentially associated with continuous cooling rates leading to partial formation of equilibrium products. Actually, dilatometric tests clearly indicate the occurrence of a bainitic transformation even when the bainitic structure occasionally exhibits more-or-less pearlitic features.

Influence of Initial Condition of Austenite It is now generally held that deforming austenite, both in the stable and metastable fields, can influence the microstructures formed during cooling. These treatments — thermomechanical working, ausforming, controlled rolling — sometimes make it possible to obtain attractive mechanical properties. We have applied a wide range of mechanical deformations to the manganese–molybdenum–boron steel VII followed by cooling at various rates. We shall successively examine the influence of deformation in three temperature ranges, one in which the austenite is stable and the other two in which it is unstable.

Deformation at Temperatures Between 950 and 830 C (1740 and 1525 F) When austenite is deformed by rolling at these temperatures, it can easily recrystallize before transformation and the structure obtained after slow cooling can even be of the ferritic–pearlitic type with a few bainitic cores. On the other hand, faster cooling produces bainitic ferrite structures similar to those previously described (Figure 15). Both optical microscopy and thin-foil examination reveal the occurrence of martensitic-austenitic areas. These structures are generally fairly homogeneous although with a preferred orientation due to the mode of formation. The thin-foil technique also makes it possible to detect ferrite with a high dislocation density as well as austenitic-martensitic areas in which differences in intensity similar to those described previously are observed (Figure 16).

Deformation at Temperatures Between 800 and 700 C (1470 and 1290 F) The structures formed here are more oriented and less homogeneous but the two types of constituents described previously can still be detected (Figure 15). In some cases, however, the

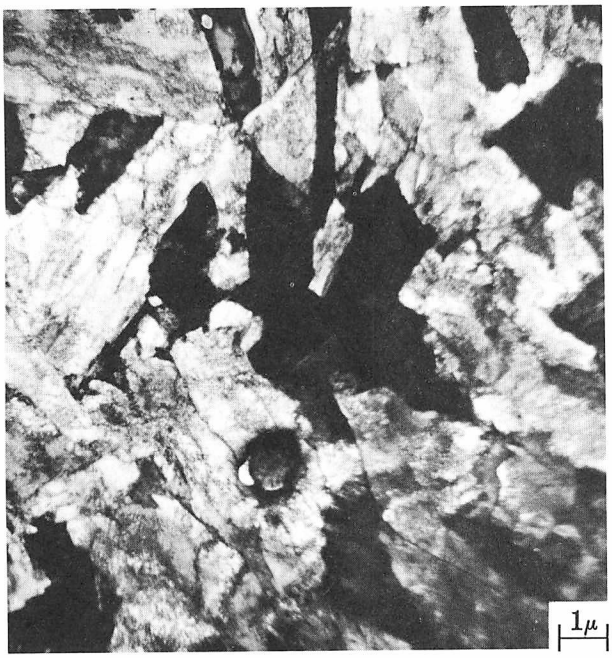

FIGURE 16. Austenitic-martensitic area with differences in intensity found in manganese–molybdenum–boron steel VII after thermomechanically treating by 30% reduction in rolling (one pass) between 950 and 830 C (1740 and 1525 F) and cooling at 30 C/min (55 F/min). Thin-foil electron micrograph

higher carbon regions occurring with intermediate cooling rates now give rise to ferrite and carbides and no longer consist of austenite and martensite (Figure 17). In other cases, a mixture of carbides and austenitic-martensitic areas in ferrite occurs. The bainite grains are often relatively small and contain a large number of dislocations. Thus, it is seen that deformation plays a relatively large role in determining structure.

Deformation at Temperatures Between 650 and 550 C (1200 and 1020 F) The structure is clearly oriented when the deformation temperature is so low. Both types of constituents — austenite-martensite and bainitic ferrite — occur in the intermediate transformation band. The austenitic-martensitic areas are much smaller than after deformation at higher temperatures but again dark regions are often found inside these areas. The dislocation content of the ferrite is particularly high and the defect density is not homogeneous (Figure 18).

It can be stated that the microstructure is markedly affected by the treatment to which the stable or metastable austenite has been subjected prior to transformation. Not only do the bainitic ferrite grains and the number and distribution of dislocations within these grains differ; but the size, arrangement and very occurrence of the austenitic-martensitic areas as well as the presence of carbides are also affected by the treatment. The influence of thermomechanical treatments on mechanical properties will be dealt with at length in the second half of this paper.

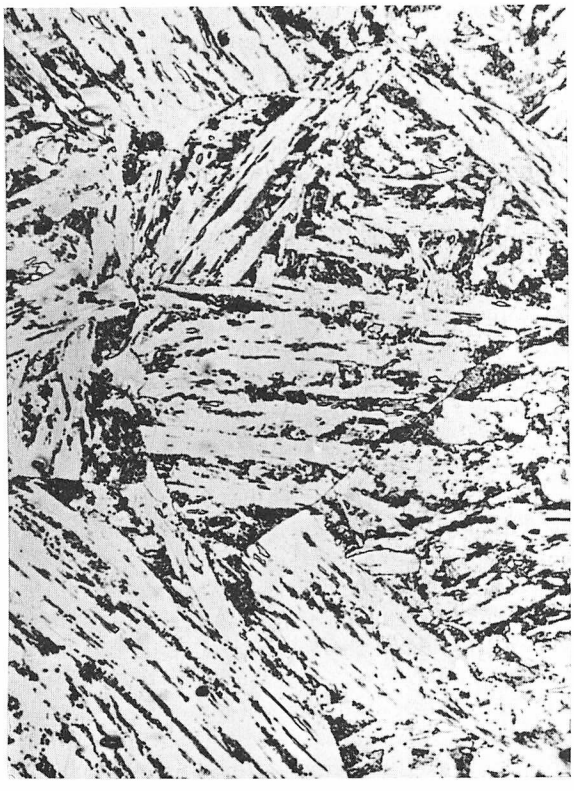

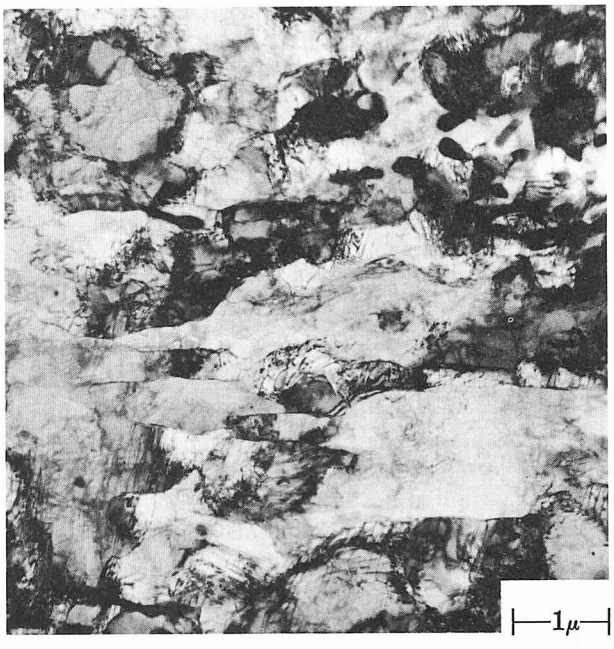

FIGURE 17. Austenitic-martensitic areas replaced by ferrite-carbide aggregates in manganese–molybdenum–boron steel VII thermomechanically treated by 30% deformation between 800 and 700 C (1470 and 1290 F) and cooled at 80 C/min (145 F/min). Optical (500 X) and thin-foil electron micrograph.

FIGURE 18. High dislocation content and inhomogeneous defect density in ferrite after thermomechanical treatment of manganese–molybdenum–boron steel VII by 30% deformation between 650 and 550 C (1200 and 1020 F) and cooling at 80 C/min (145 F/min). Thin-foil electron micrograph

Summary

It appears from the observations just described that the intermediate structures of many steels exhibit aspects differing sharply from those currently defined as upper and lower bainite. Intermediate structures of bainitic ferrite with a high density of dislocations and of high-carbon austenitic-martensitic nodules occur frequently and are produced more readily by continuous cooling than by isothermal treatment. These structures are influenced by composition, rate of cooling and thermomechanical treatment.

PROCESSES OF FORMATION OF INTERMEDIATE STRUCTURES

Transformation of Austenite

General We shall now attempt to outline a possible formation mechanism that would account for all the observations reported so far. The kinetics of the transformation of austenite into stable and metastable structures has already formed the subject of numerous investigations. One of the hypotheses (1947) evolved to explain the various transformations was based on the influence of alloying elements: namely, proeutectoid ferrite was formed by diffusion of substitutional and interstitial elements, bainite formation required only the diffusion of interstitial elements and martensite resulted from a diffusionless transformation.[26]

Numerous studies, both theoretical and experimental, on the role of lattice defects and their influence on interfaces indicate that these excessively general concepts must now be largely revised. Smith (1953)[27] and Aaronson (1962)[28] have proposed a classification of the modes of formation of the various structures based on the nature and migration characteristics of interplanar boundaries. They differentiate among:

Noncoherent or disordered boundaries have isotropic structures and diffusion takes place along them. They are mobile at high temperatures because individual atoms are rapidly transferred along or across them. Their migration depends on their structure.

Semicoherent or dislocation boundaries are made up of a nearly two-dimensional array of dislocations. In this case, appreciable volumes of the lattices on both sides of the boundary are strained and movement takes place by the migration of component dislocations perpendicularly to the boundary. Accumulation of volume strain energy is the major cause of restraint as regards the movement of this type of boundary, but Brooks[29] has pointed out that strain fields cancel each other. The mechanism of migration is relatively difficult to understand. If it is assumed that the dislocation boundaries remain planar during growth, a synchronous glide is necessary to explain the movement.

Coherent boundaries in principle contain no dislocations but strain substantial volumes of the adjacent lattices. They can move but are stopped by the accumulation of volume strain energy.

Purdy and Kirkaldy[30] demonstrated that the $\gamma \rightarrow \alpha$ reaction in an iron–carbon alloy started from a noncoherent interface and was controlled by volume diffusion of carbon. Rouze and Grube[31] established that the thickness of ferrite plates in Widmanstätten structures was distinctly less than a process controlled by carbon diffusion would have allowed. Semicoherent interfaces appear to have low mobility. In steels with a ternary element, Aaronson and Bowman[32, 33] showed in connection with the formation of proeutectoid ferrite that there was no redistribution of the ternary element, for instance chromium or molybdenum, during the formation of ferrite in the iron–chromium–carbon and iron–molybdenum–carbon systems. When studying the influence of manganese on the formation of pearlite in a manganese-containing steel, Picklesimer came to the conclusion that the coefficient for volume diffusion of this element was not the factor that controlled the transformation rate.[34] More recently, Purdy, Weichert and

Kirkaldy investigated the iron–carbon–manganese system. They established that the ferritic transformation was accompanied by a redistribution of the manganese in the case of low-manganese steels, but that no such redistribution occurred in high-manganese steels.[35]

It appears that the organization of the lattice defects, which depends on the nature of the interface, influences the mobility of the interface and that it is this mobility rather than the presence of alloying elements that accounts for the transformation rate. However, the alloying elements and the carbon dissolved in the austenite influence the nature and mobility of the interface to such an extent that certain forms of transformation become impossible.

Finally it seems that many transformations are not pure nucleation-and-growth or martensitic-diffusionless reactions but are of an intermediate nature. The coherency of the nuclei will prevail only in the early stages of growth and will be lost when the new phase becomes sufficiently large that its surface energy is lowered.

Extra strain energy is tolerated only in the acicular martensitic reaction because some coherency of the phase is essential to the mechanism of transformation. In fact, the acicular martensitic reaction occurs because there exists an easy growth mechanism, which does not require atomic diffusion and which leads to the rapid formation of a new phase accompanied by a net lowering of the free energy.

Present-Day Concepts on Transformation in the Intermediate Field Recent investigations have contributed in no small way to an understanding of conventional bainite, i.e., ferrite + carbides. The concepts currently accepted as they appear in particular in Christian's bibliographic study[8] and in the recent Iron and Steel Institute Special Report entitled Physical Properties of Martensite and Bainite[5] will help us in our attempt to explain the mechanism for the formation of the intermediate structure consisting of ferrite and austenitic-martensitic areas such as has been described above.

Conventional Bainitic Structure We have indicated the principal characteristics of this transformation at the beginning of this paper. It now appears that the bainitic transformation is similar to the martensitic transformation and implies the existence of a coherent interphase boundary in its early stages. In fact, the shear transformation starts with the migration of glissile interphase boundaries, which ensures nucleation. However, growth must be due to other phenomena related to interatomic diffusion. Actually, growth in bainite is possible only because the chemical free-energy driving force is increased by diffusion. Finally, it appears that the bainitic transformation is a nucleation-and-growth reaction.

In the case of conventional bainite, following the suggestion made by Ko and Cottrell,[36] Bowles and Barrett[37] proposed that the boundaries had a dislocation structure. As the high velocities associated with shear are reduced during the bainitic reaction, these authors suggested that a barrier was present. This barrier was assumed to be primarily the volume strain energy of the transformation. The process that controls the growth rate must therefore be able to lower the barrier. This is actually accomplished by reducing the amount of carbon in the supersaturated ferrite formed through diffusion of the excess carbon into the surrounding austenite and by its precipitation in the form of carbides.

Bowles and Barrett also suggested that the interphase boundaries could be described by an array of glissile dislocations. Transport of an atom across such a boundary is accomplished by the gliding of a dislocation in its slip plane. In order to account for a discrepancy, Christian suggested that the complexity of the structure of the broad faces of a ferrite plate is such that both sessile and glissile dislocations are needed to compensate for the misfit at these interphase boundaries. The sessile dislocations restrict the rate of migration of the boundary while the glissile dislocations do not impede the motion of the boundary but contribute to the observed relief effect.

Massive or Granular Structures in Ferrous Alloys Work by Massalski[38] and Owen[39] recently confirmed indications supplied by Greninger[40] and showed that, on cooling at intermediate rates, certain substitutional solid solutions transform very rapidly into a structure having the same composition as the parent phase. Such transformations have been observed in copper- as well as iron-base alloys. They occur on quenching from an elevated temperature; their rate of formation is generally rapid and it is impossible to analyze them by conventional isothermal techniques. The crystals of the new phase have rather irregular boundaries consisting of a certain number of straight segments.

The new phase nucleates at the grain boundaries of the parent phase and during growth has a noncoherent interface with the surrounding matrix. In Massalski's opinion, the growth mechanism must be thermally activated and the growth rate controlled by the mobility of the interface. This mechanism calls for a rapid movement, though over a short distance only, of the atoms, which are thermally activated on an individual basis. It seems that the atoms move from one phase to the other with an activation energy approximately equal to that of grain-boundary diffusion rather than to that of volume diffusion. If growth is thermally activated, the growth rate must be much greater on a pre-existing noncoherent boundary with lower activation energy for the movement of atoms.

All massive structures are not formed by the same transformation mechanism and two limiting cases have been distinguished. One of these is a massive transformation involving short-range diffusion (SRD) as described by Kurdyumov.[41,42] The massive grains grow as a result of the displacement of noncoherent interfaces, which can even extend across the boundaries of the parent phase. The other is a "massive martensitic" transformation that occurs within a given austenite grain. According to several authors,[39] this massive martensite would consist, in most cases, of plates formed by shearing. Some investigators even believe that this mode of formation is general. Rectilinear boundaries form during the growth of this massive martensite and are probably related to the presence of groups of dislocations having a low energy in the austenite. The formation of either structure depends on the composition of the parent phase, the characteristics of the austenite grain and the cooling rate. Transformation by short-range diffusion requires little undercooling (corresponding to 30/80 cal/mole). In the case of ferrous alloys, it occurs in the neighborhood of 585 C (1085 F), is thermally activated and can be suppressed by raising the cooling rate. Free energy for the massive martensitic transformation is higher (approximately 300 cal/mole) and accordingly this structure is observed at lower temperatures of the order of 440 C (825 F). Transformations starting by the first process and continuing by the second can be observed occasionally. According to some authors[5] it is possible to suppress the massive transformations not only by resorting to very high cooling rates but also by adding relatively small amounts of carbon or by avoiding the presence of excessive quantities of substitutional elements. Alloying elements seem to lower the reaction temperatures.

Influence of Condition of Austenite in Metastable Field Only a few authors[12,42,43] have considered the condition of austenite in the metastable field when attempting to explain the immediate transformations or have endeavored to detect an influence of this condition on these transformations. It was not until investigations on ausforming[44] were carried out that it became apparent that the deformation of austenite could exert a considerable influence on the structures produced by the bainitic transformations.

However, it was obvious from the start that since the austenitic grain size plays a role in these transformations, the latter must also be influenced by the inner structure of this austenite, i.e., the occurrence of groups of lattice imperfections, sub-boundaries, etc. Accordingly, attempts were made to account, at least partly, for the metastable transformations in terms of various phenomena that can occur in the austenite in the metastable condition. It proved possible to relate these phenomena to the formation of more or less ordered regions, presence of internal stresses, groups of dislocations possibly favoring carbon concentration, etc.

In quenched solid solutions, such as austenite in the metastable field of the CCT diagram, dehomogenization may actually occur since the solid solution is held at a temperature at which it should normally transform. In spite of the fact that the temperature is still relatively high, precipitation or concentration of the carbon atoms can occur on dislocation tangles in the austenite. This reaction would constitute only a preliminary step in the formation of a metastable structure consisting of supersaturated ferrite and carbon-rich austenite. Such a metastable structure can actually be located by extending the equilibrium lines in the iron–carbon diagram.

Since stabilized enriched austenite has been observed in many of the structures examined, we shall now briefly discuss present-day knowledge on austenite stabilization, which has mainly been described in connection with the martensitic transformation. Two stabilization modes have been distinguished: thermal stabilization and mechanical stabilization.[5,8]

Thermal stabilization occurs during both the athermal and the isothermal martensitic transformation of steel. It is observed only when carbon and nitrogen are present.[45] According to some authors it occurs only below the M_s temperature, at which martensite starts to form, but other investigators believe it can also take place above this point.[46] The phenomenon is attributed to modifications of the untransformed austenite where the dislocations in the austenite lattice are locked by precipitates or solute atmospheres. As a result, the structure is hardened, and direct growth of martensitic needles as well as the plastic deformation accompanying this growth are inhibited. When the martensitic transformation starts, the elastic deformation that has produced imperfections tends to reduce thermal stabilization.

Mechanical stabilization is caused by an applied plastic deformation or by the accommodation of stresses by the lattice. The M_s temperature can be modified by the action of an applied stress, whether it be a shear or hydrostatic stress. It can even reach a value, M_d, appreciably higher than M_s. It has been possible to show that a plastic deformation applied at a temperature above M_d stabilizes the austenite mechanically. In other cases, the temperature for martensite formation is lowered because the lattice defects introduced inhibit the growth and possibly destroy the coherency of the martensite nuclei. Occasionally, an opposite effect is observed. Instead of stabilizing the austenite, a small deformation causes a concentration of internal stresses that favor the nucleation of martensite or growth of existing nuclei. Finally, plastic deformation produced by accommodation stresses slows down the transformation as does any transformation above the M_d temperature.

Bearing in mind these different conditions, we shall now try to assess a process for the formation of the massive or granular structures found in the investigated steels.

Massive or Granular Structure

General Thus it appears that transformations and particularly their growth are related to displacements of noncoherent, coherent or semicoherent interfaces. These movements are possible because they decrease the free energy of the system. Their speed, i.e., the kinetics of the phenomenon, depends on the size of the free-energy variation, the diffusion rate of certain solute elements across the lattice or along the interface, etc. It is also influenced by the reaction of the dislocation network at the interface with the dislocations existing in the parent lattice.

In the case of intermediate transformations, which occur by various modes as has been shown, growth of the transformation products appears to be related very often to displacements of semicoherent interfaces. Moreover, the fact that several temperature regions, each corresponding to a different structure, can be identified tends to indicate that various mechanisms are involved. The transformation rate, however, is not very high; this indicates that the dislocation network at the interface cannot move as easily as it does in the acicular-martensitic transformation. Let us recall that the following temperature ranges were identified in the investigations reported above:

580/530 C (1075/985 F) — occurrence of massive structures at intermediate cooling rates

480/440 C (895/825 F) — formation of massive martensitic structures in ferrous alloys at intermediate cooling rates

350 C (660 F) — temperature limit between regions where conventional upper and lower bainite are formed

The fact that very often transformation does not produce the same structures under isothermal and continuous-cooling conditions shows further that, in addition to a martensitic phenomenon, time-dependent phenomena involving diffusion for instance may also be occurring.

With regard to conventional bainites, the assumption of Ko and Cottrell,[36] confirmed by the Zener-Hiller theory,[8] appears to be valid for lower bainite. The transformation nuclei would actually be martensitic but their growth would require the driving force to be increased by diffusion around the growing plate. Thus, the rate of such a transformation is restricted by the rate of carbon diffusion. It can be considered as a potentially martensitic transformation with an inadequate driving force. Actually, bainitic reactions of this type transform into conventional martensitic reactions when the driving force is increased by lowering the temperature.

Although the process described above satisfactorily accounts for the formation of conventional lower bainite and up to a certain point that of upper bainite, it is less readily applicable to the formation of massive structures. We were thus led to carry out additional investigations with a view to identifying relevant factors in the mechanism of formation of these structures.

Additional Investigations The conditions under which the massive structures of ferrite and austenitic-martensitic areas occur were summarized above. Additional investigations were carried out on the manganese–molybdenum–boron steel VII and comprised dilatometric tests on austenitized specimens held in lead baths at various temperatures and subsequently water quenched, and electron-microscopic examinations using the replica and, in some cases, the thin-foil technique, on specimens cooled at 50 C/min (90 F/min) followed by water quenching from predetermined temperatures.

Dilatometric Studies The dilatometric tests showed that a decrease in temperature at an adequate rate is practically the only factor responsible for transformation in the upper part of the bainitic range. Time at a given temperature has very little influence here as illustrated by test 3 in Figure 19. On the contrary, transformation is time dependent in the middle and lower parts of the intermediate transformation range. In test 4 (Figure 19) the specimen was observed to expand as a result of transformation during cooling between B_s and 550 C (1020 F) and perhaps during the first few moments of holding at 550 C (1020 F), after which its length remained practically constant. Subsequently when the specimen was placed in a bath at 400 C (750 F), it again expanded rapidly during some minutes. No martensite was formed when the specimen was finally water quenched. This specimen, transformed partly isothermally at the lower temperature, contained fewer and smaller austenitic-martensitic particles than the specimen from test 1, but numerous carbides.

The comparison of tests 3 and 5 with test 4 in Figure 19 confirms the effect of time at temperature indicated above. There was some transformation in test 3 before cooling was interrupted at 550 C (1020 F) but it did not progress during holding at this temperature. The subsequent water quench produced martensite, which had been influenced by the high-temperature holding. If we had air cooled instead of water quenched, transformation would have occurred during this cooling and given a structure like that in Figure 2, micrograph 4. The progress of transformation in test 5 was similar to that of test 1 except it continued to completion during isothermal holding and the resultant structure was finer with carbides. In test 6, the austenite-martensite transformed during the one-hour holding at 410 C (770 F).

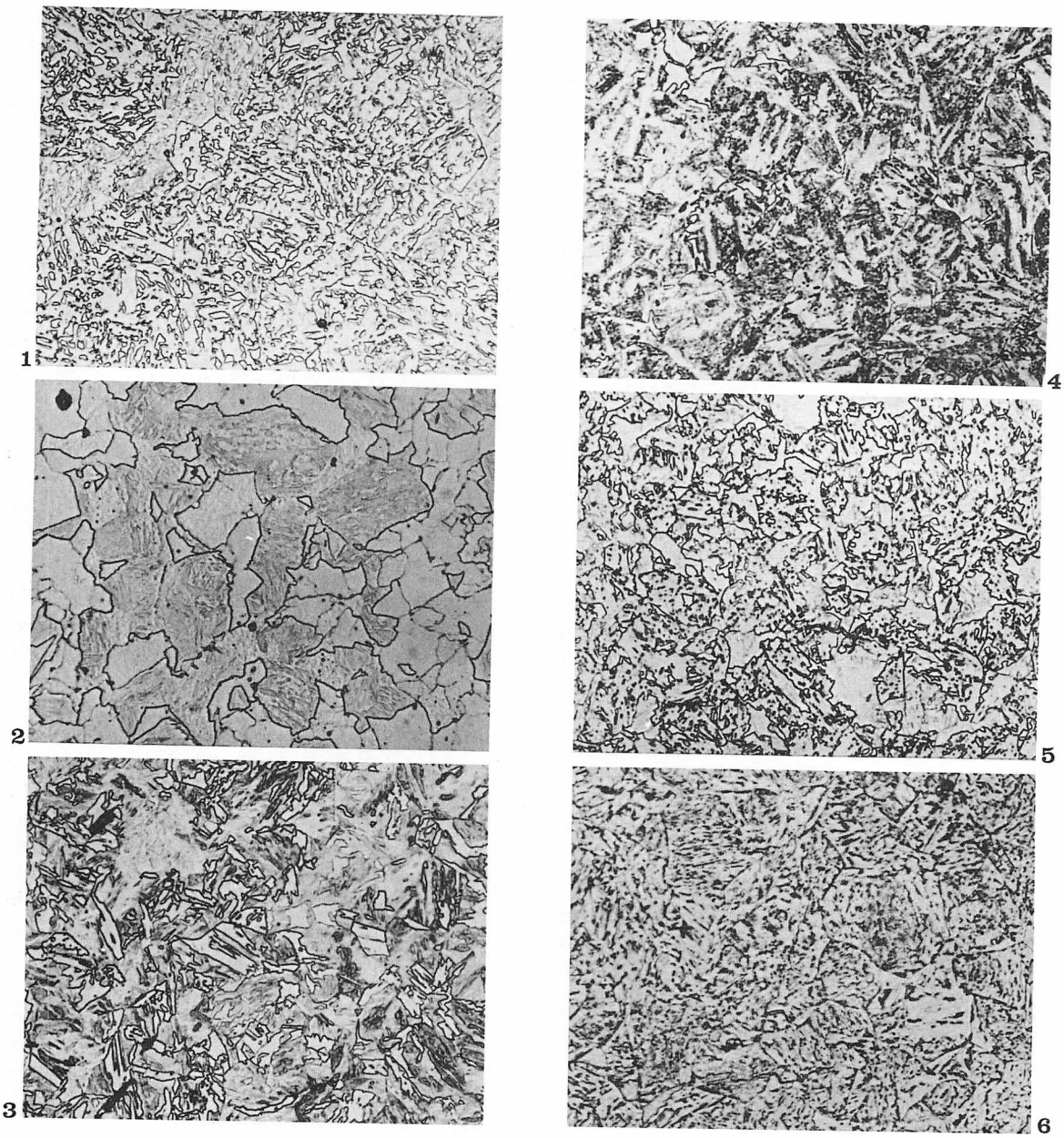

FIGURE 19.

1. uninterrupted cooling produces a mixture of bainitic ferrite and austenitic-martensitic particles
2. cooling is interrupted at 650 C (1200 F) for one hour before air cooling. curve shows that residual austenite is transformed into acicular martensite while micrograph is typical for an aggregate of propearlitic ferrite and acicular martensite
3. some transformation has taken place before interruption of cooling at 550 C (1020 F) (point A on curve). no further transformation occurs during one hour at this temperature. on subsequent air cooling, residual austenite is partially transformed to martensite as shown in curve and micrograph
4. some transformation has taken place before interruption of cooling at 550 C (1020 F) (point B on curve). no further transformation occurs during half an hour at this temperature. specimen is cooled in a few seconds to 400 C (750 F) (point C on curve) and maintained half an hour at this temperature during which time transformation proceeds to completion (CD). after subsequent water quenching, structure is complex with carbides present in ferrite but no acicular martensite
5. bainite transformation begins at about 500 C (930 F) and continues to completion during interruption of cooling at 450 C (840 F) for one hour. no further changes during subsequent air cooling
6. transformation is practically complete before interruption of cooling at 410 C (770 F). holding one hour at this temperature transforms austenitic-martensitic particles into ferrite and carbides

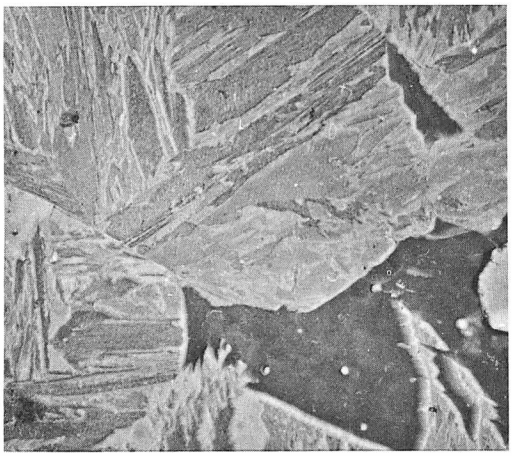

1. cooling interrupted at 575 C (1065 F)

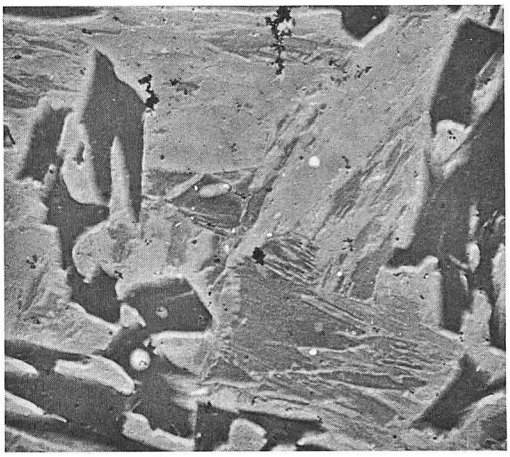

2. cooling interrupted at 550 C (1020 F)

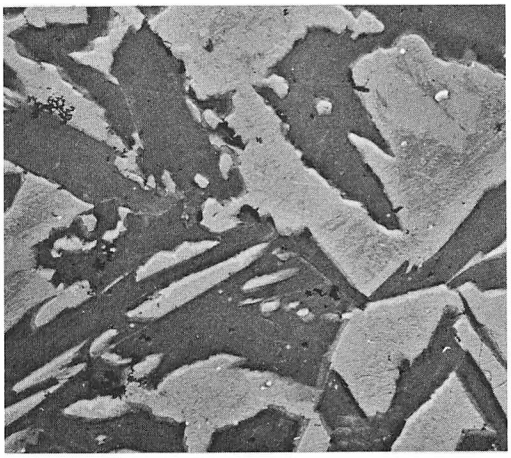

3. cooling interrupted at 500 C (930 F)

4. cooling interrupted at 450 C (840 F)

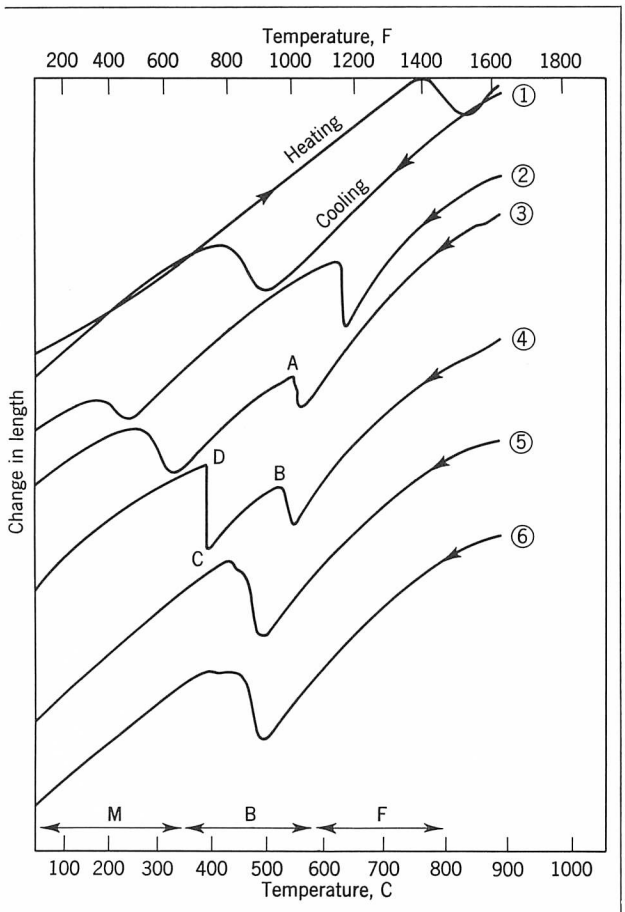

FIGURE 19. Effect of interrupted cooling on dilatometric curves and resultant structures of manganese–molybdenum–boron steel VII austenitized at 880 C (1615 F) for 15 min and cooled at 450 C/min (810 F/min). Optical micrographs on opposite page. 500 X

FIGURE 20. Effect of interrupted air cooling on structure of manganese–molybdenum–boron steel VII. After austenitizing, specimens cooled at 50 C/min (90 F/min) before cooling interrupted by water quenching. Electron micrographs, plastic negative replicas. 2000 X

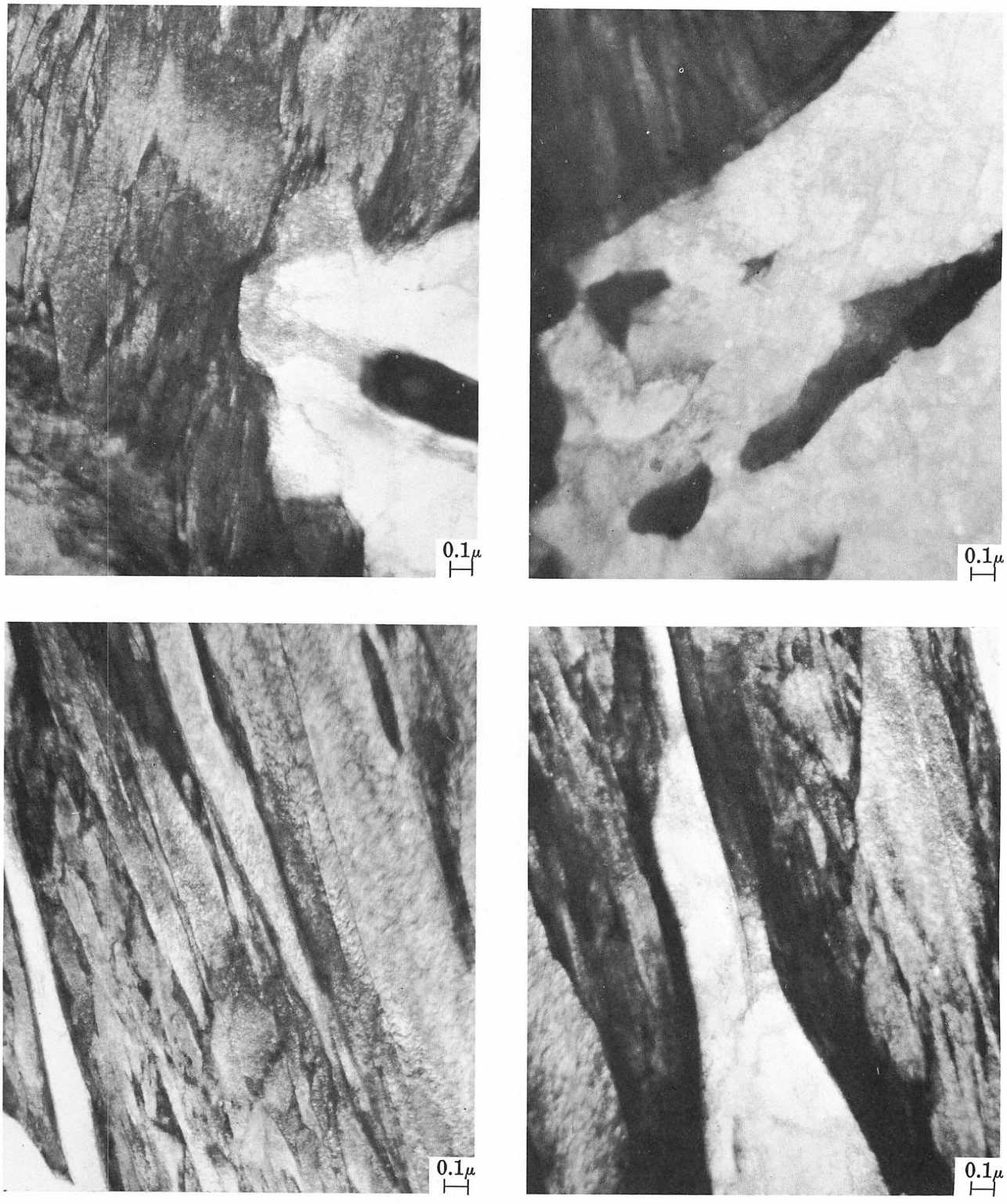

FIGURE 21. Thin-foil electron micrographs of manganese–molybdenum–boron steel VII austenitized at 880 C (1615 F) and cooled at 50 C/min (90 F/min) before water quenching from 575 C (1065 F). 40,000 X

Interrupted Air-Cooling Tests Figure 20 shows the structures obtained when the cooling process in the manganese–molybdenum–boron steel VII is interrupted by quenching from various temperatures. The untransformed region decreases with the temperature where cooling was interrupted and the fer-

ritic region increases with resultant formation of islands of the austenitic-martensitic constituent. The latter may sometimes decompose to ferrite and carbides when cooling is continued to 375 C (705 F) before quenching.

To obtain a better understanding of certain structures we examined more closely the first ferrite grains formed in the specimen cooled to 575 C (1065 F) before water quenching. The four micrographs in Figure 21 summarize our most salient observations. Ferrite with a high defect density forms along an austenite grain boundary, grows in various directions and occasionally entraps zones that appear to contain dark areas as previously described. These dark areas, which sometimes remain even when the contrast conditions are modified, are occasionally observed under the electron microscope along certain boundaries of acicular-type transformed areas. Under the magnifications used here, the zones containing the dark areas appear to be an early form of the regions that will remain austenite-martensite and that may well be chemically heterogeneous. Actually, it seems that the occurrence of such areas is also observed in the martensite formed so they would thus either exist in the parent austenite or form on quenching. In any case, such regions when they exist can be related to deformation cells inherited from austenite with a nonuniform carbon distribution and perhaps some inhomogeneity in substitutional elements,[47,48,49] and thus explain the formation of the intermediate ferrite and the course followed by transformation. If we refer to the dilatometric tests, it appears that this transformation is athermal. In fact, the phenomenon progresses extremely slowly with time at 550 C (1020 F). Actually, there would be no driving force to move the interface at this temperature but the possibility of some diffusion occurring in front of the interface must not be ruled out.

Tentative Mechanism of Massive or Granular Transformation

Two types of structures have to be taken into account in the case of ferrous materials. On the one hand, there are the structures formed in the lower temperature range: acicular martensite produced by the highest cooling rates and conventional lower bainite produced by less drastic cooling rates. The formation of the latter structure is satisfactorily explained by the Ko-Cottrell hypothesis. On the other hand, in carbon-free alloys there are the massive structures of Greninger and the massive martensite described by Owen, both produced by intermediate transformation rates, and in low-carbon alloy steels there is the aggregate consisting of ferrite and austenitic-martensitic particles, which is also produced by cooling at rates of the same order as those giving rise to massive martensite in carbon-free alloys.

It is logical, particularly in the light of the structural analyses reported above to assume that the same initial mechanism of formation applies to the latter two structures. In our opinion, two factors influence this transformation. The first pertains to the parent austenite and consists of a dehomogenization above B_s leading to the formation of regions enriched in carbon and perhaps substitutional elements.* Such dehomogenization can have many different causes, such as the existence of stresses in the metastable austenite, which would produce accumulations of dislocations on some groups of {111} planes and hence lead to a concentration of carbon in the stress fields of dislocation tangles. When endeavoring to explain some microstructures observed in the intermediate transformation range, Habraken[3] suggested that a redistribution of carbon occurred before and not during the formation of bainite. The same assumption was made by Entin[15] in attempting to explain bainitic structures. The second factor is the nucleation of carbon-depleted substitutional ferrite by a process similar to the formation of massive martensite in carbon-free ferrous alloys. The interfaces would move along some suitable oriented planes and would be stopped by the enriched regions mentioned above. Thus, the phenomenon involved would have initially a martensitic character.

When the cooling rate is low (Figure 22, curve I), large carbon-enriched clusters would be formed as explained above. Transformation would follow a path between them and would frequently entrap some of

* Complete homogenization of austenite is doubtful even under equilibrium conditions.

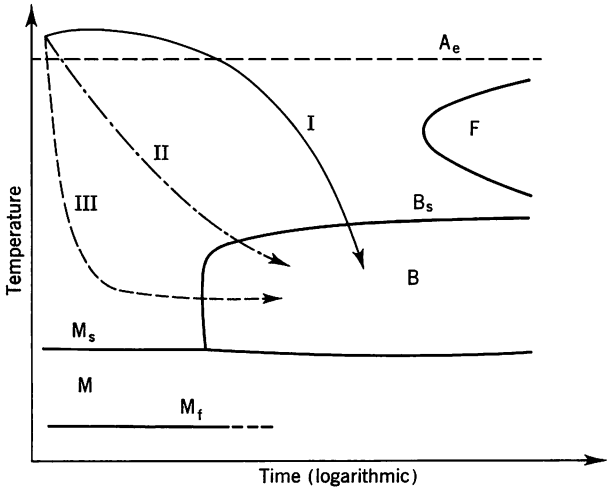

FIGURE 22. Schematic representation of transformation in a low-carbon alloy steel

I. produces a structure with ferrite and austenitic-martensitic particles

II. produces a carbide-free acicular structure or conventional upper bainite

III. produces conventional lower bainite

them. In the lower carbon steels investigated, it has even been possible to detect occasionally a transformation by short-range diffusion followed by a massive-martensitic transformation as in carbon-free ferrous alloys. The thermodynamic conditions near the interfaces or in the carbon-rich clusters are not adequate for the nucleation of the Fe_3C carbide. Some stabilization is observed at low temperatures, probably as a result of the locking of dislocations by interstitial atoms. In fact, it is not excluded that the transformation interfaces would be enriched in carbon but transformation would progress only when the driving force is sufficient, i.e., when the temperature decreases. In this case, it seems that the isothermal transformation is negligible.

When the cooling rate is higher (Figure 22, curve II), the carbon-rich clusters are smaller and more numerous, and the acicular character of the transformation is more pronounced. Transformation often starts on the austenite boundaries. The final microstructure is then similar to that described previously as carbide-free acicular ferrite or conventional upper bainite. The latter structure occurs when the carbon content of the steel is high enough. In this case it seems that the interface is able to displace carbon atoms in front of it because the driving force is sufficiently high (lower temperature). All this would tend to confirm the mechanism of double nucleation of ferrite and Fe_3C proposed by Krisement and Wever.[13] This mechanism would be enhanced by the initial local enrichment in carbon referred to above.

Finally, at the high cooling rates leading to conventional lower bainite (Figure 22, curve III), the carbon-rich clusters are very small. Transformation starts as an acicular-martensitic transformation and is not hampered by the presence of these clusters.

PART TWO. MECHANICAL PROPERTIES OF BAINITIC STRUCTURES

PRELIMINARY CONSIDERATIONS

To establish a relation between two variables or two properties, it is first necessary to define them unequivocally. Whereas the accurate definition of mechanical properties does not pose any particular problem in the case of steels, that of their microstructure is much more difficult. Indeed, the parameters chosen to characterize the microstructure of steels depend largely on the magnification at which the observation is made. In the case of bainite, for instance, optical-microscopic examination at 100 to 1000 X results in laying emphasis on the austenitic grain size, the fineness or acicularity of the microstructure, etc. When replicas are observed under the electron microscope at 2000 to 15,000 X, the major aspects considered are the bainitic grain size, size and distribution of carbides, presence of residual austenite, etc. Finally, the characteristics revealed when observing a thin foil directly under the electron microscope at 30,000 X or more are not only the nature and distribution of imperfections in the crystal lattice but also the orientation relationships between neighboring phases. This aspect of the problem of correlating mechanical properties and microstructure explains why progress in this field has closely followed improvements in metallographic techniques.

Metallographic investigations come up against a major difficulty when the problem is transferred from the qualitative to the quantitative plane. Whatever the parameter or parameters chosen to define the microstructure, they change from one area to another on the polished surface or thin foil. These changes are due to the polycrystalline nature of the metal and the different orientations of the grains with respect to the surface examined; the heterogeneous character of the nucleation phenomena; and unavoidable chemical segregation. This difficulty increases as observation methods become finer and hence as the areas observed become smaller.

SURVEY OF PREVIOUS WORK

In the following sections, a brief outline will be given of the currently prevailing notions concerning the influence of structural factors on the mechanical properties of bainite. Structures produced by isothermal transformation and continuous cooling will be considered separately since, as stated earlier, these two transformation modes can lead to morphologically different microstructures.

Isothermal Bainites

Isothermal transformation within the bainitic field has found relatively few practical applications, which are confined to small parts with very small tolerances where dimensional stability is essential. Nevertheless, the study of these structures is interesting in that it leads to a better understanding of the phenomena and prepares for the study of the continuous-cooled bainites.

The early investigations devoted to the mechanical properties of bainite were mainly centered on the comparison between these properties and those of tempered martensite and paid no particular attention

to the morphology of the bainite. The work of Delbart and Potaszkin[50] was one of the first interesting attempts to study the mechanical properties of bainite as a function of microstructure. The conclusions reached by Potaszkin and Bar-Avi on medium-carbon structural steels in two recent papers[51, 52] can be summarized as follows. Lower bainite, formed between the M_s point and 350 C (660 F) or so, exhibits tensile properties equivalent to those of tempered martensite; this similarity is also observed in the microstructures since the acicular structure of lower bainite closely resembles that of martensite. The impact strength of lower bainite is generally higher than that of tempered martensite. Formation of upper bainite between approximately 350 and 500 C (660 and 930 F) leads to a severe loss of yield strength and appreciable embrittlement. Potaszkin and Bar-Avi[52] attribute the latter on the one hand to the coarse structure of upper bainite and on the other to possible carbide precipitation on austenite grain boundaries. In fact, the embrittlement is found in upper bainite formed in the neighborhood of, but approximately 25 C (45 F) lower than, the main bay in the TTT curve corresponding to the longest transformation times. Prolonged holding at these temperatures would cause the above-mentioned precipitation.

It will thus be noted that there exists a relation between the metallographic appearance and mechanical properties,[53] although it was impossible to formulate this relation quantitatively as was done for instance for pearlite.[54, 55] In the case of globular structures, Gensamer and coworkers[55] used the mean ferrite path as the parameter defining the microstructure and demonstrated the existence of a close relation between this value and mechanical properties. However, it proved impossible to apply this criterion to bainitic structures because of the inadequate resolving power of instruments at that time.

It should be noted that the investigations mentioned above pertained to structures corresponding to the conventional definition of bainite as acicular ferrite and carbides.

Continuous-Cooled Bainites

The bainitic structures produced by continuous cooling are of considerable practical interest since they form an appreciable fraction of the microstructure of numerous heat-treated parts. Examples would be large forgings, which may contain high amounts of bainite and some such as large generator rotors are often almost entirely bainite; high-strength structural steels, which more and more frequently consist of ferrite-bainite-pearlite mixtures and sometimes as with the molybdenum–boron steels are even entirely bainitic; and some low-alloy structural steels used in the partly bainitic condition.

In spite of the practical significance of continuous-cooled bainites, so far their mechanical properties have hardly been investigated except by Irvine, Pickering and coworkers.[56-60] These authors studied a large number of compositions resulting from the addition of chromium, nickel or manganese to the same base (0.5% Mo–B). Thus a large range of bainitic structures was obtained with the same heat treatment (air cooling of 19-mm-dia bars).

Before summarizing the results reported by Irvine and Pickering, it would be useful to explain the term "transformation temperature" introduced by these authors. In the case of continuous cooling, this concept appears somewhat vague since the bainitic transformation occurs over a temperature range. Consequently, a point easy to define had to be selected within the transformation zone. Irvine and Pickering chose the temperature at which the transformation rate is highest. This temperature will be designated henceforth as "formation temperature." The choice of this temperature proved judicious since a close relation was found to exist between the formation temperature of bainite and tensile strength.

The tensile strength of the bainites obtained by continuous cooling the steels investigated by the above authors ranged from 70 to 120 kg/mm.^{2} At the lower end of this range, the bainite was characterized by the occurrence of two grain-boundary networks — the prior austenite grain boundaries and the boundaries of what Irvine and Pickering have called bainitic grains. The latter were much smaller than the former and their boundaries delineated elongated plates of bainitic ferrite. The carbides generally occurred between the plates and in clusters.

As the formation temperature decreased, the strength increased and the morphology of the structure changed. The bainitic-ferrite plates became thinner and thinner and the carbides precipitated on the sub-boundaries separating these plates. For the lowest formation temperatures and highest strengths, the bainitic-ferrite plates were very thin with carbides precipitated inside them.

When attempting to formulate quantitatively the effect of microstructure, Irvine and Pickering found that the tensile strength depended mainly on two factors: bainitic grain size and carbide density. The former played a preponderant role in lower-strength bainites since the carbides here occurred mainly at grain boundaries or in the form of clusters. Strengthening of the higher strength bainites was due mainly to a fine dispersion of carbides.

There was also a very clear correlation between impact strength and microstructure.[60] The bainites with a tensile strength near 70 kg/mm^2 had an impact-strength curve similar in shape to that encountered with ferritic-pearlitic steels. The impact strength of these bainites depended mainly on the bainitic grain size, just as did the tensile strength.

According to Irvine and Pickering, the width of the ferrite plates decreased with the bainite formation temperature but their length was always determined by the dimensions of the prior austenite grain. In addition, the carbides precipitated mainly between the ferrite plates of the bainite. Both factors account for the brittleness observed in these intermediate bainites.[59, 60] Finally, for very low formation temperatures, carbides precipitated inside the ferrite plates because the carbon diffusion was very much restricted. As a result the carbides were very finely dispersed in the ferrite so the strength increased without prohibitive sacrifice of ductility. Indeed, the carbides and dislocation tangles at the grain boundaries presented so many obstacles obliging the cleavage cracks to deviate from one cleavage point to another that an absorption of energy resulted.[60]

It should be noted that the above authors detected no residual austenite in the course of their investigations.

TEST PROCEDURES

Heat treatment of the specimens used for determining mechanical properties set two problems, that of finding a simple means of achieving a wide range of cooling rates and that of ensuring good reproducibility.

To cover the whole bainitic field of the steels investigated, it was necessary to achieve cooling rates from 0.1 to 1500 C/min (0.2 to 2700 F/min). This broad range was covered as follows:

0.1/5.5 C/min (0.2/10 F/min) — programmed cooling

5.5/25 C/min (10/45 F/min) — furnace cooling in a stream of compressed air under controlled pressure

25/50 C/min (45/90 F/min) — air cooling in a refractory muffle preheated to various temperatures

50/150 C/min (90/270 F/min) — cooling in compressed air under controlled pressure

150/1500 C/min (270/2700 F/min) — cooling by "mist quenching" with controlled water flow and air pressure

The problem of reproducibility was important because for each selected cooling rate some 20 specimens were required to determine the transition curve and tensile properties and it was impossible to treat so many samples simultaneously. The samples were treated in groups of five, with the fifth serving as a reference sample for recording the cooling curve. For this purpose, a thermocouple was welded at the bottom of a hole drilled halfway up the specimen axis. The reproducibility was found to be satisfactory and this was further confirmed by the small scatter in mechanical test results.

Tensile and impact specimens were rough machined to 12 x 12 x 70 mm from 16-mm plates with the long dimension in the direction of rolling. Identical dimensions were used for both types of specimens to ensure their receiving strictly identical heat treatments. The excess of these dimensions over those of the finished specimens was sufficient to permit removing all oxidation, decarburization or boron depletion caused by heat treatment.* In each group of four simultaneously heat-treated specimens, one was intended for a tensile test while the other three were used to determine the impact strength. Thus tensile and impact values correspond to the same heat treatment and the same microstructure.

Tensile tests were carried out on a 2.5-ton Adamel machine with specimens having a gage length of 29 mm and a diameter of 4 mm. Typical results show that the scatter was small, due partly to the good reproducibility of the heat treatment. Conventional Charpy V-notch specimens were used for the impact-strength determinations and here also the scatter in results was fairly small.

MECHANICAL PROPERTIES

The mechanical properties of five steels listed in Table I were determined systematically. The first four steels (VII to X) were of the high-strength weldable type, with or without boron additions; while the fifth (XIII) was an ultrahigh-strength nickel–cobalt steel. Mechanical properties and transformation characteristics are summarized in one diagram for each steel (Figures 23 to 27). Electron micrographs showing typical bainitic structures have been given previously in Figures 2 to 6.

Within the bainitic field, the curves representing the dependence of tensile and yield strength on cooling time have approximately the same shape for the four low-alloy steels. In addition, for some of the steels, especially steel VII, each branch of the tensile-strength–cooling-time curve corresponds to a different section of the CCT diagram (Figure 23). Such a relation does not exist in the case of steel VIII because the transition between the branches BC and DE of the tensile-strength curve occurs mainly inside the ferritic-bainitic region (Figure 24).

In the chromium–molybdenum steel VIII (Figure 24), the branch DE corresponds to a polygonal ferritic-bainitic structure in which the bainite visually resembles pseudo-pearlite. The branch BC corresponds to the pure massive or granular structure; the small amounts of polygonal ferrite detectable in this structure by physical methods are basically insig-

* It is well known that boron-containing steels are highly susceptible to "deboronization" when heat treatment is carried out in an oxidizing atmosphere.

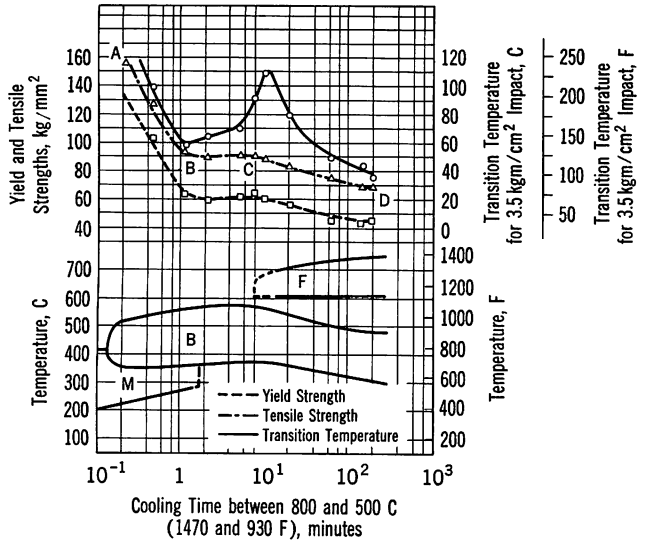

FIGURE 23. Effect of cooling rate on structure and mechanical properties of 1.5% Mn–0.5% Mo–B steel VII

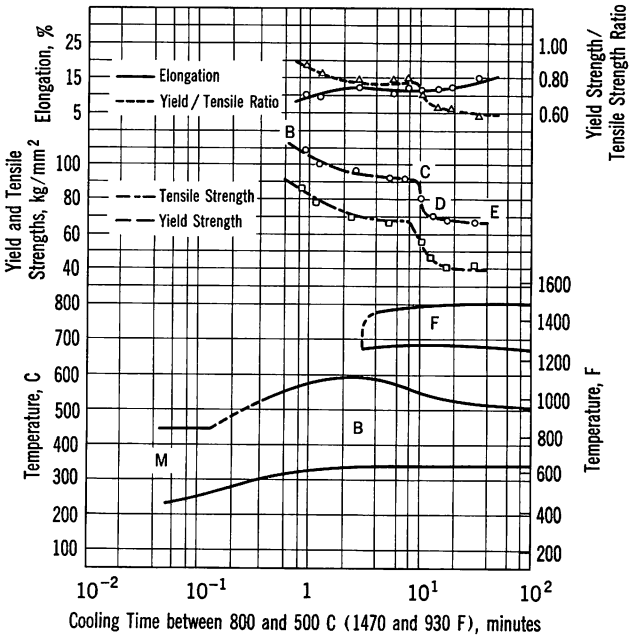

FIGURE 24. Effect of cooling rate on structure and mechanical properties of 1% Cr–0.5% Mo steel VIII

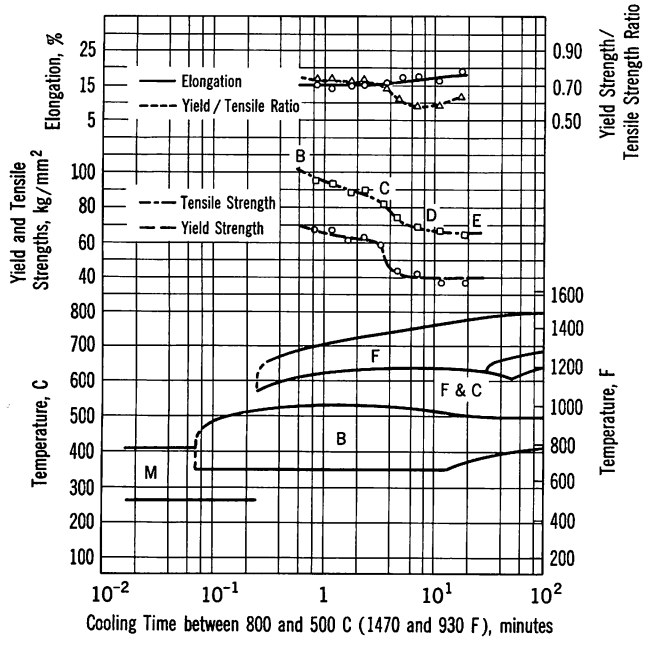

FIGURE 25. Effect of cooling rate on structure and mechanical properties of 1% Cr–0.5% Mo–B steel IX

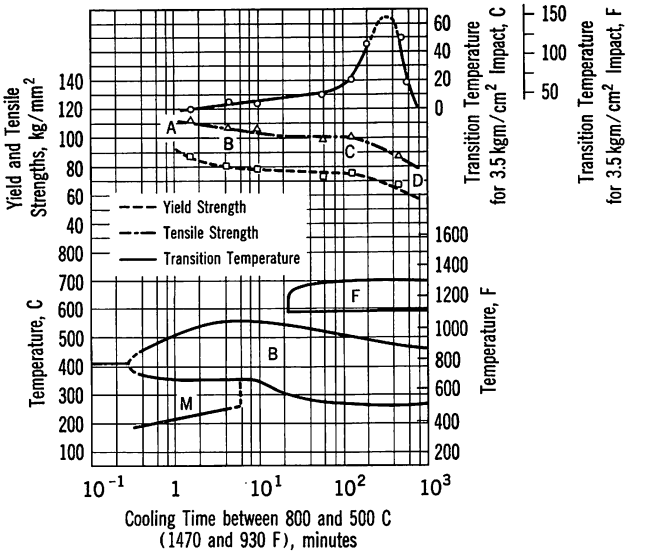

FIGURE 26. Effect of cooling rate on structure and mechanical properties of 2.7% Ni–0.9% Cr–0.25% Mo–B steel X

nificant. In some cases, the austenitic-martensitic islands have decomposed to ferrite and carbides. The branch CD corresponds to a transitional field in which polygonal ferrite disappears while massive bainite starts to occur. It is interesting to note that the ductility of this steel as typified by elongation varies only slowly over the whole of the bainitic field explored (60/100 kg/mm²). It will also be noted that the yield-strength/tensile-strength ratio is attractive (0.72) only in the ferrite-free quasi-granular bainitic field. This ratio drops to less than 0.6 as soon as proeutectoid ferrite appears.

The mechanical properties of the chromium–molybdenum–boron steel IX are summarized in Figure 25. The shape of the tensile-strength–cooling-time curve is similar to that of steel VIII but is shifted to lower cooling rates. As with steel VIII, the DE branch corresponds to a mixture of polygonal ferrite and bainite, with the appearance of the latter resembling pearlite. However, some austenitic-martensitic

islands can already be observed. The BC branch again corresponds to massive granular bainite. The formation of this structure is followed easily since it occurs over a wide range of cooling rates. At the lower end of the range, the structures consist of quasi-granular bainite where the austenitic-martensitic islands are often decomposed and give rise to carbide clusters. This decomposition is more advanced with steel IX than with steel VII, perhaps due to the fact that the same structure is produced by a much slower cooling rate.

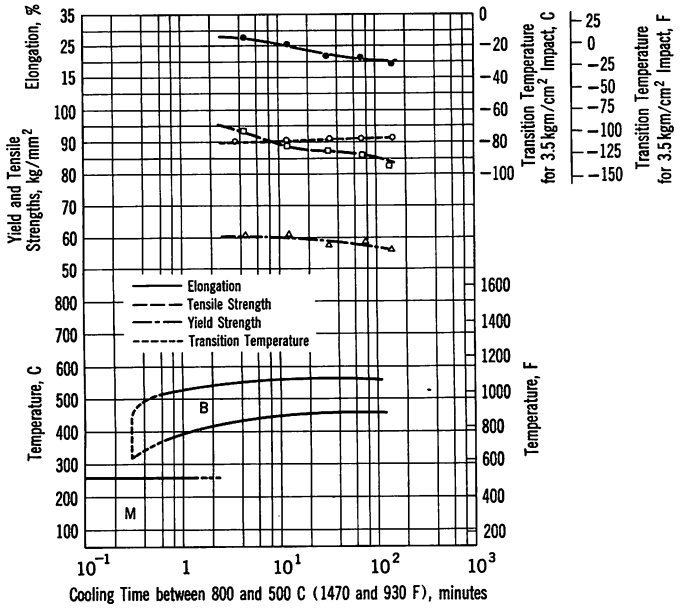

FIGURE 27. Effect of cooling rate on structure and mechanical properties of 9% Ni–4% Co ultrahigh-strength steel XIII

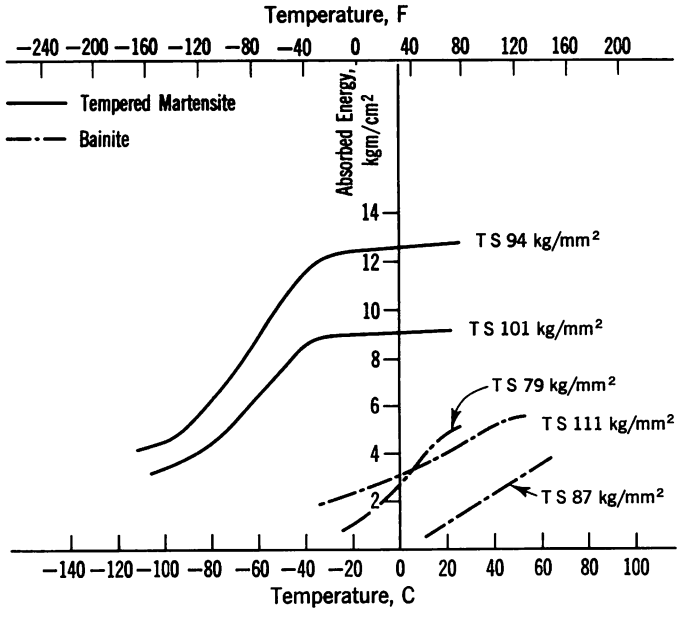

FIGURE 29. Effect of structure on impact properties of nickel–chromium–molybdenum–boron steel X

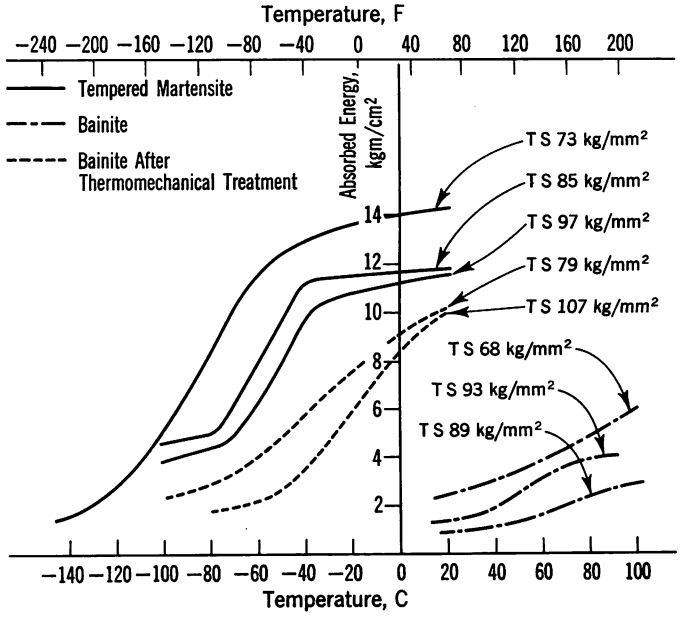

FIGURE 28. Effect of structure and thermomechanical treatment on impact properties of manganese–molybdenum–boron steel VII

The manganese–molybdenum–boron steel VII and the nickel–chromium–molybdenum–boron steel X exhibit more or less similar tensile-strength curves, the branches of which are again related to structure (Figures 23 and 26). As expected, a strength increase is observed as the amount of martensite in the bainitic-martensitic mixture increases. The influence of martensite becomes decisive with steel VII for the slowest cooling rates (Figure 23). The large strength increase observed in this bainitic-martensitic field is accompanied by a marked increase in brittleness. This increase in brittleness with increasing martensite content, which should normally be encountered in all the steels, is not observed in steel X, at least over the range of cooling rates explored. In fact, on cooling at 200 C/min (360 F/min), corresponding to 30% martensite, the strength increase is not accompanied by increased brittleness but, on the contrary, the transition temperature continues to decrease slowly (Figure 26).

In the fields where acicular martensite does not occur, transition-temperature–cooling-time curves exhibit for both steels VII and X a characteristic peak (Figures 23 and 26). In the case of steel VII, this peak coincides with the transition between the ascending branch CD and the horizontal branch BC of the tensile-strength–cooling-time curves and with the nose of the ferrite curve. On the other hand, the peak for steel X is shifted towards lower cooling rates away from the nose of the ferrite curve. As a matter of fact, it corresponds to a proeutectoid-ferrite content of approximately 30%.

The transition-temperature–cooling-time curves provide a rough indication of the susceptibility of a steel to brittle fracture. A more complete picture can be derived from an examination of the impact-energy–temperature curves. Curves shown in Figures 28 and 29 for bainite were obtained on samples transformed at cooling rates corresponding to the base and top of the transition-temperature peaks illustrated in Figures 23 and 26. The characteristic appearance of these curves for bainitic structures differs from that for ferritic-pearlitic or tempered-martensitic structures in that the slope is less steep and there is no clear transition temperature. A comparison of Figures 28 and 29 shows that the impact-energy–temperature curves for bainitic specimens are shifted to lower temperatures and higher energies in the case of the nickel–chromium–molybdenum–boron steel X regardless of the strength level or cooling rate. In other words, steel X is superior to steel VII in respect to its susceptibility to brittle fracture.

To understand the reasons for the shape of the transition temperature vs cooling time curves, we resorted to internal-friction experiments. Small specimens (150 x 1.5 x 1.5 mm) of steel VII were austenitized at 800 C (1470 F) and cooled at various rates. The results on examination in a Wert pendulum show that a Köster peak appears at 200 C (390 F) and is maximum for the specimen cooled at about 20 C/min (36 F/min) (Figure 30). In this steel the maximum brittleness in the bainitic-ferrite–austenitic-martensitic structure is also observed for specimens cooled at this rate. The brittleness is very probably related to coarsening of the microstructure and locking of the dislocations. The same coarse structures also occur in the nickel–cobalt steel XIII but it does not show the same brittleness (Figure 27) nor does it exhibit an internal-friction peak around 200 C (390 F), at any rate not under the above test conditions.

EFFECT OF THERMOMECHANICAL TREATMENTS ON MANGANESE–MOLYBDENUM–BORON STEEL

A mechanical deformation applied to austenite influences both the transformation process and the condition of the metastable austenite since it increases the number of lattice imperfections, influences their distribution and modifies the precipitates.

Zoidzee, Economopoulos and Habraken[61] recently analyzed the influence of thermomechanical treatments on one of the steels investigated here, the manganese–molybdenum–boron steel VII. Small plates (12 x 12 x 0.4 in.) were rolled on a two-high mill within three temperature ranges: 950/800 C (1740/1470 F), 800/700 C (1470/1290 F) and 650/550C (1200/1020 F), where the first temperature is that at which the material left the reheating furnace and the second temperature is that at the end of the rolling operation. The material was then cooled at given rates. In general, four cooling rates were used, all of which produced a largely bainitic structure: 80, 30, 9 and 1 C/min (145, 55, 16 and 2 F/min) corresponding to times of 3.6, 10, 33 and 300 min for cooling from 800 to 500 C (1470 to 930 F). After the thermomechanical treatments, tensile and impact specimens were machined from the rolled products with their axis parallel to the rolling direction. In addition, samples were systematically examined under the optical and electron microscope using in the latter case the thin-foil technique.

The treatments applied and the results obtained are summarized in Figure 31 for thermomechanical treatments in the temperature range where austenite is stable and in Figure 32 for treatments in the intermediate temperature range of 800/700 C (1470/1290 F) around the transformation points. The indicated reductions were obtained on one pass and the cooling times are mean values. For comparison purposes the results obtained on a normalized steel cooled at rates similar to those used after the thermomechanical treatments are included. The most salient observations are summarized below.

Deformation Above Critical Point by Rolling Between 950 and 800 C (1740 and 1470 F) (Figure 31)

The strength, impact and transition-temperature curves are similar in shape to those for specimens cooled at the same rates after austenitization. The

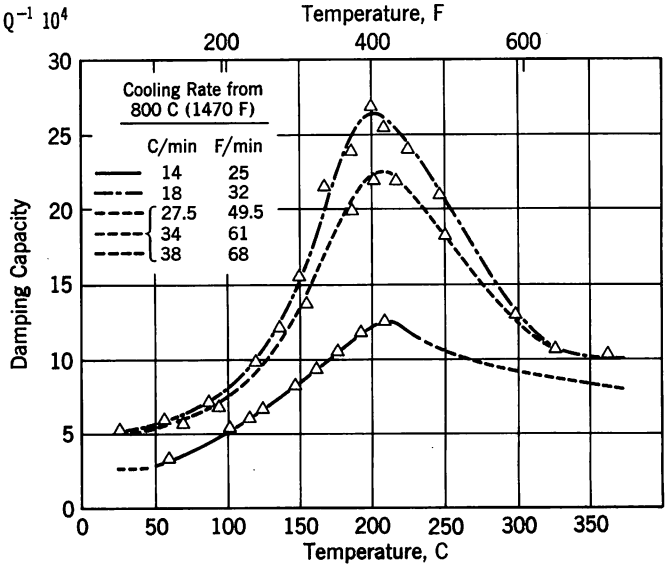

FIGURE 30. Effect of cooling rate and test temperature on internal friction of manganese–molybdenum–boron steel VII

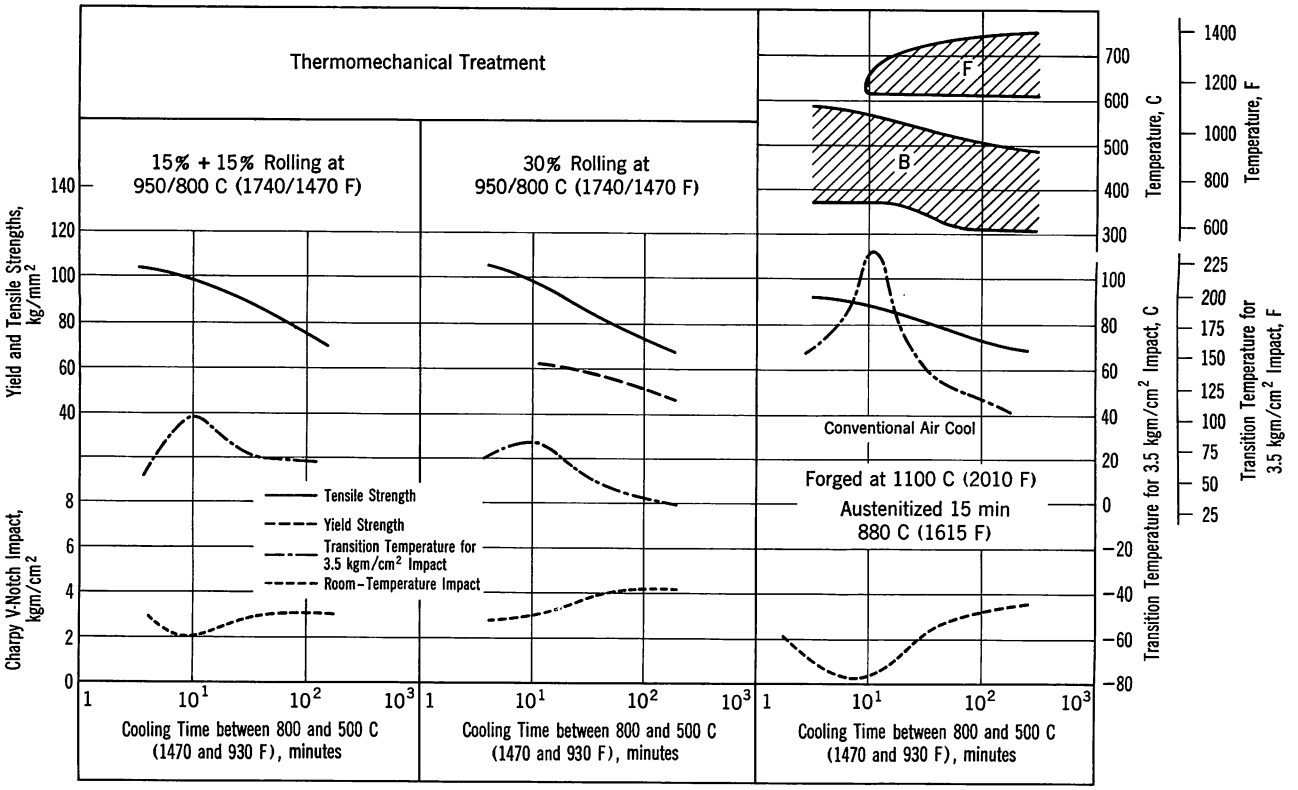

FIGURE 31. Effect of high-temperature thermomechanical treatment on mechanical properties of manganese–molybdenum–boron steel VII

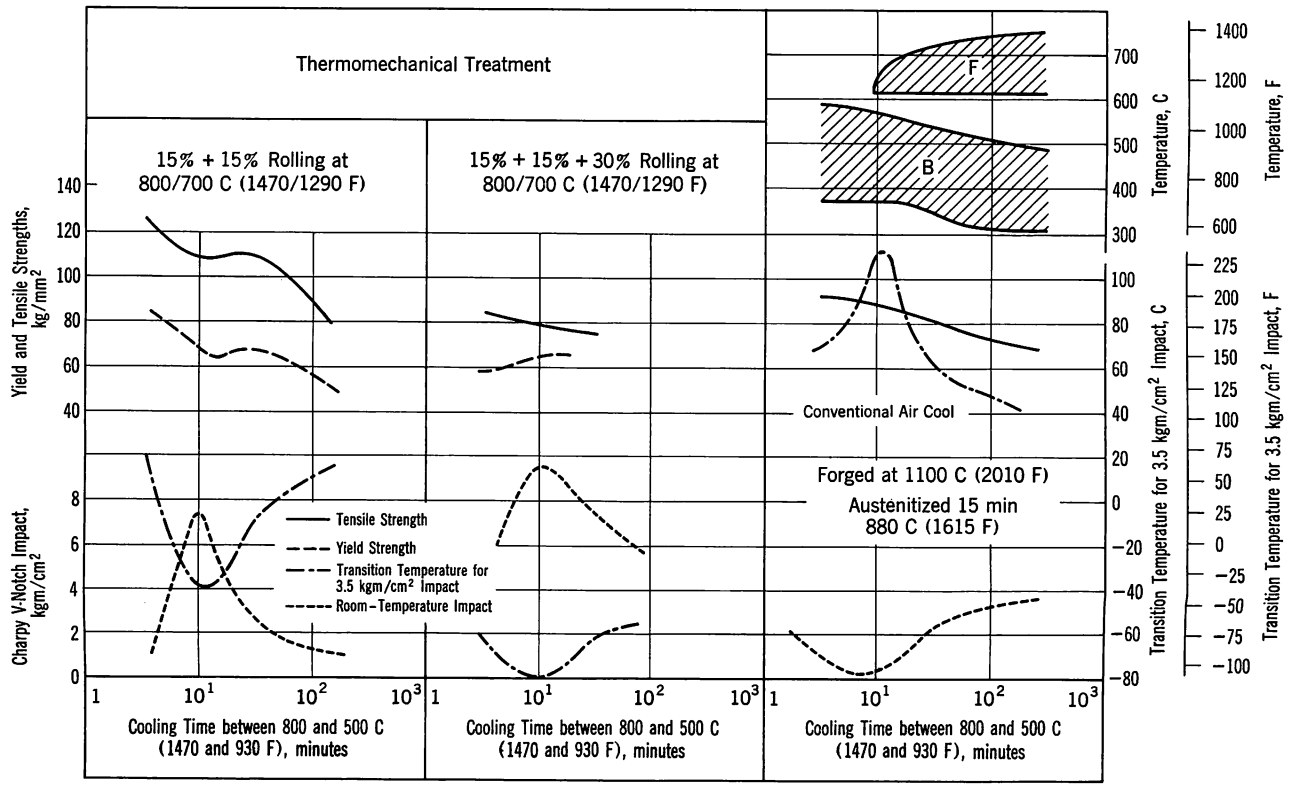

FIGURE 32. Effect of intermediate-temperature thermomechanical treatment on mechanical properties of manganese–molybdenum–boron steel VII

impact strengths, however, are higher and the peaks in the transition-temperature curves are much less apparent.

All the structures obtained are similar to those described previously. In the region of maximum brittleness, the structure consists of ferrite and austenitic-martensitic particles (Figure 16). The size of the austenite and bainitic-ferrite grains is smaller than that obtained after austenitization and the ferrite has a high density of dislocations. The undecomposed particles are also smaller but more numerous and very irregular in shape. The difference between the structures obtained by cooling at the same rates after austenitizing and after thermomechanical treatments could account for the observed difference in mechanical properties.

Thermomechanical Treatments Between 800 and 700 C (1470 and 1290 F), Below Transformation Point

Figure 32 shows that not only is the tensile strength increased by this type of thermomechanical treatment but a high impact strength is sometimes also associated with this high tensile strength. Oddly enough, the best impact strengths are obtained by cooling at 30 C/min (55 F/min), that is with a cooling time of ten minutes between 800 and 500 C (1470 and 930 F), or precisely that which produces the lowest values directly after austenitization. The percentage reduction and number of passes influence the results considerably but do not change the comparative positions of the impact and transition-temperature curves.

Optical micrographs in Figures 33 and 34 show complex structures composed of ferrite surrounding a large number of small, substantially unaligned austenitic-martensitic particles, which are partially decomposed to carbides and ferrite. Austenite grain boundaries are not visible. The structure is coarser after three passes. In both cases, the ferritic regions are typical when they are observed at a very high magnification; the grains are relatively small and the dislocations are grouped in low-energy arrays recalling a recovered structure. This ferrite is completely different from those observed so far, which were more like mechanically deformed structures. The austenitic-martensitic particles are often decomposed as shown in the electron micrographs at the intermediate magnification. The ferrite between the carbides again has many dislocations but these tend to be more disorganized than in the bainitic ferrite. Combination of the strength of the bainitic ferrite with that of the austenitic-martensitic zones partially transformed to ferrite and carbides may account qualitatively for the observed mechanical properties, especially the good impact properties.

If we analyze now the first group of curves in Figure 32, we do not observe a continuous increase in tensile strength as the cooling rate increases. Actually, a slight decrease occurs for cooling rates around 30 C/min (55 F/min). This decrease, which coincides with the highest impact properties, is related to the presence of a recovered structure as stated above. At low cooling rates (cooling time from 800 to 500 C (1470 to 930 F) about 150 min), the tensile strength is only 80 kg/mm^2. The structure consists of very large bainitic-ferrite grains with numerous randomly distributed dislocations and elongated austenitic-martensitic particles, a few of which have decomposed. At fast cooling rates (shortest cooling time between 800 and 500 C (1470 and 930 F) 3.6 min) the tensile strength is 128 kg/mm^2. The structure then consists of small ferritic grains with a high density of dislocations. The austenitic-martensitic particles are large, elongated and undecomposed. In both cases, the impact properties are very low; the intrinsic properties of the bainitic ferrite, and the size and distribution of the austenitic-martensitic particles within the ferrite are jointly responsible for this effect.

Deformation by Rolling at 650/550 C (1200/1020 F)

When such a deformation is followed by cooling at a rate sufficiently high to produce bainite, the structure consists of ferrite with a very high dislocation density (Figure 18), inside which small but numerous austenitic-martensitic particles occur. The strength is high with a tensile strength of 127 kg/mm^2 and a yield strength of 93 kg/mm^2 but naturally the impact properties are low with a Charpy V-notch impact about 1.7 kgm/cm^2.

DISCUSSION

The following discussion, based on the whole of the observations just described, is aimed at explaining the dependence of the tensile and impact properties on the observed microstructures, accounting for the vastly different impact strengths of structures having the same tensile strength and understanding the differences in behavior of isothermal bainites, which in certain cases are less brittle than tempered martensite of similar strength, and of some continuous-cooled bainites, which are much more brittle than isothermal bainites.

Influence of Structures on Correlation Between Microstructure and Mechanical Properties

In principle, the mechanical properties of bainitic steels can be accounted for in terms of the structures observed under the microscope. Our investigations, however, have shown that a complete solution of this

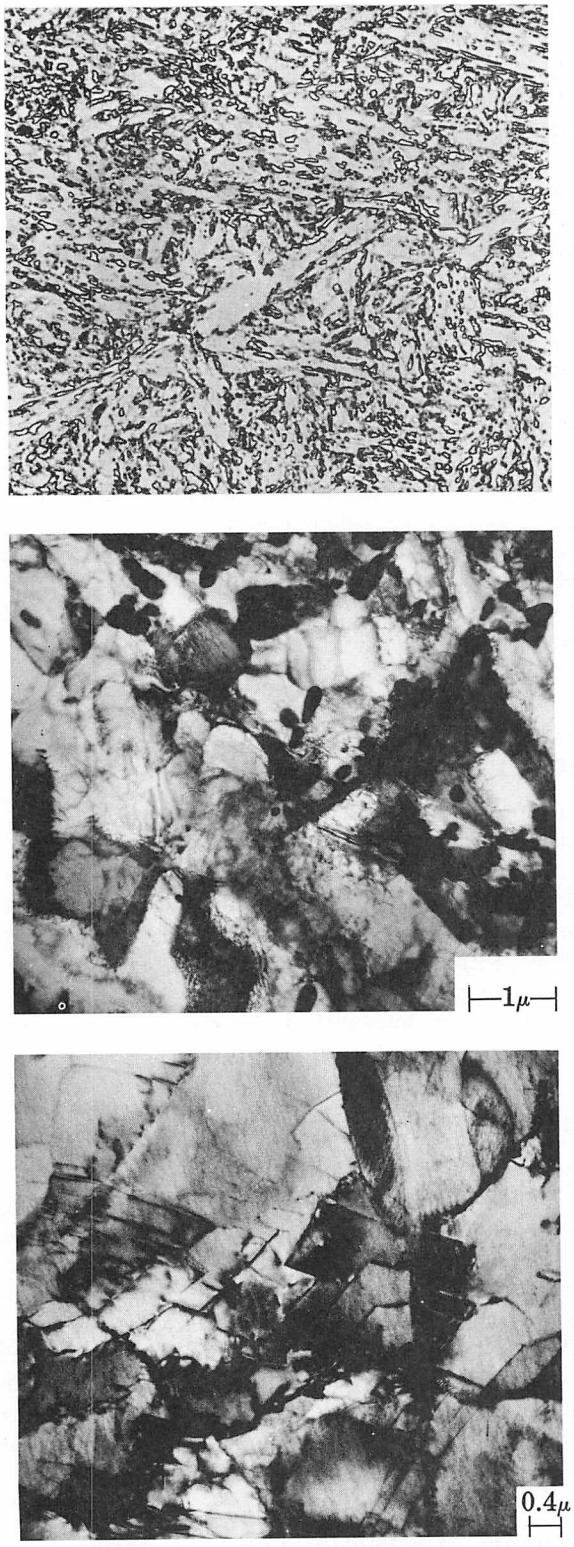

FIGURE 33. Structure of manganese–molybdenum–boron steel VII after intermediate-temperature thermomechanical treatment involving 15% + 15% deformation by rolling between 800 and 700 C (1470 and 1290 F) followed by cooling at 30 C/min (55 F/min). Optical (500 X) and thin-foil electron micrographs (12,000 and 40,000 X)

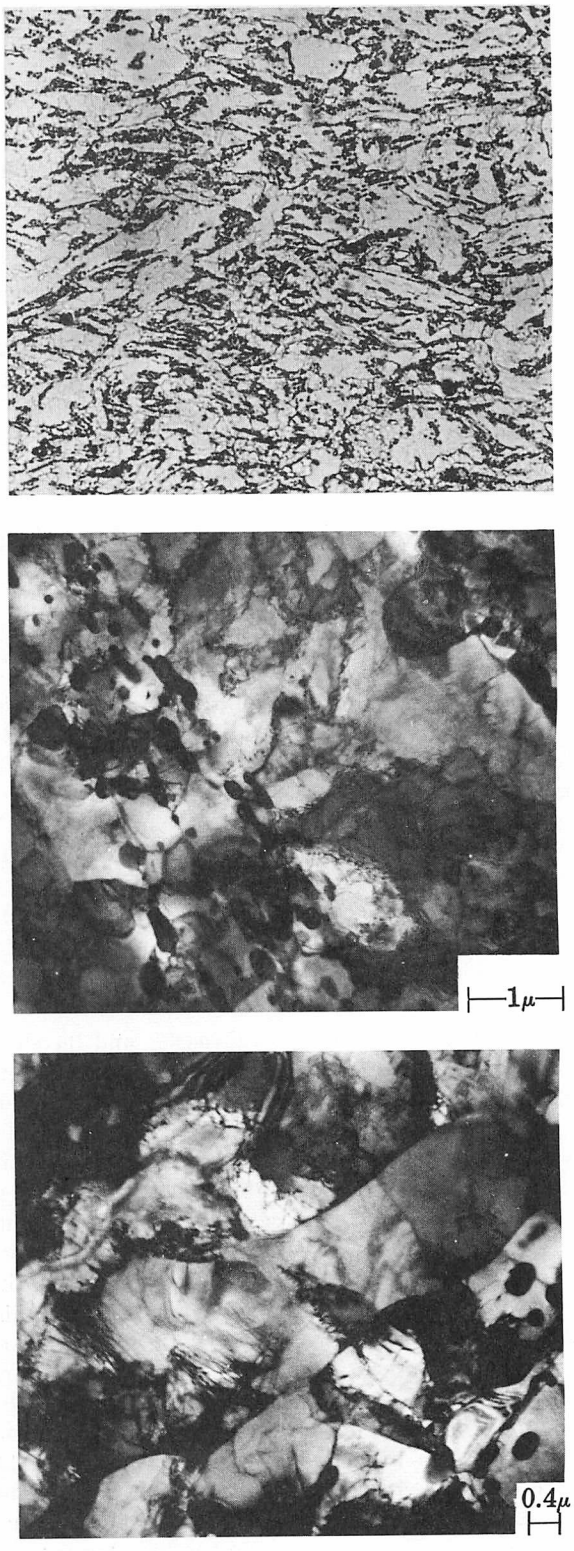

FIGURE 34. Structure of manganese–molybdenum–boron steel VII after intermediate-temperature thermomechanical treatment involving 15% + 15% + 30% deformation by rolling between 800 and 700 C (1470 and 1290 F) followed by cooling at 30 C/min (55 F/min). Optical (500 X) and thin-foil electron micrographs (12,000 and 40,000 X)

correlation problem requires quantitative data or, in other words, describing the microstructures by parameters.

Attempts in this direction have been made, particularly by Irvine and Pickering.[58] These authors have shown that the tensile strength can be satisfactorily correlated quantitatively with two structural parameters, the bainitic grain size and the carbide density. In most of the steels considered in the present paper, however, the problem is complicated by the occurrence of certain bainitic structures consisting of ferrite and austenitic-martensitic areas. For this reason, it appears that the structural parameters to be used should be much more general than those employed up to now.

Ansell[63] has shown that the problem of quantitatively correlating properties with microstructure is complex even in the case of relatively simple structures such as those consisting of a finely dispersed phase inside a homogeneous matrix. In the case of bainite or of the structures identified in the present work, the problem is considerably complicated by the fact that four constituents are often present simultaneously: bainitic ferrite, cementite, martensite and austenite. This is the reason why we shall restrict ourselves in the present discussion to some general remarks regarding a possible correlation.

For each of the constituents listed above, it is appropriate to consider on the one hand its intrinsic properties and on the other its relation with adjacent constituents. For instance, the contribution of bainitic or massive ferrite to strength will depend on the grain size, intrinsic strength of the lattice, which is related to substitutional or interstitial solid-solution hardening, precipitation hardening, etc. The strength is also influenced by the density of dislocations and vacancies present, whether arising during transformation or inherited directly from the austenite. We shall now examine successively the three structures as defined in Figure 8.

Bainitic Ferrite–Austenitic-Martensitic Structure (I) This structure, which has been shown to occur in numerous steels and to be in some cases free of precipitates, exhibits tensile strengths ranging from 50 to 100 kg/mm^2, depending on the composition of the steel. Over a whole range of cooling rates, it leads to a momentary levelling-off in the tensile-strength–cooling-time curve. This tends to indicate that the properties are little influenced by minor modifications in the distribution of the two phases. When thermomechanical treatments are applied, however, the structure becomes finer and in this case a rather large variation in tensile strength, often dependent on cooling rate, is observed. As regards impact strength, a high degree of impact brittleness is generally observed when structures of this type become very coarse whereas room-temperature tensile and elongation values are little affected. This embrittlement is more evident when elongated austenitic-martensitic particles are present.

After certain thermomechanical treatments, numerous arrays of dislocations similar to those observed in a recovered structure appear in the ferrite. When this is the case, the tensile strengths are low but impact properties are attractive even when austenitic-martensitic particles are present. The most favorable impact properties, however, are obtained when the ferrite is recovered and the austenitic-martensitic areas are small and globular.

Carbide-Free Acicular Ferrite Structure (II) This structure forms on cooling at higher rates than those giving the bainitic ferrite–austenitic-martensitic structure. In general, it is relatively acicular and much finer than that examined above. This actually accounts very often for the improved tensile properties observed. When long austenitic-martensitic plates extend across the grains, however, the impact strength may decrease fairly sharply. In many cases, this structure tends to resemble conventional upper bainite, especially when the carbides have had an opportunity to precipitate. Finally, a spectacular strength increase together with an appreciable decrease in impact strength is observed in most steels when at the end of the bainitic transformation a certain amount of acicular martensite is formed inside the acicular-bainitic regions.

Proeutectoid Ferrite and Pseudo-Pearlite (III) Generally speaking, the low strength of propearlitic ferrite is responsible in this case for an appreciable decrease in tensile strength, which often drops below 50 kg/mm^2. The grain boundaries are generally well defined and the impact strength is adequate. The mechanical properties are observed to depend in some measure on the number and extent of the bainitic areas and on the size and distribution of the precipitates. The effect of these factors is in conformity with the fundamentals of physical metallurgy.

Influence of Composition on Microstructure

The composition of the steel determines above all the position of the transformation curves. For a given austenitization treatment, it is thus possible to define the cooling conditions that will avoid the coarse and brittle structures described above. In certain cases, heavy turbine rotors for instance, selection of a suitable grade of steel is based solely on the necessity of avoiding transformations that would lead to the embrittling structures mentioned above under the cooling conditions prevailing throughout the part.

On the other hand, composition certainly modifies the amount of solid-solution hardening that can be attained in a given structure. For instance in the case of bainitic ferrite, the tensile strength varies from

60 kg/mm² for a low-alloy steel to more than 100 kg/mm² for the nickel–cobalt steel XIII in spite of an often fairly similar dislocation density. Let us emphasize that solid-solution strengthening must exert a very large influence since, in the nickel–cobalt steel XIII with 0.3% C just considered, the structure is relatively coarse and there is considerable stabilization of austenite. This does not prevent the steel from exhibiting a high tensile strength on the one hand and from retaining an adequate impact strength down to – 80 C (– 110 F) on the other. Bearing in mind the results obtained by Krön and associates[62] on a 9% Ni ferritic steel, which after heat treatment contains an appreciable amount of residual austenite, and the results of internal-friction measurements, we believe the favorable effects on impact properties are due principally to the presence of nickel in solid solution in the ferrite.

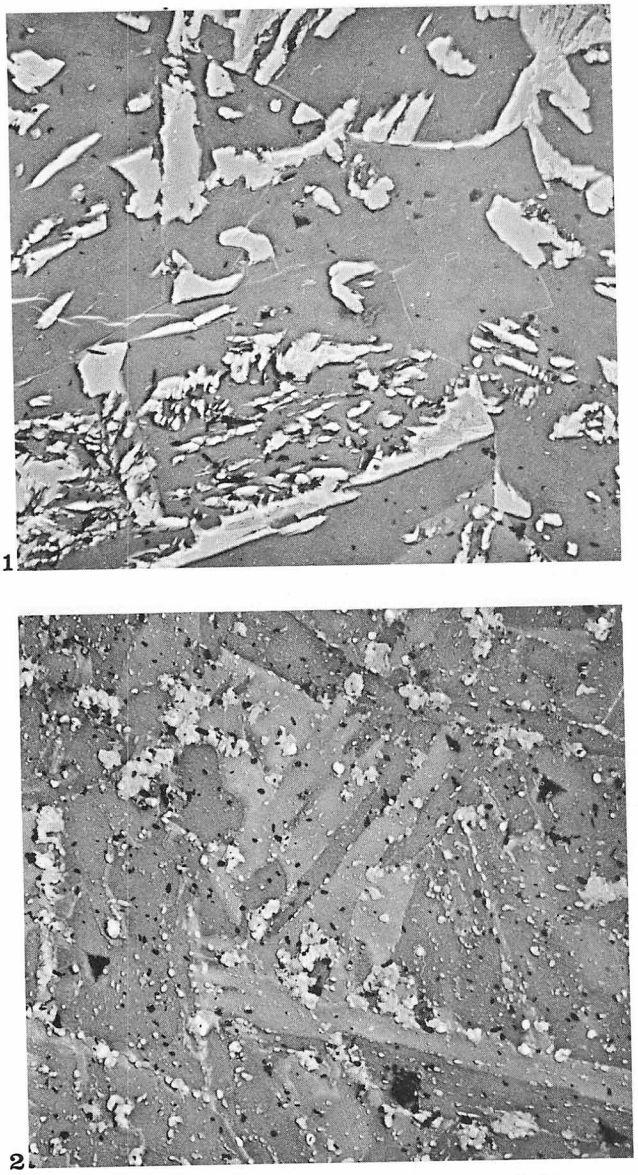

FIGURE 35. Two structures of manganese–molybdenum–boron steel VII having same tensile strength of 85 kg/mm² but different transition temperatures. Electron micrographs, plastic negative replicas. 2000 X

1. bainite produced by air cooling at 50 C/min (90 F/min) has transition temperature of 80 C (175 F)
2. tempered martensite produced by water quenching and tempering has transition temperature of – 60 C (– 75 F)

Comparison Between Bainite and Tempered Martensite

Considerations similar to the preceding ones permit an explanation as to why two microstructures of identical strength, one consisting of bainite and the other of tempered martensite, have distinctly different brittleness characteristics. Figure 35 provides a characteristic illustration of this difference. It shows two types of microstructures exhibiting the same tensile strength (85 kg/mm²); the first is bainitic with a transition temperature of 80 C (175 F) while the second is a tempered martensite with a relatively low transition temperature of – 60 C (– 75 F).

Hyam and Nutting[64] have shown that the major part of the strength of tempered martensite originates from the extremely small ferritic grain size (inherited from the fineness of the martensitic needles) and from the uniform dispersion of small carbide particles. Similarly, it is a fact that a fine ferritic grain size is highly favorable with respect to impact strength and the same applies for a fine dispersion of uniformly distributed carbides. Actually the latter constitute obstacles, which force the

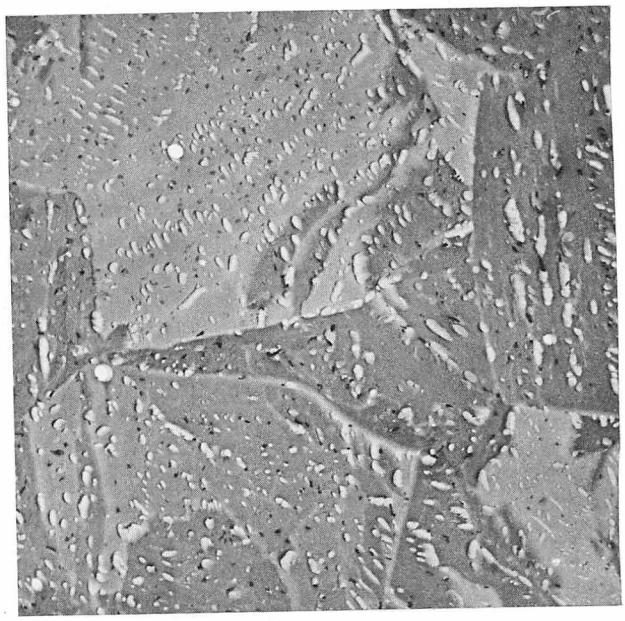

FIGURE 36. Isothermally produced bainite in manganese–molybdenum–boron steel VII. Electron micrograph, plastic negative replica. 2000 X

microcracks to deviate from one plane to another, thereby absorbing energy. The joint influence of these two favorable factors may well account for the combination of strength and high toughness found in tempered martensite.

As regards granular or massive bainite, the micrograph in Figure 35 shows that this structure has neither a fine ferritic grain size nor a homogeneous dispersion of small precipitated particles. Accordingly, other factors must be put forward to explain its strength: inherent strength of the bainitic ferrite because of its high dislocation density; solid-solution hardening of this ferrite; obstacles placed by the austenitic-martensitic islands; and presence within the structure of an appreciable percentage of martensite resulting from partial transformation of the stabilized austenite. Contrary to the situation prevailing in the case of tempered martensite, all these factors except the second are detrimental to impact strength. Actually, the large bainitic ferrite areas favor the formation and propagation of microcracks. In addition, the austenitic-martensitic islands are neither sufficiently fine nor sufficiently dispersed to constitute efficient obstacles to the propagation of cleavage cracks. Finally the presence of an appreciable amount of martensite can also contribute to brittleness.

However, let us recall that in certain cases a thermomechanical treatment produces an appreciable improvement in impact strength. This is illustrated in Figure 33, which shows that rolling at temperatures between the transformation points produces a structure in which the bainitic ferrite exhibits a large number of sub-boundaries as well as a distribution of dislocations similar to that observed in a crystal after recovery. Simultaneously the austenitic-martensitic particles become more numerous and globular with some of them dissociated into carbides and ferrite. This structure exhibits not only a high tensile strength but also impact properties that approach those of tempered martensite.

Comparison of Isothermal and Continuous-Cooled Bainites

Numerous investigations on bainites obtained by isothermal treatments have shown that in certain cases these structures can exhibit impact properties higher than those of tempered martensites of similar strength.[2] This is not true in the case of the bainitic structures obtained by continuous cooling of the steels considered in the present work. The explanation of this difference, which is particularly clearly apparent in the case of the manganese–molybdenum–boron steel VII, must be sought in the configuration of the isothermal and continuous-cooled structures (Figure 36 vs micrograph 1 of Figure 35). We have actually shown that in this steel it is practically impossible to obtain by continuous cooling a bainite with a structure similar to that of tempered martensite because of the presence of acicular martensite.

CONCLUSIONS

The various experimental facts relating to microstructure and mechanical properties described in the present paper can be summarized as follows.

Numerous steels exhibit a form of intermediate structure differing from ferrite and carbides. It consists of ferrite with a high dislocation density and austenitic-martensitic particles that are sometimes partly decomposed into ferrite and cementite. These structures form especially in low-carbon, low- and medium-alloy steels by cooling at intermediate rates from the austenitic range. It is often possible to deduce from a continuous-cooling diagram the austenitization conditions and cooling rate that will give these carbide-free structures. However can these structures still be called bainites? They are frequently encountered in continuous-cooling diagrams but seldom occur in isothermal diagrams. Early indications on their kinetics of formation suggest that these structures are related in several respects to the massive structures described previously in carbon-free ferrous alloys. In the light of the experiments described, it appears reasonable to assume that their formation is preceded by some kind of dehomogenization of the austenite. The same structures also occur in the steels investigated after certain thermomechanical treatments but they are then largely influenced by the nature of the treatment.

The comparative study of mechanical properties as a function of microstructure has revealed the existence of a qualitative correlation in all the steels investigated. In view of the fact that numerous factors such as the intrinsic properties of each phase, their arrangement with respect to each other, the boundary effect etc., are involved, it appears difficult to evaluate at the present time the relative importance of each of these factors.

In any case, all the steels except the nickel-containing ones present some analogies. The coarsest structures, which are obtained in a well-defined range of cooling rates, often lead to brittleness related to the form, size and number of the austenitic-martensitic particles. A notable difference is observed between the impact strength of the bainitic structures and that of tempered martensite with the latter displaying a distinct superiority. In some cases, thermomechanical treatments lead to a finer or recovered structure and improve the impact strength of this bainite almost up to the level found in tempered martensites of similar strength.

ACKNOWLEDGMENTS

The authors wish to express their thanks to Mrs. D. Coutsouradis, V. Leroy, J. M. Drapier and Miss N. Lambert from the CNRM and the Metallurgical Department of the University for help in experimental work and useful discussions.

REFERENCES

1. E. S. Davenport and E. C. Bain, Trans. AIME *90*. 117 (1930)
2. ASTM Subcommittee XI of Committee E-4, "Electron Microstructure of Bainite in Steel," Second Progress Report, ASTM Proc. *52*. 543 (1952)
3. L. Habraken, Compt. Rend. de Recherches — IRSIA — Belgique, No. 19, (1957)
4. R. F. Hehemann and A. R. Troiano, Metal Progr. *70*. (2). 97 (1956)
5. *Physical Properties of Martensite and Bainite*, Special Report 93, The Iron and Steel Institute (London), 1965
6. F. Wever and A. Rose, *Atlas of the Heat Treatment of Steels*, Verlag Stahleisen, Düsseldorf, 1954-56-58.
7. *ASM Metals Handbook*, American Society for Metals, Metals Park, Ohio, 8th Edition, Vol. 1, 1961
8. J. W. Christian, *The Theory of Transformation in Metals and Alloys*, Pergamon, New York, 1965
9. P. Coheur and L. Habraken, Rev. Universelle Mines *7*. 107 (1951)
10. G. R. Speich, "Growth Kinetics of Bainite in a Three Per Cent Chromium Steel," *Decomposition of Austenite by Diffusional Processes*, edited by V. F. Zackay and H. I. Aaronson, Interscience, New York, 1962, 353
11. J. Pomey, Mem. Sci. Rev. Met. (Paris) *63*. (6). 509 (1966)
12. L. Habraken, "Some Special Aspects of the Bainitic Structure," Proc. 4th Conf. on Electron Microscopy, Berlin, Vol. 1, 1958, 621
13. O. Krisement and F. Wever, "Bainite Reaction in High-Carbon Steels," *Symposium on the Mechanism of Phase Transformations in Metals*, Inst. Metals (London), Monograph and Rept. Ser. No. 18, 1956, 253
14. L. Habraken, *Symposium on the Mechanism of Phase Transformations in Metals*, Inst. Metals (London), Monograph and Rept. Ser. No. 18, 1956, Discussion
15. R. I. Entin, "The Elementary Reactions in the Austenite → Pearlite and the Austenite → Bainite Transformations," *Decomposition of Austenite by Diffusional Processes*, edited by V. F. Zackay and H. I. Aaronson, Interscience, New York, 1962, 295
16. D. N. Shackleton and P. M. Kelly, "Morphology of Bainite," *Physical Properties of Martensite and Bainite*, Special Report 93, The Iron and Steel Institute (London), 1965, 126
17. L. Habraken, *Sur la Métallographie Electronique*, edited by V. Carmanne, Liège, 1953
18. M. Economopoulos and T. Greday, Met. Report — CNRM, No. 1, 1964, 45
19. M. Economopoulos, T. Greday and L. Habraken, Rev. Met. (Paris) *62*. 687 (1965)
20. M. Economopoulos, T. Greday and L. Habraken, Mem. Sci. Rev. Met. (Paris) *60*. (1). 11 (1963)
21. L. Habraken and M. Economopoulos, Struktura a Wasnosci Mechaniczne Metali, Tom. 1, Polska Akad. Nauk. Gliwice, 1965
22. M. Economopoulos and J. Delatte, Acta Tech. Belg. Met. *3*. (2). 27 (1962) N. Lambert and M. Economopoulos, Met. Rep. — CNRM, No. 5, 65 (1965)
23. M. Economopoulos, Metaux (Corrosion-Ind.) *39*. (461). 1 (1964)
24. F. Galere and M. Economopoulos, Met. Report — CNRM, No. 4, 41 (1965)
25. N. Lambert and M. Economopoulos, Mem. Sci. Rev. Met. (Paris) *64*. (1). 1 (1967)
26. A. Hultgren, Trans. ASM *39*. 915 (1947)
27. C. S. Smith, Trans. ASM *45*. 533 (1953)
28. H. I. Aaronson, "The Proeutectoid Ferrite and the Proeutectoid Cementite Reactions," *Decomposition of Austenite by Diffusional Processes*, edited by V. F. Zackay and H. I. Aaronson, Interscience, New York, 1962, 387
29. H. Brooks, "Theory of Internal Boundaries," *Metal Interfaces*, American Society for Metals, Cleveland, Ohio, 1952, 20
30. G. R. Purdy and J. S. Kirkaldy, Trans. AIME *227*. 1255 (1963)
31. S. Rouze and W. L. Grube, quoted by H. I. Aaronson, "The Proeutectoid Ferrite and the Proeutectoid Cementite Reactions," *Decomposition of Austenite by Diffusional Processes*, edited by V. F. Zackay and H. I. Aaronson, Interscience, New York, 1962, 510
32. H. I. Aaronson, Trans. AIME *224*. 870 (1962)
33. F. E. Bowman, Trans. ASM *36*. 61 (1946)
34. M. L. Picklesimer, D. L. McElroy, T. M. Kegley, Jr., E. E. Stansbury and J. H. Frye, Jr., Trans. AIME *218*. 473 (1960)
35. G. R. Purdy, D. H. Weichert and J. S. Kirkaldy, Trans. AIME *230*. 1025 (1964)
36. T. Ko and S. A. Cottrell, J. Iron and Steel Inst. (London) *172*. 307 (1952)
37. J. S. Bowles and C. S. Barrett, "Crystallography of Transformations," *Progress in Metal Physics*, edited by B. Chalmers, Interscience, New York, 1952, Vol. 3, 1
38. T. B. Massalski, Acta Met. *6*. 243 (1958)
39. W. S. Owen, E. A. Wilson and T. Bell, "The Struc-

ture and Properties of Quenched Iron Alloys," *Proc. Berkeley Intern. Mater. Conf.*, 2nd, Berkeley, Calif., 1964, 167

40. A. B. Greninger, Trans. AIME 133. 204 (1942); Trans. ASM *30*. 1 (1942)
41. G. V. Kurdyumov, Probe, met. fiz. met. (1952)
42. G. V. Kurdyumov, *International Conference on the Peaceful Uses of Atomic Energy*, Vol. 15, 1955, p. 81
43. G. Krauss, Jr., Acta Met. *11*. 499 (1963)
44. R. Phillips and W. E. Duckworth, "The Effect of Alloying Additions on the Ausforming Response of Steels," BISRA Rep. MG/A/108/64, 1964, Aug./Sept.
45. J. Philibert and C. Crussard, J. Iron and Steel Inst. (London) *180*. 39 (1955)
46. S. G. Glover, J. Iron and Steel Inst. (London) *200*. 102 (1962)
47. E. P. Abrahamson, II and M. W. Dumais, Trans. AIME *236*. 1743 (1966)
48. I. A. Oding and M. G. Lozinsky, Izv. Akad. Nauk SSSR, Otd. Tekhn. Nauk *1953*. (7). 1035
49. B. Edmondson, Acta Met. *5*. 208 (1957)
50. G. Delbart and R. Potaszkin, J. Iron and Steel Inst. (London) *157*. 527 (1947)
51. R. Potaszkin and K. Bar-Avi, Mem. Sci. Rev. Met. (Paris) *55*. 346 (1958)
52. R. Potaszkin and K. Bar-Avi, Mem. Sci. Rev. Met. (Paris) *60*. 335 (1963)
53. M. Gensamer, E. B. Pearsall and G. V. Smith, Trans. ASM *28*. 380 (1940)
54. G. E. Pellissier, M. F. Hawkes, W. A. Johnson and R. F. Mehl, Trans. ASM *30*. 1049 (1942)
55. M. Gensamer, E. B. Pearsall, W. S. Pellini and J. R. Low, Jr., Trans. ASM *30*. 983 (1942)
56. K. J. Irvine, F. B. Pickering, W. C. Heselwood and M. Atkins, J. Iron and Steel Inst. (London) *186*. 54 (1957)
57. K. J. Irvine and F. B. Pickering, J. Iron and Steel Inst. (London) *187*. 292 (1957)
58. K. J. Irvine and F. B. Pickering, J. Iron and Steel Inst. (London) *188*. 101 (1958)
59. K. J. Irvine and F. B. Pickering, J. Iron and Steel Inst. (London) *201*. 518 (1963)
60. K. J. Irvine, Metallurgia *58*. 13 (1958)
61. V. Zoidzee, M. Economopoulos and L. Habraken, to be published
62. M. Krön, A. Constant, A. Clerc, J. Plateau, G. Henry, M. Robert and C. Crussard, Mem. Sci. Rev. Met. (Paris) *58*. 901 (1961)
63. G. S. Ansell, "Theory of Strengthening Due to Precipitate Phases," *Precipitation from Iron-Base Alloys*, edited by G. R. Speich and J. B. Clark, Gordon and Breach, New York, 1965, 231
64. E. D. Hyam and J. Nutting, J. Iron and Steel Inst. (London) *184*. 148 (1956)

ORAL DISCUSSION OF

Bainitic Microstructures in Low-Carbon Alloy Steels and Their Mechanical Properties

Presented by L. HABRAKEN

B. R. BANERJEE (Crucible Steel Company). I believe you had a transmission micrograph showing equiaxed retained austenite grain structure, where certain portions of the austenite exhibited darker contrast than the rest of the retained austenite. If I understood you correctly, you suggested that the dark contrast was due to variation in carbon content, which in effect, created regions of different thickness, during specimen thinning. Is this correct?

AUTHOR'S REPLY. This is correct.

B. R. BANERJEE. This bothers me because of several reasons: (1) In a crystalline specimen of this thickness, I would not expect such a pronounced absorption contrast effect; I suspect this would not be expected from theoretical principles. (2) On the other hand, if you did indeed have varying thicknesses within these regions, then you should expect to see thickness fringes. Because of varying carbon content, you'd have a wedge, and this would give rise to thickness fringes, which of course, you can measure. Alternately, if the contrast is due to orientation, then, by tilting and dark-field experiments you could sort it out. Perhaps you have done these experiments and can explain this behavior.

AUTHOR'S REPLY. In fact, the unusual contrast effect which is observed is similar to that observed some years ago by Phillips.* As in Phillips' work on ferrite, the dark contrast has been found to be relatively insensitive to tilting and we think that it is a mass thickness rather than a diffraction contrast effect. We suggest that this effect could be attributed to a segregation of impurities, especially carbon.

E. NACHTMAN (LaSalle Steel Company). It might be interesting to comment that this same effect on lowering the transition temperature of bainite by using a thermomechanical working technique has also been seen after thermomechanically deforming the martensite; you can lower the transition temperature there as well. Maybe you can see some relationship between these effects.

*V. A. Phillips, Acta Met. *11*. 1139 (1963)

AUTHOR'S REPLY. I thank Mr. Nachtman for his comment. We have not worked in the field of deformed martensite. What appears in our tests and could explain the valuable impact resistance is that imperfections in bainitic ferrite are grouped more as in a polygonized structure than in a "worked structure."

F. B. PICKERING (United Steel Companies, Ltd.). Dr. Habraken has shown some extremely interesting and important effects in his paper, particularly in showing that carbon and alloy element enrichment in the remaining austenite, when bainitic ferrite is formed, can lead to the presence of large quantities of martensite of varying carbon content, and even retained austenite, in continuously cooled specimens. Of particular importance is the evidence that, once transformation to bainitic ferrite has commenced, partitioning effects to the untransformed austenite so alter the transformation characteristics of that austenite that it can behave entirely differently from the original austenite. This being the case, one has to be very careful about the interpretation of the transformed structures, and this is particularly important when one is dealing with the kinetics of the transformation, because the kinetics may be continually altering as the analysis of the untransformed austenite alters during the progress of transformation.

I was particularly interested in the internal friction work in which a Köster peak had been observed in specimens which I believe showed poor impact properties. I think it was suggested that such an internal friction effect, which is often interpreted as being due to interstitial-dislocation interaction, could be evidence that the poor impact properties are the result of interstitial-dislocation locking. Whilst I would agree that Köster peaks can be obtained in bainitic ferrite in low carbon steel, they are usually quite small in magnitude. In martensite, however, such Köster peaks can be very pronounced, and their magnitude increases with increasing carbon content of the martensite. In the specimens which showed poor impact properties, I believe that you had appreciable quantities of martensite, together with bainitic ferrite in the granular bainitic structure. Do you think that the Köster peak was largely due to the martensite present, rather than to the bainitic ferrite, particularly as the martensite would be high carbon martensite? In fact, does the intensity of the internal friction peak correlate with the presence of martensite in the structure? It is possible that the Köster peak height may not increase as the amount of martensite in the structure increases, due to the variation in the carbon content of the martensite itself. A further question which I would like to ask is what effect you think the martensite in the granular bainite has upon the impact properties.

AUTHOR'S REPLY. We agree with the remarks of Dr. Pickering, but as isothermal and continuous cooling transformations do not give the same structure in the intermediate range, it seems useful to study the properties of structure appearing in the whole range of transformation, even if a part of the final structure is proeutectoid ferrite.

Concerning the internal friction peak, we have reviewed all the results we have obtained and we have completed the test in the martensitic region. We agree with the idea that this peak could be mainly related to the martensite in the austenite–martensite regions. We have now* found similar peaks in other steels examined after the conference. It is not excluded that the peak is also partly connected with some effect of residual interstitials in the bainitic ferrite.

F. B. PICKERING. We have observed this sort of thing in retained austenite–martensite structures, and we do find that it is possible to correlate the peak with the percentage of martensite in the structures.

AUTHOR'S REPLY. At this moment, we have not found a direct correlation with the percentage of martensite in the structure.

*April 1967, after reviewing the text of the discussions

The Structure and Properties of Bainite in Steels

F. B. PICKERING
The United Steel Companies Ltd.
Moorgate, Rotherham, Great Britain

INTRODUCTION

Ever since the initial work of Davenport and Bain,[1]* the bainitic microstructure has excited a continuing interest in metallurgical research over more than 30 years. Gradually, more and more information has been accumulated on bainitic structures, but this has only served to reveal their complex nature, and this can be shown by the fact that there are at least two[2,3] and possibly three[4,5] forms of bainite in many steels. These can vary quite appreciably in morphology with increasing carbon content. The effect of alloy content may further complicate the situation, but systematic data on the effect of alloy content on the morphology, crystallography and kinetics of the bainite structure and reaction have not yet been determined.

The properties of bainitic structures have also excited considerable interest. In some cases, very clear advantages have been claimed for a bainitic structure,[6] but often the strict basis for a comparison between bainite and for example martensite or tempered martensite, has not been established.[7] Also, quite contradictory opinions are frequently held regarding the low carbon bainites, which in some forms can have very inferior ductility and toughness compared with other ferrous microstructures of similar strength.[8,9] Some attempts have however been made to discover the basis of the strength of bainite,[10] and to begin to put such a basis in quantitative terms. Such work however is not yet very highly developed.

Despite the lack of a fundamental understanding of many features of the bainitic structures and the bainitic reaction itself, low carbon steels containing bainitic structures have been successfully developed,[8,11-15] and some higher carbon bainitic steels have also found a commercial application.[16] While the development of these commercial bainitic steels has been in progress, work has also been carried out on the morphology and crystallography of certain features of the bainite reaction, and on the relationships between the microstructure of bainite and its mechanical properties. It is not the intention in this paper to try to review the general literature of the bainite reaction, but rather to present the results of some of the studies which have been initiated during the development of commercially acceptable bainitic steels.

*See references.

THE MICROSTRUCTURE OF BAINITIC STEELS

It has long been known that there are two major forms of bainite, namely upper and lower bainite.[2,17] In many steels there has been shown to be a distinct microstructural difference between these two forms. In upper bainite the carbides frequently form elongated particles between the bainitic ferrite grains, while in lower bainite, the carbides tend to precipitate at an inclined angle to the major growth direction, or longitudinal axis, of the bainitic ferrite grain. There is also evidence of a difference in the reaction kinetics of the upper and lower bainite transformations,[18-22] particularly in high carbon steels, and attempts have been made to reconcile these differences with the morphology of the microstructures and the mechanisms of their formation. The formation of bainite, both in the case of upper and lower bainite, has been shown to occur by a shear mechanism,[22-25] and from this it would be anticipated that there is an orientation relationship between the bainitic ferrite and the austenite from which it forms. Such orientation relationships have been described,[26] but much more work is required to confirm them.

Morphology of Bainitic Structures

A systematic investigation has been made of the morphology of both upper and lower bainite in steels of varying carbon content. The structure of both continuously cooled and isothermally transformed

TABLE I Analyses of Steels*

Steel No.	% C	% Mn	% Si	% Cr	% Mo	% Soluble B	Series
1	0.10	0.52	0.11	—	0.54	0.0033	
2	0.20	0.59	0.22	—	0.52	0.0033	
3	0.32	0.46	0.22	—	0.53	0.0034	
4	0.41	0.62	0.23	—	0.54	0.0034	0.5% Mo-B
5	0.61	0.53	0.36	—	0.53	0.0023	
6	0.83	0.50	0.35	—	0.53	0.0014	
7	0.93	0.63	0.29	—	0.49	0.0042	
8	1.06	0.48	0.34	—	0.54	0.0017	
9	0.12	0.52	0.27	1.08	0.54	0.0038	
10	0.22	0.57	0.21	1.05	0.51	0.0038	
11	0.32	0.63	0.29	1.03	0.49	0.0040	
12	0.42	0.59	0.28	0.99	0.52	0.0024	1% Cr-
13	0.53	0.50	0.15	1.30	0.55	0.0012	0.5% Mo-B
14	0.65	0.50	0.46	1.01	0.52	0.0032	
15	0.82	0.51	0.41	1.18	0.52	0.0034	
16	0.96	0.66	0.37	1.00	0.53	0.0040	
17	1.04	0.65	0.57	1.08	0.50	0.0030	

*Weight percent.

specimens was examined in order to try to establish the sequence of structural changes during transformation, which eventually led to the fully transformed structure. Both optical and electron microscopical techniques were used, and the electron microscopical examinations employed both replicas and thin foils. The steels used were 0.5% Mo-B or 1% Cr-0.5% Mo-B alloys containing carbon contents up to 1%. These were selected as being typical of a wide range of bainitic alloy steels. The combinations of carbon and alloy content enabled the transformations to be studied over a wide range of temperature, while the boron present not only facilitated the experiments by retarding the transformation in the lower carbon steels, but also enabled bainite to be formed during continuous cooling, where this was deemed necessary. The analyses of the steels used are shown in Table I.

Upper Bainite

The first stages of transformation to upper bainite in the low carbon steels consisted of the formation

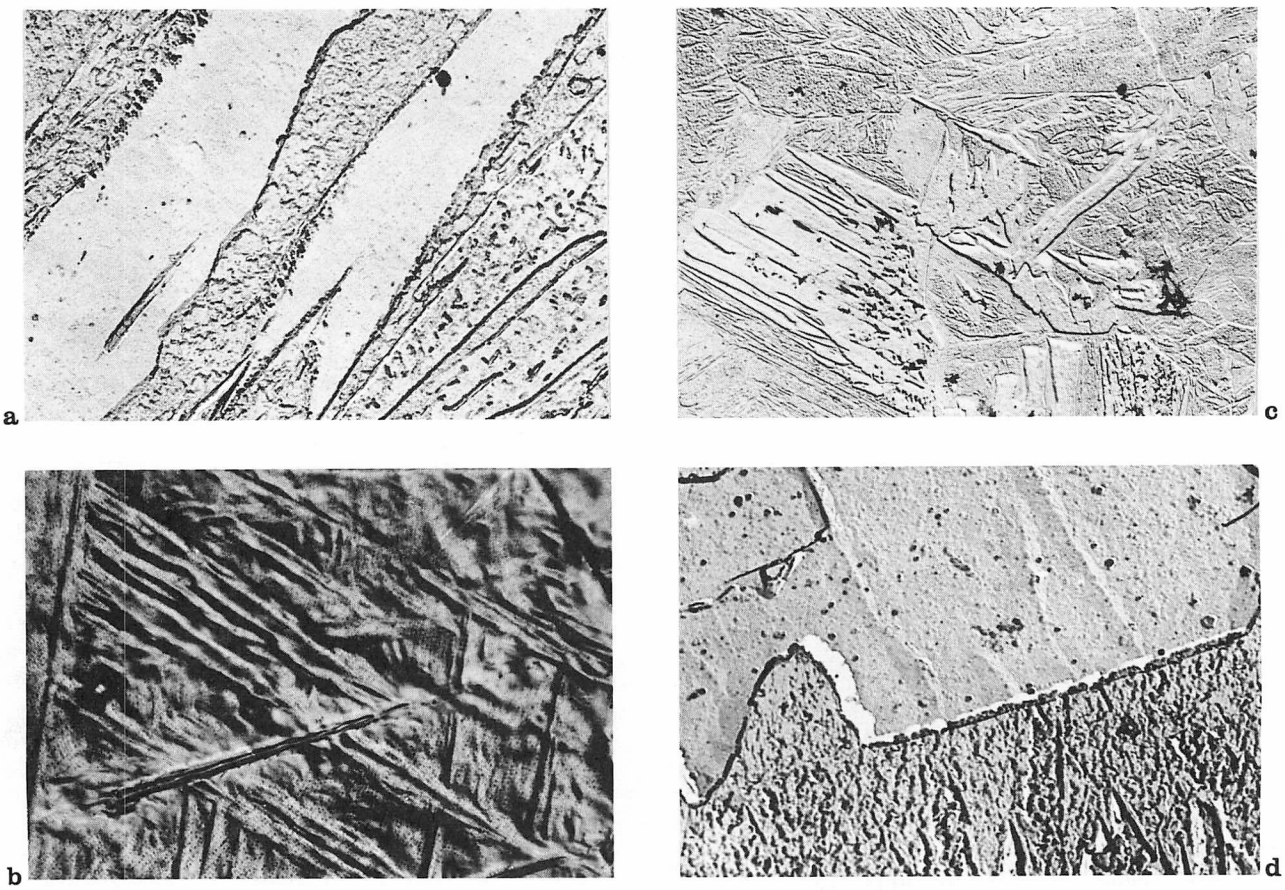

FIGURE 1. Upper bainitic structures

a. upper bainitic ferrite laths in 0.1% C steel; electron micrograph, replica, 15,000 X

b. surface shear due to upper bainite formation in 0.1% steel; optical micrograph, 750 X

c. side-by-side nucleation of upper bainitic ferrite in 0.2% C steel; electron micrograph, replica, 3000 X

d. carbon enrichment at ferrite–austenite interface in 0.1% C steel; electron micrograph, replica, 15,000 X

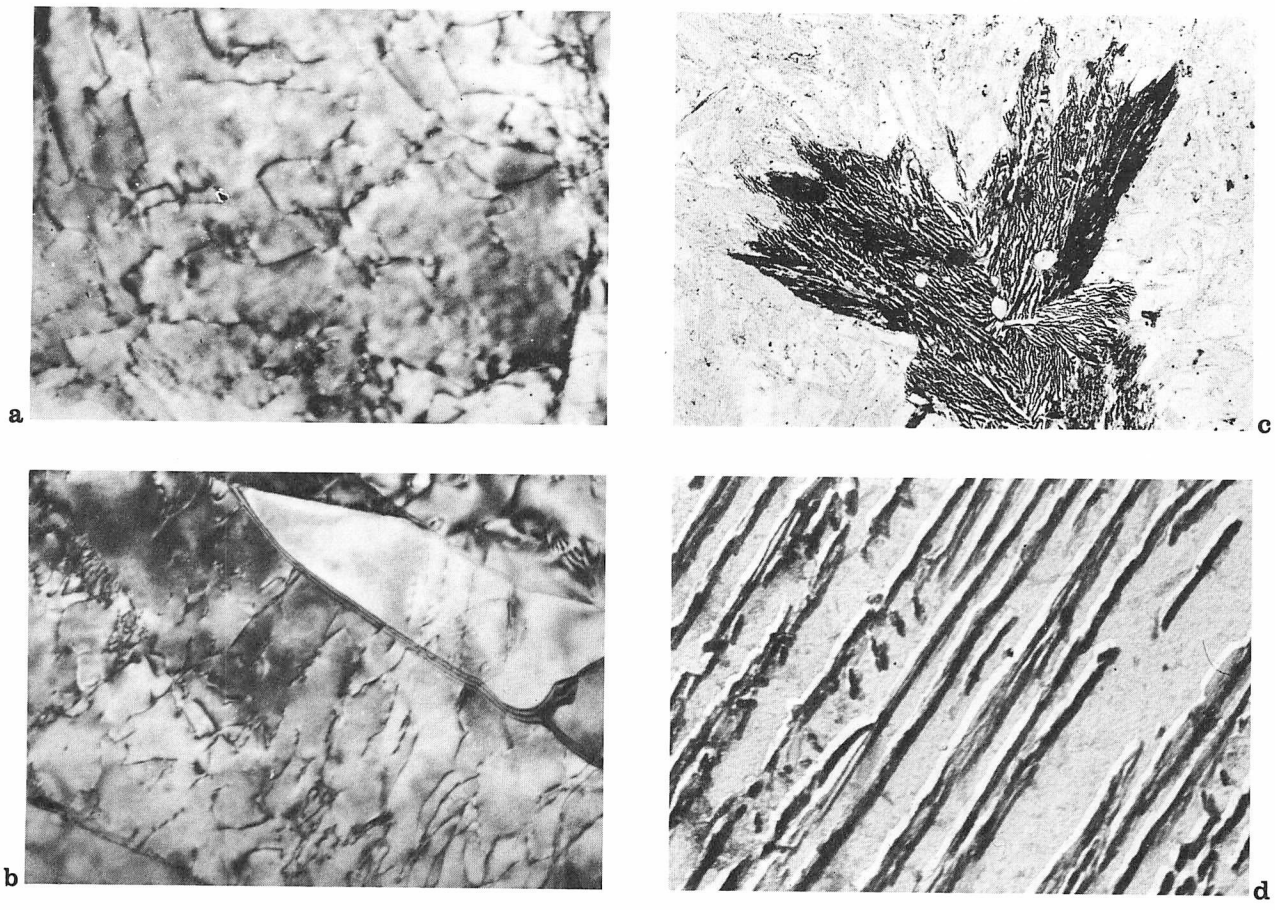

FIGURE 2. Upper bainitic structures

a. 0.1% C steel transformed at 600 C (1110 F) showing dislocations in ferrite; thin foil electron micrograph, 75,000 X

b. 0.1% C steel transformed at 500 C (930 F) showing higher dislocation density; thin foil electron micrograph, 75,000 X

c. 1.0% C steel transformed at 450 C (840 F) with spear-like upper bainite morphology; electron micrograph, replica, 3000 X

d. lamellar upper bainite structure in 0.6% C steel transformed at 500 C (930 F); electron micrograph, replica, 15,000 X

of a lath of ferrite from the austenite, Figure 1(a). This was a shear transformation product, as shown by the surface relief produced on a polished surface, Figure 1(b). Frequently a cooperative transformation phenomenon was observed in which fairly rapid side-by-side nucleation of the ferrite laths occurred, to form a sheaf of parallel laths by a sympathetic nucleation effect. This feature became more frequent with increasing carbon content, Figure 1(c). As the ferrite laths grew, the carbon diffused away in front of the ferrite-austenite interface, and so enriched the surrounding austenite in carbon. This effect is shown in Figure 1(d), in which the carbon content of the surrounding austenite has been so enriched that the local M_s temperature has been lowered. This has occurred to such an extent that the martensite formation on quenching from the transformation temperature has stopped short of the bainitic ferrite–austenite interface.

In some cases, this carbon enrichment can cause the retention of untransformed austenite, particularly when the austenite occurs between two ferrite laths which are growing together. Many workers have established the presence of such retained austenite in apparently fully transformed upper bainitic structures.[27]

With decreasing transformation temperature in the upper bainite range, the laths of ferrite became more narrow, probably because the sideways growth of the laths was restricted by diffusion of carbon. The axial length of the laths did not seem to be affected so much, and in many cases appeared to be controlled by the dimensions of the austenite grain size, or by the space between already formed bainite volumes in which the new bainitic ferrite laths were nucleating and growing. The side-by-side sympathetic nucleation effect also became more apparent, and with decreasing transformation temperature the

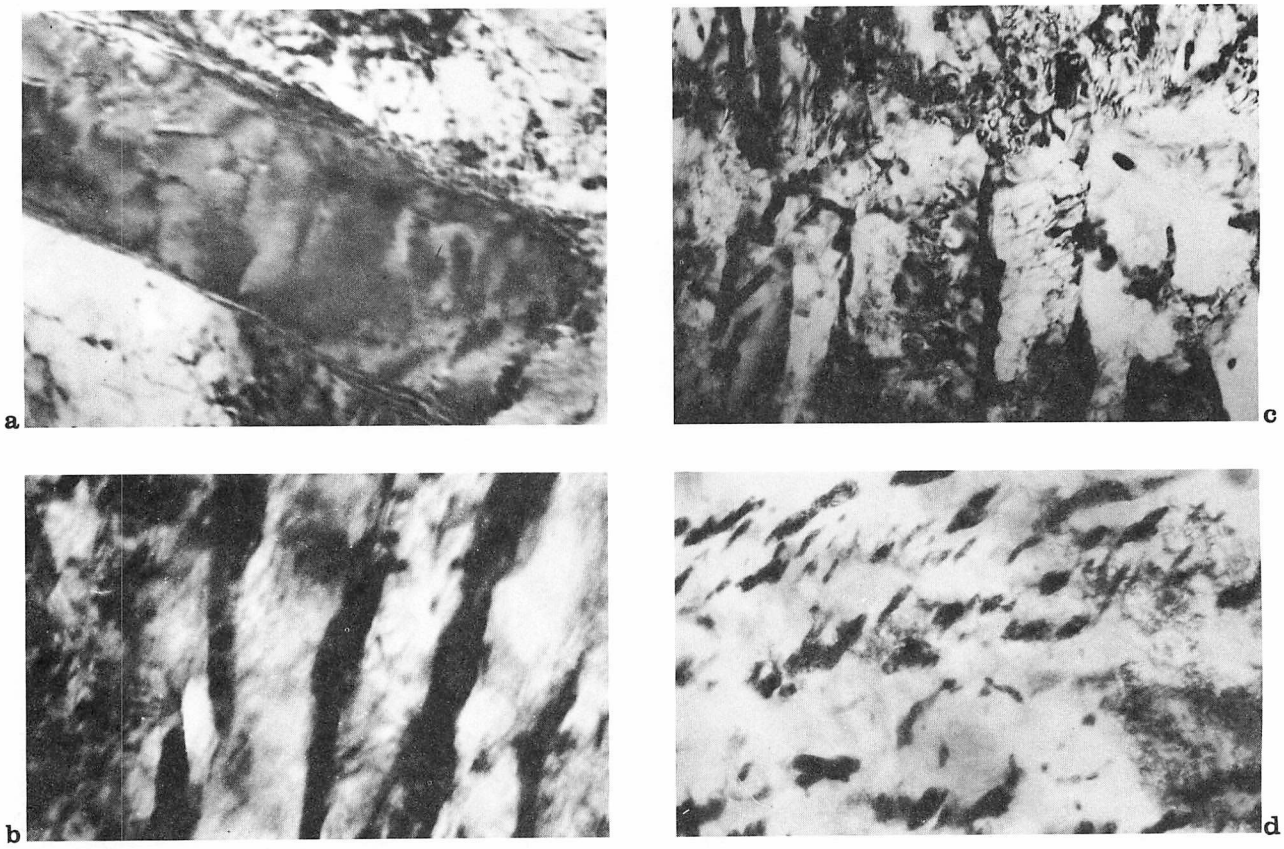

FIGURE 3. Upper bainitic structures

a. carbides between bainitic ferrite laths in 0.2% C steel; thin foil electron micrograph, 75,000 X

b. more extensive carbides between bainitic ferrite in 0.4% C steel; thin foil electron micrograph, 60,000 X

c. finer structure of carbides between bainitic ferrite in 0.6% C steel; thin foil electron micrograph, 60,000 X

d. unusual morphology caused by sectioning in 0.6% C steel; thin foil electron micrograph, 75,000 X

dislocation density in the bainitic ferrite increased, Figures 2(a) and (b). As the transformation temperature was lowered still further, lower bainite began to be formed, and this will be described later.

With increasing carbon content, the upper bainitic ferrite laths also became thinner as the diffusion gradient down which the carbon in the austenite must diffuse, became less steep. As was the case for lowering the transformation temperature, so increasing the carbon content tended to cause more extensive sympathetic nucleation of the bainitic ferrite laths, in a side-by-side manner. As the carbon content of the steel increased, so the formation of carbide during the upper bainite reaction was accelerated, and in steels near to the eutectoid carbon content it was not possible to establish whether ferrite or carbide was the first nucleated phase in the transformation sequence. As will be discussed later, it is suggested that when the steel contains more than about 0.5% C, cementite (Fe_3C) may well be the primarily nucleated phase. In fact the rapid side-by-side nucleation caused a spear-like growth of alternate ferrite laths and cementite, Figure 2(c), and the fully transformed structure may well have a lamellar appearance in certain orientations, Figure 2(d).

Due to the carbon enrichment between the side-by-side nucleated ferrite laths, regions of high carbon austenite were entrapped by the bainitic ferrite, and transformed eventually to carbides, which occurred generally along the boundaries between adjoining ferrite grains, Figure 3(a). With either increasing carbon content or decreasing transformation temperature the width of the bainitic ferrite laths decreased and consequently the carbides lying between them were closer together, i.e., the structure became much finer, Figures 3(b) and (c). Also, particularly with increasing carbon content, the amount of carbide increased and the cementite films between the ferrite laths became more continuous, forming long films at the bainitic ferrite boundaries. In some orientations, such structures have almost a pearlitic

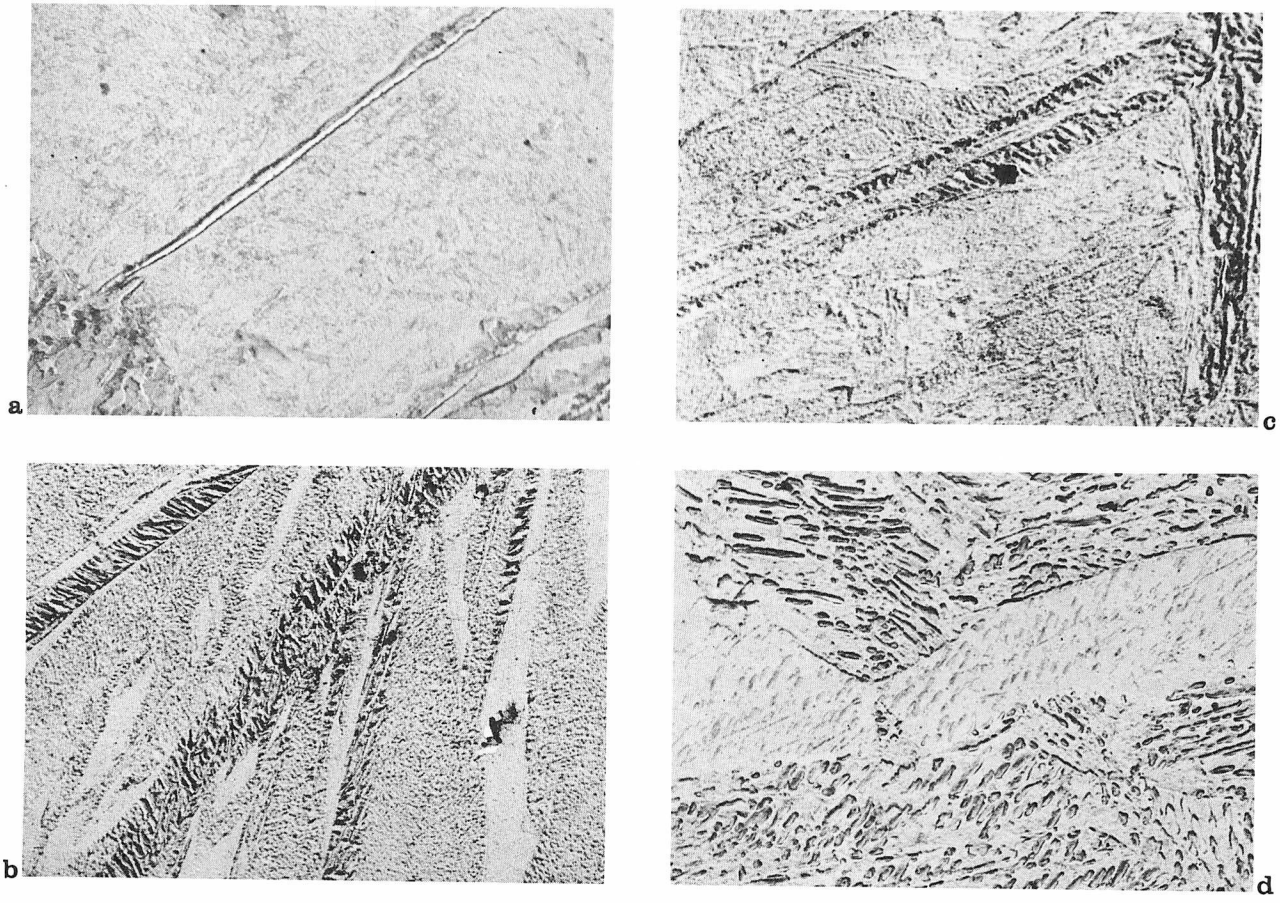

FIGURE 4. Lower bainitic structures

a. first formed bainitic ferrite lath in 0.6% C steel; electron micrograph, replica, 15,000 X

b. several lower bainite laths with carbides in 1.0% C steel; electron micrograph, replica, 15,000 X

c. side-by-side nucleation of lower bainite in 0.6% C steel; electron micrograph, replica, 15,000 X

d. 0.6% C steel fully transformed to lower bainite at 300 C (570 F); electron micrograph, replica, 15,000 X

appearance, as noted by Shackleton and Kelly,[3] while sectioning effects can produce a wide range of apparent morphologies as shown by Figure 3(d). In many cases when more or less continuous films of cementite were formed at the bainitic ferrite boundaries, the boundaries themselves were no longer visible. Sometimes there may be in effect no boundary if the side-by-side nucleated ferrite laths have identical orientations, but usually a slight misorientation can be established by electron diffraction from the ferrite on either side of such a cementite film. The significance of this observation will be discussed later.

The way in which the carbon enriched austenite entrapped between growing bainitic ferrite plates transformed to cementite in the lower carbon steels suggests that the cementite precipitated directly from the austenite. An orientation relationship might therefore be expected between the austenite and the cementite, which would be identical with that produced if, as is suggested for the steels containing more than 0.5% C, the cementite is the primarily nucleated phase. Evidence for this will be presented later.

Lower Bainite

The sequence of events during the transformation to lower bainite was observed to be the same at all carbon contents. Initially a bainitic ferrite plate or lath was formed, which because of the relatively slow rate of diffusion of carbon at the temperatures at which lower bainite forms, was very thin. There is evidence in the literature[18] which indicates that such an initial bainitic ferrite lath is supersaturated in carbon. The growth of such a supersaturated ferrite region can only proceed if the supersaturation is decreased by carbide precipitation, and it was observed that cementite rapidly precipitated within the bainitic ferrite lath, Figure 4(a) which could then grow laterally. This was accompanied by further cementite precipitation. Many such bainite

laths were nucleated within an austenite grain, Figure 4(b), but the side-by-side nucleation of this bainitic ferrite was by no means so apparent, although a few such sympathetically nucleated laths were sometimes seen, Figure 4(c). The growth of the individual lower bainite laths, with their internal carbide precipitation, seemed to be relatively slow or restricted, and generally more such nuclei were formed within the remnant untransformed matrix until the fully transformed structure was developed, Figure 4(d).

There did not seem to be a very great effect of carbon content on the lower bainitic structure, except to increase the amount of carbides which were precipitated, as indicated in Figures 5(a) and (b). Decreasing the transformation temperature however, appeared to cause the bainite laths to become thinner, but as in the case of increasing carbon content also, the precipitation of carbide became so rapid that it was virtually impossible to observe a bainitic ferrite lath which did not contain internally precipitated carbides. As shown in Figure 4, the cementite tended to precipitate across the bainitic ferrite at a relatively constant angle to the longitudinal or axial direction of the lath. This is further shown by a series of thin foil electron micrographs in Figure 5, in which the effect of increasing the carbon content on the number of the carbide precipitates is clearly shown, together with apparent structural variations brought about by sectioning effects. The cementite precipitates themselves seemed to be in the form of rods or small plates, and the mode of precipitation indicated an orientation relationship between the cementite and the bainitic ferrite. In fact it has been suggested[3] that the cementite precipitates on twins in the bainitic ferrite, but no observations of such twins have been made. Shackleton[3] suggests that the precipitation of carbides on the twins would remove the twins.

Temperature of the Change from Upper to Lower Bainite

In high carbon steels, there is much published information to show that at transformation temperatures above 350 C (660 F) upper bainite is formed,

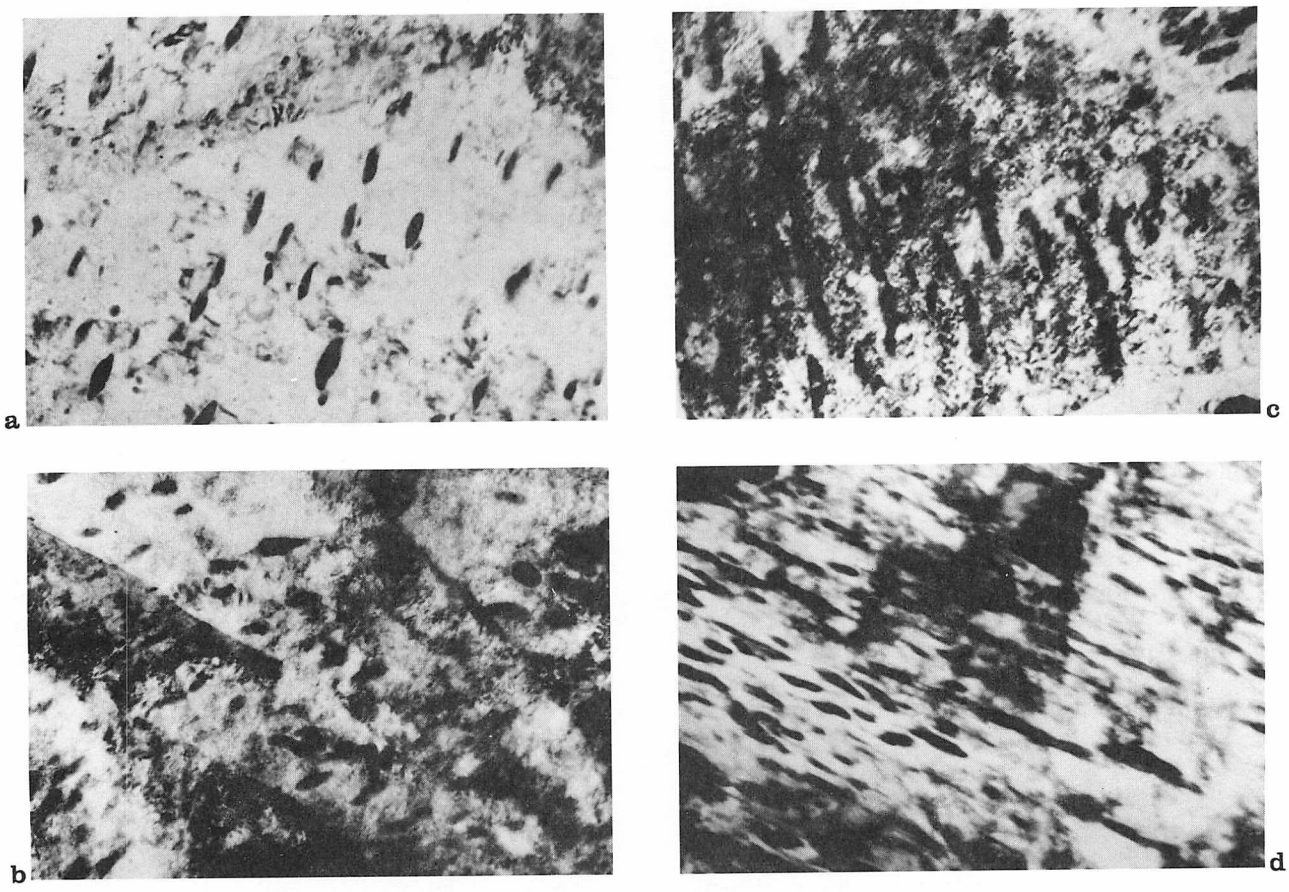

FIGURE 5. Effect of carbon content on lower bainite

a. 0.1% C steel transformed at 450 C (840 F); thin foil electron micrograph, 75,000 X

b. 0.4% C steel transformed at 350 C (660 F); thin foil electron micrograph, 45,000 X

c. 0.6% C steel transformed at 300 C (570 F); thin foil electron micrograph, 75,000 X

d. 1.0% C steel transformed at 250 C (480 F); thin foil electron micrograph, 75,000 X

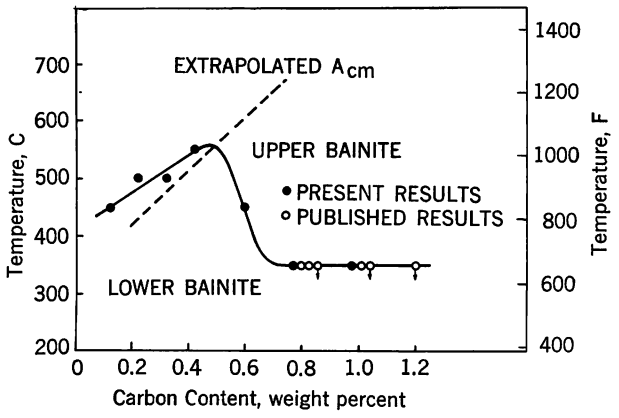

FIGURE 6. Effect of carbon on the temperature of change from upper to lower bainite

but at temperatures below 350 C (660 F), lower bainite is formed. The results of the present investigation are in agreement with this. In the lower carbon steels however, the change from upper to lower bainite occurred at rather higher temperatures than 350 C (660 F). It should be pointed out however that this change from upper to lower bainite occurred over a range of temperatures, and at some temperatures a mixture of both upper and lower bainite can occur. A similar effect was observed by Shackleton.[3] The maximum temperature for this change, above which lower bainite was never observed, is shown as a function of carbon content in Figure 6. It can be seen that the maximum temperature above which lower bainite was never observed, increased with increasing carbon content up to about 0.5% and then rapidly decreased to 350 C (660 F), at which temperature it remained constant with a further increase in carbon content. The data for the high carbon steels is in excellent agreement with the previously published data. The extrapolation of the A_{cm} line is also shown in Figure 6. It is significant that when the steel became supersaturated with respect to cementite, the temperature of the change from upper to lower bainite abruptly decreased and then remained constant for all higher carbon compositions. This observation has a marked bearing on the mechanism of the bainite reaction, which will be postulated later in the paper.

THE CRYSTALLOGRAPHY OF BAINITES

The morphology of lower bainite indicated that the cementite precipitates were related crystallographically to the bainitic ferrite in which they precipitated. Similarly if the cementite in upper bainite formed from the carbon enriched austenite between the bainitic ferrite laths, or precipitated directly from the austenite, it might be expected that the cementite would then exhibit an orientation relationship with the original austenite in which it precipitated. Shackleton and Kelly[3] have shown that these orientation relationships can be observed, and moreover have suggested that the orientation relationship which thus exists between the cementite and ferrite in bainite is as distinctive of the upper and lower bainite structures as are their respective morphologies. Some crystallographic analyses were therefore made of the electron diffraction patterns from cementite and ferrite in both upper and lower bainite in steels of different carbon contents. It should be emphasized that, while the steels used for this work were low alloy steels, the carbide observed in the bainitic structures was always cementite (Fe_3C) and at no time was an alloy carbide observed in the structures produced by transforming even at high temperatures in the bainite range. This was probably because the isothermal transformation times were relatively short. Also, even at the lowest temperatures investigated in the bainite range, namely 250 C (480 F), epsilon carbide was not observed.

Orientation Relationship between Bainitic Ferrite and Cementite in Upper Bainite

No clearly defined orientation relationship was observed between the cementite and bainitic ferrite. However, as observed by Shackleton and Kelly,[3] if the ferrite and cementite were both assumed to precipitate directly from the parent austenite with their respective orientation relationships, then the observed orientation relationships between the cementite and the bainitic ferrite could be rationalized.

In the present work, the Nishiyama-Wassermann[28, 29] orientation relationship between austenite and ferrite was used:

$$(0\bar{1}1)_\gamma \;//\; (001)_\alpha$$
$$[\bar{1}11]_\gamma \;//\; [\bar{1}10]_\alpha$$
$$[211]_\gamma \;//\; [110]_\alpha$$

It should be stated however that within the accuracy of the electron diffraction patterns, the Kurdyumov-Sachs orientation relationship[30] would be equally valid.

The orientation relationship between the cementite and the austenite which was used was that determined by Pitsch[31]:—

$$(010)_z \;//\; (110)_\gamma$$
$$[001]_z \;//\; [\bar{2}25]_\gamma$$
$$(100)_z \;//\; (5\bar{5}4)_\gamma$$

This is very close to the general relationship:—

$$(010)_z \;//\; (110)_\gamma$$
$$[001]_z \;//\; [\bar{1}12]_\gamma$$
$$[100]_z \;//\; [1\bar{1}1]_\gamma$$

which more readily facilitates the analysis.

Using the observed orientations of the cementite and the bainitic ferrite in the electron diffraction pattern, and the appropriate variant of their respec-

tive orientation relationships with austenite, it was possible to show that both phases could be generated from a common orientation of the austenite from which they formed. All the examples of upper bainite which were investigated conformed to this analysis. This very clearly indicated that the assumption made, namely that in upper bainite both the cementite and bainitic ferrite precipitated directly from the austenite, was valid. In no case was an orientation relationship observed between cementite and upper bainitic ferrite which was typical of that of cementite precipitated directly from the ferrite.

Orientation Relationship between Bainitic Ferrite and Cementite in Lower Bainite

With decreasing transformation temperature, the lower bainitic morphology became more predominant, and in these structures the orientation relationship between the cementite and the lower bainitic ferrite was always:

$$\begin{array}{lll} (001)_Z & // & (11\bar{2})_\alpha \\ [100]_Z & // & [1\bar{1}0]_\alpha \\ [010]_Z & // & [111]_\alpha \end{array}$$

This relationship[32] is that obeyed by the precipitation of cementite from martensite during tempering, and also for cementite in quench aged ferrite. None of the varied orientation relationships described for upper bainite were observed, and the evidence strongly indicates that in lower bainite the cementite precipitated directly from the bainitic ferrite. This is to be expected from the increased supersaturation of carbon reported in lower bainitic ferrite,[18] and the general morphological aspects of lower bainite confirm this.

Of particular interest in view of the dependence of the temperature of the change from upper to lower bainite on the carbon content, was the fact that in 0.1% C and and 0.2% C steels transformed at 450 C (840 F) the morphology and orientation relationship typical of lower bainite were observed.

It should be pointed out however that this orientation relationship, as shown by Shackleton and Kelly,[3] can also be one of the variants derived from the mutual orientation relationships between ferrite and austenite and cementite and austenite. This means that it can be obtained from either upper or lower bainite, but mainly from the latter. However, all other orientations which are mutually related through a common austenite orientation, are indicative of upper bainite. The orientation relationship between cementite and lower bainitic ferrite is that observed when cementite precipitates on twins in the higher carbon martensites; the morphology also suggests precipitation on twins. However, as stated previously, there is no positive evidence for twins in lower bainite. It might be possible to produce further evidence for the presence of twins in lower bainite by establishing the habit plane of the precipitating cementite, because Tekin and Kelly[35] have shown that the habit plane of cementite precipitated on twins in martensite is $\{112\}_\alpha$.

Orientation Relationship between Bainitic Ferrite and Austenite

Very little work has been reported on the orientation relationship between the bainitic ferrite and the austenite from which it forms. The fact that it occurs by a shear transformation[22-25] suggests that some clearly defined orientation relationship does exist, and Smith and Mehl,[26] using X-ray pole figure techniques, showed that the orientation relationship was the Nishiyama relationship[28] in upper bainite, but the Kurdyumov-Sachs relationship[30] in lower bainite. Also, the habit plane of the bainitic ferrite changed progressively from $\{111\}\gamma$ in upper bainite, through $\{225\}\gamma$ towards $\{259\}\gamma$ in lower bainite, in a eutectoid steel. More work is required to confirm these trends, and electron diffraction of the bainitic ferrite and martensite in partially transformed structures would probably be useful, relating the austenite orientation to that of the martensite by means of one of the well known orientation relationships.

The inferences from the work of Smith and Mehl are that bainitic ferrite formation is similar in its crystallographic features to that of martensite, and the lower bainites in eutectoid steels have habit planes similar to those of the higher carbon martensites, which are known to be extensively twinned.[34] This tends to suggest that high carbon lower bainitic ferrite may well be twinned prior to the cementite precipitation. A further difficulty however arises in explaining why lower bainite should be twinned when formed at transformation temperatures such that a carbon martensite with a similar M_s temperature would contain few, if any, twins. Also the spacing of the cementite in lower bainite is very much wider than the normally observed twin spacings in martensite.[34,36] This suggests that either the cementite precipitates preferentially only on certain twin interfaces or that the twins, if present in bainitic ferrite, are not strain accommodation twins in the sense of martensitic twinning, but are more likely to be the more widely spaced deformation or growth twins, which are occasionally observed in the lower carbon martensites.

Misorientation between Neighboring Bainitic Ferrite Grains

As has already been described, many bainitic ferrite laths are nucleated within any one austenite grain, and sheaves of these laths are frequently formed

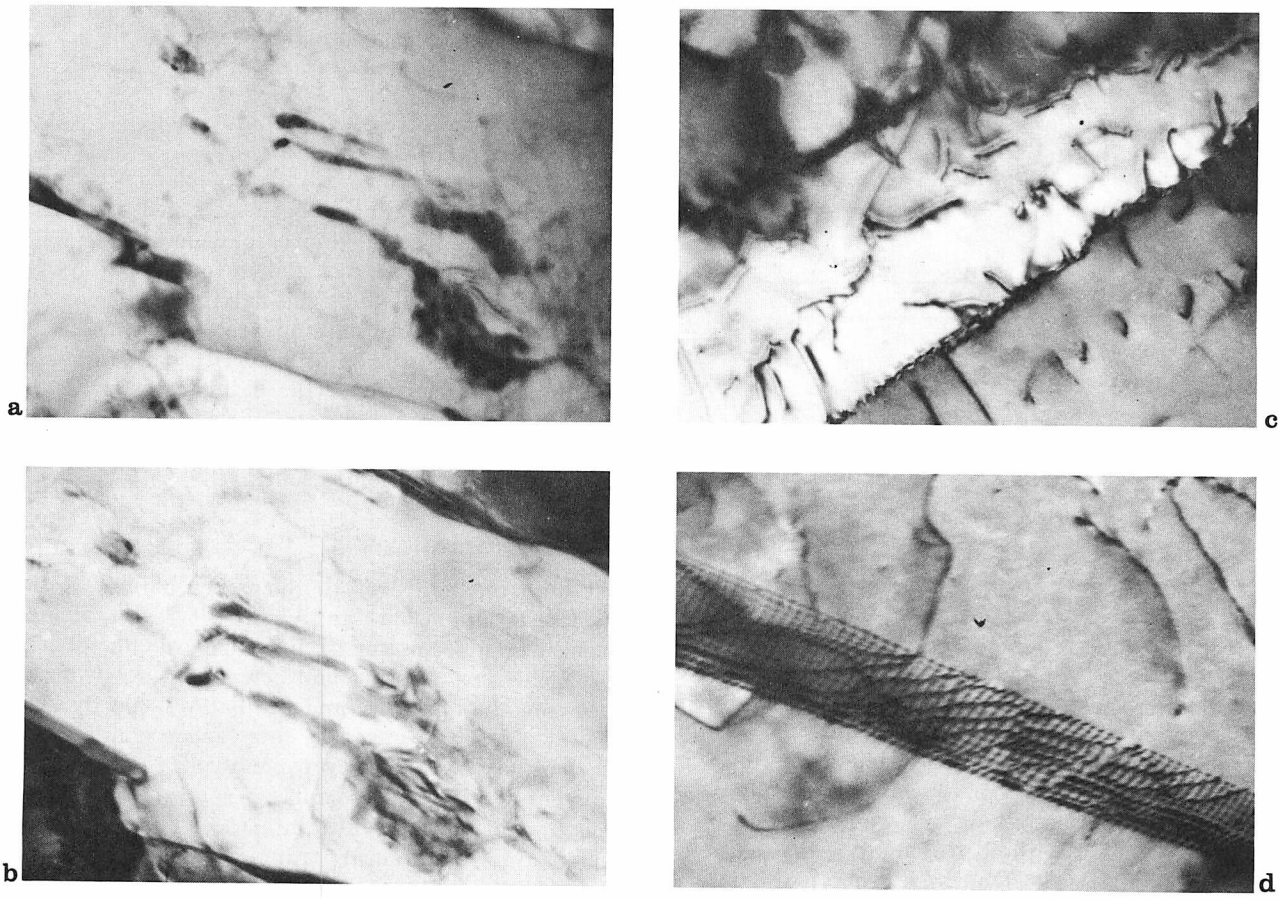

FIGURE 7. Misorientation between bainitic ferrite grains in 0.1% C steel

a. upper bainite showing bainitic ferrite boundaries; thin foil electron micrograph, 75,000 X

b. as a, but tilted to show orientation differences; thin foil electron micrograph, 75,000 X

c. low angle boundary between bainitic ferrite laths; thin foil electron micrograph, 75,000 X

d. low angle boundary between bainitic ferrite laths; thin foil electron micrograph, 75,000 X

very rapidly by a cooperative side-by-side nucleation effect. In the upper bainitic structure, this effect is particularly evident and the carbide forms from the entrapped austenite between the laths of ferrite. This carbide is usually coincident with the grain boundary, and in the higher carbon upper bainites, the carbide may occur as continuous films between the bainitic ferrite grains and often completely obliterates any evidence of the boundary. In some structures, little or no evidence of the boundary can be obtained, but careful tilting experiments can usually reveal a slightly different orientation on either side of the entrapped carbide. However, in some cases, the bainitic ferrite within a colony of the higher carbon upper bainite appears to be continuous and in such circumstances it is suggested that the carbide is first nucleated and then the ferrite forms around the carbides. This process then is repeated but the ferrite simply forms by growth of the earlier ferrite, so that a single orientation of ferrite is produced, which contains the elongated carbide films or plates, which were precipitated directly from the austenite.

Usually however, orientation differences between neighboring ferrite grains can be observed, Figures 7(a) and (b) and many pairs of such grains were examined by electron diffraction to determine the extent of this misorientation. It was found that the misorientation was generally quite small, as shown by some of the more clearly resolved boundaries in very low carbon upper bainite, Figures 7(c) and (d), and varied between 6° and 18° for angular tilts measured on the {110} planes.

In the orientation relationships between bainitic ferrite and austenite, there are many possible variations for the orientation of a ferrite grain formed from an austenite grain of a given orientation. Using the Nishiyama-Wassermann orientation relationship, the possible spread of orientation of the {110} ferrite planes which could be produced from a given austenite grain was plotted on a stereographic projection, Figure 8. It was found that six groups of

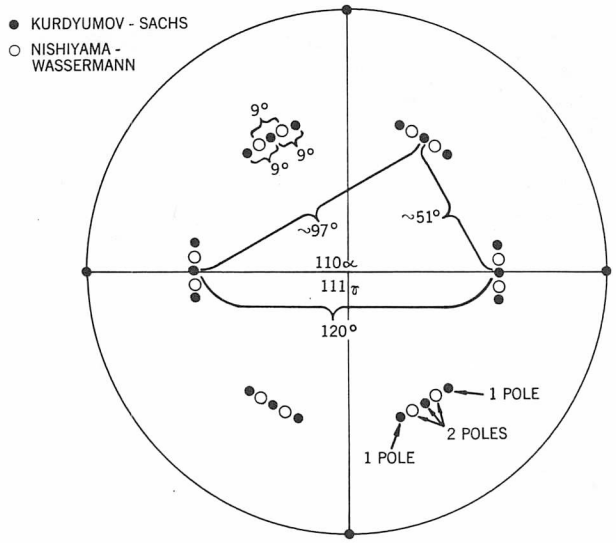

FIGURE 8. $\{110\}\alpha$ Variants from α/γ orientation relationships

such planes occurred, in which there were two distinct orientations. Two variants of the relationship coincided on each of these two orientations in each group. The misorientation within any group was about 9° and between groups was either ~51°, ~97° or ~120°. For the Kurdyumov-Sachs relationship, the angular spread within a group is about 18°. The observed misorientation across the boundary of neighboring bainitic ferrite grains indicates that within a set of side-by-side nucleated ferrite laths, the orientations all lie within any one of the six groups of possible orientations, but do not vary from group to group. It thus seems that the transformation occurs with a selection of the orientation variants such that the boundaries between adjacent bainitic ferrite grains are low angle, i.e., of low energy. This is also indicated by the fact that on tempering, such low angle boundaries are not readily annealed out and consequently bainitic steels, especially the low carbon steels, show appreciable tempering resistance because growth of the ferrite grains is slow.

It is suggested that in the cooperative transformation in which many bainitic ferrite laths are nucleated side-by-side in rapid succession, the transformation strains may determine the orientation variant chosen by the successively nucleated ferrite grains. A further interesting feature of this analysis is that the orientations within a group of bainitic ferrite grains may well be generated from a twinning effect, neighboring grains being more or less twin related. Further and more detailed work is required to investigate this effect. A similar analysis, using the Kurdyumov-Sachs orientation relationship gives generally the same overall result as the Nishiyama-Wassermann relationship, Figure 8, but with modifications introduced by the small differences between the two relationships.

THE MECHANISM OF THE BAINITE REACTION

The results which have been obtained from the morphology of the structures and crystallographic observations enable a mechanism for the bainite reaction to be postulated. The driving force for the reaction is the difference in free energy between the austenite and the bainitic ferrite. This increases as the carbon content of the bainitic ferrite is decreased.[37] There is thus some carbon content of the bainitic ferrite at which the driving force is insufficient for the reaction to continue.

Upper Bainite

At high temperatures in the upper bainite range, ferrite laths nucleate and grow, the reaction being a shear transformation having the Kurdyumov-Sachs or Nishiyama-Wassermann orientation relationship between the austenite and the bainitic ferrite. The bainitic ferrite contains a low carbon content, but carbon has a sufficiently rapid rate of diffusion in austenite to be able to diffuse away ahead of the moving ferrite–austenite interface. The strains accompanying the shear transformation appear to cause cooperative nucleation of many bainitic ferrite laths, side-by-side. There is a particular and restricted set of variants of the orientation relationship for the ferrite thus formed from any given austenite grain, so that neighboring ferrite grains have a minimum misorientation between them. This misorientation does not seem to exceed 18°. As the

FIGURE 9. High carbon upper bainite produced by enrichment of austenite in carbon in a low carbon steel; thin foil electron micrograph, 60,000 X

ferrite laths grow together, the carbon content in the austenite trapped between them is increased until it exceeds the solubility of carbon in the austenite. When this happens, cementite is precipitated directly from the austenite with the Pitsch orientation relationship, and is related in orientation to the bainitic ferrite through the Kurdyumov-Sachs or Nishiyama-Wassermann relationships. The extent to which carbon enrichment occurs before cementite forms directly from the austenite will depend upon the transformation temperature and the carbon content of the steel. The lower the transformation temperature, or the higher the carbon content of the steel, the less will be the enrichment in carbon required for this to occur. Also, the higher the carbon content or the lower the transformation temperature, the larger will be the regions of austenite enriched in carbon, which give rise to the carbide aggregates often seen in upper bainitic structures in low carbon steels, and which are actually regions of higher carbon upper bainite. A typical example of this type of mixed low carbon and high carbon upper bainite structure is shown in Figure 9.

With decreasing transformation temperature, the rate at which carbon can diffuse in front of the ferrite–austenite interface decreases, and so the sideways growth of the ferrite laths is slowed down, resulting in narrower ferrite laths. Also the increased strain associated with the reaction probably restricts the edgewise growth of the ferrite plates in the initial part of the shear reaction. Both these effects lead to a smaller bainitic ferrite grain size. The slower rate of diffusion of carbon away from the bainitic ferrite–austenite interface also means that the ferrite tends to become more supersaturated with carbon. It has been shown[18] that with decreasing transformation the bainitic ferrite becomes more supersaturated in carbon, and further evidence for this from internal friction studies will also be presented.

Lower Bainite

Eventually a temperature is reached at which the carbon diffuses so slowly that it can no longer diffuse away adequately in front of the bainitic ferrite. Also the carbon content dissolved in the ferrite is too high for the reaction to continue. When this occurs, upper bainite can no longer form, and it is replaced by lower bainite. In this structure the initial bainitic ferrite forms by shear with the normal orientation relationship with the austenite, but the laths are very thin, and before they can grow laterally, carbides must be precipitated in the ferrite with an orientation relationship similar to that between carbide and ferrite in tempered twinned martensite. Only when this precipitation has lowered the carbon content of the ferrite sufficiently, is the driving force restored to a level which allows the bainitic ferrite to grow. The new growth again produces supersaturated ferrite, and again carbide precipitation is required within the ferrite for the bainite to continue to grow. This process of carbide precipitation and growth is continuous until the growing plate impinges on an adjacent plate. Similarly, cementite may well precipitate on twins, thus resulting in the observed morphology, but such twins in lower bainite have not yet been observed. Also, with decreasing transformation temperature, the carbon supersaturation in the bainitic ferrite increases although prolonged holding after completion of transformation will cause this supersaturation to be lowered.

It is observed that in lower bainite, there is less tendency for cooperative or sympathetic nucleation of the bainitic ferrite, and in this respect the transition from upper to lower bainite tends to parallel the change from low to high carbon martensite, i.e., the change from high to low M_s temperatures.

Effect of Carbon Content

The temperature at which upper bainite is replaced by lower bainite is about 450 C (840 F) in steels containing 0.1% C but increasing the carbon content up to about 0.5% causes the maximum temperature of the change from lower to upper bainite to increase to about 550 C (1020 F). With a still further increase in carbon content there is a sharp decrease in this temperature down to an almost constant level of 350 C (660 F). The effect of carbon content on the temperature for the change from upper to lower bainite is shown in Figure 6, and the similarity between the relationship up to 0.5% C and the extrapolated A_{cm} line is obvious.

The results shown in Figure 6 may be explained by the mechanism of bainite formation which has already been discussed.

The temperature at which upper bainite gives way to lower bainite is that at which the rate of carbon diffusion is so slow that it can no longer diffuse away in front of the growing bainitic ferrite, and so the supersaturated ferrite has to precipitate carbide for growth to continue. This occurs at about 450 C (840 F) in 0.1% C steels. With increasing carbon content in the austenite, the more shallow diffusion gradient resulting from the higher carbon content in the austenite, see Figure 10, means that the rate of diffusion of carbon away from the bainitic ferrite–austenite interface will be less rapid. Therefore precipitation of carbide within the supersaturated bainitic ferrite (i.e., the lower bainite morphology) is necessary at higher temperatures than in a lower carbon steel, in order for the reaction to proceed. This means that with increasing carbon content the temperature at which lower bainite forms instead of upper bainite is increased, as shown in Figure 6. At a carbon content of about 0.5% it can be seen that the extrapolated A_{cm} line intersects the curve denot-

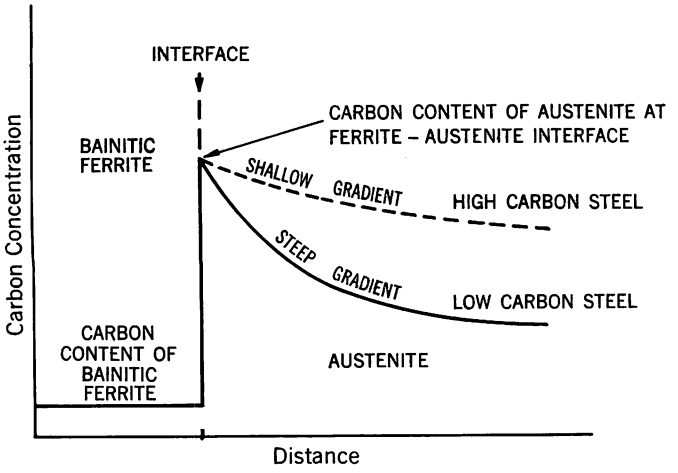

FIGURE 10. Carbon concentration gradients during bainite formation (schematic)

ing the upper temperature limit of lower bainite formation. When this occurs, primary cementite becomes capable of nucleating and precipitating directly from the austenite. This situation applies to any steel containing more than about 0.5% C at temperatures below about 550 C (1020 F). This mode of carbide precipitation is that for upper bainite. It is suggested that the primary carbide precipitation produces low carbon contents adjacent to it, which give rise to bainitic ferrite formation, the local carbon content having then been lowered to the left of the extrapolated A_{cm} line. Consequently, with carbon contents greater than 0.5%, there is a sharp decrease in the temperature at which upper bainitic structures can be formed. Only at as low a temperature as 350 C (660 F) is the rate of cementite precipitation from the austenite so slow that, kinetically, the formation of supersaturated ferrite and the precipitation of cementite from the supersaturated ferrite is a more favorable process, i.e., lower bainite is formed. With all steels containing more than 0.5% C these same conditions apply, as all are supersaturated with respect to cementite, and so there is no reason why the temperature for the change from upper to lower bainite, i.e., 350 C (660 F), should alter with carbon contents above 0.5%.

It must be borne in mind however that for many carbon contents greater than 0.5% at temperatures below 550 C (1020 F), ferrite is also capable of nucleating and precipitating from the austenite, from the point of view of supersaturation, just as is cementite as already discussed. It is suggested that the reason why cementite forms directly from the austenite in preference to ferrite is that the carbon content dissolved in the ferrite would be high, as may be indicated by the extrapolation of the line denoting the solubility of carbon in ferrite. It seems probable that this carbon content is high enough to cause the driving force for ferrite precipitation to be less than that for cementite precipitation, and that despite the fact that the austenite is supersaturated with respect to both ferrite and cementite, the cementite precipitates preferentially. Also it is suggested that the criterion for whether cementite or ferrite nucleates upper bainite may not be governed by the extrapolation of the A_{cm} line, but rather by the locus of the eutectoid composition with regard to carbon content during undercooling.

It seems therefore, that a reasonably consistent explanation may be possible of the effect of carbon content on the observed temperature of the change from upper to lower bainite, and this can be correlated with both the morphology and orientation relationships which are observed for both upper and lower bainite.

STRENGTHENING MECHANISMS IN BAINITIC STRUCTURES

While much work still remains to be done before the strengthening mechanisms in bainite are fully understood, and at present there are no quantitative relationships which can be suggested, the strength of bainite obviously depends on a number of different effects.

Bainitic Ferrite Grain Size

With decreasing transformation temperature it can readily be seen that the bainitic microstructure becomes finer, and in fact this is mainly due to a decrease in the grain size of the bainitic ferrite. An attempt was made to obtain a quantitative estimation of the effect of the bainitic ferrite grain on the strength of low carbon (0.05/0.20%) steels in which the transformation had occurred at different temper-

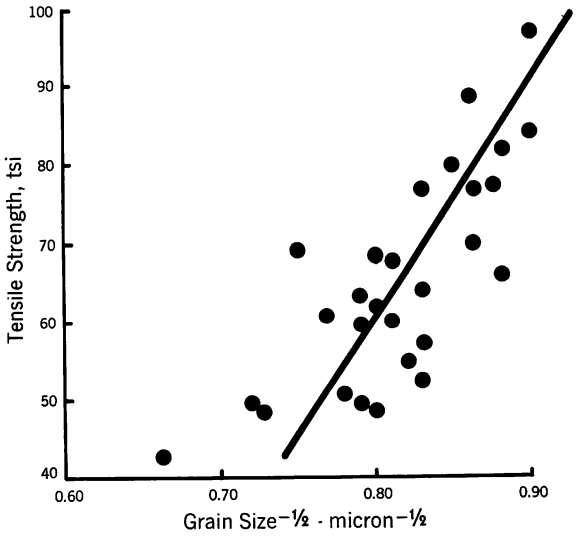

FIGURE 11. Effect of grain size on strength of bainitic steels

atures. A quantitative estimate of the bainitic ferrite grain size was made, using lineal analysis techniques applied to electron micrographs of surface carbon replicas. The results are shown, plotted against the tensile strength,* in Figure 11. It can be seen that there was a clearly defined relationship in which the tensile strength increased linearly with an increasing value of the reciprocal of the square root of the bainitic ferrite grain size. A similar effect was found by Siriwardene.[38] The scatter in the results about the mean line in Figure 11 is due to the inherent errors associated with the assessment of an elongated grain size and to the fact that the grain dimensions are also dependent upon the size of the untransformed austenite regions in which the bainitic ferrite can grow. In a bainitic structure there will always be a variable bainitic ferrite grain size because the bainitic ferrite nucleated later in the progress of transformation will invariably show a smaller grain size. Nevertheless, it is clear that the bainitic ferrite grain size is one of the factors which controls the strength, and it is interesting to note that the low angle boundaries forming the great majority of the bainitic ferrite boundaries are apparently capable of exerting a strengthening effect. In upper bainite of course, these bainitic ferrite boundaries are also the sites of the carbide particles.

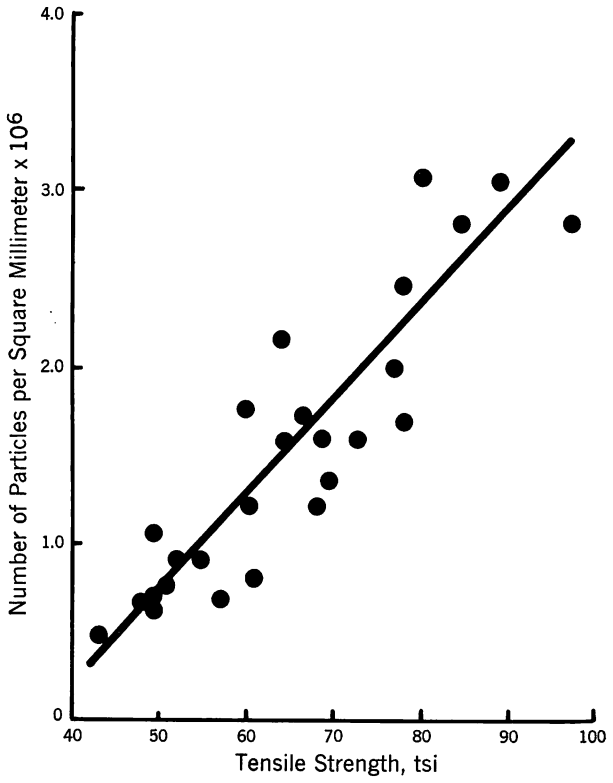

FIGURE 12. Effect of number of particles on strength of bainitic steels

*1 tsi = 2240 psi = 15.4 MN/m².

Dispersion of Carbides

With decreasing transformation temperature, the carbides in the bainitic structure for a given carbon content in the steel, tend to become smaller and to increase in number. It is to be expected that this change will cause an increase in the dispersion strengthening brought about by the carbide. Measurements were made of the number of carbides in the structure of low carbon bainites with different transformation temperatures and therefore different strengths. Surface carbon replicas were used for this work, to eliminate the possibility of over-extraction in an extraction replica giving too high values. The results are shown in Figure 12, in which the number of carbide particles intersecting a unit area of a polished and etched surface is plotted against the tensile strength. There is a clearly defined effect for an increasing number of carbides to be associated with increasing strength, and this reflects the increasing amount of dispersion strengthening with decreasing transformation temperature. Dispersion strengthening by the bainitic carbides therefore plays a part in the strength of bainite.

Internal Stress

With decreasing transformation temperature there is a greater expansion during the bainitic transformation, and this must lead to a higher level of internal stress especially as there will be less tendency for the thermal relief of such internal stresses at the lower transformation temperatures. These internal stresses may well contribute to the strength of the structure, but this effect is probably of secondary importance compared with other strengthening mechanisms. However it must be borne in mind that the apparently more effective strengthening mechanisms might exert their influence partly through the medium of internal stresses. The presence of internal stresses in bainite can be shown by the facts that, when bainite is present in an otherwise polygonal ferrite structure, an anomalously low yield or proof stress value is obtained, and the effect of increasing internal stress with decreasing transformation temperature in bainitic structures results in a decreasing yield strength/tensile strength ratio.

Dislocation Density

The greater the dislocation density in a metal, the greater is the strength, due to larger stresses being required to force a slip dislocation through the structure. It has been shown in the present work that all bainites even those formed in low carbon steels at high temperature, contain a higher dislocation density than polygonal ferrite, due to the strains associated with the shear transformation. These not only cause dislocations to be generated in the bainitic ferrite, but also in the adjacent austenite.

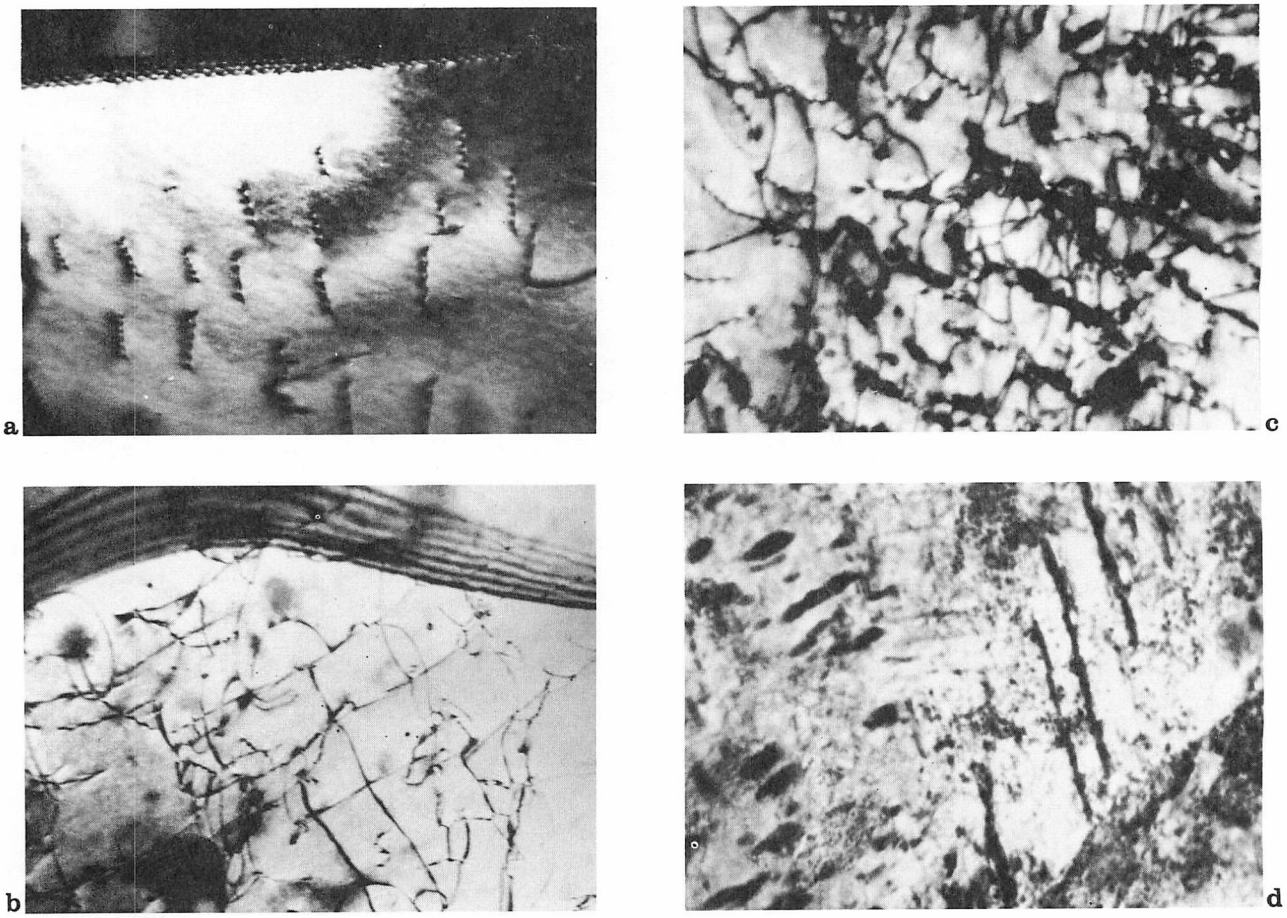

FIGURE 13. Dislocation density of bainitic ferrite

a. 0.1% C steel transformed to upper bainite at 650 C (1200 F) with few dislocations; thin foil electron micrograph, 75,000 X

b. 0.1% C steel transformed to upper bainite at 550 C (1020 F) with more dislocations present; thin foil electron micrograph, 75,000 X

c. 0.1% C steel transformed to lower bainite at 450 C (840 F) showing still heavier dislocation density; thin foil electron micrograph, 75,000 X

d. 0.6% C steel transformed to lower bainite at 300 C (570 F) with many unresolvable dislocations; thin foil electron micrograph, 75,000 X

The dislocation density of the bainitic ferrite increases with decreasing transformation temperature, presumably due to the greater strains accompanying the transformation, and because there is less chance for the dislocations to be annealed out, Figure 13. Consequently, this increased dislocation density can also contribute to the higher strength of bainite with decreasing transformation temperature. As will be shown later, there is evidence which suggests that many of these dislocations are associated with "atmospheres" of carbon atoms.

Another interesting feature of the dislocation structure in bainite is that lower bainite, in which the carbides are precipitated directly from the ferrite, seems to contain a very much higher dislocation density than upper bainite. A possible reason for this is that the precipitation of carbides produces sufficient stress to generate dislocations, and the interface between the cementite and bainitic ferrite will act as a source for such dislocations. This will also be assisted by strains produced by the differential contraction of the bainitic ferrite and the carbide during cooling from the transformation temperature, and by strains imposed on existing bainite regions during the progress of the transformation.

Carbon Dissolved in Bainitic Ferrite

It has been shown[18] that with decreasing transformation temperature, more carbon remains dissolved in the bainitic ferrite. This will tend to produce solid solution strengthening which may partly be due to an association of the dissolved interstitial carbon atoms and the dislocations in the structure. Such an association of carbon atoms with dislocations is shown by internal friction experiments. The Köster[39] peak, which occurs at a frequency ~1 cps at 220 C (430 F), is generally interpreted to be the result of

a carbon–dislocation interaction, and is very pronounced in martensitic structures.[40] It was found that with decreasing transformation temperature in the bainite range in steels containing 0.1% and 0.4% C, the intensity of the Köster peak increased, Figure 14. This shows an increased interaction between carbon and dislocations, which is believed to be mainly due to the increased carbon in solution in the bainitic ferrite at the lower transformation temperatures. It is interesting to note that there is no clear discontinuity in the curve shown in Figure 14, which can be related to the change from upper to lower bainite.

The intensity of the Köster peaks observed in bainitic structures is much less than those occurring in martensitic structures. This may partly be due to tempering of the bainite during the reaction period, and also to a lesser extent to precipitation during heating to the peak temperature of 220 C (430 F). A comparison of the internal friction effects in tempered martensite and bainite indicates, however, very much less carbon–dislocation interaction in bainitic than in martensitic structures. It is not possible at present to relate quantitatively the Köster peak intensity to either dislocation density or the dissolved carbon content in bainite, but the increasing carbon–dislocation interaction with decreasing transformation temperature must be exerting an influence on the strength. The evidence also suggests that the Köster peak intensity is not dependent on the carbon content of the steel for a given transformation temperature.

Despite the fact that the quantitative effects of the various strengthening mechanisms in the bainitic structure are not known, it is nevertheless possible to predict the strengths available in steels which can be air cooled to form bainitic structures, simply from the chemical composition of the steel. As shown in Figure 15, over the range of bainitic structures there is a linear relationship between the strength and the transformation temperature. The transformation temperature on continuous cooling in a steel which exhibits a wide range of bainitic hardenability is closely related to the B_{50} temperature, which has also been shown to be linearly related to chemical analysis.[41] Consequently the tensile strength is related linearly to the chemical composition of the steel, and a regression equation of the following type can be used for carbon contents up to about 0.25% :

$$\text{Tensile Strength (tsi)} = 16 + 125(\%C) + 15(\%Mn+\%Cr) + 12(\%Mo) + 6(\%W) + 8(\%Ni) + 4(\%Cu) + 25(\%V+\%Ti)$$

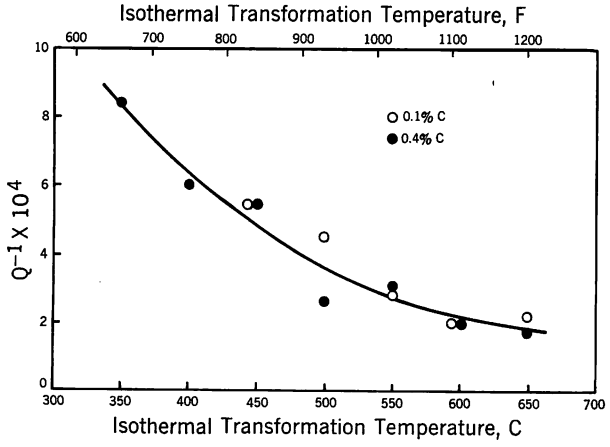

FIGURE 14. Effect of transformation temperature on the Köster peak in bainite

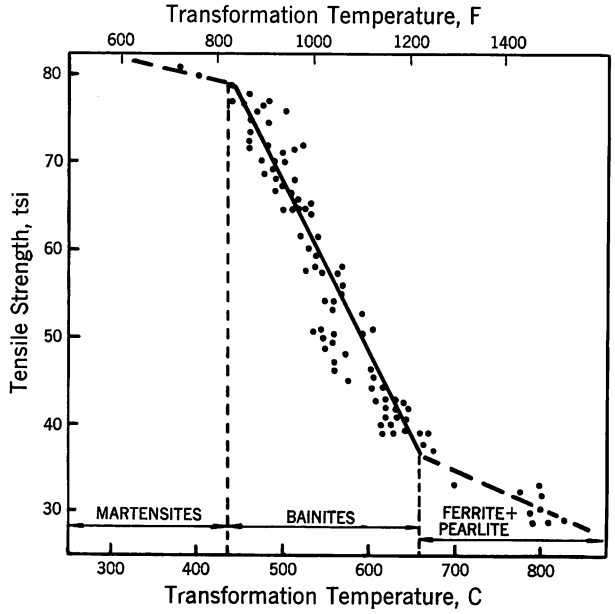

FIGURE 15. Effect of transformation temperature on tensile strength

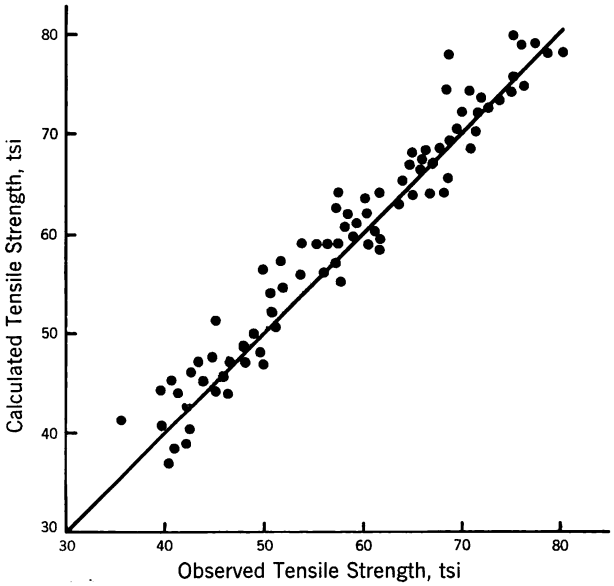

FIGURE 16. Calculated vs observed tensile strength of bainitic steels

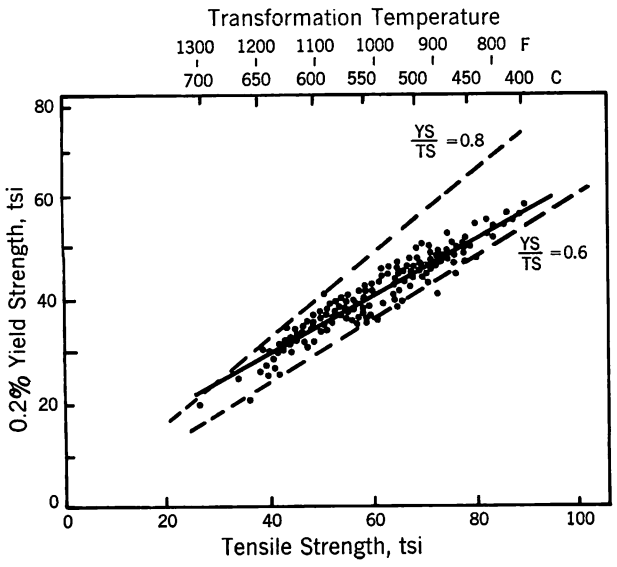

FIGURE 17. Relationships between yield strength, tensile strength and transformation temperature

The accuracy of the prediction from such an equation is shown in Figure 16, and from the relationship shown between yield strength and tensile strength, Figure 17, the yield strength can also be obtained.

DUCTILITY AND IMPACT PROPERTIES OF BAINITIC STEELS AND SOME ASPECTS OF THEIR FRACTURE

Tensile Ductility

The tensile ductility of bainitic structures is generally related to their tensile strength; the higher the strength, the lower being the ductility. In general the percent elongation and reduction of area values are of the same order of magnitude with respect to tensile strength[42] as those reported by several workers for quenched and tempered low alloy steels.[43, 44] The bainitic structures however tend to have slightly superior tensile ductilities, particularly in the high strength lower bainitic structures with strengths above ~55 tsi. Consequently a knowledge of the tensile strength of a bainitic steel, as derived by the regression equation given in the preceding section, enables a reasonably accurate prediction to be made of the tensile ductility.

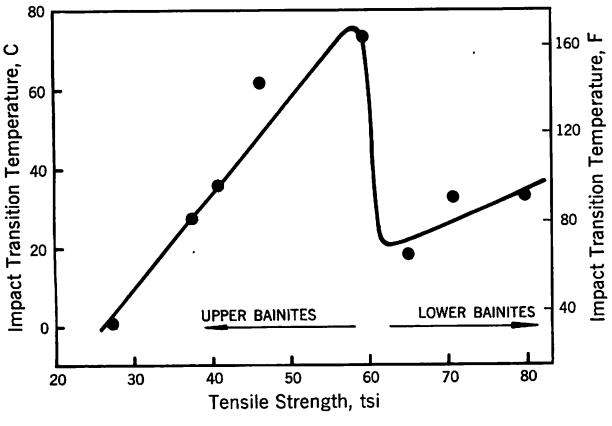

FIGURE 18. Effect of tensile strength on impact transition temperature in bainitic steels

Impact Properties and Fracture Characteristics

A study of the impact properties of bainitic structures of the low carbon variety[8] showed that as the strength increased the impact transition temperature increased up to a tensile strength of about 60 tsi. With a further increase in strength, the impact transition temperature showed a sharp decrease, and then continued to increase again with a still further increase in strength. This behavior is shown in Figure 18, and the discontinuity in the relationship occurs at a tensile strength which is equivalent to the transformation temperature at which there is the major change in structure from upper to lower bainite. It appears therefore that upper bainite has a generally higher impact transition temperature despite its lower strength, than does lower bainite. This effect has also been reported in the literature.[9] At the same time the transition temperature curve changes from an upright form for upper bainite to a very wide transition temperature range in lower bainite.

The reason for this change is believed to be due to the difference in carbide dispersion in lower and upper bainite, although other factors such as the dislocation density may exert an influence. In upper bainite, it is suggested that the carbides at the bainitic ferrite boundaries do not greatly obstruct the propagation of a cleavage crack. This is particularly the case in the lower carbon steels (0.1%) under consideration, in which the carbides are relatively widely spaced. Also, there is evidence that the low angle boundaries between neighboring ferrite grains do not cause any major obstruction to the propagation of a cleavage crack. Optical microstructures of such fractures show that the cleavage cracks deviate but little in direction on crossing from one bainitic ferrite grain to another within a group of side-by-side nucleated laths. Only at the boundaries between different sheaves of laths, or at prior austenite grain boundaries, is there a major change in the direction of the cleavage crack, when some tearing and energy absorption can occur. Microfractographs show a similar effect. At the low angle bainitic ferrite boundaries the cleavage crack either changes direction slightly if the boundary is predominantly tilt, Figure 19(a), produces a number of river markings at a predominantly twist boundary, Figure

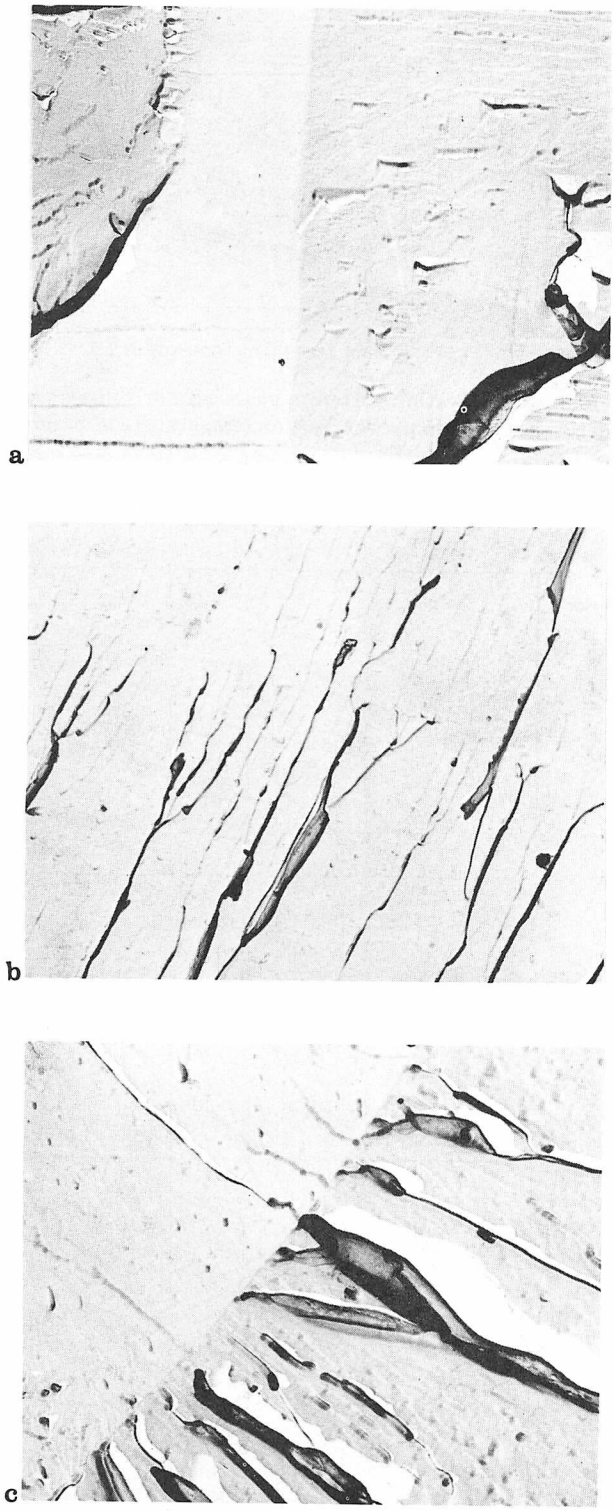

FIGURE 19. Fracture across low angle bainitic ferrite boundaries

a. tilt type boundary; carbon replica fractograph, 15,000 X

b. twist type boundary; carbon replica fractograph, 15,000 X

c. tilt-twist type boundary; carbon replica fractograph, 15,000 X

19(b), or gives a combination of these effects at more complex boundaries, Figure 19(c). Once initiated therefore, the brittle cleavage crack spreads rapidly over a large number of bainitic ferrite grains in any prior austenite grain, and mainly encounters an obstruction when it meets a prior austenite grain boundary. Thus the transition temperature range is narrow and the impact transition temperature curve has an upright form. These observations are further confirmed by the fact that the cleavage fracture facets are larger than the bainitic ferrite grains. With increasing strength or decreasing transformation temperature in the upper bainitic range of structures, the increased dislocation density and the

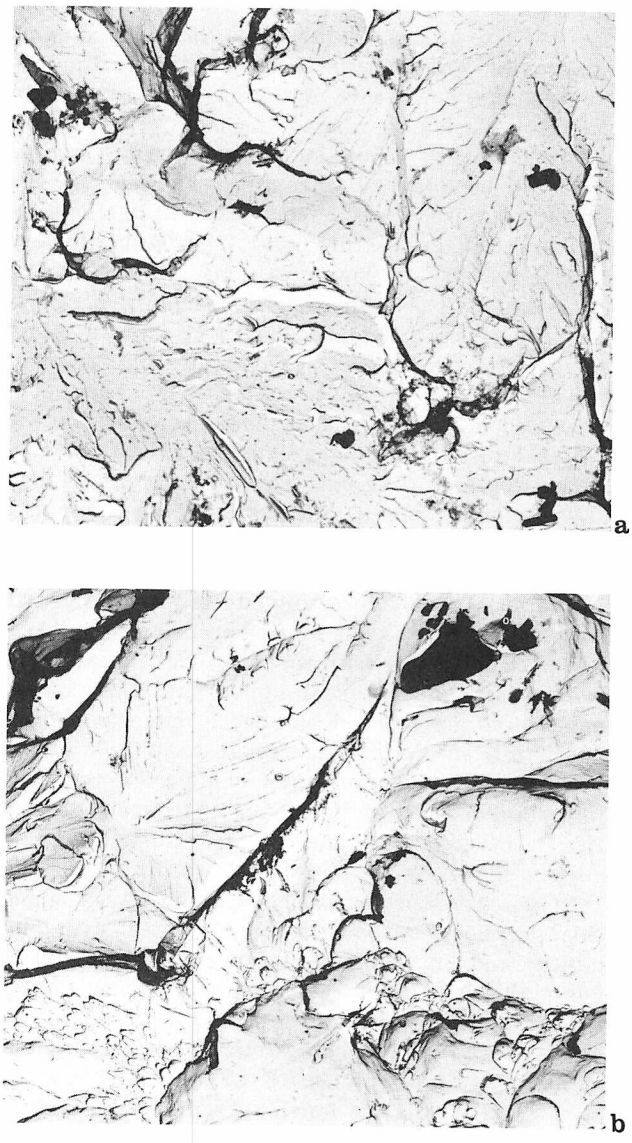

FIGURE 20. Fracture in lower bainitic structures of 0.1% C steel

a. brittle fracture; carbon replica fractograph, 3000 X

b. mixed ductile-brittle fracture; carbon replica fractograph, 3000 X

greater number of low angle boundaries brought about by the finer bainitic ferrite grain size, give rise to a much greater number of river markings in the microfractograph.

In lower bainite however, the increased dislocation density, but more particularly the considerable increase in the number of dispersed carbides, causes the crack to intersect and propagate through or around, or actually fracture, many more carbides. The cleavage surface as revealed by the microfractograph becomes more irregular with many river markings and cleavage steps, which absorb energy as they tear together, Figure 20(a). Thus the cracks tend to be arrested, so that while the higher strength bainitic structure may more readily initiate a brittle cleavage crack, it does not allow such easy propagation of these cracks. The result is that when a crack is arrested, some deformation and ductile fracture occur until a new cleavage crack is initiated, due to the work hardening raising the flow stress; unless the temperature is low enough for many cleavage cracks to be initiated when they can join up by a ductile fracture. These effects result in ductile dimples and cleavage fracture occurring together in very close proximity in lower bainites, Figure 20(b). Consequently the transition temperature range is very considerably extended, and while brittle cleavage failure may initiate at higher testing temperatures than in an upper bainitic structure, the measured impact transition temperature appears to decrease due to the wider temperature range over which the ductile–brittle transition occurs. In fact at some temperatures, lower bainites can have much greater impact strengths than do upper bainites of much lower strength.

There are some interesting effects which originate from the very different impact properties exhibited by upper and lower bainitic structures. Because the brittle cleavage fracture in upper bainite can spread unhindered across most bainitic ferrite boundaries, but mainly encounters a major obstacle to its propagation at the prior austenite boundaries, the most important method of improving the impact properties is therefore to refine the prior austenite grain size, as shown by curve (b) in Figure 21. The commercially developed bainitic steels contain boron and this necessitates that they are treated with aluminum and/or titanium in order to fix the nitrogen;[11] they are therefore fine grained. The only other method of further refining the prior austenite grain size is to lower the finishing rolling temperature, but as shown in Figure 21, the higher the strength of the steel, the lower is the finishing rolling temperature required to give an acceptable level of the impact transition temperature. With tensile strengths much greater than about 45 tsi, this method cannot be used to produce impact transition temperatures below room temperature, because the requisite low finishing temperatures are difficult to achieve commer-

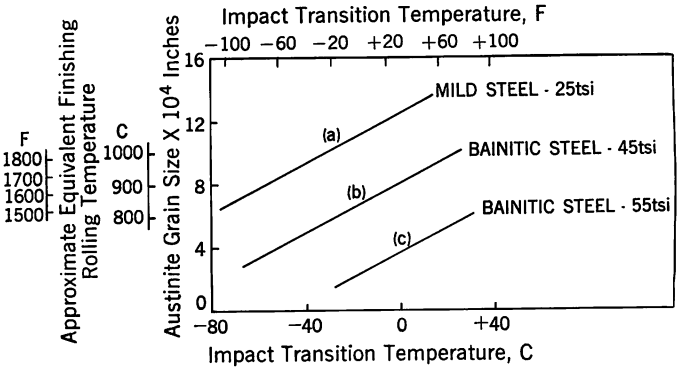

FIGURE 21. Effect of austenite grain size or rolling temperature on the impact transition temperature of bainitic steels

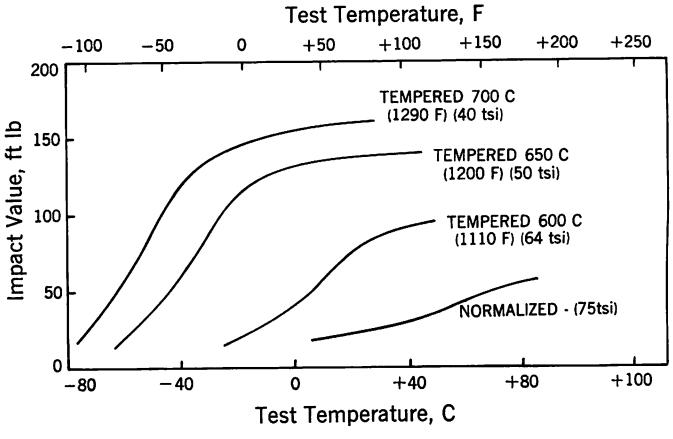

FIGURE 22. Effect of tempering on the impact transition curves of a 75 tsi high strength bainitic steel

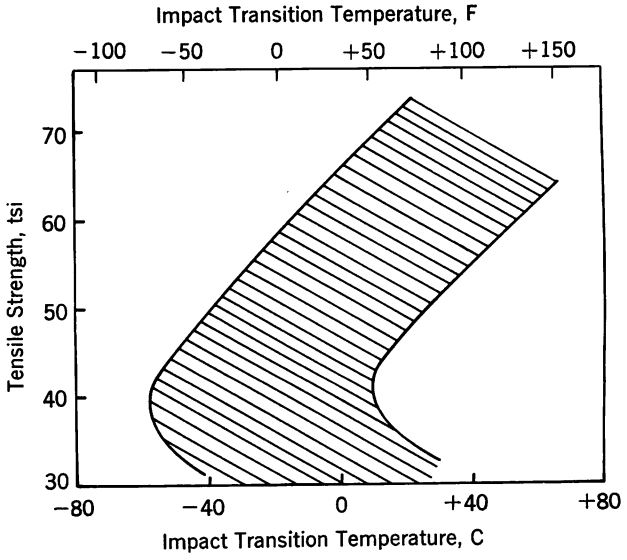

FIGURE 23. Relationship between tensile strength and transition temperature in tempered high strength bainitic steels

cially without considerable economic disadvantages. Also, in low carbon upper bainitic structures, tempering has little or no effect unless very high tempering temperatures are used. This is because of the low energy bainitic ferrite boundaries, which are very slow to migrate unless high tempering temperatures are used. The tempering effect which occurs at high temperatures is a fairly rapid ferrite grain growth, and this is detrimental to the impact properties.

Because of the good impact properties of lower bainitic structures however, which also are associated with higher strength levels, it is possible to temper these structures to lower the strength. This is readily achieved, and yet the beneficial structure containing many dispersed carbides is maintained. The lower strength produced by such a tempering treatment results in an improvement of the impact properties, as shown in Figure 22, and the general relationship between tensile strength and impact transition temperature after tempering is shown in Figure 23. This shows the band of results for many different types and compositions of bainitic steels, and it can be seen that the optimum combination of properties which can be produced is 45 tsi tensile strength with an impact transition temperature of −40 C (−40 F).

DEVELOPMENTS IN BAINITIC STEELS

The aims in a steel designed to have a bainitic structure have been:

(1) to use a low carbon content in order to obtain good welding properties. This also gives a benefit in terms of impact properties.

(2) to provide steels of varying tensile strength from 40 to 75 tsi. This gives a range of yield strength values from 30 to about 60 tsi.

(3) to obtain these properties in the air cooled condition, either directly from the finishing rolling temperature or by a simple normalizing treatment. It was appreciated that to obtain certain properties for specific applications, a tempering treatment would have to be used.

(4) to obtain the required properties, with a minimum of variation, over a wide range of section sizes.

These requirements necessitated that the steel should show a metastable austenite bay between the polygonal ferrite and the bainite C curves in the isothermal transformation diagram, for the bainite reaction to be relatively rapid, and yet for the polygonal ferrite reaction to be retarded as much as possible. Also the bainite reaction would have to exhibit a very flat topped C curve. These requirements are illustrated schematically in Figure 24. It was

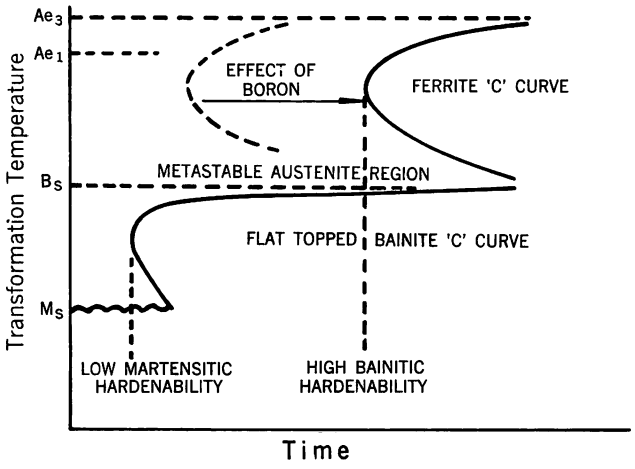

FIGURE 24. Schematic diagram of requirements for a bainitic steel with respect to transformation characteristics

found that they were best achieved, most economically, in a low carbon, 0.5% Mo steel containing an addition of boron. It was also found that by introducing other alloying elements, the B_s-B_f range could be so lowered in temperature that a range of strengths could be achieved simply because the transformation temperature during cooling had been depressed. However, there was a limit to the amount of alloying element which could be introduced because of:

(1) the danger of lowering the end of transformation on cooling to martensite, as occurs in a weld, so that the weldability of the steel was impaired and cracking resulted.

(2) the bainite reaction itself became so retarded that the steel became martensitic air hardening in the smaller section sizes. This effect became of even greater importance in the development of higher carbon bainitic steels.[16]

However, steels were successfully developed, and the low carbon steels have been used for the main structural components of aircraft engines, boilers and pressure vessels, heavy moving machinery, load transporters, lifting equipment, excavators, fans, light transportable bridges, structural supports in mining operations, etc. The steels have good high temperature properties, and a British Standard specification is being prepared incorporating them. The high carbon version, containing about 0.55% C, has found an application as a die block material.

It is interesting to consider the possible further developments which can be made in bainitic steels. It seems possible that the use of very low finishing temperatures in thin sections might improve both the strength and ductility particularly with respect to a fracture toughness aspect in sheet materials. Preliminary work, using finishing temperatures

down to as low as 500 C (930 F) has indicated that there was only a slight increase in strength, possibly because the bainitic ferrite grain size was not very dependent on the prior austenite grain size. However, the impact ductility showed an interesting feature in that while the impact properties of the lowest strength upper bainitic structures were not appreciably altered, the impact properties of the higher strength upper bainitic structure did show a marked improvement which was more evident as the strength increased up to ~55 tsi. This is undoubtedly due to some further refinement of the prior austenite grain size, which has been shown to control the impact properties in upper bainitic structures. The transition temperature however was never lower than that of the lowest strength bainitic steel, but the results do indicate that the detrimental effects of increasing strength in upper bainite can be largely counteracted by a refinement of the prior austenite grain size.

Furthermore, it was observed that the most beneficial effects were produced if the deformation, during for example hot rolling, was carried out in a narrow temperature range just above the B_s temperature of the steel. This is in effect an ausforming treatment, and further results on ausforming have shown that the increase in strength during ausforming bainitic steels is relatively small and is very dependent on the transformation temperature of the steel. The increase in strength after ausforming becomes smaller as the transformation temperature of the steel increases. It is suggested that this feature is associated with recovery effects in the austenite and possibly with self annealing effects in the bainitic structure either during or after transformation.

It may also be possible to use a precipitation reaction in a bainitic steel, and such a reaction would be most beneficial if it could be made to increase the strength in air cooled materials. The use of columbium might be anticipated, and while this would give a slightly higher strength in the as rolled condition, any benefit would be lost in the normalized condition because of the limited solubility of columbium in the austenite at the normalizing temperature. The maximum possible effect of columbium precipitation strengthening however would be quite small, probably not more than an increase of 5 tsi on the yield strength, and such an increase would be very marginal, particularly in the higher strength steels. An alternative age hardening addition which might be considered is copper. This could give approximately a 10 tsi increase in the yield strength, but in steels containing about 1.5% Cu, a separate aging treatment would be necessary. If however as much as 3% Cu could be accommodated in a bainitic steel without altering radically the transformation characteristics, this would result in age hardening occurring during normalizing or in the as rolled structure. However, such an effect could only be produced if the transformation temperature was above the temperature at which copper precipitates, namely about 500 C (930 F). Consequently such a phenomenon could only be applied to the lower strength steels, but the possible effects of copper itself on the B_s temperature would require careful study.

Finally it seems reasonable to suggest that a bainitic steel could be used in the quenched and tempered condition in plate. This would enable any lack of hardenability to be counteracted by the fact that even in the air cooled condition, bainite would be formed. Thus inefficient quenching would not be so deleterious and the properties across the section might be anticipated to be more uniform.

ACKNOWLEDGMENTS

The author wishes to thank Dr. F. H. Saniter, O.B.E. Director of Research, The United Steel Companies Limited, for permission to publish this paper, and to acknowledge the many instructive discussions with colleagues, Dr. T. Gladman and Messrs. S. R. Keown and B. R. Clark.

REFERENCES

1. E. S. Davenport and E. C. Bain, Trans. AIME *90*. 117 (1930)
2. "Electron Microstructure of Bainite in Steel," 2nd Progress Report by Subcommittee XI of Committee E-4, ASTM Proc. *52*. 543 (1952)
3. D. N. Shackleton and P. M. Kelly, "Morphology of Bainite," *Physical Properties of Martensite and Bainite*, Special Report 93, The Iron and Steel Institute (London), 1965, 126
4. L. Habraken, Discussion, *Physical Properties of Martensite and Bainite*, Special Report 93, The Iron and Steel Institute (London), 1965, 148
5. K. A. Ridal and J. McCann, Discussion, *Physical Properties of Martensite and Bainite*, Special Report 93, The Iron and Steel Institute (London), 1965, 147
6. E. S. Davenport, Trans. AIME *209*. 677 (1957)
7. K. J. Irvine, Discussion, *Physical Properties of Martensite and Bainite*, Special Report 93, The Iron and Steel Institute (London), 1965, 151
8. K. J. Irvine and F. B. Pickering, J. Iron and Steel Inst. (London) *201*. 518 (1963)

9. T. Boniszewski, Discussion, *Physical Properties of Martensite and Bainite*, Special Report 93, The Iron and Steel Institute (London), 1965, 147
10. F. B. Pickering, "Mechanism of Bainite Formation in Low-Alloy Steel Containing up to 0.4% Carbon," *Proceedings of the Fourth International Conference on Electron Microscopy*, Berlin, Vol. 1, 628 (1958), pub. 1960
11. W. E. Bardgett and L. Reeve, J. Iron and Steel Inst. (London), *163*. 277 (1949)
12. K. J. Irvine, F. B. Pickering, W. C. Heselwood and M. Atkins, J. Iron and Steel Inst. (London), *186*. 54 (1957)
13. K. J. Irvine and F. B. Pickering, J. Iron and Steel Inst. (London), *187*. 292 (1957)
14. K. J. Irvine and F. B. Pickering, J. Iron and Steel Inst. (London), *188*. 101 (1958)
15. K. J. Irvine and F. B. Pickering, J. Iron and Steel Inst. (London), *194*. 137 (1960)
16. K. J. Irvine and F. B. Pickering, "High-Carbon Bainitic Steels," *Physical Properties of Martensite and Bainite*, Special Report 93, The Iron and Steel Institute (London), 1965, 110
17. L. Habraken, Compt. Rend. Rech. Trav. du Centre National de Recherches Métallurgiques, Nov. 1957, No. 19
18. P. Vasudevan, L. W. Graham and H. J. Axon, J. Iron and Steel Inst. (London), *190*. 386 (1958)
19. S. V. Radcliffe and E. C. Rollason, J. Iron and Steel Inst. (London), *191*. 56 (1959)
20. J. S. White and W. S. Owen, J. Iron and Steel Inst. (London), *195*. 79 (1960)
21. A. E. Austin and C. M. Schwartz, Proc. ASTM *52*. 592 (1952)
22. R. H. Goodenow, S. J. Matas and R. F. Hehemann, Trans. AIME *227*. 651 (1963)
23. T. Ko and S. A. Cottrell, J. Iron and Steel Inst. (London), *172*. 307 (1952)
24. G. R. Speich and M. Cohen, Trans. AIME *218*. 1050 (1960)
25. R. H. Goodenow, R. H. Barkalow and R. F. Hehemann, "Bainite Transformations in Hypoeutectoid Steels," *Physical Properties of Martensite and Bainite*, Special Report 93, The Iron and Steel Institute (London), 1965, 135
26. G. V. Smith and R. F. Mehl, Trans. AIME *150*. 211 (1942)
27. J. M. Wheatley and R. G. Baker, Brit. Welding J. *10*. (1). 23 (1963)
28. Z. Nishiyama, Sci. Rep. Tohoku Univ. *23*. 637 (1934)
29. G. Wassermann, Arch. Eisenhüttenw. *6*. 347 (1933)
30. G. Kurdyumov and G. Sachs, Z. Physik *64*. 325 (1930)
31. W. Pitsch, Acta Met. *10*. 897 (1962)
32. Yu. A. Bagaryatskii, Doklady Akad. Nauk SSSR *73*. 1161 (1950)
33. W. Pitsch and A. Schrader, Arch. Eisenhüttenw. *29*. 485 (1958)
34. P. M. Kelly and J. Nutting, J. Iron and Steel Inst. (London), *192*. 246 (1959)
35. E. Tekin and P. M. Kelly, "Precipitation from Iron Base Alloys," AIME Met. Soc. Conf. Vol. 28, 1965, Gordon and Breach, New York, 173
36. R. H. Richman, Trans. AIME *227*. 159 (1963)
37. R. F. Hehemann and A. R. Troiano, Trans. AIME *200*. 1272 (1954)
38. P. P. L. G. Siriwardene, PhD Thesis, Cambridge University, 1955
39. W. Köster, L. Bangert and R. Hahn, Arch. Eisenhüttenw. *25*. (11/12). 569 (1954)
40. T. Gladman and F. B. Pickering, J. Iron and Steel Inst. (London), *204*. 112 (1966)
41. W. Steven and A. G. Haynes, J. Iron and Steel Inst. (London), *183*. 349 (1956)
42. F. B. Pickering, "Metallurgical Achievements," Pergamon Press, London, 1965, 199
43. W. G. Patton, Metal Progress *43*. 726 (1943)
44. E. J. Janitzky and M. Baeyertz, *ASM Metals Handbook*, 1939, 515

ORAL DISCUSSION

The Structure and Properties of Bainite in Steels

Presented by F. B. PICKERING

C. L. MAGEE (Ford Motor Company). I'd like to ask a question about how you were able to vary the grain size of your bainitic structure because I am struck by the very large variation of strength with grain size that you report. If you obtained these results by varying the transformation temperature, isn't it probable that a good part of the effect is due to changes in dislocation density, or more generally the effect of substructure buried in an apparent grain size effect?

AUTHOR'S REPLY. The bainitic ferrite grain size was varied both by varying the prior austenite grain size and by varying the transformation temperature. The strength of bainite depends on a number of features, and dislocation density is equally as important, if not more so, than the bainitic ferrite grain size. The evidence I presented was only intended to illustrate that grain size has a strengthening effect, but the strength no doubt also contains a contribution from the dislocation density. The bainitic ferrite grain size is, in fact, the substructure size you refer to.

H. I. AARONSON (Ford Motor Company) These very attractive results on the crystallography of sheaves were qualitatively forecast in the paper in which the sheaf morphology was first reported (H. I. Aaronson and C. Wells, "Sympathetic Nucleation of Ferrite," Trans. AIME *206*. 1216 (1956); see also H. I. Aaronson, *Decomposition of Austenite by Diffusional Processes*, John Wiley and Sons, New York (1962) 481-490).

In this paper, it was suggested that sheaves are built up by the repeated "sympathetic nucleation" of ferrite plates at the broad faces of ferrite plates previously formed. Since such nucleation occurs under conditions of low supersaturation, it becomes exceptionally important that the net interfacial free energy required to form a ferrite nucleus be minimized. On the standard formalism of heterogeneous nucleation theory, this is accomplished in part by nucleation at the edge of a ledge, but with a broad face of the lath- or plate-shaped nucleus in contact with the broad face of the ledge. (The edge of a ledge is considered to have a high specific interfacial free energy; the broad face of a full-grown plate and the broad face of a nucleus are taken to have low, though probably different, interfacial energies.) The area of the nucleus not in contact with the ferrite plate against which it forms should also be bounded insofar as practicable by low interfacial energy facets. In order to achieve this geometry, the orientation relationship of the lattice of the nucleus should be parallel or nearly parallel to that of the lattice of the plate against which it forms. This accounts for the rather low angle boundaries observed between adjacent ferrite plates in a sheaf. The finding of Mr. Pickering that the plates comprising a sheaf are nonetheless discrete crystals — a result which Drs. Oblak and Hehemann have also presented at this Symposium in more qualitative fashion — strongly supports the view that sheaves are actually formed by sympathetic nucleation, rather than by polygonization of one big ferrite single crystal, as has sometimes been suggested.

AUTHOR'S REPLY. I entirely agree with Dr. Aaronson, that in low carbon bainitic ferrite the ferrite comprises many sympathetically-nucleated laths of ferrite, each individual ferrite lath being formed quite separately from the austenite. The fully transformed structure therefore consists of impinged lath-like ferrite grains. This structure has been referred to sometimes as a substructure, and this has led to the misconception that, as Dr. Aaronson says, it formed by a substructure developed within a large ferrite grain, as occurs during deformation. This, however, is not the case, each "substructural" unit being more properly termed a bainitic ferrite grain. The relatively restricted orientation differences across the bainitic ferrite grain boundaries are caused by the peculiarities of the mechanism of the transformation from austenite to bainitic ferrite. In assessing the bainitic ferrite grain size, it is this so-called "substructure" which is being measured, and it is found that this bainitic ferrite grain size is one of the features which govern the strength.

G. R. SRINIVASAN (Cornell University). I would like to refer to the question whether cementite forms as plates or rods in bainite. Our thin-foil studies in an Fe–3.32% Cr–0.66% C alloy show that the electron diffraction pattern from cementite in lower bainite consists of streaking of the cementite reflections in the [001] cementite or [112] ferrite direction. This would occur if cementite forms as thin plates and is oriented such that the plates are parallel to the electron beam with the thin direction along the streaking direction. Since this streaking occurs in this specific direction, we believe that the ferrite (112) planes correspond to the cementite habit in this alloy.

Also, I would like to know if Mr. Pickering observed the same frequency of the ferrite–cementite relationship in upper bainite as Shackleton and Kelly reported in

their Scarborough paper.* They observed that more than two-thirds of the relationships were the standard tempering relationships and they attributed the crystallographic differences between the carbide in upper and lower bainite to differences in the cementite habit plane rather than in the cementite–ferrite orientation relationship.

AUTHOR'S REPLY. I agree that the orientation relationship itself is not sufficient to define whether a structure is upper or lower bainite. As you point out, the normal orientation relationship for the precipitation of carbide from ferrite or tempered martensite, is one of those which can be obtained from relating the cementite and ferrite orientations through a common austenite orientation. We certainly found that in upper bainite, this orientation occurred much more frequently than one would expect. I also agree with your statement that the habit plane of the cementite is as important as the orientation relationship in deciding whether a structure is upper or lower bainite. However, there is often a large scatter in the results of such habit plane determinations, as shown by recent work by Kelly and Shackleton, possibly because the cementite does not have a well defined plate-like morphology.

G. R. SRINIVASAN. Another point I wanted to make concerns the existence of internal twins in lower bainite. To the best of my knowledge no one has found twins in the bainite plate. This is confirmed by our own studies. Furthermore, as I mentioned in the discussion to Professor Hehemann's paper, twinning can not explain the crystallographic features of lower bainite, such as the habit plane and the austenite–ferrite orientation relationship. In fact, this was shown by Bowles and Kennon in 1960 in their theoretical paper on the crystallography of bainite transformation.** Our results show that the crystallography of bainite in a Fe–7.9% Cr–1.1% C alloy is consistent with the lattice invariant deformation being a pencil glide along the usual bcc slip direction.

AUTHOR'S REPLY. I agree also with you about the existence of twins in bainite. I believe I make the matter quite clear in my paper. I do not know of anyone finding positive evidence for twins, but the matter has been speculated upon from time to time, in order to explain the morphology of lower bainite. Not only has there been no positive evidence for twins in lower bainite, but as I also pointed out in the paper, the whole concept of such twins does introduce many problems. At present, I prefer to think that lower bainite is not twinned at any stage of its formation.

G. R. SRINIVASAN. The last point I want to make is that by choosing a suitable alloy we have been able to get reflections from ferrite, cementite, and the parent austenite. These three structures are related uniquely.

*D. N. Shackleton and P. M. Kelly, *Physical Properties of Martensite and Bainite*, Special Report 93. The Iron and Steel Institute (London), 1965, 126.

**J. S. Bowles and N. F. Kennon, J. Aust. Inst. Met. 5. 106 (1960)

WRITTEN DISCUSSION

M. COHEN (Massachusetts Institute of Technology). Mr. Pickering has given us a comprehensive picture of the structural characteristics and properties of bainitic steels. His paper will prove extremely valuable to those participating in this intriguing field. The only question that I am raising here has to do with the mechanism of the transformation of austenite to lower bainite.

It is evident that Mr. Pickering believes the initially-formed bainite to be supersaturated ferrite. If there is sufficient driving force for this to happen, one may then wonder why it is necessary (as Mr. Pickering states) for carbides to precipitate from the ferrite in order for the growth process to proceed. Mr. Pickering mentions that "Only when this precipitation [carbides from supersaturated bainitic ferrite] has lowered the carbon content of the ferrite sufficiently, is the driving force restored to a level which allows the bainitic ferrite to grow. The new growth again produces supersaturated ferrite, and again carbide precipitation is required within the ferrite for the bainite to continue to grow."

I am curious to know how such carbide precipitation can enhance the driving force for the transformation of austenite to supersaturated ferrite, if the carbides precipitate *after* the supersaturated ferrite has started to form. If the supersaturated ferrite can come into existence in the first place, then the increment of driving force corresponding to the subsequent conversion of supersaturated ferrite to low-carbon ferrite and precipitated carbides should not be necessary for the continued growth of supersaturated ferrite from the austenite.

A corollary question also arises as to the degree of supersaturation that is inferred. If the first-formed ferrite has the same composition as that of the parent austenite, the reaction temperature must be below T_0, for only then can the driving force be sufficient for diffusionless growth. If this process can start as presumed, it should continue rapidly without waiting for, or without being controlled by, carbide precipitation from the ferrite. Of course, the nucleated ferrite may have something less than this high degree of supersaturation, but then the carbon would have to redistribute itself between the ferrite and the surrounding austenite, thereby setting up concentration gradients. Perhaps this situation is what Mr. Pickering has in mind, but here carbon diffusion in the austenite or ferrite should control the kinetics of growth, with the precipitation of carbides being only incidental. Alternatively, the interface between the bainitic ferrite and austenite may become pinned by carbon atmospheres, thereby introducing a growth barrier that could be relieved intermittently through carbide precipitation, but this kinetic process would not be governed by the driving force of the initial reaction.

In other words, if the carbides are visualized to precipitate from the supersaturated ferrite *after* its formation, it is not easy to see what kind of a model will permit the precipitation of carbides to control the bainitic growth merely through driving-force considerations. On

the other hand, carbide precipitation could play an important role in the growth kinetics if this phase were to form *simultaneously* with the ferrite, supersaturated or otherwise, or if the growth were interface-controlled by interstitial locking. Growth could also be favored thermodynamically by the precipitation of carbides from the *austenite* just ahead of the advancing interface, this being a way of reducing the carbon build-up in the surrounding austenite either continuously or discontinuously. However, this would be quite a different process from the one described by Mr. Pickering.

I should welcome having Mr. Pickering's clarification of his views on these matters.

AUTHOR'S REPLY. Professor Cohen has raised some very pertinent questions to which there are probably no fully satisfactory answers in the present state of knowledge. There seems to be little doubt that it is experimentally observed that much of the carbide in lower bainite precipitates from the ferrite. This is confirmed by Professor Hehemann's paper in the present Symposium. There is also some evidence that at the very earliest stages in its formation, the bainitic plate does not contain carbides, but this evidence requires much further confirmation.

It is not suggested that the first-formed bainitic ferrite has the same carbon content as the parent austenite, but rather that it has a lower carbon content. If this is the case there will be a carbon concentration in the austenite immediately ahead of the bainitic ferrite, and so the bainite is trying to grow into austenite of locally higher carbon content than the mean carbon content of the original austenite. The energy required to do this could become available if the intensity of the carbon supersaturation in the ferrite was reduced by precipitation of carbide within the ferrite. An alternative possibility is that the carbon concentration in the austenite ahead of the bainite interface may be reduced. There are several mechanisms by which this could occur. One would be the diffusion of carbon away into the austenite, and such a situation would not depend on the precipitation of carbides in the bainitic ferrite, nor on carbon diffusion in the ferrite, as Professor Cohen points out. Another is that the rate of diffusion of carbon away into the austenite is so slow that carbides first start to precipitate in the supersaturated bainitic ferrite. This would lower the degree of supersaturation in the bainitic ferrite and, depending on the actual levels of carbon in the ferrite which contains carbides, in the carbon enriched austenite, and in the matrix austenite remote from the bainite, and also on the diffusion rates in ferrite and austenite, could allow carbon to diffuse back across the interface from the austenite into the ferrite. This would enhance the carbide precipitation in the ferrite, decrease the carbon enrichment at the interface, and allow the bainite to grow. In this case, it would be diffusion of carbon in ferrite which is the controlling factor, and this would be dependent on the precipitation of carbides in the ferrite.

The further possibility mentioned by Professor Cohen is that the bainitic–ferrite interface is pinned by carbon atmospheres, possibly resulting from the carbon enrichment in the austenite at this interface. As he says, the relief of this pinning would not be governed by the driving force for the initial reaction, but would depend on precipitation of carbides in the austenite at or slightly ahead of the interface. This suggestion may have some validity, as we have recently observed lower bainite in which carbides appear to cross the bainite–austenite interface, but again much more confirmatory evidence for this effect is required.

One final point is concerned with the measurements of the rates of reaction in lower bainite formation. I think that most of the techniques used only measure the rate after the reaction is proceeding, i.e., when ferrite and carbide are, in the aggregate as a whole, forming together. It would be, I think, exceedingly difficult to establish the kinetics of the initial reaction, and consequently it seems necessary to fall back on morphological and possibly crystallographic evidence to investigate this reaction.

Transformation Kinetics in Marage Type Fe–18% Ni Steels

B. R. BANERJEE† and J. J. HAUSER
Hunter Research Laboratories
Crucible Steel Company of America
Pittsburgh, Pennsylvania

INTRODUCTION

In order to strengthen a ductile material, plastic flow must be inhibited by introducing barriers which restrict dislocation motion. But at the same time, to avoid notch brittleness and catastrophic failure, plastic flow—through motion of large numbers of dislocations—must redistribute any localized high material stresses around both internal and external stress concentrators. This seemingly contradictory requirement imposes rather stringent conditions on the development of alloys that are simultaneously strong and ductile, and leads to the frequent observation of strength varying inversely with toughness. Because of the high strength and toughness combinations achievable in the marage steels, these materials have been intensively studied in recent years. But, in spite of this effort, we have not yet achieved a satisfactory understanding of the basic physical metallurgy and transformation kinetics responsible for the unique properties combination in these intermetallic-strengthened martensitic alloys.

This is particularly true of the important Fe–18% Ni–Co–Mo alloys, additionally hardened with titanium and aluminum. Indeed the basic hardening mechanisms involved are still open to question. For example, though synergistic effects of cobalt–molybdenum interactions have been suggested,[1]* no clearly defined mechanism for this has yet been demonstrated. Matrix hardening by cobalt through an ordering reaction was speculated,[1] and recently, some neutron diffraction data[2] on a related material—i.e., Fe–23% Ni–19% Co alloy—indirectly suggests a possibility of ordering. In a recent paper,[3] the major effects of cobalt were attributed to a vaguely defined "matrix hardening," because only a small amount of cobalt is present in the precipitate. The high toughness of molybdenum-containing iron–nickel alloys was attributed[4] to an absence of precipitation or segregation at grain boundaries, though this was experimentally confirmed only by light metallography and electron fractography. Cobalt was also believed[4] to decrease the solubility of Ni_3Mo in the martensite, and produce a more finely dispersed Ni_3Mo precipitate; hence increasing the strength of the aged alloy.

The age-hardening constituents themselves are still controversial. The major precipitate is believed by some[5-8] to be Ni_3Mo (in a ribbon-like morphology), with a second spherical precipitate of Ni_3Ti; while others[3] suggest Fe_2Mo and Ni_3Ti as the principal precipitate phases causing hardening of the marage steels.

In our research programs,[9] a variety of iron–nickel binary, ternary, quaternary, and more complex alloy systems of high purity were explored for detailed fine structural and property correlations, with a view to developing a better understanding of their basic strengthening mechanisms.

MATERIALS AND PROCEDURE

The chemical compositions of the alloys studied are given in Table I. The alloys were vacuum induction melted (using pure starting materials) in 50 and 30-pound (three- and two-way) split heats, to produce the basic iron–nickel binary, the iron–nickel–cobalt and iron–nickel–molybdenum ternary, and the iron–nickel–cobalt–molybdenum quaternary alloys, along with a comparable marage composition. Titanium and aluminum were singly added to the iron–nickel binary composition at two preselected levels. The cast ingots (2½ in. cross section) were soaked for 16 hr at 815 C (1500 F), and directly reheated to 1245 C (2275 F) for 3½ hr. The ingots were hot press forged

* See references.

† Now at The Franklin Institute Research Laboratories, Philadelphia, Pennsylvania.

TABLE I—Chemical Composition*

% C	% Mn	% P	% S	% Si	% Ni	% Cr	% Mo	% Co	% Ti	% Al	% N	% O	H (ppm)
0.004	0.03	0.002	0.005	0.02	18.20	—	—	—	—	—	0.004	0.013	0.09
0.005	0.02	0.002	0.005	0.01	18.10	—	—	**2.86**	—	—	0.002	0.014	0.07
0.004	0.01	0.002	0.005	0.07	18.05	—	**1.24**	**2.89**	—	—	0.002	0.011	0.03
0.004	0.01	0.002	0.005	0.01	17.85	—	—	**7.91**	—	—	0.002	0.023	0.02
0.004	0.01	0.002	0.005	0.01	17.75	—	**4.03**	**7.80**	—	—	0.002	0.033	1.2
0.004	0.01	0.002	0.005	0.02	17.75	—	**4.03**	**7.84**	**0.37**	**0.07**	0.003	0.017	1.1
0.031	0.01	0.002	0.005	0.02	17.95	None	**1.31**	—	—	—	0.001	0.006	0.5
0.020	0.01	0.002	0.005	0.03	17.70	None	**4.64**	—	—	—	0.001	0.017	1.3
0.016	0.01	0.002	0.004	0.04	17.30	—	—	—	**0.56**	—	0.002	0.005	0.5
0.016	0.01	0.002	0.008	0.04	17.30	—	—	—	**1.12**	—	0.001	0.003	0.2
0.010	<0.01	0.002	0.009	0.05	17.55	—	—	—	—	**1.00**	0.002	0.001	0.2
0.013	<0.01	0.002	0.007	0.05	17.45	—	—	—	—	**2.56**	0.001	0.0008	0.5

* Weight percent analysis on ingot stock.

into 2 x 2 in. billets. The billets were reheated four hours at 1205 C (2200 F), air cooled, then hot rolled from 1095 C (2000 F) into 1 x 2 in. sheet bars, which were further hot rolled with a 1095 C (2000 F) reheat to 0.15-in. thick strips.

Bulk samples (⅝ by ¾ by ⅛ in.) were heat treated in neutral salt baths; samples for thin-section electron microscopy (0.6 by 0.7 by 0.003 in.) were sealed in evacuated quartz capsules and heat treated. Samples were austenitized at 815 C (1500 F) for one hour, and air cooled; they were refrigerated in liquid nitrogen for 15 min to minimize retained austenite. A higher austenitizing temperature (1150 C (2100 F) for one hour and water quench) was used, in selected cases, to better dissolve carbides and intermetallic compounds. Alloys were aged from 315/540 C (600/1000 F) for times to 100 hr; but the 480 C (900 F) and 540 C (1000 F) aging treatments were emphasized. The hardening response of the alloys was studied in detail both isochronally (three-hour aging at temperatures from 315/540 C, 600/1000 F), and isothermally near the critical age-strengthening region (425/540 C, 800/1000 F, from ½ to 100 hr). However, in this discussion, only the isochronal studies will be emphasized.

Rockwell hardness of the bulk samples and Vickers DPH hardness for the thin-section samples gave the aging response. Hot stage metallography was used for martensite transformation temperatures; while thermal arrest curves gave the austenite reversion temperatures. X-ray integrated intensity measurements gave quantitative measures of reverted austenite.

Uranium shadowed parlodion surface replicas were used. Extraction replicas were prepared by stripping plastic replicas from lightly etched surfaces, carbon coating the stripped replicas and subsequently dissolving the plastic backing, leaving a carbon film containing the precipitate; specimens were lightly etched to avoid pickup of reverted austenite. For X-ray diffraction, extraction replicas were placed on the end of a glass fiber; while for electron probe microanalysis[10] of extraction replicas, stacked multiple layers (15–20) were mounted on a carbon block. The quantitative probe data,* in every case, was corrected for absorption and fluorescence effects.[10]

Some samples for transmission electron microscopy were prepared using a virtual cathode electrolytic polishing technique.[9] However, a simpler "window technique," with an edge-coated sample as anode suspended between two flat cathodes in a beaker of electrolyte produced equally satisfactory thin areas, and required less time. Foils 0.001 in. thick were directly thinned by this technique; the electrolyte was a 10:1 chromic-acetic acid solution. Thicker samples

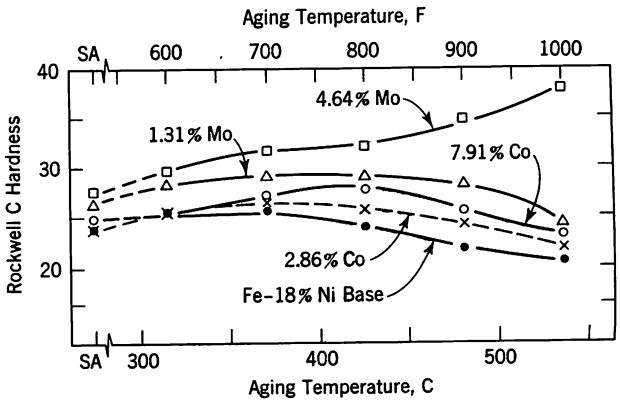

FIGURE 1. Aging curves showing effects of cobalt and molybdenum on the Fe–18% Ni binary base. Aging time three hours

* The precision of these measurements is estimated to be better than 5% of the amount present; cobalt (only 2% in the precipitate) is an exception, where the precision is 10% of the amount present.

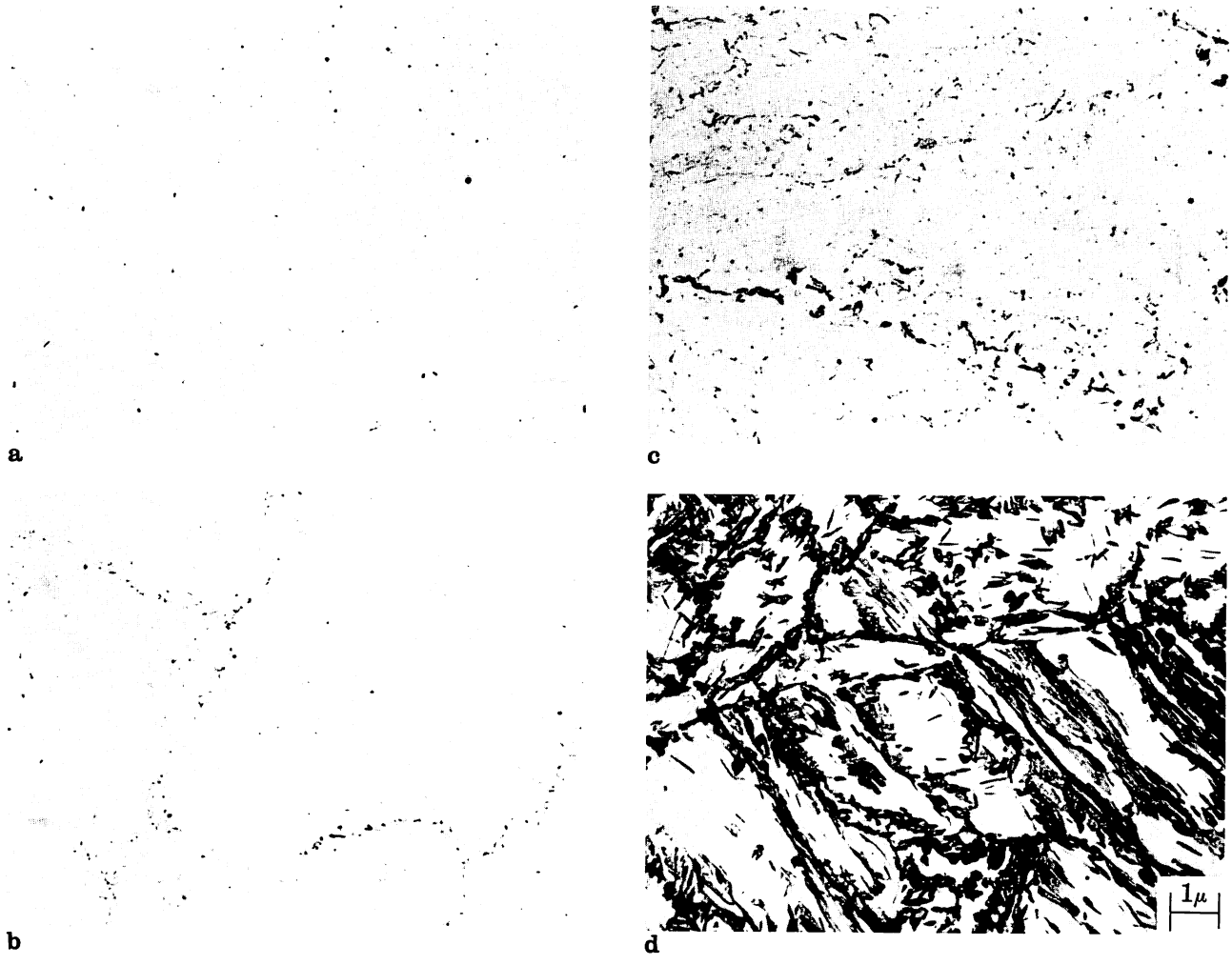

FIGURE 2. Extraction replica micrographs of quenched and aged Fe–18% Ni binary base

a. quenched
b. aged at 425 C (800 F) for three hours
c. aged at 480 C (900 F) for three hours
d. aged at 540 C (1000 F) for three hours

were first mechanically ground to 0.002 in., and chemically thinned to 0.001 in., in a 50% solution of hydrogen peroxide (30% concentration) and phosphoric acid (ortho, 85% concentration), prior to the final electrolytic polishing step.

RESULTS

The high-strength 18% Ni marage alloy is a complex six-component material where the strengthening mechanism and age-hardening constituents still remain controversial. Recent electron diffraction data[11,12] from extraction replicas of the commercial alloy failed to uniquely identify the hardening precipitates because of the superposition of diffraction lines from various possible intermetallic precipitates. Therefore, the individual effect of each element on binary and ternary compositions was investigated.

Iron–Nickel Binary

The iron–nickel binary alloy, upon isothermal aging at various temperatures, showed a gradually declining hardness, as seen in Figure 1. Correspondingly, the extraction replica micrographs from the binary alloy showed no general precipitation until 425 C (800 F), when some reversion to austenite began; reversion was further accelerated at higher temperatures (see Figure 2). The M_s temperature of the iron–nickel binary was 290 C (555 F).

Cobalt and Molybdenum

Because both cobalt and molybdenum are major matrix strengtheners, these two elements and their interactions must be examined together.

Cobalt Adding 3 and 8% Co (see Figure 1) produces no perceptible solid-solution hardening, but definitely retards the softening upon heating at temperatures up to 425 C (800 F). Extraction replica micrographs, taken from the ternary alloy, after aging at temperatures up to 540 C (1000 F), showed

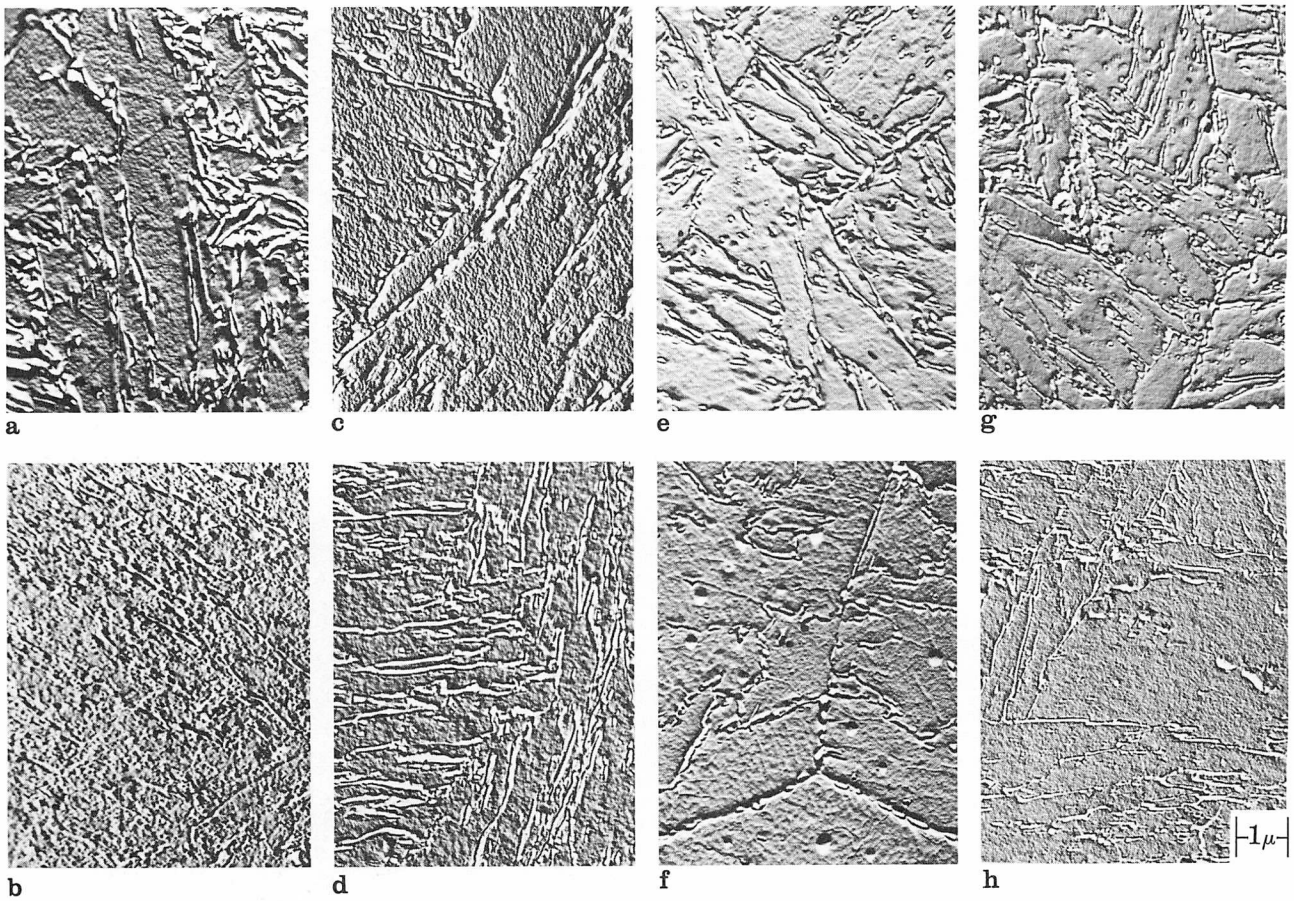

FIGURE 3. Surface replica micrographs of Fe–18% Ni binary base alloys with various added elements after aging three hours at 540 C (1000 F)

a. Fe–18% Ni base
b. marage composition
c. base + 1% Mo
d. base + 4% Mo
e. base + 3% Co
f. base + 8% Co
g. base + 1% Mo + 3% Co
h. base + 4% Mo + 8% Co

TABLE II Interplanar Spacings of Precipitates from Extraction Replicas of the Molybdenum—Ternary and Molybdenum—Cobalt Quaternary Alloys

Base + 4% Mo[a]			Base + 4% Mo + 8% Co[b]			Standard σ Fe Mo[c]	
Electron Diffraction d(Å)	X-Ray		Electron Diffraction d(Å)	X-Ray			
	d(Å)	I		d(Å)	I	d(Å)	I
	2.40	VW		2.35	VVW	2.35	50
2.17	2.20	S	2.19	2.19	S	2.21	100
	2.14	M		2.14	M	2.13	60
	2.08	VW		2.07	M	2.08	60
2.04	2.0	M (Broad)	2.03	2.03	M	2.04	70
				2.00	M	1.99	100
			1.92	1.91	VVW	1.93	60
				1.89	VVW	1.90	30
1.29	1.28	VW	1.29	1.28	VW	1.28	100
	1.24	VW	1.25	1.24	VW	1.246	70
1.07			1.07			1.068	100

[a] Quenched from 1150 C (2100 F) and aged 22 hr at 540 C (1000 F).
[b] Quenched from 1150 C (2100 F) and aged 6 hr at 540 C (1000 F).
[c] ASTM X-ray data.

no general precipitates; and the replicas were essentially similar to Figure 2. But the reversion reaction is definitely retarded (see Figure 3).

Molybdenum Adding 1 and 4% Mo to the iron–nickel binary alloy introduces increasing solid-solution hardening (see Figure 1). With 1% Mo, the solid-solution hardening was retained throughout the aging sequence; but with 4% Mo, the hardness substantially increased throughout the aging sequence up to 540 C (1000 F), and the alloy did not overage at 480 C (900 F) up to 100 hours of aging (see Figure 11). Molybdenum also effectively retards reversion (see Figure 3); although, on a weight percent basis, cobalt seems to be more potent.

In addition to retarding reversion and strengthening the solid-solution, molybdenum is also effective as a precipitation strengthener. X-ray and electron diffraction data from the aged molybdenum ternary showed an intermetallic compound, σFeMo; Table II illustrates the observed interplanar spacings. Electron probe microanalysis of somewhat overaged* precipitates showed a calculated stoichiometry of $(Ni_{0.3}\ Fe_{0.7})Mo$. This corresponds to the diffraction-identified structure of σFeMo. The morphology of the σFeMo precipitate begins with a ribbon-like form at 480 C (900 F), but changes to a spheroidal form at 540 C (1000 F) aging (see Figure 4).

Because the role of the individual alloying elements was unresolved, certain elements have sometimes been assigned special attributes. Thus, molybdenum was claimed[4] to improve toughness of the marage alloys because it prevents segregation or precipitation at the boundaries, thereby lowering the propensity to grain-boundary cracking. However, the apparent absence of grain boundary etching in molybdenum-containing alloys seems to be an etchant dependent artifact. The marked difference in etching behavior of the Fe–18% Ni–4.64% Mo alloy, when etched with nital and with picral, is shown in Figure 5. Nital delineates the prior austenite grain boundaries, while the martensitic structure remains indistinct. In contrast, picral reveals the blocky martensite in excellent relief, but the prior austenite boundaries are indistinguishable, except by inference.

Surface replica electron microscopy provides the reasons for this difference. Figure 6 shows the austenite boundaries delineated by a nital etch; but only martensite relief is shown by a picral etch. The boundaries are selectively attacked by nital because of the fine undissolved residual molybdenum carbides (M_6C), present (Figure 6) in them; but picral does not readily attack these carbides, and this accounts for the marked etchant-dependent difference. This

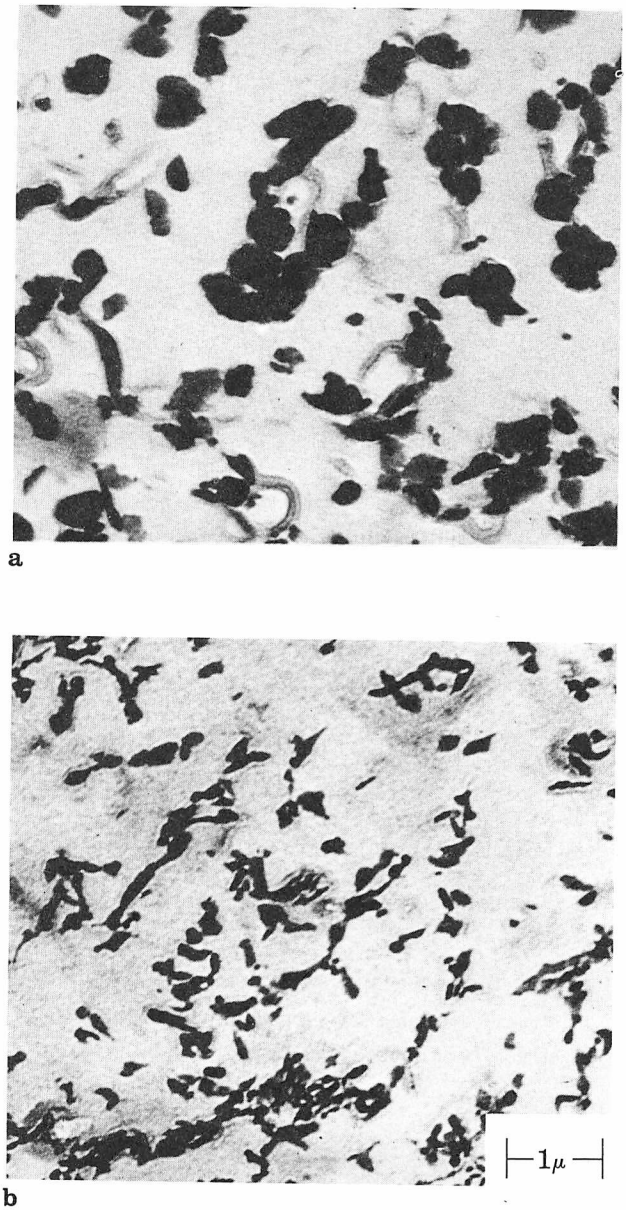

FIGURE 4. Extraction replica micrographs of σ FeMo precipitate in Fe–18% Ni binary base + 4% Mo alloy as quenched from 1150 C (2100 F) and aged three hours

a. aged at 540 C (1000 F)

b. aged at 480 C (900 F)

etching difference, if properly interpreted, can be used to identify the carbide. But, the grain boundaries are clearly not immune to precipitation, and some other explanation must be sought for the toughness achieved with molybdenum.

Cobalt Plus Molybdenum Cobalt and molybdenum, simultaneously added to the Fe–18% Ni binary, produce additive hardening effects. Three percent cobalt, added to the 1% Mo ternary alloy, produces

* Quenched from 1150 C (2100 F) with six hour aging at 540 C (1000 F).

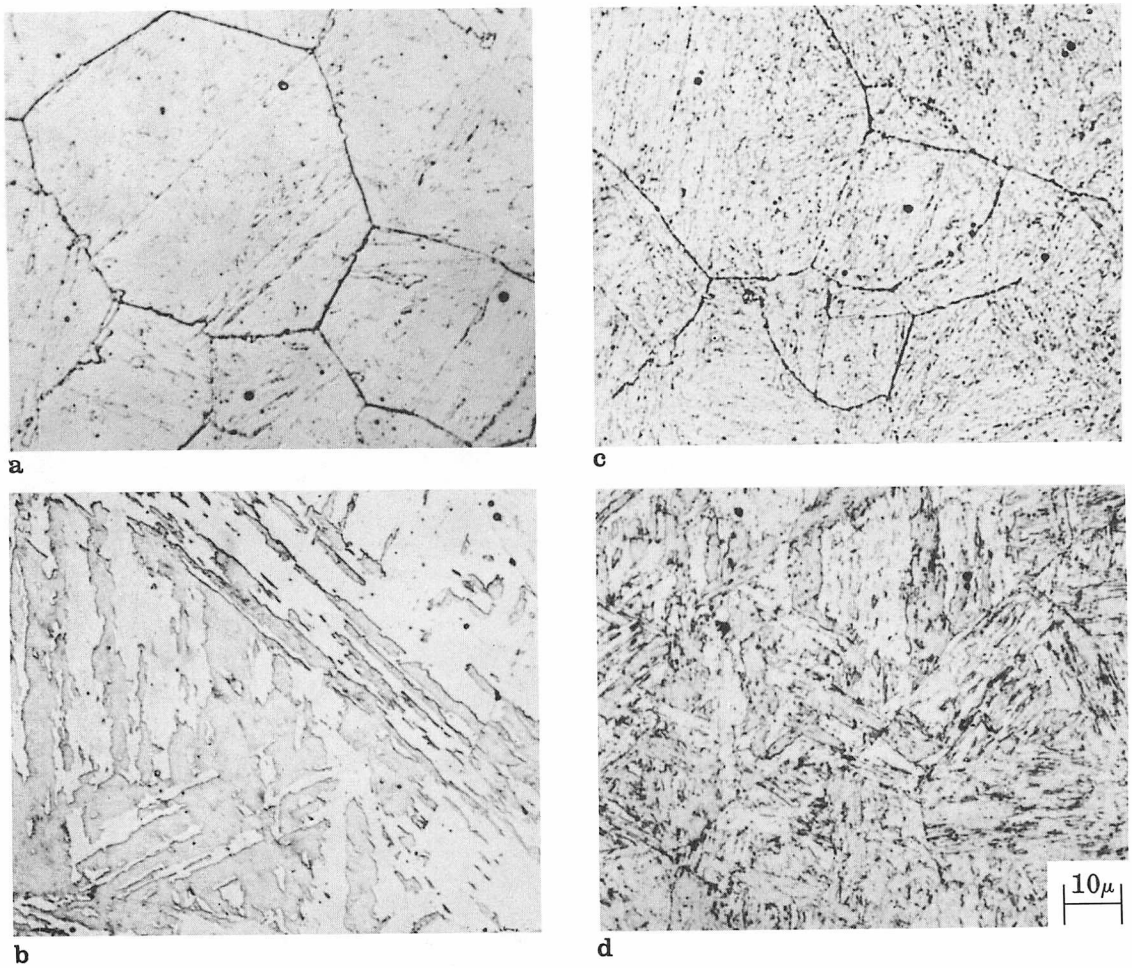

FIGURE 5. Etch-dependent structures in Fe–18% Ni binary base + 4% Mo alloy

a. structure as quenched etched with 3% nital
b. structure as quenched etched with picral/HCl
c. structure as quenched and aged three hours at 480 C (900 F) etched with 3% nital
d. structure as quenched and aged three hours at 480 C (900 F) etched with picral/HCl

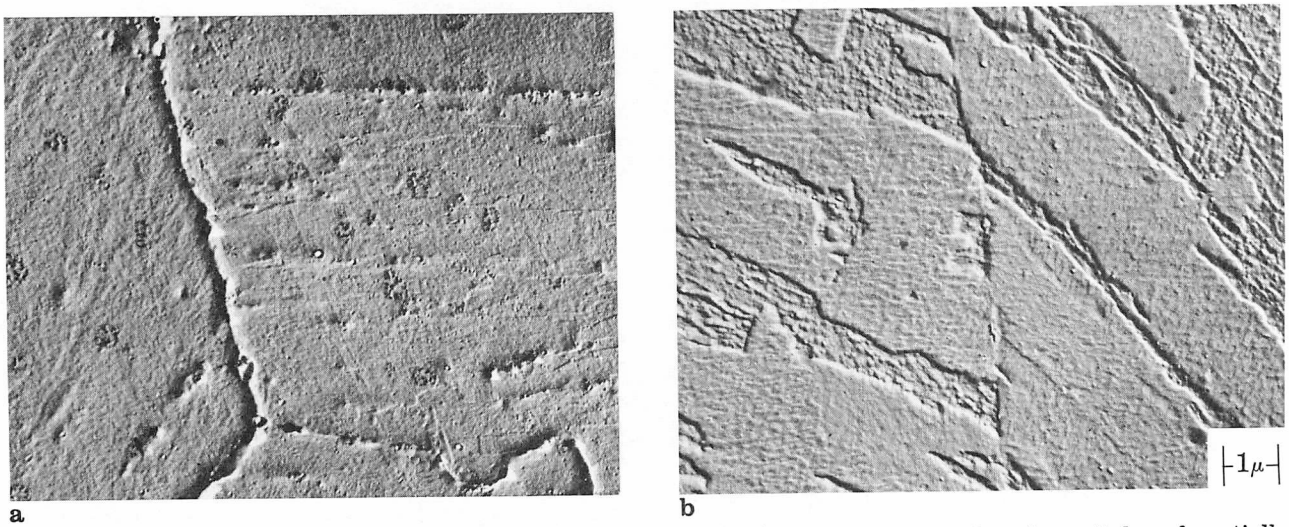

FIGURE 6. Surface replica micrographs of unaged Fe–18% Ni binary base + 4% Mo alloy show nital preferentially attacks boundaries while picral reveals the martensite laths

a. nital etchant
b. picral + two drops HCl etchant

little additional change (see top graph Figure 7). But, 8% Co, added to the 4% Mo ternary, slightly hardens the solid-solution; also, some increased resistance to softening is observed on aging above 370 C (700 F). On the other hand, adding 1 and 4% Mo substantially age-strengthens the cobalt

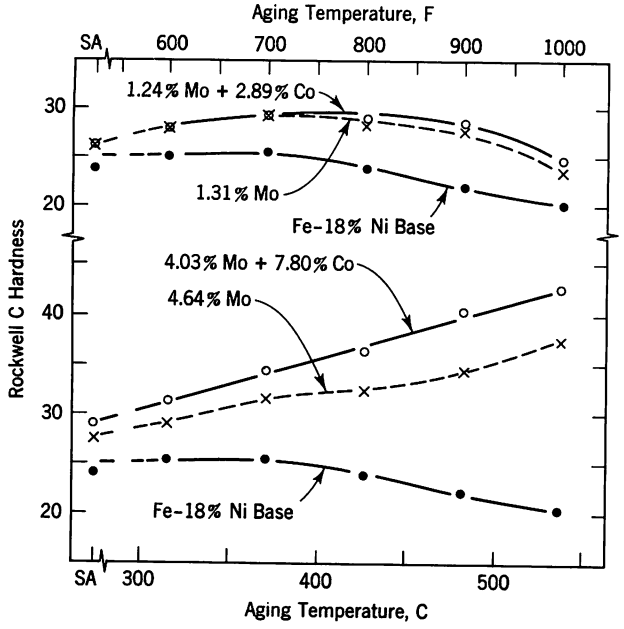

FIGURE 7. Aging curves showing effect of adding cobalt to the molybdenum ternary alloys. Aging time three hours

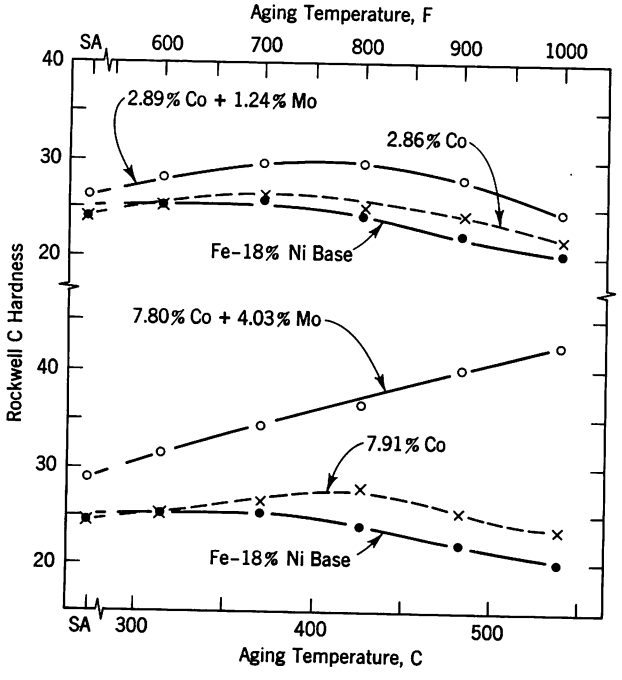

FIGURE 8. Aging curves showing effect of adding molybdenum to the cobalt ternary alloys. Aging time three hours

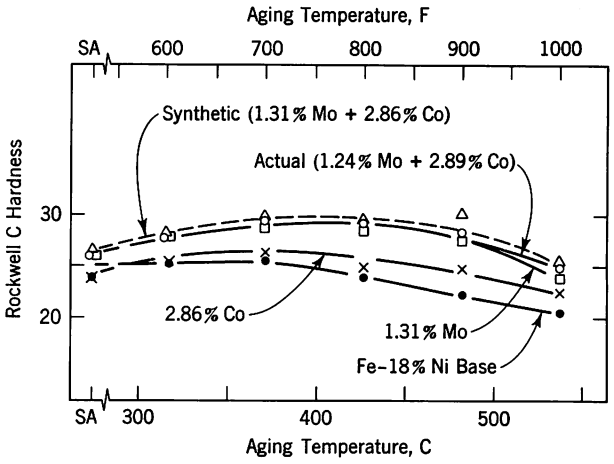

FIGURE 9. Aging curves showing simple additive role of cobalt and molybdenum. Aging time three hours

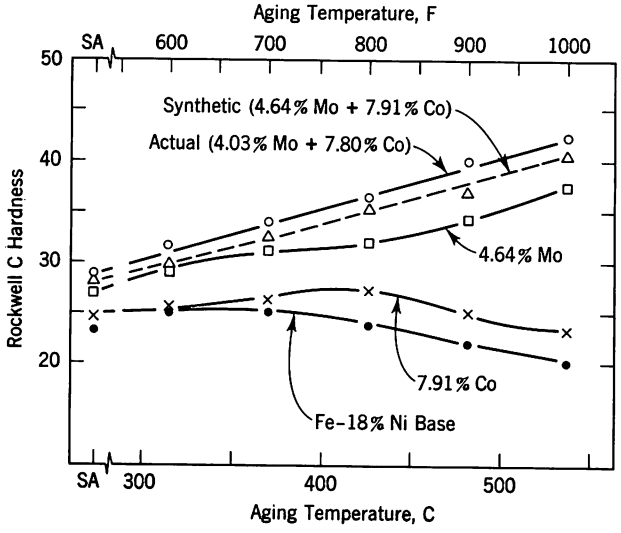

FIGURE 10. Aging curves showing simple additive role of cobalt and molybdenum. Aging time three hours

ternary compositions (see Figure 8), analogous to the effects of molybdenum on the iron–nickel binary.

The additive hardening of cobalt and molybdenum is further explained in Figures 9 and 10. In Figure 9, the top solid curve shows the aging response of the 1% Mo–3% Co quaternary alloy, while the dashed curve is obtained by summing the differential hardening due to the two lower curves corresponding to the 3% Co and 1% Mo alloys respectively. Similarly, Figure 10 shows the summed synthetic and actual curves for the 4% Mo and 8% Co contributions. In each case, the synthetic curve almost coincides with the actual, demonstrating the simple additive contributions of the alloy elements, rather than a synergistic effect.

Synergism is defined as "the cooperative action of

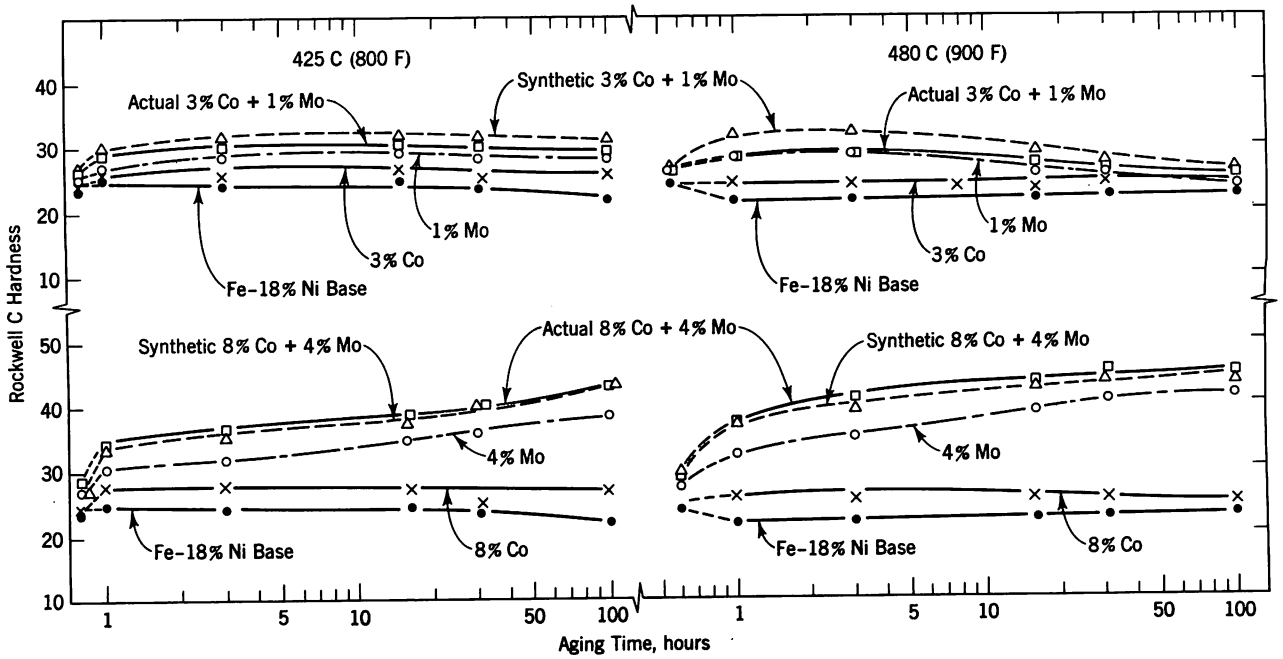

FIGURE 11. Isothermal aging curves of the cobalt and molybdenum ternary alloys and the cobalt–molybdenum quaternary alloys

TABLE III Maximum Age Hardening of Cobalt and Molybdenum Alloys

Nominal Addition to Fe–18% Ni Base	425 C (800 F)		480 C (900 F)	
	Time hr	Maximum Hardness Rockwell C	Time hr	Maximum Hardness Rockwell C
8% Co	1	28.3	16	25.8
4% Mo	100	39.3	100	40.5
Actual 8% Co + 4% Mo	100	43.6	32	44.9
Synthetic 8% Co + 4% Mo	—	42.5	—	44.7
3% Co	16	27.1	100	25.3
1% Mo	16	29.3	3	28.5
Actual 3% Co + 1% Mo	32	30.6	1	28.4
Synthetic 3% Co + 1% Mo	—	32.1	—	31.7

discrete agencies such that the total effect is greater than the sum of the two effects taken independently." Decker et al[1] derived the synergistic effect of molybdenum–cobalt interactions by comparing the maximum hardness from age hardening at 425/480 C (800/900 F) of a 7% Co–4% Mo, and a 7% Co–5.5% Mo alloy with a hardness maximum curve for various molybdenum contents in iron–nickel binary alloys. But the separate contribution of cobalt in retarding the normal softening of the iron–nickel binary may have been neglected.

Analogous data on maximum age-hardening of the cobalt and molybdenum ternary alloys, as well as the cobalt–molybdenum quaternary alloys derived from isothermal hardening curves (Figure 11) are shown in Table III. In this table, the "synthetic" cobalt plus molybdenum hardness values were derived from the hardness maximum at each aging temperature of the isothermal aging curve according to the following formula: (maximum hardness of cobalt ternary alloy minus maximum hardness of iron–nickel binary) plus maximum hardness of molybdenum ternary alloy. Again, simple additive (nonsynergistic) hardening contributions are confirmed. Similarly, by plotting the isothermal hardening curves themselves, Figure 11 shows the 3% Co–1% Mo, and the 8% Co–4% Mo curves almost coincide with the summed synthetic curves throughout the aging period of 0.5 to 100 hr at temperatures of 425 and 480 C (800 and 900 F). Thus, both isochronal and isothermal data,

as well as hardness maximum data demonstrate the simple additive contributions of cobalt and molybdenum; and there is no synergism.

Cobalt and molybdenum, together, quite effectively retard reversion (Figure 3); the reversion kinetics in these alloys favorably compare with those of the marage composition. Correspondingly, both cobalt and molybdenum raise the A_s temperature of the iron–nickel alloys. For the 18% Ni binary the A_s temperature is 580 C (1080 F), while with 8% Co it is 667 C (1233 F), and with 4% Mo it is 623 C (1154 F).

As previously indicated, X-ray and electron diffraction data from the aged cobalt–molybdenum quaternary alloys were similar to those of the aged molybdenum ternary alloys (compare data in Table II), and showed the presence of an intermetallic compound corresponding to σFeMo. Also, the calculated stoichiometry of the intermetallic compound, from microprobe analysis, was $(Ni_{0.4}\,Fe_{0.6}\,Co_{0.05})Mo$ for these precipitates. Neither Ni_3Mo nor Fe_2Mo appears to form in these systems; upon adding cobalt to the iron–nickel–molybdenum ternary, the σFeMo structure persists, with some (about 2 weight percent) cobalt dissolved in the precipitate.

The precipitate morphology of the molybdenum–cobalt quaternary alloy is also the same as that of the molybdenum ternary. But with similar aging treatments, the precipitate size remains significantly smaller, though the number of particles is greater in the quaternary alloy, particularly at the 480 C (900 F) aging (compare Figures 12 and 4). Thus cobalt seems to favor an increased nucleation rate.

Titanium

Titanium—a strong carbide former—exhibits solute-depletion softening (see Figure 13) in the unaged condition at low substitutional solute concentrations (e.g., 0.56% Ti). This suggests solute (titanium) depletion in the solid-solution by forming titanium–carbon–nitrogen complexes during solution treating at 815 C (1500 F). Analogous effects were observed[9] for other carbide formers, such as columbium, chromium, etc. However, with an excess of the solute, as with the 1.12% Ti alloy, the solid-solution hardness returns to that of the Fe–18% Ni binary level. Additionally, titanium is a potent precipitation hardening agent, as seen in Figure 13.

Titanium raises both the M_s and the A_s temperatures, raising the M_s temperature to 303 C (578 F) with 1.2% Ti, and retarding reversion to the extent of only 1% reverted austenite after aging for three hours at 540 C (1000 F).

Electron diffraction data for an aged iron–nickel–titanium alloy, Table IV, correspond to the hexagonal Ni_3Ti precipitate; however, there is one extra line of weak intensity at 1.44Å, which remained unidentified. The diffraction patterns of this intermetallic

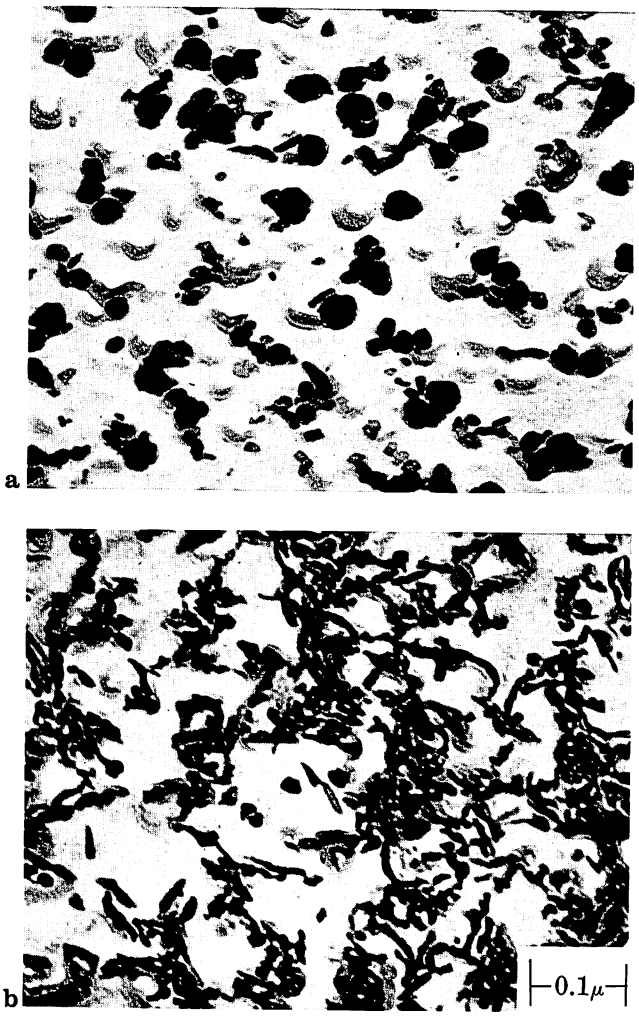

FIGURE 12. Extraction replica micrographs of σFeMo precipitate in Fe–18% Ni binary base + 4% Mo + 8% Co alloy as quenched from 1150 C (2100 F) and aged three hours

a. aged at 540 C (1000 F) b. aged at 480 C (900 F)

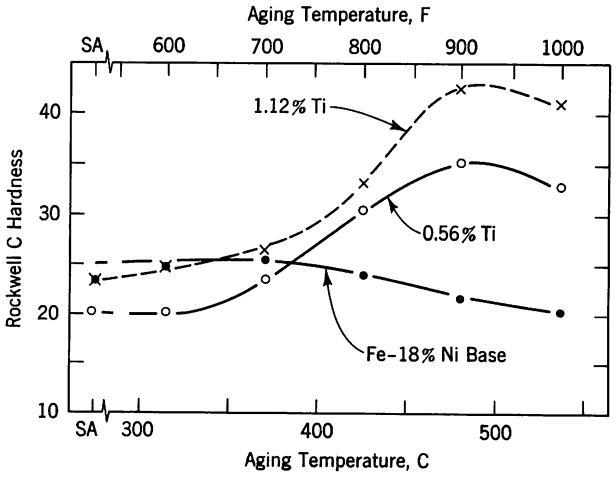

FIGURE 13. Aging curves showing effect of titanium on the Fe–18% Ni binary base. Aging time three hours

TABLE IV Interplanar Spacings of Precipitate from Extraction Replicas of 18% Ni–1% Ti Alloy [a]

Electron Diffraction		Standard Ni_3Ti [b]	
d(Å)	I	d(Å)	I
2.20	MS	2.21	20
2.10	S	2.13	50
		2.07	50
1.99	VS	1.95	100
1.76	W	1.72	20
1.44	W		
1.29	MS	1.276	50
1.18	M Broad	1.173	20
1.09	MS	1.095	10
0.87	W		
0.82	MW		

[a] Quenched from 1150 C (2100 F) and aged 6 hr at 540 C (1000 F).
[b] ASTM X-ray data.

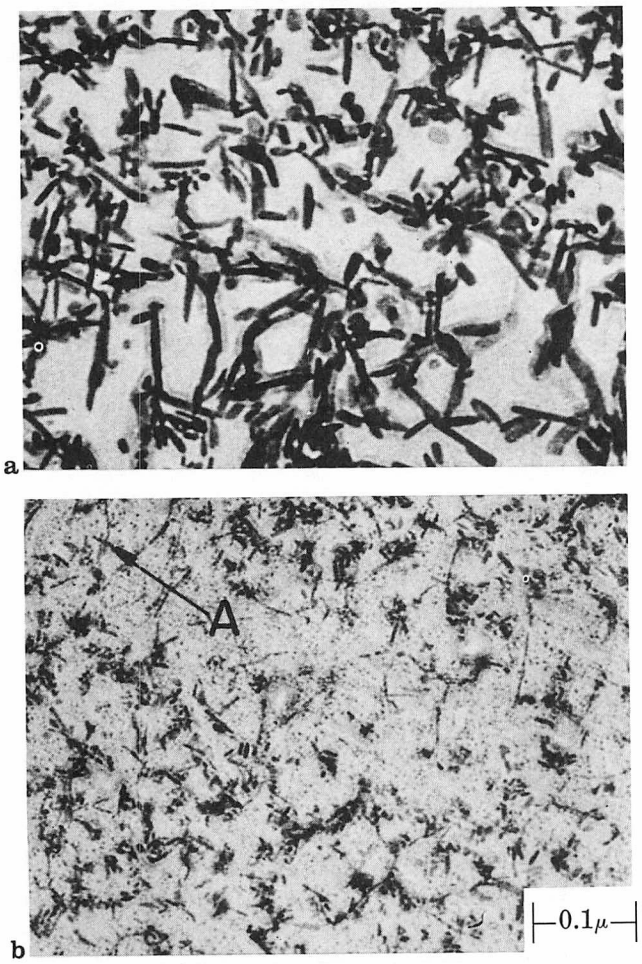

FIGURE 14. Extraction replica micrographs of η Ni_3Ti precipitate in Fe–18% Ni binary base + 1% Ti alloy as quenched from 1150 C (2100 F) and aged three hours

a. aged at 540 C (1000 F) b. aged at 480 C (900 F)

compound, unlike those from the iron–nickel–molybdenum–cobalt alloy, show arcing of the diffraction lines, suggesting a preferred orientation of the precipitate. Electron probe microanalysis established the precipitate composition as $(Ni_{2.9}\,Fe_{0.1})Ti$. The Ni_3Ti precipitate morphology is shown in Figure 14; an irregular stringer morphology predominates at 480 C (900 F), but at 540 C (1000 F) a flat ribbon form is observed. The irregular stringers at 480 C (900 F) may be aggregates of fine spheroidal particles which are seen throughout the structure. In specific areas (A), the stringers are clearly aggregates of spherical particles, which may have precipitated upon dislocation lines.

Aluminum

Aluminum contributes both marked solid-solution strengthening and age-hardening to the Fe–18% Ni

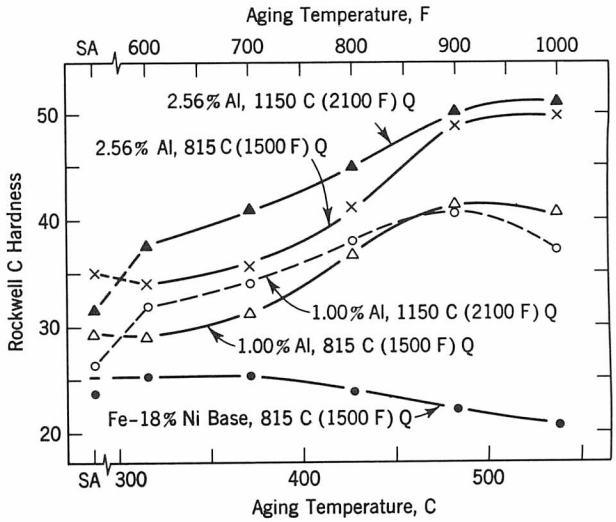

FIGURE 15. Aging curves showing effect of aluminum on the Fe–18% Ni binary base. Aging time three hours

TABLE V Interplanar Spacings of Precipitate from Extraction Replicas of 18% Ni–3% Al Alloy [a]

Electron Diffraction	X-Ray		Standard NiAl [b]	
d(Å)	d(Å)	I	d(Å)	I
	2.85	VVW	2.87	40
2.02	2.03	VS	2.02	100
	1.66	VVW	1.66	20
1.43	1.43	VVW	1.43	20
	1.28	VVW	1.28	10
1.17			1.17	70
1.01			1.015	20

[a] Quenched from 1150 C (2100 F) and aged 22 hr at 540 C (1000 F).
[b] ASTM X-ray data.

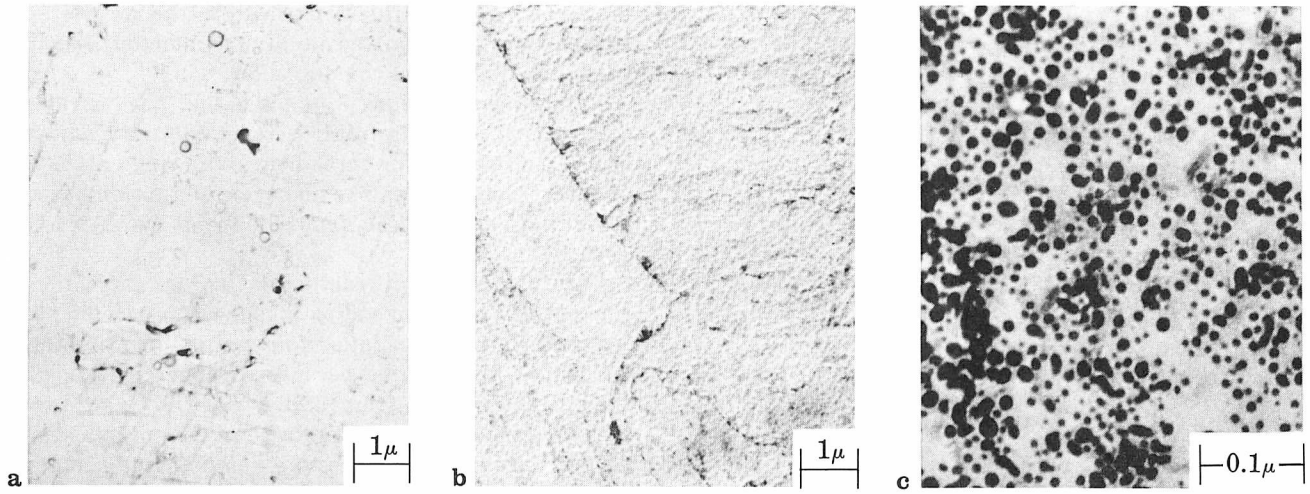

FIGURE 16. Extraction replica micrographs of Fe–18% Ni binary base + 2.56% Al alloy as quenched from 1150 C (2100 F)

a. aged at 480 C (900 F) for 3 hr b. aged at 540 C (1000 F) for 3 hr c. aged at 540 C (1000 F) for 22 hr

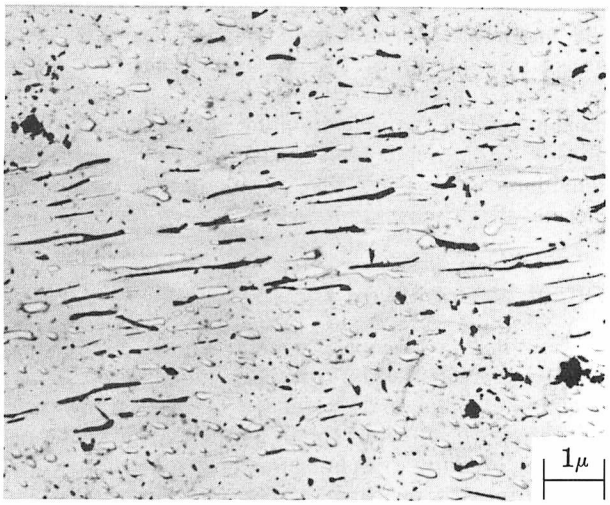

FIGURE 17. Extraction replica micrograph of Fe–18% Ni binary base + 2.56% Al alloy showing lathlike precipitates as quenched from 815 C (1500 F)

binary base (see Figure 15). Using a 1150 C (2100 F) solution treating temperature, all of the aluminum can be held in solid-solution, and aging produces a high hardness. However, if a standard 815 C (1500 F) solutionizing temperature is used, the aging is less pronounced.

Aluminum raises the M_s temperature to 316 C (589 F) at 2.56% Al, but has no observed effect on the reversion.

Electron diffraction data (Table V) from extraction replicas of 1150 C (2100 F) austenitized plus somewhat overaged specimens show an NiAl precipitate. Electron probe microanalysis established the precipitate composition as $(Ni_{0.7}\ Fe_{0.3})$ Al. The NiAl precipitates, formed at aging temperatures of 480 C or 540 C (900 F or 1000 F), have a spheroidal morphology, as seen in Figure 16. The precipitate in the 480 C (900 F) three-hour aged condition is extremely fine; however, with some overaging, the precipitates were resolvable.

It will be recalled that solution treating at 815 C (1500 F) produced a lower age-strengthening potential (see Figure 15). Extraction replicas from specimens directly quenched from 815 C (1500 F) showed some lathlike precipitates (see Figure 17) which were identified by electron diffraction as NiAl, and analyzed by the electron probe as $(Ni_{0.7}\ Fe_{0.3})$ Al. Thus, the commercial solutionizing treatment of 815 C (1500 F) in the marage alloy may well combine precipitates of this lathlike NiAl formed during the solution treatment, in addition to NiAl precipitates with a spheroidal morphology subsequently formed during aging at 480 C (900 F). Although we must remember that aluminum, added as a deoxidizer, is maintained at <0.15%, therefore the actual amount of NiAl in a commercial marage alloy would be small, if any.

Marage Composition

The age-hardening response of a commercial marage-type composition (4.03% Mo, 7.84% Co, 0.37% Ti, 0.07% Al, 18% Ni, balance iron) is compared in Figure 18 to the quaternary equivalent, and the Fe–18% Ni binary composition. While the 4% Mo–8% Co quaternary alloy has a linear response to aging throughout the aging sequence of 315/540 C (600/1000 F); the titanium–aluminum additions reduce the solid-solution hardness—analogous to the effects of titanium on the binary iron–nickel base (discussed in an earlier section). In fact, the hardness of the marage composition does not cross the quaternary aging curve until an aging temperature of 400 C (750 F)

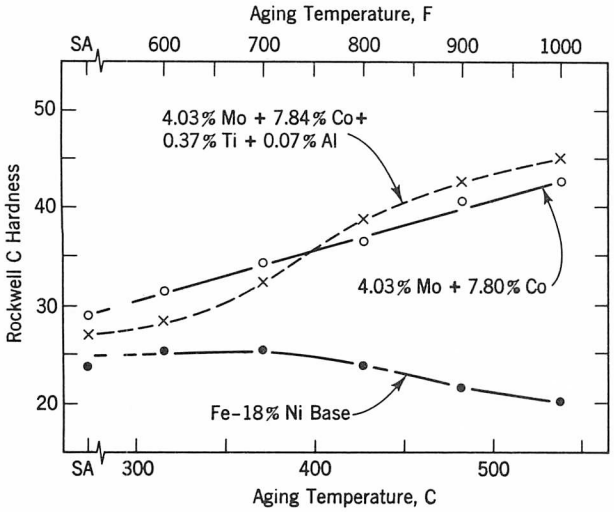

FIGURE 18. Aging of the marage alloy compared with that of the Fe–18% Ni binary base and the base + 4% Mo + 8% Co alloy. Aging time three hours

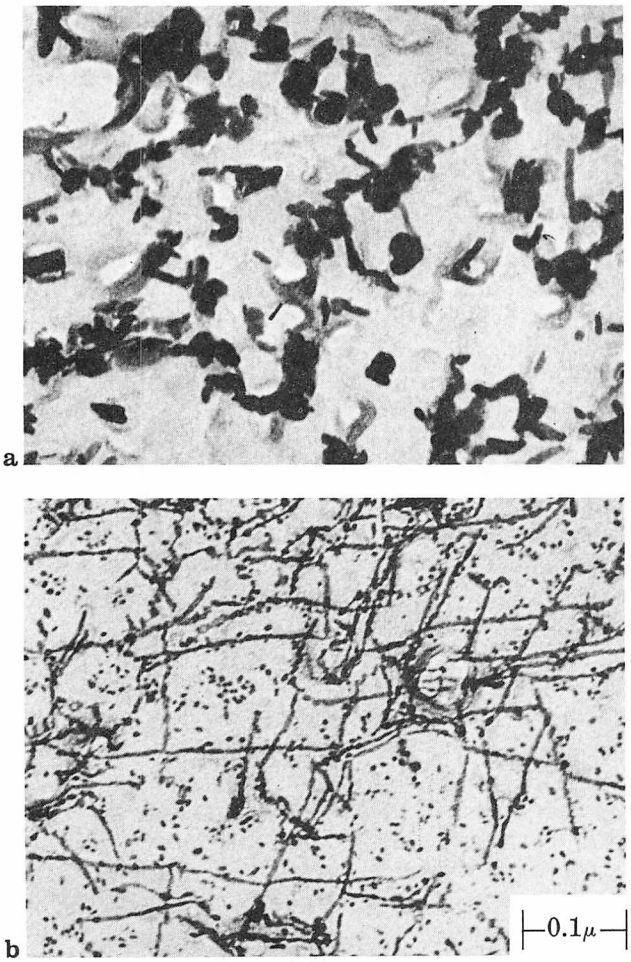

FIGURE 19. Extraction replica micrographs of precipitate in marage composition as quenched from 1150 C (2100 F) and aged three hours

a. aged at 540 C (1000 F) b. aged at 480 C (900 F)

is reached. Beyond this temperature, the precipitation agents (titanium and aluminum) add to the final hardness of the aged complex alloy.

Referring to Figure 3, we see that the marage composition markedly retards reversion upon aging at 540 C (1000 F) for three hours, showing only 5% of reverted austenite. The marage composition has a somewhat depressed M_s temperature of about 261 C (505 F).

Careful electron diffraction data from extraction replicas of the marage alloy (made from pure starting materials) again failed to definitely identify the hardening precipitates because of superposition of the diffraction lines from similarly diffracting intermetallic structures (see Table VI). The morphology of precipitates in the marage composition (4.03% Mo–7.84% Co–0.37% Ti–0.07% Al) is illustrated in Figure 19. In the 480 C (900 F), three-hour aged condition, the precipitates are mainly individual spherical particles, or stringers of particles, suggesting precipitation upon dislocation lines. The diffraction pattern does not clearly identify the precipitates, and the spherical morphology could represent several precipitates; but both σFeMo, and the Ni_3Ti precipitates are consistent with the observed precipitate morphology in the marage alloy. Thus, the observed phases, σFeMo, and Ni_3Ti, with some NiAl must be considered as possible precipitates in the aged commercial alloy.

Effect of Cobalt on the Matrix

So far, the role of cobalt, which seems to produce no definite precipitates, but provides added strength and hardness to the matrix, has remained a mystery. Therefore, the effect of cobalt on the matrix structure was explored by transmission electron microscopy.

Cobalt, with an estimated stacking fault energy (SFE) of about 20 erg/cm^2, [13,14] may be expected to lower the stacking fault energy of the iron–nickel (estimated 75 erg/cm^2) matrix. That this is indeed the case for the face centered cubic structure is illustrated in Figure 20. The 8% Co ternary alloy, upon aging 32 hr at 540 C (1000 F), shows stacking fault contrast of substantial width in the reverted austenite compared to the similarly aged iron–nickel binary alloy which shows only dislocation tangles. The striations parallel to the partials are a moiré pattern produced probably by alloy element segregation and consequent change in lattice parameter at the fault regions. The presence or absence of stacking faults in the face centered cubic structure does not mean that a corresponding effect on the stacking fault energy must persist in the body centered cubic phase. Therefore, observable parameters in the bcc structure, which significantly depend upon the stacking fault energy, were carefully explored. Thus, cell size was directly measured in quenched and cold-

worked martensitic structures; and twin-density was determined in the low-temperature deformed matrix.

Figure 21 shows a well developed cell structure in the quenched martensite of the 18% Ni binary alloy, with increased dislocation density in the cell walls, and relatively low density in the cell interiors; and this remains substantially unaltered upon adding 4% Mo to the binary alloy—as seen at the top center. But cobalt retards cell development in the ternary, producing a more uniform dislocation density throughout the structure (see Figure 21). Though some cell structure is still seen in the cobalt–molybdenum quaternary alloy, the average cell is smaller.

Similarly, as shown in Figure 22, upon cold rolling these alloys (about 5% rolling deformation at room temperature), cell structures are well developed in the iron–nickel and the iron–nickel–molybdenum alloys, but in the cobalt-containing ternary and quaternary alloys the cells are again smaller. Low-temperature deformations (15% rolling reduction at −196 C, −320 F) produced[9] similar results, with the cobalt-containing alloys having a higher dislocation density, and smaller average cell size.

The average cell size in the foils is given in Table VII as a function of rolling reductions at room and liquid-nitrogen rolling temperatures. The data were obtained from measurements on three micrographs (at 74,000X) for each; between 250 and 300 intercepts for each condition provided the statistics. The cell size remained relatively independent of reduction or rolling temperature, but was consistently smaller for alloys containing cobalt than for those free from cobalt. The ratio of cell size in the cobalt-free to cobalt-containing alloys varied from 1.2 to 1.9.

Low-temperature impact deformation produced deformation twins (see Figure 23) in the 4% Mo alloy, and the 4% Mo–8% Co alloy. Specimens, solution treated at 1150 C (2100 F) and water quenched, were similarly hammer deformed at −196 C (−320 F) and metallographically examined. Twin frequency was measured on 12 to 15 micrographs at 500X. On each alloy, about 800 twins were counted for the twins/mm² values, and about 700 twins for the twins per martensite lath data.

Alloy	Twins/mm²	Twins/Martensite Lath
Fe–Ni + 4% Mo	1.40×10^3	5.56
Fe–Ni + 4% Mo + 8% Co	1.52×10^3	7.77

TABLE VI Interplanar Spacings of Precipitate from Extraction Replicas of Marage Composition Compared with Those of Standards[a]

Electron Diffraction Data on 18% Ni Marage Alloy		Standards[b]									
		Ni_3Mo		Ni_3Ti		Fe_2Ti		Fe_2Mo		σFeMo	
d(Å)	I[c]	d(Å)	I	d(Å)	I	d(Å)	I	d(Å)	I	d(Å)	I
				2.56	10						
						2.40	50	2.36	60	2.35	50
2.19	M	2.22	M	2.21	20	2.20	75	2.18	100	2.21	100
2.10	S	2.11	S	2.13	50					2.13	60
				2.07	50	2.04	100	2.05	60	2.08	60
										2.04	70
		1.97	S								
2.00	M	1.95	VS	1.95	100	2.00	100	2.02	100	1.99	100
						1.96	50	1.98	60	1.93	60
						1.83	50				
				1.72	20	1.77	35				
						1.62	10				
1.53	M	1.52	M	1.54	10						
				1.51	20					1.43	50
				1.33	20	1.38	10	1.37	60	1.37	60
						1.34	75	1.33	60	1.30	70
1.30	M	1.28	M	1.28	50	1.30	85	1.29	100	1.28	100
						1.25	85	1.23	60	1.25	70
						1.22	60			1.22	60
						1.20	85				
1.20/1.16	M	1.19	M	1.17	20			1.18	60	1.18	60
										1.17	60
1.10/1.07	M	1.09	M	1.09	50			1.09	60	1.10	60
1.03				1.05	20			1.04	100	1.07	100
										1.04	100

[a] Samples aged 3 hr at 540 C (1000 F).
[b] Ni_3Mo standard from: S. Saito and P. Beck, AIME Trans, *215*, (1959) 938. all others from ASTM X-ray data.
[c] Lines are broad.

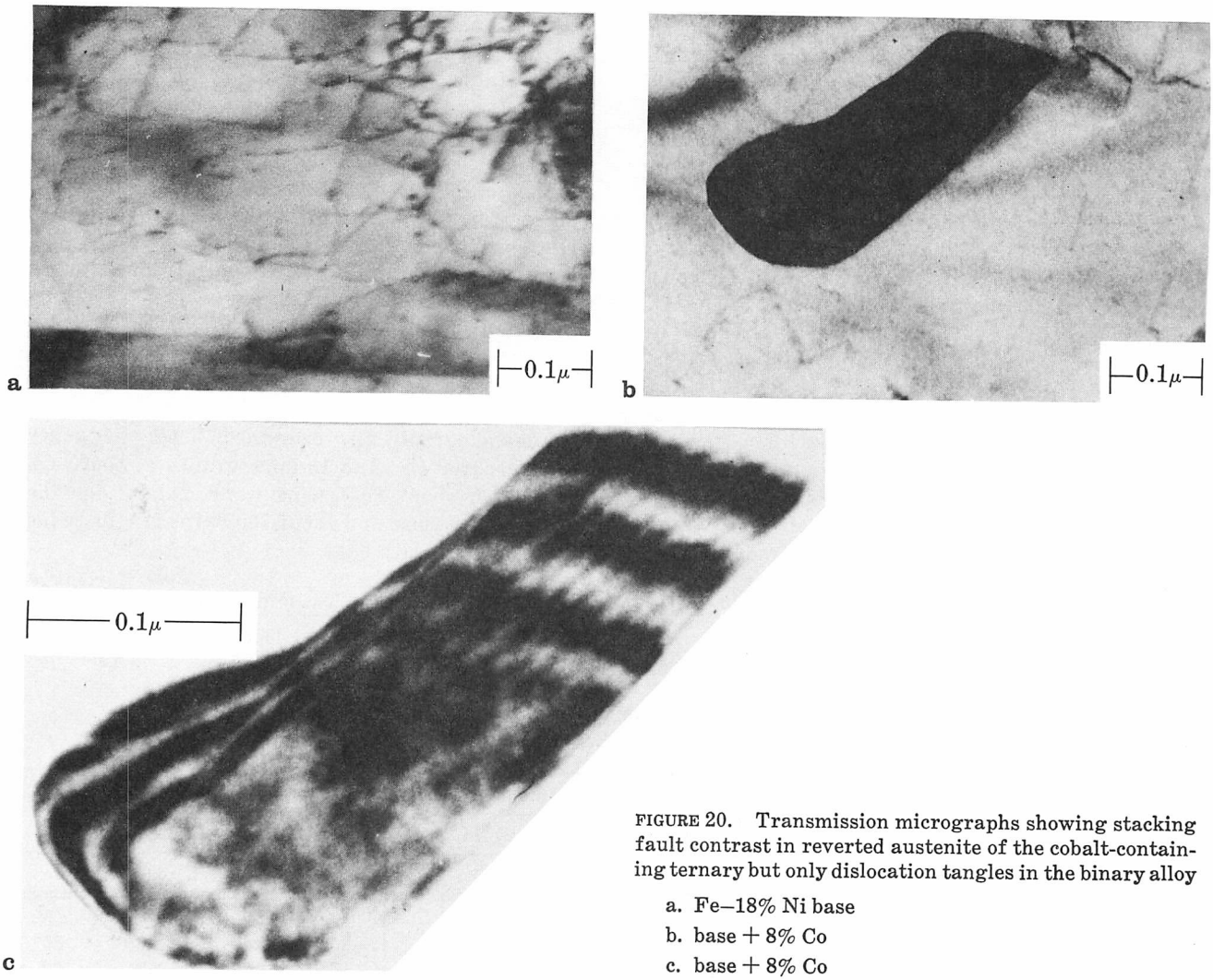

FIGURE 20. Transmission micrographs showing stacking fault contrast in reverted austenite of the cobalt-containing ternary but only dislocation tangles in the binary alloy

a. Fe–18% Ni base
b. base + 8% Co
c. base + 8% Co

TABLE VII Average Cell Size in Cold Rolled Foils

Nominal Reduction %	Fe–18% Ni Binary Base μ	Base + 8% Co μ	Ratio	Base + 4% Mo μ	Base + 4% Mo + 8% Co μ	Ratio
Cold Reduced at 22 C (72 F)						
0	0.33	0.20	1.65	0.24	0.19	1.26
3	0.25	0.19	1.32	0.24	0.19	1.26
5	0.25	0.21	1.19	0.27	0.18	1.50
15	0.26	0.18	1.44	0.23	0.15	1.53
30	0.24	0.17	1.41	0.26	0.18	1.44
Cold Reduced at −196 C (−320 F)						
0	0.33	0.20	1.65	0.24	0.19	1.26
3	0.26	0.19	1.37	0.24	0.20	1.20
5	0.28	0.23	1.22	0.26	0.19	1.37
15	0.25	0.14	1.78	0.29	0.15	1.93
30	0.30	0.18	1.67	0.32	0.19	1.68

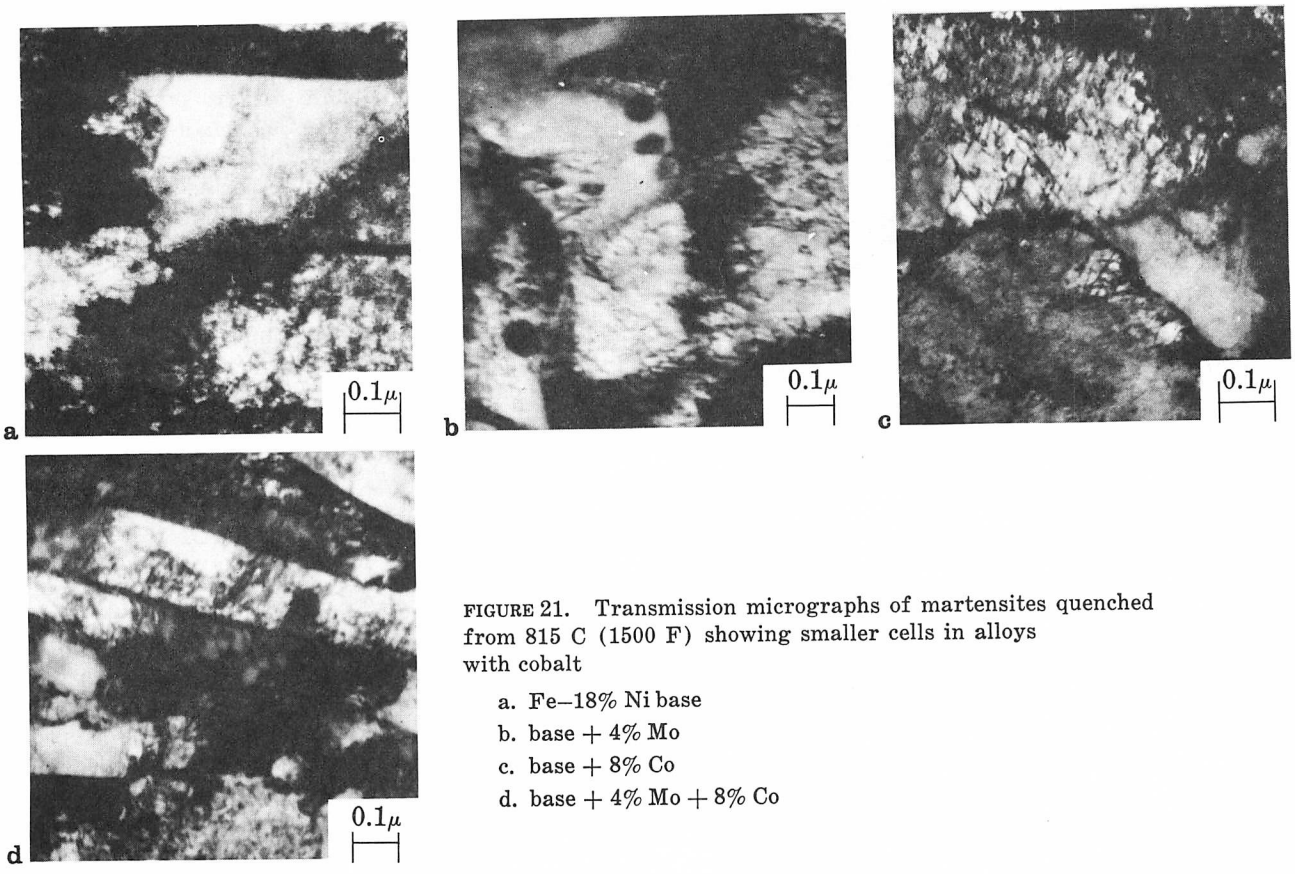

FIGURE 21. Transmission micrographs of martensites quenched from 815 C (1500 F) showing smaller cells in alloys with cobalt

a. Fe–18% Ni base
b. base + 4% Mo
c. base + 8% Co
d. base + 4% Mo + 8% Co

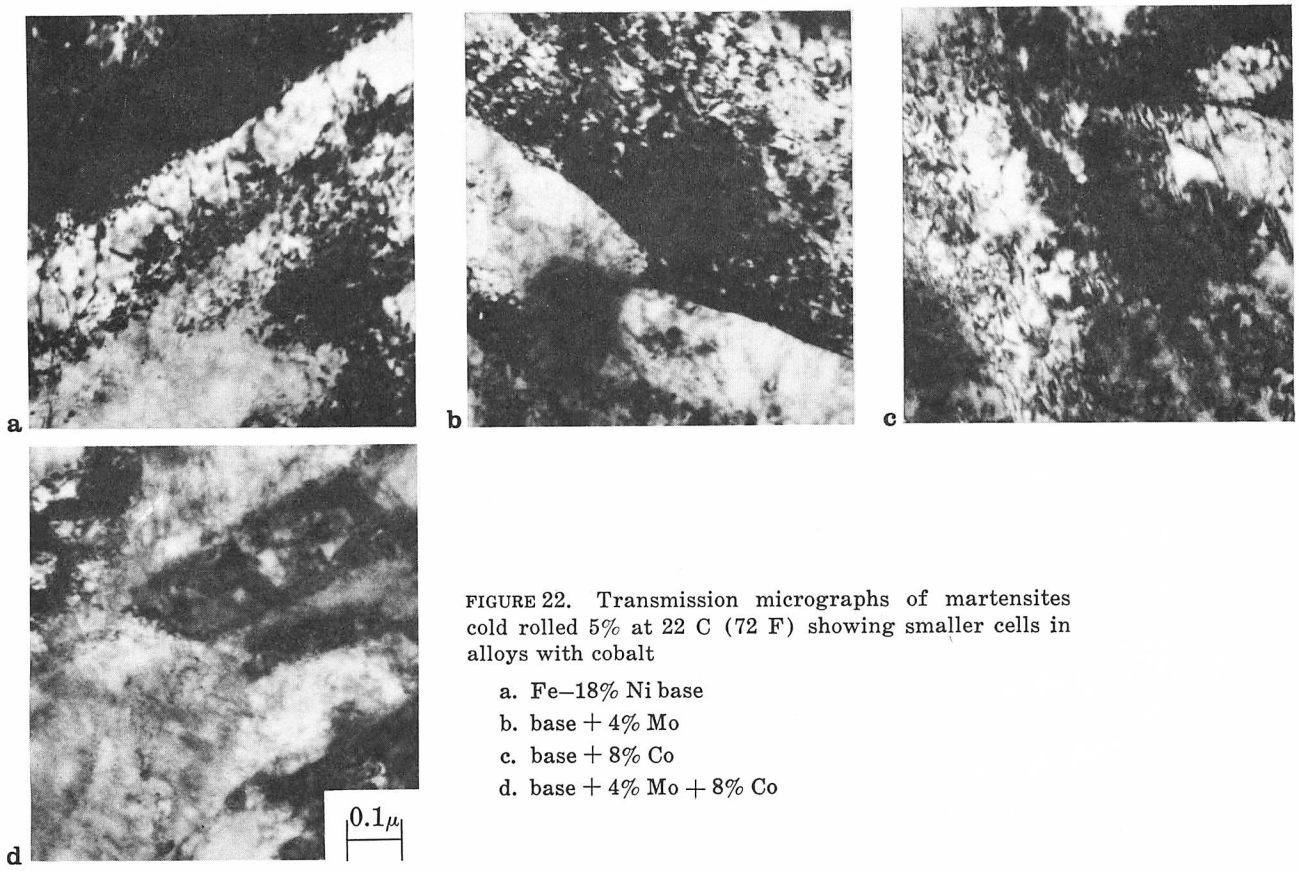

FIGURE 22. Transmission micrographs of martensites cold rolled 5% at 22 C (72 F) showing smaller cells in alloys with cobalt

a. Fe–18% Ni base
b. base + 4% Mo
c. base + 8% Co
d. base + 4% Mo + 8% Co

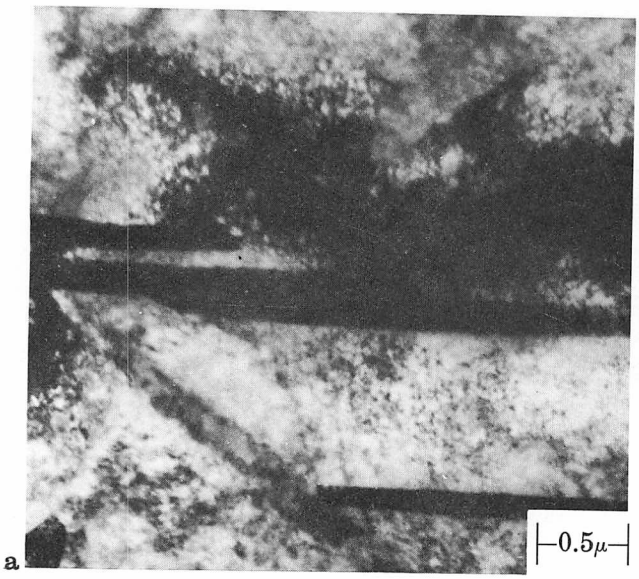

FIGURE 23. Transmission micrographs of deformation twins in molybdenum and molybdenum–cobalt alloys

a. base + 4% Mo b. base + 4% Mo + 8% Co

Both the numbers of twins per mm², and twins per martensite lath, were greater for the cobalt-containing alloy. The observed trend toward increased twin frequency in the cobalt-containing alloys is another indication of lowered stacking fault energy in them.

These data can be simply interpreted in terms of the stacking fault energy lowered by cobalt additions. Because of the lowered SFE, twin deformation is encouraged in the martensite; and cross slip becomes more difficult, which impedes the development of cell structure. Cross slip requires the two partials of a dissociated dislocation to recombine, hence, the energy for cross slip increases with decrease in SFE, making cross slip more difficult; the resulting cell size becomes smaller, and the average dislocation density increases.

The increased dislocation density provides more nucleation sites for the age-hardening precipitates. Figure 24 shows transmission electron micrographs of the molybdenum ternary and cobalt–molybdenum quaternary alloys after 3 and 32 hr aging at 480 C (900 F). The molybdenum ternary on the top has coarser precipitates than the cobalt–molybdenum quaternary on the bottom; this is more clearly apparent after the longer aging period of 32 hr. The higher dislocation density in the cobalt-containing alloy favors an increased nucleation rate, producing a larger number of more finely dispersed precipitates. Thus, through lowering the stacking fault energy, cobalt provides more nucleation sites where precipitation may occur. And the more numerous precipitate particles tend to stabilize the dislocation forest, and to interfere with dislocation motion—producing increased strength and hardness in the aged condition.

SUMMARY AND CONCLUSIONS

This research was undertaken in view of the importance of combining high strength with toughness, and the present lack of basic understanding of the strengthening mechanisms underlying the important, strong and tough 18% Ni marage steels. Iron–nickel binary, ternary, quaternary, and more complex alloys of high purity were explored for detailed fine structural and property correlations. The individual effect of each element was investigated. This was related to their effects on the matrix structures, stacking faults, martensite morphology, etc.; the interaction of precipitates and substructures was also studied. This investigation permits the following conclusions:

Adding cobalt to the iron–nickel binary alloy produces no solid-solution hardening, but suggests a retardation of the age softening. However, adding molybdenum to the iron–nickel binary produces solid-solution, as well as age-hardening. Simultaneously adding both cobalt and molybdenum to the iron–nickel binary produces hardening responses analogous to those obtained by adding the individual elements; and their cumulative effects are additive. No synergism is observed. Also, contrary to previous claims, grain boundary precipitates do occur in molybdenum-containing alloys, but were probably missed in previous studies because of etching specificity.

Diffraction and quantitative (corrected) electron probe data on extraction replicas show that σFeMo, and Ni_3Ti (with probably small amounts of NiAl, from the residual aluminum) are the most likely age-hardening precipitates in commercial high strength Fe–18% Ni marage steels. The calculated stoichiometry of the intermetallic compounds are: $(Ni_{0.4}\,Fe_{0.6}\text{-}Co_{0.05})\,Mo$, $(Ni_{0.3}\,Fe_{0.7})\,Mo$, $(Ni_{2.9}\,Fe_{0.1})\,Ti$, and $(Ni_{0.7}\,Fe_{0.3})\,Al$ for the precipitates in the iron–nickel–molybdenum–cobalt, iron–nickel–molybdenum, iron–nickel–titanium, and iron–nickel–aluminum alloys respectively. Thus, cobalt does not enter

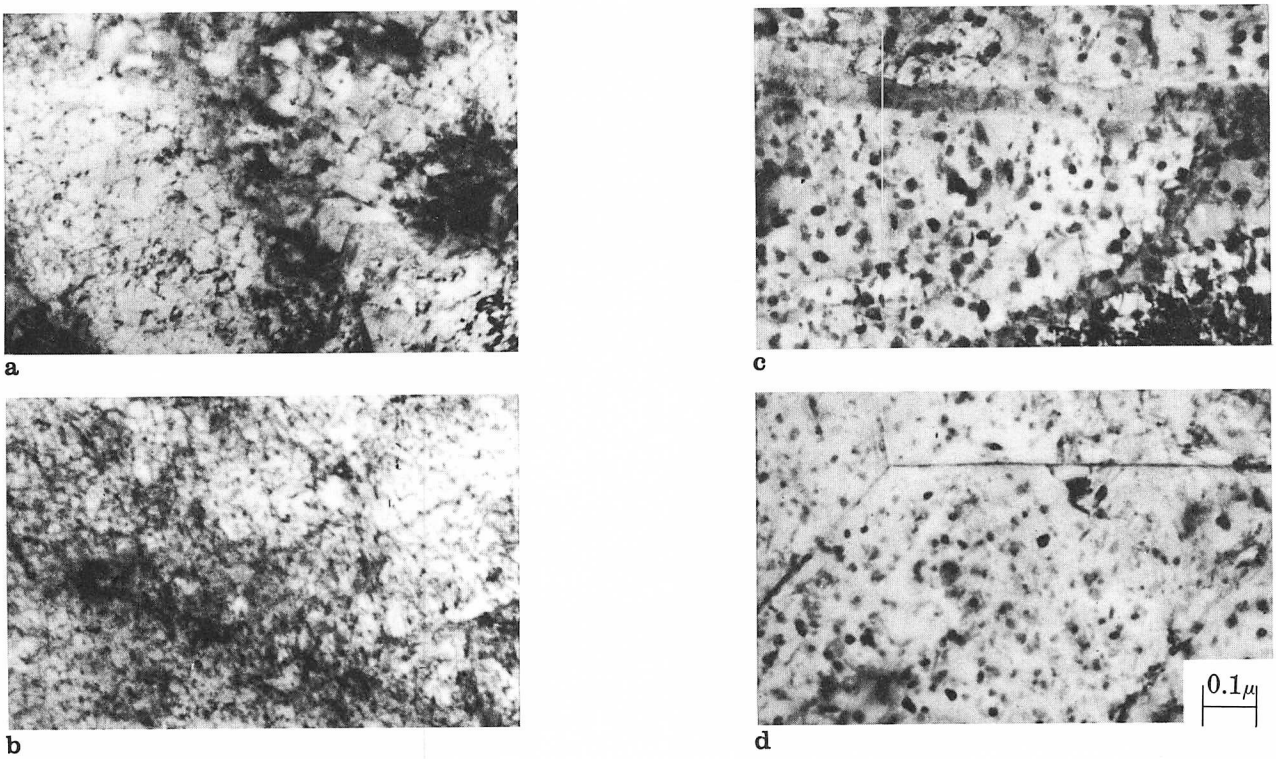

FIGURE 24. Transmission micrographs showing increased precipitation sites in the cobalt-containing alloy

a. base + 4% Mo aged at 480 C (900 F) for three hours

b. base + 4% Mo + 8% Co aged at 480 C (900 F) for three hours

c. base + 4% Mo aged at 480 C (900 F) for 32 hr

d. base + 4% Mo + 8% Co aged at 480 C (900 F) for 32 hr

the precipitate phase to any significant extent. Fine structures of these alloys show cobalt increasing the precipitate-nucleation rate.

The long-sought mystery of the effect of cobalt on matrix strengthening is resolved, in terms of the cobalt lowering the stacking fault energy (SFE) of the matrix; the lowered SFE is proven through observations of smaller cell size and increased twin frequency in the cobalt-containing alloys. The lowered SFE discourages cross slip and retards cell growth. Thus, the average dislocation density is increased, which provides more nucleation sites for precipitation, as is indeed shown by transmission microscopy. The resulting stabilization of the dislocation forest, and increased interference with dislocation motion are responsible for the observed strengthening.

ACKNOWLEDGMENTS

We are pleased to acknowledge the able assistance of many staff members of Crucible's Hunter Research Laboratories. In particular, J. M. Capenos, W. D. Bingle, A. Bossar, F. S. Snyder, E. J. Fiore, M. M. Saunders and L. J. Bench have made substantial contributions to this effort. The support of the Wright Patterson Air Force Base, United States Air Force, through Contract AF33(657)-10337, is also gratefully acknowledged.

REFERENCES

1. R. F. Decker, J. T. Eash and A. J. Goldman, Trans. ASM, *55*. 58 (1962)
2. J. R. Mihalisin, Trans. ASM, *59*. 60 (1966)
3. G. P. Miller and W. I. Mitchell, J. Iron and Steel Inst. (London), *203*. 899 (1965)
4. S. Floreen and G. R. Speich, Trans. ASM, *57*. 714 (1964)
5. B. G. Reisdorf and A. J. Baker, "The Kinetics and Mechanisms of Strengthening of Maraging Steels," AFML-TR-64-390, Wright-Patterson Air Force Base, Ohio, Jan. 1965
6. B. G. Reisdorf, Trans. ASM, *56*. 783 (1963)
7. A. J. Baker, ASM Metals Eng. Quarterly, *6*. 24 (1966)

8. R. F. Decker, "Maraging Steels: Structure Property Relationship," NPL Symposium No. 15—*Relation between Structure and Mechanical Properties of Metals*, HMSO (London), 1964, 648

9. B. R. Banerjee and J. J. Hauser, "Hardening Mechanisms and Delamination Studies of 18% Ni Marage Steels," 9FML-TR-66-166, Wright-Patterson Air Force Base, Ohio, March 1966

10. B. R. Banerjee and W. D. Bingle, "Electron Probe Microanalysis of Submicroscopic Precipitates in Stainless Steel," *The Electron Microprobe*, J. Wiley and Sons, Inc., New York, 1964, 653

11. B. R. Banerjee and J. J. Hauser, "Fracture Micromechanics in High-Strength Steels and Titanium," ML-TDR-64-182, Wright-Patterson Air Force Base, Ohio, July 1964

12. B. R. Banerjee, J. M. Capenos and J. J. Hauser, "Structure and Properties of 18-Ni Marage Steel," *Fourth Maraging Steel Project Review*, ML-TDR-64-225, Wright-Patterson Air Force Base, Ohio, July 1964, 95

13. A. Seeger, "Stacking Faults in Close Packed Lattices," *Bristol Conf. Defects in Crystalline Solids*, Phys. Soc. (1955), 328

14. E. Votava, Acta Met., *8*. 901 (1960)

ORAL DISCUSSION OF

Transformation Kinetics in Marage Type Fe–18% Ni Steels

Presented by B. R. BANERJEE

R. F. DECKER (The International Nickel Company, Inc.). In commenting on Dr. Banerjee's paper, I find that there are several new thoughts in his paper. These thoughts certainly are worthy of very careful examination and consideration against the prior art and science of maraging steels.

Our maraging team at Sterling Forest reviewed the recent AFML report on the same research. We had two or three major points that we thought we would open for discussion before the audience. I don't mean to detract from the rest of the important observations by emphasizing these three.

1. Since this is a molybdenum conference, I shall refer to Figure A from Floreen and Speich[1] on the molybdenum effect, emphasizing a most important role of molybdenum. Illustrated are impact energy versus yield strength curves of quaternary alloys based on Fe–18% Ni–8% Co, with a quaternary addition listed in the figure. The important thing to notice is the retention of impact energy to high levels of strength with molybdenum additions in contrast to the other elements that are used for age-hardening. More recently, this sort of comparison has been carried into the stainless maraging steels, and again molybdenum provides a very important role of increasing toughness at high strength levels. This toughening effect is accomplished by retarding precipitation at the grain boundaries. In many respects it parallels the role of molybdenum in preventing temper embrittlement in conventional steels; but of course, the exact mechanism may be different. I would like to leave that as a most important practical mechanism for molybdenum and the reason that molybdenum will be found quite universally in maraging steels.

[1]S. Floreen and G. R. Speich, Trans. ASM *57*. 714 (1964)

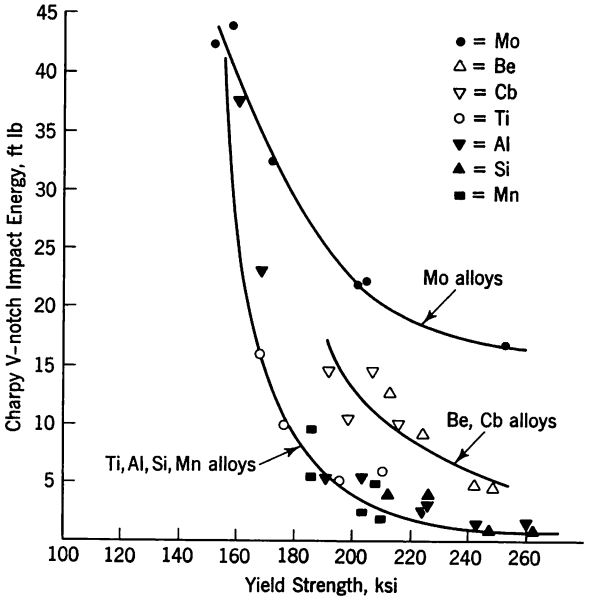

FIGURE A. Charpy V-notch impact energy vs yield strength of quaternary alloys. Base composition of Fe–18% Ni–8% Co with quaternary addition listed in box and on curves

2. Figure B and C bear on the cobalt–molybdenum synergism. These results are from recent studies by Dr. Dale Peters of our laboratory,[2] comparing the aging of ternary Fe–18% Ni–5% Mo with quaternary Fe–18% Ni–8% Co–5% Mo. Here are plotted the maximum aged hardness values versus aging temperature comparisons. In this very careful study, Dr. Peters noticed an extra aging behavior in the quaternary alloy below about 480 C (900 F) (see Figure B). Thinking of extra precipitates, he ran classical precipitate reversion studies using resistivity measurements, which turned out to be very sensitive to molybdenum in solution.

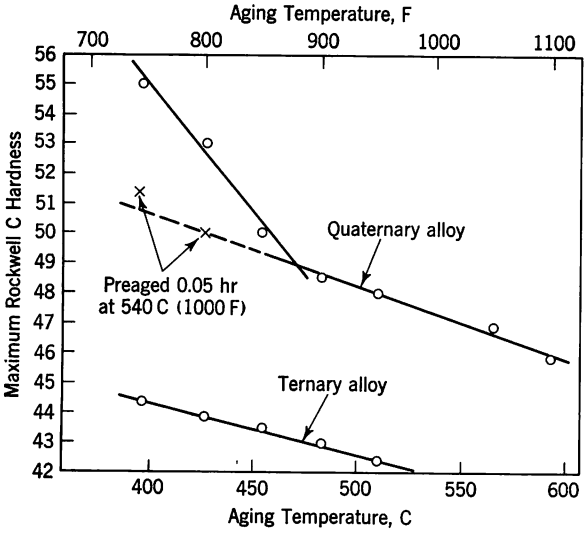

FIGURE B. Effect of aging temperature on peak hardness of ternary (Fe–18% Ni–5% Mo) and quaternary (Fe–18% Ni–8% Co–5% Mo) alloys

Figure C shows some of the results plotted as degree of precipitate reversion as measured by resistivity changes versus first aging temperature. Aging was conducted at T_1, and then the aging temperature was raised to T_2, which was 55 C (100 F) higher and resistivity was monitored to watch degree of reversion. It can be seen that with the ternary alloy, a horizontal line is plotted indicating little precipitate-reversion. But with the quaternary alloy, a precipitate formed below 480 C (900 F) which was reverted by going 55 C (100 F) higher. Analysis of this type and the fact that addition of cobalt accelerates the precipitation reaction just as with increasing molybdenum led Dr. Peters to conclude that the mechanism of cobalt–molybdenum synergism was the decrease of the solubility of molybdenum by cobalt and addition of an extra homogeneously nucleated precipitate at the higher supersaturation. The decrease in molybdenum solubility by cobalt argument was supported by Floreen and Speich[1] and Mitchell and Miller.[3]

This extra precipitate may be more homogeneously nucleated precipitate between the ribbons as you saw in Dr. Banerjee's micrographs. The ribbons would be heterogeneously nucleated on dislocations and present in both ternary and quaternary alloys.

To round out the experiment, Peters preaged at 540 C (1000 F) before exposing at lower temperature, thinking that this would cause all heterogeneous dislocation precipitation and wipe out the extra homogeneous precipitation. Indeed, this was observed in Figure B where it can be seen that the extra aging effect below 480 C (900 F) was wiped out. Thus, the entire mechanism seems to be quite consistent with the data.

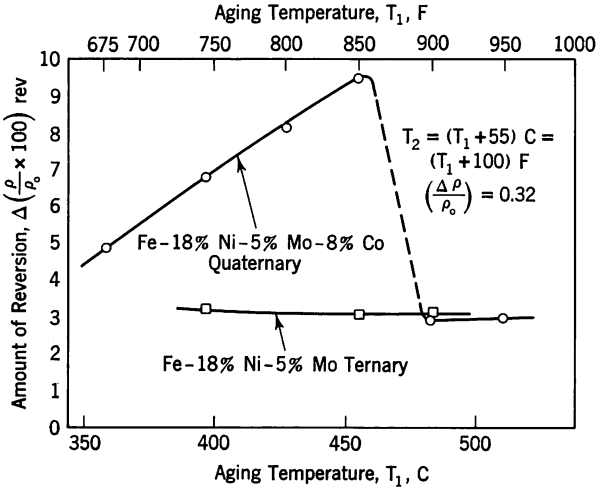

FIGURE C. Amount of reversion at T_2 as a function of the aging temperature T_1 for the ternary and quaternary alloys

3. Dr. Banerjee had a very good thought on the effect of cobalt on reversion and that has been a very important mechanism for cobalt. Also, the raising of the M_s temperature is an important mechanism for cobalt. These latter two factors make possible highly alloyed materials such as the new 18 Ni 350 maraging steel with higher cobalt to prevent retained austenite and reversion problems. I might conclude by asking Dr. Banerjee if he thinks there is any connection between the observations of Dr. Peters and his on stacking faults.

AUTHOR'S REPLY. I couldn't comment on your new data right now; I'd like to look at your data in more detail, and discuss this with you subsequently. I think these are interesting pieces of information that should add up to a final picture. I think all of this says that we have indeed a very complex system, in which certainly further studies are needed for complete understanding.

I'd like to ask a question on this. Do you find another precipitate that appears between the dislocation nucleated precipitates and if so, is it a different precipitate or the same one, or haven't you had a chance to determine its nature?

R. F. DECKER. I don't think we can safely go too far in that direction; it is suspected that it might contain

[2]D. T. Peters, to be published

[3]G. P. Miller and W. I. Mitchell, "Structure and Hardening Mechanisms of 18% Ni-Co-Mo Maraging Steel," J. Iron and Steel Inst., (London) *203*. 899 (1965)

more molybdenum than the ribbon precipitation, which we think is Ni_3Mo. We could speculate that this extra phase is the molybdenum zone suggested by Hornbogen[4] in his research on Fe–Mo alloys.

C. F. JATCZAK (The Timken Roller Bearing Company). Was the measurement of particle or cell size made by harmonic analysis of x-ray diffraction line shapes or by some other method?

AUTHOR'S REPLY. No, we did not make a quantitative particle size measurement at all. When I say finer particles, I am referring to data based on electron microscopy — both extraction replica and transmission.

DISCUSSER. I was a little disturbed by your picture on the stacking fault in the cobalt — it looked to me like a precipitate with uneven interfacial dislocations added. My question is, what density of stacking faults did you observe, and did you apply dark field techniques to validate?

AUTHOR'S REPLY. Let me answer that question in two ways: (1) We could not find any precipitate reflections from these regions, and (2) we did look at dark field and confirmed a stacking fault contrast. There must be some sort of alloy segregation in order to darken the partials themselves, which become visible; but normally the partials don't produce contrast. Of course, you can see the contrast parallel to the fault intersection with the foil. The additional contrast parallel to the partials disturbed us; however, we concluded that this contrast must be due to alloy-element segregation and not a precipitation because we couldn't find any diffraction spots attributable to the precipitates.

DISCUSSER. But what about the frequency of the stacking faults?

AUTHOR'S REPLY. The stacking fault frequency is not very high. You have to look for them.

C. S. SIMCOE (Simonds Steel Division, Wallace Murray Corporation). Since the work-hardening rate or the strain-hardening exponent of maraging steels is very low, it would indicate that perhaps the precipitates are coherent, and all of the strengthening is by coherency hardening; do you have any comment?

AUTHOR'S REPLY. I can comment only indirectly on that, and offer a negative answer. One finds only rare cases of typical coherency contrast in the transformation pictures from these precipitates. So it would be rather odd to conclude that the hardening is entirely due to coherency.

J. W. SPRETNAK (Ohio State University). Along that line, do you have an estimate of the dislocation density in your fully-hardened condition?

AUTHOR' REPLY. No dislocation density is so high in these materials in the aged condition that I don't know how you would make a valid density measurement; I would estimate an order of magnitude of about 10^{13} lines/cm, but you can't really measure it.

G. E. PELLISSIER (United States Steel Corporation). The first comment I would like to make is about the rate of work-hardening; actually, for low levels of stress and strain in these alloys, the rate of work-hardening is very high. It is only in the region of large strains that the rate becomes low; so, I think that the question of coherency could be turned around. The second point is that we have repeatedly identified the major precipitate in the commercial grades of maraging steel as Ni_3Mo. Recently, we have completed another more sophisticated diffraction study which verifies our original finding that the precipitate is Ni_3Mo. However, in titanium-free steels of this kind, I think overaging does produce the sigma phase, Fe–Mo. Three different methods of analysis: (1) extraction replication with powder electron diffraction, (2) thin metal foil with transmission electron diffraction, and (3) bulk extraction of precipitate with microchemical analysis, have all independently shown the major precipitate to be Ni_3Mo.

AUTHOR'S REPLY. I am not sure that there is a basic inconsistency between your observations and ours. I indicated that as far as the commercial alloy is concerned, we are only drawing inferences based on analogies in the component systems, because when I see the diffraction pattern (Table VI in our paper) we get from the commercial alloy, we cannot uniquely identify any single precipitate phase, because of the co-presence of the various intermetallics. But if you have worked this thing out, I will have to take your word for it.

G. E. PELLISSIER. In the titanium-free composition?

AUTHOR'S REPLY. Both in the ternary and in the quaternary, which are titanium-free, of course, we were able to clearly establish the sigma Fe–Mo precipitate.

G. E. PELLISSIER. We still find Ni_3Mo, until we overage, and then we also find the sigma Fe–Mo. There is another precipitate in the titanium-free steels which also contributes to the strengthening, and that is an M_6C carbide.

AUTHOR'S REPLY. Yes, there is a carbide precipitate; but this is a residual rather than a carbide formed during aging treatments.

G. E. PELLISSIER. Yes, but it still effects some strengthening.

AUTHOR'S REPLY. Yes, it probably contributes some, though because of its size the effect would be small.

WRITTEN DISCUSSION

C. L. MAGEE (Ford Motor Company). One of the major new proposals contained in this paper is the hypothesis that cobalt affects the strength of maraging steels by lowering the stacking fault energy of the matrix. How-

[4]E. Hornbogen, "Precipitation from Binary Substitutional Solid Solutions of Alpha Iron," *Precipitation from Iron-Base Alloys*, Gordon and Breach Science Publishers, New York, 1965, 1

ever, it should be pointed out that this proposal may involve unwarranted extrapolation.

As previous discussers have pointed out, it is not unequivocally established that Dr. Banerjee's micrograph demonstrates that cobalt lowers the austenite stacking fault energy. However, even if it does, it does not follow that the lower fcc stacking fault energy is relevant to the aging response of the bcc martensite. Therefore, it is the "stacking fault energy of the bcc phase" — as discussed by Dr. Banerjee — which must be considered in the explanation for the cobalt effect.

Dr. Banerjee proposes that cobalt lowers the bcc stacking fault energy — but is unclear what kind of faults are being referred to. Despite this uncertainty, the authors apply standard arguments for fcc metals (in which Shockley partials and well known faults are involved) to the case of the bcc structure. For example, the authors argue that lower bcc stacking fault energy leads to inhibition of cross slip and that lower stacking fault energy results in more deformation twinning. However, I would suggest that these assertions are rather speculative in regards to the unspecified bcc fault. As far as this discusser knows, stacking faults have not been observed in any bcc material. Furthermore, the faults which have been theoretically postulated for bcc structures have not been shown to have an important role in deformation (inhibition of cross slip) nor has anyone demonstrated a relationship between the energy of these faults and deformation twinning. Since the only evidence Dr. Banerjee advances for cobalt lowering the "bcc stacking fault energy" is enhancement of deformation twinning, his arguments are open to considerable question and I would suggest that a more direct rationale of the cobalt effect — e.g., as outlined by Dr. Decker — seems more plausible.

AUTHOR'S REPLY. We have been careful to indicate that stacking faults in the fcc phase (which we have demonstrated) do not establish a lowering of SFE in the bcc phase. The combined evidence of increased twin frequency, and decreased cell size in the bcc structures does, in our opinion, suggest and support the proposed mechanism. The supportive evidence, in this case, is just as good as any other alternative so far suggested.

Transformation Characteristics and Hardenability of Carburizing Steels

A. ROSE and H. P. HOUGARDY
Max-Planck-Institut für Eisenforschung
Düsseldorf, Germany

INTRODUCTION

It takes courage to present a paper in the USA on transformation characteristics and hardenability of carburizing steels. As justification, however, we might point out the extremely large amount of work that has already been done and published on this subject even in our much smaller country.[1]*

The very old idea of producing a "tool steel" composition by carburizing the parts of a structural steel exposed to wear would be a stroke of genius if it could be ascribed to a specific inventor. It is fascinating to picture how on hardening the transformation of an entire series of steel compositions occurs consecutively or simultaneously over the cross section and thus produces a structure giving the required properties at predetermined areas of the part.

CONTINUOUS-COOLING TRANSFORMATION DIAGRAMS FOR GAS-CARBURIZED CARBURIZING STEELS

Continuous-cooling transformation (CCT) diagrams were used in an attempt to represent the course of this transformation from the surface to center. The procedure for determining such diagrams is well known. Dilatometric methods[2] on 4-mm-dia specimens were used for cooling rates in the range 0.004/20 C/sec (0.007/36 F/sec) and qualitative thermal analysis on discs with a diameter of 4 mm and a thickness of 1 to 2 mm was applied for cooling rates over 20 C/sec (36 F/sec) to 500 C/sec (900 F/sec). In the latter method, electronic means were used to produce a differential cooling curve and the cooling rate as a function of temperature was recorded with a Sanborn x-y U-V instrument. Thus the curve was immediately visible.[3]

The extension of the investigation to the high cooling rate of 500 C/sec (900 F/sec) is necessary not only to determine the martensitic transformation of the unalloyed carburizing steel but also to see what changes in the structure of martensite — for example, in the retained-austenite content or in the pre-precipitation of carbides and thereby in the hardness — are still feasible in the supercritical cooling range.

The investigation was carried out on commercial German carburizing grades. The standard German designation is included with the compositions in Table I.

For constructing the CCT diagram, the small specimens described above were carburized to a predetermined carbon content by an endothermic carrier-gas process with introduction of propane. This guaranteed that the CCT diagrams for all carbon contents of any one grade refer to the same heat. The specimens were carburized through to about 0.3, 0.6, 0.9, 1.2 and 1.5% C in such a manner that the difference in carbon content over the section was less than 10% of the average. For the 1.2 and 1.5% C levels, all steels were carburized together with controlled carbon potential, measured on a pure iron wire. For the rest of the carbon levels, the Ck 15, 16 MnCr 5, 15 CrNi 6 and 18 CrNi 8 steels were carburized in one group and the 20 MoCr 4, 25 MoCr 4, 14 NiCr 14 and 20 NiMoCr 6 steels in another. Table II shows the carbon contents obtained by carburizing. In spite of simultaneous carburizing, it can be seen that the steels have different carbon contents, due to the effect of the alloying elements on carbon activity. The highest carbon contents were found in the steels with high contents of carbide-forming elements.

*See references.

TABLE I Chemical Composition of Steels Investigated*

DIN Designation	% C	% Mn	% Si	% P	% S	% Cr	% Cu	% Mo	% Ni	% Al	% B	% N
Ck 15	0.15	0.39	0.29	0.012	0.026	0.12	0.22	...	...	0.003	.....	0.007
16 MnCr 5	0.16	1.12	0.22	0.030	0.008	0.99	0.22	0.02	0.12	0.015	.....	....
20 MoCr 4	0.22	0.66	0.30	0.018	0.011	0.56	0.18	0.44	0.15	0.049	<0.0005	0.020
25 MoCr 4	0.27	0.67	0.20	0.017	0.022	0.50	...	0.45	0.11	0.034	0.002	0.005
15 CrNi 6	0.13	0.51	0.31	0.023	0.009	1.50	0.22	0.06	1.55	0.010	.....	....
18 CrNi 8	0.16	0.50	0.31	0.013	0.014	1.95	0.20	0.03	2.02	0.030	.....	....
14 NiCr 14	0.13	0.46	0.26	0.013	0.012	0.78	0.16	0.04	3.69	0.012	.....	....
20 NiMoCr 6	0.20	0.62	0.15	0.015	0.020	0.47	...	0.48	1.58	0.015	<0.0005	....

*Weight percent.

TABLE II Carbon Contents after Gas Carburizing

Ck 15	0.15	0.30	0.46	0.90	0.98	1.75
16 MnCr 5	0.16	0.33	0.53	1.00	1.20	3.00
20 MoCr 4	0.22	0.28	0.57	0.88	1.00	2.35
25 MoCr 4	0.27	0.31	0.60	0.92	1.18	2.60
15 CrNi 6	0.13	0.32	0.50	0.97	1.07	2.60
18 CrNi 8	0.16	0.34	0.56	1.10	1.15	3.20
14 NiCr 14	0.13	0.25	0.53	0.81	1.03	1.80
20 NiMoCr 6	0.20	0.28	0.58	0.90	1.14	2.25

A typical CCT diagram is shown in Figure 1 for unalloyed Ck 15 steel carburized to 0.3% C. It is to be read along the cooling curves, which in the following will be referred to in terms of the cooling time in seconds to 500 C (930 F). The time scale is logarithmic. The heavy-dash line indicates the start of the proeutectoid-ferrite precipitation and, at an infinitely long time, should meet the A_3 temperature. The solid line shows the start and finish of the pearlite formation, which at an infinitely long time should meet the A_1 temperature, while the short-dash line denotes the initiation of bainite formation. The lower solid line indicates the beginning of the martensitic transformation. The formation of bainite causes a marked increase in the carbon content of the remaining austenite and thus shifts the martensite forma-

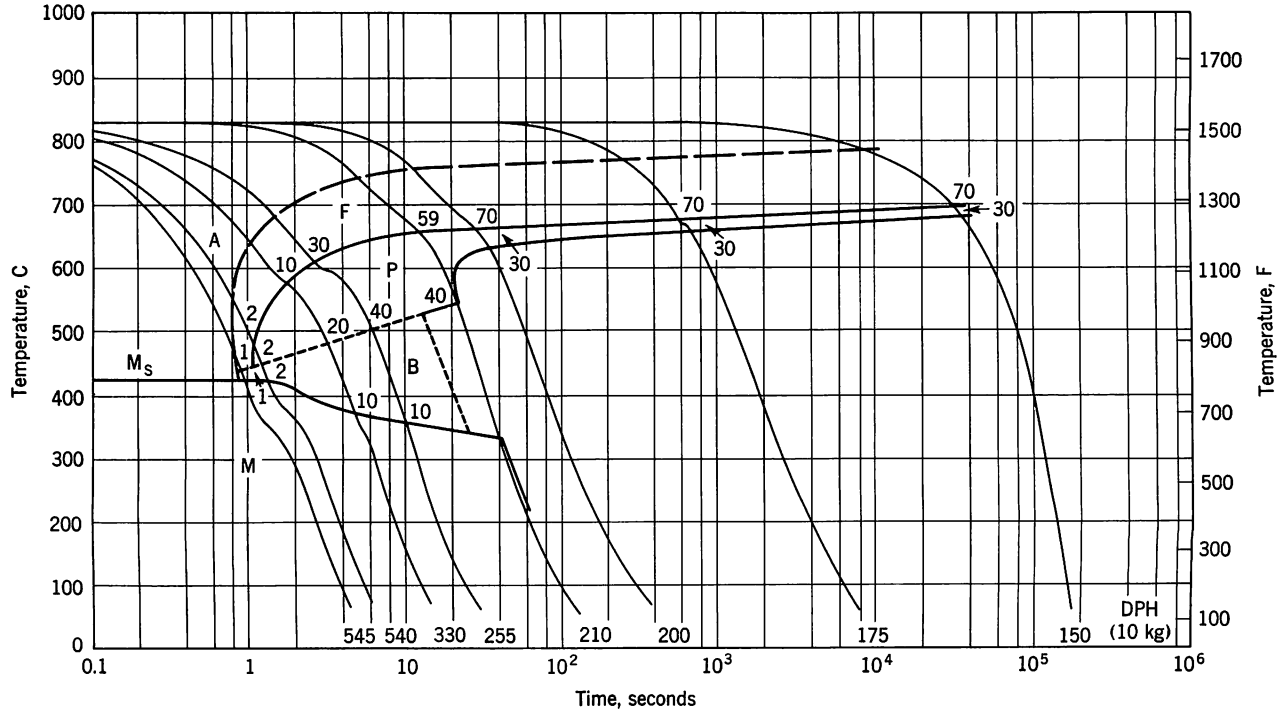

FIGURE 1. Continuous-cooling transformation diagram for Ck 15 steel, carburized to 0.30% C and austenitized at 830 C (1525 F) for 15 min

tion to lower temperatures. The numbers appearing in the individual areas give the percent of the structure formed down to this temperature while the numbers at the end of the cooling curves represent the DPH hardness. From this diagram we can derive the following parameters, which summarize the transformation characteristics: K_m, the limiting cooling time to 500 C (930 F) for formation of martensite alone, is 0.65 sec; K_f for the start of ferrite formation is in this case the same as K_m; K_p denoting the fastest cooling rate that gives a pearlitic structure and the slowest rate that produces any martensite in the structure, is 26 sec. With alloy steels, the beginning of bainite formation generally coincides with K_m and the end — with a few exceptions — with K_p.

The diagram does not contain all the test data needed for its construction. A large number of tests are required to establish the position of the start of transformation and also serve as a basis for Figure 2, showing the equalized structural and hardness values as a function of cooling time to 500 C (930 F). The type of line corresponds to that used in the CCT diagram for the same structure. Although Figure 1 shows that bainite is formed over a wide range of cooling rates, the maximum amount formed is no more than 10%. Only pearlite and martensite are

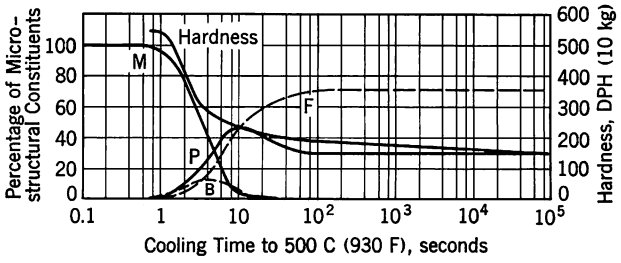

FIGURE 2. Microstructure and hardness as a function of cooling time to 500 C (930 F) for Ck 15 steel, carburized to 0.30% C and austenitized at 830 C (1525 F) for 15 min

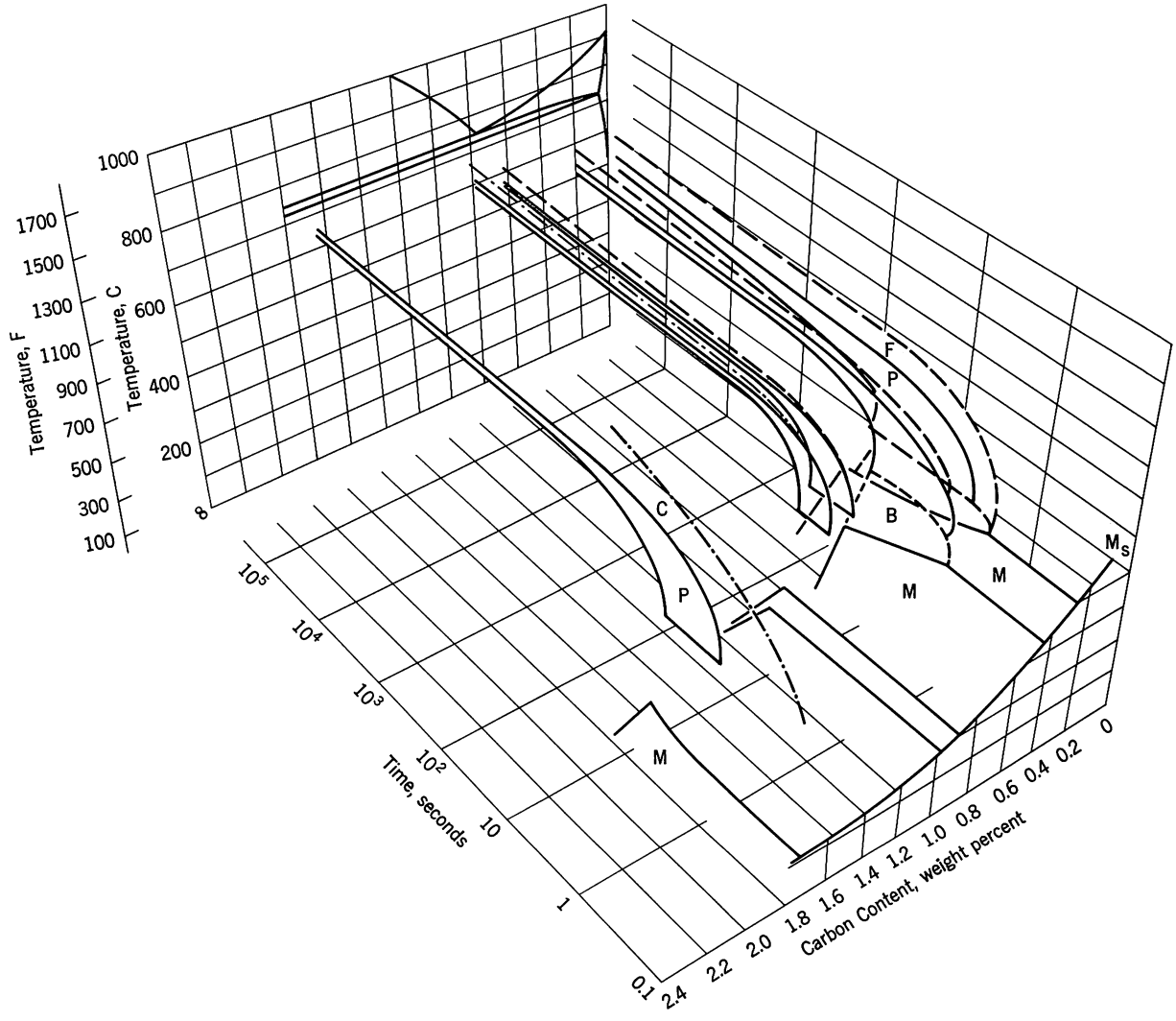

FIGURE 3. Continuous-cooling transformation diagrams as a function of carbon content for Ck 15 steel carburized to 1.75% C

formed with over 0.5% C. The significant information on the hardness values obtainable with different alloy steels — how they are affected by cooling rate and structure — can be derived from analogous diagrams for different steels and carbon contents.

For any specific carburizing steel, the CCT diagrams for different carbon contents can be assembled into a three-dimensional diagram with carbon content, cooling time and temperature as coordinates. An example is given in Figure 3 for the unalloyed Ck 15 steel. In the background, the CCT diagrams for long times approach the equilibrium diagram. The latter is a multicomponent iron–carbon diagram with small contents of manganese and silicon where the A_1 line has been expanded to a section of a three-phase area. To make the diagram more easily understandable, the cooling curves have been deleted from the individual CCT diagrams.

Starting from the side corresponding to high cooling rates or the beginning of transformation, we can see how extraordinarily rapidly the proeutectoid-ferrite precipitation — which here forms the boundary next to martensite formation — is suppressed by increasing carbon content. The steels with the most sluggish transformation behavior lie in the eutectoid region, where the carbide precipitation — shown here as a dot-dash line — succeeds the proeutectoid-ferrite precipitation without a transition. The transformation to bainite is limited to the hypoeutectoid region. The surface at the right representing the formation of martensite is shifted extremely rapidly to lower temperatures as the carbon content increases. The M_s temperature is decreased by prior bainite formation but increased by prior carbide precipitation.

This diagram gives in summary form information on the hardenability of the different compositions over a range of carbon contents, the effect of proeutectoid precipitations and the successive transformations from the core to the hardened case. As an example for the use of this graph, let us follow the course of transformation over the cross section of a 50-mm-dia bar carburized to 0.9% C on the surface. For the layer near the surface we must follow the cooling curve with a cooling time of four seconds in the diagram for 0.9% C. (All these cooling times refer to the intersection of the cooling curves starting at 830 C (1525 F) with the 500 C (930 F) level.) At a depth of two millimeters under the surface, transformation proceeds along a cooling-rate curve corresponding to a cooling time of seven seconds and lies — based on the carbon content–depth curve — on the 0.4% C graph. The graph for the uncarburized condition applies to transformation in the core with a cooling time of about 25 sec.

A comparison of the different transformation paths shows clearly that transformation begins in the area from the core to two millimeters below the surface with the formation of ferrite, pearlite and

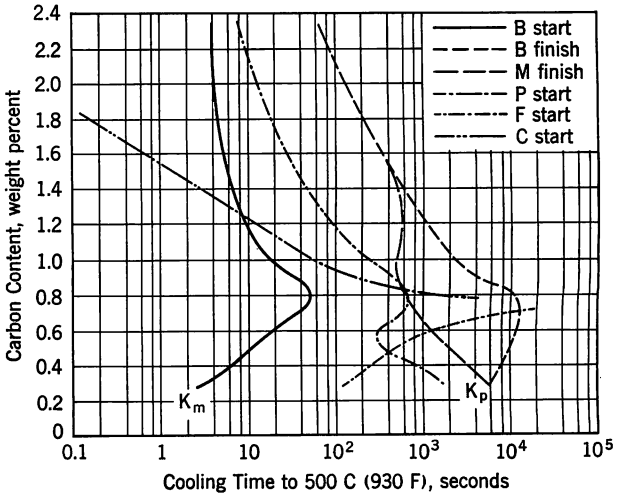

FIGURE 4. Critical cooling times for the various microstructural constituents in 20 MoCr 4 steel, carburized to 2.35% C and austenitized at 830 C (1525 F) for 15 min

bainite. These transformations start at about 760 C (1400 F) and finish at about 300 C (570 F). Subsequently, martensite is formed in the carburized case and causes compressive stresses at the surface because of the large volume expansion.

The two-dimensional projection of such a three-dimensional presentation on the cooling time–concentration plane at 500 C (930 F) is shown in Figure 4 for the sluggish-transforming steel 20 MoCr 4 after austenitizing at 830 C (1525 F). The K_m curve indicates the change in critical cooling time for the formation of pure martensite as a function of carbon content while the K_p curve gives the boundary for a pure ferritic-pearlitic structure. At 0.3/0.4% C, this structure adjoins bainite while the last martensite is formed at shorter times. It is only with higher carbon contents that — as with most steels — the ends of the bainite and martensite formations coincide. The proeutectoid precipitation of ferrite runs from short cooling times at low carbon contents to infinitely long times at higher carbon contents; that is, it disappears at the eutectoid carbon content of about 0.7% just as does the curve for cementite precipitation, which starts down from high carbon contents and short times. There is a fundamental similarity with the unalloyed steel in respect to the sluggish behavior in the eutectoid region, but there are also characteristic differences in regard to the incubation times, which are prolonged by an order of magnitude, and the proeutectoid-ferrite precipitation, which is shifted towards longer times by two orders of magnitude.

Each of the eight grades investigated has been represented in this way for six different carbon levels and two austenitizing temperatures. Austenitizing for 15 min at 830 C (1525 F) corresponds to the hardening treatment for the carburized case,

while austenitizing for 30 min at 930 C (1705 F) is a direct-hardening treatment. These 96 CCT diagrams (8 x 6 x 2) will be published elsewhere.

Before analyzing and comparing the large number of results, we must ask ourselves what conclusions of practical importance may be drawn from such a broad and yet simple basic investigation. We do not expect to discover anything new but perhaps for the first time we can see all phenomena occurring from surface to core of carburizing steels after carburizing and transforming from one common viewpoint of transformation behavior. Thereby all the basic predictions of the transformation diagrams have been obtained under established and reproducible physical conditions on specimens free from uncontrollable heat-to-heat variations.

The following properties are expected from carburizing steels:

- good wear and abrasion resistance on the surface as a result of adequate hardness
- ability to withstand high surface pressures as a result of adequate strength throughout a sufficiently thick case
- adequate fatigue strength as a result of suitable stress distribution and finally
- sufficient strength and toughness in the core to meet service requirements

The first property, wear resistance, raises questions about the relation between attainable maximum hardness and the carbon and alloy content, the amount of retained austenite and the quantity and distribution of carbides; the second — the case depth and again the retained austenite; the third — the distribution of residual stresses resulting from cooling and transformation; and finally the fourth property involves core transformation.

MAXIMUM HARDNESS IN CARBURIZED CARBURIZING STEELS

A broad view of the maximum attainable hardness values for martensite in the individual grades can be gained by comparing the hardness in the martensite range shown in the microstructure curves (such as given in Figure 2 for an unalloyed steel after carburizing to 0.3% C) for all carbon contents attainable in carburizing. The amount of untransformed austenite and any premature carbide precipitates should be taken into consideration, especially with hypereutectoid steels, to explain any hardness variations in this range. Such predictions for hardness and retained-austenite content, which in the past have often been contradictory, can be confirmed only when the hardness changes can be observed over a sufficiently wide range of cooling rates leading

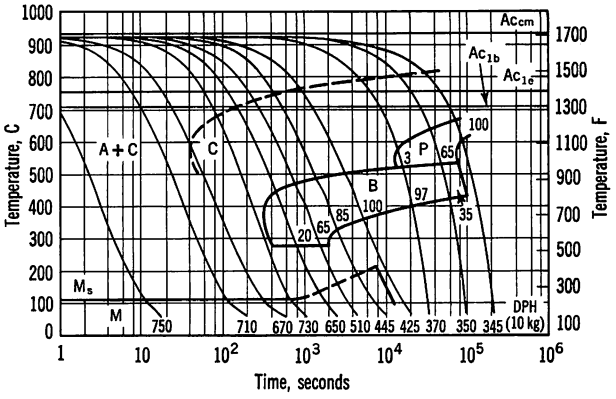

FIGURE 5. Continuous-cooling transformation diagram for 20 NiMoCr 6 steel, carburized to 1.14% C and austenitized at 930 C (1705 F) for 30 min

to the formation of martensite. Without excessive test expenditures, this can best be done with very sluggish steels. Figure 5 shows the continuous-cooling transformation diagram for 20 NiMoCr 6 steel, carburized to 1.14% C and austenitized 30 min at 930 C (1705 F). A comparison with Figure 1 indicates that this steel transforms considerably more slowly than the unalloyed Ck 15 steel. So, for instance, K_m is 200 sec for 20 NiMoCr 6 vs 0.65 sec for the unalloyed steel. Furthermore, a shift of the pearlite range to longer times than the bainite range, a characteristic unique for molybdenum-containing steels, is most pronounced. Figure 6 gives the relevant data for microstructure and hardness. The large amount of bainite for cooling times around 10,000 sec is particularly noticeable. The proeutectoid-carbide precipitation has not been shown since the generally very small amounts could not be determined on the metallographic section with adequate accuracy. Only the location where the carbide precipitation begins to be evident with decreasing cooling rate is indicated by a "C."

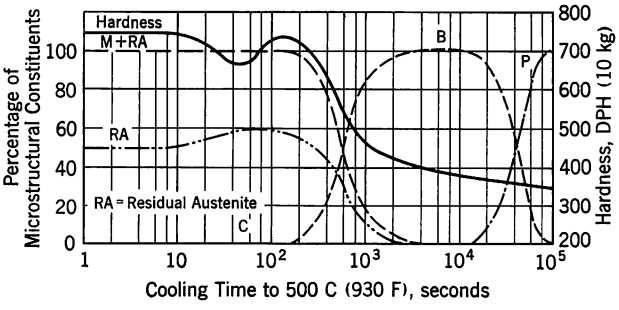

FIGURE 6. Microstructure and hardness as a function of cooling time to 500 C (930 F) for 20 NiMoCr 6 steel, carburized to 1.14% C and austenitized at 930 C (1705 F) for 30 min

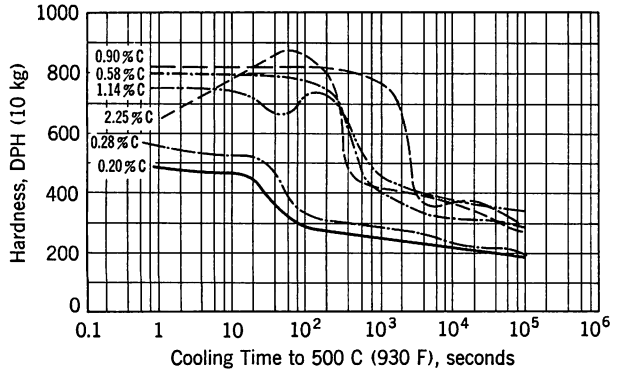

FIGURE 7. Hardness as a function of carbon content and cooling time to 500 C (930 F) for 20 NiMoCr 6 steel, carburized up to 2.25% C and austenitized at 930 C (1705 F) for 30 min

The hardness curve in the range of hypercritical cooling rates is surprising. The first peak is reached when the bainite disappears in favor of martensite; afterwards the hardness decreases by about 20 DPH and then increases with increasing cooling rate. The cause for this hardness decrease in the hypercritical range seems to be an increase in the retained austenite, which in turn is caused by increasing supersaturation of the austenite by growing suppression of the proeutectoid-carbide precipitation. The second increase of hardness at high cooling rates appears to be related to a decrease in the amount of retained austenite, which probably results from diminishing austenite stabilization with higher cooling rates.

Figure 7 summarizes the effect of cooling time on hardness for 20 NiMoCr 6 carburized to various degrees. In following the change of hardness from right to left (that is, towards shorter cooling times), the sharp rise from the area of mixed structures shows clearly that the slowest transforming carburized layer lies at about 0.9% C. Here, just as with 0.6% C, the hardness values show practically no change with increasing cooling rate although the amount of residual austenite appears to decrease. In the hypoeutectoid layers (0.20 and 0.28% C), the hardness value increases at shorter times; for example, in the case of 0.28% C, the increase is from 525 to 575 DPH. Increasing suppression of the self-tempering effect appears to be the only possible explanation.[4] The unusual hardness curve for the hypereutectoid composition with 1.14% C was already explained in Figure 6. With the much higher carbon content of 2.25%, the hardness first reaches a maximum at 880 DPH and then falls steadily to 650 DPH at the highest attainable speed corresponding to a cooling time of about one second. Here, as with 1.14% C, the hardness decrease is related to an increase in the retained-austenite content, which is caused by growing suppression of the proeutectoid carbide precipitation. With this carbon content, complete prevention of this carbide precipitation is impossible even with the highest feasible cooling rate.

In line with these considerations, the attainable hardness after hypercritical quenching of the steel is influenced by various factors other than carbon content. The self-tempering effect, which decreases with increasing cooling rate, and the simultaneous decreased stabilization of the residual austenite lead to an increase in hardness. With high carbon contents the decrease in the amount of proeutectoid carbide precipitated with decreasing cooling time causes an increase in the amount of retained austenite and thus a decrease in hardness. In turn each of these three factors is dependent on the carbon content of the steel. Their superposition determines the course of the hardness curve in the supercritical range, as typified by Figure 7. The same basic change of hardness is observed with all steels. It is, however, less evident with rapidly transforming steels when the limit of detectability approaches the critical rate. This means that the maximum attainable hardness of a series of alloy steels can be correctly compared only for equivalent structure or for equivalent cooling conditions. The maximum hardness values as given in Figures 8 and 9 fall somewhat in the first category. As shown in Figure 8, the unalloyed steel reaches a maximum hardness of about 900 DPH at about 0.9% C after quenching from either 830 C (1525 F) or 930 C (1705 F). On austenitizing at the lower temperature, 16 MnCr 5 attains a maximum of 900 DPH at 1.2% C and after austenitizing at the higher temperature, 840 DPH at 0.6% C. On quenching from 930 C (1705 F), the hardness drops sharply at carbon contents over 0.7% along with increasing supersaturation and growth of the residual-austenite content. The fact that the hardness of both Ck 15 and 16 MnCr 5 increases to 1.2% C on quenching from the austenite + carbide field at 830 C (1525 F) indicates that either the carbide must contribute to the hardness or the composition of the austenite in the multiphase field does not remain constant with increasing carbon content.

The maximum hardness determined from the carburized Jominy specimen is also shown in all these hardness graphs. With the two steels described above, these curves show characteristic deviations. With lower carbon contents the values are higher than those derived from the CCT diagram and with higher carbon contents they are lower. The reasons are the following.

The cooling curves of the Jominy specimens show a systematic variation from those of the CCT diagrams; the austenitizing treatment is different; the more sluggish areas can be nucleated by previously transformed areas; and, finally, stresses and deformation of the Jominy specimen can influence the transformation. From this it can be seen that the extent of the hardness deviation depends on the transformation characteristics of the individual grade.

The occurrence of stresses would be an explanation if the stress pattern in the Jominy specimen were such that tensile stresses at the surface would suppress the self-tempering effect during formation of martensite and compressive stresses in the residual austenite would facilitate its stabilization.

For the two molybdenum–chromium steels in Figure 8, the maximum hardness of about 900 DPH in the eutectoid range is reached with the relatively low carbon content of around 0.6% C. With 20 MoCr 4 steel, it increases still further to 930 DPH at 1.0% C after quenching from 830 C (1525 F). The hardness decrease with increasing supersaturation after austenitizing at 930 C (1705 F) is relatively slight. With these two steels, the maximum hardness value of the end-quenched case-hardenability tests drops to lower values only with hypereutectoid carbon contents.

Figure 9 compares the maximum hardness of chromium–nickel and nickel–chromium steels with that of 20 NiMoCr 6 steel having about the same hardenability. With the chromium–nickel and nickel–chromium steels the maximum hardness is found at about 0.7% C but with the nickel–molybdenum–chromium steel at 0.8% C. After quenching from 830 C (1525 F), the hardness values of the first two types are generally somewhat higher than those of the nickel–molybdenum–chromium steel used for comparison but this difference vanishes on quenching from 930 C (1705 F). This means that the hardness differences resulting from the two different austenitizing treatments are greater for 15 CrNi 6 and 18 CrNi 8 than for 14 NiCr 14 and 20 NiMoCr 6. In two cases the hardness values from the case-hardenability curves deviate towards higher values for lower carbon contents and in three cases to lower values at higher carbon contents.

HARDENABILITY OF CARBURIZED CARBURIZING STEELS

Comparative transformation characteristics of the steels investigated after carburizing — that is, their hardenability or depth of hardening, which is important in connection with the need for resistance to surface pressures — can best be comprehended in terms of the cooling times representing the limits of continuous-cooling transformation to pure martensite (K_m) and to a ferritic-pearlitic structure (K_p) as indicated in Figure 10. This graph is similar to that shown in Figure 4 but with the coordinates reversed for readier comparison of the four steels. Figure 10 permits the comparison of Ck 15 and 16 MnCr 5 with the two molybdenum-containing steels (20 MoCr 4 and 25 MoCr 4) on quenching from 830 C (1525 F) for hardening the case as well as for a direct-hardening treatment from 930 C (1705 F). All cooling times, however, are figured from 830 C (1525 F).

The effect of proeutectoid precipitates in accelerating transformation is clear for all steels and both austenitizing temperatures. Increasing the carbon content over the eutectoid value leads to a very definite decrease in the time for start of transformation in the case of the alloy steels. This may be due to the fact that the alloying elements present in the carbides of these steel are not uniformly distributed in the austenite after solution during the austenitizing treatment so the austenite is still very inhomogeneous when cooling starts. The value K_m describes the start of bainite formation in the molybdenum steels over the entire range of carbon contents, but in the manganese–chromium steel only in the hypoeutectoid range and in the carbon steel just for a restricted carbon range of about 0.3/0.5%.

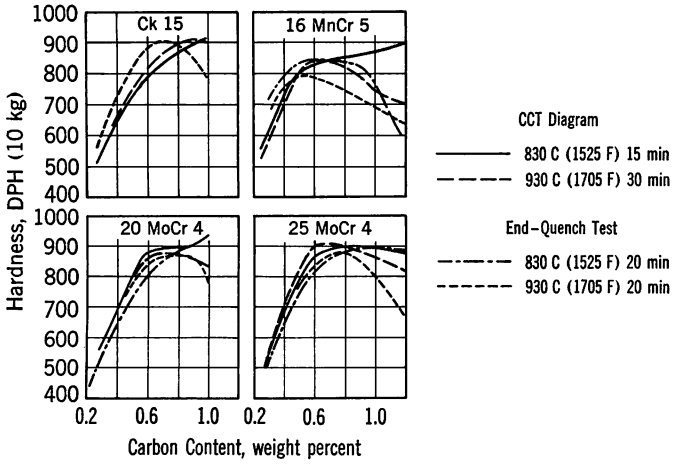

FIGURE 8. Maximum hardness of carburized Ck 15, 16 MnCr 5, 20 MoCr 4 and 25 MoCr 4 steels as a function of carbon content and method of determination

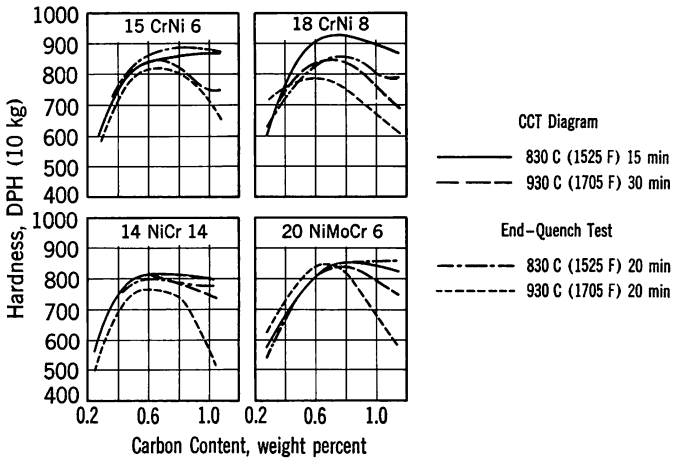

FIGURE 9. Maximum hardness of carburized 15 CrNi 6, 18 CrNi 8, 14 NiCr 14 and 20 NiMoCr 6 steels as a function of carbon content and method of determination

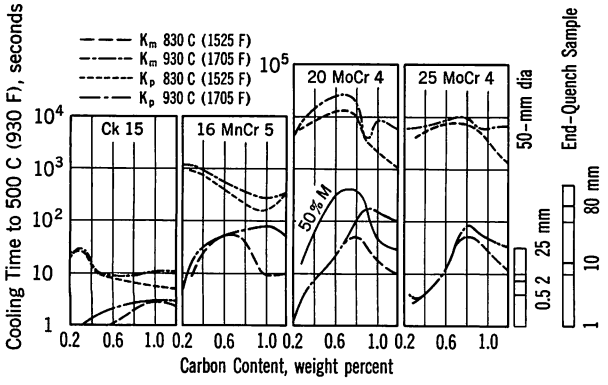

FIGURE 10. Critical cooling times of carburized Ck 15, 16 MnCr 5, 20 MoCr 4 and 25 MoCr 4 steels as a function of carbon content and austenitizing temperature

The time required for the start of ferrite formation (not shown on the graph) increases in the following order: Ck 15, 16 MnCr 5, 20 MoCr 4 and 25 MoCr 4. These times for the manganese–chromium specimens are ten-times those for unalloyed steel while for the molybdenum steels they are 100 times. In general, K_p, the time for conclusion of the formation of a mixed structure, decreases in the unalloyed and manganese–chromium steels as the effect of ferrite formation diminishes but again increases with formation of cementite. On the other hand, K_p for the molybdenum–chromium steels increases up to the eutectoidal composition and then decreases in the range where carbide precipitation is a factor.

Increasing the austenitizing temperature from 830 to 930 C (1525 to 1705 F) increases the K_m values up to the eutectoidal composition only in those cases where the formation of martensite is limited by ferrite. This is probably largely the result of grain growth. As soon as bainite is the limiting constituent for the formation of martensite, as is the case with the manganese–chromium and particularly with the molybdenum steels, there is no prolongation of the initiation times since bainite is not nucleated preferentially at the grain boundaries but is formed by a single-phase decomposition. The effect of austenitizing temperature on transformation is considerably greater in the hypereutectoid range because of differences in the amount of undissolved carbides. The times for the end of transformation remain almost constant for the unalloyed steel after austenitizing at 930 C (1705 F). With the manganese–chromium and the molybdenum steels however, the transformation starts after significantly longer times than after austenitizing at 830 C (1525 F). It is noteworthy that the analogous 25 CrMo 4 steel containing boron shows the least effect of austenitizing temperature.

Evaluation of the effect of alloying elements must be based on a specific carbon content or a definite stage in transformation. In general, the effect of an alloying addition is quite different in the eutectoidal range from that in the proeutectoidal transformations. The same applies for the effect of raising the austenitizing temperature.

The critical cooling times K_m for the carbon concentration giving the best hardenability after austenitizing at 830 C (1525 F) increase from three seconds at 1.0% C in the unalloyed steel to 50 sec at 0.60% C for the 16 MnCr 5 steel and the same time but about 0.8% C for the two molybdenum steels. With direct hardening the highest hardenability for the manganese–chromium steel is shifted to about 1.0% C and 80 sec, about the same time but 0.8% C for the 25 MoCr 4 steel with boron and to 180 sec at about 0.9% C for the 20 MoCr 4 steel. It appears that greater grain growth had already taken place here. The carbon content corresponding to the best hardenability remains relatively low for the molybdenum steels and the carbon range for this optimum hardenability comparatively narrow.

With the aid of these graphs it is possible to estimate the depth of hardening in specific sections if the cooling times over the section are known. The cooling time of a 50-mm-dia bar is given on the right for water quenching: 4 sec for a depth of 0.5 mm; 7 sec for 2 mm, the usual carburizing depth; and 25 sec in the core. Therefore, at a depth of 0.5 mm after direct hardening, a substantially martensitic structure will be obtained in the unalloyed steel at carbon contents over 0.8%, but in the manganese–chromium steel at carbon contents as low as 0.25% and in the two molybdenum steels with carbon contents over 0.35%. Ferrite-pearlite is found at the core of the unalloyed steel but a mixed structure occurs with the other steels.

The bar furthest to the right in Figure 10 gives the cooling times in a Jominy specimen for 1, 10 and 80 mm from the quenched end. Thus, the course of the Jominy hardenability curve can be estimated to a first approximation. With the high-hardenability molybdenum steels, the cooling rate of the Jominy specimens is slowed down further by setting a cap on the end. This prolonged cooling time corresponds to the top mark on the bar.

The cooling times for 50% martensite taken from the CCT diagram for an austenitizing temperature of 830 C (1525 F) have been indicated in the section of Figure 10 pertaining to 20 MoCr 4. The 50% martensite values determined from the carburized Jominy specimen give about the same shape curve but with somewhat shorter times. This difference corresponds to the hardness differences in Figure 8.

A very characteristic difference between the manganese–chromium steel and the molybdenum–chromium steels is the width of the cooling-rate band corresponding to formation of a mixed structure, that is, the difference between K_m and K_p. In the highest hardenability region, this is about 200 sec for the manganese–chromium steel and about 10^4 sec for the molybdenum–chromium steels.

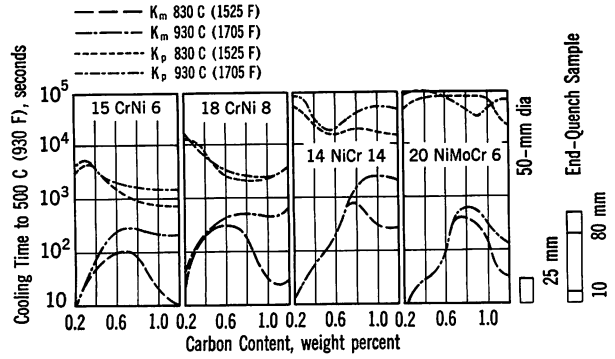

FIGURE 11. Critical cooling times of carburized 15 CrNi 6, 18 CrNi 8, 14 NiCr 14 and 20 NiMoCr 6 steels as a function of carbon content and austenitizing temperature

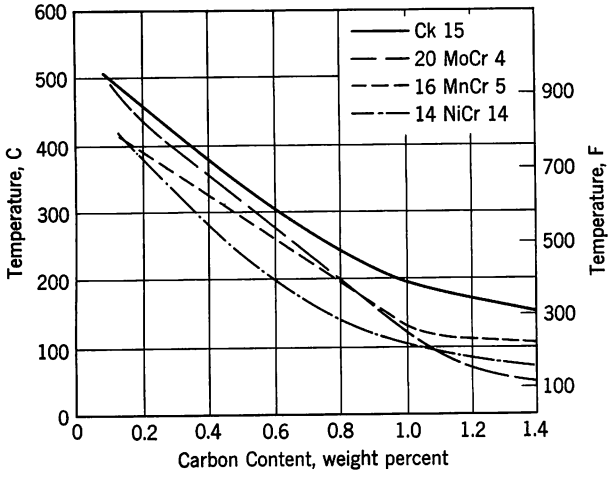

FIGURE 12. M_s temperatures of carburized Ck 15, 20 MoCr 4, 16 MnCr 5 and 14 NiCr 14 steels austenitized at 930 C (1705 F) for 30 min as a function of carbon content

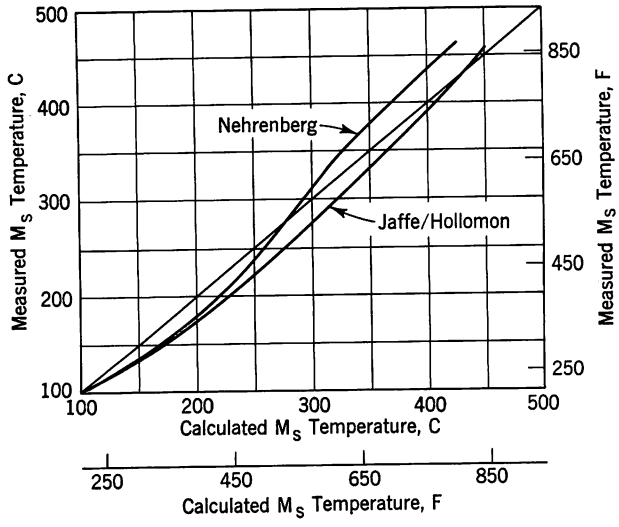

FIGURE 13. Correlation between measured and calculated M_s temperatures

The transformation characteristics of 20 NiMoCr 6 steel are compared with those of chromium–nickel and nickel–chromium steels in Figure 11, where the vertical scale has been shifted towards longer cooling times by one cycle. Here also it is clearly evident how much broader the mixed-structure zone is for the molybdenum-alloyed steel, how much narrower the range of compositions around the eutectoidal value corresponding to the highest hardenability is and how slight is the influence of higher austenitizing temperature. This steel behaves basically the same as the 25 MoCr 4 steel, especially after direct hardening from 930 C (1705 F). On direct hardening, the chromium–nickel steels retain the maximum hardenability reached at 0.6% C almost unchanged up to 1.2% C as does the nickel–chromium steel over 0.8% C. In this range, therefore, the factors slowing down transformation such as grain size and alloy content of the austenite counterbalance the factors promoting transformation, greater supersaturation and entrance into the multiphase region.

Figure 12 summarizes the M_s temperatures of various steels as a function of carbon content. The upper curve covers the unalloyed steel, while the next applies to both molybdenum–chromium steels. The curve for 16 MnCr 5 coincides with that for the considerably higher alloyed 20 NiMoCr 6 and the lowest curve is representative of the chromium–nickel and nickel–chromium steels. The Jaffe-Hollomon formula[5] gives as good agreement as the Nehrenberg formula[6] when the corrections indicated in Figure 13 are applied. Calculations of the M_s temperature are based on the premise that the composition of the solid solution capable of transformation does not deviate from that of the steel because of the presence of undissolved or previously precipitated phases. For all the steels investigated the equilibrium diagrams show three and more components. Consequently, even with the same alloy content, a change of the carbon content in the two-phase region austenite + carbide can result in a change in the content of other alloying elements in the solid solution capable of transformation. Therefore, even in the two-phase region the M_s temperatures are dependent on carbon content.

RESIDUAL STRESSES AFTER CARBURIZING

The third property requirement pertains to improved fatigue characteristics through compressive stresses at the surface. An analysis of the evolution of residual stresses through superposition of thermal contractions and expansions during transformation on cooling can also clarify the conditions under which the case may crack or spall.

The formation of the thermal stresses caused by thermal contraction can be seen in Figure 14. Here the cooling curves for surface and center of a 100-

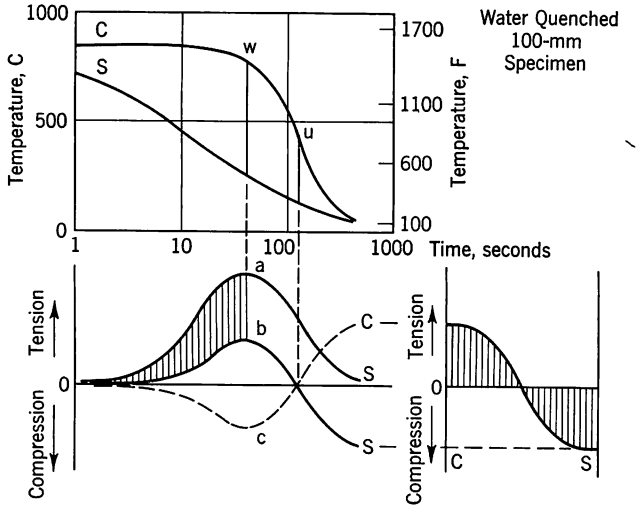

FIGURE 14. Formation of thermal stresses on cooling

mm-dia bar have been entered in the coordinate system of a CCT diagram. At the start of cooling the surface temperature "S" drops considerably faster than the core temperature "C." The maximum temperature difference of about 600 C (1080 F) occurs at a time indicated by W. At this point the thermal contraction of the surface is about 0.5% as compared to the almost unchanged core. This contraction, however, cannot take place because it is prevented by the rest of the cross section. Consequently tensile stresses are formed in the case and compressive stresses in the core as indicated in the lower left diagram for longitudinal stresses. If all these stresses could be absorbed elastically, they would increase to a point "a," corresponding to W in the upper diagram, and then would again decrease to zero when all portions of the cross section would have the same temperature. Stresses, however, are possible only for values up to the hot elastic limit so plastic deformation will occur. As a result the core will contract and the stresses will follow curve "b" where a reversal of stresses will take place at "u." The ultimate outcome, as shown in the lower right sketch, will be residual stresses with reversed sign, that is compression at the surface and tension at the core.

With a shallow-hardening tool steel containing about 1.3% C, the expansion due to transformation is superimposed upon the above pattern so the thermal stresses are increased. Thus it can happen, as shown in Figure 15, that the core is cracked by tensile stresses at regular intervals. This unfavorable addition of transformation and thermal stresses occurs when the formation of pearlite in the core takes place before the stress reversal indicated in Figure 16 at a time when compressive stresses already exist in the core and when the case transforms to martensite with a large expansion of volume after the stress reversal. Both transformations augment the thermal stress pattern of compression at the surface and tension in the core as indicated schematically in the two bottom diagrams.[7]

The creation of stresses on hardening a carburized part of a carburizing steel is entirely comparable. In Figure 17 the cooling curves for the surface at depths of 0.5, 2 and 5 mm as well as for the core of a 50-mm-dia bar are entered in the coordinates of a CCT diagram, which shows the transformation behavior of the uncarburized Ck 15, 20 MoCr 4 and 20 NiMoCr 6 steels after austenitizing at 930 C (1705 F) to indicate conditions at the core on direct hardening. The 25-mm curve for cooling of the core indicates that transformation goes to completion in

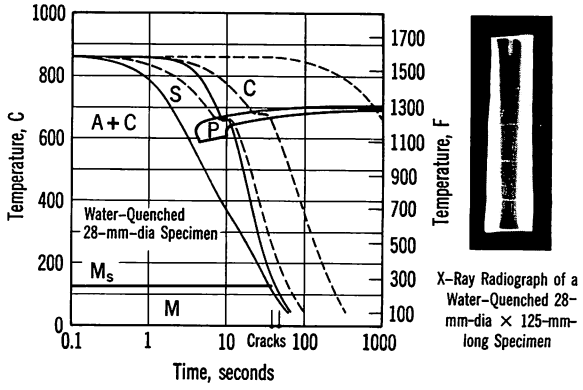

FIGURE 15. Transformation characteristics and formation of cracks in a shallow-hardening tool steel with 1.3% C austenitized at 860 C (1580 F)

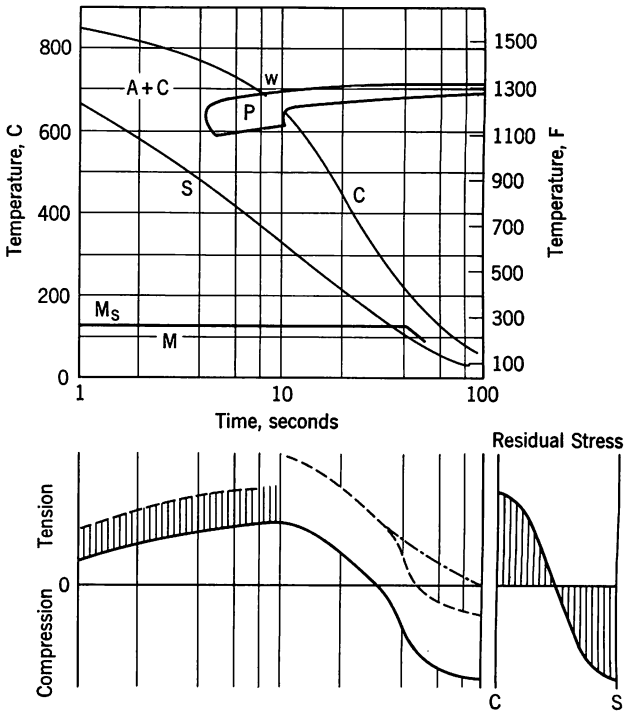

FIGURE 16. Formation of residual stresses in a 28-mm-dia bar of a 1.3% C steel, water quenched to give a shallow outer hardened layer

the ferrite and bainite regions and that the amount of bainite increases with increasing sluggishness, that is with increasing hardenability of the steel. Only the M_s lines for carbon contents from 0.40 to 1.2% are needed to judge the conditions in the carburized case on hardening. Actually, the M_s temperatures for the unalloyed steel would be somewhat higher than the indicated lines for carbon contents over 0.2% and those of the nickel–molybdenum–chromium steel would be somewhat lower.

Transformation in the core is largely completed before transformation in the case and also prior to the stress reversal, just as with the shallow-hardening steel in Figure 16. This transformation, therefore, accentuates the tensile stresses in the case resulting from thermal stresses, which become compressive stresses after reversal. With carbon contents around 0.8% C, the transformation to martensite in the case with its large volume expansion occurs at a temperature under 200 C (390 F) after the stress reversal and consequently again adds to the compressive stresses in the case. But with the 50-mm-dia bar described, the transformation to martensite in the case would not start on the surface with 0.8% C. If a carbon content of about 0.4% is assumed to be present at a depth of two millimeters, the martensite formation would then start here at about the time indicated by W. As cooling progresses, it would extend in a few seconds to the surface.

A decrease in diameter has the same effect on the course of transformation as a change to a steel with more sluggish transformation characteristics but the same diameter. If the diameter is also increased with a steel having very high hardenability, it can happen that the core would transform after the case. This would lead to tensile stresses and probably longitudinal cracks in the case.

Case depth plays a very important role. If the case depth is such that a carbon content of 0.4% C is found two millimeters below the surface, then the formation of martensite occurs here about five seconds before the outer surface with over 0.8% C. Thus the austenite untransformed at that time can be deformed but no deleterious effects are to be expected. But if the case is so thick that the 0.4% C level is at a depth of five millimeters, the formation of martensite takes place over the entire case almost simultaneously as indicated in Figure 17. Because of the abrupt expansion in volume of the case, which is being hardened at the same time, this can lead to high radial stresses that will result in spalling of the case. This effect is increased further if the steel was carburized to give hypereutectoid carbon contents so the M_s temperature no longer decreases appreciably as indicated in Figure 12. Under unfavorable conditions of this type, very characteristic cracks are also produced on deep-carburized Jominy specimens when only the cylindrical surface and not the end are carburized and when the end is water

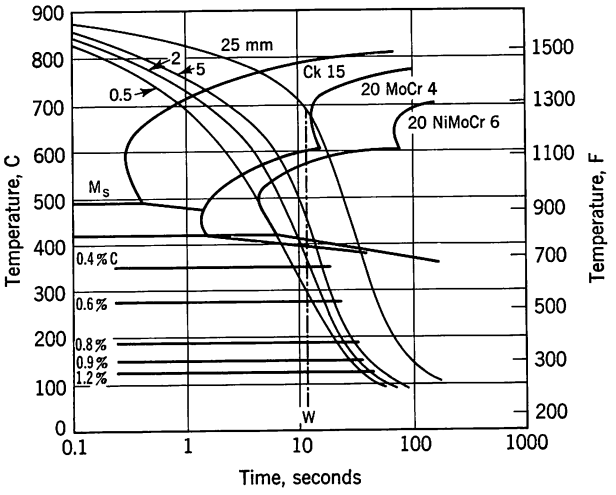

FIGURE 17. Transformation in carburized 50-mm-dia bars of Ck 15, 20 MoCr 4 and 20 NiMoCr 6 steels

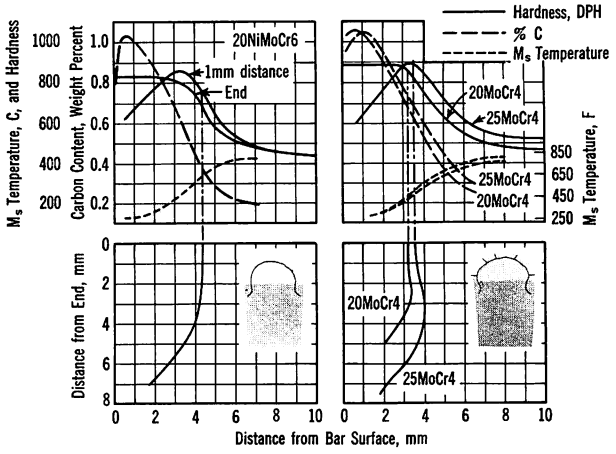

FIGURE 18. Correlation between cracking, depth of hardening and carbon content. 20 MoCr 4 quenched from 830 C (1525 F); 25 MoCr 4 and 20 NiMoCr 6 from 930 C (1705 F)

quenched as usual. In this case, the formation of martensite at the quenched end starts at the axis of the specimen and progresses outward at increasing speeds. The radial stresses set up in this way can lead with all steels to complete separation of the case in the form of a hollow cylinder.

Figure 18 shows the propagation of such cracks longitudinally from the quenched end of a molybdenum–chromium and a nickel–molybdenum–chromium steel. The top part of this graph indicates the carbon content, hardness and M_s temperature as a function of distance from the surface. The quenched end shows not only a concentric crack but also radial cracks starting along the inner surface of the separated case. These cracks indicate that the final portions of the case to transform caused tangential tensile stresses in the underlying areas that had already transformed.

SUMMARY

The aim of our research was to gain information about the technical behavior of carburizing steels from a broad basic investigation of their transformation characteristics at different carbon levels. For this purpose continuous-cooling transformation diagrams were determined on specimens of the various steels gas carburized to specific carbon contents and austenitized at temperatures corresponding to hardening of the case as well as direct hardening from the carburizing temperature.

The hardenability of the various grades as a function of carbon content as well as the structural changes in the transition from the hardened case to the core and the maximum attainable hardness could be derived from these CCT diagrams. It was found that even in the martensitic range hardness changes occurred depending on the cooling rate and these in turn were influenced by the carbon content. Thus it can be concluded that a valid comparison of the hardening characteristics of these steels must be based on a specific cooling rate or a definite structure.

The carburizing steels investigated differed not only in the maximum hardness for specific carbon contents but particularly in the amount of hardness loss caused by retained austenite in hypereutectoid compositions. Carbon content likewise has a very characteristic effect on hardenability with a maximum in the eutectoidal range. This effect differs quite characteristically for the different types of alloy steel.

From the representation of the transformation characteristics of carburizing steels in CCT diagrams and the cooling curves over the cross section of the parts it is possible to draw conclusions as to the formation and distribution of residual stresses in carburized parts. The estimation of the magnitude of these stresses is significant because of their influence on fatigue properties as well as cracking.

REFERENCES

1. K. Bungardt, E. Kunze and H. Brandis, DEW Tech. Ber. *5.* 1 (1965)
   L. Rademacher, Härterei-Tech. Mitt. *20.* 246 (1965)
   H. Tauscher and E. Stecher, Härterei-Tech. Mitt. *20.* 263 (1965)
   R. Chatterjee-Fischer and O. Schaaber, Härterei-Tech. Mitt. *21.* 186 (1966)
   A. Randak and E. Kiderle, Härterei-Tech. Mitt. *21.* 190 (1966)
2. *Atlas for the Heat Treatment of Steels*, edited by Max-Planck-Institut für Eisenforschung in Cooperation with Werkstoffausschuss des Vereins Deutscher Eisenhüttenleute; Part I by F. Wever and A. Rose; Part II by A. Rose, W. Peter, W. Strassburg and L. Rademacher, Verlag Stahleisen, Düsseldorf, 1954/56/58
3. H. P. Hougardy and A. Rose, *Neuere metallkundliche Untersuchungsverfahren*, Verlag Stahleisen, Düsseldorf, in print
4. A. Rose, Stahl und Eisen, *85.* 1229 and 1267 (1965)
5. L. D. Jaffe and J. H. Hollomon, Trans. AIME *167.* 617 (1946)
6. A. E. Nehrenberg, Trans. AIME *167.* 494 (1946)
7. A. Rose, Berg- und Hüttenmänn. Monatsh. *110.* 393 (1965)
   A. Rose, Härterei-Tech. Mitt. *21.* 1 (1966)

ORAL DISCUSSION OF

Transformation Characteristics and Hardenability of Carburizing Steels

Presented by A. ROSE

L. PORTER (United States Steel Corporation). Yesterday, we heard some of the effects of pressure on shifting the transformation diagram. I wonder if in a carburized steel of this type, you see some effect of pressure in shifting the diagram and therefore changing the structures which you would get and the results you would infer from observations on transformation in small specimens.

AUTHOR'S REPLY. We have not evaluated the effect of pressure per se on the transformation; however, we have noted that plastic deformation of the parent austenite does affect the subsequent transformation products. Specifically, we have seen that the microstructures of conventional steels transformed by continuous cooling are different, depending upon whether the parent austenite was plastically deformed and therefore stressed, or stress-free.

D. J. BLICKWEDE (Bethlehem Steel Corporation). I believe that Carney has shown similar results.

E. S. ROWLAND (The Timken Roller Bearing Company). I would like to commend Dr. Rose on a most interesting paper. To an old timer to whom stacking fault energy is not necessarily the most vibrant, living entity, this was a most refreshing change of pace. Also, I can quite easily name a couple of dozen in the audience who have the job of getting the most out of carburizing steels for the almighty dollar, and the kind of data which you have presented is most valuable in this regard. We are at the point where composition is already established by the cost of the steel, and unless we can find ways and means of controlling residual stresses and getting them to work for us in carburized components, we have not achieved what we are all trying to do.

D. J. BLICKWEDE. I am sure that all people who will be dealing with practical things will look forward to this paper appearing in print.

W. WILSON (A. Finkl and Sons Company). Are the discrepancies between the Jominy test results and the continuous cooling transformation due to the shapes of the cooling curves?

AUTHOR'S REPLY. This assumption is correct. In most cases, the change in the result of the transformation can be determined by the type of change in the cooling curves. It is also possible that the deformation processes which lead to the formation of internal stresses in the Jominy specimen during transformation may have an effect.

A Pearlite Hardenability Concept as a Basis for Alloy Development

R. D. MANNING, H. M. REICHHOLD and J. M. HODGE
United States Steel Corporation
Applied Research Laboratory
Monroeville, Pennsylvania

INTRODUCTION

The term "pearlite hardenability," as it is used here, means the hardenability necessary for a steel to transform to a desired pearlitic microstructure at a given depth in a particular section on cooling from a temperature in the austenitic range. Several years ago, Hollomon and Jaffe[1]* coined the terms "pearlitic hardenability" and "bainitic hardenability" to distinguish between the types of high-temperature transformation that interfere with the formation of martensite on cooling — that is, the transformations that affect martensite hardenability, the hardenability with which metallurgists and engineers are more generally familiar. In the present discussion, however, we are concerned with an aspect of hardenability involving transformation to pearlitic microstructures rather than to martensitic microstructures.

This is an important consideration, despite the recent trend toward wider use of quenched and tempered constructional steels, because large tonnages of both carbon and alloy steel in the form of bars, plates, forgings, and structural shapes are marketed for use in the pearlitic condition — that is, in the hot-rolled or normalized condition. For example, many tons of low-carbon pearlitic plates are used for bridges, earthmoving equipment, ships, and pressure vessels. Similarly, many tons of medium-to-high-carbon steels are used in the pearlitic condition for applications such as railroad axles, wheels, and rails.

The present discussion will deal chiefly with the effect of alloying elements on pearlite hardenability in steels containing about 0.20% C. The alloying elements studied include manganese, silicon, copper, nickel, chromium, molybdenum, and vanadium. The general effect of alloys on pearlite hardenability is illustrated schematically in Figure 1. In the diagram on the left, transformation occurs at about 675 C (1250 F) — coarse pearlite; in the diagram on the right, representing an alloy steel, transformation occurs at about 600 C (1100 F) — fine pearlite.

Quite a few years ago, Gensamer[2] and his associates showed that in eutectoid steel, fine pearlite exhibited a much better combination of strength and ductility than did coarse pearlite. This observation also applies, in general, to the properties of 0.20% C steels with microstructures of ferrite and pearlite. Furthermore, we believe that the low-temperature notch toughness of 0.20% C steels with fine-pearlite microstructures and fine ferrite grain size is better than that of similar steels with coarse-pearlite microstructures. Therefore, since the mechanical properties of steels with fine-pearlite microstructures may be expected to be better than those of steels with coarse-pearlite microstructures, we should be interested in how to obtain the desired microstructures by controlling the composition of the steel.

In the past, several investigators[3] have devised formulas and charts for use in calculating the strength of air-cooled steels from chemical composition. These methods usually require separate charts or factors for each different cooling rate or section size. On the other hand, the calculation, in terms of Grossmann's ideal-diameter concept,[4] of the chemical composition that will yield a desired pearlitic microstructure would eliminate the need for separate charts or factors. In the Grossmann method of determining multiplying factors for each of the alloying elements[5] and determining base hardenability values for iron–carbon alloys, one calculates an ideal diameter from the chemical composition of a steel and then determines what size bar of this steel can be hardened to the center in a given cooling medium

* See references.

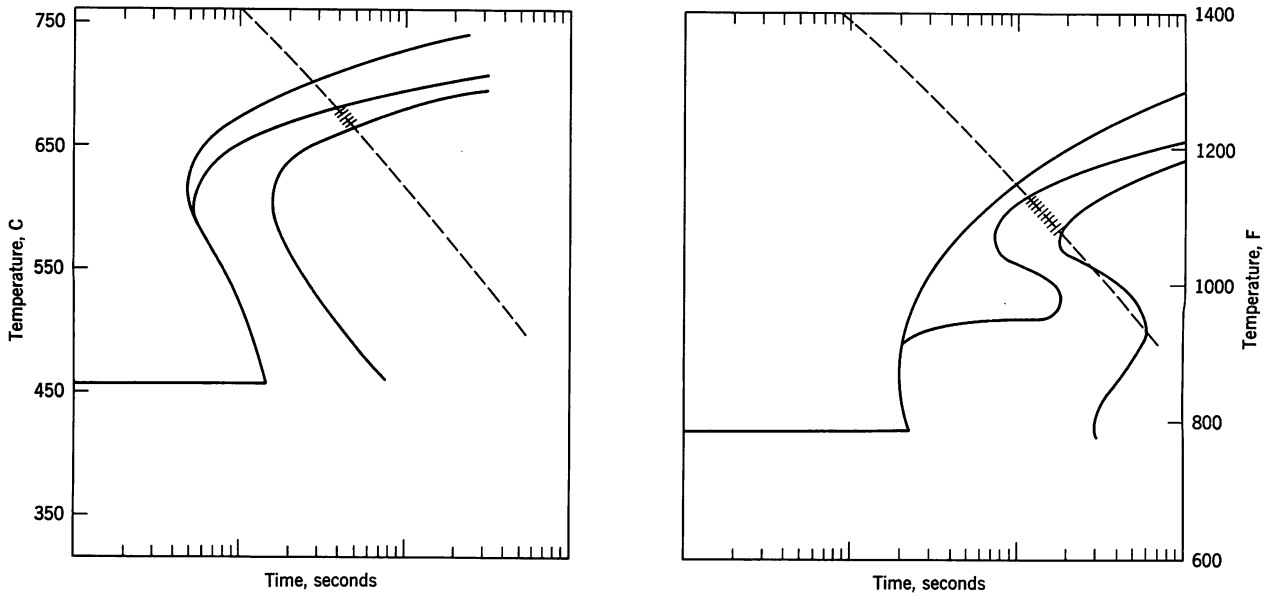

FIGURE 1. Schematic representation of an increase in pearlite hardenability

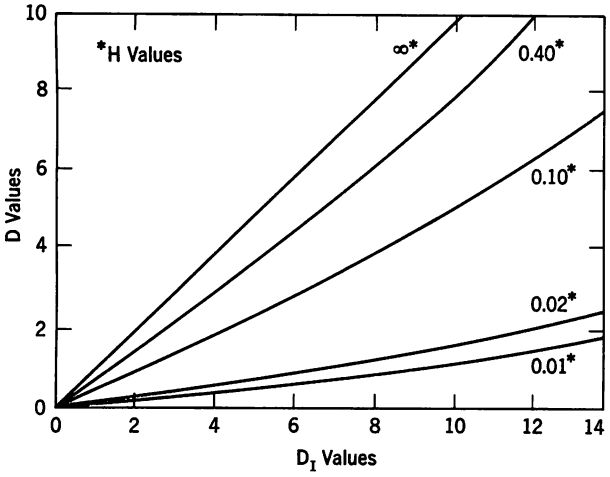

FIGURE 2. Curves showing relationships among ideal diameter, bar diameter, and severity of quench

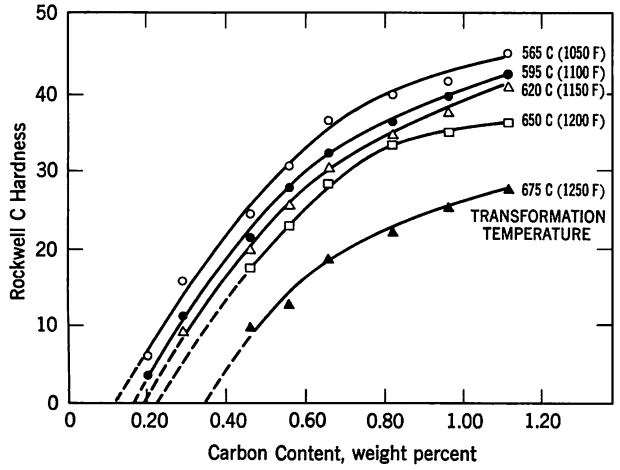

FIGURE 3. Effect of carbon content on the hardness of pearlitic microstructures formed at indicated temperatures

from a chart like that shown in Figure 2. We will be particularly interested in a curve similar to the one shown for H = 0.02, the approximate quenching severity for air cooling.

DETERMINATION OF PEARLITE-HARDENABILITY FACTORS FOR ALLOYING ELEMENTS

The investigation of pearlite-hardenability effects was based on the assumption that the hardness corresponding to complete isothermal transformation at a given temperature, such as at 595 C (1100 F), is equivalent to the hardness at the center of a continuously cooled bar or plate when the average temperature of transformation is 595 C (1100 F). Although a microstructural criterion is much to be preferred to a hardness criterion, there are several difficulties involved — for example, it is quite difficult to distinguish between say 595 C (1100 F) and 620 C (1150 F) pearlite, at least with the light microscope. Despite the limitations imposed by the hardness criterion, it was chosen because of its simplicity and because within certain limits, the results could be used satisfactorily.

First, the effect of carbon content on the hardness of plain carbon steels isothermally transformed at several temperatures in the pearlite range was determined. In Figure 3 are shown effects that have been known for a long time — that the hardness of steel with a microstructure of pearlite and ferrite increases with increasing carbon content and that for a given carbon content, the hardness increases as the temperature of transformation decreases.

Similarly, the hardening effect of each of the alloying elements to be studied was determined by isothermally transforming steels with alloy additions

at 565 C (1050 F) and 595 C (1100 F) to the fine pearlite in which we are most interested. This effect is illustrated in Figure 4 for nickel, copper, and vanadium. Hardening effects were also observed for chromium and molybdenum, Figure 5, but the hardening effects of manganese and silicon in the ranges studied were negligible.

With a quantitative evaluation of the hardening effects of carbon and the alloying elements, one can determine from end-quench hardenability curves the location at which the hardness characteristic of the desired pearlitic microstructure occurs. For example, an end-quench hardenability curve for a steel containing 0.20% C, 0.90% Mn, 0.21% Si, and 0.08% V is shown in Figure 6. If one is interested in 1100 F pearlite, then from the charts shown in the previous figures, the hardness corresponding to 0.20% C is 3 Rockwell C, and the hardness increase from 0.08% V is 8 Rockwell C. Therefore, the critical hardness for 595 C (1100 F) pearlite in this steel is 11 Rockwell C, and from the curve in Figure 6 it may be seen that 11 Rockwell C occurs 11/16 in. from the quenched end.

Now, a curve is needed to relate distance from the quenched end to ideal diameter, and such a curve is shown in Figure 7. This relationship was calculated from the heat-flow tables of Russell[6] and from the cooling rates along an end-quench hardenability specimen determined by Russell and Williamson,[7]

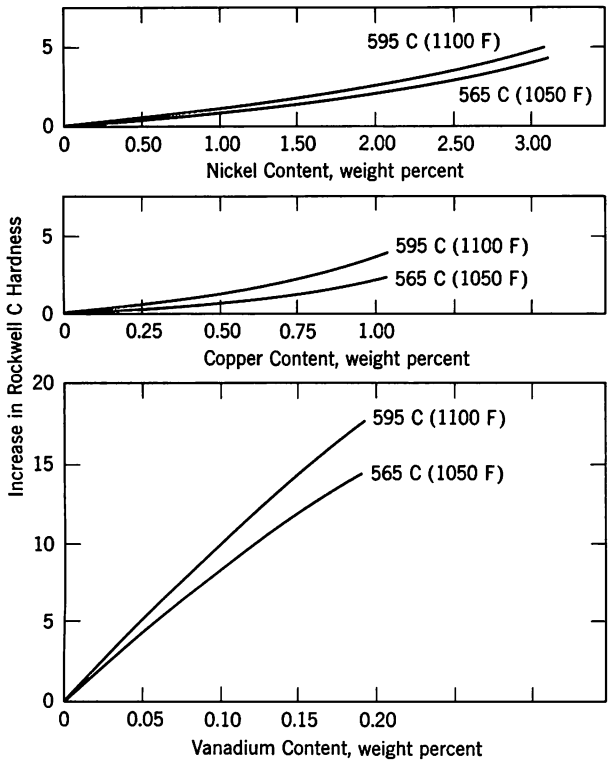

FIGURE 4. Hardening effect of nickel, copper, and vanadium in 0.20% C steels with fine-pearlite microstructures

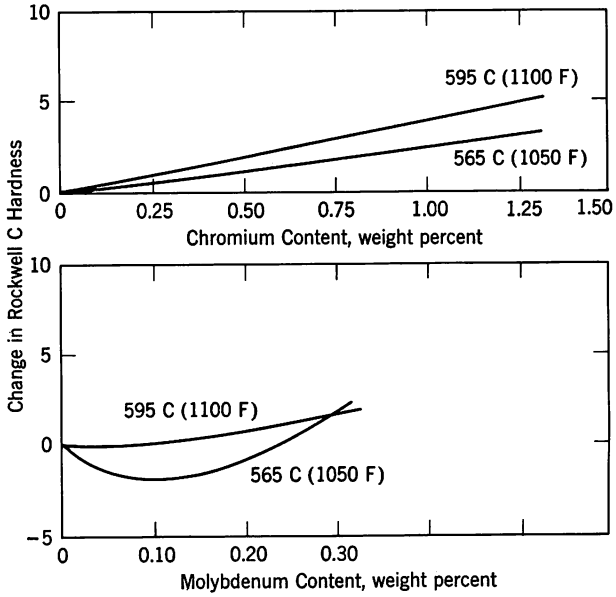

FIGURE 5. Hardening effect of chromium and molybdenum in 0.20% C steels with fine-pearlite microstructures

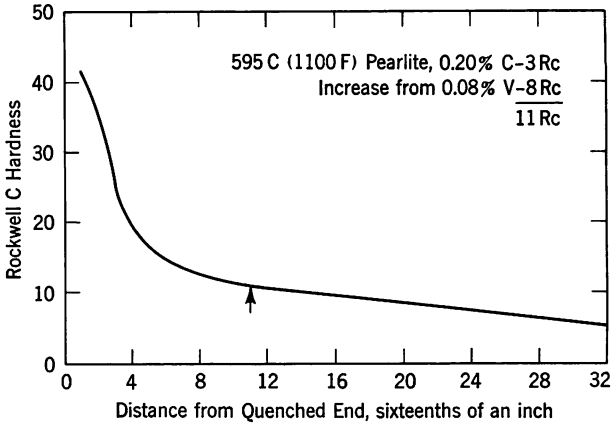

FIGURE 6. End-quench hardenability curve for an 0.20% C manganese–vanadium steel

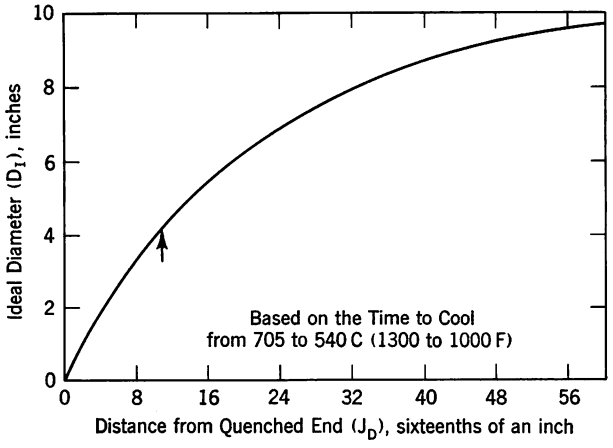

FIGURE 7. Relationship between ideal diameter and distance from quenched end, based on the time to cool from 705 to 540 C (1300 to 1000 F)

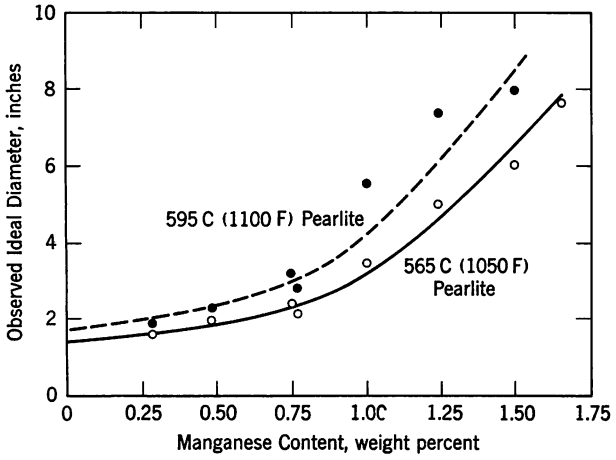

FIGURE 8. Observed ideal diameters for the manganese steels

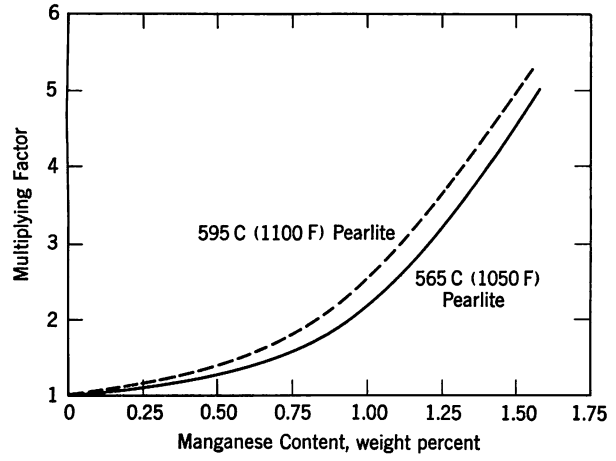

FIGURE 9. Pearlite-hardenability factors for manganese

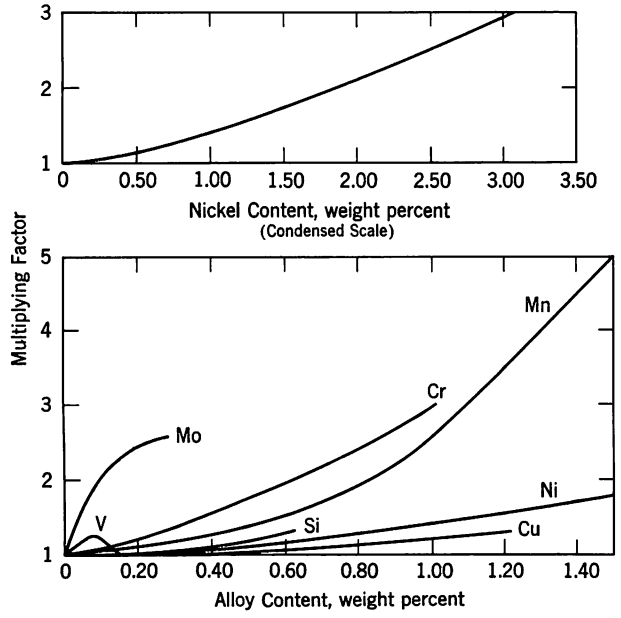

FIGURE 10. Pearlite-hardenability factors for several alloying elements

the cooling criterion being the time to cool from 705 to 540 C (1300 to 1000 F). In Figure 7, the 11/16-in. distance corresponds to an ideal diameter of about 4.1 in.

Ideal-diameter (D_I) values were obtained in this way for several series of steels, only one of the previously mentioned elements being varied in each series. The ideal diameters for different amounts of a particular alloying element were plotted against the alloy content, and the best line was drawn through the points as shown in Figure 8 for manganese. The curves were extrapolated to 0% Mn, and these intercept values were assumed to represent the respective pearlite hardenabilities for a steel with no manganese. To obtain multiplying factors for manganese, D_I values selected from these curves at various points (such as 0.25, 0.50, 0.75, 1.00%, and so forth) were divided by the respective intercept values. The factors thus obtained were plotted against manganese content as shown in Figure 9. These factors are the values that are used to indicate quantitatively the effect of manganese on transformation during continuous cooling to 565 or 595 C (1050 or 1100 F) pearlite. The marked effect on pearlite hardenability of manganese contents over about 0.75% is evident.

Factors for the other elements were determined in a similar way, and a summary of the effects on pearlite hardenability of all the elements studied is shown in Figure 10. As might be expected, molybdenum shows the greatest pearlite hardenability effect. Although the effect of vanadium is small and goes through a maximum, vanadium has the next greatest effect. Chromium is next and then manganese. It is interesting to note that up to 0.60%,

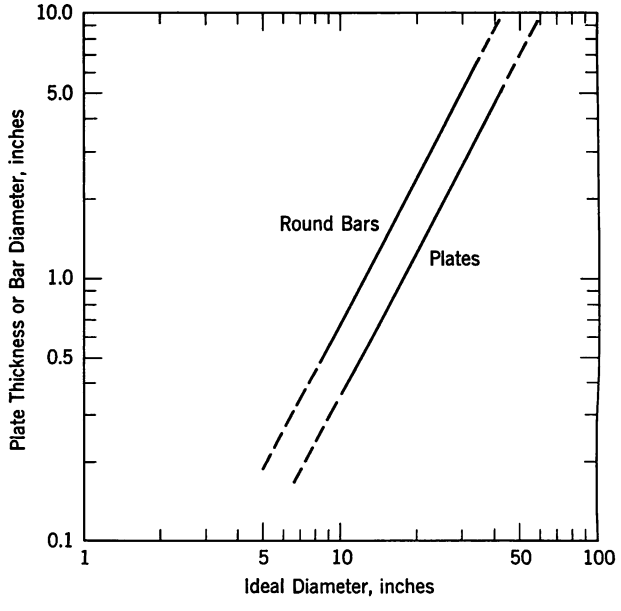

FIGURE 11. Ideal diameters for air-cooled plates of various thicknesses and for bars of various diameters

silicon has about the same effect on pearlite hardenability as has manganese. For alloy contents of less than 1%, nickel and copper exhibit minor pearlite-hardenability effects. Greater amounts of nickel, however, as drawn to the condensed scale in the upper part of the figure, show significant pearlite-hardenability effects.

Once the factors for several alloying elements were determined, base hardenability values were needed for iron–carbon alloys containing about 0.20% C. These values were obtained by dividing the ideal diameters for several of the steels, with different alloy contents, by the product of the factors determined for the various alloying elements present. The average of the resulting quotients then gave an ideal diameter for an 0.20% C iron–carbon alloy. A value of 1.2 was obtained for 565 C (1050 F) pearlite and a value of 1.45 for 595 C (1100 F) pearlite.

It was then possible to calculate an ideal diameter for pearlite microstructures, but this ideal diameter must be related to the air cooling of plates and bars. Figure 11 shows such a relationship; the line for round bars is similar to Grossmann's curve for air cooling, shown in Figure 2. These data were obtained from a calculated plot of ideal diameter versus time to cool from 705 to 540 C (1300 to 1000 F), and from a plot of experimental data on bar diameter versus the time to cool from 705 to 540 C (1300 to 1000 F). The latter cooling time for plates was calculated from the known heat-flow relationships between round bars and plates.[6] Thus, if the ideal-diameter equivalent to an air-cooled ½-in.-thick plate is desired, this plot is used and a value of about 11.5 in. is observed. Of course, as the plate or bar size increases, the ideal-diameter values become quite large — well beyond the range of the conventional end-quench test.

APPLICATION OF THE PEARLITE-HARDENABILITY CONCEPT

For an example of how this method might be used, suppose a low-carbon steel exhibiting the following properties in the hot-rolled condition is desired: a minimum tensile strength of 110,000 psi* in ¼- to ⅜-in.-thick plates, and a minimum tensile strength of 105,000 psi in plates heavier than ⅜-in.-thick to ½-in.-thick. First, it was determined from Figure 11, that the D_I equivalent to a ½-in.-thick air-cooled plate is about 11.5 in., and that the D_I equivalent to a ¼-in.-thick plate is about 8 in. Then, the pearlite-hardenability factors were used to determine a composition that would give a D_I of about 8 to 11.5. First, however, by referring to Figure 3, showing hardness as a function of carbon content, it is observed that at 0.20% C, both 565 C (1050 F) and 595 C (1100 F) pearlite are much too soft (3 to 7 Rockwell C) to meet the desired strength requirement (about 18 Rockwell C), so that an element which contributes a significant hardening effect is needed. Also, at about 0.23% C, 595 C (1100 F) pearlite exhibits a hardness of about 8 Rockwell C. Since the attainment of 595 C (1100 F) pearlite requires less alloy than the attainment of 565 C (1050 F) pearlite, the composition of the desired steel was based on 595 C (1100 F) pearlite and a carbon content of 0.20 to 0.25%. With a base hardness of 8 Rockwell C, a hardness increase of about 10 Rockwell C is required for tensile strengths of 105,000/110,000 psi. From Figure 4, it may be noted that 0.10% V gives about the required hardness increase. The following composition range, in percent, was then established on the basis of the pearlite-hardenability factors:

C	Mn	Si	Ni	V
0.20	1.20	0.20	0.40	0.08
0.25	1.50	0.35	0.70	0.13

Calculations indicated that a steel at the middle of this range has a D_I for 595 C (1100 F) pearlite of 10.3 in., more than needed for the ¼-in.-thick plates and a little less than needed for the ½-in.-thick plates.

An investigation of the properties and microstructure of hot-rolled plates from induction-furnace heats at the top and bottom of the proposed composition range, indicated that the steel would meet the mechanical-property requirements. The data for typical plates from a small *production* heat are shown in Figure 12. Here, a moderately fine pearlitic micro-

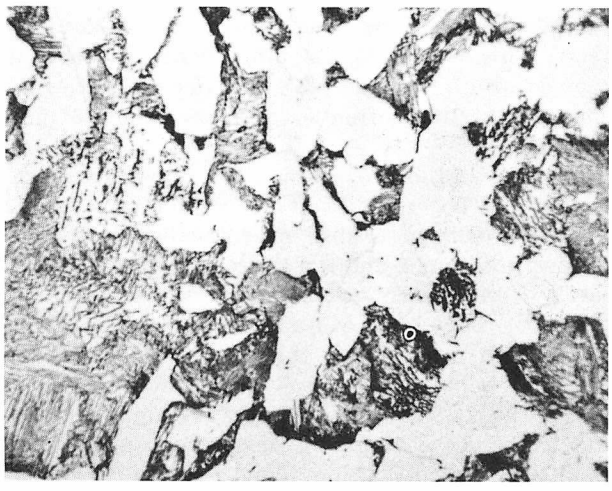

%C	%Mn	%Si	%Ni	%V
0.26	1.32	0.25	0.56	0.17

	Yield Point, psi	Tensile Strength, psi	Elongation in 2 in., %
¼ in.	94,700	118,900	29
⅜ in.	92,000	116,100	31

FIGURE 12. Microstructure and properties of commercial hot-rolled plates. 1000 X

*1000 psi = 6.9 MN/m².

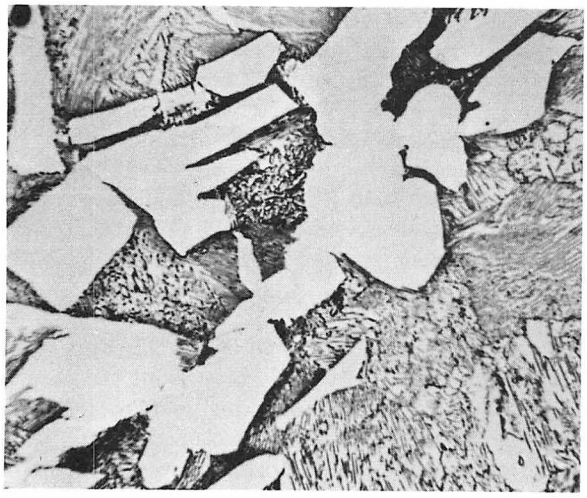

%C	%Mn	%Si	%Ni	%V
0.22	1.22	0.25	0.43	0.11

Fine Pearlite
¼ in. — 19.5 Rockwell C
½ in. — 17.5 Rockwell C

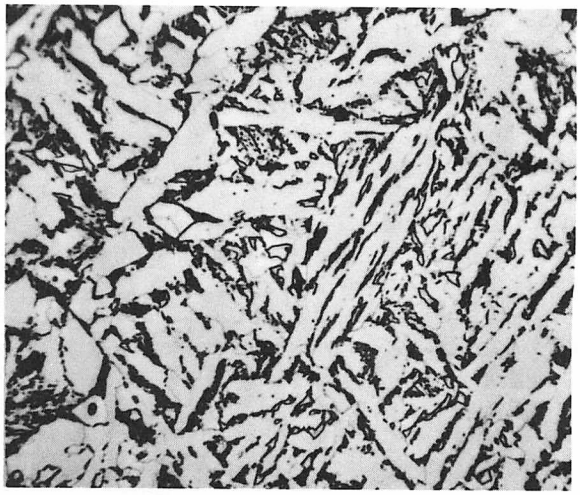

%C	%Mn	%Si	%Ni	%V
0.25	1.51	0.27	0.64	0.13

Bainite
¼ in. — 20.5 Rockwell C
½ in. — 24.0 Rockwell C

FIGURE 13. Microstructure of ¼-in.-thick experimental plates representing about the lower and upper limits of the proposed composition range. 1000 X

structure is observed at the center of a ¼-in. plate of the indicated composition, which is somewhat high in carbon and in vanadium. The tensile strength of both ¼- and ⅜-in. plates of this steel is well above the desired minimum of 110,000 psi, and the plates exhibit good ductility.

A good illustration of the effect of relatively large amounts of alloying elements in shifting the transformation from fine pearlite to upper bainite was furnished by the previously mentioned laboratory heats. This is one of the limitations of practical application of the method, since the properties of upper bainite may often be inferior to those of fine pearlite.

In Figure 13, one observes the microstructure of ferrite and fine pearlite at the center of a ¼-in. hot-rolled plate of a steel near the bottom of the composition range, and the microstructure of upper bainite (and some martensite) at the center of a ¼-in. hot-rolled plate of a steel near the top of the composition range. Note that the hardness of the bainitic steel is only one Rockwell C unit higher than that of the pearlitic steel. Because the higher carbon and vanadium contents of this steel should have resulted in higher hardness, and because its higher manganese and nickel contents should have resulted in greater hardenability (finer pearlite), a greater hardness difference might have been expected. Indeed, the ½-in. plate of the high-composition steel exhibited a pearlitic microstructure and as shown, a higher hardness (24 Rockwell C) than the ¼-in. plate (20.5 Rockwell C), whereas a slightly lower hardness might have been expected for the ½-in. plate, as was the case for the low-composition steel. Despite this limitation, the method has proved successful, and considerable tonnages of plates meeting the desired requirements have been made. Furthermore, it has been used successfully in other steel composition developments.

SUMMARY

In summary, a method of estimating quantitatively the chemical composition that will permit transformation to a desired pearlitic microstructure in a particular air-cooled section has been described and an example has been presented to show how the pearlite-hardenability concept can be used as a guide in selecting the compositions that will result in optimum properties in low-carbon, low-alloy steels.

REFERENCES

1. J. H. Hollomon and L. D. Jaffe, Trans. AIME *167*. 601 (1946)
2. M. Gensamer, E. B. Pearsall and G. V. Smith, Trans. ASM *28*. 380 (1940)
3. F. M. Walters, Jr., Trans. AIME *154*. 407 (1943) L. A. Carapella, Trans. ASM *35*. 435 (1945) I. R. Kramer, P. D. Gorsuch and D. L. Newhouse, Trans. AIME *172*. 244 (1947)
4. M. A. Grossmann, M. Asimow and S. F. Urban, "Hardenability, its Relation to Quenching, and Some Quantitative Data," *Hardenability of Alloy Steels*, ASM, 1939, 124
5. M. A. Grossmann, Trans. AIME *150*. 150 (1942)
6. T. F. Russell, "Some Mathematical Considerations on the Heating and Cooling of Steel," *Special Report No. 14*, Iron and Steel Institute (London), 1936, 149
7. T. F. Russell and J. C. Williamson, "Surface Temperature Measurements during the Cooling of a Jominy Test-Piece," *Special Report No. 36*, Iron and Steel Institute (London), 1946, 34

ORAL DISCUSSION OF

A Pearlite Hardenability Concept as a Basis for Alloy Development

Presented by R. D. MANNING

H. I. AARONSON (Ford Motor Company). The microstructures considered by the authors contain substantial proportions of proeutectoid ferrite. Since proeutectoid ferrite is mechanically weak and precipitates preferentially at the austenite grain boundaries, it can seriously degrade mechanical properties, as has long been known. If the carbon and alloy contents and the heat treatment were to be adjusted so as to obtain as nearly completely pearlitic microstructures as practicable, much more efficient use would be made of the strengthening effects of the carbide phase.

AUTHOR'S REPLY. Well, are you saying, Dr. Aaronson, that you want to make pearlite that isn't 0.80% C? One wants the low carbon to make the best use of the low carbon steel.

H. I. AARONSON. J. M. Robertson showed in 1929 that a 100% pearlitic microstructure can be obtained with an 0.35% C steel.

D. J. BLICKWEDE (Bethlehem Steel Corporation). I bet you can't weld it.

H. I. AARONSON. My point is to try to remove the proeutectoid ferrite reaction as far as you can from the picture, and to get as nearly 100% pearlite as you can, within the boundary conditions imposed by other service requirements.

AUTHOR'S REPLY. The mechanical properties will, of course, depend predominantly on the ferrite, what's dissolved in it, and on its grain size.

D. J. BLICKWEDE. I'd like to add a footnote to Dr. Aaronson's comment: A lot of work is being done to refine the proeutectoid ferrite structure in steels of this type by finishing them on the rolling mills at much lower temperatures, thereby improving ductility and to a degree, the strength. Furthermore, this isn't the only way to harden as-rolled steels or normalized steels. One can also accomplish this by small additions of other elements, which act in a synergistic way, such as vanadium and nitrogen, or columbium and nitrogen. These have essentially no effect on the pearlite reaction, but result in hardening through a precipitate of finely dispersed nitrides.

H. W. PAXTON (Carnegie Institute of Technology). Do you have any idea as to how much your factors are influenced by austenite grain size?

AUTHOR'S REPLY. No, we don't; we made a compromise and used an austenitizing temperature of 955 C (1750 F), but as you see, we are talking about using this to predict properties or compositions for hot-rolled plates, the slabs of which will have been heated considerably hotter and may or may not finish rolling in that temperature, but we haven't looked at that.

H. W. PAXTON. Do you have any indication of scatter in your results which might have come about from variation in grain size?

AUTHOR'S REPLY. No, I don't recall of any.

A. ROSE (Max-Planck-Institut für Eisenforschung). In a steel of eutectoid carbon concentration, that is, without proeutectoid phases, the hardness of pearlite, which is the basis of this so-called "pearlite hardenability," depends on the spacing of the cementite lamellae. We know this function but we were unable to observe spacings smaller than 0.1μ with increasing undercooling temperature. In spite of this, hardness increases further.

To explain this, I will show two pictures of a steel with 0.4% C: Figure A, a replica, shows that there are only pearlite lamellae with distances of nearly 0.1μ without any proeutectoid ferrite; Figure B, an extraction replica of higher magnification, shows that the cementite lamellae of the first picture are not massive but of a feathery shape.

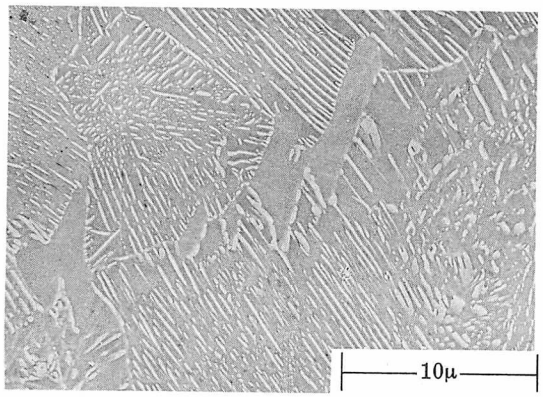

FIGURE A

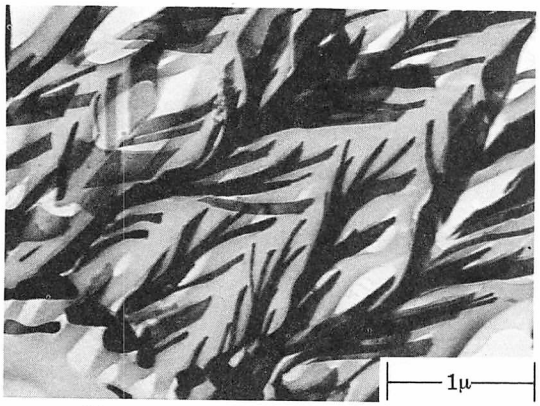

FIGURE B

J. FIELD (Bethlehem Steel Corporation). Incidentally, have you worked with boron as far as these steels are concerned?

AUTHOR'S REPLY. No, we haven't.

C. F. JATCZAK (The Timken Roller Bearing Company). Did you compare your factors with Kramer's? They seem to have the same general value for nickel and manganese.

AUTHOR'S REPLY. Yes, but Kramer et al are calculating tensile strength as such, rather than a concept of hardenability; they are generally similar, yes.

C. F. JATCZAK. They are calculating a 50% transformation which is ferrite and pearlite, and yours are for a 100% ferrite and pearlite — they look better, right? They have the same shape, though, right?

DISCUSSER. I noticed that your silicon contents were about 0.20%, or slightly higher; are your factors all based on fully-killed fine-grain steels?

AUTHOR'S REPLY. Yes, they are.

W. WILSON (A Finkl and Sons Company). What is the D_I range of the Jominy test defined in the new way?

AUTHOR'S REPLY. I forget now what D_I would correspond to the air-cooled end of the Jominy bar. It's still well below what one might choose from the plot of the actual diameter or plate thickness against ideal diameter or plate thickness. One must use it until we develop a satisfactory, high hardenability test that can complement the Jominy test.

S. V. RADCLIFFE (Case Institute of Technology). One of the questions which is interesting to an academic person is to what extent do the economic parameters mentioned in the talk influence the metallurgical decision. For example, given the different price structures for various alloying additions, what then would be the choice of the minor alloying addition you would make?

AUTHOR'S REPLY. I think that within the limits, it would be as you indicated, Dr. Radcliffe, that the economics would dictate, if one had a choice of combination of alloying elements to achieve the same goal. One thing, the molybdenum curve looked best on the plot, but actually, the amount of molybdenum that can be used is very limited because over about 0.20 or 0.25% gets you into the situation similar to the upper bainitic transformation illustrated or into suppression of pearlite and great enrichment of the remaining austenite so that you end up with a microstructure that has significant amounts of untempered martensite, which isn't good.

D. J. BLICKWEDE. Vic, I suspect that what they are doing is making controlled additions of "residuals" to steel.

M. COHEN (Massachusetts Institute of Technology). I am somewhat amused by the questions that are professed to be academic. I should now like to raise a really academic question. The terminology you are using as a member of the U. S. Steel Research Laboratory should be consistent with the brilliant work of Marcus Grossmann. The definitions established by Dr. Grossmann are now well ingrained in the metallurgical literature. The term "hardenability" in ferrous physical metallurgy means the ability to generate martensite, and "pearlitic hardenability" or "pearlite hardenability" means the ability to avoid the formation of pearlite and thereby produce martensite. You have been using the term "pearlite hardenability" in an entirely different context, and this is bound to cause pedagogic confusion because of the vast distinction you are making between the slightly different terms "pearlite hardenability" and "pearlitic hardenability."

Furthermore, are you not talking about ferrite–pearlite aggregates, and not pearlite alone, as a transformation product?

AUTHOR'S REPLY. Yes.

M. COHEN. This again has further difficulties.

D. J. BLICKWEDE. I think that what he means is pearlite controllability.

M. COHEN. Well, they will find the words.

D. J. BLICKWEDE. As a Bethlehem representative, I thought I would get the word first.

J. HODGE (United States Steel Corporation). I'd like to make one comment on Morris Cohen's comment. I thought that Dick mentioned in his presentation that he called this pearlite hardenability and that he clearly distinguished between pearlite hardenability and pearlitic hardenability. I would like to say that, in general, U. S. Steel Corporation prefers to think about hardenability in relationship to specific microstructures, rather than in relationship to hardness, and not necessarily in relation to martensite. This viewpoint undoubtedly complicates the nomenclature question, but I think the viewpoint justifies the complications.

J. W. SPRETNAK (Ohio State University). I'd like to ask whether or not using a hardness criterion gives you a variation in the ratio of ferrite to pearlite, and also in the state of aggregation of the ferrite–pearlite aggregate.

AUTHOR'S REPLY. Yes, we are talking about a bulk hardness of a ferrite–pearlite microstructure that is going to vary depending on each of the alloying elements and the amount of them. Averaging, perhaps, is an oversimplification.

J. W. SPRETNAK. Do you get considerable change in the distribution of ferrite at that hardness criterion?

AUTHOR'S REPLY. Well, once we decided to use the hardness criterion, we then did not investigate the microstructure of each of the individual steels.

F. B. PICKERING (United Steel Companies, Ltd). Can this method of hardenability calculation be applied to semi-killed or even rimming steels? Also, when the strength is largely dependent on the ferrite grain size, such as in fine-grained, control-cooled, low carbon steels, how applicable is the pearlite hardenability concept?

AUTHOR'S REPLY. I don't really know; we've used it primarily with what we define as the alloy steels and low-alloy steels, not the low-alloy high-strength class. All of these steels are normally fully-killed, and therefore, the laboratory heats that we used in the development work were all fully-killed, so I can't answer your question.

Structure, Hardenability and Toughness of Low-Carbon High-Strength Steels

A. J. McEVILY, R. G. DAVIES, C. L. MAGEE and T. L. JOHNSTON
Metallurgy Department
Scientific Laboratory
Ford Motor Company
Dearborn, Michigan

INTRODUCTION

This paper is concerned with three important factors which influence the strength–toughness characteristics of low carbon steels. The first of these is the nature and stability of the transformation-induced substructure which can contribute significantly to strength. To obtain substantial substructural strengthening it is necessary that the phase transformation, per se, induces extensive shear deformation and that the transformation occurs at a temperature sufficiently low that the resulting substructure does not anneal out on further cooling. The desired substructure consists of dislocation arrays and cells which are similar to those observed in maraging steels.[1]* However, in contrast to the maraging steels, which utilize further heat treatment to develop ultra-high strength, we will be primarily interested in the properties obtainable in as-transformed alloys.

The second factor is hardenability. In order to obtain the desired transformation structure upon cooling, decomposition of austenite to proeutectoid ferrite must be suppressed. This of course can usually be achieved through rapid quenching, but practical applications become feasible when the desired transformation can be obtained at much slower cooling rates, for then it is possible to obtain the substructural strengthening in thick sections. Since quenching stresses can therefore be avoided, an improvement in impact properties is realized.

The third factor is the size and distribution of carbides, which are particularly important in relation to fracture toughness. It is well known that the presence of carbides (which may have a beneficial effect on strength) invariably leads to a decrease in fracture toughness — perhaps to an unsatisfactorily low level. When carbides are present, particularly large ones, they tend to crack under stress when they block slip bands.[2,3] At a sufficiently low temperature the formation of a crack in a carbide can in turn trigger cleavage failure of the ferrite matrix. Even above the brittle range these particles can lower resistance to ductile failure, as evidenced by a decrease in the upper shelf energy of the Charpy impact curve. Therefore the danger of brittle failure, as well as low energy tear failure, is increased by the presence of carbide particles. Thus, to optimize toughness at a given strength level it is desirable to maintain the carbon at a minimum level, consistent with strength considerations. The superior toughness of maraging steels as compared to carbide

* See references.

strengthened steels of the same strength level probably is due in large measure to their low carbon content, of the order of 0.03 w/o.[4]

Using the above considerations as guidelines, we have developed a new series of strong, tough, low-carbon steels, containing 3% Ni and 3% Mo as alloying additions. The yield strength of these steels is in excess of 100,000 psi and is attained through a combination of solid solution and substructural strengthening. Charpy V notch impact values of 150 ft lb at −40 C (−40 F) and transition temperatures below −75 C (−100 F) are readily obtained. An important feature of this class of steels is that they possess sufficient hardenability to obtain these properties in thick, as-rolled sections. A prototype of these steels has the composition: Fe–3% Ni–3% Mo–0.7% Mn–0.3% Si–0.05% Cb–0.02% C. The structure, hardenability and toughness of this type of steel will be described, with particular reference to the transformation features and structures of related ferrous alloys of simpler compositions. Such comparisons were useful in delineating the contributions of alloying elements and transformation mode on structure and properties.

ALLOYS AND PREPARATION

The various alloys which were investigated, including details of composition, melting practice and heat treatments, are listed in Table I.

TABLE I Experimental Alloys and Heat Treatment

Alloy Number	Chemical Composition* % Ni	% Mo	% Mn	% Si	% Al	% V	% Cb	% C	Heat Size lb	Melting Practice	Heat Treatment
1	2.99	...	...	...	...	0.49	....	0.002	20	vacuum	Initially, alloys with vanadium were annealed at 980 C (1800 F) for one hour and furnace cooled to 480 C (900 F) to precipitate vanadium carbides *Air Cooled Condition* 980 C (1800 F) for one hour followed by air cooling *Water Quenched Condition* Air cooled treatment followed by austenitizing at 925 C (1700 F) and water quenching
2	3.07	2.96	...	...	...	0.49	....	0.012	20	vacuum	
3	8.81	...	...	...	...	0.48	....	0.005	20	vacuum	
4	8.87	2.97	...	...	...	0.49	....	0.006	20	vacuum	
5	8.71	...	...	...	...	...	....	0.040	20	vacuum	
6	3.00	2.82	0.68	0.28	0.063	...	0.047	0.002	20	vacuum	For I-T diagram determination samples were first austenitized at 1040 C (1900 F) for ½ hr before cooling to the transformation temperature
7	2.82	2.82	0.69	0.27	0.055	...	0.046	0.0398	20	vacuum	
8	2.90	2.90	0.73	0.30	...	...	0.046	0.026	20	vacuum	Tested in as-rolled condition with a finish rolling temperature of 775 C (1425 F)
9	3.05	2.95	0.66	0.31	...	...	0.033	0.014	20	air	Tested in as-rolled condition with a finish rolling temperature of 940 C (1725 F)
10	2.95	2.75	0.66	0.30	...	...	0.03	0.003	20	vacuum	See Figures 3 and 5
11	3.07	3.07	0.71	0.26	...	...	0.07	0.03	1500	vacuum	Tested in as-rolled condition with a finish rolling temperature of 900 C (1650 F)
12	3.30	2.95	0.68	0.37	0.04	...	0.026	0.01	20	vacuum	See Figure 4
13	3.10	3.10	0.75	0.30	...	...	0.07	0.018	20	vacuum	

*Weight percent.

In our laboratory 20 lb vacuum melts, the starting charge was electrolytic iron and electrolytic nickel and all other alloying additions were made in elemental form. Alloy 11 is a 1500 lb vacuum heat melted for us by the Latrobe Steel Company. For this melt, and the 20 lb air melt (alloy 9), the starting material was Armco iron rather than electrolytic iron. The carbon concentrations shown in Table I were determined by a conductometric technique.[6] The detailed effects of various processing variables on the properties of the steels (alloys 6 to 12) will be presented elsewhere.[7] Vanadium was added to some alloys to remove residual carbon from solid solution, presumably as vanadium carbides.

STRUCTURES

The nature of the isothermal transformation diagram for the steels of interest herein is shown in Figure 1. Two transformation ranges separated by a metastable austenite bay are indicated. In this paper the term hardenability will be used to indicate the ability to avoid transformation to the upper transformation product on cooling from the austenitic region. The substructural morphology above and below the metastable austenite bay differs considerably in these low carbon alloys. The simple 3% Ni alloys are representative of those undergoing upper temperature transformation to proeutectoid ferrite whereas 9% Ni alloys can transform at a lower temperature at which transformation shear is quite pronounced.

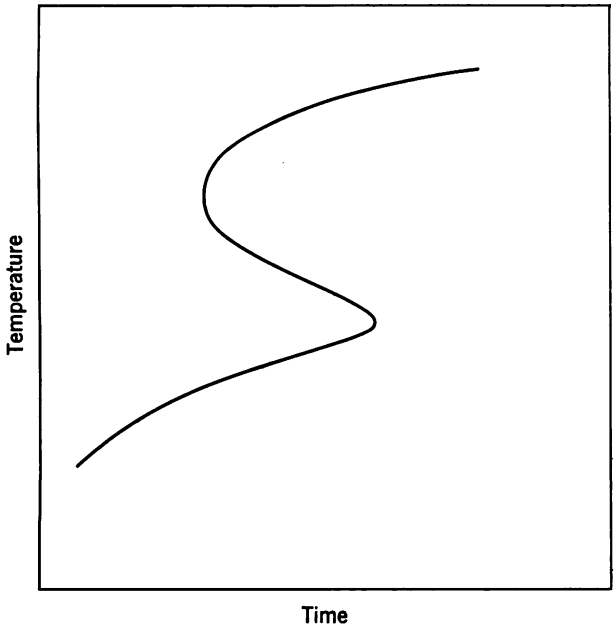

FIGURE 1. Schematic isothermal transformation diagram showing upper and lower transformation regions separated by a metastable austenite bay

Massive Ferrite

The ferritic structure formed above the bay is known in the Dubé morphological terminology[8] as massive ferrite. Based upon the work of Aaronson et al[9] it is expected that for the alloys investigated the growth of this phase occurs without partition of substitutional alloying elements. Growth occurs by a short range diffusion (SRD) of atoms across the ferrite–austenite interface which is of an incoherent type.[10] If the ferrite rejects carbon, the rate of diffusion of this carbon away from the interface into the austenite will influence the growth rate.

During the transformation process there is, of course, an attendant volume increase, the approximate extent of which is shown as a function of transformation temperature in Figure 2. This volume change is substantial, approximately 2% at 650 C (1200 F) and increasing as the transformation temperature is decreased through alloying. In order to accommodate this volume increase, plastic deformation of the remaining austenite and of the already formed ferrite must occur. Examination of prepolished specimens, austenitized in vacuo at 1315 C (2400 F) for 24 hours, and transformed during subsequent air cooling, clearly revealed evidence of plastic deformation, particularly near the prior austenite grain boundaries. This deformation occurs as a result of the volume change accompanying transformation to massive ferrite.

The equiaxed grain structure obtained upon isothermal transformation at 650 C (1200 F) for 24 hours to this massive ferrite structure is shown in Figure 3. Transformation induced dislocations arrayed in networks are still evident after this prolonged hold, indicating that the dislocations are in a low energy array and therefore difficult to anneal out. The carbon content of this particular specimen was 0.003%, and a few small, unidentified particles which may be carbides are seen on the dislocations.

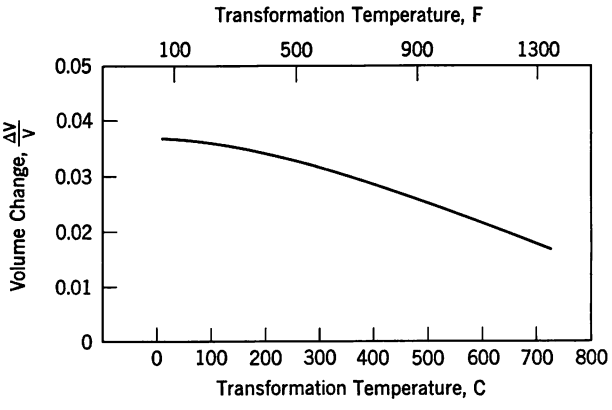

FIGURE 2. Volume change, ΔV, associated with transformation from austenite to ferrite as a function of transformation temperature, which is varied by change in composition

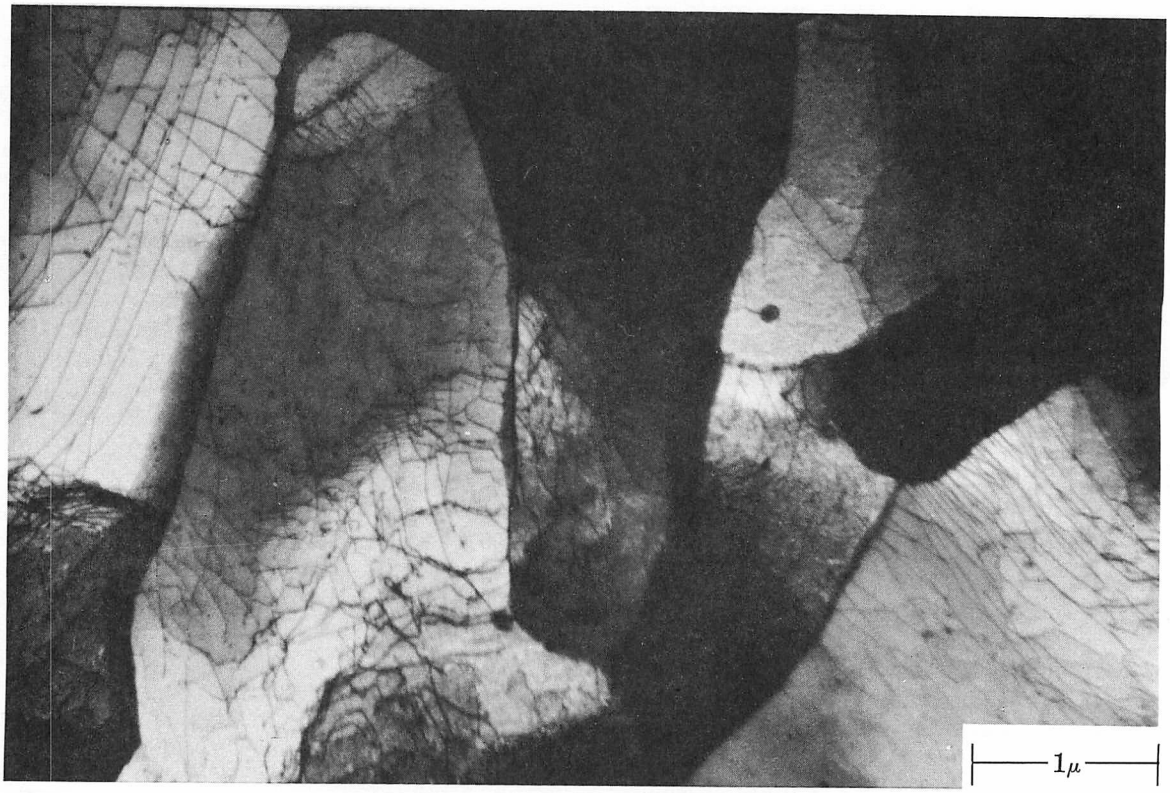

FIGURE 3. Structure of a 3% Ni–3% Mo steel (alloy 10) after isothermal transformation at 650 C (1200 F) for 24 hr following austenitizing at 955 C (1750 F) for one hour

Structures Formed Below the Bay

The role of shear during transformation is much more apparent in transformations which occur below the bay. For example, Figure 4 indicates the surface distortion which occurs on air cooling through the lower temperature transformation range and is significantly different from the deformation markings observed in the higher temperature transformation region. Four sets of sheaves are present within one prior austenite grain, a circumstance which has been interpreted to indicate that the sheaths are parallel to $\{111\}_\gamma$. [11] Grain boundaries act as barriers to the growth of any tilt element in contrast to the growth of massive ferrite, and usually the entire grain is transformed. In addition the interface is semicoherent during this transformation.

The typical substructure produced by this transformation is shown in Figure 5a. In this instance the specimen had been water quenched, but quite similar substructures are produced by cooling this particular steel at rates of 3 C/min (6 F/min) or higher.[7] The substructure is characterized by irregular, elongated dislocation cells about 1 μ wide, which are often termed laths, within which additional dislocations are observed. Because of the obviously heavy shear deformation taking place in transformation to this structure we refer to this transformation as "shear dominated." At higher magnification, Figure 5b, the

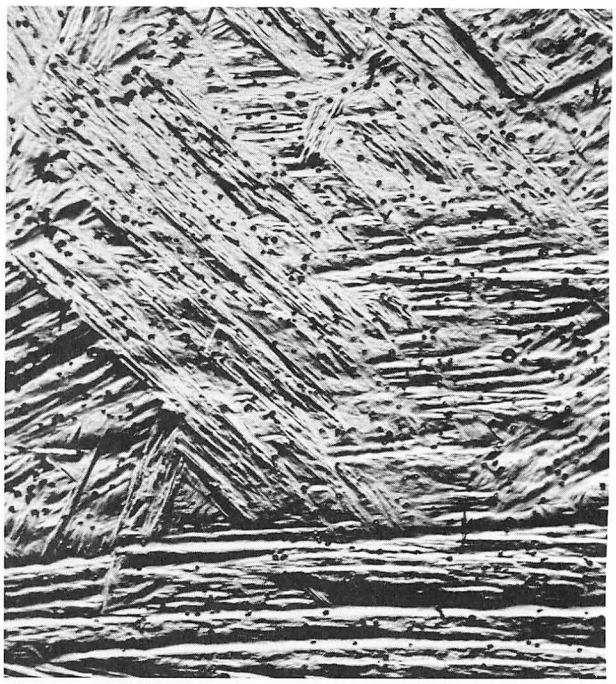

FIGURE 4. Appearance of a prepolished surface of a 3% Ni–3% Mo steel (alloy 12) after air cooling from an austenitizing treatment at 1315 C (2400 F) for one hour. 250 X

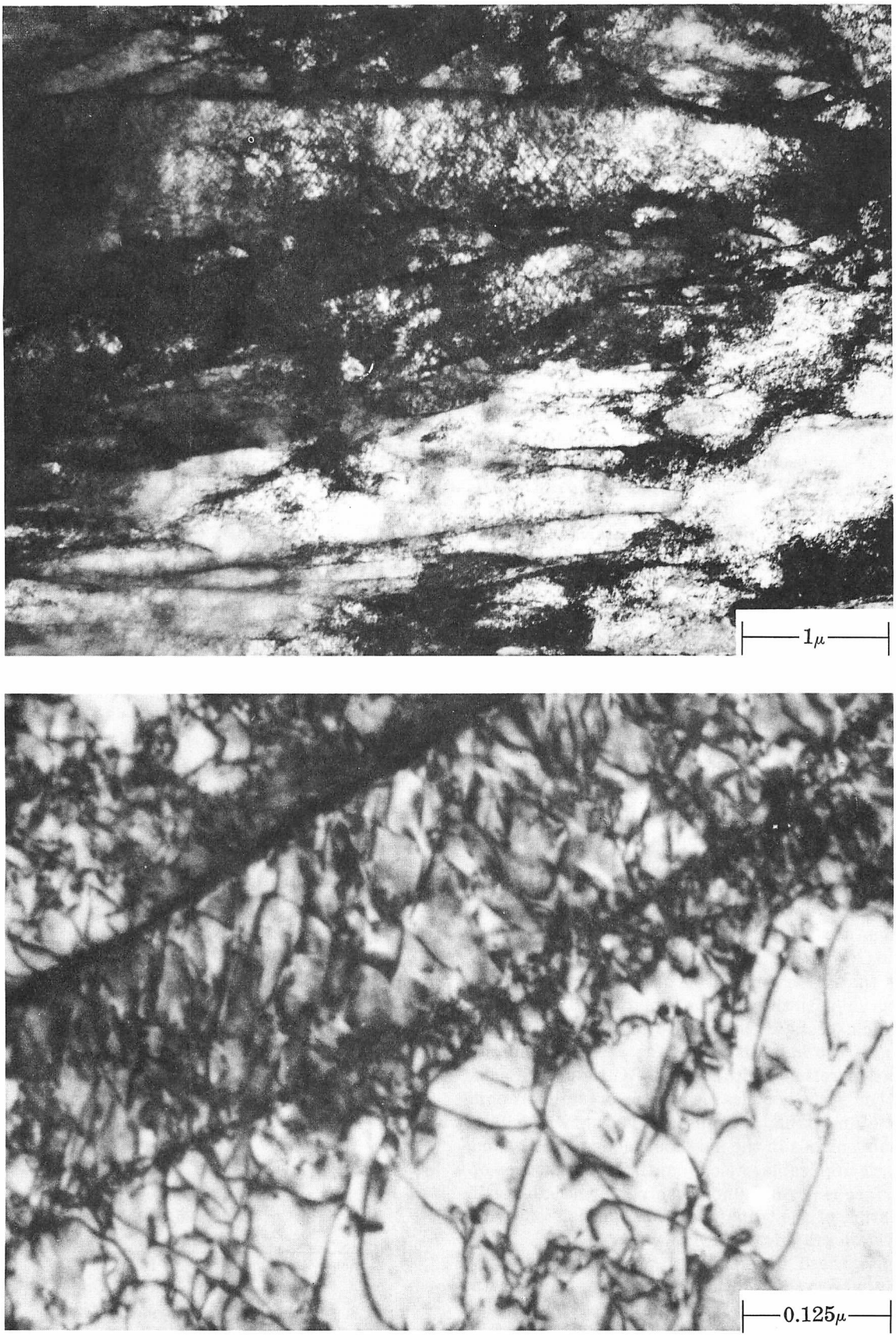

FIGURE 5. Structure at different magnifications of a 3% Ni–3% Mo steel (alloy 10) after water quenching from an austenitizing treatment at 955 C (1750 F) for one hour

lath boundaries in this structure appear to be quite sharp in some regions, but in others they are more diffuse. Because of the complexity of these tangles the nature of the dislocations of which they are comprised has not been established. In some of our low carbon alloys small particles which may be carbides are sometimes observed within these boundaries. Comparison of Figures 3 and 5 indicates the sharp, characteristic differences in structural features between the upper temperature massive ferrite transformation and the lower temperature, shear-dominated transformation product.

Owen and his co-workers[12,13,14] have described the conditions under which these two types of transformation can be obtained in binary iron–nickel alloys. Their work shows that the shear dominated transformation readily occurs above 10% Ni.

The product of this shear-dominated transformation has been the subject of much semantic uncertainty. It has been called variously: upper bainite in 9% Ni–0.01% C alloys transformed at 400 C (750 F),[15] bainitic ferrite in 0.15% C carbon steels,[16] massive martensite in Fe–20% Ni alloys,[17] and lath martensite in low carbon, iron–carbon binary alloys.[17,18] Furthermore as the carbon content approaches zero, it is not clear how any distinction between bainite and martensite can exist. However, despite the confusion in terminology, the structural features are quite characteristic, as shown in Figure 5 and the surface characteristics (Figure 4) are reproducible among the different alloys.

In contrast to the structural characterization, the mechanistic nature of the transformation is quite unsettled, which is probably why the name for the transformation product is still under debate. Direct observations[15,19] of development of surface relief during transformation have shown that carbon diffusion is not the only controlling process. Such observations do not eliminate the possibility that the reactions are truly "martensitic" because the isothermal formation of martensite at 77 K demonstrates that other relaxation processes can occur in conjunction with these transformations. The crystallographic aspects of the transformation are also uncertain. If the habit is $\{111\}_\gamma$ as reported and the orientation relationship is of the Kurdyumov-Sachs type, then it is not clear that the crystallographic theory of martensitic transformations, which predicts habit planes in the neighborhood of $\{259\}_\gamma$ and $\{225\}_\gamma$, is applicable. Also, quantitative measures of the surface relief have not been performed to see if this feature of the transformation is consistent with the crystallographic theory.

Despite these uncertainties, we adopt the view already expressed by others[10,15,20] that the growth process is dependent upon the motion of glissile dislocations as an inherent rather than incidental aspect of the transformation process. In this interpretation the mechanism of transformation below the bay dif-

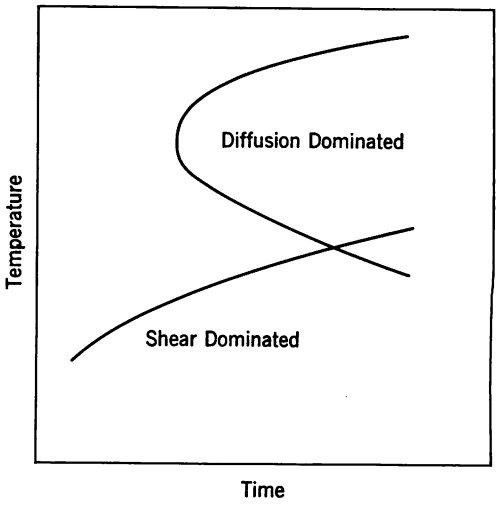

FIGURE 6. Schematic isothermal transformation diagram indicating short range diffusion (SRD) dominated and shear dominated ranges

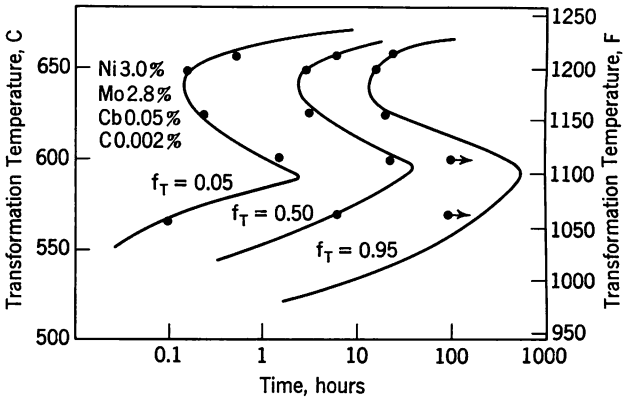

FIGURE 7. Isothermal transformation diagram for alloy 6 where f_T refers to the fraction transformed at the indicated time

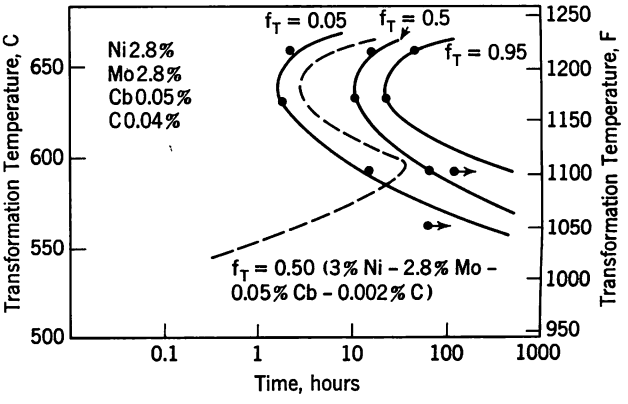

FIGURE 8. Isothermal transformation diagram for alloy 7 where f_T refers to the fraction transformed at the indicated time. The dashed curved is the 50% transformed line from Figure 7, alloy 6

fers from that above the bay; the former being shear dominated and the latter controlled by short range diffusion as indicated in Figure 6. A word of caution, however, is in order for Aaronson[21] has interpreted the results of his studies of the transformation process to indicate that even in this range the growth process is diffusion controlled rather than shear controlled. In view of the possible intermediate nature of this transformation perhaps the term "quasi-military" is somewhat descriptive of the transformation and "shear" or "lath structure" of its morphology.

HARDENABILITY

In the light of the above discussion, it may be anticipated that the role of alloying elements in influencing hardenability, i.e., in avoiding the upper temperature transformation to massive ferrite, becomes an important feature of the alloys under discussion. Indeed one of the important effects of molybdenum additions is to increase the hardenability of the low carbon, nickel steels.

I-T Diagrams

The isothermal transformation diagram of a 3% Ni–3% Mo–0.7% Mn–0.3% Si–0.05% Cb–0.002% C steel obtained by a dilatometric technique is shown in Figure 7. Despite the low carbon content of this alloy there is an appreciable time interval (20 min) before significant transformation to the massive ferrite structure occurs. Thus this transformation regime can be bypassed readily to obtain a shear dominated transformation at lower temperature. It is significant to note that studies with other alloys have shown that elimination of manganese, silicon and columbium results in a loss of hardenability.

Figure 8 indicates that the effect of an increase in carbon content to the 0.04% level on isothermal transformation characteristics. Comparison between Figures 7 and 8 reveals the effect of carbon in increasing hardenability in terms of the suppression of the proeutectoid ferrite reaction. Also, it is seen that the temperature at which the shear dominated transformation starts is noticeably reduced. The transformation characteristics of such an alloy indicate that it would be fairly easy to cool thick sections from the austenite range without obtaining significant amounts of transformation to massive ferrite.

Effect of Strength on Hardenability

From the isothermal transformation results it is found that the two transformation regions are clearly separated by a metastable austenite bay. As indicated by Kinsman and Aaronson[22] the reasons for the presence of a bay may not yet be clearly understood. They showed that molybdenum, which is a ferrite former, slightly raises the temperature at which the ferrite phase is first observed. Nevertheless, at lower temperatures, where the thermodynamic driving force is higher and rapid diffusion of carbon (0.1% in their alloys) can still occur, the growth rate of alloys containing molybdenum is decreased with the result that a high temperature C-curve develops. We note that even in an alloy such as shown in Figure 7 which contains but 0.002% C (which may be in solution at the temperature of the bay or even tied up in the form of a carbide) a bay is observed. In the alloys which we have investigated, carbon may not be necessary for the presence of a bay, but obviously carbon, when present, has a strong effect as can be seen by comparing Figures 7 and 8. We suggest that a factor not usually or easily incorporated into thermodynamic treatments of transformation kinetics may contribute to the development of a bay. This factor is the plastic work done during transformation. As previously noted, plastic deformation resulting from the attendant volume change accompanies the transformation to ferrite. If the resistance to plastic deformation is particularly high, as may be the case when sufficient molybdenum is present, then a bay may develop as the transformation temperature is reduced. A further effect of a high resistance to plastic deformation may be to cause a shift in transformation mode at temperatures below the bay. The suggestion that the strength of the austenite influences transformation characteristics and kinetics is not altogether new. Consideration of the strength of austenite has been applied previously to the bainite and martensite transformations by a number of investigators,[15,23,24] and it has been shown that the deformation work term can lead to a C curve.[25] Here we are suggesting that the strength of the austenite may be important over the entire range of transformation. Its influence becomes more apparent in the case of low carbon alloys such as shown in Figure 7.

The suggested influence of the strength of the austenite on the plastic work term and the development of a bay is as follows: As the temperature of transformation is reduced both the volume change associated with transformation as well as the flow strength of the austenite increase. If the dislocations introduced during transformation do not immediately anneal out, then it will not be the initial flow stress of the austenite but rather the work-hardened strength which will be involved, a quantity which is not constant but increases as the transformation process proceeds. The product of the volume change and the flow stress represents the additional work term which must be overcome for growth to continue. For those alloys in which no significant strengthening of the austenite occurs in the temperature range of transformation no high temperature bay will develop; i.e., the usual diffusional C-curve behavior will be obtained at lower temperatures. For those alloys in which the plastic work term does be-

come significant, nucleation and growth are retarded, that is, the atom-by-atom short range diffusion process associated with the formation of massive ferrite is arrested and a bay develops. At lower temperatures, under the influence of the increased chemical driving force, a new mode of transformation, dominated by shear, becomes activated. This mode involves the advance of the interface by glissile dislocation motion and the coordinated group behavior of large numbers of atoms.

It, therefore, was of interest to determine whether any differences in elevated temperature strength characteristics of our alloys existed which might influence the transformation kinetics. Tensile specimens were austenitized at 980 C (1800 F) and their flow strengths (0.2% offset) were determined as a function of decreasing temperature. Only one specimen was used for a given test run, and it remains for future study to determine the importance of history effects in these tests. Figure 9 shows the results obtained for two 9% Ni alloys with and without 3% Mo; the cooling rate in these tests was approximately 5 C/min (10 F/min) and the strain rate was approximately 0.05 in./in./min. It is seen that at 925 C (1700 F) the strength of both alloys is similar but as the test temperature is reduced the molybdenum containing alloy increases somewhat more in strength and its transformation begins some 110 C (200 F) lower in temperature. We note also that the strength attained when the molybdenum containing alloy does transform is much higher than that of the molybdenum-free alloy, and that transformation to the upper transformation product is suppressed. It is interesting that, over the temperature range of about 550/450 C (1020/840 F), the alloy without molybdenum becomes somewhat stronger than the Mo containing alloy. Within this temperature range, the 9% Ni alloy without molybdenum has already undergone transformation to ferrite containing transformation induced dislocations and exhibits a higher yield strength than the austenite of the 9% Ni–3% Mo alloy.

These same effects are also evident in three nickel alloys as shown in Figures 10a and 10b. The 3% Ni–3% Mo–0.5% V alloy undergoes a split transformation, that is, it only partially transforms to massive ferrite on cooling. The 3% Ni–0.5% V is the weakest

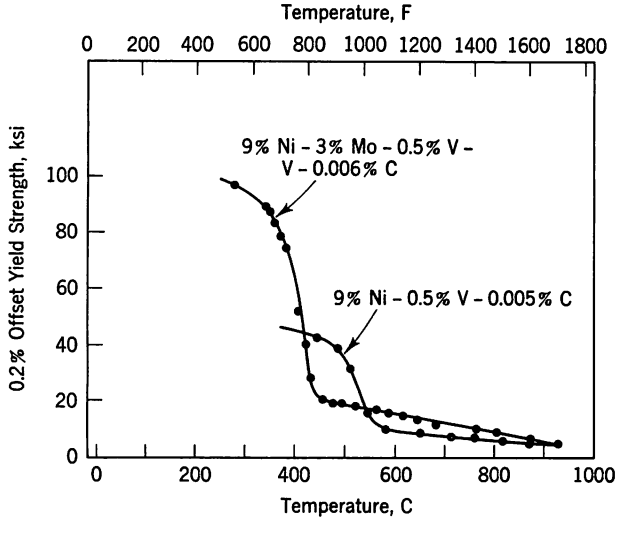

FIGURE 9. Yield strength (0.2% offset) of two 9% Ni alloys (alloys 3 and 4) as a function of temperature starting at 980 C (1800 F) and determined at successively lower temperatures through the transformation range. Strain rate approximately 0.05 in./in./min

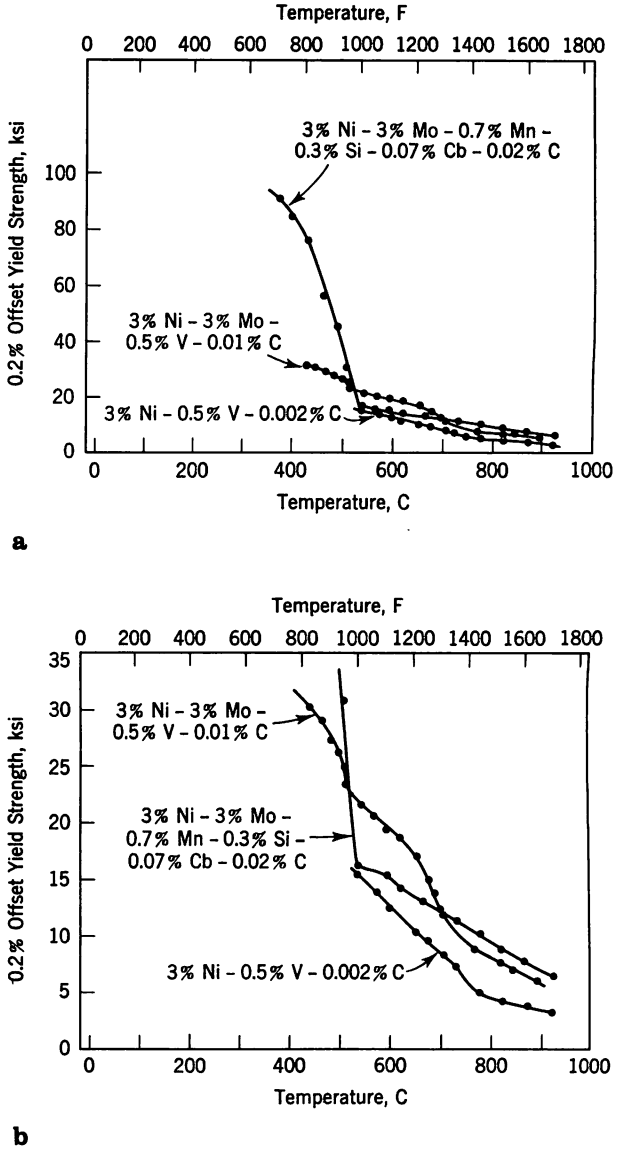

FIGURE 10. Yield strength (0.2% offset) of three 3% Ni alloys (alloys 1, 2 and 13) as a function of temperature starting at 980 C (1800 F) and determined at successively lower temperatures through the transformation range. Strain rate approximately 0.05 in./in./min

a. over entire stress range studied

b. detail of lower stress region

of the three alloys shown and transforms entirely to massive ferrite at a relatively high temperature. The 3% Ni–3% Mo–0.7% Mn–0.3% Si–0.05% Cb–0.02% C alloy does not undergo appreciable transformation except in the lower temperature range. These data indicate, as well, that manganese, an austenite stabilizer, has contributed appreciably to hardenability. All of the high temperature deformation results are consistent with the hypothesis that the strength of the austenite is a factor in influencing transformation kinetics, since as we have shown, stronger alloys transform less readily. However, we recognize that these results do not unequivocally prove the importance of the work term in inhibiting ferrite formation nor do they eliminate other suggested possibilities for the effect of molybdenum.[22]

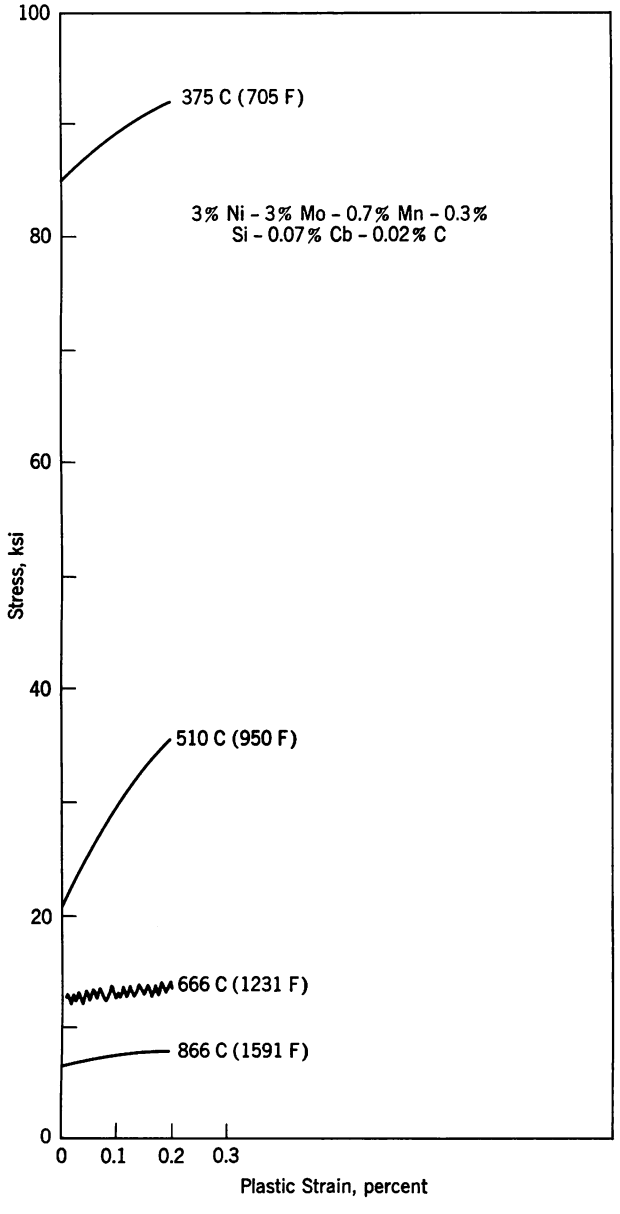

FIGURE 11. Appearance of stress–strain curves of alloy 13 at various test temperatures

The nature of the stress–strain curves obtained during the austenite deformation tests are also of interest. Those for the prototype steel are shown in Figure 11. At the highest temperature, the form of the curve is descriptive of austenite deformation. At a test temperature, e.g., 666 C (1231 F), where the upper transformation would occur at long holding times, a serrated curve, indicative of stress induced transformation in this alloy is obtained which provides further support for the suggestion that the strength of the austenite is important. It would follow that if stress can induce transformation, then some barrier to transformation, i.e., the strength of the austenite, must pre-exist.

In the temperature range of transformation to the shear dominated product, e.g., 510 C (950 F), rapid strain hardening is observed. This strain hardening may contribute to the phenomenon of transformation plasticity. Just prior to the onset of this region, a slight decrease in flow stress was sometimes detected, suggesting that the first shear dominated transformation occurs readily but that the work hardened austenite (and ferrite) provides a rapidly increasing resistance to transformation at a given temperature in this range.

Below the transformation range, the flow stress can be quite high, and for the case of the highly strengthened, low carbon steels, the stress-strain curves take on the character of cold-worked alloys.

MECHANICAL PROPERTIES

Ferrous Alloys

The contrast in fine structure between that of massive ferrite, produced at temperatures above the bay and that of the highly dislocated lath product formed at lower temperatures has been emphasized above. The consequent contrast in mechanical behavior of these transformation products will now be considered. As pointed out previously, the reduction of the carbon level is a prerequisite for high toughness through the elimination of relatively large particles of cementite. The sacrifice of carbon as a strengthening element, focuses attention on the need to evaluate the solution strengthening effects, in the two types of transformation product, of those elements that play a key role in hardenability. Two base alloys were investigated: Fe–3% Ni and Fe–9% Ni with and without 3% Mo respectively. Molybdenum, among its other attributes, has been shown to improve the toughness of maraging steels by minimizing the deleterious effects of grain boundary segregation and precipitation.[5]

The stress–strain curves of these alloys in both the air cooled and water quenched condition are shown

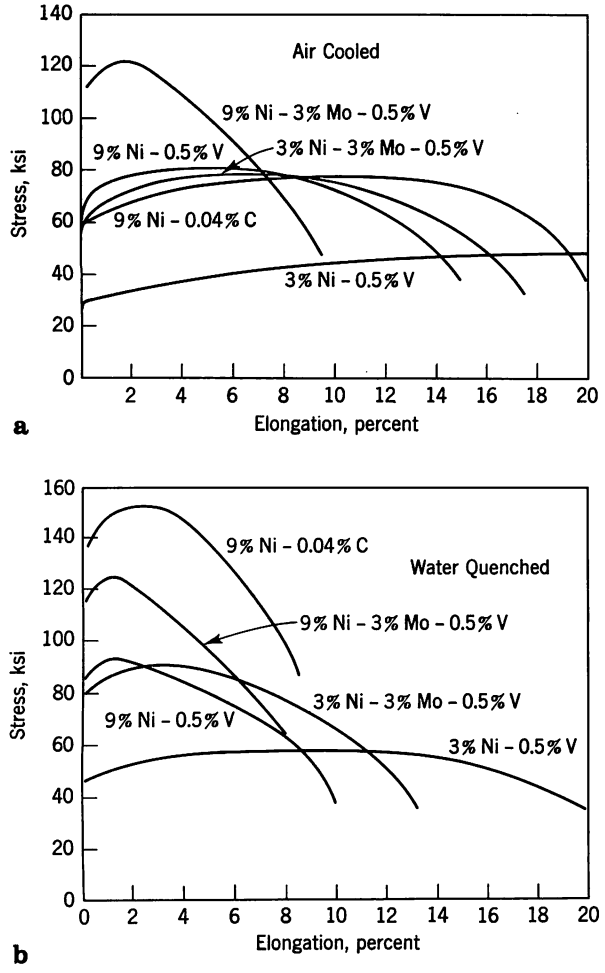

FIGURE 12. Stress–strain curves for 3% Ni and 9% Ni alloys (alloys 1 to 5)
a. air cooled
b. water quenched

in Figures 12a and 12b. The curves for the 3% Ni alloy which transforms to massive ferrite on air cooling, and the 9% Ni–3% Mo alloy which transforms to a lath structure represent two extremes observed. The uniform plastic elongation of the 3% Ni alloy is much larger than that of the 9% Ni–3% Mo alloy. The former is typical of an annealed material whereas the latter is more typical of a cold worked structure. The difference in stress–strain behavior between these two alloys is a manifestation of the striking difference in their transformation induced substructures. Only the 9% Ni–3% Mo alloy has sufficient hardenability such that the stress–strain properties are insensitive to cooling rate. Table II, which compares yield strengths of the alloys in the air cooled and water quenched conditions, demonstrates this point clearly; for all alloys except the 9% Ni–3% Mo alloy the more rapid quench leads to a marked increase in yield strength. For alloys of lesser hardenability the more rapid quench reduces

TABLE II A Comparison of Yield Strengths

Alloy	0.2%-Offset Yield Strength, ksi*	
	Air Cooled	Water Quenched
3% Ni–0.5% V	30	44
3% Ni–3% Mo–0.5% V	58	79
9% Ni–0.5% V	66	85
9% Ni–3% Mo–0.5% V	111	114
9% Ni–0.1% C	58	135

* 1000 psi = 6.9 MN/m^2

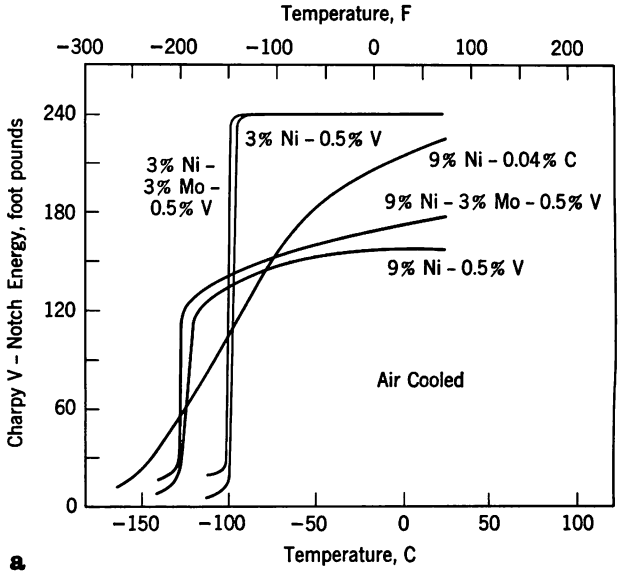

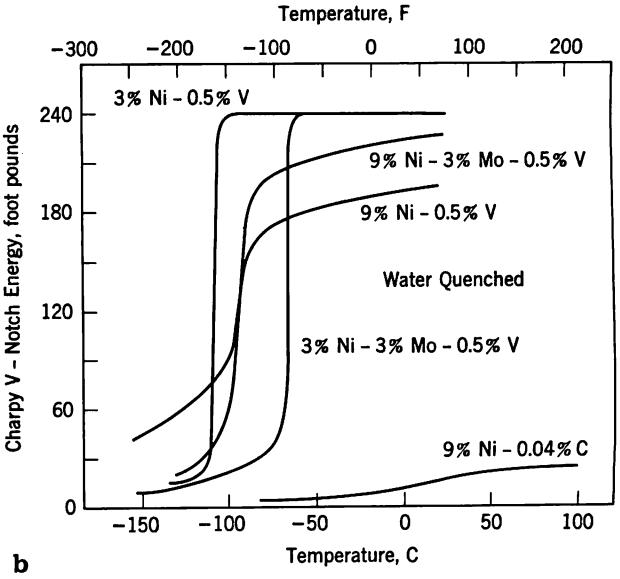

FIGURE 13. Impact properties for 3% Ni and 9% Ni alloys (alloys 1 to 5)
a. air cooled
b. water quenched

both the amount of massive ferrite and the transformation start temperature, and thereby increases the amount of "lath structure" and the average dislocation density. The increase in yield strength associated with substructure was assessed in a 3% Ni–3% Mo alloy which was isothermally transformed at 650 C (1200 F) and then air cooled. The yield strength in this condition was 40,000 psi as compared to 79,000 psi in the water quenched state indicating that substructural strengthening contributes about 40,000 psi to the yield strength of the quenched alloy. A similar conclusion has been reached with respect to the substructural contribution to the strength of iron–nickel–vanadium alloys.[26] Comparison of the yield strengths of quenched alloys with and without molybdenum indicates that this element at the 3% level contributes about 20,000 psi. Molybdenum in solid solution and substructural strengthening together therefore account for at least 75% of the strength of the molybdenum containing nickel alloys.

Figure 13 shows the Charpy V notch transition temperature curves for the simpler alloys.* The 3% Ni alloys exhibit a rather sharp transition temperature, whereas the 9% Ni alloys do not. The reason for this effect has not been established. It is noted also that the shelf energy is very high in these alloys, reaching the full capacity of the impact machine for the low carbon alloys. The benefits of minimizing the deleterious effects of carbon are clearly evident. The adverse effects of carbon on toughness are indicated also in the case of the water quenched 9% Ni–0.04% C alloy. The absence of carbon gettering elements such as molybdenum, columbium and vanadium has reduced the toughness of this alloy, but quenching stresses and a high yield strength may also be responsible for the lower impact strength. The fact that water quenching improves the impact resistance of the 3% Ni alloy may be associated with reduction in grain size as a consequence of a lowering of the transformation temperature. The impact resistance of the 3% Ni–3% Mo alloy, which is less sensitive to quench rate in terms of tensile properties, is adversely affected by water quenching. Again, internal stresses introduced on rapid quenching are probably responsible. These divergent results illustrate the difficulties of making a priori predictions of impact behavior.

High Toughness Steel

It is quite clear that transformation induced substructure and a combination of nickel and molybdenum in solid solution can together produce a substantial increase in yield strength in the effective

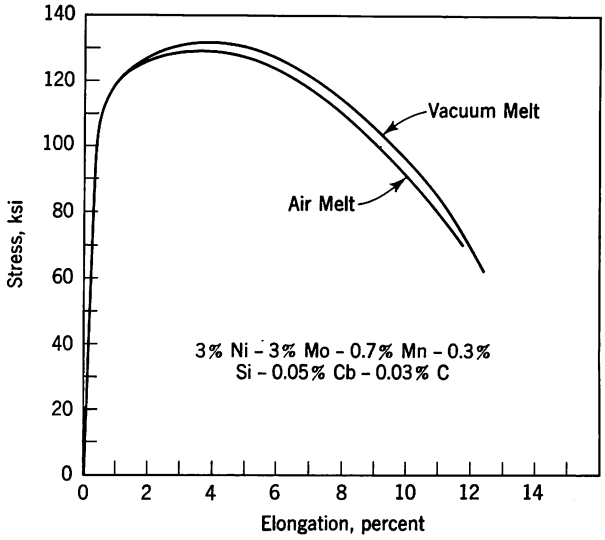

FIGURE 14. Stress–strain curves for vacuum and air melted alloys with nominal composition of 3% Ni–3% Mo–0.7% Mn–0.3% Si–0.05% Cb–0.03% C. See Table I, alloys 8 and 9 for detailed composition

absence of carbon. We have found that a 3% Ni–3% Mo steel containing 0.03% C, 0.7% Mn, 0.3% Si and 0.05% Cb has indeed a remarkable combination of high yield strength of 110,000 psi and toughness at −75 C (−100 F). The I–T diagram in Figure 8 indicates that this combination of properties can be obtained over a wide range of cooling rates. The stress–strain curves of vacuum melted and air melted laboratory heats of this steel, in the as-rolled condition, are shown in Figure 14. We note that melting procedure has little influence on these curves. The reduction in area for the air melt was 59%, that for the vacuum melt 65%. The yield strength of these alloys, 112,000 psi, is quite similar to those obtained for the 9% Ni–3% Mo alloy but a higher tensile strength of 130,000 psi and a greater extension to necking are observed, demonstrating a greater strain hardening capacity. If these alloys are furnace cooled at a very low rate of 1 C/min (2 F/min) the strength level drops to 69,000 psi, as a consequence of a loss of substructure hardening.[7]

The impact properties of this steel are shown in Figure 15, and it is seen that the toughness is high particularly in view of the strength level involved. As might be expected the toughness in the vacuum melted condition is superior to that of the air melted condition. The impact strength of the air melt is somewhat lower, probably because of oxides and nitrides introduced during alloy preparation. It is important to emphasize that for a given chemistry, if the cooling rate is such as to produce the "lath" structure, the yield strength is relatively insensitive to melt practice and hot working conditions; however

* Specimens taken in longitudinal direction with respect to rolling directions; the base of the notch is parallel to the face of the plate.

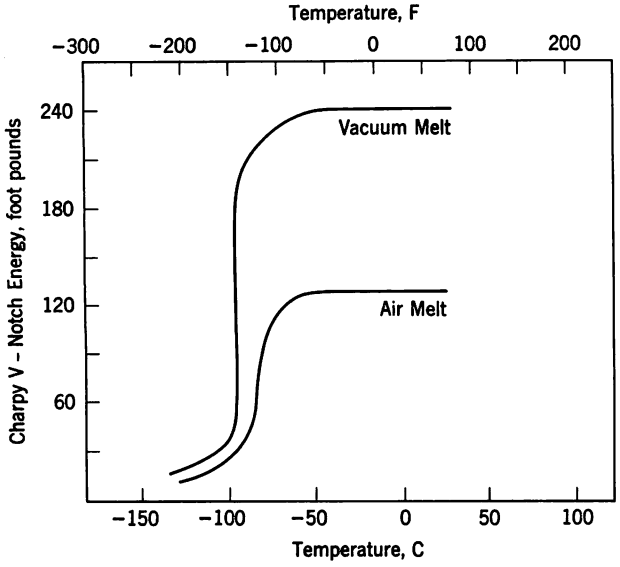

FIGURE 15. Impact properties of vacuum and air melted 3% Ni–3% Mo steels (alloys 8 and 9)

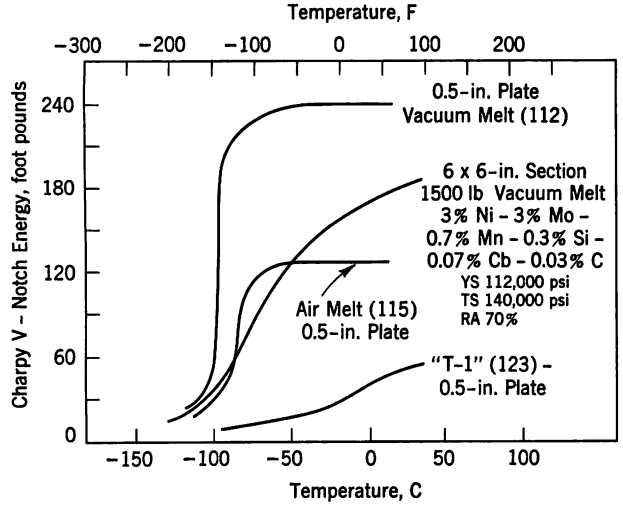

FIGURE 16. Impact properties of 1500 lb heat of 3% Ni–3% Mo steel (alloy 11) as rolled. Also shown for purposes of comparison are the results for smaller (20 lb) laboratory heats (alloys 8 and 9) and for a quenched and tempered high strength structural steel, "T–1." The long dimension of all specimens was in the rolling direction with the base of the notch parallel to the rolling plan. Yield strengths in ksi are indicated in parentheses

this is not the case for the impact properties which are much more structure sensitive.

The mechanical properties thus far described have been representative of small (20 lb) laboratory heats. The indicated hardenability suggested that similar properties should be attainable in much larger section sizes in the as-rolled and air cooled condition. This was in fact confirmed with a 1500 lb vacuum induction melt of composition 3% Ni–3% Mo–0.7%

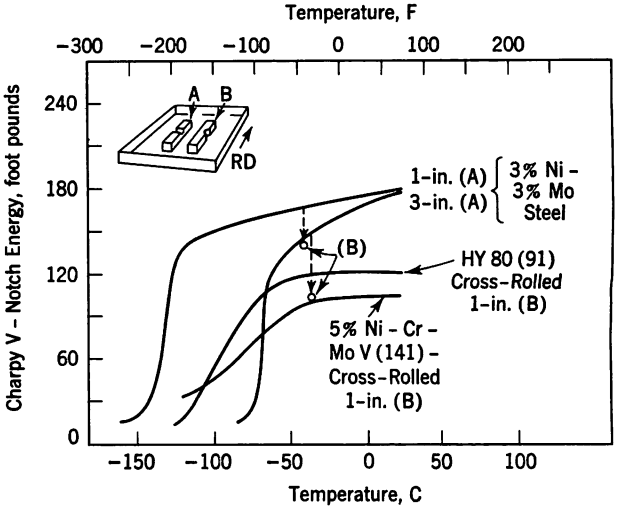

FIGURE 17. Impact properties of 3 and 1-in. plate from the 1500 lb heat of 3% Ni–3% Mo steel with a yield strength of 112,000 psi. The long dimension of all specimens was in the rolling direction with the base of the notch oriented as shown in the insert. Also shown are the impact properties of HY-80 and 5% Ni steels.[27] Yield strengths in ksi are indicated in parentheses

Mn–0.3% Si–0.07% Cb–0.03% C prepared for us by Latrobe Steel Company. A 6 × 6-in. section was rolled from this heat, and its toughness and strength properties (uniform throughout the section) are shown in Figure 16 and compared with the impact data of Figure 15 and with a quenched and tempered commercial alloy of high strength. While vacuum melting would result in some improvement for the commercial quenched and tempered steel, much less of a benefit would be expected then for the case of the 3% Ni–3% Mo steel since the commercial steel contains at least 0.1% C.

The impact properties of this 1500 lb heat after rolling to 3-in. and 1-in. plate form are shown in Figure 17 together with reported [27] results for two other steels of high toughness. The curve for the 3-in. plate is similar to that of the 6 × 6-in. rolled section shown in Figure 16. A reduction from 3-in. to 1-in. thickness improves the impact toughness for longitudinal specimens, indicating that a beneficial fibering effect has been introduced. It is noted that for both the 3-in. and 1-in. plate the impact values are reduced somewhat when the base of the notch is perpendicular rather than parallel to the plate. The extent of this anisotropy is being investigated for other orientations. Preliminary results indicate that the anisotropy is a function of processing history, plate thickness, carbon content and residual impurities. For these reasons, comparisons with published data are not straightforward since the details of processing and chemistry can have a significant effect.

SUMMARY

1. A shear dominated transformation can lead to substantial substructural strengthening in low carbon, iron-base alloys. Combinations of solid solution plus substructural strengthening can result in yield strengths in excess of 100,000 psi. In these alloys, the substructural contribution is almost 50%.
2. At low carbon levels (< 0.04 w/o) the high hardenability of these alloys is due to the presence of nickel, manganese and molybdenum. Low carbon steels containing 3% Ni–3% Mo–0.7% Mn–0.3% Si–0.05% Cb have been investigated in some detail. A 6 × 6-in. rolled section of such a steel can be air cooled after rolling without substantial transformation to massive ferrite. Problems associated with quenching such as warpage, internal stresses, and the attainment of through-section properties are therefore minimized.
3. At strength levels in excess of 100,000 psi, the fracture toughness of the low-carbon alloys is high. This toughness is directly related to the minimization of the deleterious effects of carbides on fracture toughness. The fracture toughness of vacuum melted low carbon alloys is superior to that of air melted alloys.

The characteristics of this new class of steels suggest potential application in areas where high strength and superior fracture toughness in thick sections are desired, for example in the construction of nuclear reactor pressure vessels.

ACKNOWLEDGMENT

The authors express their appreciation of the contributions of Drs. R. H. Bush and R. C. Boettner to this work; the helpful discussions with Dr. H. I. Aaronson; the encouragement of Mr. J. J. Harwood; and the technical assistance of Mr. J. Ingall.

REFERENCES

1. S. Floreen, Trans. AIME *230*. 842 (1964)
2. G. T. Hahn, B. L. Averbach, W. S. Owen and M. Cohen, "Initiation of Cleavage Microcracks in Polycrystalline Iron and Steel," *Fracture*, edited by B. L. Averbach, D. K. Felbeck, G. T. Hahn and D. A. Thomas, Wiley, New York, 1959, 91
3. C. J. McMahon, Jr. and M. Cohen, Acta Met. *13*. 591 (1965)
4. A. J. Birkle, D. S. Dabkowski, J. P. Paulina and L. F. Porter, Trans. ASM *58*. 285 (1965)
5. S. Floreen and G. R. Speich, Trans. ASM *57*. 714 (1964)
6. E. J. Violante, Anal. Chem. *36*. 856 (1964)
7. A. J. McEvily, R. C. Boettner and T. L. Johnston, to be published
8. C. A. Dubé, H. I. Aaronson and R. F. Mehl, Rev. Met. (Paris) *55*. 201 (1958)
9. H. I. Aaronson and H. A. Domian, Trans. AIME *236*. 781 (1966)
10. J. W. Christian, "Military Transformations: An Introductory Survey," *Physical Properties of Martensite and Bainite*, Special Report 93, The Iron and Steel Institute (London), 1965, 1
11. R. F. Mehl and G. Derge, Trans. AIME *125*. 482 (1937)
12. W. S. Owen, E. A. Wilson and T. Bell, "The Structure and Properties of Quenched Iron Alloys," *High-Strength Materials*, edited by V. F. Zackay, Wiley, New York, 1965, 167
13. W. S. Owen and E. A. Wilson, "A Note on Massive Structures," *Physical Properties of Martensite and Bainite*, Special Report 93, The Iron and Steel Institute (London), 1965, 53
14. E. A. Wilson, *Metallurgical Developments in High-Alloy Steels*, Special Report 86, The Iron and Steel Institute (London), 1964, 155, discussion
15. R. H. Goodenow, S. J. Matas and R. F. Hehemann, Trans. AIME *227*. 651 (1963)
16. K. J. Irvine and F. B. Pickering, J. Iron and Steel Inst. (London) *201*. 518 (1963)
17. A. B. Greninger and A. R. Troiano, Trans. AIME *140*. 307 (1940)
18. P. M. Kelly and J. Nutting, J. Iron and Steel Inst. (London) *197*. 199 (1961)
19. R. B. G. Yeo, Trans. ASM *57*. 48 (1964)
20. T. Ko and S. A. Cottrell, J. Iron and Steel Inst. (London) *172*. 307 (1952)
21. H. I. Aaronson, "The Proeutectoid Ferrite and the Proeutectoid Cementite Reactions," *Decomposition of Austenite by Diffusional Processes*, edited by V. F. Zackay and H. I. Aaronson, Interscience, New York, 1962, 387
22. K. R. Kinsman and H. I. Aaronson, this symposium
23. B. Edmondson and T. Ko, Acta Met. *2*. 235 (1954)
24. H. R. Woehrle, W. R. Clough and G. S. Ansell, Trans. ASM *59*. 784 (1966)
25. C. L. Magee and H. W. Paxton, to be published
26. R. G. Davies, to be published
27. S. T. Rolfe, R. P. Haak and J. H. Gross, ASM Metals Eng. Quart. *5*. (1). 33 (1965)

ORAL DISCUSSION OF

Structure, Hardenability and Toughness of Low-Carbon High-Strength Steels

Presented by A. J. McEVILY

F. B. PICKERING (United Steel Companies Limited). The structure shown by Mr. McEvily is very typical of a low carbon bainite, and thus the tensile and proof-stress value should be calculable from the analysis of the steel, using the type of relationships described in our own work (see present Symposium). Such a calculation gave a tensile strength of about 170,000 psi and a proof stress value of 110,000 to 120,000 psi. These may be compared with your quoted values, and a very close agreement is observed in the proof stress, but the calculated tensile strength is about 30,000 psi too high. I ascribe this discrepancy in the calculated and observed tensile strength to the very low carbon content of the steel; the relationships upon which the calculations were based were 0.1% C steels. It is well known that with very low carbon contents, the tensile strength is considerably decreased, even though the proof stress value is not greatly affected.

AUTHOR'S REPLY. In your calculation what is the contribution of the substructure to strength level?

M. COHEN (Massachusetts Institute of Technology). It does suggest though, Mr. Pickering, that a good part of the strengthening in the bainite is due to the substructure rather than to the carbides. Is this one of the microstructural parameters that you have measured quantitatively? In the strain hardening of iron and low-carbon steels up to very high plastic strains, almost the entire strengthening can be accounted for in terms of the size of the cells, i.e., the subgrains that are generated. It is like getting extreme grain refinement. Furthermore, the strength of these subboundaries is almost as high as the strength of regular grain boundaries. Therefore, the cell structure in bainite should not be overlooked as one of the principal components in the strengthening of the bainitic steels, in addition to the other factors that you have mentioned.

F. B. PICKERING. The strength of a bainitic structure depends, amongst other factors, on the grain size, carbide dispersion effects, dislocation density, carbon in solution, etc. In my paper I presented evidence to show that all these effects were operative. There is no doubt that the grain size is most important, and in this respect, the bainitic ferrite grain size which we measure is in fact the substructure cell size illustrated in the micrographs of Mr. McEvily. However, it is virtually impossible at the present time to quantify these individual strengthening effects in low carbon bainitic structures. All these strengthening effects, however, are related to the actual transformation temperature at which the bainite forms. There is a linear relationship between this transformation temperature and the strength. If, therefore, the transformation temperature can be predicted, so can the strength. During continuous cooling of these types of steels, which show a considerable bay in the TTT diagram and a flat top to the bainite C curve, the transformation temperature is directly related to the B_s temperature, which in turn can be calculated from linear functions of the analysis of the steel, and so too can the strength. The chemical analysis therefore, by controlling the transformation temperature, also controls the sum total of the various individual strengthening mechanisms, and consequently it is possible to predict the strength from the analysis without reference to the individual strengthening effects of different microstructural features.

WRITTEN DISCUSSION

G. R. SRINIVASAN (Cornell University). It is well known that three types of martensite structures (acicular martensite, massive martensite and surface martensite) occur in a narrow composition range of 25 to 30 w/o Ni in binary iron–nickel alloys.[1,2,3] While the details of one of these structures, namely that of the acicular martensite, are fairly well recognized, those of the other two are not well understood.

The massive martensite consists of a rectangular slab-like structure which has roughly equal dimensions in width and thickness, both of which are smaller than its length. The two-surface composite micrograph in Figure A shows that this slab-like structure is made up of a packet of sheets which lie parallel to the sides of the slab. Figure B shows the geometry of these internal sheets within a single, prior austenite grain. Single surface trace analysis shows that the plane of the sheets is a {111} plane of the austenite or very nearly so. This result is consistent with the trace analysis results of Bryans et al.[4] who find that the sides of the slab are parallel to or nearly parallel to the octahedral planes of austenite. They have also found that the internal structure observed in surface relief corresponds very well with the internal structure beneath the surface. Thus

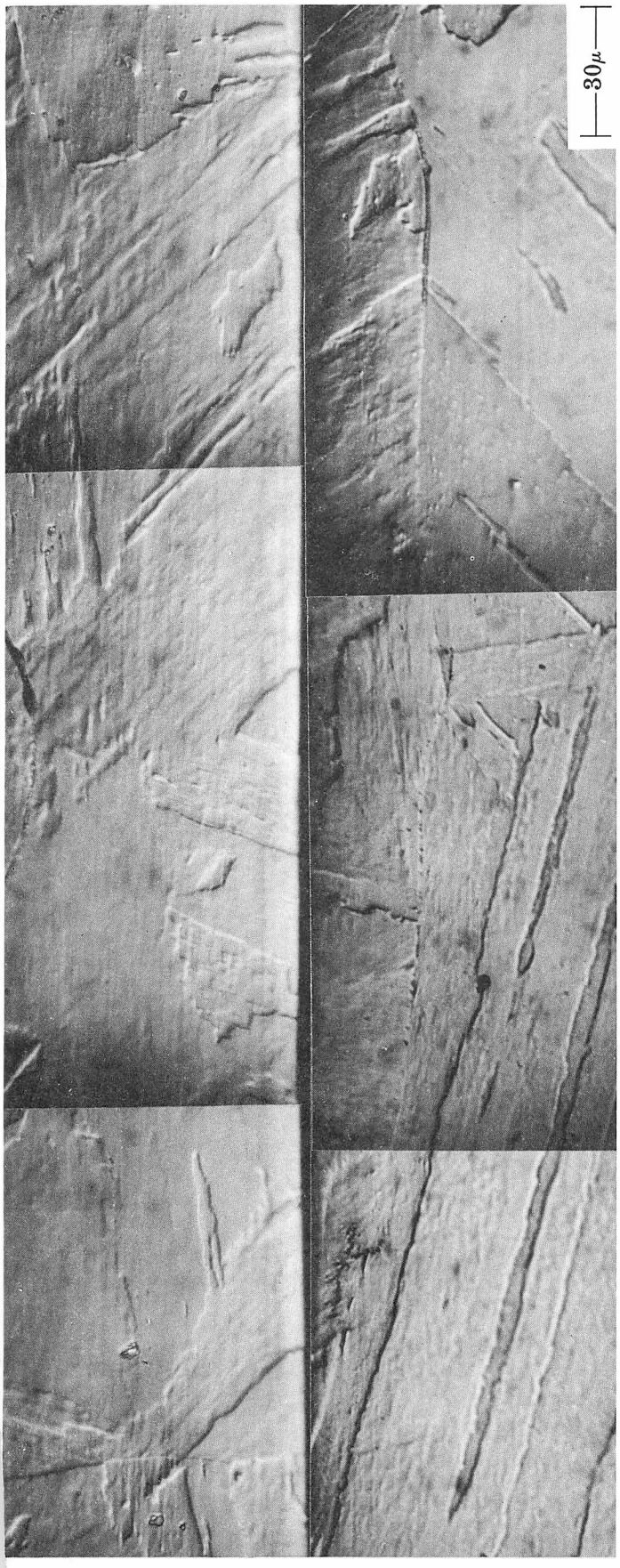

FIGURE A. Two-surface composite micrograph of massive martensite in an Fe–25% Ni alloy

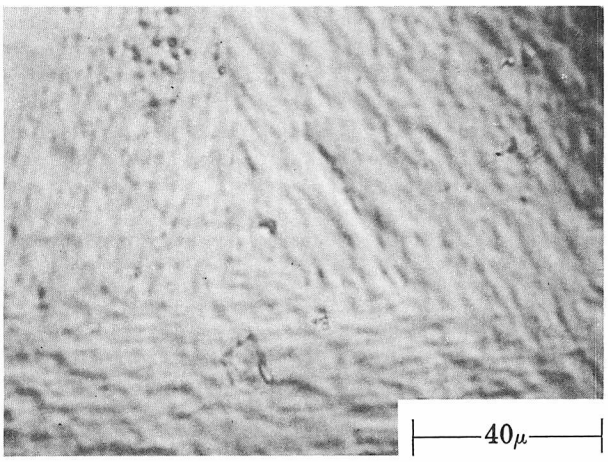

FIGURE B. Geometry of the massive martensite packets in a single prior austenite grain. Acetic – nitric etch

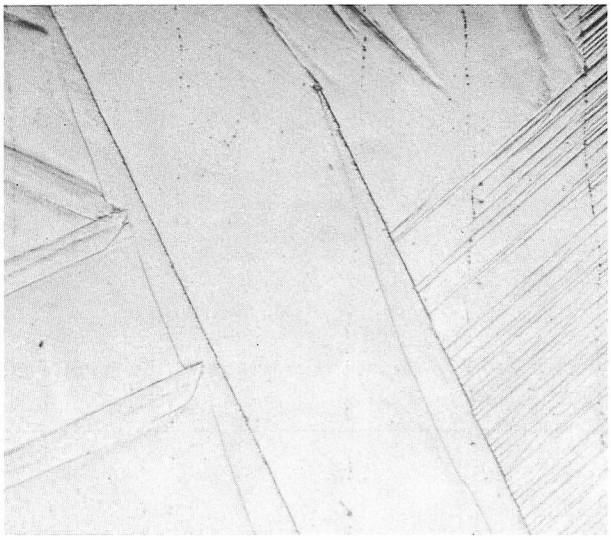

300 X

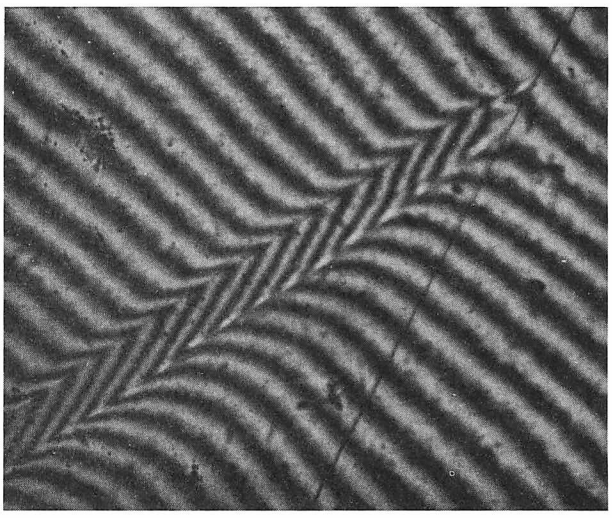

600 X

FIGURE C. Surface martensite and its interferogram in an Fe–28% Ni alloy. Note the straight edge on one side of the "plate"

the parallel sheets probably represent individual shear units or "shear plates." (In order to bring out clearly the etched structure of the massive martensite, the following solution is found suitable: 65% glacial acetic acid, 34% HNO_3, and 1% HCl. The solution is used at about 70 C (160 F) for etching, and at boiling temperature for chemical polishing.)

The surface martensite formed in these alloys, on the other hand, exhibits a structure very different from that of massive martensite. Figure C shows a typical surface martensite "plate." The accompanying interference pattern shows that the shape deformation of the surface martensite resembles that of the acicular martensite. In fact, it is very easy to confuse the surface and plate (acicular) martensite, unless one looks at a second surface. This is shown in Figure D, where the surface martensite can be seen to penetrate the second surface by not more than 10-20μ. At present, it is not clear how a surface needle such as is shown in Figure D can result in a shape deformation approximating to an invariant plane strain.

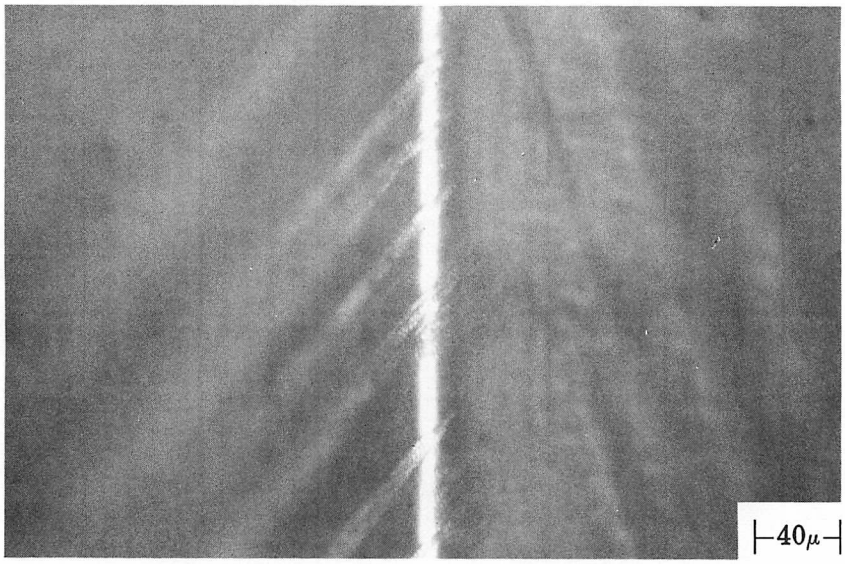

FIGURE D. Two-surface micrograph of the surface martensite viewed from the specimen edge

REFERENCES

1. W. S. Owen, E. A. Wilson and T. Bell, "The Structure and Properties of Quenched Iron Alloys," *Proc. Berkeley Intern. Mater. Conf.*, 2nd, Berkeley, Calif., 1964, 167

2. C. M. Wayman, "Ferrous Martensite," *Physical Properties of Martensite and Bainite*, Special Report 93, The Iron and Steel Institute (London), 1965, 153

3. R. P. Reed, Acta Met., *15*. 1287 (1967)

4. R. G. Bryans et al., to be published

Effects of Carbon and Austenitic Grain Size on the Hardenability of Molybdenum Steels

R. V. FOSTINI and F. J. SCHOEN
Climax Molybdenum Company of Michigan (Incorporated)
Ann Arbor, Michigan

INTRODUCTION

Since the publication of the first isothermal transformation diagrams by Bain and Davenport in 1930,[1]* many investigators have contributed to what is now an extensive amount of literature on transformation of steel. These studies are of great value to the metallurgist since they shed light on how alloying elements and carbon content affect the transformation of austenite.

Prior to 1938, when Jominy[2] developed the end-quench hardenability test for low-hardenability steels, little or no specific data were available on the influence of alloying elements on the continuous cooling transformation of austenite. The Jominy test, although originally used qualitatively, is highly regarded for its ability to show the relative hardenability of low-alloy steels.

In 1942, Grossmann[3] proposed a method of calculating the hardenability of steel from its chemical composition. From his investigation, Grossmann derived a system of factors for alloying elements that, when multiplied by the ideal critical diameter (D_I) of the iron–carbon base composition, gives an estimate of the ideal critical diameter of the alloy steel. The Grossmann system, however, is based on the assumption that there are no interactions between carbon and the alloying elements or between the various alloying elements.

Subsequent investigators[4-15] derived alloy and carbon factors for medium-carbon and 1% C steels. Some of these investigators[5-9,12,14,15] supported the Grossmann concept but disagreed over the values assigned to the factors; others[4,11,13] concluded that there must be interactions between carbon and the alloying elements and/or interactions between the alloying elements.

The rather large differences reported for the molybdenum factors of hypoeutectoid and hypereutectoid steels suggested that the value of the factor depended on the carbon content.

The hardenability effect of molybdenum was also discussed by Hollomon and Jaffe[12] who introduced a concept in which they differentiated between pearlitic and bainitic hardenability. This concept suggested that the hardenability contribution of each element, i.e., the multiplying factors, may differ between steels whose hardenability is governed by the pearlite and/or ferrite transformation and steels whose hardenability is limited by the bainite transformation.

The austenitic grain size is another factor that significantly affects hardenability. Increasing the austenitic grain size has been reported to have an appreciable effect in retarding the ferrite and pearlite reactions but a small, if any, effect in retarding the bainite reaction.[16,17,18] These results suggest that steels heat-treated to produce large austenitic grains would have a greater chance to transform to bainite, and thus the bainite reaction would control the hardenability of the steel. Under such conditions, the alloy multiplying factors for steels having small austenitic grains may very well be different from the factors for steels having large austenitic grains.

This paper presents the results of a systematic investigation performed to determine the effects of carbon and austenitic grain size on the molybdenum multiplying factor.

* See references.

EXPERIMENTAL PROCEDURES

Preparation of Steels

The chemical compositions of the steels that were air-induction-melted for this investigation are listed in Table I. Sixty-pound, aluminum-killed melts were split to produce systematic variations in molybdenum and carbon content with a constant base composition of 0.5% Mn and 0.3% Si. Since relatively high purity melting stock was employed, the steels are low in extraneous residual elements. The ingots were forged to 1⅛-in.-dia bar stock. The bars were normalized for one hour and then machined into standard Jominy end-quench specimens.

Ideal Critical Diameter and Grain Size Measurements

The effects of carbon and molybdenum variations on the ideal critical diameter were established from metallographic analyses of Jominy end-quench specimens quenched from the austenitizing temperatures listed in Table I. The austenitizing temperatures for the hypoeutectoid steels were, in general, selected on the basis of the carbon content of the steel. The austenitizing temperature employed for the hypereutectoid steels (0.75 to 1.20% C) was 925 C (1700 F), which corresponds to the temperature employed for carburizing steels.

Figure 1 shows representative curves of hardness versus Jominy distance for steels containing 0.19, 0.42, 0.61, and 0.96% C.

The nominally 0.30, 0.40, and 0.60% C steels that contained 0, 0.50, and 1.0% Mo were also used to investigate the effect of austenitic grain size on hardenability. Variations in the austenitic grain size were produced by heating Jominy specimens for 1½ hr at selected temperatures between 980 and 1260 C (1800 and 2300 F), cooling to the normal austenitizing temperature for the steel composition, holding at temperature for 20 min, and end quenching.

Each Jominy flat was polished and etched and metallographically examined to determine quantitatively the amount of transformation product as a function of distance from the quenched end, and the austenitic grain size. The amount of nonmartensitic transformation was determined by a point-counting procedure employing a minimum of six determinations for any one Jominy distance. The Jominy distances corresponding to 99, 95, 90, and 50% martensite were converted to D_I values with the D_I versus Jominy distance curve revised by Carney.[19]

The D_I values obtained for a given amount of martensite were adjusted for minor composition differences to correspond to the D_I values for steels containing 0.50% Mn and 0.30% Si. Within each group of steels at specified carbon levels, corrections were also made for deviations from the specified carbon content.

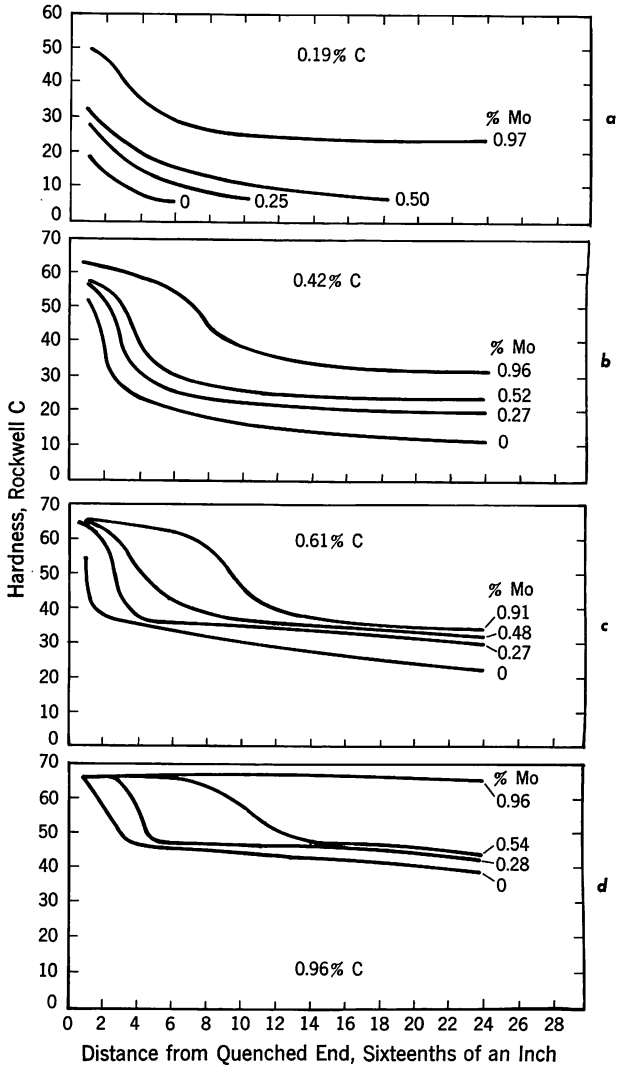

FIGURE 1. Effect of molybdenum and carbon on the Jominy hardenability curves of steels containing 0.5% Mn and 0.3% Si

a. 0.19% C. average ASTM grain size no. 8.9. quenched from 925 C (1700 F)
b. 0.42% C. average ASTM grain size no. 9.3. quenched from 845 C (1550 F)
c. 0.61% C. average ASTM grain size no. 9.0. quenched from 845 C (1550 F)
d. 0.96% C. average ASTM grain size no. 7.6. quenched from 925 C (1700 F)

The line intercept method, based on a 100-mm datum line, was used to determine the austenitic grain size on each Jominy flat. The grain sizes, converted to ASTM grain size numbers, appear in Tables I and II.

The austenitic grain sizes of all specimens used in the study of effects of carbon content ranged from 7.5 to 9.5 on the ASTM scale. However, for any given series of steels having the same nominal carbon con-

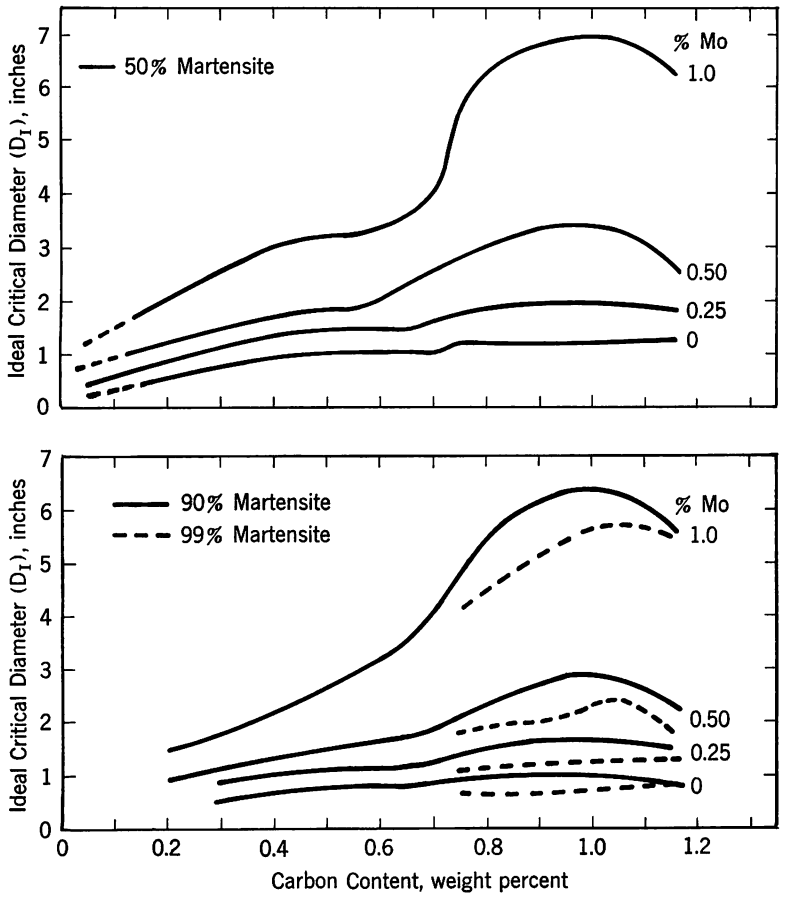

FIGURE 2. Effect of carbon and molybdenum on the ideal critical diameter of steels containing 0.50% Mn and 0.30% Si

tent, the maximum deviation of ASTM grain sizes from the mean values did not exceed ±½ unit on the ASTM scale of grain size numbers. Consequently, the hardenability data were not adjusted for the minor grain size differences that existed between the steels at any one carbon level.

RESULTS AND DISCUSSION

In this section, the data will be treated in two groups. The first group will pertain to the influence of carbon content on the molybdenum multiplying factor. The second group will have to do with observed variations in hardenability caused by changes in austenitic grain size.

Effects of Carbon Content

Ideal Critical Diameter The adjusted values of ideal critical diameter for various criteria are plotted in Figure 2 as a function of carbon content at four molybdenum levels. Figure 2 shows:

1. In the carbon range of 0 to 0.50%, the ideal critical diameter of all the steels increases with the carbon content. The increase is somewhat more pronounced at higher molybdenum levels.
2. In the carbon range of 0.50 to 0.70%, the ideal critical diameter of molybdenum-free steels remains essentially constant. On the basis of published data on the effect of carbon on hardenability, this behavior was unexpected and the reason for it is not known.
3. In the carbon range of 0.70 to 1.20%, the effectiveness of molybdenum additions passes through a maximum and then decreases. The maximum value of the ideal critical diameter is reached at approximately 1.0% C.

Molybdenum Multiplying Factors The molybdenum multiplying factors at the three levels of martensite were derived from plots of D_I versus molybdenum content.* The molybdenum multiplying factor is defined as the ratio of the adjusted D_I value for a steel containing a particular molybdenum content to the adjusted D_I value for a steel not containing molybdenum. The following equation expresses this relationship for a specific martensite criterion:

$$f\text{Mo} = \frac{D_I^* \text{ at X\% Mo}}{D_I^* \text{ at 0\% Mo}}$$

where

fMo = the molybdenum multiplying factor,

D_I^* = adjusted D_I.

* See representative curves in Fig. A-1 in the Appendix.

TABLE I—Summary of Data on Compositions, Heat Treatments, Grain Sizes, and Ideal Critical Diameters

Heat No.	Analyses of Steels*				Normalizing Temperature		Austenitizing Temperature		Austenitic Grain Size (ASTM No.)	Experimentally Observed Ideal Critical Diameter** (in.) for Indicated Criterion				Experimentally Determined Ideal Critical Diameter (in.)†			
	% C	% Mn	% Si	% Mo	C	F	C	F		99% M‡	95% M	90% M	50% M	99% M	95% M	90% M	50% M
3825A	0.045	0.44	0.29	—	955	1750	955	1750	—	—	—	—	—	—	—	—	—
3825B	0.042	0.44	0.28	0.25	955	1750	955	1750	—	—	—	—	0.42 (0.042)	—	—	—	0.45
3825C	0.047	0.44	0.28	0.48	970	1775	970	1775	—	—	—	—	0.67 (0.07)	—	—	—	0.72
3825D	0.049	0.45	0.27	0.64	980	1800	980	1800	7.5	—	—	—	0.77 (0.082)	—	—	—	0.82
3825E	0.044	0.46	0.28	0.80	1010	1850	1010	1850	7.3	—	—	0.73 (0.074)	1.02 (0.11)	—	—	0.77	1.09
3837A	0.066	0.50	0.30	0.98	1010	1850	1010	1850	8.7	0.67 (0.07)	0.80 (0.086)	0.88 (0.095)	1.20 (0.14)	0.67	0.80	0.88	1.20
3826A	0.092	0.48	0.28	—	955	1750	955	1750	8.2	—	—	—	0.26 (0.026)	—	—	—	0.262
3826B	0.097	0.51	0.29	0.26	955	1750	955	1750	8.2	—	—	—	0.54 (0.055)	—	—	—	0.534
3826C	0.10	0.51	0.30	0.52	955	1750	955	1750	8.1	—	—	—	0.88 (0.095)	—	—	—	0.87
3826D	0.10	0.52	0.30	0.65	955	1750	955	1750	8.2	—	—	—	1.0 (0.11)	—	—	—	0.978
3826E	0.10	0.50	0.30	0.85	955	1750	955	1750	7.4	—	—	—	1.20 (0.14)	—	—	—	1.20
3837B	0.11	0.57	0.32	0.96	955	1750	955	1750	—	—	—	1.24 (0.15)	1.54 (0.20)	—	—	1.17	1.45
3827A	0.17	0.51	0.29	—	925	1700	925	1700	8.9	—	—	—	0.37 (0.037)	—	—	—	0.37
3827B	0.17	0.49	0.32	0.26	925	1700	925	1700	8.9	—	—	—	0.80 (0.084)	—	—	—	0.81
3827C	0.17	0.50	0.33	0.50	925	1700	925	1700	9.0	—	—	—	1.15 (0.13)	—	—	—	1.16
3827D	0.16	0.51	0.32	0.63	925	1700	925	1700	9.0	0.84 (0.090)	0.92 (0.100)	1.05 (0.12)	1.37 (0.17)	0.84	0.92	1.05	1.37
3827E	0.17	0.51	0.32	0.65	925	1700	925	1700	8.1	0.95 (0.104)	1.0 (0.110)	1.10 (0.13)	1.45 (0.18)	0.95	1.0	1.10	1.45
3837C	0.18	0.55	0.34	0.96	925	1700	925	1700	9.1	1.13 (0.13)	1.33 (0.16)	1.48 (0.19)	1.80 (0.24)	1.08	1.27	1.41	1.72
3828A	0.19	0.46	0.25	—	925	1700	925	1700	9.1	—	—	—	0.45 (0.044)	—	—	—	0.47
3828B	0.19	0.46	0.25	0.25	925	1700	925	1700	9.1	—	—	—	0.85 (0.090)	—	—	—	0.88
3828C	0.19	0.47	0.26	0.50	925	1700	925	1700	9.1	—	—	0.92 (0.10)	1.16 (0.14)	—	—	0.94	1.18
3828D	0.20	0.44	0.25	0.66	925	1700	925	1700	9.2	—	0.92 (0.10)	1.03 (0.12)	1.33 (0.16)	—	0.97	1.08	1.39
3828E	0.21	0.46	0.25	0.85	925	1700	925	1700	8.6	1.10 (0.13)	1.20 (0.14)	1.33 (0.16)	1.64 (0.21)	1.13	1.24	1.39	1.69
3837D	0.21	0.53	0.33	0.97	925	1700	925	1700	9.0	1.15 (0.14)	1.37 (0.17)	1.45 (0.18)	1.85 (0.25)	1.13	1.35	1.42	1.82
3829A	0.29	0.49	0.28	—	900	1650	870	1600	9.6	—	—	—	0.67 (0.071)	—	—	—	0.68
3829B	0.29	0.49	0.29	0.27	900	1650	870	1600	9.4	—	—	0.89 (0.096)	1.10 (0.13)	—	—	0.90	1.11
3829C	0.30	0.48	0.30	0.51	900	1650	870	1600	9.3	0.76 (0.08)	0.95 (0.11)	1.08 (0.12)	1.34 (0.16)	0.77	0.96	1.09	1.35
3829D	0.29	0.48	0.27	0.66	900	1650	870	1600	9.6	1.05 (0.12)	1.20 (0.14)	1.32 (0.16)	1.64 (0.21)	1.06	1.21	1.33	1.66
3829E	0.30	0.49	0.28	0.85	900	1650	870	1600	9.5	1.37 (0.17)	1.58 (0.20)	1.68 (0.22)	2.00 (0.28)	1.39	1.60	1.70	2.02
3837E	0.31	0.55	0.34	0.97	900	1650	870	1600	9.3	1.53 (0.20)	1.74 (0.23)	1.84 (0.25)	2.30 (0.34)	1.48	1.68	1.78	2.22
3830A	0.41	0.50	0.31	—	870	1600	845	1550	9.4	—	—	0.75 (0.08)	1.0 (0.11)	—	—	0.75	1.00
3830B	0.41	0.51	0.32	0.27	870	1600	845	1550	9.3	0.88 (0.095)	1.02 (0.11)	1.11 (0.13)	1.40 (0.17)	0.88	1.01	1.10	1.38
3830C	0.43	0.49	0.32	0.52	870	1600	845	1550	9.4	1.03 (0.12)	1.22 (0.14)	1.34 (0.16)	1.65 (0.22)	1.03	1.22	1.34	1.65
3830D	0.42	0.48	0.32	0.66	870	1600	845	1550	9.5	1.17 (0.14)	1.39 (0.17)	1.56 (0.20)	1.95 (0.27)	1.18	1.40	1.57	1.96
3830E	0.42	0.47	0.32	0.82	870	1600	845	1550	9.1	1.74 (0.23)	1.93 (0.27)	2.05 (0.29)	2.52 (0.39)	1.77	1.96	2.08	2.56
3837F	0.43	0.54	0.33	0.96	870	1600	845	1550	9.2	2.00 (0.28)	2.24 (0.33)	2.35 (0.35)	2.86 (0.47)	1.95	2.19	2.30	2.80
3879A	0.44	0.46	0.24	—	870	1600	845	1550	9.1	—	—	—	0.95 (0.11)	—	—	—	1.00
3879B	0.44	0.49	0.26	0.24	870	1600	845	1550	9.1	—	—	—	1.40 (0.17)	—	—	—	1.43
3879C	0.44	0.45	0.24	0.46	870	1600	845	1550	9.2	—	—	—	1.67 (0.22)	—	—	—	1.74
3879D	0.44	0.47	0.24	0.87	870	1600	845	1550	—	—	—	—	2.63 (0.42)	—	—	—	2.71

TABLE I—Summary of Data on Compositions, Heat Treatments, Grain Sizes, and Ideal Critical Diameters (continued)

Heat No.	Analyses of Steels*				Normalizing Temperature		Austenitizing Temperature		Austenitic Grain Size (ASTM No.)	Experimentally Observed Ideal Critical Diameter** (in.) for Indicated Criterion				Experimentally Determined Ideal Critical Diameter (in.)†			
	% C	% Mn	% Si	% Mo	C	F	C	F		99% M‡	95% M	90% M	50% M	99% M	95% M	90% M	50% M
3880A	0.54	0.45	0.25	—	870	1600	845	1550	9.0	—	—	—	1.00 (0.11)	—	—	—	1.07
3880B	0.54	0.49	0.28	0.27	870	1600	845	1550	9.0	—	—	—	1.45 (0.18)	—	—	—	1.48
3880C	0.55	0.49	0.29	0.52	870	1600	845	1550	9.1	—	—	—	1.95 (0.27)	—	—	—	1.98
3880D	0.55	0.47	0.29	0.98	870	1600	845	1550	—	—	—	—	2.98 (0.51)	—	—	—	3.08
3881A	0.61	0.47	0.27	—	870	1600	845	1550	9.1	—	—	0.75 (0.080)	1.0 (0.11)	—	—	0.78	1.04
3881B	0.61	0.50	0.29	0.27	870	1600	845	1550	8.9	—	—	—	1.46 (0.18)	—	—	—	1.47
3881C	0.61	0.49	0.29	0.48	870	1600	845	1550	9.1	—	—	1.55 (0.20)	2.04 (0.29)	—	—	1.58	2.08
3881D	0.62	0.49	0.29	0.91	870	1600	845	1550	—	—	—	2.80 (0.45)	3.16 (0.55)	—	—	2.86	3.22
3967A	0.68	0.51	0.30	—	870	1600	845	1550	8.3	—	—	—	1.09 (0.12)	—	—	—	1.08
3967B	0.70	0.50	0.32	0.26	870	1600	845	1550	7.2	—	—	—	1.65 (0.22)	—	—	—	1.64
3967C	0.69	0.51	0.33	0.50	870	1600	845	1550	—	—	—	—	2.38 (0.36)	—	—	—	2.34
3967D	0.69	0.50	0.33	0.93	870	1600	845	1550	—	—	—	—	3.71 (0.72)	—	—	—	3.65
3868A	0.72	0.51	0.31	—	870	1600	845	1550	7.5	—	—	—	1.10 (0.12)	—	—	—	1.07
3868B	0.72	0.52	0.31	0.24	870	1600	845	1550	—	—	—	—	1.66 (0.22)	—	—	—	1.62
3868C	0.71	0.51	0.33	0.48	870	1600	845	1550	—	—	—	—	2.49 (0.38)	—	—	—	2.44
3868D	0.73	0.52	0.33	0.90	870	1600	845	1550	—	—	—	—	4.12 (0.85)	—	—	—	4.01
3740A	0.76	0.44	0.30	0.02	925	1700	925	1700	8.3	0.70 (0.072)	0.82 (0.087)	0.92 (0.10)	1.15 (0.13)	0.74	0.86	0.96	1.21
3740B	0.76	0.46	0.32	0.28	925	1700	925	1700	7.5	1.13 (0.13)	1.35 (0.17)	1.47 (0.18)	1.83 (0.25)	1.16	1.38	1.51	1.88
3740C	0.77	0.46	0.32	0.50	925	1700	925	1700	7.7	1.80 (0.26)	2.05 (0.29)	2.21 (0.32)	2.70 (0.43)	1.85	2.10	2.25	2.77
3740D	0.74	0.47	0.32	0.95	925	1700	925	1700	7.5	3.48 (0.65)	4.10 (0.85)	4.24 (0.94)	5.02 (1.17)	3.54	4.17	4.31	5.10
3741A	0.86	0.45	0.32	0.02	925	1700	925	1700	7.8	0.65 (0.067)	0.87 (0.094)	0.94 (0.10)	1.15 (0.13)	0.67	0.90	0.97	1.18
3741B	0.86	0.48	0.32	0.27	925	1700	925	1700	7.5	1.21 (0.14)	1.40 (0.17)	1.51 (0.19)	1.92 (0.27)	1.22	1.42	1.54	1.94
3741C	0.84	0.48	0.33	0.51	925	1700	925	1700	7.4	1.95 (0.27)	2.21 (0.32)	2.55 (0.40)	3.19 (0.56)	1.96	2.22	2.56	3.21
3741D	0.85	0.47	0.33	0.93	925	1700	925	1700	7.4	4.45 (0.98)	5.2 (1.24)	5.35 (1.32)	6.12 (1.74)	4.56	5.22	5.36	6.14
3742A	0.97	0.45	0.30	0.02	925	1700	925	1700	7.9	0.74 (0.077)	0.85 (0.091)	0.90 (0.098)	1.14 (0.13)	0.79	0.91	0.963	1.22
3742B	0.97	0.46	0.30	0.28	925	1700	925	1700	7.6	1.18 (0.14)	1.43 (0.18)	1.55 (0.20)	1.87 (0.25)	1.25	1.52	1.65	1.99
3742C	0.96	0.47	0.30	0.54	925	1700	925	1700	7.3	2.35 (0.35)	2.75 (0.44)	2.90 (0.48)	3.45 (0.64)	2.48	2.90	3.06	3.64
3742D	0.95	0.47	0.30	0.96	925	1700	925	1700	7.5	4.83 (1.10)	5.50 (1.40)	5.65 (1.50)	6.13 (1.75)	5.05	5.75	5.90	6.40
3743A	1.06	0.47	0.30	0.03	925	1700	925	1700	7.6	0.72 (0.075)	0.97 (0.11)	1.06 (0.12)	1.17 (0.14)	0.75	1.00	1.10	1.21
3743B	1.06	0.47	0.31	0.27	925	1700	925	1700	7.4	1.27 (0.15)	1.48 (0.19)	1.56 (0.20)	1.78 (0.24)	1.31	1.53	1.61	1.84
3743C	1.07	0.48	0.31	0.51	925	1700	925	1700	7.4	2.35 (0.35)	2.55 (0.40)	2.75 (0.44)	3.25 (0.58)	2.41	2.62	2.82	3.34
3743D	1.07	0.48	0.31	0.93	925	1700	925	1700	7.4	5.08 (1.19)	5.50 (1.40)	5.80 (1.60)	6.18 (1.78)	5.22	5.65	5.95	6.35
3746A	1.15	0.48	0.30	—	925	1700	925	1700	7.1	0.85 (0.09)	1.00 (0.11)	1.07 (0.12)	1.25 (0.15)	0.87	1.02	1.10	1.28
3746B	1.15	0.47	0.32	0.28	925	1700	925	1700	7.4	1.28 (0.15)	1.50 (0.19)	1.61 (0.21)	1.82 (0.25)	1.33	1.55	1.66	1.87
3746C	1.15	0.47	0.33	0.52	925	1700	925	1700	7.5	1.85 (0.25)	2.19 (0.32)	2.35 (0.35)	2.74 (0.44)	1.89	2.24	2.40	2.80
3746D	1.18	0.49	0.33	0.94	925	1700	925	1700	7.6	4.54 (1.00)	4.86 (1.15)	5.15 (1.23)	5.52 (1.43)	4.48	4.80	5.08	5.48

*Weight percent.

**Values in parentheses are distances (in.) on the Jominy bar.

†Adjusted to 0.50% Mn and 0.30% Si for indicated criterion.

‡Martensite.

TABLE II—Data on Composition, Heat Treatment, Grain Size, and Jominy Hardenability Pertaining to Study of Effect of Austenitic Grain Size

Heat No.	% C	% Mo	Austenitizing Temperature: Maximum C	Maximum F	Quench C	Quench F	Austenitic Grain Size (ASTM No.)	Experimentally Determined Ideal Critical Diameter* (in.) for Indicated Criterion: 50% Martensite		90% Martensite	
3828A	0.19	—	925	1700	925	1700	9.1	0.45	(0.044)	—	
			1095	2000	925	1700	4.2	0.89	(0.096)	0.72	(0.075)
			1150	2100	925	1700	6.3	0.80	(0.082)	0.60	(0.062)
			1260	2300	925	1700	1.6	1.15	(0.14)	0.90	(0.095)
3828C	0.19	0.50	925	1700	925	1700	9.1	1.15	(0.14)	0.92	(0.10)
			1095	2000	925	1700	7.5	1.32	(0.16)	0.95	(0.10)
			1150	2100	925	1700	4.3	1.53	(0.19)	1.10	(0.13)
3837D	0.21	0.97	925	1700	925	1700	9.0	1.85	(0.25)	1.45	(0.18)
			980	1800	925	1700	6.9	1.87	(0.26)	1.45	(0.18)
			1095	2000	925	1700	4.5	2.22	(0.32)	1.55	(0.20)
			1260	2300	925	1700	2.9	2.25	(0.33)	1.80	(0.24)
3830A	0.41	—	845	1550	845	1550	9.4	1.0	(0.11)	0.75	(0.08)
			980	1800	845	1550	8.3	1.10	(0.13)	0.72	(0.074)
			1040	1900	845	1550	7.7	1.10	(0.12)	0.92	(0.10)
			1095	2000	845	1550	1.2	1.60	(0.21)	1.20	(0.14)
3830C	0.43	0.52	845	1550	845	1550	9.4	1.65	(0.22)	1.34	(0.16)
			1095	2000	845	1550	5.9	2.18	(0.31)	1.57	(0.20)
			1150	2100	845	1550	5.5	1.74	(0.23)	1.46	(0.18)
			1260	2300	845	1550	3.2	2.30	(0.35)	1.75	(0.23)
3837F	0.43	0.96	845	1550	845	1550	9.2	2.86	(0.47)	2.35	(0.35)
			1095	2000	845	1550	4.3	3.65	(0.70)	2.95	(0.50)
			1150	2100	845	1550	4.8	3.68	(0.71)	3.00	(0.50)
			1260	2300	845	1550	1.5	3.80	(0.75)	3.22	(0.57)
3881A	0.61	—	845	1550	845	1550	9.1	1.0	(0.11)	0.75	(0.080)
			1095	2000	845	1550	8.2	1.20	(0.14)	0.90	(0.098)
			1150	2100	845	1550	3.0	1.46	(0.18)	1.10	(0.13)
			1260	2300	845	1550	0.27	1.46	(0.18)	1.09	(0.12)
3881C	0.61	0.48	845	1550	845	1550	9.1	2.04	(0.29)	1.55	(0.20)
			1095	2000	845	1550	7.5	2.57	(0.39)	1.95	(0.27)
			1150	2100	845	1550	6.7	2.50	(0.39)	1.97	(0.27)
			1260	2300	845	1550	2.9	2.65	(0.42)	1.99	(0.28)
3881D	0.62	0.91	845	1550	845	1550	9.3	3.16	(0.55)	2.80	(0.45)
			1095	2000	845	1550	6.9	4.05	(0.83)	3.36	(0.62)
			1150	2100	845	1550	6.6	4.00	(0.82)	3.43	(0.64)
			1260	2300	845	1550	4.0	3.97	(0.80)	3.37	(0.62)

* Values in parentheses are distances (in.) on the Jominy bar.

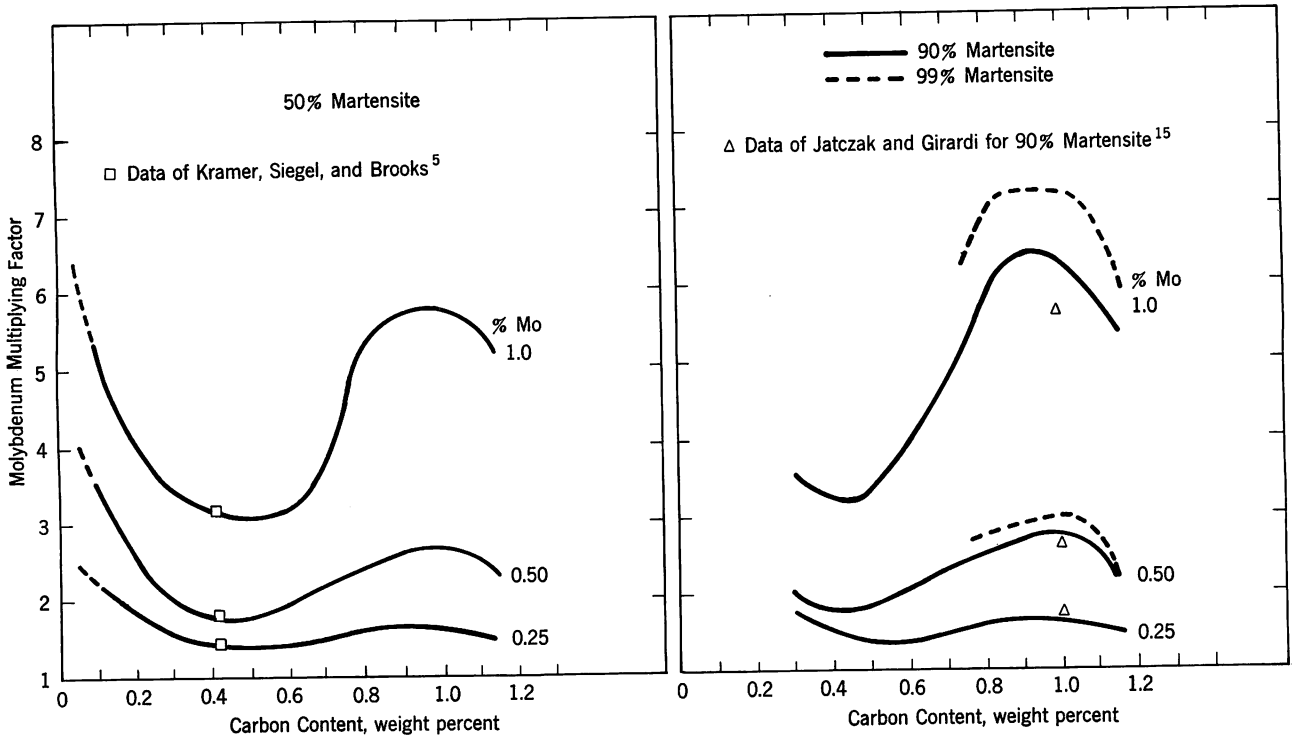

FIGURE 3. Effect of carbon and molybdenum on the molybdenum multiplying factor in steels containing 0.50% Mn and 0.30% Si

Figure 3 brings out a most significant relationship. It summarizes the multiplying factors based on 50-, 90-, and 99%-martensite criteria as a function of carbon content. It is evident that the molybdenum multiplying factor varies over a wide range as the carbon content is varied from 0.05 to 1.2%. For low-carbon steels, the factors decrease with increasing carbon content, reaching a minimum value at about 0.45% C. At the 0.45% C level, the factors are in excellent agreement with those reported by Kramer, Siegel, and Brooks.[5] As the carbon content increases above 0.45%, the value of the molybdenum factor increases, reaching a peak at approximately 1.0% C. At this carbon level, the factors are in good agreement with those reported by Jatczak and Girardi.[15]

The published molybdenum factors usually used to compute the hardenability for hypoeutectoid steels were determined using medium-carbon steels. These factors, however, underestimate the contribution of molybdenum to hardenability at both the lower and the higher carbon levels.

Figure 3 also shows the extent to which the molybdenum multiplying factor of the higher carbon steels is influenced by the amount of martensite specified in the hardenability criterion. At molybdenum contents of 0.50 and 1.0%, the molybdenum factor increases as the specified martensite content increases. This effect is most pronounced at 1% Mo.

These results imply that a molybdenum–carbon interaction exists and that the interaction causes the molybdenum factor to vary markedly with the carbon content. It is evident that this interaction affects the multiplying factors regardless of which criterion is employed in their derivation.

Effects of Austenitic Grain Size

From a practical point of view, a fine austenitic grain size is desirable for good toughness. At the same time, it is essential that the hardenability of a fine grain steel be adequate. Therefore, the hardenability contribution of any alloying element would be of greater practical importance for fine grain sizes than for coarse grain sizes.

Influence of Grain Size on Ideal Critical Diameter The variation of ideal critical diameter with austenitic grain size is shown in Figure 4 for 0.19% C steels. The D_I values decrease progressively as the ASTM grain size number increases, i.e., as the austenitic grain size decreases. The rate of decrease in hardenability (D_I) with decreasing grain size is greatest for the molybdenum-free steel (Figure 4). In fine-grained specimens, the nonmartensitic transformation products were ferrite and pearlite. The nonmartensitic transformation products in the 0.50 and 0.97% Mo steels contained considerably more bainite than was noted in the molybdenum-free steel.

As shown in Figure 5, similar results were obtained for the 0.43% C steels except that the hardenability of the 0.52 and 0.96% Mo steels tends to drop

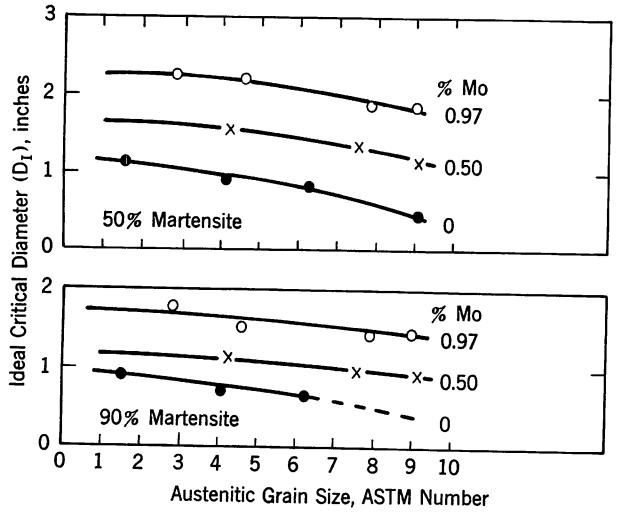

FIGURE 4. Effect of austenitic grain size and molybdenum content on the ideal critical diameter of 0.19% C steels containing 0.50% Mn and 0.30% Si

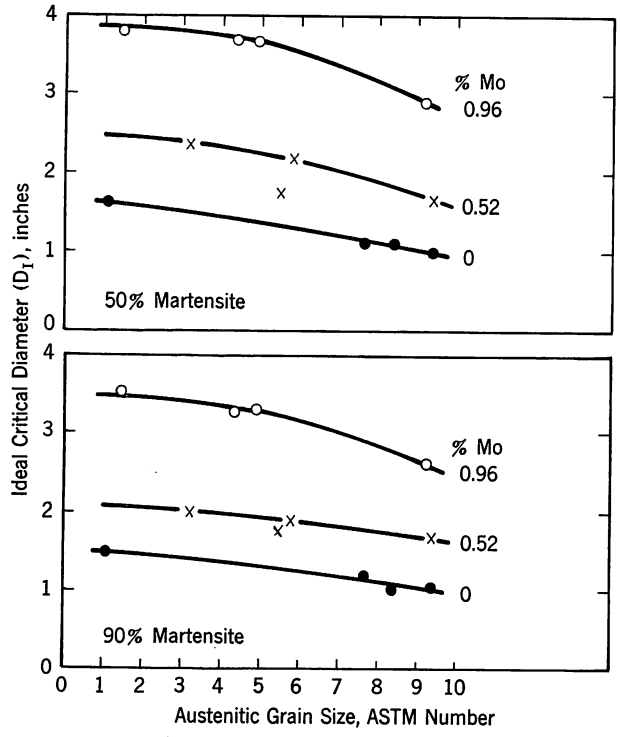

FIGURE 5. Effect of austenitic grain size and molybdenum content on the ideal critical diameter of 0.43% C steels containing 0.50% Mn and 0.30% Si

off more rapidly with decreasing grain size. No explanation is advanced for these results. Since the microstructures at the 50- and 90%-martensite Jominy distances contained appreciable amounts of bainite in the two molybdenum steels, it appears that the increase in grain-size dependency can not be simply explained on the basis of a transition from ferrite plus pearlite to bainite in the nonmartensitic part of the microstructure.

The hardenability results obtained for the 0.61% C steels (Figure 6) show essentially constant D_I values for grain sizes larger than ASTM no. 7. As the grain size becomes finer than ASTM no. 7, the hardenability becomes progressively more and more dependent on grain size.

Variation of Molybdenum Multiplying Factor with Grain Size The molybdenum multiplying factor for the 0.19% C steels (Figure 7(a)) is strongly dependent on the austenitic grain size, viz., as the austenitic grain size decreases (or the ASTM number increases), the multiplying factor increases progressively.

Similar trends were obtained for the 0.43% C steel (Figure 7(b)) except that the differences between the factors at the coarse and fine grain sizes were less than those observed for the 0.19% C steels. The nonmartensitic transformation product for the 0.43% C steels contained more pearlite and bainite than was observed in the lower-carbon alloys.

Except for steels containing 0.25% Mo,* the molybdenum multiplying factors for the 0.61% C steels (Figure 7(c)) show a greater dependency on grain size than the 0.43% C steels.

In steels that contain 1% Mo the multiplying factors for the 90%-martensite criterion are greater than those for the 50%-martensite criterion. This difference, as can be seen in Figure 7, increases in magnitude with increasing carbon content. At 0.19% C, the difference between the 90%- and the 50%-martensite factor diminishes with increasing grain size (i.e., decreasing ASTM number). At 0.43 and 0.61% C, the 90%-martensite factor is greater than the 50%-martensite factor at all grain sizes.

It is interesting to note that the molybdenum factors for the fine-grained steels were based on measurements of ideal critical diameter in steels having nonmartensitic transformation products that were mainly ferrite and pearlite. Consequently, these multiplying factors represent the contribution of molybdenum to pearlitic hardenability. In addition, the multiplying factors obtained for the coarse-grained steels were based on the values of the ideal critical diameter in steels having nonmartensitic transformation products that were largely acicular ferrite for the lower-carbon steels and bainite for the higher-carbon steels. Therefore, these factors represent the contribution of molybdenum to bainitic hardenability if the formation of carbide-free acicular ferrite is assumed to be a part of the bainite transformation.

*The 0.25% Mo curves were obtained by interpolation from curves drawn through points determined for the 0, 0.50, and 1.0% Mo (nominal) steels.

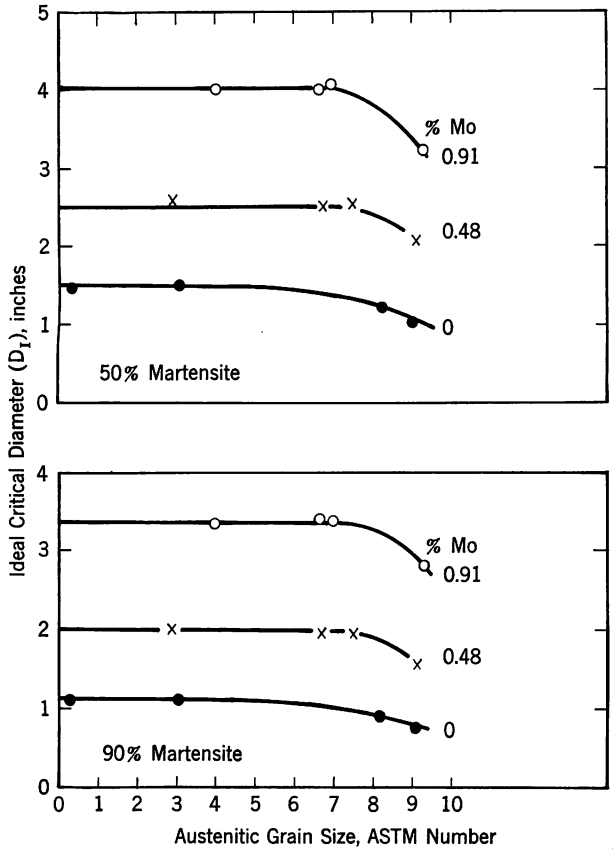

FIGURE 6. Effect of austenitic grain size and molybdenum content on the ideal critical diameter of 0.61% C steels containing 0.50% Mn and 0.30% Si

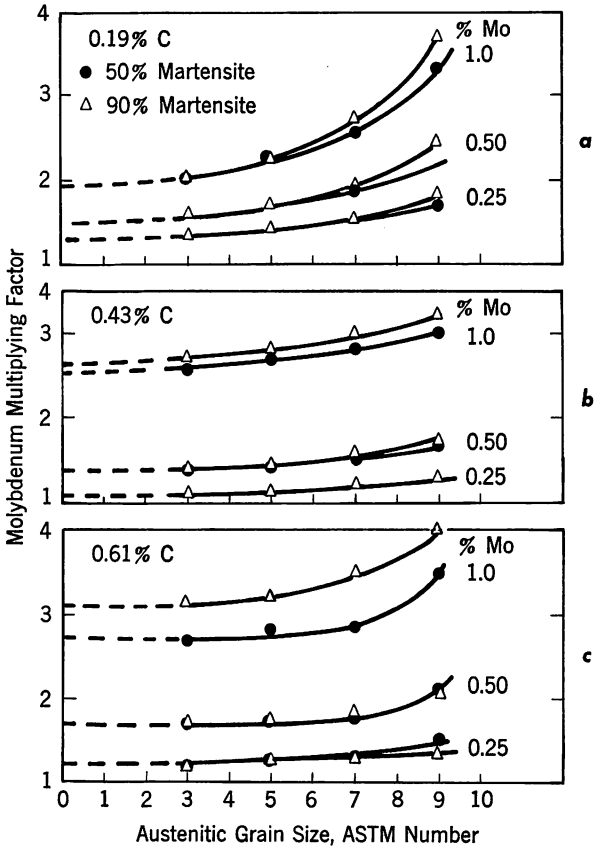

FIGURE 7. Effect of austenitic grain size on the molybdenum multiplying factor at various levels of molybdenum and carbon in steels containing 0.50% Mn and 0.30% Si

CONCLUSIONS

The effect of molybdenum on hardenability is not a simple function of the molybdenum content. Instead, the molybdenum multiplying factor varies with the carbon content and the austenitic grain size.

The addition of molybdenum to low-carbon steels enhances the pearlitic hardenability (50% martensite) to a much greater extent than would be predicted by published factors based on steels containing 0.45% C.

For a given molybdenum content, the molybdenum multiplying factor often increases as the amount of martensite specified in the hardenability criterion increases.

The molybdenum multiplying factors derived for fine-grained steels were larger than those for coarse-grained steels.

The results demonstrate that, regardless of the nature of the nonmartensitic transformation product, an interaction affecting the hardenability of the steel occurs between carbon and molybdenum.

In contrast to the tentative conclusion reached by Hollomon and Jaffe[12] that molybdenum has no effect on bainitic hardenability, the results of this study show that molybdenum does indeed increase the bainitic hardenability of steels, i.e., the hardenability where the nonmartensitic transformation product is bainite.

APPENDIX

Detailed data are presented here on the effects of variations in composition and grain size studies.

Composition Effects

Relation between Ideal Diameter and Molybdenum Content The adjusted D_I values obtained for the various amounts of martensite and for representative carbon levels are plotted versus the molybdenum content of the steel in Figure A-1.

Relation between Molybdenum Multiplying Factor and Molybdenum Content The relation between the molybdenum factor and molybdenum content for several carbon contents and martensite criteria is shown in Figure A-2.

Relation between Ideal Critical Diameters for Various Percentages of Martensite The ideal critical diameter (D_I) for 90, 95, and 99% martensite criteria are plotted in Figure A-3 as a function of the ideal critical diameter for the 50% martensite cri-

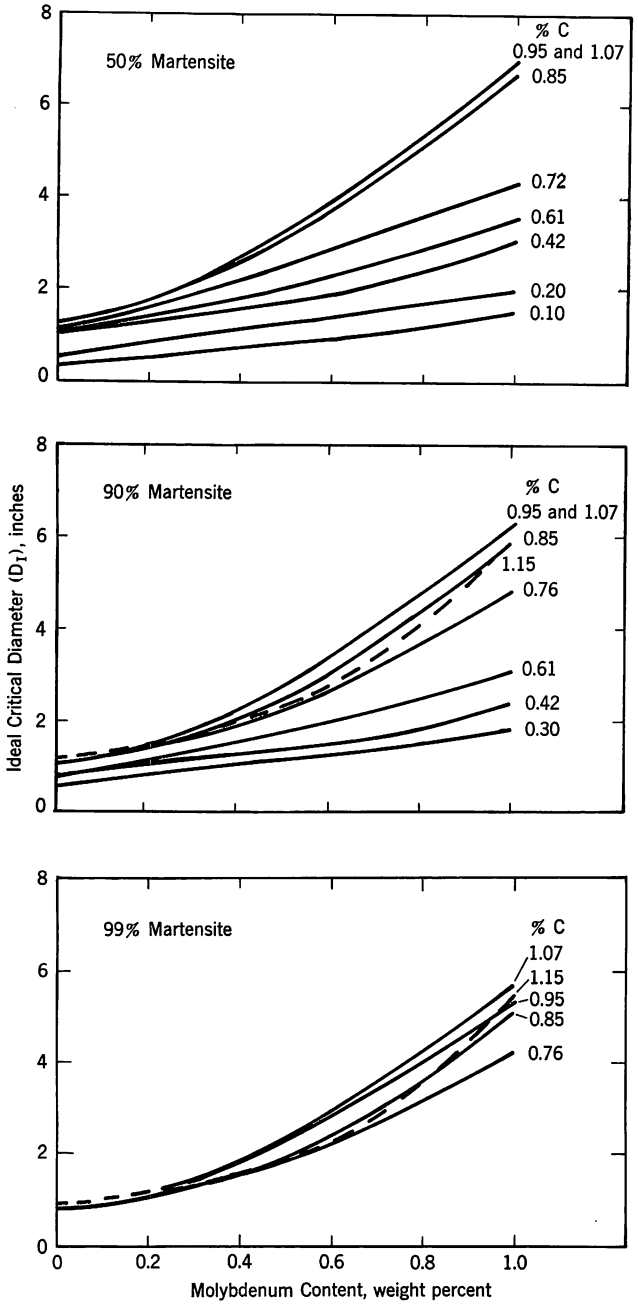

FIGURE A-1. Effect of molybdenum on the ideal critical diameter at various carbon contents in steels containing 0.50% Mn and 0.30% Si

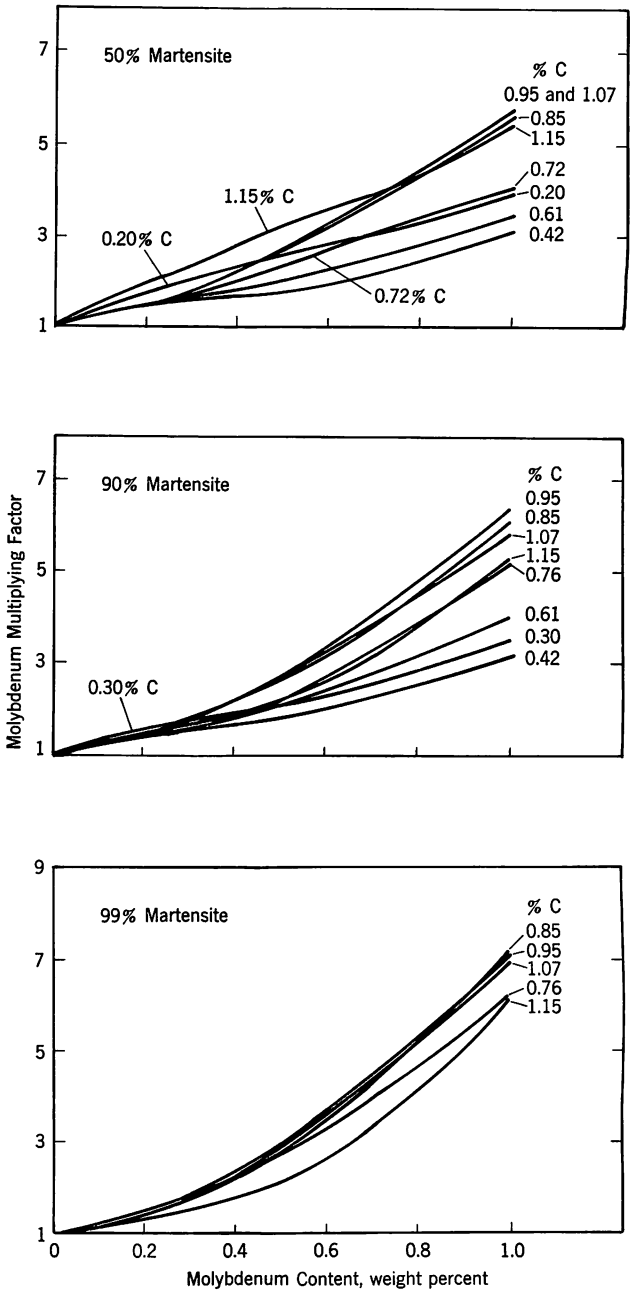

FIGURE A-2. Variation of molybdenum multiplying factor with molybdenum content for various carbon contents and hardenability criteria. All data adjusted to 0.50% Mn and 0.30% Si

teria. All of the values for this plot were obtained from metallographic examination of the Jominy specimens. The results for D_I values based on a 90% martensite criterion agree with those reported by Hodge and Orehoski[7] for D_I (50% M) values less than three; however, at higher D_I (50% M) values, the curve obtained in the present investigation lies above the relationship developed by Hodge and Orehoski.

In an effort to reconcile these differences, the carbon effect was examined. Values of the D_I (50% M)/D_I (90% M) ratio from the earlier work, as well as those from the present investigation, are plotted versus the carbon content in Figure A-4.

Most of the steel compositions studied by Hodge and Orehoski had carbon contents which fell in a narrow range even though the steels varied in alloy content. When the entire range of carbon contents

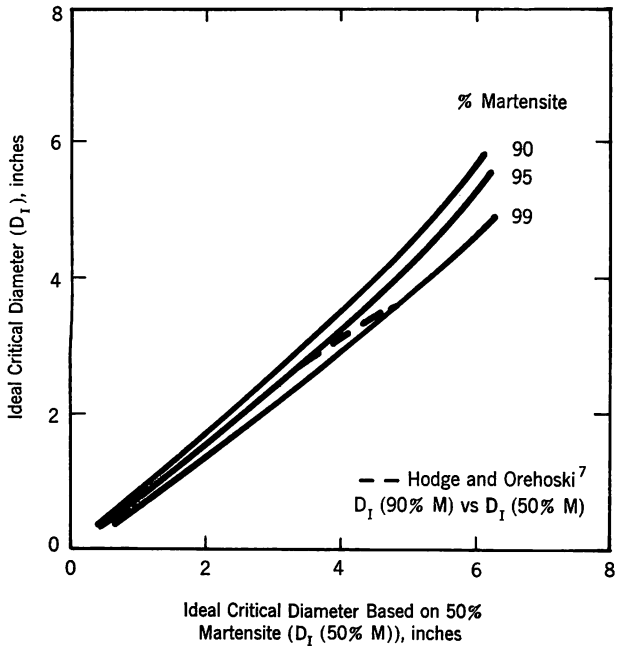

FIGURE A-3. Relation between the ideal critical diameters based on 90, 95 and 99% martensite and the ideal critical diameter based on 50% martensite

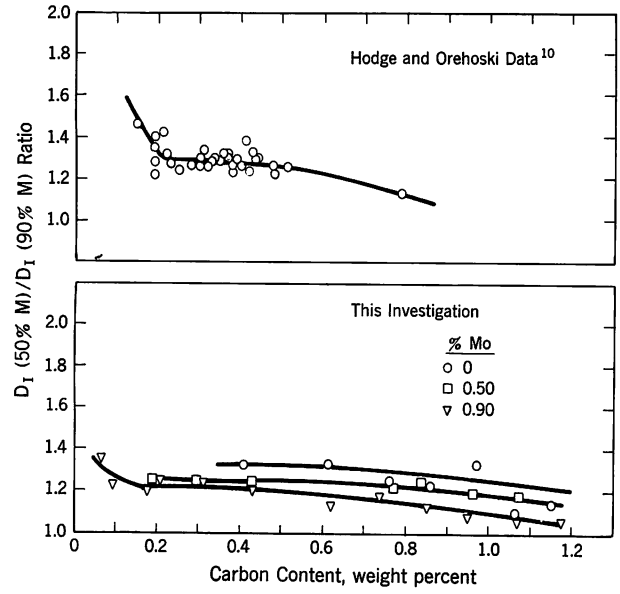

FIGURE A-4. Relation between the ratio of the ideal critical diameter based on 50% martensite to the ideal critical diameter based on 90% martensite and the carbon content

in their steels is considered, however, the low carbon steels exhibit significantly higher ratios of D_I(50% M)/D_I (90% M) than the high carbon steels.

The results obtained for the steels studied in this investigation indicate that the D_I(50% M)/D_I (90% M) ratio depends on the molybdenum as well

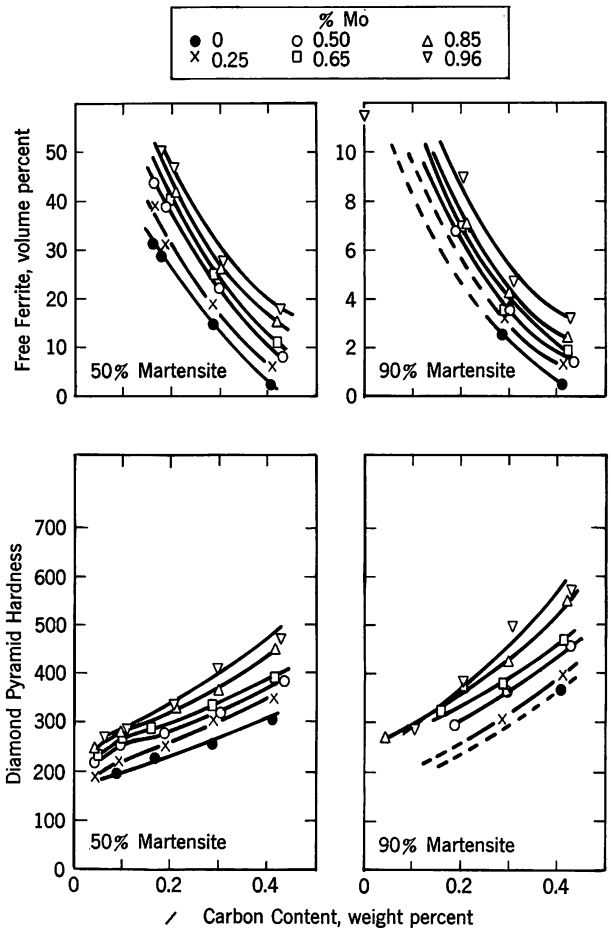

FIGURE A-5. Effect of carbon and molybdenum contents on the ferrite volume and hardness at the Jominy positions corresponding to 50 and 90% martensite

as on the carbon content, i.e., the D_I(50% M)/D_I (90% M) ratio was found to decrease as either the molybdenum content or the carbon content increased.

Relation between Hardness and Microstructure

The molybdenum multiplying factors plotted in Figure 3 of the main text show a continuous and pronounced increase as the carbon content is reduced below approximately 0.45%. The hardness and the volume percent of "free" ferrite* at the 50- and 90%-martensite Jominy distances are listed in Table A-I and plotted as functions of carbon content in Figure A-5.

The diamond pyramid hardness values were found to be dependent on the carbon and molybdenum contents. For a given molybdenum content, the hardness increases with the carbon content; and for a given carbon content, the hardness increases with the molybdenum content.

The effects of carbon content and molybdenum con-

*"Free" ferrite as used in this paper includes all ferrite —polygonal and acicular—that is not intimately mixed with carbides.

TABLE A-I–Data Used in Figure A-5

Heat No.	Analyses of Steels*				D_I–50% Martensite (in.)	Data at 50%–Martensite Jominy Distance		D_I–90% Martensite (in.)	Data at 90%–Martensite Jominy Distance	
	% C	% Mn	% Si	% Mo		Hardness (DPH)	Free Ferrite (Vol %)		Hardness (DPH)	Free Ferrite (Vol %)
3830A	0.41	0.50	0.31	—	1.00	305	2.5	0.75	370	0.5
B	0.41	0.51	0.32	0.27	1.40	350	6	1.11	400	1.3
C	0.43	0.49	0.32	0.52	1.65	385	8	1.39	460	1.5
D	0.42	0.48	0.32	0.66	1.95	385	11	1.56	470	1.9
E	0.42	0.47	0.32	0.82	2.52	450	15	2.05	550	2.4
3837F	0.43	0.54	0.33	0.96	2.86	475	18	2.35	575	3.2
3829A	0.29	0.49	0.28	—	0.67	248	15	—	—	2.6
B	0.29	0.49	0.29	0.27	1.10	282	19	0.89	310	3.2
C	0.30	0.48	0.30	0.51	1.34	320	22	1.08	365	3.6
D	0.29	0.47	0.27	0.66	1.64	340	25	1.32	400	3.6
E	0.30	0.49	0.28	0.85	2.00	365	26	1.68	425	4.2
3837E	0.31	0.55	0.34	0.97	2.30	410	28	1.84	500	4.8
3828A	0.19	0.46	0.25	—	0.45	242	29	—	—	—
B	0.19	0.46	0.25	0.25	0.85	260	31	—	—	—
C	0.19	0.47	0.26	0.50	1.16	280	39	0.92	300	6.6
D	0.20	0.44	0.25	0.66	1.33	288	40	1.03	310	6.1
E	0.21	0.46	0.25	0.85	1.64	325	42	1.33	375	7
3837D	0.21	0.53	0.33	0.97	1.85	325	46.5	1.45	375	9
3827A	0.17	0.51	0.29	—	0.37	230	31.5	—	—	—
B	0.17	0.51	0.29	0.26	0.80	255	39	—	—	—
C	0.17	0.50	0.33	0.50	1.15	260	44	—	—	—
D	0.16	0.51	0.32	0.63	1.37	287	50	1.05	325	—
E	0.17	0.51	0.32	0.65	1.45	305	50	1.10	345	—
3837C	0.18	0.55	0.34	0.96	1.80	315	50	1.48	345	10
3826A	0.092	0.48	0.28	—	0.25	197	50	—	—	—
B	0.097	0.51	0.29	0.26	0.54	225	50	—	—	—
C	0.10	0.51	0.30	0.52	0.88	255	50	—	—	—
D	0.10	0.52	0.30	0.65	1.00	260	50	—	—	—
E	0.10	0.50	0.30	0.85	1.16	275	50	—	—	—
3837B	0.11	0.57	0.32	0.96	1.54	275	50	1.24	295	10
3825A	0.045	0.44	0.29	—	—	—		—	—	—
B	0.042	0.44	0.28	0.25	0.42	193	50	—	—	—
C	0.047	0.44	0.28	0.48	0.67	192	50	—	—	—
D	0.049	0.45	0.27	0.64	0.77	227	50	—	—	—
E	0.044	0.46	0.28	0.80	1.02	244	50	0.73	265	10
3837A	0.066	0.50	0.30	0.98	1.20	245	50	0.88	265	10

* Weight percent.

tent on the amount of free ferrite in the nonmartensitic transformation products is apparent from the plot. For a given molybdenum content, the amount of free ferrite increases as the carbon content decreases; and for a given carbon content, the amount of free ferrite increases as the molybdenum content increases. In many of these steels and especially those having low carbon and high molybdenum contents, the free ferrite constituent had a predominantly acicular morphology.

The resemblance between Figure 3 and the free ferrite curves in Figure A-5 suggests that the molybdenum multiplying factor might be related to the amount of free ferrite in the nonmartensitic transformation product.

At first glance, these results appear to contradict the hardness versus carbon data (Figure A-5). One might expect the hardness at a given carbon content to decrease as the amount of free ferrite increases. The results indicate that increased free ferrite content actually results in an increase in hardness.

These observations, however, can be rationalized as follows:

1. For a given carbon content, increasing molybdenum contents increase the amount of free ferrite, thereby increasing the amount of carbon enrichment of the remaining austenite.
2. The martensite formed from the carbon-enriched austenite is, therefore, harder than would be predicted on the basis of the overall carbon content of the steel.

Based on hardness and metallographic data, it is concluded that molybdenum increases the hardness of the 50- and 90%-martensite microstructures by promoting the formation of free ferrite, resulting in carbon enrichment of the austenite that subsequently transforms to martensite, and the hardness of these microstructures is governed by the hardness of the martensite. It is also concluded that for steels containing less than 0.45% C the molybdenum multiplying factor is in some way related to the volume percent of free ferrite in the nonmartensitic transformation product.

Relation between Hardness at 90% and 50% Martensite Figure A-6 shows the hardness values at the 90%-martensite Jominy distance plotted against the hardness values at the 50%-martensite Jominy distance as well as similar hardness data reported by Hodge and Orehoski for 35 commercial heats. Hodge and Orehoski's[10] data (represented by the shaded area) brackets the solid circles obtained in the present study. Figure A-6 makes it possible to predict hardenability in terms of D_I values for a 90%-martensite criterion when the hardness at the 50%-martensite Jominy distance is known.

Grain Size Effects

Interrelation Involving D_I Values for Coarse Grain versus Fine Grain Steels From the published literature, it would be expected that the dominant factor controlling the effect of grain size on hardenability would be the nature of the nonmartensitic transformation product. It appears from the present study that the carbon content may have a significant influence on the dependency of hardenability on grain size by altering the nonmartensitic transformation product.

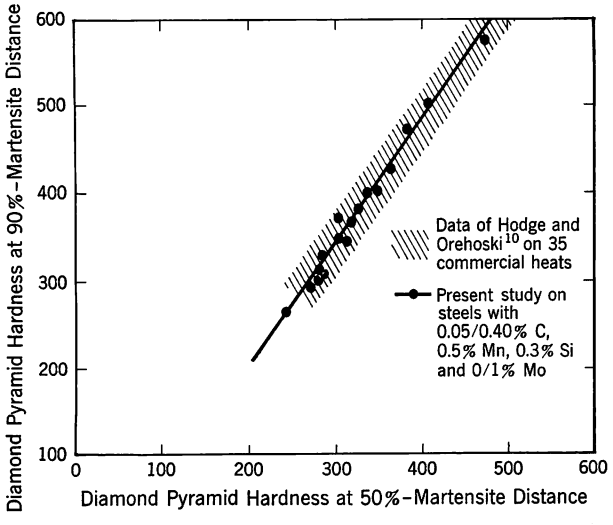

FIGURE A-6. Relation between the hardness at the Jominy position corresponding to 90% martensite and that at the Jominy position corresponding to 50% martensite

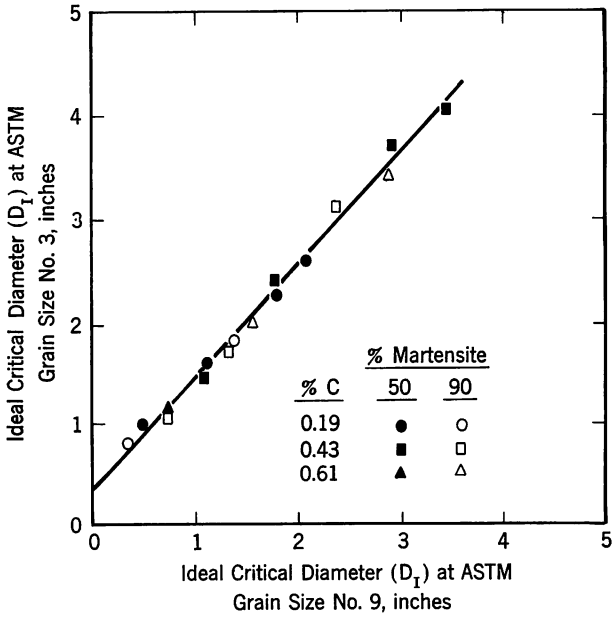

FIGURE A-7. Relation between ideal critical diameters for coarse grain (ASTM no. 3) and fine grain steels (ASTM no. 9). Steels contained 0/1.0% Mo

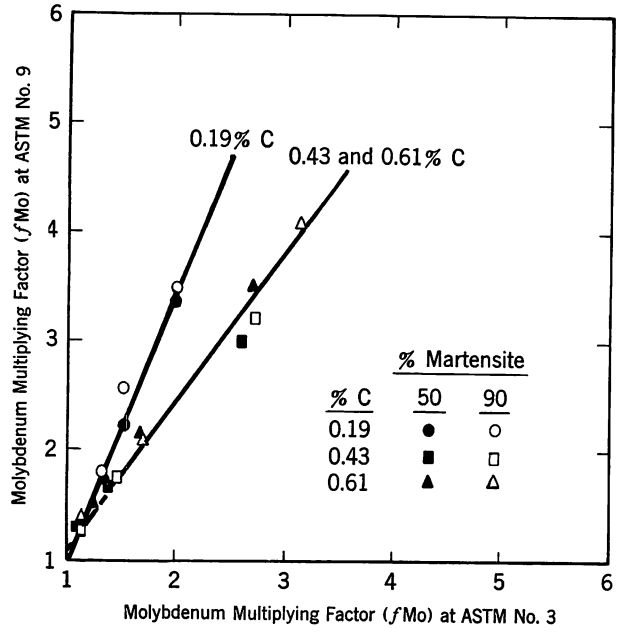

FIGURE A-8. Relation between molybdenum multiplying factors obtained on fine grain (ASTM no. 9) and coarse grain (ASTM no. 3) steels. Steels contained 0/1.0% Mo

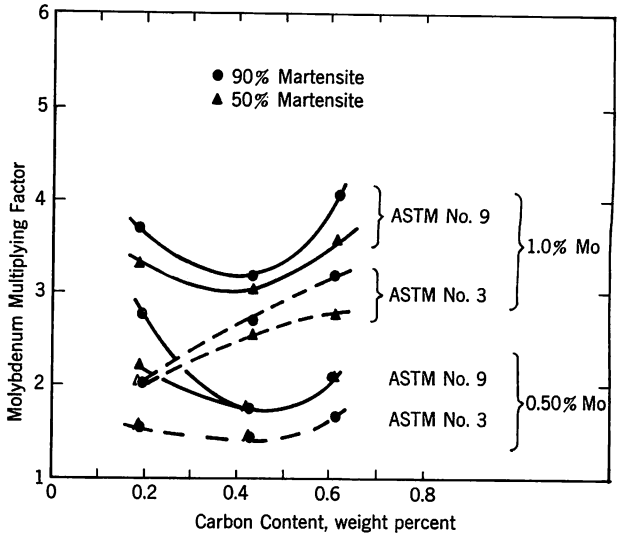

FIGURE A-9. Effects of carbon content, martensite percentage and austenitic grain size on the molybdenum multiplying factor for steels containing 0.50% Mn and 0.30% Si

The hardenability of fine-grained steels is usually limited by the transformation to pearlite and ferrite. The hardenability of coarse-grained steels is usually governed by transformation to bainite. Obviously, mixtures of these nonmartensitic transformation products exist in these steels. Therefore, with coarsening of the austenite grains and increasing molybdenum content, one would expect more bainite in the microstructure and a change in the relationship between the D_I values at the coarse and fine grain sizes.

Two important effects can be seen from Figure A-7, where the D_I value for grain size no. 3 (representing the hardenability of a coarse-grain steel) is plotted against the D_I value for grain size no. 9 (representing the hardenability of a fine-grain steel). The D_I values associated with the fine-grain steels vary in a linear manner with the D_I values derived for coarse-grain steels, and this relation is independent of composition, microstructure, or the amount of martensite specified in the hardenability criterion.

Interrelation Involving Molybdenum Multiplying Factors for Coarse-Grain versus Fine-Grain Steels

A plot of the molybdenum multiplying factors for grain size no. 9 versus the factors for grain size no. 3 should give some indication of the relation between pearlitic and bainitic factors for molybdenum. Figure A-8 indicates that the grain size effect is dependent upon the carbon content. The one possible reason is that low carbon contents cause the nonmartensitic transformation product to be largely polygonal ferrite or acicular ferrite, resulting in carbon enrichment of the austenite during transformation. In the higher carbon steels the nonmartensitic transformation products contain a large amount of carbon in the form of carbides in pearlite or bainite; therefore, extensive enrichment of the austenite in carbon did not occur.

The data permit a qualitative evaluation of the effect of carbon content and austenitic grain size on the molybdenum multiplying factor. Although the carbon contents of the steels employed for the grain size studies covered only a limited range, the results do supply some indication of how molybdenum factors vary with grain size and carbon content. The divergence between the coarse-grain factors (ASTM no. 3) and the fine-grain factors (ASTM no. 9) in Figure A-9 is least in the vicinity of 0.45% C and is greatest at lower and higher carbon contents.

The results show that carbon and molybdenum interact to affect the hardenability of a steel regardless of whether the nonmartensitic transformation products are predominantly bainite, ferrite, or pearlite.

REFERENCES

1. E. S. Davenport and E. C. Bain, Trans. AIME *90*. 117 (1930)
2. W. E. Jominy and A. L. Boegehold, Trans. ASM *26*. 574 (1938)
3. M. A. Grossmann, Trans. AIME *150*. 227 (1942)
4. G. R. Brophy and A. J. Miller, Trans. AIME *167*. 654 (1946)
5. I. R. Kramer, S. Siegel and J. G. Brooks, Trans. AIME *167*. 670 (1946)
6. I. R. Kramer, R. H. Hafner and S. L. Toleman, Trans. AIME *158*. 138 (1944)
7. J. M. Hodge and M. A. Orehoski, Trans. AIME *167*. 502 (1946)
8. W. Crafts and J. L. Lamont, Trans. AIME *158*. 157 (1944)
9. L. H. Boyd and J. Field, "Calculation of the Standard End-Quench Hardenability Curve from Chemical Composition and Grain Size," *Contributions to the Metallurgy of Steel*, No. 12, American Iron and Steel Institute, New York, 1946, 25pp
10. J. M. Hodge and M. A. Orehoski, Trans. AIME *167*. 627 (1946)
11. J. M. Hodge, J. L. Giove and R. G. Storm, Trans. AIME *185*. 218 (1949)
12. J. H. Hollomon and L. D. Jaffe, Trans. AIME *167*. 601 (1946)
13. C. F. Jatczak and R. W. Devine, Trans. ASM *47*. 748 (1955)
14. E. J. Whittenberger, R. R. Burt and D. J. Carney, Trans. AIME *206*. 1008 (1956)
15. C. F. Jatczak and D. J. Girardi, Trans. ASM *51*. 335 (1959)
16. E. S. Davenport, Trans. ASM *27*. 837 (1939)
17. R. A. Grange, Trans. ASM *59*. 26 (1966)
18. G. Bandel and H. C. Haumer, Stahl und Eisen *84*. 932 (1964)
19. D. J. Carney, Trans. ASM *46*. 882 (1954)

ORAL DISCUSSION OF

Effects of Carbon and Austenitic Grain Size on the Hardenability of Molybdenum Steels

Presented by R. FOSTINI

C. F. JATCZAK (The Timken Roller Bearing Company). The results of this work should certainly discourage attempts at calculation of hardenability factors for the various alloying elements by the expeditious use of the computer. It should be obvious that normalized statistics would be completely fouled up by the unpredictable synergistic effects which occur so frequently between some elements in multialloyed compositions. The influence of carbon on the molybdenum factor is an example of this problem.

One question is directed to the writers regarding the dip in the molybdenum hardenability factor shown at high molybdenum contents and fine grain sizes. Could this drop perhaps be explained by the probability that in heat treating to achieve the fine grain size of 9 and above, the austenitizing temperature got so low as to precipitate molybdenum carbides? $M_{23}C_6$ carbides would definitely be present if such temperatures were below 845 C (1550 F).*

AUTHOR'S REPLY. We haven't investigated this area as yet, and I have no explanation for this effect. The small grain sizes were obtained by austenitizing these steels at temperatures dictated by the particular carbon content of the steel.

C. F. JATCZAK. Do you go below 800 C (1470 F) maybe?

AUTHOR'S REPLY. No, the 0.40 and 0.60% C steels were austenitized at 845 C (1550 F).

C. F. JATCZAK. Well, then you had carbides?

AUTHOR'S REPLY. If we had carbides present, they were not visible under the light microscope.

*R. F. Campbell, S. H. Reynolds, L. W. Ballard and K. G. Carroll, Trans. AIME *218*, 723 (1960)

J. HODGE (United States Steel Corporation). It seems to me that this paper further emphasizes the problem that Morris Cohen brought up as to the definition of hardenability. Similarly, these effects have reached a distinction between bainitic and pearlitic hardenability which is obviously a very significant factor in the behavior you are talking about, but when you get down to the lower carbon ranges, down to 0.2% C or below, I think neither of these categories are particularly significant. I think the most significant thing at low carbon contents is probably what I suppose you might call ferritic hardenability, but the significant behavior is the austenite enrichment that occurs when the ferrite comes out, and it seems to me that it is logical to look most critically at the hardenability in this carbon content range in relation to this behavior. In this respect, I was wondering if you looked at these things, say on a 5 or 10% ferrite basis rather than on a 90 or 95 or 50% martensite basis, what would the results be?

AUTHOR'S REPLY. When you say 5 or 10% ferrite basis, what is the remaining transformation product?

J. HODGE. I don't know. It will vary quite markedly, depending on the enrichment behavior.

AUTHOR'S REPLY. I have to agree with you that the carbon enrichment of the remaining austenite is one of the most important factors that contributes to the hardenability of these low-carbon steels. I have looked a little bit into it, and I have concluded that as you decrease your carbon content and maintain a constant martensite criterion, the carbon enrichment becomes progressively greater and greater as you go lower in carbon content. The reason for the enrichment is that you are forming more ferrite. If we assume the ferrite to be supersaturated with respect to carbon, let's assume the carbon content to be about 0.02% and work backwards; you can then estimate the carbon content of the untransformed austenite. From this type of calculation, you can get an idea of how much carbon enrichment occurs. Of course, the degree of carbon enrichment is quite significant at the lower carbon contents, and this will have a greater stabilization effect at the lower than at the higher carbon contents. This in turn will have an appreciable effect on the transformation rate of carbon-enriched austenite.

J. HODGE. As far as application of measurements and evaluations go, I would be inclined towards using some small amount of ferrite as a criterion and then use the hardenability evaluation to establish what alloy content is needed to assure that minimum level of ferrite in the microstructure, and corresponding minimum degree of enrichment. That leads to a generalization, but this is the predominant significant factor in the 0.20% C and low-carbon steels. In the 0.40% and 0.50% C steels though, the predominant harmful thing is the bainite and it is bainitic hardenability that is of primary concern. We seldom really worry about pearlite in such steels, at least when you have molybdenum in them, and the same sort of thing applies to the higher carbon steels, so this may suggest that one should think about different criterions, depending upon the carbon regions of interest. So at any rate, I still believe that the criterion should be based strictly on specific microstructures, and should be based on what is known about the relationships between microstructure and properties and what has to be limited in the ferritic microstructures to obtain the desired properties.

AUTHOR'S REPLY. I agree with that.

A. J. MCEVILY (Ford Motor Company). At high carbon levels your slides indicated that the effect of molybdenum on hardenability went through a maximum and then started decreasing with increase in carbon content. At low carbon levels hardenability increased monotonically with decrease in carbon content below 0.1% carbon. On the basis of the work which we have just described, it appears that a maximum may be present at very low carbon contents as well as at high carbon contents.

AUTHOR'S REPLY: It may be; that end of the curve is uncertain as far as we are concerned at this time.

H. I. AARONSON (Ford Motor Company). These effects you have shown are very interesting, and in attempts to understand them, it would be valuable to have TTT diagrams determined by the isothermal method. Do you have this information?

AUTHOR'S REPLY. No, this is something I would like to see done.

Closing Remarks

R. F. MEHL
University of Delaware

I am one of those chaps referred to by a speaker yesterday who had done a great deal of work years and years ago and who surprisingly is still here. I don't propose to do anything about this, despite some very strong suggestions made to me last evening by some old friends!

It should be useful as research in a field progresses to try to identify the critical areas of ignorance — to name those aspects of a field that are most puzzling. A few years ago I was invited to give the tenth-anniversary lecture of the Tubal Cain, student metallurgical society of the Technische Hochschule in Delft. I chose to speak on pearlite, particularly on what is not known or not understood. Afterwards, everyone in the audience told me that my speech had been very successful — they had been convinced that there was a great deal that I did not know about pearlite! Possibly it might now be useful to regard bainite in this way.

The subject of this conference is the classical one in physical metallurgy with a long history stretching far back into the centuries. It surely reached a point of high excitement in this country in the 1930's and to that scene the research workers at Climax made important contributions. It was in this period following the derivation of the TTT curve that bainite was recognized and received its name. Sitting beside Dr. Rowland today, we recalled that high tide of activity and some of the people who took part: Bain, Sauveur, McQuaid, Grossmann, and the rest. Professor Sauveur was of the old school, of the days of heroes, and the days when troostite, sorbite, hardenite, etc., etc., were daily words to the metallurgist. He invited me, in 1938, to lecture on bainite at Harvard. As Professor Hehemann remarked yesterday, I had at that time proposed that there are probably two bainites, upper bainite and lower bainite; there was but little evidence for this at the time, chiefly that based on the obviously different microscopic appearance. Research since has confirmed the guess — which I suppose proves that it is better to be lucky than to be smart! So it came about that I lectured on upper and lower bainite at Harvard. Professor Sauveur, that great gentleman, arose when I had finished and said, "For years I have held that there is no such thing as bainite, and now an old associate of mine tells me that there are two of the things!"

Despite the beautiful research work on bainite that has been done in recent years by Professor Hehemann and others, some serious questions remain. If these can be identified in such a way as to suggest research projects for the future, there would be a gain; at least one can try.

Why is it that upper bainite forms needles while lower bainite forms plates? There is otherwise so much similarity between them. The formation of needles in solid–solid reactions is not a new phenomenon; Dr. Marzke demonstrated in 1930 that alpha brass forms from the beta phase at high temperatures as needles, and we now know that the same reaction conducted at low temperatures produces plates, a loose analogy to the steels. This is by no means the only example of the formation of needles or laths, as reference to the extremely voluminous literature on this subject will show. I do not understand this. Allied is the curious fiber structure in some precipitates; for example, Fe_3C formed from austenite, and others. It would seem that crystallographic directions in the cooperating lattice are sometimes as important as crystallographic planes, for reasons we do not see.

Old work seemed to show that the orientation of the ferrite lattice with respect to the matrix austenite *in space* is essentially the same in the two bainites (and in martensite), independent of the temperature of reaction, though the habit plane (or direction) changes gradually with temperature, from proeutectoid ferrite down to and including martensite. There are two old publications on this, giving the same result; perhaps it should be repeated at more frequent temperature intervals, to more surely trace the continuity, or perhaps to identify discontinuities, in this crystallography — a curious fact.

There are other similar interesting major puzzles in this field. Why is it, as Professor Hehemann pointed out in a discussion at the recent Scarborough Conference, that particles of alpha brass, growing rapidly along a direction, grow laterally too but only on one side, with the other side of the precipitate remaining inactive; why are there such inactive plane interfaces? Why as one lath or plate forms is another and still more encouraged to form next to it — the phenomenon which Dr. Aaronson, who has done so much in this field, calls "sympathetic nucleation"?

Perhaps we should reconsider the nucleation and growth mechanism of the bainite reaction. The recent work of Garwood, reported at the Scarborough Conference, provides strong evidence that the initial nucleus is the same in the two bainites and that they differ only in the growth stage; the argument is based on a rough approximation of activation energies, and it seems good. There are direct measurements of the rate of growth of bainite, (and these show some peculiarities) but there is very little direct quantitative evidence on the rate of nucleation; we should have some. The beautiful work of Professor Hornbogen on age-hardening at U. S. Steel and more recently at Göttingen, is germane and worthy of study by those who concern themselves with bainite.

Habit planes (or directions) in all solid–solid reactions remain puzzling. Stray references in the age-hardening field identify the habit plane of the precipitate as that for which the value of Young's modulus perpendicular to the plate is a maximum; in aluminum alloys this is the [100] direction; yet in the aluminum–silver system, almost certainly with the similar elastic properties, the habit plane of the platelet precipitate is matrix (111), not (100). There is something amiss. It has become arguable in recent years whether habit planes in solid–solid reactions are truly rational in the sense of crystallographic indices. Certainly there is real doubt on this for martensite, and for bainite too. How should one approach this awkwardness?

I would suggest that the key lies in the elastic moduli of both matrix and precipitate. As a first approximation, a precipitate with a given orientation in space with the matrix should form plates lying on some matrix plane which will create the least strain energy; this might be enough, though it is well known that plastic strain is involved too. To argue that the elastic properties of the matrix alone is important is hardly convincing — if this were the case, why do habit planes vary from system to system with the same base metal?

In the case of bainite with the habit plane probably always irrationally changing with temperature, could not elastic anisotropy of the matrix and precipitate vary so with temperature as to vary the habit plane? Both gamma and alpha iron at room temperature are highly anisotropic with respect to both Young's modulus and the shear modulus exhibiting extreme anisotropy by a factor of approximately three. If there be merit in this, then it would seem advisable to determine these elastic properties of the two phases as a function of temperature, in single crystals of course. This has not been done. And with this, knowing the volume changes, to calculate the elastic strain energies for all possible habit planes, hopefully finding that the habit plane observed is indeed that which would give a minimum value. These studies would be difficult but as surely worthy. One could go on, but not today!

My main purpose, gentlemen, in arising at the very end of this conference is to thank the Climax Molybdenum Company in the persons of Mr. Herzig and his associates, and also the University of Michigan, for their warm hospitality — all in behalf of this large and grateful audience. The conference has been marvelously organized and operated, and I hope that the results have proved pleasing to our hosts.